3D Printed Polymeric Drug-Eluting Implants for Personalized Therapy

Athina Liaskoni

Pharmacist, MSc

Thesis submitted to the University of Nottingham for the degree of Doctor of Philosophy

October 2021

Μηδὲν τῆς τύχης ἀλλὰ πάντα τῆς εὐβουλίας εἶναι
καὶ τῆς προνοίας.

Nothing depends on luck, but all on good judgment
and diligence.

Plutarch,
47-120 AD, Ancient Greek historian

Declaration

Unless acknowledged otherwise, the work presented in this thesis is my own. No part of this work has been submitted for another degree at the University of Nottingham, or any other institute of learning.

Athina Liaskoni
October 2021

Acknowledgements

I would like to express my deep gratefulness to my supervisors, Prof. Clive Roberts and Prof. Ricky Wildman who gave me the golden opportunity to do this wonderful project on the topic of "3D printed personalised polymeric implants" that helped me to do a lot of research and explore new scientific fields.

However, I would particularly like to thank my principal supervisor, Prof. Clive Roberts, for his marvellous support, exemplary guidance, invaluable advice and contribution to this work. Our meaningful discussions throughout my PhD and his constructive feedback were making me feel more confident in my abilities, opening my mind and always aiming to the highest peak. It is a great privilege and honour to have been supervised by such a brilliant and inspiring professor, scientist and person that contributed much to shaping my personality and character for my future career as a formulation scientist.

I am indebted to Prof. Ricky Wildman, as well, for his constant encouragement, prompt inspiration and timely suggestions, but also for always guiding me so positively and believing in me even in the most challenging moments of my academic journey. His support was essential to the accomplishment of this demanding task, the completion of my PhD.

I am deeply grateful to the technical team of the Boots Science Building, School of Pharmacy, Paul Cooling and Esme Ireson, for the training and support in the laboratory equipment and especially, Douglas Crackett for very effectively and quickly setting up and training me on the USP4 "flow through" dissolution tester at a very critical stage of my research project. I would also like to thank Dr. Graham Rance for his assistance with Raman analysis and nmRC (University of Nottingham) for kindly providing me access to the SEM instrument. Lastly, I am extremely thankful to the technical team of the Centre for Additive Manufacturing in the Advanced Manufacturing Building, Mark East and Mark Hardy, for always being available to give a solution to the amusingly unexpected machine malfunctions that I was experiencing.

I would like to express my eternal appreciation for my fellow PhD students and colleagues in the A09 office in Boots Science Building, School of Pharmacy for providing such a nice atmosphere for working by being supportive and helping me to have a laugh even when stressed and sometimes disappointed with my research

data. I, also, thank profusely all the members of the Additive Manufacturing group for their valuable assistance and fantastic company and for making my PhD journey so enjoyable at the best of times, and bearable at the worst of times.

I am deeply thankful to my beloved brother, Athanasios, for his continuous moral support, immense patience, tireless encouragement and his motivating words that were helping me to never lose hope, but always pursue my dreams. I am extremely grateful to my fiancé, François, for patiently dealing with my frustration throughout my research, for never once wavering in his complete support and encouragements, as well as, for our endless discussions any time of the day or night and for filling my life with happiness and goofiness. Finally, I owe profound gratitude to my parents, Konstantinos and Alkmini, to whom this thesis is dedicated, for always having confidence in my ability to succeed and being there for me from the very first steps of my research in Greece at an undergraduate level until now, the obtainment of my PhD in the UK. Without them, I would not have accomplished all my ambitious goals and would not be the person I am today. Thank you for never stop believing in me, as I never stop believing in you!

ABSTRACT

Conventional oral drug delivery systems, such as tablets, capsules and solutions, are widely used today and is the most commonly selected mode of administration for patient treatment. These systems can, however, demonstrate limitations, including the need for their frequent administration so that drug therapeutic levels can effectively be achieved and maintained. This can lead to reduced patient compliance, especially in populations having multiple and multiplex conditions, that need to be treated with several active ingredients contained in different formulations - in the UK, patients over 65 years of age take on average 5 to 8 different medications per week. For certain clinical needs, this requirement for frequent administration can be avoided by the use of long-acting implants. In addition, personalised medicine is a new approach that can reduce medication burden, since the fabrication of bespoke dosage forms is based on an individual's health status, needs, genetic and physical factors.

Implants represent formulations with great potential to be applied in patient-centric therapies and can be manufactured with a variety of materials and processing technologies. 3D Printing is a manufacturing technology with increasing popularity in various fields, including pharmaceuticals. Its versatility and the high degree of design freedom make feasible the production of different types of personalised formulations with unique attributes matching each patient characteristics, needs and preferences.

In the present study, the fabrication of sustained drug release dosage forms using a solvent-free method at a relatively low printing temperature by a pressure assisted microsyringe 3D printer is demonstrated. The selected materials for the implant manufacture were polycaprolactone (PCL) – a polymer that is considered promising due to its properties; biodegradability, biocompatibility and processability – and lidocaine (LDC) – the model drug with a melting point close to the polymer's.

The first stage of this work was the investigation of the printability of PCL with two molecular weights - 25 kDa and 50 kDa - using a pressure assisted microsyringe (PAM) 3D printer and a Fused Deposition Modelling (FDM) 3D printer. FDM polymeric filaments for printing were produced by a Hot Melt Extruder (HME). The impact of the extrusion on the thermal and crystalline properties of the polymer was explored.

The next step in this study was the manufacture of lidocaine loaded PCL implants, with and without a PCL barrier-shell with various lidocaine loading using the PAM 3D printer. Physical and chemical characterization (SEM, DSC, XRD, FTIR, Raman) in the printed formulations have been performed to investigate potential changes in their thermal and crystalline properties, their chemical structure or potential interactions after their mixing and 3D printing process.

In the final phase of this work, the drug release rate of the differently printed implants was evaluated using a USP4 flow-through cell apparatus. The structural integrity of the studied dosage forms after the four-day long dissolution studies was explored by SEM. Drug release kinetics were studied by fitting the drug release data to four standard mathematical models; zero-order, first-order, Higuchi model and Korsmeyer-Peppas model.

PCL extrudability in an HME was demonstrated with the addition of 1% w/w plasticizer, triethyl citrate, and by a suitable combination of the extrusion parameters, temperature in heat zones and screw speed. Both molecular weight PCLs have been extruded in fine filaments at low temperatures, close to the polymer melting point. The printability of these filaments has subsequently been investigated in an FDM 3D printer. After optimization of the printing parameters – print temperature, print speed, nozzle diameter – applied, a basic triangle geometry, with a high printing resolution has been manufactured.

The printability of PCL was shown to be successful without the addition of any other material – excipient or solvent – when a pressure-assisted microsyringe (PAM) 3D printer was used. Optimization of the printing procedure was also needed due to the high viscosity of the polymer, especially of the 50 kDa molecular weight PCL. In this 3D printer type, though, the fabrication of a predetermined shape with PCL has been achieved at a lower print temperature (110 ^{o}C) compared to the temperature applied during the FDM 3D printing (180 ^{o}C).

DSC and XRD characterization of the filaments, as well as, of the 3D printed test shapes showed that the polymers were crystalline after the extrusion and 3D printing. The crystalline nature of the investigated materials was not affected by the various extrusion and printing parameters applied.

The fabrication of encased and non-encased lidocaine loaded PCL implants has successfully been achieved using the Pressure Assisted Microsyringe 3D printer. Optimization of the printing process, regarding the print temperature, print speed, bed temperature, extrusion width and pressure, was required to accommodate the impact of formulation changes. Specifically, the addition of lidocaine led to a decreased formulation viscosity.

The versatility of the selected 3D printing method was proven by the successful manufacture of a PCL barrier–shell lidocaine loaded polymeric implant without any particular material preparation prior to their loading to the cartridge of the printer or any post–printing processing.

DSC and XRD characterization of the 3D printed PCL lidocaine implants revealed that the blending and extrusion processes did not significantly affect the thermal behaviour of the materials used with PCL and that lidocaine crystals were present in the fabricated formulations at a low level indicating the formation of solid dispersion for the majority of the drug in the polymer matrix.

FTIR and Raman analysis demonstrated that the blending and printing processing did not result in detectable modifications in the materials chemical structures or interactions between PCL and LDC. Moreover, Raman spectra indicated the presence of both materials on the surface of the printed formulations. Nevertheless, this did not lead to a significant burst drug release suggesting that the active agent remained sufficiently physically associated with the polymer to control release.

Sustained lidocaine release has been attained both when PCL was used as a matrix or as a barrier-shell in the fabricated dosage forms due to its slow degradation rate. The use of the PCL barrier enabled delayed and slower drug release that can be tuned by control of barrier size.

The Korsmeyer-Peppas model was shown as the best fit to drug release profiles for all the produced encased and non-encased implants indicating that drug release was controlled by combined transportation mechanisms, diffusion and polymeric chain relaxation.

The early stages of PCL degradation were also shown by SEM imaging of the lidocaine loaded and lidocaine free PCL formulations after four days of dissolution, where the appearance of some surface holes was detected.

This work has demonstrated that PCL has a significant potential for the production of prolonged drug release formulations by 3D printing, both as a matrix and as a barrier-shell to enable predictable and programmable delayed drug release. Solid drug dispersions can successfully be manufactured with hot melt extrusion-based 3D printing broadening its applications in the pharmaceutical field. It has, also, been shown that drug loading can be varied in a bespoke fashion for each implant, showing that personalisable implants can be manufactured by 3D printing and, thereby, address some limitations of conventional pharmaceutical dosage forms.

TABLE OF CONTENTS

LIST OF FIGURES

LIST OF TABLES

ABBREVIATIONS

.stl (file)	STereoLithography (file)
ΔH	Enthalpy Change
ΔH_f	Enthalpy of fusion
2D	Two Dimensional
3D	Three Dimensional
3DP	Three Dimensional Printing
ABS	Acrylonitrile Butadiene Styrene
ADME	Absorption, Distribution, Metabolism and Excretion
AIDS	Acquired Immune Deficiency Syndrome
AM	Additive Manufacturing
API	Active Pharmaceutical Ingredient
ATR	Attenuated Total Reflectance
BMS	Bare Metal Stents
CAD	Computer Aided-Design
CIJ	Continuous Inkjet
CMV	Cytomegalovirus
Da	Dalton
DDS	Drug Delivery System
DEEP	Data-Enriched Edible Pharmaceuticals
DES	Drug Eluting Stents
DLP	Digital Light Processing
DoD	Drop-On-Demand
DSC	Differential Scanning Calorimetry
e.w.	Extrusion Width
EBM	Electron Beam Melting
EC	Ethylcellulose
EG	Ethylglycine
EU	European Union
EVA	Ethylene Vinyl Acetate
FDA	Food and Drug Administration
FDM	Fused Deposition Modelling
FFF	Fused Filament Fabrication
FTIR	Fourier-Transform Infrared (spectroscopy)

GC-MS	Gas Chromatography-Mass Spectroscopy
GI	Gastrointestinal
GRAS	Generally Recognised As Safe
GX	Glycinexylidide
HIPS	High Impact Polystyrene
HIV	Human Immunodeficiency Virus
HME	Hot Melt Extrusion
HMW	High Molecular Weight
HPC	Hydroxypropyl cellulose
HPMC	Hydroxypropyl methyl cellulose
HPMCAS	Hydroxypropyl methylcellulose acetate succinate
HZ	Heating Zone
IDDS	Implantable Drug Delivery System
K_0	Zero-order release rate constant
K_1	First-order release rate constant
K_{K-P}	Release rate constant of Korsmeyer-Peppas
K_H	Release rate constant of Higuchi
kDa	Kilodalton
kPa	Kilopascal
LDC	Lidocaine
LMW	Low Molecular Weight
MCC	Microcrystalline cellulose
MEC	Minimum Effective Levels
MEGX	Monoethylglycine xylidide
MHRA	Medicines and Healthcare products Regulatory Agency
MIT	Massachusetts Institute of Technology
MTC	Maximum Toxic Levels
n	Drug release exponent
PAA	Polyaspartic acid
PAM	Pressure Assisted Microsyringe
PBS	Phosphate Buffered Saline
PC	Polycarbonate
PCL	Poly (ε-caprolactone)
PCPP	1,3-bis(carboxyphenoxypropane)
PEG	Polyethylene glycol
PEO	Polyethylene oxide

PET	Polyethylene Terephthalate
PET-G	Polyethylene terephthalate glycol-modified
PEVA	Polyethylene vinyl acetate
PGA	Polyglycolic Acid
pH	Potential of Hydrogen
PHB	Polyhydroxybutyrate
PLA	Polylactic Acid
PLGA	Polylactic-co-Glycolic Acid
PLLA	Poly(L-lactide)
POC	Point Of Care
PPSF	Polyphenylsulfone
PU	Polyurethanes
PVA	Poly Vinyl Alcohol
PVP	Polyvinylpyrrolidone
PVP-VAc	Polyvinylpyrrolidone-Vinyl Acetate copolymer
QR	Quick Response
RP	Rapid Prototyping
SA	Sebacic Acid
SBF	Simulated Body Fluid
SEM	Scanning Electron Microscopy
SFF	Solid Free-Form
SLA	Stereolithography
SLM	Selective Laser Melting
SLS	Selective Laser Sintering
SSE	Semi-Solid Extrusion
T_m	Melting Point
TEC	Triethyl citrate
TPU	Thermoplastic polyurethane
UK	United Kingdom
US	United States
USP	United States Pharmacopeia
UV	Ultraviolet
UV-Vis	Ultraviolet-Visible
X_C %	Crystallinity degree/percentage
XRD	X-Ray Diffraction

CHAPTER 1: INTRODUCTION

Conventional drug dosage forms, such as tablets, capsules and solutions, are widely used today, even though they exhibit limitations that mean some therapeutics are not possible or are limited in their functionality. One disadvantage relates to their normal manufacturing route of mass manufacture and hence, lack of personalisation to meet individual patient needs, characteristics and preferences. The purpose of this introduction is to highlight the reasons why more individualized medicines are required to be developed and the benefits that they could offer to patients. Implantable drug delivery systems will, then, be presented since they can appropriately be modified by additive manufacturing (3D printing) and be used in personalized therapy. Implants design approaches, drug release mechanisms and categories will be discussed, with a focus on degradable dosage forms that are the devices of interest of this work and they demonstrate the most benefits to long-term patients therapies compared with the other categories of implants. The personalization of these formulations is not feasible with the current mass manufacturing processes. 3D printing offers a solution because of the design freedom that it provides for each individual product manufactured; the most popular additive manufacturing technologies in the pharmaceutical field will be presented. The formulation materials used in this 3D printing study – polycaprolactone as a matrix polymer and lidocaine as a model drug, as well as, the properties that led to their selection, will be introduced.

The aim of the present research is the manufacture of drug-eluting polymeric implants using a thermal extrusion based 3D printing process demonstrating the required attributes to be applied in personalized therapies for sustained drug release. A secondary aim is to use the minimum thermal stress possible in the manufacture without the addition of any solvents or other materials. The aims and objectives of this work will be discussed more extensively in the final section of this Chapter.

A part of this thesis has been published with the relevant publication included in ***Appendix 2*** (Liaskoni, Wildman and Roberts, 2021).

1.1. DRUG DELIVERY SYSTEMS

1.1.1. Introduction

A drug delivery system (DDS) is a formulation or a device that makes feasible the introduction of a therapeutic compound to the body and its subsequent release with a defined rate, often at a predetermined place and time, enhancing or enabling drug efficacy and safety (Liu *et al.*, 2016) (Shaik, Korsapati and Panati, 2012). Drug absorption, distribution, metabolism and excretion (ADME) profiles should also be improved (Abu-thabit and Makhlouf, 2018) (K. K. Jain, 2008). A DDS plays, thus, the role of the interface between the patient and the drug with the aim to eliminate the complications caused by the active agent (K. K. Jain, 2008). The selected method of DDS administration is, usually, closely associated with its effectiveness (Abu-thabit and Makhlouf, 2018).

An ideal DDS should demonstrate the following properties (Langer, 1993) (Deshpande *et al.*, 1996) (Maiti and Sen, 2017) (K. K. Jain, 2008) (Liu *et al.*, 2016) (Abu-thabit and Makhlouf, 2018) (Langer and Peppas, 1981) (Bhowmi*k et al*., 2012):

1) Inert, biocompatible and mechanically strong.
2) Comfortable for the patient, reliable and cost-effective.
3) Increase drug bioavailability.
4) Capable of achieving the required drug loading.
5) Decrease drug concentration fluctuations in blood between the minimum effective levels (MEC) and maximum toxic levels (MTC) and contribute to more stable plasma/blood drug concentration levels.
6) Be able to achieve controlled drug delivery for a predetermined period of therapy.
7) Be stable after its administration in the human body, while the delivery of the active substance should not be affected unduly by physiological variables.
8) Contribute to high dispersion of the active agent.
9) Be able to be used for various active compounds.
10) Easy administration and removal (if needed) from a patient.
11) Exhibit high safety in case of accidental release.
12) Easy to manufacture and sterilize.
13) Free of leachable impurities.

1.1.2. Conventional Drug Delivery Systems

Tablets, capsules, solutions, elixirs, emulsions, suspensions, cachets, lozenges are included in conventional drug delivery systems and are overwhelmingly used today. Oral drug formulations, where immediate release of the active ingredient and rapid absorption occur, represent more than 50% of the available dosage forms today (Langer and Peppas, 1981) (Deshpande *et al.*, 1996) (Abu-thabit and Makhlouf, 2018). Oral ingestion is largely selected as a mode of administration since it is considered more natural, convenient and safe for the patients. The most important advantages of the oral dosage forms are the following: they are broadly accepted by patients, easy to administer and cost-effective to manufacture and distribute (Deshpande *et al.*, 1996) (Ummadi *et al.*, 2013).

However, these systems exhibit some limitations, often including the need for frequent administration for the desired therapeutic effect. This can lead to reduced patient adherence, while the chances of missing a dose in a treatment scheme increase, especially in populations that have multiple and complex conditions and need to be treated with several active compounds contained in different formulations. This is particularly important in cases where active agents with a short half-life are administered (Modi *et al.*, 2013) (Ummadi *et al.*, 2013) (Robles-Martinez *et al.*, 2019).

Other issues include fluctuations in the *in vivo* drug concentrations outside of the desired therapeutic window, especially for substances with a narrow therapeutic index (Langer and Peppas, 1981) (Vadlapudi *et al.*, 2014) (Ummadi *et al.*, 2013) (Modi *et al.*, 2013) (Bikiaris, Koutris and Karavas, 2007). This makes it more difficult for a steady state condition to be achieved, and can mean more frequent administration is required (Yang and Pierstorff, 2012) (Ummadi *et al.*, 2013) (Langer and Peppas, 1981). Minimum effective levels and/or maximum toxic levels are, hence, commonly observed with the conventional drug formulations (***Figure 1.1***) (Vadlapudi *et al.*, 2014) (Shaik, Korsapati and Panati, 2012) (Langer and Peppas, 1981). An important issue from this is the increased risk of causing unwanted additional side effects to the patients due to the initial high concentrations reached on immediate release (Bikiaris, Koutris and Karavas, 2007) (Langer and Peppas, 1981).

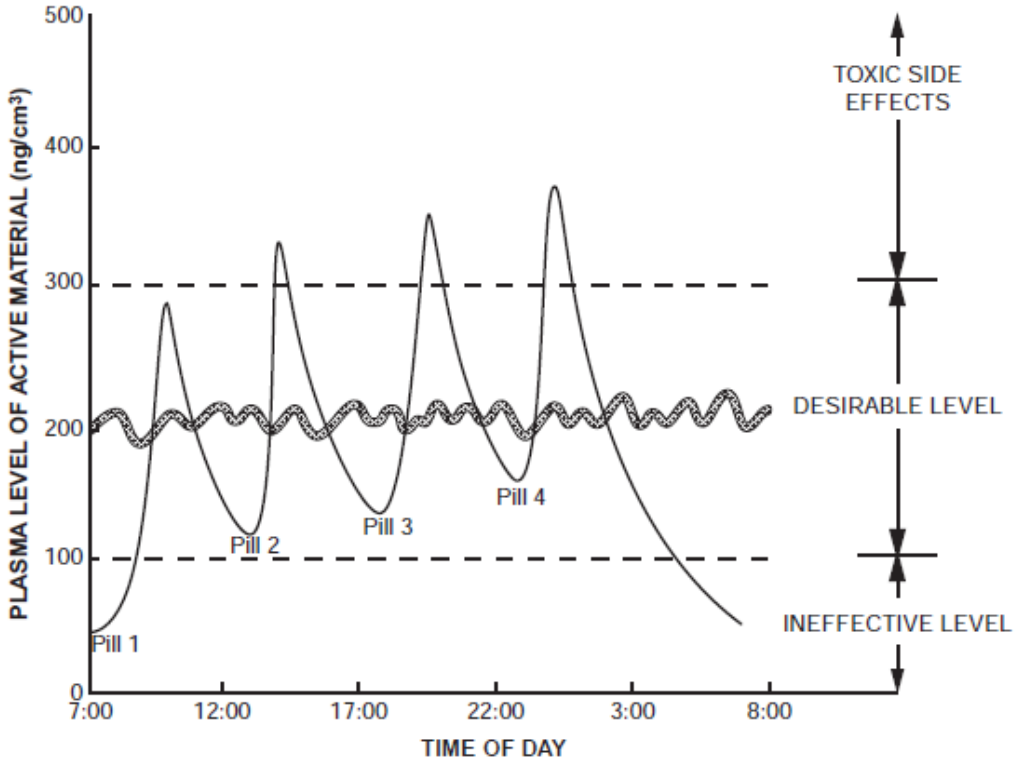

Figure 1.1: *Drug levels in the blood after the administration of conventional drug delivery systems. This figure is reproduced from Vadlapudi et al. (Vadlapudi et al., 2014).*

Another drawback of the traditional drug delivery forms is that apart from cases where a local effect can be achieved (for example in the GI tract) the systemic biodistribution of the active agent in the body after its administration is uncontrolled, potentially leading to the metabolism and degradation of the drug and the reduction of its plasma levels before it reaches its target (Langer and Peppas, 1981) (Liu *et al.*, 2016) (Vadlapudi *et al.*, 2014) (Abu-thabit and Makhlouf, 2018).

Consequently, the administration route, the type of the medication, the pharmacokinetic properties of each active agent, its distinct characteristics, as well as, the various responses of each patient or even the same patient under different conditions cannot efficiently be addressed with the traditional dosage forms (Maiti and Sen, 2017) (Paolino *et al.*, 2006).

To overcome these limitations, the preparation of non-conventional drug delivery systems is an option. Two potential ways to achieve the optimization of patients' treatment and quality of life are either by developing new, better, and safer drugs with a longer half-life and larger therapeutic indices or by effective and safer use of the already existing drugs via concepts and techniques of sustained/controlled and targeted drug delivery systems (Bhowmi*k et al*., 2012). The goal of non-conventional drug delivery systems is, thereby, to improve the efficacy of the active compound and patients compliance by reducing the frequency and the required amount of the active ingredient that needs to be administered; to reduce the chances of missing or erring a dose; to reduce treatment cost; to reduce side effects, especially in the non-diseased areas by enhancing targeted delivery and biocompatibility (Paolino *et al.*, 2006) (Uhric*h et al*., 1999) (Ummad*i et al*., 2013) (Huang and Brazel, 2001) (Yang and Pierstorff, 2012) (Siegel and Rathbone, 2012).

1.2. PERSONALISED DRUG THERAPY

1.2.1. Introduction

A person's wellbeing is impacted upon by their health and thus, the success of medicines and dosage schemes are important (Sandler and Preis, 2016). Nevertheless, patients are generally receiving the same dose of a specific active compound contained in a conventional drug delivery system, such as oral dosage forms, while their clinical conditions and the disease state are not considered at an individual level and therefore, might be less effective than desired (Acosta-Vélez and Wu, 2016). Many parameters affect a person's response to an active ingredient like the health status, such as organ functions, infections and genetic factors; metabolism, such as age, gender and diet; or other physical factors, such as body weight and race (K. Jain, 2008) (Dincer *et al.*, 2017) (Shafiee and Atala, 2016) (Han *et al.*, 2018) (Kotta, Nair and Alsabeelah, 2018) (Beg *et al.*, 2020).

Personalized medicine, also referred to as individualized or individual-based or patient-centric drug therapy, is considered a promising approach to take into consideration these parameters to maximize the treatment effects and benefits to each patient. This concept is closely associated with both genomics and individualisation of the choice and dose of active substances in a safely and

effectively fashion contrasted with the mass-oriented traditional drug delivery systems (Nagpal, 2018) (Sandler and Preis, 2016) (Alomari *et al.*, 2015) (Kotta, Nair and Alsabeelah, 2018) (Haris *et al.*, 2020) (Norman *et al.*, 2017).

Human being diversity makes necessary the development of not only efficacious drug therapies, but also effective and safe drug delivery carriers which will meet the requirements of continuous dosing needs that vary among the patients and the patient groups (Alomari *et al.*, 2015) (Norman *et al.*, 2017) (Konta, García-Piña and Serrano, 2017) (Acosta-Vélez and Wu, 2016). Different aged patients, such as newborns, children, adolescents, adults and older people, can demonstrate a diverse response to the same dosage scheme (Sandler and Preis, 2016). High diversity of indications of traditional drug delivery systems is another commonly observed phenomenon, which results in either less effective treatments or the development of side effects (Konta, García-Piña and Serrano, 2017) (Palo *et al.*, 2017) (Acosta-Vélez and Wu, 2016) (Haris *et al.*, 2020).

The principles of personalised medicines follow the advice of Hippocrates, "to treat the person, not the disease", since the purpose of their fabrication is to suit each patient's needs, characteristics and preferences (Goole and Amighi, 2016) (Alom*ari et al*., 2015) (Sarah J. Trenfield *et al.*, 2018) (Eshkalak *et al.*, 2020) (Zema *et al.*, 2017) (Shende and Agrawal, 2018). The production of a custom-shaped drug delivery system loaded with one or more APIs can significantly improve patients' clinical outcomes, as the frequency of drugs administration and adverse effects can be reduced, and their adherence will, thus, be enhanced (Shafiee and Atala, 2016) (Zema *et al.*, 2017) (Sandler and Preis, 2016) (Peng *et al.*, 2017). As a result, the costs related to the "trial-and-error" approaches in the treatment schemes can considerably be reduced (Acosta-Vélez and Wu, 2016) (Nagpal, 2018) (Shafiee and Atala, 2016).

Individualization of the treatment is a versatile way to achieve more efficient patient outcomes and more appropriate management of an illness as it significantly contributes to a better and faster diagnosis and therapy of disease. Progress in various scientific fields, such as pharmacogenomics, metabolomics and pharmacogenetics, provided more accurate methods of understanding how a specific disease affects each person's body based on its unique molecular and genetic profile. In this way, better tailoring of the treatment scheme can be achieved. Moreover, these areas can contribute to a more precise prediction of which active agents will be safe and effective for each patient and which will not

be, for a maximum therapeutic efficacy to be attained (Nagpal, 2018) (K. K. Jain, 2008) (Sandler and Preis, 2016) (Palo *et al.*, 2017) (Aquino *et al.*, 2018) (Lamichhane, Bashyal, *et al.*, 2019) (Zema *et al.*, 2017).

One of the fundamental concepts of personalised drug therapy is "the right drug for the right patient at the right dose and time". Therefore, after the diagnosis of a disease, a patient-centric therapy can be designed where the active agent, dose, dosage intervals and cure duration will properly be adjusted to each patient's needs, genetic makeup and disease state to improve the quality of each person's treatment and hence, life (***Figure 1.2***) (Aquino *et al.*, 2018) (Dincer *et al.*, 2017) (Beg *et al.*, 2020) (Nagpal, 2018) (Sarah J. Trenfield *et al.*, 2018) (Acosta-Vélez and Wu, 2016) (Jamróz, Szafraniec, *et al.*, 2018).

Currently, dose adjustment with conventional solid dosage forms, such as tablets, is done by splitting them; this can lead, though, to a variation in drug content as the equal subdivision is difficult and can result in the administration of higher or lower than the desired doses (Alomar*i et al*., 2015) (Jamróz, Szafraniec, *et al.*, 2018) (Goole and Amighi, 2016). Tablet splitting by hand, knife, scissors or tablet splitter has been proven to be less effective than expected, while the various characterization parameters of the obtained tablet parts did not meet the Pharmacopoeial requirements (Alomari *et al.*, 2015) (Haris *et al.*, 2020) (Vaz and Kumar, 2021). Moreover, this method affects the coating of the tablets (enteric coating, coating for modified/delayed release, moisture protection film coating) and leads to dose alterations (Sarah J. Trenfield *et al.*, 2018) (Shaikh *et al.*, 2018).

Liquid dosage forms also represent potentially promising candidates for individualization of patients treatment schemes through calculation of the dose based on the volume. Dosing aids, which were provided with the medicines at a reasonable cost, were used for this purpose. However, inaccuracies of several types have occurred, such as errors in drop counting and confusion with the grades in syringes or cups. Various shapes of spoons used for the dose adjustment, also, resulted in inaccurate dosing. Furthermore, the patient's and/or carer's dexterity and cognition were particularly important for the accurate and precise measurement of the dose (Goole and Amighi, 2016) (Haris *et al.*, 2020) (Alomar*i et al*., 2015) (Haris *et al.*, 2020).

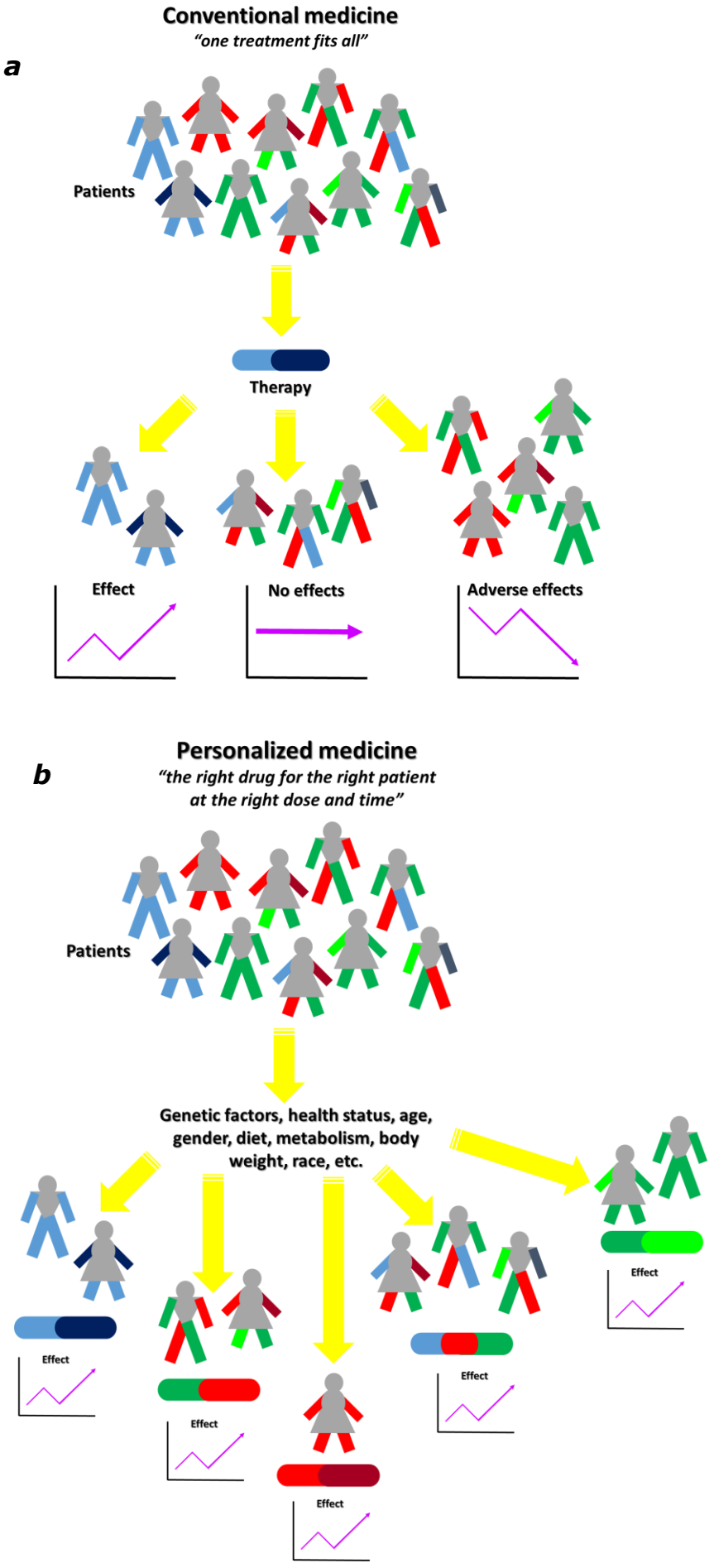

Figure 1.2: *From* ***(a):*** *generalized therapy using conventional drug delivery systems to* ***(b):*** *patient-centric therapy.*

1.2.2. Regulatory Aspects of Personalised Medicine

Personalized Medicine is a particularly promising approach for the more effective treatment of patients according to their health status, lifestyle, characteristics, such as age, gender, body weight, race and metabolism. However, it only recently started attracting more attention, as the need for its application increased. Therefore, legislation defining the manufacturing requirements for the wide use of precision medicines is required; only this year these aspects were covered for the first time by the new regulatory framework issued in the UK (UK Legislation, 2021).

The UK was following the EU legislation – Directive 2001/83/EC of the European Parliament and of the Council of 6 November 2001 on the Community code relating to medicinal products for human use – since it joined the EU and until the end of its transition period of exit from the EU, end of December 2020 (Gov.UK, 2020). At the beginning of 2021, a new regulatory framework has been issued in the UK entitled "Medicines and Medical Devices Act 2021" (UK Legislation, 2021). In this Bill, for the first time the requirements for the manufacture of novel bespoke formulations at the point of care, such as hospitals or clinics, with innovative pharmaceutical processing methods, such as 3D printing, are determined. Guidelines for the combination of more than one active agent in one patient-specific dosage form and quality controls for the fabrication procedures are also included. The patient group to which the administration of personalized formulations will apply is another element that has been addressed (UK Legislation, 2021) (Gov.UK, 2021).

The EU regulatory framework for pharmaceuticals, Directive 2001/83/EC, currently used in the EU does not cover the manufacture and administration of bespoke medicines. However, it is now under review, while in 2022 a new legislation is anticipated to be issued concerning the fabrication procedures and wider use of personalized dosage forms (EU Legislation, 2021) (Wiring, 2020) (Kerrels *et al.*, 2021).

1.2.3. Future Applications

The manufacturing of custom-made dosage forms, apart from considering each patient's genetic profile, phenotypic response and pathophysiology and aiming to include one or several active compounds in the doses that each person needs, will also be of benefit to individuals with intolerances in certain excipients, such as lactose or sucrose (Zema *et al.*, 2017) (Eshkala*k et al*., 2020) (Acosta-Vélez and Wu, 2016).

Possible applications of personalized medicine are with active ingredients with known pharmacokinetic variability or with a high risk of causing side effects, such as toxicity, or with narrow therapeutic windows, where frequent drug administrations are required. Antibiotics, antidepressants, antipsychotics, caffeine, immunosuppressive, antiepileptic agents for chronic treatments and also drugs aimed for the treatment of cardiovascular diseases, such as antiarrhythmic and antihypertensive agents, or diabetes are included in one or more of the above mentioned categories (Goole and Amighi, 2016) (Dince*r et al*., 2017). Moreover, individualized therapy seems very promising for the treatment of complex illnesses, like epilepsy, Alzheimer's disease and cancer (Be*g et al*., 2020).

Personalisation of the treatments is highly needed for the paediatric and geriatric population, as well. Body weight, age, physiological and metabolic functions of the former group rapidly change, while in the latter group, changes in the body fat, renal clearance and pathology of the gastrointestinal tract frequently occur (Sarah J. Trenfield *et al.*, 2018) (Norman *et al.*, 2017) (Jamróz, Szafraniec, *et al.*, 2018) (Sandler and Preis, 2016) (Pal*o et al*., 2017) (Goole and Amighi, 2016).

Polypharmacy is another phenomenon that reduces the efficacy of the currently applied treatment schemes and it is common amongst older people. The majority of this patient group suffer from several diseases which require long term drug administration; over 65 years old patients take on average 13 medicines and as many as 28 at the same period (Vaz and Kumar, 2021) (Han *et al.*, 2018). In the UK, patients over 65 years of age are on average 5 to 8 medications each week, while as the age of the patients increases the number of their prescribed medicines is at least 10 (Rawle *et al.*, 2018) (Petchey *et al.*, 2018) (NHS England, 2020).

The phenomenon of polypharmacy, thereby, makes patients' therapy more complex due to interactions among the administered active substances or the

diseases with the active agents (Zema *et al*., 2017) (Konta, García-Piña and Serrano, 2017) (Alomari *et al.*, 2015). Poor patient adherence and the likelihood of dosing errors are aftereffects of the traditional therapeutic approaches. It is, hence, highlighted how necessary is for a strict dose adjustment to quickly be established for the elimination of potential interactions and the enhancement of the illnesses treatment (Alomar*i et al*., 2015) (Haris *et al.*, 2020) (Vaz and Kumar, 2021). Another patient-centric dosing concept, which seems particularly promising to address polypharmacy issues, is the fabrication of a multi-drug dosage form which will contain all the medications that the patient needs each day or even for a specific period (Norman *et al.*, 2017) (Konta, García-Piña and Serrano, 2017).

1.3. IMPLANTABLE DRUG DELIVERY SYSTEMS

1.3.1. Introduction

Implantable drug delivery systems (IDDSs), also called implantable drug-eluting devices, are single-unit formulations designed to release the loaded active agent usually close to the desired site of action at a therapeutically desired rate for extended periods of time, often months or even years. They represent promising dosage forms for bespoke therapies, while the reasons for that will be discussed below (Kumar and Pillai, 2018) (Shende and Agrawal, 2018) (Major *et al.*, 2020) (Vadl*apudi et al*., 2014) (Danckwerts and Fassihi, 1991) (Santos *et al.*, 2014) (Stewart *et al.*, 2018).

The concept of implants firstly appeared in modern medicine in 1938 when Deansby and Parkes presented a paper in the Royal Society of Medicine in London regarding the effect of compressed pellets of pure crystalline oestrogen in livestock in which the pellets were subcutaneously implanted (Parkes, 1938). These novel formulations displayed that the release of the hormone was continuous for at least three months after the implantation (Dash and Cudworth II, 1999) (Kumar and Pillai, 2018) (Vadlapudi *et al.*, 2014) (Danckwerts and Fassihi, 1991). This work triggered another study performed by P.M.F. Bishop at Guy's Hospital in London later that year. Compressed oestrogen pellets were also used, but this time they were subcutaneously implanted in a young woman for the treatment of premature menopausal symptoms. The results were particularly

encouraging as they exhibited that the hormone replacement was occurring for about five weeks after the initial insertion of these formulations (Vadlapudi *et al.*, 2014) (Kaurav and Kapoor, 2017). The hormonal implantation method was widely used in the 1950s and resulted in the augmentation of the growth and feed efficiency of cattle (Dash and Cudworth II, 1999).

In 1964, Folkman and Long developed implantable drug delivery capsules in which the drug release rate was controlled by a polymeric membrane. Silicone rubber (Silastic) was explored for its potential to achieve long-term drug delivery at a systemic level. Controlled drug delivery was indeed achieved after the insertion of the capsules in the cardiac muscle of dogs, while silicone rubber caused very little inflammatory response (Folkman and Long, 1964). This technology drew considerable interest and was applied in the implantation of pure drug-compressed pellets using various active substances and especially, steroid hormones (Emmens, 1941) (Thom, Collins and Studd, 1981) (Handelsman, Conway and Boylan, 1990) (Kelleher *et al.*, 2004). Further investigation in this field revealed that the implanted hormones were released by two simultaneous mechanisms, erosion and diffusion. The release rate was considerably influenced by the surface area of the formulation, the particle size and the solubility of the active compound in the fluids of the human body (Danckwerts and Fassihi, 1991) (Vadlapudi *et al.*, 2014).

These early studies demonstrated the capability of the implantable drug-eluting formulations to address the limitations of traditional drug delivery systems linked with oral administration, such as drug bioavailability, stability, and toxic drug levels. IDDSs were designed to reduce the frequency of drug administration, extend the timespan of their action, improve patient adherence and eliminate the adverse effects. These characteristics placed them as particularly promising candidates in the field of personalised drug therapy since they can easier be manufactured to meet each patient's needs and phenotypic characteristics (Kumar and Pillai, 2018) (Meng and Hoang, 2012) (Stewart *et al.*, 2018).

The insertion of implant formulations in the human body can be performed in various manners by medical personnel; by using a specific insertion device, such as needles; alternatively with a surgical operation (Stewart *et al.*, 2018) (Danckwerts and Fassihi, 1991) (Kumar and Pillai, 2018) (Majo*r et al*., 2020). Some of these procedures are relatively convenient for patients. After the implantation, only a small bump under the skin can be felt, while the daily

activities of the patient are not particularly affected. Many implants are subcutaneous in an inconspicuous region. They are, thus, nearly invisible as there is no opening in the skin. These facts also improve the patients psychology as they feel less anxious for their treatment scheme (Ranade, 1990) (Paolino *et al.*, 2006).

Implantable systems can be applied for systemic or local drug delivery. For the former, these drug delivery devices are usually administered subcutaneously, intramuscularly or intravenously, where the loaded active compound is released from the IDDS and subsequently, absorbed into the blood circulation. High fat content in subcutaneous or intramuscular tissues makes them ideal regions for the implantation of these systems since slow drug absorption is feasible, the pain felt by the patients is minimal, the hemoperfusion in these areas is good and the likelihood of an inflammation to occur is very low. When foreign to the body materials are inserted through these tissues, they very rarely lead to a reaction and subsequently, to unwanted side effects. Besides these locations, others have already successfully been used for the insertion of implants, especially for the delivery of an active substance to the local tissue, such as intravaginal, intravascular, intraocular, intrathecal, intracranial and peritoneal (Kumar and Pillai, 2018).

When a local therapeutic effect is the goal, the implantation of these systems is performed in the relevant body region, where the active agent is required; intravaginal, intravesicular, intratumoral, intraocular. An insignificant amount of the released drug is absorbed into the systemic circulation (Kumar and Pillai, 2018) (Stewart *et al.*, 2018). In this way, the therapeutic efficacy of the loaded active agent is considerably enhanced, while the systemic toxicity is greatly decreased (Dash and Cudworth II, 1999) (Huang *et al*., 2007).

An ideal implantable drug delivery system should have the following attributes (Kumar and Pillai, 2018) (Vadlapudi *et al.*, 2014) (Dash and Cudworth II, 1999) (Santos *et al.*, 2014) (Kaurav and Kapoor, 2017):

1) Be biocompatible with the human body and the human environment, safe, chemically inert, non-carcinogenic, nonimmunogenic and hypoallergenic. It should not cause any inflammatory response in the implantation region. The biomaterials used for their fabrication and the breakdown products should not provoke any thrombogenicity.

2) Not modify the pharmacological activity of the incorporated active agent.
3) Decrease the requirement for frequent drug administration over the treatment duration and enhance at the same time patient adherence.
4) Be mechanically stable; no physical (no loss of their shape) or chemical modification should be triggered by the tissue in the implantation area.
5) Be sterile – easy to be sterilized.
6) Easy to be implanted or removed, if necessary, by healthcare staff for the treatment to begin or discontinue.
7) Enable the release of the active agent to be performed in a controlled manner at an optimal dose and the desired site of action.
8) Easy to manufacture.
9) Suitable for direct administration.
10) Be cost-effective for the prescribed treatment duration: patients with chronic illnesses will not need to be continuously monitored by medical personnel or spend extended periods in hospitals.
11) Enhance the stability and the protection of the incorporated active ingredient from the body until it is the right time to be released.

Nowadays, the most common implantable formulations, are biodegradable and can release macromolecular and micromolecular active agents (Danckwerts and Fassihi, 1991). Sustained release has been attained and can last from a few hours up to 5 years, while no frequent patients monitoring is necessary compared to the conventional drug formulations (Danckwerts and Fassihi, 1991) (Dash and Cudworth II, 1999). Small mechanical implants have also been developed in which their release rate is triggered by external stimuli, such as temperature, light, electrical stimulation, magnetic field; impulse doses have been activated and a zero-order release has been achieved (Yasin *et al.*, 2014) (Prodanov and Delbeke, 2016) (Wang *et al.*, 2019) (Bijukumar *et al.*, 2016) (Lee *et al.*, 2019).

Another advantage of implantable systems is that they can be loaded with active substances that cannot be administered through traditionally used modes of administration (Dash and Cudworth II, 1999) (Danckwerts and Fassihi, 1991) (Kompbella, Kadam and Lee, 2011) (Vadlapudi *et al.*, 2014) (Ranade, 1990) (Paolin*o et al*., 2006). Furthermore, active ingredients loaded in the IDDSs are protected against rapid metabolism or degradation; the incorporated drug will not go through the gastrointestinal and hepatobiliary systems before it reaches its target and therefore, no rapid degradation will occur. First-pass hepatic effects, which also lead to the rapid degradation of the drug, will be avoided.

Macromolecules, such as peptides and proteins, with short *in vivo* half-life, low permeability and/or high susceptibility to enzymatic degradation are, as well, more efficiently protected when incorporated in implantable formulations (Paolino *et al.*, 2006) (Zaki Aj. *et al.*, 2012) (Kumar and Pillai, 2018) (Vadlapudi *et al.*, 2014) (Dash and Cudworth II, 1999) (Danckwerts and Fassihi, 1991).

An additional benefit to the patients is that the implantation of drug delivery devices in their body represents a more appropriate and less painful alternative for the intravenous administration of active compounds, such as insulin, chemotherapeutics, antibiotics, analgesics, contraceptives, heparin steroids, which need to be administered long term (Kumar and Pillai, 2018) (Paolino *et al.*, 2006) (Dash and Cudworth II, 1999) (Danckwerts and Fassihi, 1991) (Ranade, 1990) (Meng and Hoang, 2012) (Yang and Pierstorff, 2012).

Implantable formulations offer, also, the flexibility of selecting the materials that will be used for their manufacturing, their fabrication method, the amount of the active agent that will be loaded - a significant amount of drug can be loaded in these systems to fit the needs of the patients and the duration of the treatment. The rate with which the incorporated active compound will be released can more effectively be regulated in these systems (Vadlapudi *et al.*, 2014) (Zaki Aj. *et al.*, 2012). Drug release kinetics of the loaded active ingredient usually follows the principles of the zero-order release, enhancing, thus, more controlled levels of the active substance to be obtained at the target area of action (Vadlapud*i et al*., 2014) (Meng and Hoang, 2012) (Kaurav and Kapoor, 2017).

An important advantage of the implantable drug-eluting systems is the fact that they can contain several compartments which can be loaded with various active substances either in a liquid or solid form. The drug release can occur independently in each reservoir in a controlled fashion; continuous or pulsatile release can be achieved. This implants attribute is particularly essential for certain treatment schemes since the release profile is not influenced by factors such as the reservoir geometry, the incorporated active compound or the release mechanism (Kumar and Pillai, 2018).

However, implantable drug-eluting devices present some disadvantages which might affect the patient acceptability and compliance. As already mentioned, minor or major surgery is sometimes required for their placement into the human body and potentially their removal. Allied healthcare personnel are performing the

implantation instead of surgeons and therefore, proper training is required to be given. Moreover, this procedure is time-consuming for both the patients and the medical staff, while it can be traumatic to the patients. In some cases, a scar can be formed at the placement site or surgery-related complications can occur (Kumar and Pillai, 2018) (Zaki Aj. *et al.*, 2012) (Vadlapudi *et al.*, 2014) (Danckwerts and Fassihi, 1991) (Yang and Pierstorff, 2012).

The removal of the implants can be avoided if biodegradable materials are selected for their manufacture. The breakdown products of these materials, though, can be harmful in some cases. Furthermore, depending on the size of the fabricated formulations, the surgical operation can be replaced by another implantation method, less invasive. The smaller the size the less the discomfort caused to the patient and the better his compliance is. However, in these formulations, the size is a factor that considerably affects their drug loading capacity (Kumar and Pillai, 2018) (Vadlapudi *et al.*, 2014) (Danckwerts and Fassihi, 1991) (Zaki Aj. *et al.*, 2012).

Another limitation of these systems is the fact that their design and production is quite time-consuming and expensive, especially compared with the widely used and much simpler oral dosage formulations. Consequently, that makes necessary the development of novel technologies which will contribute to the decrease of their fabrication cost (Zaki Aj. *et al.*, 2012) (Kumar and Pillai, 2018) (Vadlapud*i et al*., 2014).

1.3.2. Design approach

Implantable devices can be manufactured in various shapes, such as rods, films, plugs, pellets and discs, while their size is at the millimetre or centimetre scale (Kumar and Pillai, 2018) (Yasukawa *et al.*, 2006) (Yang and Pierstorff, 2012). Even though the most commonly chosen design is the rod, implants with more complex architecture can be fabricated to achieve more complex and personalised release profiles (Stewart *et al.*, 2018).

A large number of the produced implantable formulations belong to the category of reservoir-based drug delivery systems where the active agent is incorporated in a polymer matrix or is surrounded by a polymeric film. Many factors impact the

release of the active and they should be considered during the design of the IDDSs; implant shape, thickness of the polymeric membrane, properties of the polymer, such as the polymer composition and molecular weight, the physicochemical properties of the loaded active substance, such as its molecular weight, side effects, solubility and particle size, the targeted release area, as well as, the disease (Yang and Pierstorff, 2012) (Kumar and Pillai, 2018) (Langer, 1990). The majority of the reservoir type implantable devices are manufactured in a cylindrical shape (Paolino *et al.*, 2006).

In the case of biodegradable implants which are in the main interest of the current study, the rate of degradation of the polymeric matrix is one of the most essential factors that is considered during the design process. The degradation rate of the polymer controls the release of the active agent from the matrix and is influenced by several factors, such as variations in pH or temperature (Liechty *et al.*, 2010) (Kumar and Pillai, 2018) (Langer and Peppas, 1981). Implant surface area is another important factor that has an essential impact on matrix degradation. When the degradation is occurring throughout the device's volume and not only on its surface, the overall ratio of the surface area to volume is increasing (Liechty *et al*., 2010) (Uhrich *et al.*, 1999). The latter has as a result the enhancement of the degradation rate since the original monolithic system degrades into smaller parts. If surface erosion is the only degradation mechanism, then the total surface area exposed to erosion will progressively be reduced. Consequently, the degradation of the polymer will become slower. This demonstrates, therefore, that during the design process of the IDDSs, the shape and the general form that they will have after the first stages of their *in vivo* degradation should be taken into consideration (Kumar and Pillai, 2018) (Liechty *et al.*, 2010) (Uhrich *et al.*, 1999).

Geometry can be used to achieve a uniform and constant release. For example, a flattened slab-like shape is selected to attain a zero-order release kinetics profile, as these do not have any significant edges available for erosion (Langer and Peppas, 1981) (Vadlapudi *et al.*, 2014) (Zaki Aj. *et al.*, 2012). Implantable formulations with more complex architectures, such as an inert, biodegradable core, are coated with a blend of the active ingredient within a polymer matrix to eliminate any surface alterations during erosion (Vadlapudi *et al.*, 2014) (Kumar and Pillai, 2018) (Zaki Aj. *et al.*, 2012) (Langer and Peppas, 1981).

1.3.3. Mechanisms of drug release from implantable drug delivery systems

Drug release mechanisms are categorised into five main groups: matrix degradation, controlled swelling, osmotic pumping, passive diffusion and externally stimulated. A combination of usually two mechanisms leads to the release of the active ingredient from implantable devices (Stewart *et al.*, 2018) (Kumar and Pillai, 2018) (Langer, 1990).

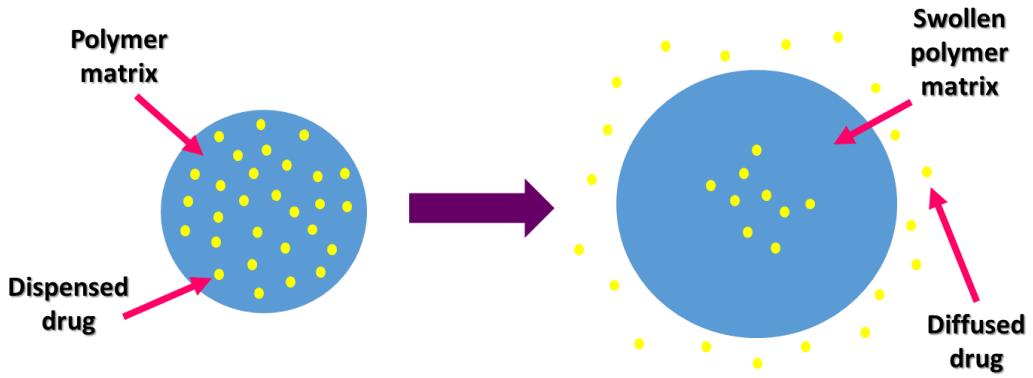

Figure 1.3: *Schematic representation of a swelling controlled implantable drug eluting system.*

When the driving force for the release of the incorporated active substance is controlled swelling, the penetration rate of the external solvent into the implant matrix regulates the rate of the release. More specifically, the insertion of the biological fluid into the implant matrix at a controlled rate leads to the swelling of the formulation and the release of the enclosed active compound from that compartment (***Figure 1.3***) (Danckwerts and Fassihi, 1991) (Kumar and Pillai, 2018) (Uhrich *et al.*, 1999). In most systems, this process is considerably slower than the passive diffusion of the active agent and results in a far lower release rate (Danckwerts and Fassihi, 1991) (Stewart *et al.*, 2018) (Langer and Peppas, 1981). Even though diffusion is the main drug release mechanism when the matrix is swelling, matrix degradation can be another method through which the delivery of the loaded active substance can be performed in the desired site of action (Langer, 1990) (Stewart *et al.*, 2018) (Langer and Peppas, 1981).

Mechanisms for the attainment of a linear release of active agents from implants are osmotic pumping and passive diffusion. In this way, the amount of an active compound that is released is directly proportional to the square root of the release time and thereby, a linear relationship is obtained after fitting of the drug release data versus the square root of time (Stewart *et al*., 2018) (Kumar and Pillai, 2018) (Ranade and Hollinger, 2015).

Osmosis is the phenomenon in which the water is moving from a solution with a low concentration to a solution with a higher concentration through a partially permeable membrane. Hydrostatic pressure is, then, developed between these areas due to the water transfer. Osmotic pumping is based on this process for the control of the release rate of the active ingredient in designated conditions. The water which is absorbed by the implantable system has as a result, the creation of osmotic pressure that subsequently leads to the constant release of the active compound (Siegel and Rathbone, 2012) (Uhrich *et al.*, 1999) (Kumar and Pillai, 2018) (Stewart *et al.*, 2018) (Langer, 1990).

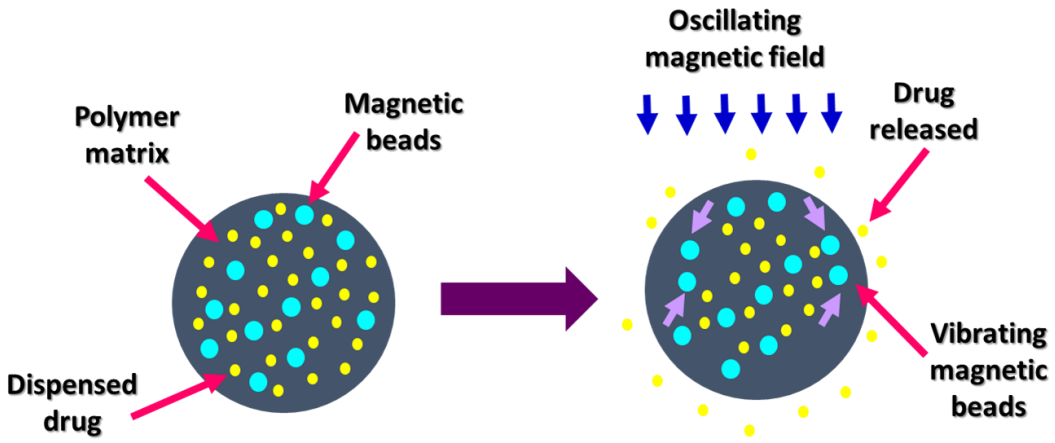

Figure 1.4: *Schematic representation of a magnetically controlled implantable drug eluting system.*

Externally activated drug release can achieve very specific release profiles, for example using magnetic fields. In such formulations, not only the active agent but also magnetic beads are homogeneously dispersed within a, usually polymeric, matrix (Langer and Peppas, 1981) (Danckwerts and Fassihi, 1991) (Yasin *et al.*,

2014). When this system is exposed to an aqueous medium, the enclosed active substance is normally released through diffusion due to a concentration gradient. However, in this case with the application of an oscillating external magnetic field, the drug release rate can be increased (***Figure 1.4***) (Danckwerts and Fassihi, 1991) (Langer and Peppas, 1981) (Uhrich *et al.*, 1999) (Dash and Cudworth II, 1999) (Langer, 1990) (Paolino *et al.*, 2006). The main advantage of this mechanism is the capability of better adjustment of the drug release kinetics with an external stimulus (Dash and Cudworth II, 1999).

When the release mechanism of an active compound from an implantable formulation is controlled by matrix swelling, osmotic pressure or passive diffusion, various properties of the material used for the implants fabrication or the incorporated active agent have a significant impact on the drug release kinetics; the solubility and diffusion coefficient of the active ingredient in the matrix; the amount of the loaded drug in the device; the *in vivo* degradation rate of the material of which the matrix consists (Stewar*t et al*., 2018) (Kumar and Pillai, 2018).

1.3.4. Classification of implantable drug delivery systems

The classification of the implantable formulations is not straightforward since some of these systems are hybrid and belong in more than one group. Nonetheless, they can be divided into two main categories, passive and active implantable devices. Formulations included in the first group are further classified into two categories, biodegradable and non-biodegradable implants, usually polymeric (Stewar*t et al*., 2018) (Paolino *et al.*, 2006). In contrast, in active implants, the release of the incorporated active agent is achieved by methods relying on energy, such as electromechanical systems and systems controlled by osmotic pressure gradients. The most frequently used materials for this category are metals (Stewart *et al.*, 2018) (Kumar and Pillai, 2018).

1.3.4.1. Active Implantable Drug Delivery Systems

In the dynamic or active IDDSs, a positive driving force controls the release of the active substance and thereby, can be regulated in these systems more precisely than in passive implants (Stewart *et al.*, 2018) (Kumar and Pillai, 2018) (Dash and Cudworth II, 1999). Their disadvantages, though, are associated with their structural complexity and high cost of manufacture. Mainly electronic systems belong in this category, while the materials used for their fabrication are predominantly metals, even though polymers are also selected in some cases (Kumar and Pillai, 2018) (Stewar*t et al*., 2018). Further classification of active implants divides them into more categories, which will be discussed in the following sections.

1.3.4.1.1. Implantable pump systems

External control of drug administration is required for several active agents. Even though this is hard to be achieved when biodegradable or nonbiodegradable formulations are used, pump systems offer this feature. The release of the active agent from implantable pumps can be controlled in several ways, such as osmosis, propellant-driven fluids or gasses, piezoelectric disc benders, oscillating pistons or electromechanical drives for the generation of pressure gradients (Kumar and Pillai, 2018) (Ranade, 1990) (Dash and Cudworth II, 1999) (Vadlapudi *et al.*, 2014) (Santos *et al.*, 2014) (Langer, 1990).

In ***Table 1.1***, the osmotic pump types are presented, as well as, their structural characteristics and the delivery mechanism of the enclosed active substance.

Constant drug release and thus, zero order release kinetics are achieved with osmotic pumps that are maintained until the incorporated active compound is completely released. No initial burst effect has been observed in previous studies with these pumps (Dash and Cudworth II, 1999) (Stewart *et al.*, 2018). Even though this release rate is the preferred one, the drug loading capacity in this implant type is particularly low (Stewar*t et al*., 2018) (Kumar and Pillai, 2018) (Vadlapud*i et al*., 2014) (Dash and Cudworth II, 1999). Moreover, the release rate of the active ingredient cannot easily be regulated as the semipermeable membrane is responsible for that. Consequently, this device needs to completely

be removed from the implantation site for the structure of the membrane to be altered (Dash and Cudworth II, 1999) (Vadlapudi *et al.*, 2014).

In the case of the mini-osmotic pumps, even though constant administration of the incorporated active substance is attained, the drug release rate can easily be regulated based on the patient's treatment scheme. The delivery of the active agent might be performed in various timespans by attaching to the pump a catheter displacement tube including a preadjusted schedule of intervals for drug release. An inert liquid is contained in the pump, while the displacement catheter might be shaped into a tight coil around the pump after the application of temperature. In this manner, a compact device is created and it can subsequently be inserted into the human body (Ranade, 1990) (Santos *et al.*, 2014) (Langer, 1990).

Table 1.1: *Types of osmotic implantable pump systems with their structural characteristics and mechanism of drug release.*

Implantable pump type	Structural characteristics	Mechanism of drug release	References
Osmotic pump	▪ capsular shape ▪ drug reservoir enclosed by a semipermeable, usually, polymeric membrane, which allows the constant movement of the external medium through that, but not of the active ingredient ▪ diameter of orifice (drug portal) in the membrane controls the drug release rate	Osmotic action or direct mechanical movement generate hydrostatic pressure in the drug reservoir and that leads to the release of the active compound through the drug portal in the membrane.	*(Stewart et al., 2018) (Langer, 1983) (Ranade and Hollinger, 2015) (Theeuwes and Yum, 1976)*
Miniature osmotic pump	▪ capsular shape ▪ catheter connected to the membrane orifice	Delivery of the active substance to a region further away from the implantation location is achieved through the catheter.	*(Santos et al., 2014) (Paolino et al., 2006) (Langer, 1990)*

To address the drug loading limitation of the osmotic implantable drug eluting systems, propellant infusion pumps are an alternative option (***Table 1.2***). The main advantage of this method is that no external power source is required to activate the pump (Vadlapud*i et al*., 2014) (Danckwerts and Fassihi, 1991) (Dash and Cudworth II, 1999).

Table 1.2: *Propellant infusion pump systems with their structural characteristics and mechanism of drug release.*

Implantable pump type	Structural characteristics	Mechanism of drug release	References
Propellant infusion pumps	Pump comprises a disc-shaped canister containing collapsible welded bellows.	Propellant gas (such as fluorocarbon) is used instead of an osmotic agent for the production of constant positive pressure for zero order release to be obtained. At body temperature, vapour pressure above atmospheric pressure is generated by the propellant gas and causes the release of the active compound from the compartment in which is incorporated. The drug passes through a filter and a flow regulator which enables the attainment of constant infusion of the active substance at a specific temperature.	*(Meng and Hoang, 2012) (Vadlapudi et al., 2014) (Danckwerts and Fassihi, 1991)*

Even though osmotic and propellant infusion pumps can successfully be used when small amounts of active substances are needed for patient therapy, they demonstrate limited capability of application for the treatment of specific chronic conditions where a daily infusion of the active agent is needed for extended periods of time. Larger implants are needed for this purpose where the incorporated active compound can be replenished when it reaches a low level while the device remains implanted in the body (Kumar and Pillai, 2018).

Table 1.3: *Controlled release micropumps with their structural characteristics and mechanism of drug release.*

Implantable pump type	Structural characteristics	Mechanism of drug release	References
Controlled release micropumps	Foam disc is compressed by the coated, mild steel piston without the presence of any valves. The piston is the core of a cylinder and the compression is triggered by the application of current to the cylindrical coil.	Basal delivery is attained through diffusion across a rate-controlling membrane, whilst a quickly oscillating piston is acting on a compressible foam disc to enhance the release of the active ingredient.	*(Dash and Cudworth II, 1999)* *(Ranade, 1990)*

Controlled release micropumps are another category of implantable devices, where no external power source is needed for the activation of the release of the enclosed active substance (***Table 1.3***) (Ranade, 1990) (Vadlapudi *et al.*, 2014) (Danckwerts and Fassihi, 1991).

Electrically powered mechanical pumps are also used and include moving parts and advanced control systems (Kumar and Pillai, 2018). In this manner, the pump rate, the flow rate and the dose of the active agent can be regulated in contrast with the pump type devices (Danckwerts and Fassihi, 1991) (Meng and Hoang, 2012). Larger implants can be applied in these cases that can be refilled with the active substance when their drug loading is running low, while the pumps will remain implanted in the human body (Kumar and Pillai, 2018) (Langer, 1990).

Peristaltic pumps represent a characteristic example since their operation relies on a battery and electronics (Khan and Gillespie, 2013) (Dash and Cudworth II, 1999) (Danckwerts and Fassihi, 1991). These devices demonstrate several advantages; they can be used for long periods of time, even for many years, depending on the life span of the battery; an external remote system can be used to adjust the release rate of the active substance; they are considered safe implantable devices since the drug administration can be stopped anytime as it is controlled by an external remote control system. The main disadvantage of the peristaltic pumps is the high cost required for their manufacture and this makes their applications more limited and rare (Vadlapud*i et al*., 2014) (Dash and

Cudworth II, 1999). Another disadvantage of the peristaltic pumps and in general, of mechanical pumps is that a mechanical or electrical failure can lead to the release of the incorporated active ingredient at a higher rate than the pre-regulated one. Consequently, this will influence the performance of this device and the patients' acceptability regarding its safety (Ranade, 1990) (Khan and Gillespie, 2013).

Positive displacement pumps belong, as well, in the group of electrically powered mechanical pumps since the release of the enclosed active compound is achieved upon the application of voltage (***Table 1.4***) (Danckwerts and Fassihi, 1991) (Dash and Cudworth II, 1999) (Meng and Hoang, 2012) (Ranade, 1990). A major disadvantage of electrically powered mechanical pumps is that their sterilization is challenging. This process is essential to secure patient safety as microorganisms inside this device can result in unexpected side effects, such as inflammation or allergic reactions. The sterilization of the external parts of the pump is not sufficient to prevent this (Ranade, 1990).

Table 1.4: *Positive displacement pump systems with their structural characteristics and mechanism of drug release.*

Implantable pump type	Structural characteristics	Mechanism of drug release	References
Positive displacement pumps	comprise delicate discs, made of flexible piezoelectric material that form a bellows	The application of voltage leads to the bending of the piezoelectric discs and the release of the active substance from the reservoir. The release rate can be regulated through the application of electrical pulses.	*(Meng and Hoang, 2012) (Danckwerts and Fassihi, 1991)*

1.3.4.2. Passive Implantable Drug Delivery Systems

Passive implantable drug delivery devices are generally simple systems and they do not include any moving parts, unlike the active implantable devices. The release of the incorporated active substance mainly relies on passive diffusion. Biocompatible polymers are the chosen materials for the manufacture of the

passive implantable systems contrasted with metals that are usually selected for the fabrication of the active IDDSs. The release profile in the former systems can be controlled by proper adjustment of various parameters, such as the type of the active compound, its amount loaded in the implants, the type of the used polymer, the design attributes of the device, as well as, its surface properties. Passive implantable drug delivery systems are further divided into two groups depending on the biodegradability of the selected polymer; non-biodegradable and biodegradable systems (Stewart *et al.*, 2018) (Kompbella, Kadam and Lee, 2011) (Kumar and Pillai, 2018) (Paolino *et al.*, 2006) (Yang and Pierstorff, 2012) (Yasukawa *et al.*, 2006).

1.3.4.2.1. Non-biodegradable Polymeric Implantable Systems

Non-biodegradable implantable devices consist of non-biodegradable, inert and biocompatible polymers, while the release of the incorporated active agents occurs through swelling or diffusion. Swelling controlled formulations are fabricated by water-soluble, cross-linked polymers (Dash and Cudworth II, 1999) (Stewart *et al.*, 2018) (Santos *et al.*, 2014) (Yang and Pierstorff, 2012) (Langer, 1990). These systems are designed to avoid any initial burst release of the active agent after the implantation of these devices, while the release rate of the active substance can be controlled by proper adjustment of the polymeric membrane thickness and permeability, the polymeric surface area and the solubility of the enclosed active substance (Wang *et al.*, 2013) (Yang and Pierstorff, 2012) (Christoforidis *et al.*, 2012).

There are two types of diffusion-controlled implants: reservoir and matrix (***Figure 1.5***) (Vadlapudi *et al.*, 2014) (Langer, 1990) (Wang *et al.*, 2013) (Kumar and Pillai, 2018) (Dash and Cudworth II, 1999) (Santos *et al.*, 2014). The former type comprises a polymeric matrix containing a homogeneously dispersed active compound. The latter type is made of a compact drug core surrounded by a permeable non-biodegradable polymeric membrane. Both types demonstrate a resilient and robust structure over their life span and they can be used for long-term therapeutic applications (Santos *et al.*, 2014) (Stewar*t et al*., 2018) (Dash and Cudworth II, 1999) (Ranade, 1990).

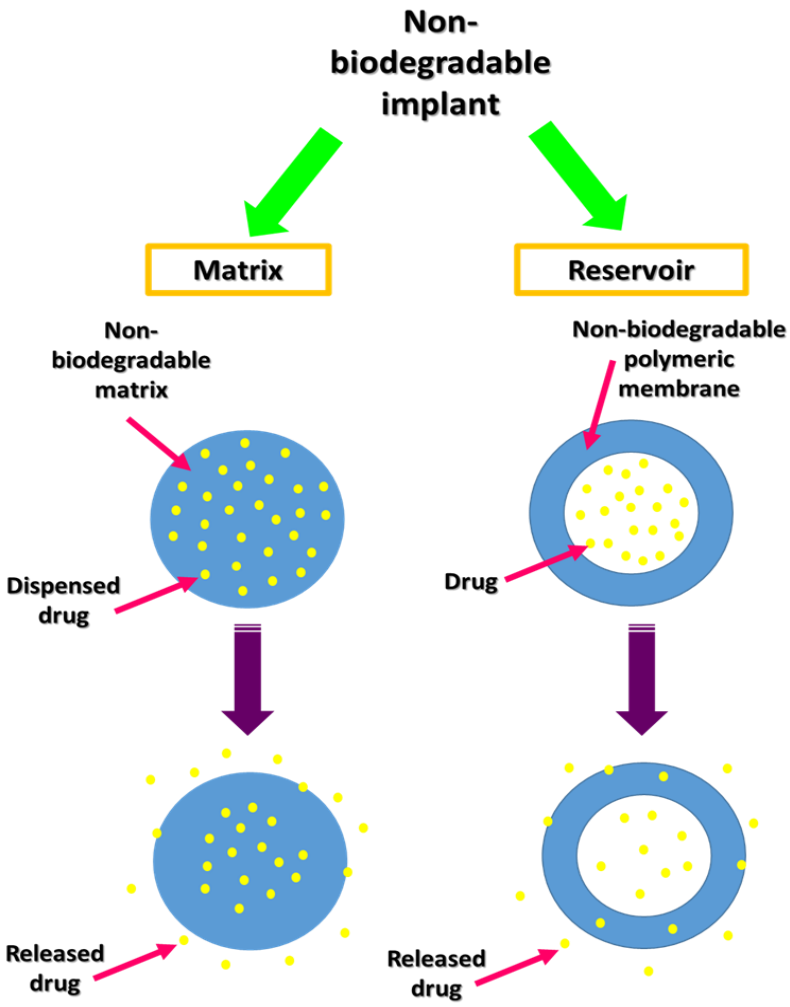

Figure 1.5: *Schematic illustration of reservoir and matrix types of non-biodegradable implantable systems.*

More specifically, in the reservoir systems the polymeric membrane, which encloses the drug core, acts as a diffusional barrier to the drug flow efficiency (***Figure 1.5***) (Dash and Cudworth II, 1999) (Langer and Peppas, 1981) (Kumar and Pillai, 2018) (Paolino *et al.*, 2006). A constant release rate and hence, zero-order release kinetics can be maintained in these devices since the release rate is not affected by a concentration gradient, but predominantly by the thickness of the membrane and the permeability of the active ingredient through the membrane (Vadlapud*i et al.*, 2014) (Kumar and Pillai, 2018) (Danckwerts and Fassihi, 1991) (Yang and Pierstorff, 2012) (Yasukawa *et al.*, 2006).

The main advantages of this non-biodegradable implant type are its simplicity, long lifetime and the capability of attaining steady-state pharmacokinetics (Langer, 1990) (Dash and Cudworth II, 1999). Nevertheless, a reservoir device where the constant release of the enclosed compound needs to occur is hard to be manufactured due to the poor diffusion of the active substances through the polymeric membrane (Vadlapudi *et al.*, 2014) (Langer and Peppas, 1981). These systems exhibit more disadvantages; similarly, to all the types of non-biodegradable systems, necessary removal after the completion of the therapy. Furthermore, "drug dumping" is possible with these implants in case of breakage of the polymeric membrane (Danckwerts and Fassihi, 1991) (Langer, 1990) (Vadlapudi *et al.*, 2014) (Dash and Cudworth II, 1999) (Langer and Peppas, 1981).

In matrix systems, also termed monolithic systems, the implant consists of a polymer with an active agent homogeneously dispersed or dissolved in it; the medium basically regulates the release rate of the active compound (***Figure 1.5***) (Vadlapudi *et al.*, 2014) (Dash and Cudworth II, 1999) (Yasukawa *et al.*, 2006) (Langer and Peppas, 1981) (Kumar and Pillai, 2018) (Danckwerts and Fassihi, 1991) (Paolino *et al.*, 2006). In this implant type, the driving force for the release of the active substance is Fickian diffusion through the non-biodegradable fibrous polymeric network and is influenced by several factors, such as the length of the diffusion, the swelling degree and the concentration gradient (***Figure 1.5***) (Vadlapudi *et al.*, 2014) (Langer and Peppas, 1981) (Stewart *et al.*, 2018) (Paolino *et al.*, 2006) (Dash and Cudworth II, 1999).

If an active agent is encapsulated in a matrix where it demonstrates low solubility, its release mainly occurs through a solution diffusion mechanism. The release of active ingredients insoluble in the matrix is governed by leaching through intergranular gaps in the polymeric matrix (Danckwerts and Fassihi, 1991) (Paolino *et al.*, 2006) (Vadlapudi *et al.*, 2014).

The amount of the remaining active agent in the matrix plays a significant role in the release kinetics; the release of the active substance is directly proportional to the concentration of the incorporated drug in the polymeric matrix. Drug release rate and diffusion decrease continuously with time as the concentration of the active agent in the matrix decreases. At the same time, though, the surface area of the matrix exposed to biological fluids increases and in this way, the length of

the diffusion path is compensated (Danckwerts and Fassihi, 1991) (Kumar and Pillai, 2018) (Dash and Cudworth II, 1999) (Stewart *et al.*, 2018).

The degree of matrix swelling is another factor that influences solute movement. Slow diffusion of the active compound through tortuous interconnecting pores of the polymer can enable sustained drug release (Paolino *et al.*, 2006) (Stewar*t et al*., 2018) (Danckwerts and Fassihi, 1991) (Vadlapudi *et al.*, 2014) (Kumar and Pillai, 2018) (Dash and Cudworth II, 1999). Contrasted with the reservoir type systems, the fabrication cost for the matrices is low, while drug leakage is less likely to happen. The major disadvantage of these devices, similar to the reservoir systems, is their necessary minor surgical implantation and removal that affect patient adherence and acceptance (Danckwerts and Fassihi, 1991) (Vadlapudi *et al.*, 2014) (Dash and Cudworth II, 1999) (Stewart *et al.*, 2018) (Langer and Peppas, 1981).

Even though the used polymers demonstrate long-term biocompatibility, they might cause infections, damage in tissues or cosmetic deformation (Stewar*t et al*., 2018). These possible adverse effects combined with the fact that these materials do not degrade over time, but instead, are accumulating in the human body, make necessary their removal after the completion of the treatment and the release of the loaded active substance (Stewart *et al.*, 2018) (Ranade, 1990) (Kumar and Pillai, 2018).

Polymers usually selected for the fabrication of non-biodegradable implants are silicones, polyurethanes (PU), polysulfones, polyacrylates or copolymers, such as polyethylene vinyl acetate (PEVA), poly vinyl alcohol (PVA), polymethylmethacrylate and vinylidenefluoride (Santos *et al.*, 2014) (Langer and Peppas, 1981) (Kaurav and Kapoor, 2017) (Major *et al.*, 2020) (Christoforidis *et al.*, 2012) (Langer, 1993) (Yasukaw*a et al*., 2006) (Paolino *et al.*, 2006) (Uhrich *et al.*, 1999) (Yang and Pierstorff, 2012).

1.3.4.2.2. Biodegradable Polymeric Implantable Systems

Biodegradable implantable devices were developed to address the limitations of non-biodegradable systems for the generation of more patient-friendly formulations. The release of the active compound from the biodegradable implants is regulated by polymer degradation (Santos *et al.*, 2014) (Dash and Cudworth II, 1999) (Yang and Pierstorff, 2012). The inert polymers or block copolymers used for their manufacture can be broken down into smaller fragments which will, then, easily be excreted or absorbed by the human body after their purpose is fulfilled (Santos *et al.*, 2014) (Yasukawa *et al.*, 2006) (Stewart *et al.*, 2018) (Vadlapudi *et al.*, 2014) (Dash and Cudworth II, 1999) (Kumar and Pillai, 2018). These are occurring through phagocytosis of the small particles by macrophages and/or chemical dissolution. The surgical explantation of the biodegradable implants, after their therapeutic purpose is achieved, is, thus, not necessary and this is their essential advantage (Langer and Peppas, 1981) (Stewart *et al.*, 2018) (Santos *et al.*, 2014) (Danckwerts and Fassihi, 1991) (Major *et al.*, 2020) (Yasukawa *et al.*, 2006). This results in the enhancement of patients acceptance and compliance, as well as, in the decrease of potential complications associated with their removal, as previously mentioned (Danckwerts and Fassihi, 1991) (Kumar and Pillai, 2018) (Vadlapudi *et al.*, 2014) (Dash and Cudworth II, 1999).

The degradation rate of biodegradable formulations is a function of their shape, size, contact with the body fluids, the implantation site, temperature, motion, the molecular weight and the crystallinity of the materials that they consist of, but also, the amount of the incorporated active agent; the higher the loading of the active compound, the faster its release (Major *et al.*, 2020) (Kumar and Pillai, 2018). For a stable drug release profile to be attained throughout their application, a constant degradation rate of the formulation is required (Major *et al.*, 2020) (Dash and Cudworth II, 1999). Their drawback, though, is that their fabrication methods are more complex than in the case of non-biodegradable devices and their production is expensive (Kumar and Pillai, 2018) (Liechty *et al.*, 2010) (Langer and Peppas, 1981). An initial burst release is usually observed after their implantation, which can be a major disadvantage of these systems when constant drug release kinetics is needed for the whole duration of the treatment scheme (Yang and Pierstorff, 2012). Moreover, fewer materials can be used for their manufacture due to the required mechanical strength, biodegradation and their breakdown products that remain in the human body and can be toxic,

immunogenic or carcinogenic (Langer and Peppas, 1981) (Kumar and Pillai, 2018) (Dash and Cudworth II, 1999) (Stewart *et al.*, 2018) (Liechty *et al.*, 2010). There are strict regulatory requirements that need to be met for the fabrication of safe biodegradable devices and therefore, more research should be performed for new materials (Stewart *et al.*, 2018) (Major *et al.*, 2020).

Similarly to the non-biodegradable implants, there are two types of biodegradable devices: monolithic systems, where the drug is uniformly dispersed in the polymer and reservoir systems, where a polymeric membrane encloses the active agent. In the reservoir-type systems, a solution of the active agent is surrounded by a biodegradable polymeric membrane. The release rate of the incorporated active compound is a function of the polymer degradation rate or the drug dissolution rate and then, diffusion through the polymeric membrane, or a combination of both mechanisms. In most cases, the degradation rate of the membrane is slower than the release rate of the active substance and this is a challenge that should be addressed when active agents with a narrow therapeutic index are incorporated in these devices. However, this indicates that the polymeric membrane remains intact until the release of the total amount of the enclosed active compound. In the end, the membrane will degrade *in vivo* through biological procedures and its removal is, thus, not required (Yasukawa *et al.*, 2006) (Danckwerts and Fassihi, 1991) (Vadlapudi *et al.*, 2014) (Dash and Cudworth II, 1999) (Stewart *et al.*, 2018) (Christoforidis *et al.*, 2012).

In matrix-type systems, where the active ingredient is homogeneously dispersed into a biodegradable polymeric matrix, one or a combination of mechanisms regulate the release of the active agent; diffusion, swelling, erosion and cleavage of covalent linkage in the polymer (Christoforidis *et al.*, 2012) (Dash and Cudworth II, 1999) (Vadlapudi *et al.*, 2014) (Langer and Peppas, 1981) (Ranade, 1990). Several factors affect the release of the active substance from the polymeric matrix, such as the solubility and the permeability of the drug through the polymeric material, the chemical nature of the polymer, the amount of the incorporated active agent, as well as, the *in vivo* degradation of the polymeric matrix (Stewar*t et al*., 2018) (Christoforidis *et al.*, 2012) (Dash and Cudworth II, 1999).

In both biodegradable implant types, the release rate of the active substance can, thus, be controlled by proper adjustment of the membrane thickness or the polymeric surface area in biodegradable implantable devices (Christoforidis *et al.*,

2012). The release of the active compound is performed either through degradation of the polymer after the implantation of the device in the predetermined location of the human body or through diffusion; a combination of both procedures is also likely to occur (Christoforidis *et al*., 2012) (Santos *et al.*, 2014) (Kumar and Pillai, 2018) (Stewart *et al.*, 2018) (Vadlapudi *et al.*, 2014). The drug release mechanism is governed by polymer degradation when the diffusion rate of the active substance is slower than the degradation or erosion rate of the polymeric vehicle. The release of the active agent occurs at the same time as the polymer degrades and hence, sigmoidal release profiles are obtained (Santos *et al.*, 2014) (Kumar and Pillai, 2018).

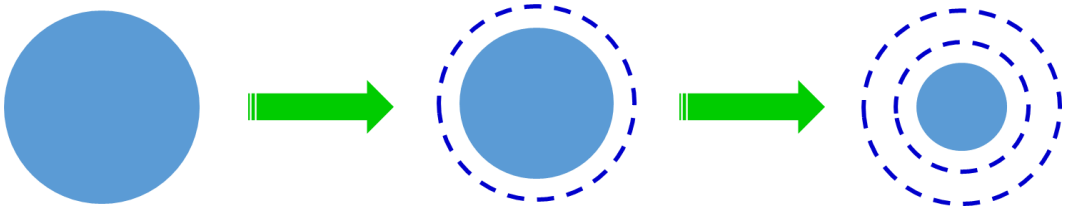

Figure 1.6: *Schematic illustration of an ideal surface erosion.*

Degradation is a chemical process and it is usually associated with bond cleavage, while erosion is a physical process and is linked to dissolution and diffusion (Uhrich *et al.*, 1999) (Liechty *et al.*, 2010). The mechanism of polymer erosion can be categorised into two approaches: surface-degrading and bulk-degrading. Surface-to-volume ratio, as well as, the shape and size of the implants play an important role in the drug release profiles of the biodegradable implants where the driving force for their degradation is surface-erosion (Lee, 2015) (Yasukawa *et al.*, 2006) (Kumar and Pillai, 2018) (Uhrich *et al.*, 1999) (Langer, 1990) (Santos *et al.*, 2014). In this case, the erosion is happening faster than the water penetration into the polymer bulk and hence, the polymer degradation is happening from the outer surface of the formulation towards its inside compartments (Uhrich *et al.*, 1999) (Yasukawa *et al.*, 2006) (Lee, 2015) (Langer, 1993). The polymer matrix is gradually eliminated from the surface, while the fraction of the polymer volume remains moderately stable (Yang and Pierstorff, 2012). The likelihood of dose dumping is very low in surface-erosion controlled biodegradable systems. The release rate of the active compound can be adjusted by altering the thickness of the polymeric formulations or the amount of the incorporated drug; thicker

systems have more extended lifespans and enhanced safety (Langer, 1993) (Uhrich *et al.*, 1999). Zero-order drug release can be obtained with these devices if their shape remains constant and the release of the enclosed active agent is limited (***Figure 1.6***) (Uhrich *et al.*, 1999).

On the contrary, when bulk-erosion occurs the polymer degradation is nearly uniform throughout the material, while water penetration into the bulk polymer matrix occurs faster than its erosion (Santos *et al.*, 2014) (Langer, 1990) (Uhrich *et al*., 1999) (Kumar and Pillai, 2018) (Lee, 2015). The volume of the matrix and not its thickness controls the erosion process; the size of the formulation does not exhibit any particular alterations until it is completely degraded, while the amount of the remaining polymer in the system decreases during this process. Drug delivery systems with different thicknesses exhibit the same lifespan (Langer, 1993) (Liechty *et al.*, 2010) (Yang and Pierstorff, 2012). In this erosion mechanism, the interaction of the water with the incorporated in the matrix active agent before its release can have as a result its destruction before its delivery. Burst release can also be observed in case the matrix is degraded rapidly and a pore is created through which the active substance can be released in an uncontrolled fashion (Yasukawa *et al.*, 2006) (Lee, 2015).

In both erosion processes and especially for polymers susceptible to hydrolytic degradation, water access to the polymer has a significant impact on its degradation and consequently, the drug release kinetics (Santos *et al.*, 2014) (Kumar and Pillai, 2018) (Langer, 1993) (Liechty *et al.*, 2010) (Yang and Pierstorff, 2012) (Lee, 2015). Nevertheless, both mechanisms of erosion are usually observed in biodegradable systems due to the hydrophilic nature of the majority of the materials used for biomedical applications (Langer and Peppas, 1981) (Lee, 2015) (Uhrich *et al.*, 1999). The chemical structure of the materials used for the fabrication of these devices influences the extent of the erosion (Uhrich *et al.*, 1999) (Lee, 2015).

The shape and the surface area of the implantable formulation are altered when bioerosion of the polymer occurs and that can have an impact on the drug release kinetics, as well as, the surface to volume ratio. Geometrical shapes are promising candidates for the development of biodegradable implants with the aim to achieve a more uniform and constant release, since their surface area is not changing over time during erosion. Zero order release is obtained with a flattened-slab type shape as it does not have any edge erosion. These elements should also be

considered during the development of biodegradable formulations for a more uniform and constant release of the loaded active compound to be attained (Danckwerts and Fassihi, 1991) (Langer, 1993) (Vadlapudi *et al.*, 2014) (Zaki Aj. *et al.*, 2012) (Dash and Cudworth II, 1999) (Langer and Peppas, 1981).

Polymer degradation which leads to the release of the active compound might happen through one or more processes; hydrolysis, during which bonds, such as ester bonds, in the polymer backbone are breaking down; enzyme degradation, during which hydrolytically susceptible bonds, such as amide bonds, degrade when a catalyst is present; oxidation; physical degradation which occurs when bonds are breaking due to the application of physical forces, such as swelling or mechanical loading. Each polymer type has a different degradation time which is affected by its molecular weight, crystallinity and surface properties (Danckwerts and Fassihi, 1991) (Stewart *et al.*, 2018) (Kumar and Pillai, 2018) (Langer, 1990) (Major *et al.*, 2020). Consequently, this can lead to various release profiles. *In vivo* factors, such as the environmental pH and temperature, have also an impact on the polymer degradation rate. It is, hence, crucial the *in vivo* degradation time of the polymer that will be used for the manufacture of a biodegradable implantable device to be fully studied and characterised prior to the wider use of the implants (Stewar*t et al*., 2018) (Dash and Cudworth II, 1999) (Vadlapudi *et al.*, 2014). The age of the patient, as well as, the state of the disease are other factors that influence the *in vivo* degradation kinetics of the polymer (Kumar and Pillai, 2018).

The ideal biodegradable polymer should be fully biocompatible, degraded to non-toxic fragments, highly reproducible, easily metabolised and excreted by physiological pathways, inert and free from any inflammatory response *in vivo*. However, no polymer demonstrates all the above mentioned characteristics and hence, the selection of the material for the implant manufacture will be based on the wanted drug release rate and mechanism. Sometimes, a combination of two or more polymers is chosen for the fabrication of an implantable device with the desired attributes (Stewar*t et al*., 2018) (Kumar and Pillai, 2018) (Ranade, 1990).

Biodegradable polymers can be used for the manufacture of simple and homogeneous drug-eluting systems that comprise an active ingredient either enclosed homogeneously within a plain polymer matrix or a polymeric matrix mixed with additives. Depending on the required properties of the final formulation, a polymer with suitable properties is selected; if sustained drug

release is the ultimate goal, then a polymer with slow degradation is the most appropriate material. Other materials, additives, can also be contained in the biodegradable device, such as plasticizers, fillers, stabilizers and excipients, to improve the mechanical properties of the device or decrease the cost of its production (Major *et al.*, 2020) (Langer, 1993) (Uhrich *et al.*, 1999).

Biodegradable polymers that can be used for the fabrication of implants include natural polymers, such as gelatin, collagen, starch, cellulose and chitosan; thermoplastic aliphatic polyesters, such as polylactic acid (PLA), polyglycolic acid (PGA), polylactic-co-glycolic acid (PLGA), and polycaprolactone (PCL); polyhydroxybutyrate (PHB); polyaspartic acid (PAA); hydroxypropyl methyl cellulose (HPMC) (Langer, 1993) (Paolin*o et al*., 2006) (Zaki Aj. *et al.*, 2012) (Yasukawa *et al.*, 2006) (Major *et al.*, 2020) (Santos *et al.*, 2014) (Langer and Peppas, 1981) (Ranade, 1990) (Uhrich *et al.*, 1999) (Yang and Pierstorff, 2012). Extensive research has already been performed in these materials regarding their biodegradability, the safety of their degradation products, biocompatibility and mechanical strength (Stewar*t et al*., 2018) (Kumar and Pillai, 2018) (Langer, 1993). Another advantage of these materials is that they are approved by the FDA for biomedical applications (Kumar and Pillai, 2018). Their degradation periods vary from one month up to several years. Factors, such as the polymer hydrophilicity, glass transition temperature, crystallinity and molecular weight, as well as, the environmental conditions, like the pH and the temperature, play a significant role in their degradation rate (Stewar*t et al*., 2018) (Langer, 1990).

Collagen exhibits several advantages to support its use for the manufacture of biodegradable drug delivery implants, such as biocompatibility, non-toxicity, efficiency, as well as, easy isolation and purification procedures of large amounts. Nevertheless, collagen causes immunogenic reactions in some patients that restrict its wide application (Yang and Pierstorff, 2012).

Aliphatic polyesters are popular materials for the fabrication of biodegradable implantable formulations due to their simple manufacturing methods; hot melt extrusion, solvent evaporation, compression molding from powder or pellet form (Kumar and Pillai, 2018). The degradation of this polymer type is achieved through bulk erosion (Langer, 1990) (Uhrich *et al.*, 1999).

Polylactic acid (PLA) belongs to the groups of biodegradable and bioresorbable polymers and it is produced through the polymerisation of lactic acid obtained

from natural feedstock, such as corn, rice or potato starch (Stewart *et al*., 2018) (Talebian *et al.*, 2018) (Yang and Pierstorff, 2012) (Uhrich *et al.*, 1999) (Langer, 1990). It is the second most widely used polymer as it demonstrates promising properties for biomedical applications and similar mechanical properties compared with other synthetic polymers (Stewart *et al.*, 2018) (Yang and Pierstorff, 2012). It is an inexpensive polymer with high versatility, abundance, biodegradability, biocompatibility and hydrophobicity. The latter property contributes to its slow degradation rate, which can last from to 1 to 5 years (Langer, 1993) (Talebian *et al.*, 2018) (Uhrich *et al.*, 1999) (Lee, 2015) (Stewart *et al.*, 2018) (Major *et al.*, 2020) (Yang and Pierstorff, 2012) (Christoforidis *et al.*, 2012). It is semipermeable to oxygen and water and these enable its bulk biodegradation contrasted with other biomedical polymers. Its breakdown products, lactic acid, demonstrate biocompatibility and ease of elimination from the human body (Talebian *et al.*, 2018) (Kumar and Pillai, 2018) (Christoforidis *et al.*, 2012) (Yang and Pierstorff, 2012). PLA is approved by the US Food and Drug Administration (FDA) for direct contact with biological fluids since it is generally recognised as safe (GRAS) material (Stewart *et al.*, 2018) (Talebian *et al.*, 2018) (Kumar and Pillai, 2018) (Major *et al.*, 2020) (Christoforidis *et al.*, 2012). This polymer can be used in various manufacturing technologies, including extrusion, film casting, blow moulding and fibre spinning, due to its exceptional thermal processability; its melting point is approximately 145 – 200 ^{o}C, while its glass transition temperature is ranging from 35 to 65 ^{o}C (Qian *et al.*, 2016) (Hung *et al.*, 2013) (Stewart *et al.*, 2018) (Major *et al.*, 2020) (Uhrich *et al.*, 1999) (Johari *et al.*, 2016) (Tee *et al.*, 2013).

Polyglycolic acid (PGA) is a polyester produced by the polymerisation of glycolic units. This polymer is one of the first biodegradable polymers ever used for drug delivery purposes and is approved by the FDA (Yang and Pierstorff, 2012) (Stewart *et al.*, 2018) (Major *et al.*, 2020) (Christoforidis *et al.*, 2012). It shows remarkable mechanical properties, even better than those of PLA, and a high melting point, 145 – 200 ^{o}C. Its glass transition temperature is ranging from 35 to 65 ^{o}C (Stewart *et al.*, 2018) (Major *et al.*, 2020). Its degradation occurs quite fast contrasted with PLA, while its acidic breakdown products can result in inflammation in the surrounding tissues (Lee, 2015) (Kumar and Pillai, 2018) (Stewart *et al.*, 2018) (Uhrich *et al.*, 1999) (Christoforidis *et al.*, 2012). These attributes are the main reasons that PGA is not used as a lone polymer in biomedical applications (Lee, 2015) (Stewart *et al*., 2018).

Polylactic-co-glycolic acid (PLGA) is another FDA approved biodegradable and biocompatible copolymer of PLA and PGA (Major *et al.*, 2020) (Lee, 2015) (Talebian *et al.*, 2018) (Langer, 1993) (Stewart *et al.*, 2018) (Christoforidis *et al.*, 2012). It is the most commonly used polymer for the manufacture of biodegradable drug-eluting devices (Christoforidis *et al.*, 2012) (Yang and Pierstorff, 2012). Depending on its PLA and PGA ratios, PLGA degradation period varies, from two to six months. This copolymer, is hence, more suitable for short-term drug release applications (Talebian *et al.*, 2018) (Yasukawa *et al.*, 2006) (Stewart *et al.*, 2018) (Christoforidis *et al.*, 2012) (Major *et al.*, 2020) (Lee, 2015) (Langer, 1993). Unlike the PGA, this copolymer is not broken down into acidic fragments during its degradation (Stewar*t et al*., 2018).

Polycaprolactone (PCL) represents a particular promising polymer for the fabrication of biodegradable implants due to its biocompatibility, biodegradability, non-toxicity and relatively low production cost. It is an FDA approved material for drug delivery purposes (Major *et al.*, 2020) (Stewart *et al.*, 2018) (Christoforidis *et al.*, 2012). Its breakdown products are safe and they are easily metabolised or eliminated through phagocytosis (Christoforidis *et al.*, 2012) (Stewart *et al.*, 2018). PCL is a hydrophobic polymer and thus, water cannot penetrate this material. This attribute is responsible for its extended degradation rate, even longer than other polymers, such as PLA, PGA or PLGA, with a range of many months to several years. Its glass transition temperature is -55 to -68 ºC, while its melting point is considered quite low, 55 – 60 ºC (C. Wu, 2005) (Sayyar *et al.*, 2012) (Talebian *et al.*, 2018) (Stewart *et al.*, 2018) (Benjamin H*o et al*., 2017) (Christoforidis *et al.*, 2012) (Major *et al.*, 2020) (Bae *et al.*, 2006) (Danafar *et al.*, 2014). The latter enables its mixing with a variety of active agents and the fabrication of implants through temperature-driven processes, such as extrusion, without leading to the decomposition of the drug (Stewar*t et al*., 2018). These are the main reasons that PCL is the selected polymer for the current study, while its properties will further be discussed in ***Chapter 2***.

Other biodegradable polymers, less popular, can also be used for the manufacture of polymeric implants, such as polyparadioxane, polyamides, polyanhydrides, polyphosphazenes, polyorthoesters, polyvinylpyrrolidone, polyaminoacids, polyalkyl cyanoacrylates, polyphosphoesters and polydioxanone (Langer, 1993) (Uhrich *et al.*, 1999) (Kaurav and Kapoor, 2017) (Liechty *et al.*, 2010) (Yang and Pierstorff, 2012) (Langer, 1990) (Paolino *et al.*, 2006) (Langer and Peppas, 1981) (Christoforidis *et al.*, 2012).

Polyanhydrides are great candidates for short-term controlled drug delivery formulations since their degradation time is fast due to their low hydrolytic stability (Stewart *et al.*, 2018) (Uhric*h et al*., 1999) (Langer, 1993). Their degradation occurs through surface erosion, while their breakdown products are monomers that are metabolized and then, excreted from the human body. This degradation mechanism enables better control of the incorporated active agent contrasted with active substances released through bulk erosion. Several classes of polyanhydrides are available for use as drug delivery vehicles, aliphatic, unsaturated and aromatic, with different degradation times each. Aliphatic polyanyhdrides exhibit a very short degradation period, only a few days, while some aromatic polyanhydrides demonstrate slow degradation, up to several years. The various degradation times of the classes of polyanhydrides and the capability of combining them for the production of copolymers make them promising candidates for the fabrication of implantable systems where the release of the active agent will happen for a predetermined period of time (Talebian *et al.*, 2018) (Langer, 1990) (Uhrich *et al.*, 1999) (Christoforidis *et al.*, 2012).

The most commonly used copolymer of polyanhydrides is 1,3-bis(carboxyphenoxypropane) (PCPP) and sebacic acid (SA). PCPP is aromatic and hydrophobic and degrades very slow through surface erosion, for over three years, while SA is aliphatic and hydrophilic with a far slower degradation time, a few days only. The obtained copolymer will have a slow degradation lifetime like the sebacic acid (Langer, 1993) (Christoforidis *et al.*, 2012) (Uhrich *et al.*, 1999) (Talebian *et al.*, 2018).

1.3.5. Methods of Manufacture of Implantable Drug Delivery Devices

Several technologies are available today for the manufacture of implantable drug delivery devices, such as compression moulding, solvent casting, hot melt extrusion and injection moulding. The selection of the most suitable technique is affected by a series of factors including material properties, cost, efficiency of the technique, and the desired properties of the final implant. Thermoplastic polymers, such as PLA, PLGA or PCL can be used in technologies where heat is applied, such as hot melt extrusion, injection moulding and 3D printing.

Formulations fabricated by different techniques will have in most cases different microporous structure and degradation time and hence, different *in vitro* and *in vivo* release profiles (Stewar*t et al*., 2018) (Yasukaw*a et al*., 2006) (Santos *et al.*, 2014).

The main advantage of the compression manufacturing method is the fact that no heat or solvents are used for the production of implants. A closed container is used for the formation of the predetermined shape after the materials compression. Consequently, this technology can be applied for heat or solvent sensitive substances, such as peptides, proteins or drugs (Yasukawa *et al.*, 2006) (Stewart *et al.*, 2018). Nevertheless, implantable formulations produced with compression usually demonstrate rapid release compared with the products of the other manufacturing techniques where the materials are heated and are in a molten phase before the formation of the final architectures. The application of heat for material melting during injection molding or hot melt extrusion results in the manufacture of products with a smooth surface with only a few cracks or apertures. In contrast, implants fabricated via compression exhibit a particularly irregular surface with many cavities. The latter could act as channels facilitating the penetration of the dissolution medium increasing, in this way, the materials degradation and the release of the encapsulated active agent (Stewart *et al.*, 2018) (Fialho, Cunha and Cunha, 2005). Extended drug release can be achieved with the combination of another method for the coating of the implant (Stewar*t et al*., 2018) (Yasukawa *et al.*, 2006).

Another method that is used for the fabrication of implantable devices is solvent casting in which a solvent is selected for the adequate dissolution of the polymer. The obtained solution is, then, placed into a mould where the solvent is evaporated. This technique is usually applied for the production of films or laminar implants. The major drawback of solvent casting is the large amounts of organic solvents that are used which might influence the stability of the incorporated active compounds, as well as, the toxicity of the final device (Yasukawa *et al.*, 2006) (Stewar*t et al*., 2018) (Makadia and Siegel, 2012).

On the other hand, hot melt extrusion does not require the use of any solvent for the manufacture of an implantable drug eluting system. During this method, the melting, mixing and forcing of the loaded materials through an aperture, also termed die, with predetermined dimensions and shape, occur continuously (Cunha-Filho *et al.*, 2017) (Yasukawa *et al.*, 2006). In this manner, high

throughput rates can be achieved. Only thermoplastic polymers, such as PLA, PGA, PLGA and PCL, can be used in this technology. The disadvantage of hot melt extrusion is the application of high temperatures which might lead to the decomposition of active ingredients (Stewar*t et al*., 2018) (Patil, Tiwari and Repka, 2016). Commonly extrusion is usually combined with a downstream post processing technique to ensure that the final object has the desired architecture. Injection moulding is a melt process that can be coupled with hot melt extrusion for implant fabrication (Cunha-Filh*o et al*., 2017) (Maniruzzaman *et al.*, 2012). In injection moulding, the molten extrudate is injected into a mould with the desired shape and dimensions where it is allowed to solidify. Implants produced with this method demonstrated a slower degradation rate compared with the extruded ones (Stewart *et al.*, 2018) (Rothen-Weinhold *et al.*, 1999).

Therefore, new techniques are needed for the fabrication of implantable drug delivery devices with an appropriate structure which will enable better adjustment of the polymer degradation rate for the desired release profile to be obtained.

1.3.6. Applications of Implantable Drug Delivery Devices

Implantable drug-eluting devices can be applied for long-term sustained release of different types of active compounds for the treatment of patients with chronic diseases. The areas of their applications include women's health, cardiovascular diseases, ocular diseases, oncology, diabetes, pain management, infectious diseases and central nervous systems disorders (Langer, 1993) (Vadlapudi *et al.*, 2014) (Stewart *et al.*, 2018) (Kumar and Pillai, 2018) (Dash and Cudworth II, 1999) (Wang *et al.*, 2013) (Christoforidis *et al.*, 2012) (Yang and Pierstorff, 2012). The most commonly incorporated active agents in commercially available implants include contraceptive steroids, anticancer agents, narcotic analgesics, ocular therapeutics, proteins, antibiotics, hormones and anti-inflammatory active substances (Major *et al.*, 2020) (Ranade, 1990) (Yasukawa *et al.*, 2006) (Vadlapud*i et al*., 2014) (Zaki Aj. *et al.*, 2012) (Stewart *et al.*, 2018) (Kompbella, Kadam and Lee, 2011) (Danckwerts and Fassihi, 1991) (Meng and Hoang, 2012) (Lee, 2015). Several implants have already been approved by the FDA and some of them will further be discussed below.

Contraceptive implants are the most commonly known applications of implantable devices since these formulations exhibited a great influence on women's health (Danckwerts and Fassihi, 1991). They have been fabricated using both biodegradable and non-biodegradable materials. They have demonstrated exceptional effectiveness with an annual pregnancy rate lower than 1%. Norplant (Wyeth Pharmaceuticals, Madison, NJ), Jadelle (Bayer Pharmaceuticals), Implanon (Organon International, Oss, the Netherlands), Estring (Pfizer), NuvaRing (Merck, Whitehouse Station, NJ) and Nexplanon (Merck, Whitehouse Station, NJ) represent examples of FDA approved contraceptive implantable devices (Langer, 1990) (Zaki Aj. *et al.*, 2012) (Paolino *et al.*, 2006) (Ranade, 1990) (Vadlapudi *et al.*, 2014) (Stewart *et al.*, 2018) (Kumar and Pillai, 2018).

Norplant is the first contraceptive implant that reached the market in 1990 and it is loaded with crystalline levonorgestrel. It has a cylindrical shape and is placed under the skin of the upper arm. It belongs in the category of reservoir type formulations, while a non-degradable silicone elastomer was the material used for its manufacture. The active agent is released through slow diffusion for more than 5 years (Dash and Cudworth II, 1999) (Langer, 1993) (Vadlapudi *et al.*, 2014) (Stewar*t et al*., 2018) (Ranade, 1990) (Paolino *et al.*, 2006) (Kumar and Pillai, 2018) (Zaki Aj. *et al.*, 2012). The disadvantage of Norplant is associated with its difficult insertion and removal procedures (Kumar and Pillai, 2018).

Implanon is a rod-shaped subdermal implantable reservoir formulation incorporating etonogestrel and it was approved by the FDA in 2006 (Kumar and Pillai, 2018) (Vadlapudi *et al.*, 2014). It was designed to address the decreasing patients acceptance for Norplant; easier subcutaneous implantation and explantation processes enhanced patients compliance (Kumar and Pillai, 2018). PEVA is the non-degradable polymer selected for its fabrication, while sustained release for more than 3 years has been achieved (Kumar and Pillai, 2018) (Vadlapud*i et al*., 2014).

Estring is a silicone intravaginal ring commercially available for the treatment of symptoms linked with menopause. It is loaded with estradiol which is released for a period of 90 days (Kumar and Pillai, 2018).

NuvaRing is another intravaginal ring available in the market in which etonogestrel and ethinyl estradiol are loaded. The release period of the enclosed active compounds is approximately 3 weeks (Kumar and Pillai, 2018).

Nexplanon is the new version of Implanon and it also has a cylindrical shape. It is subcutaneously implanted in the arm, similarly to Norplant and Implanon, while the loaded etonogestrel is released over a period of 3 years (Kumar and Pillai, 2018).

Drug-eluting stents (DES) are the most representative examples of implantable devices for the therapy of vascular diseases. More specifically, these devices have been developed to replace the bare-metal stents (BMS) that lead to restenosis. The new versions of stents are composed of a BMS coated with a polymer that contributes to the progressive release of the incorporated active agent to hinder cell proliferation which results in restenosis. Cypher stent (Boston Scientific) was the first approved DES in 2003, while Taxus stent (Abbott Vascular) was later approved, in 2004 (Kumar and Pillai, 2018).

Ocular implantable drug delivery devices illustrate particularly effective systems for localized sustained drug release for several ocular diseases, such as glaucoma, cytomegalovirus renitis, macular degeneration, uveitis, since the delivery of active agents in the posterior segment of the eye with the conventional formulations is hard due to the very specific anatomical and physiological barriers of the ocular environment (Stewart *et al.*, 2018) (Vadlapudi *et al.*, 2014) (Lee, 2015) (Wang *et al.*, 2013). The latter is related to poor permeation and retention of the active substance in the eye due to lacrimation, tear dilution and tear turnover. Moreover, poor patient adherence and the complicated use of the ocular devices make necessary the development of other systems for the treatment of ocular conditions (Stewart *et al.*, 2018).

Various types of ocular implants are commercially available today and they overcome the majority of the previously mentioned limitations: Ocusert Pilo (ALZA Corporation, Mountain View, CA), Vitrasert (Bausch & Lomb, Inc., Rochester, NY), Retisert (Bausch & Lomb), Surodex (Allergan, Inc., Irvine, CA), Ozurdex (Allergan Inc.), Illuvien (Alimera Sciences Inc., Alpharetta, GA; pSivida Inc., Watertown, MA), Verisome (Icon Biosciences Inc., Sunnyvale, CA), Prosert (IOL Tech) and Lacrisert (Valeant Pharmaceuticals North America LLC, Aliso Viego, CA) (Wan*g et al*., 2013) (Langer and Peppas, 1981) (Vadlapud*i et al*., 2014) (Kumar and Pillai, 2018) (Zaki Aj. *et al.*, 2012) (Yang and Pierstorff, 2012) (Langer, 1993) (Christoforidis *et al.*, 2012) (Lee, 2015) (Yasukawa *et al.*, 2006).

Occusert was the first ocular implantable system that was distributed in the market in 1976. PEVA copolymer was used for the manufacture of a release rate-controlling membrane of its reservoir in which pilocarpine and alginic acid were enclosed. This formulation is implanted beneath the tarsus of the lower eyelid, while its therapeutic efficacy lasts for one week. Occusert exhibits easy implantation, removal and the development of only a few adverse effects (Langer, 1993) (Zaki Aj. *et al.*, 2012) (Vadlapudi *et al.*, 2014) (Kumar and Pillai, 2018) (Langer and Peppas, 1981) (Yasukaw*a et al*., 2006). Although its advantages enhance patient adherence, it is more expensive than the use of topical eye drops. The latter resulted in its reduced application in the therapy of glaucoma (Langer, 1990) (Vadlapud*i et al*., 2014).

Vitrasert is an intravitreal drug-eluting implant approved by the FDA in 1996 for the treatment of AIDS-associated cytomegalovirus retinitis (CMV). Its polymeric membrane consists of PVA and PEVA, while ganciclovir is incorporated in its core (Wang *et al.*, 2013) (Yasukaw*a et al*., 2006) (Christoforidis *et al.*, 2012) (Kumar and Pillai, 2018) (Lee, 2015) (Yang and Pierstorff, 2012). Long-term sustained release of the active ingredient is obtained for a period of at least 5 to 8 months. Even though no systemic toxicity has been observed with this implant and its cost is particularly low, the risk of endophthalmitis, development of cataract and cystoid macular oedema with epiretinal membrane, vitreous haemorrhage and rhegmatogenous retinal detachment is quite high (Kompbella, Kadam and Lee, 2011) (Lee, 2015) (Yasukawa *et al.*, 2006) (Wang *et al.*, 2013) (Vadlapud*i et al*., 2014) (Kumar and Pillai, 2018) (Christoforidis *et al.*, 2012).

Retisert is the first ocular implant approved by the FDA in 2005 for the therapy of chronic non-infectious uveitis affecting the posterior segment of the eye. PVA and silicone laminates have been used for the manufacture of the polymeric membrane of its reservoir containing fluocinolone acetonide (Vadlapudi *et al.*, 2014) (Lee, 2015) (Christoforidis *et al.*, 2012) (Yang and Pierstorff, 2012) (Wan*g et al*., 2013) (Yasukawa *et al.*, 2006) (Kompbella, Kadam and Lee, 2011). Its sustained release lasts for approximately 3 years and it contributes to the control of inflammation, the decrease of repeated events of uveitis and the enhancement of vision acuity. Its disadvantages, though, are associated with the development of cataract and high intraocular pressure (Christoforidis *et al.*, 2012) (Vadlapud*i et al*., 2014) (Yasukaw*a et al*., 2006) (Lee, 2015) (Rodríguez Villanueva, Rodríguez Villanueva and Guzmán Navarro, 2017).

Illuvien is another FDA approved non-biodegradable implantable system containing fluocinolone acetate in a PLGA matrix within a polyimide tube. It is used for treating patients with diabetic macular oedema, while the release period of the active agent is over 3 years (Lee, 2015) (Christoforidis *et al.*, 2012) (Kompbella, Kadam and Lee, 2011) (Wan*g et al*., 2013). The side effects, appearing after the implantation of this device are the development of cataract and high intraocular pressure (Kompbella, Kadam and Lee, 2011) (Christoforidis *et al.*, 2012).

Surodex is a matrix type implant made of biodegradable polymers, PLGA and hydroxylpropyl methylcellulose (HPMC) loaded with dexamethasone. Its FDA approval is for the treatment of postoperative inflammation after cataract surgery with a long-lasting effect for a period of 7 to 10 days (Vadlapud*i et al*., 2014) (Wang *et al.*, 2013) (Kompbella, Kadam and Lee, 2011) (Christoforidis *et al.*, 2012) (Lee, 2015).

Ozurdex is another FDA approved biodegradable intravitreal implantable system incorporating dexamethasone in a PLGA matrix. It is a rod-shaped formulation used for treating macular oedema connected with retinal vein occlusion after approval in 2009, while in 2010 became the second FDA approved formulation for the therapy of non-infectious posterior uveitis. The release of the active agent lasts for over a period of 4 months (Rodríguez Villanueva, Rodríguez Villanueva and Guzmán Navarro, 2017) (Christoforidi*s et al*., 2012) (Kompbella, Kadam and Lee, 2011) (Yang and Pierstorff, 2012) (Lee, 2015) (Wan*g et al*., 2013).

Polymer implantable drug delivery systems represent a promising less invasive solution for a more effective and safe localized cancer chemotherapy. They can be directly inserted into the tumour, either subcutaneously or intramuscularly. In this fashion, localized delivery of the enclosed active compound is achieved without any adverse effects in healthy organs, cells or tissues, eliminating at the same time the need for repeated injections (Dash and Cudworth II, 1999) (Danckwerts and Fassihi, 1991). Various implantable formulations are available in the market today for the treatment of prostate, breast and bladder cancer: Zoladex (AstraZeneca Pharmaceuticals, London, U.K.), Lupron Depot (Abbott Laboratories, Abbott Park, IL), Gliadel Wafers (Eisai Inc., Woodcliff Lake, NJ), Eligard (Sanofi-Synthelabo Inc., Bridgewater, NJ), Profact or Superfact Depot (Sanofi-Aventis Inc., Canada), Lupron depot (Takeda), Vantas (Endo Pharmaceutical), Prostap SR and OncoGel (Protherics, a BTG PLC Company, UT) (Vadlapud*i et al*., 2014) (Kumar and Pillai, 2018) (Stewar*t et al*., 2018) (Langer, 1990) (Zaki Aj. *et al.*,

2012) (Danckwerts and Fassihi, 1991) (Ranade, 1990) (Majo*r et al*., 2020) (Yang and Pierstorff, 2012) (Paolino *et al.*, 2006).

Zoladex is a biodegradable matrix type implant composed of PLGA or PLA loaded with goserelin acetate (Danckwerts and Fassihi, 1991) (Langer, 1993). This cylinder-shaped formulation, manufactured through hot melt extrusion, has received FDA approval for the treatment of hormone-responsive prostate cancer and advanced breast cancer. It is subcutaneously inserted into the anterior abdominal wall, while the release period of the enclosed active agent is influenced by its loaded amount and it can last from 28 days to 12 weeks. Goserelin acetate is released via diffusion through aqueous pores created by the degradation of the PLGA or PLA matrix (Zaki Aj. *et al.*, 2012) (Paolino *et al.*, 2006) (Yang and Pierstorff, 2012) (Vadlapud*i et al*., 2014) (Kumar and Pillai, 2018).

Profact or Superfact Depot is another commercially available implantable device approved for the treatment of hormone-responsive cancers, such as prostate cancer, breast cancer and assisted reproduction. PLGA is the biodegradable drug vehicle in this formulation which is loaded with buserelin acetate. Its sustained drug release is ranging from 2 to 3 months depending on the relative ratio of polymer and active compound in the device (Kumar and Pillai, 2018).

Eligard is an in situ forming biodegradable implantable system approved by the FDA for the palliative treatment of prostate cancer. PLGA is the selected biodegradable material for its manufacture and it is dissolved in a biocompatible solvent, N-methyl-2-pyrrolidone. Leuprolide acetate is added to the polymer solution prior to the implantation. After the injection of this solution in the body, the solvent diffuses away, while the system is penetrated by water. The latter has as a result the PLGA precipitation and in this manner, an implant depot is created. Depending on the amount of the loaded active ingredient, sustained drug release varies from 1 to 6 months (Vadlapud*i et al*., 2014).

Vantas is another implantable device targeting prostate cancer. It is inserted subcutaneously, while it is used for the delivery of the enclosed histrelin acetate for up to 12 months (Kumar and Pillai, 2018).

Lupron depot is the first FDA approved device for the controlled release of a peptide for the therapy of prostate cancer or endometriosis. It is composed of

PLGA and it is loaded with leuprolide acetate with a long-lasting effect of over 30 days (Langer, 1990) (Zaki Aj*. et al*., 2012) (Langer, 1993).

Gliadel Wafers is one of the first FDA approved biodegradable implants; it has been approved in 1996 for the therapy of malignant glioma. It is inserted during brain resection surgery on tumour surface for the controlled delivery of carmustine for approximately 3 weeks (Vadlapud*i et al*., 2014) (Kumar and Pillai, 2018) (Christoforidis *et al.*, 2012) (Yasukawa *et al.*, 2006) (Paolino *et al.*, 2006) (Major *et al.*, 2020). The biodegradable materials used for its manufacture are 80% w/w 1,3-bis(carboxyphenoxypropane) (PCPP) and 20% w/w sebacic acid (SA) (Christoforidis *et al.*, 2012) (Kumar and Pillai, 2018). Gliadel is also used for the therapy of recurrent Hodgkin's lymphoma and multiple myeloma (Christoforidis *et al.*, 2012).

Implantable drug delivery systems can be particularly effective in the management of chronic pain, as well, and address the limitations of oral and parenteral formulations that require frequent administration, the development of side effects, the mortality from overdosing and the increased likelihood of addiction (Danckwerts and Fassihi, 1991) (Dash and Cudworth II, 1999). Implants subcutaneously inserted into the human body for the prolonged release of active agents are already available in the market; hydromorphine is released from 30 to 90 days from implants for the treatment of patients with cancer or HIV/AIDS-induced neuropathic chronic pain; LiRis is a silicone made implant incorporating lidocaine which is continuously released for the therapy of interstitial cystitis/bladder pain syndrome; baclofen is delivered from an infusion pump for the treatment of muscle spasticity; Probuphine is an implantable device composed of a polyethylene vinyl acetate matrix containing buprenorphine hydrochloride which is released for a period of 6 months for treating patients with opioid abuse problems (Ranade, 1990) (Kumar and Pillai, 2018) (Stewart *et al.*, 2018).

IDDSs can offer a promising solution also for the treatment of infectious diseases, such as tuberculosis, where long-term drug administration is needed. The latter combined with the adverse effects hinder patients lifestyle and lead to reduced adherence, failure of the therapeutic scheme and the development of strains resistant to already used active compounds (Danckwerts and Fassihi, 1991) (Vadlapudi *et al.*, 2014) (Stewart *et al.*, 2018).

Neurology and central nervous system diseases, such as schizophrenia, are additional areas where implants can be applied since the commercially available formulations are associated with low patient compliance and high risk of hospitalization, relapse and other harmful effects (Vadlapudi *et al.*, 2014) (Stewart *et al.*, 2018). A subcutaneously implanted system has already been approved for the prolonged release of risperidone for the treatment of patients with schizophrenia (Vadlapud*i et al*., 2014).

Another application of implantable devices can be for the treatment of diabetes, where long-term insulin administration is needed. Several studies have been performed to date, while DUROS technology has shown promising results in clinical trials. No implant for this therapeutic area is yet available in the market, though (Danckwerts and Fassihi, 1991) (Paolino *et al.*, 2006) (Kumar and Pillai, 2018) (Zaki Aj. *et al.*, 2012) (Dash and Cudworth II, 1999) (Ranade, 1990).

Implantable pump systems exhibit considerable accuracy and predictability regarding the release of the enclosed active substance and therefore, extensive research has been performed for their potential human and veterinary applications. These systems include ALZET osmotic pump (DURECT Corporation, Cupertino, CA), OSMET, L-OROS SOFTCAP, L-OROS HARDCAP (Alza Corporation, Vacaville, CA), SCOT (Andrx Pharmaceuticals, Fort Lauderdale, FL), EnSoTrol (Supernus Pharmaceuticals, Inc., Rockville, MD), Osmodex (Osmotica Pharmaceutical, Wilmington, NC), controlled porosity osmotic pump, DUROS (DURECT Corporation, Cupertino, CA), Veterinary Implantable Therapeutic System (VITS), and Ruminal Therapeutic System (RUTS) (Alza Corporation, Vacaville, CA) (Meng and Hoang, 2012) (Dash and Cudworth II, 1999) (Vadlapud*i et al*., 2014) (Ranade, 1990) (Paolino *et al.*, 2006).

ALZET osmotic pumps belong in the category of miniature implantable pumps and have been used for research applications. Several types of active compounds can be loaded to them, such as small drugs, peptides, proteins, bioactive macromolecules, while their sustained release can last from 1 day to 6 weeks (Ranade, 1990) (Kumar and Pillai, 2018) (Meng and Hoang, 2012) (Dash and Cudworth II, 1999) (Vadlapud*i et al*., 2014) (Zaki Aj*. et al*., 2012).

DUROS osmotic pumps are cylindrically shaped and made of an inert titanium alloy. They can be loaded with various types of therapeutic agents, including growth factors, addictive drugs, cytokines, chemotherapeutic drugs, steroids,

antibodies, peptides and proteins, that need to be delivered for extended periods of time for the treatment of chronic diseases (Zaki Aj. *et al.*, 2012) (Kumar and Pillai, 2018) (Paolino *et al.*, 2006). Their main advantage is that no batteries, switches or other electromechanical parts are required for their operation. Sustained drug release is achieved with these systems for various periods, ranging from months to one year. The titanium shell is protecting the formulation from enzymatic, hydrolytic degradation and other metabolic clearance procedures activated after exposure to body fluids. This device has been approved by the FDA in 2000 with a commercial name Viadur (Bayer Healthcare, Leverkusen, Germany) for the palliative therapy of prostate cancer through the delivery of leuprolide acetate (Meng and Hoang, 2012) (Vadlapud*i et al*., 2014) (Paolino *et al.*, 2006) (Zaki Aj. *et al.*, 2012).

1.4. 3D PRINTING

1.4.1. Introduction

Three Dimensional Printing (3DP), also known as additive manufacturing (AM), rapid prototyping (RP) or solid free-form technology (SFF), is a computer controlled technology in which the fabrication of the desired objects is achieved by the deposition of materials in a layer fashion way according to a digital design (Sandler and Preis, 2016) (Zema *et al.*, 2017) (Choonara *et al.*, 2016) (Vaz and Kumar, 2021) (Akmal *et al.*, 2018) (Norman *et al.*, 2017) (Konta, García-Piña and Serrano, 2017) (Moulton and Wallace, 2014) (Patterson, Collopy and Messimer, 2015) (Sarah J. Trenfield *et al.*, 2018) (Capel *et al.*, 2018) (Jamróz, Kurek, Łyszczarz, Brniak, *et al.*, 2017).

The concept of Additive Manufacturing was firstly mentioned by Pierre A. L. Ciraud at the beginning of 1970s when he presented a new method to fabricate objects; a powdered material can be deposited and properly shaped on a platform in a layer fashion through the application of a high energy beam. The solidification of each layer was following until the production of the desired structure. Promising materials for use in this innovative technology can be plastics or metals that are melting when high temperature is applied. That was only the start of the development and commercialization of various 3D printing methods (Jamróz, Szafraniec, *et al.*, 2018).

The first time that an additive manufacturing technique reached the market was in 1984 when Charles Hull, also recognized as the pioneer of this technology, invented and later commercialized and patented the first 3D printer, known as Stereolithography (SLA). This 3D printing technology was using an ultraviolet (UV) laser source for the photopolymerisation of light sensitive liquid polymers, resins, for the production of a predetermined architecture (Hull, 1986). Charles Hull also introduced the .stl format for the 3D design files that is still in use today (Sadia, Alhnan, *et al.*, 2018) (Hull, 1986) (Vithani, Goyanes, Jannin, Abdul W Basit, *et al*., 2019b). Later, in 1986, another 3D printing technique was developed and after 4 years was patented by Carl Deckard and Joseph Beaman from the University of Texas. The manufacture of objects with that new technology was based on powder fusion achieved through a computer-controlled laser; this technology was called Selective Laser Sintering (SLS) (Beaman and Deckard, 1990) (Vaz and Kumar, 2021) (Jamróz, Szafraniec, *et al.*, 2018) (Beg *et al.*, 2020) (Sadia, Alhnan, *et al.*, 2018) (Eshkalak *et al.*, 2020) (Shende and Agrawal, 2018).

1989 was the year that many more 3D printing techniques were introduced to the public. Scott and Lisa Crump, founders of the company Stratasys, introduced and later patented (in 1992) a different from the previously presented 3D printing techniques, Fused Deposition Modelling (FDM). The principle of this equipment was relying on the heating and extrusion of usually a plastic material –metals can also be applied- through a heated nozzle on a printing stage, where each layer of the deposited material solidified (Crump, 1979) (Eshkalak *et al.*, 2020) (Vithani, Goyanes, Jannin, Abdul W Basit, *et al*., 2019b) (Beg *et al.*, 2020) (Ani Jose and Christopher GV, 2018). In 1989, as well, Hans Lager introduced Selective Laser Melting (SLM) in which a laser beam was employed directly to metal, paper or plastic to cut it for the manufacture of a predetermined structure (Shende and Agrawal, 2018) (Beg *et al.*, 2020) (Vaz and Kumar, 2021). Emanuel Sachs and his colleagues at MIT presented the same year, 1989, another 3D printing system in which an inkjet 3D printer was used for the deposition of a layer of ink on a powder platform for the ultimate binding of the powder. This process was repeated for the fabrication of the desired object layer by layer, while the unbound powder was removed in the end. This technique, known today as binder jetting, is the first 3D printing method applied for the production of formulations, while it was patented in 1993 (Sachs *et al.*, 1993). The professors from MIT were the ones who first introduced the term of 3D printing (Sadia, Alhnan, *et al.*, 2018) (Dumitrescu *et al.*, 2018) (Goole and Amighi, 2016) (Jamró*z et al*., 2018) (Beg *et*

al., 2020) (Vitha*ni et al*., 2019b) (Khatri, Shah and Vora, 2018) (Ani Jose and Christopher GV, 2018) (Palo *et al.*, 2017). Nowadays, there are more than ten different types of 3D printers available in the market and many more are currently being developed (Sanghavi *et al.*, 2016) (Vaz and Kumar, 2021) (Vithani *et al.*, 2019b) (Lamichhane, Bashyal, *et al.*, 2019) (Afsana *et al.*, 2018) (Han *et al.*, 2018).

The differences in the additive manufacturing instruments are associated with the material types that can be used –polymers, ceramics, resins, metals, composites, plastic, various forms of food, growth factors, biological materials or living cells- and their forms, such as powders, filaments, liquids, gels or binder solutions, the method of deposition, the fashion with which each layer is created and the characteristics of the end object, such as resolution, morphology, texture, surface, thermal, mechanical or conductivity properties (Zema *et al.*, 2017) (Hoque, Chuan and Pashby, 2011) (Patterson, Collopy and Messimer, 2015) (Lamichhane, Bashyal, *et al.*, 2019) (Stansbury and Idacavage, 2016) (Choonara *et al.*, 2016) (Shende and Agrawal, 2018) (Jasiuk *et al.*, 2018). Nevertheless, the main principles of operation in all the instrument types follow the 3D's of 3D printing; Design, Develop and Dispense (Sarah J. Trenfield *et al.*, 2018) (Beg *et al.*, 2020).

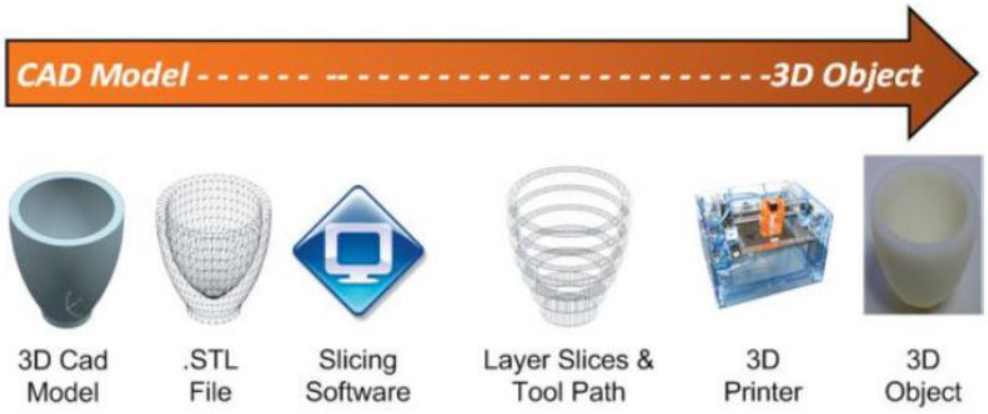

Figure 1.7: *Schematic illustration of the basic steps of the 3D printing process. This figure is reproduced from Patterson, Collopy and Messimer (Patterson, Collopy and Messimer, 2015).*

"Design" is the first step of the 3D printing process and is associated with the generation of a computer aided-design (CAD) file, which will then be converted

into a .stl file. 3D printing software is "slicing" the information in the .stl file regarding the architecture –size and shape- and the characteristics of the final product, the printer set up and the parameters needed for the manufacture of the desired object into well-defined printable layers (Khatri, Shah and Vora, 2018) (Goole and Amighi, 2016) (Vithani, Goyanes, Jannin, Abdul W Basit, *et al*., 2019b) (Hoque, Chuan and Pashby, 2011) (Ramya, 2016) (Aquino *et al.*, 2018) (Capel *et al.*, 2018). The final file is, then, loaded to the printer in a proper format, .gcode, to be successfully read in a 2D manner. The printed layers, are built on top of each other and then, are fused together for the production of the desired 3D structure (***Figure 1.7***) (Patterson, Collopy and Messimer, 2015) (Jamróz, Kurek, Łyszczarz, Brniak, *et al.*, 2017) (Akash *et al.*, 2016) (Shende and Agrawal, 2018) (Lamichhane, Bashyal, *et al.*, 2019) (Berman, 2012) (Capel *et al.*, 2018) (Sarah J. Trenfield *et al.*, 2018) (Sadia, Alhnan, *et al.*, 2018) (Zema *et al.*, 2017). The quality or the resolution of the 3D printed object is influenced by the number of the cross sections (Hsiao *et al.*, 2018) (Zhang *et al.*, 2018) (Ligon *et al.*, 2017) (Hoque, Chuan and Pashby, 2011) (Sadia, Alhnan, *et al.*, 2018).

The second D, "Develop", comprises the selection of the most appropriate technique, excipients and printer settings depending on the properties of the used active compound, the chosen equipment and excipients and the desired characteristics of the final product (Trenfiel*d et al*., 2018) (Khatri, Shah and Vora, 2018). More specifically, the physical, chemical and mechanical properties of the materials loaded to the instrument play a significant role in the 3D printing process and they should be considered during the preformulation or development stage. Each AM technique requires the loading of the raw materials in a specific form, such as powder, liquid, paste or solid, while the materials physical properties will affect the final fabricated architecture (Beg *et al.*, 2020) (Sandler and Preis, 2016) (Kotta, Nair and Alsabeelah, 2018) (Aquino *et al.*, 2018). Any chemical interactions or modifications, degradation or changes in the thermal stability and photocurable properties of the materials used are factors that should also be considered. Particular focus should be given to the improvement of the materials mechanical properties, such as the stiffness, hardness and viscosity, for the successful manufacture of a dosage form. The selection of the proper combination of printing parameters, such as print speed, infill density, building platform temperature, layer thickness, can influence the resolution of the predetermined structure and the printing time (Zhang *et al.*, 2018) (Khatri, Shah and Vora, 2018) (Jamróz, Szafraniec, *et al.*, 2018) (Haris *et al.*, 2020).

"Dispense" is the stage where the chosen materials are loaded to the 3D printer for the fabrication of the predetermined architecture. After the completion of the 3D printing process, the final product will be removed from the printing platform, while post-processing, such as removal of any support, polishing, drying or smoothing, will follow, if required (Khatri, Shah and Vora, 2018) (Sarah J. Trenfield *et al.*, 2018) (Eshkalak *et al.*, 2020) (Haris *et al.*, 2020). Waste material can be reused for another 3D printing process (Berman, 2012) (Lin*d et al*., 2017) (Vithani, Goyanes, Jannin, Abdul W Basit, *et al*., 2019b). It is noteworthy that the whole fabrication process occurs continuously, while any modifications in the produced object can be performed in the digital file (Sarah J. Trenfield *et al.*, 2018) (Zema *et al.*, 2017) (Zhan*g et al*., 2018) (Jamróz, Kurek, Łyszczarz, Brniak, *et al.*, 2017). A brief introduction of the various 3D printing methods will follow in the next section of this Chapter.

Additive Manufacturing has numerous applications in various fields, such as automotive, aerospace, military, energy, consumer electronics, buildings construction, architecture, entertainment, food, chemical, toy and fashion industry (for the production of clothes, shoes), art, jewellery and in healthcare industries for the fabrication of scaffolds, medical prosthetics, implants, stents, transdermal, rectal and vaginal devices, artificial tissues and organs or even dosage forms (Shende and Agrawal, 2018) (Ventola, 2014) (Palo *et al.*, 2017) (Norman *et al.*, 2017) (Beg *et al.*, 2020) (Sadia, Alhnan, *et al.*, 2018) (Tappa and Jammalamadaka, 2018) (Vaz and Kumar, 2021) (Akmal *et al.*, 2018) (Choonara *et al.*, 2016) (Khatri, Shah and Vora, 2018) (Liang, Brambilla and Leroux, 2019) (Ramya, 2016) (Pandey *et al.*, 2020) (Han *et al.*, 2018) (Bahnini *et al.*, 2018).

3D Printing has gained considerable popularity in the past years as its versatility and the potential of fabricating structures with predetermined permeability, porosity, hydrophobicity/hydrophilicity or functionality can lead to a revolutionary change in the drug delivery field and the treatment schemes. Dosage forms that can be applied in personalised medicine and hence, address the limitations of the widely used traditional formulations can easily be manufactured with this technology (Lamichhane, Bashyal, *et al.*, 2019) (Eshkalak *et al.*, 2020) (Khatri, Shah and Vora, 2018) (Goole and Amighi, 2016). Extensive research has recently been performed for the potential application of 3D printing in the manufacture of various formulations, such as controlled release tablets, polypills, implants, immediate release tablets, multiphase release dosage forms, monolithic sustained release tablets, pulsatile drug release tablets, biphasic release tablets, enteric

release tablets, orodispersible films, gastrofloating tablets, self-emulsifying drug delivery systems, microneedles and transdermal patches (Vaz and Kumar, 2021) (Vithani, Goyanes, Jannin, Abdul W Basit, *et al*., 2019b) (Khatri, Shah and Vora, 2018) (Ju *et al.*, 2019). Polypharmacy, where patients are taking more than five tablets a day for the treatment of multiple diseases, can be replaced by the fabrication of a polypill, a single 3D printed tablet loaded with the right amount of the active agents that each patient needs, at the point-of-care (Zhang *et al.*, 2018) (Sadia, Alhnan, *et al.*, 2018) (Haris *et al.*, 2020) (Shende and Agrawal, 2018) (Awad *et al.*, 2018) (Babu and Devaprakasam, 2019) (G. Chen *et al.*, 2020) (Gioumouxouzis, Karavasili and Fatouros, 2019) (Vaz and Kumar, 2021). Implantable drug delivery devices can also be produced with this technology with higher accuracy and speed, and lower production costs and material loss (Afsan*a et al*., 2018) (Zema *et al.*, 2017) (Han *et al.*, 2018) (Preis and Öblom, 2017) (Kotta, Nair and Alsabeelah, 2018) (Vit*hani et al*., 2019b) (Jasiuk *et al.*, 2018) (Sanghavi *et al.*, 2016).

Unlike the traditional mass-manufacturing pharmaceutical techniques, 3D printing offers a high degree of design freedom; cost-efficiency; high yield; the capability of fabricating customized products in various shapes (such as spherical, cylindrical, pyramidal, cubic), densities and diffusivities, complex internal architecture (such as solid, hollow, pierced, honeycomb, network, gyroid, multilayer, coated, multi-compartment, gradient systems and relevant combinations); loaded with more than one active agent, with tunable drug release profiles in one dosage form; a localized, immediate, delayed and/or sustained drug release can be attained (Jasiu*k et al*., 2018) (Han *et al.*, 2018) (Afsana *et al.*, 2018) (Zema *et al.*, 2017) (Moulton and Wallace, 2014) (Sandler and Preis, 2016) (Shende and Agrawal, 2018) (Horst, 2018) (Gioumouxouzis, Karavasili and Fatouros, 2019) (Norma*n et al*., 2017) (Haris *et al.*, 2020) (Sarah J. Trenfield *et al.*, 2018) (Sanghavi *et al.*, 2016).

More specifically, no mold or cast is required for the fabrication of the desired structure contrasted with the conventional pharmaceutical processing methods and that enables the production of objects in any shape, size, internal and external geometry (Moulton and Wallace, 2014) (Lamichhane, Bashyal, *et al.*, 2019) (Eshkalak *et al.*, 2020) (Pandey *et al.*, 2020) (Palo *et al.*, 2017) (Bahnini *et al.*, 2018) (Ventola, 2014) (Rahman *et al.*, 2018) (Berman, 2012) (Jamróz, Kurek, Łyszczarz, Brniak, *et al.*, 2017). A notable advantage of this technology is the fact that low amounts of materials can be used for the production of the desired object,

while accurate spatial distribution can be achieved (Kotta, Nair and Alsabeelah, 2018) (Vithani, Goyanes, Jannin, Abdul W Basit, *et al*., 2019b) (Ju *et al.*, 2019) (Awa*d et al*., 2018) (Haris *et al.*, 2020). Even though products with high complexity can be manufactured, the fact that the design is in a digital form, no preliminary research regarding their architecture, planning of their fabrication or any manual handling is required. All these features lower significantly the production times and costs, while they enhance at the same time the potential of 3D printing to be applied for on-demand manufacture of dosage forms for better medical care to be provided to the patients, with reduced burden pill and enhancement of patient compliance (Sandler and Preis, 2016) (Vaz and Kumar, 2021) (Jamróz, Kurek, Łyszczarz, Brniak, *et al.*, 2017) (Beg *et al.*, 2020) (Lin*d et al*., 2017) (Kotta, Nair and Alsabeelah, 2018) (Norman *et al.*, 2017) (Zem*a et al*., 2017) (Choonara *et al.*, 2016).

Compared with the conventional pharmaceutical fabrication processes - compression/injection molding, melt/solvent casting, porogen leaching, electrospinning- which are time-consuming, labour intensive and dose inflexible, 3D printed objects can easily be modified in CAD files for precise deposition of a specific amount of one or several active ingredients in each layer (Palo *et al.*, 2017) (Trivedi *et al.*, 2018) (Liang, Brambilla and Leroux, 2019) (Vithani, Goyanes, Jannin, Abdul W Basit, *et al*., 2019b) (Gioumouxouzis, Karavasili and Fatouros, 2019) (Beg *et al.*, 2020) (Awad *et al.*, 2018) (Pandey *et al.*, 2020) (Capel *et al.*, 2018) (Shafiee and Atala, 2016). It should be noted that not only very low amounts of active substances can be used for the 3D printing process, but also formulations with high drug loading can be fabricated (Dumitrescu *et al.*, 2018) (G. Chen *et al.*, 2020).

Commercially available formulations are fabricated with the existing technologies in only specific dose strengths not meeting the needs of all the patients. Additive manufacturing provides a solution to this issue with the production of patient-specific dosage forms containing the exact amount of the active ingredient each patient needs (Moulton and Wallace, 2014) (Zhang *et al.*, 2018) (Vaz and Kumar, 2021) (Lepowsky and Tasoglu, 2018) (Eshkalak *et al.*, 2020) (Lamichhane, Bashyal, *et al.*, 2019) (Shafiee and Atala, 2016) (Preis and Öblom, 2017) (Beg *et al.*, 2020) (Aquino *et al.*, 2018). This feature combined with the fact that the drug loading capacity of the 3D printed formulations is higher than in the widely used dosage forms are particularly useful properties for the production of drug delivery systems for patients with multiple chronic diseases, such as diabetes, neurologic

disorders, hyperlipidemia, chronic pain, cardiovascular diseases, psychiatric disorders (Ventola, 2014) (Ani Jose and Christopher GV, 2018) (Trivedi *et al.*, 2018) (Goole and Amighi, 2016).

Furthermore, with this innovative technique incompatible active agents can be incorporated in the same formulation as compartmentalisation is feasible to be obtained; each drug can be placed in a different area of the dosage form. The specific site of location of each active compound in the formulation can properly be selected compared with the traditional manufacturing methods. Each area can even exhibit a unique release profile, reducing in this way the frequency of drugs administration and the likelihood of a dosage error to occur (Capel *et al.*, 2018) (G. Chen *et al.*, 2020) (Lepowsky and Tasoglu, 2018). In this manner, improved distribution and absorption of the active ingredient are attained with the drug efficacy and safety to be enhanced contributing at the same time to the improvement of patient adherence. Moreover, fluctuations in plasma concentrations are eliminated with the design of formulations with controlled release kinetics (Shende and Agrawal, 2018) (Dumitrescu *et al.*, 2018) (Beg *et al.*, 2020) (Goole and Amighi, 2016) (Aquino *et al.*, 2018) (Pandey *et al.*, 2020) (Ani Jose and Christopher GV, 2018) (Liang, Brambilla and Leroux, 2019) (Horst, 2018) (Ventola, 2014).

A remarkable benefit of this technique is that the use of specific excipients, such as lactose or sucrose, that cause intolerances can be avoided (Dumitrescu *et al.*, 2018) (G. Chen *et al.*, 2020). More efficient taste masking is feasible, while swallowing difficulties usually appearing in geriatric and paediatric populations can be solved (Trivedi *et al.*, 2018) (G. Chen *et al.*, 2020). The development of adverse effects can, thereby, be reduced, while the patient adherence can be enhanced with the administration of 3D printed dosage forms (Trenfiel*d et al*., 2018) (Rahman *et al.*, 2018) (Eshkalak *et al.*, 2020) (Ha*n et al*., 2018) (Kotta, Nair and Alsabeelah, 2018) (Be*g et al*., 2020) (Palo *et al.*, 2017) (Haris *et al.*, 2020) (Zema *et al.*, 2017) (Vaz and Kumar, 2021).

Contrasted with the traditional pharmaceutical fabrication methods already in use for more than 200 years, additive manufacturing considerably contributes to the decrease of the process time, the production cost, the required space for the fabrication of formulations, the number of the operation units needed as several manufacturing steps –mixing, granulation, drying, milling, compaction, compression, coating- are combined; objects with more complex internal and

external geometries can quickly be produced with high precision; orifices or cavities that can result in more efficient localized drug release can be introduced during the 3D printing procedure; the coating of the core can easily be included in this manufacturing process (Gioumouxouzis, Karavasili and Fatouros, 2019) (Awad *et al.*, 2018) (Afsana *et al.*, 2018) (Patterson, Collopy and Messimer, 2015) (Khatri, Shah and Vora, 2018) (Jasiuk *et al.*, 2018) (Zhang *et al.*, 2018) (Kotta, Nair and Alsabeelah, 2018) (Hsiao *et al.*, 2018) (Haris *et al.*, 2020).

Another advantage of this technology is that the cost of the patient treatment can significantly be decreased with the application of more suitable and cost effective medications. Moreover, poorly water soluble active compounds, poor and high metabolizers, peptides, proteins, orphan drugs, potent active substances or active agents with a narrow therapeutic index can efficiently be delivered with 3D printed formulations (Afsana *et al.*, 2018) (Awad *et al.*, 2018) (Ventola, 2014) (Vithani, Goyanes, Jannin, Abdul W Basit, *et al*., 2019b) (Ani Jose and Christopher GV, 2018) (Gioumouxouzis, Karavasili and Fatouros, 2019) (Haris *et al.*, 2020) (Han *et al.*, 2018).

Accurate dosing and predetermined release kinetics can be achieved with additive manufacturing by proper selection of one or more polymers, adjustment of the formulation dimensions and geometry, the layer thickness, infill percentage and pattern, as well as, the design of individual compartments. In this way, a better approach is available in the pharmaceutical field to address the differences detected in each patient during the metabolism and absorption of the released active substances (Preis and Öblom, 2017) (Norman *et al.*, 2017) (Pande*y et al*., 2020) (Afsana *et al.*, 2018) (Palo *et al.*, 2017) (Aquino *et al.*, 2018) (Sandler and Preis, 2016) (Zema *et al.*, 2017) (Sarah J. Trenfield *et al.*, 2018) (Kotta, Nair and Alsabeelah, 2018) (Han *et al.*, 2018). Furthermore, dosage forms tailored for patients with a pharmacogenetic polymorphism can successfully be manufactured with this method. Other parameters, such as age, gender, weight, race, comorbidities, pharmacokinetics or disease state can be considered for the production of a bespoke 3D printed formulation that is hard to be performed with the currently used mass-manufacturing technologies that follow the "one-size-fits-all" approach (***Figure 1.8***) (Trivedi *et al.*, 2018) (Kotta, Nair and Alsabeelah, 2018) (Be*g et al*., 2020) (Liang, Brambilla and Leroux, 2019) (Ani Jose and Christopher GV, 2018) (Dumitrescu *et al.*, 2018) (Capel *et al.*, 2018) (Ventola, 2014) (Pandey *et al.*, 2020) (Aquino *et al.*, 2018) (Shafiee and Atala, 2016) (Haris *et al.*, 2020).

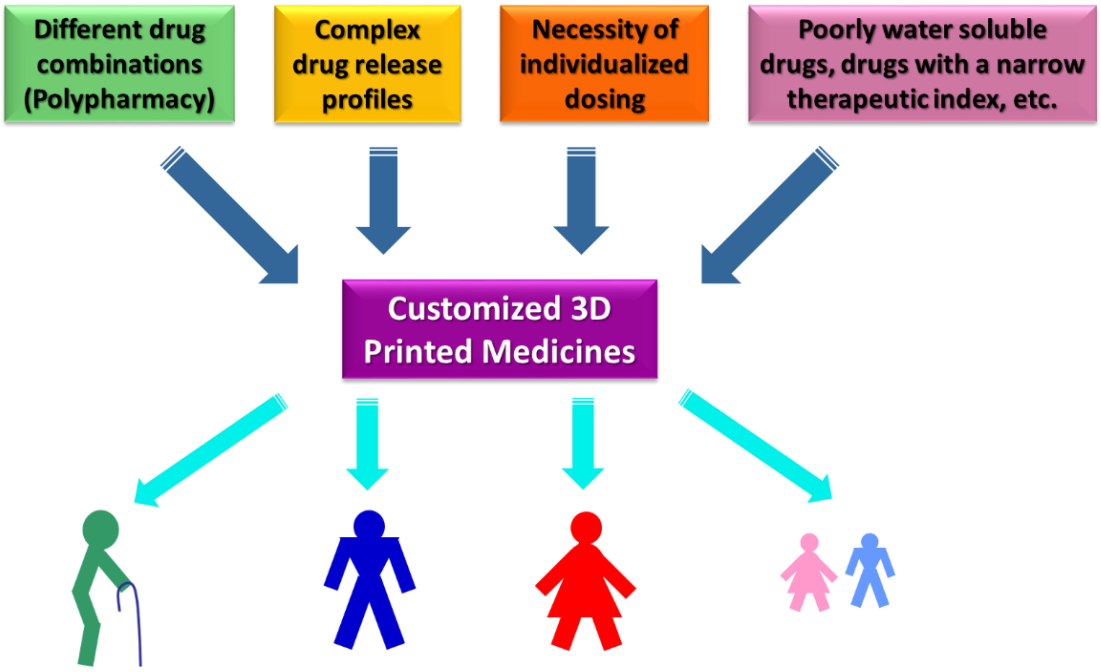

Figure 1.8: *The potential applications of 3D printed dosage forms in individualized medicine based on the needs and characteristics of each patient.*

Additive Manufacturing is providing a means to achieve on-demand formulations fabrication in small pharmacies, hospitals or even in remote locations, such as space expeditions or war zones (Capel *et al.*, 2018) (Liaw and Guvendiren, 2017) (Lepowsky and Tasoglu, 2018) (Lind *et al.*, 2017) (Seoane-Viaño *et al.*, 2021). In this approach, the pharmacist can rapidly manufacture a complete dosage form based on the individualized patient prescription as issued by a clinician (Dumitrescu *et al.*, 2018) (Eshkala*k et al*., 2020) (Liaw and Guvendiren, 2017) (Awad *et al.*, 2018) (Vithani, Goyanes, Jannin, Abdul W Basit, *et al*., 2019b) (Khatri, Shah and Vora, 2018) (Beg *et al.*, 2020) (Liang, Brambilla and Leroux, 2019).

Nevertheless, the major disadvantage of 3D printing is that the applied temperature during the manufacturing process can result in the decomposition of thermolabile active compounds and that restricts the range of active ingredients that can be used in 3D printers (Afsana *et al.*, 2018) (Goole and Amighi, 2016) (Awad *et al.*, 2018) (Haris *et al.*, 2020) (Liang, Brambilla and Leroux, 2019) (Shende and Agrawal, 2018) (Dumitrescu *et al.*, 2018) (Vaz and Kumar, 2021).

The relatively low print speed, software issues, as well as, the high cost of the equipment and mass production are additional limitations of this technology (Patterson, Collopy and Messimer, 2015) (Pandey *et al.*, 2020) (Eshkalak *et al.*, 2020) (Aquino *et al.*, 2018) (Berman, 2012) (Ventola, 2014) (Trivedi *et al.*, 2018) (Haris *et al.*, 2020) (Jasiuk *et al.*, 2018). Moreover, only a few materials are currently available for use in this technology since they need to have specific properties, such as biocompatibility, safety for human use and adequate mechanical strength (Palo *et al.*, 2017) (Gioumouxouzis, Karavasili and Fatouros, 2019) (Berman, 2012) (Tappa and Jammalamadaka, 2018) (Eshkalak *et al.*, 2020) (Ani Jose and Christopher GV, 2018). Printability is another essential material attribute that is associated with the gelation approaches, the rheological and viscoelastic properties of the compounds (Eshkalak *et al.*, 2020) (Trivedi *et al.*, 2018).

The ideal material that can be used as a matrix or vehicle for the production of dosage forms with additive manufacturing needs to be compatible with the selected active agent; biocompatible and inert, which means it should not trigger the development of any undesired systemic or local effects from the human body; physically and chemically stable; easy to be printed with adjustable degradation rates, while it should not produce any toxic compounds during its processing in the equipment (Capel *et al.*, 2018). It also needs to demonstrate appropriate thermal conductivity, viscosity and thermomechanical properties depending on the required features of the final object (Ligon *et al.*, 2017) (Ani Jose and Christopher GV, 2018) (Pal*o et al*., 2017) (Vaz and Kumar, 2021) (Berman, 2012) (Tappa and Jammalamadaka, 2018) (Be*g et al*., 2020) (Gioumouxouzis, Karavasili and Fatouros, 2019) (Lamichhane, Bashyal, *et al.*, 2019).

The efforts and advances of additive manufacturing in the pharmaceutical field are accredited by the FDA approval of the first 3D printed drug dosage form, Spritam® which was manufactured by Aprecia Pharmaceuticals with the ZipDose® technology for the treatment of epilepsy, in 2015 (West and Bradbury, 2019) (Jamróz, Kurek, Łyszczarz, Brniak, *et al.*, 2017) (Preis and Öblom, 2017) (Konta, García-Piña and Serrano, 2017) (Afsana *et al.*, 2018) (Zhang *et al.*, 2018) (Kotta, Nair and Alsabeelah, 2018) (Ani Jose and Christopher GV, 2018) (Norman *et al.*, 2017) (Sandler and Preis, 2016) (Han *et al.*, 2018). The pharmacological activity of this orodispersible tablet loaded with 1000 mg of levetiracetam, an antiepileptic drug, was similar to the pharmacological activity of the commercially available formulations, tablets. Nevertheless, its solubilisation time was significantly

decreased; the tablet dissolved in only a few seconds after its contact with an aqueous solution because of its highly porous structure (Vaz and Kumar, 2021) (West and Bradbury, 2019) (Pandey *et al.*, 2020) (Lamichhane *et al*., 2019) (Jamróz, Szafraniec, *et al.*, 2018) (Palo *et al.*, 2017). The high porosity of Spritam® and its rapid disintegration in the mouth without any water made it the ideal formulation for epileptic patients who face swallowing issues (Liang, Brambilla and Leroux, 2019) (Trivedi *et al.*, 2018) (West and Bradbury, 2019) (Liaw and Guvendiren, 2017). Moreover, orodispersible tablets loaded with high amounts of active agents exhibit most of the times issues during the manufacturing and quality control process; with 3D printing, these limitations were easily overcome, as seen in the case of Spritam® (Jamróz, Szafraniec, *et al.*, 2018) (West and Bradbury, 2019) (Dumitrescu *et al.*, 2018).

The ZipDose® technology was based on a powder bed fusion 3D printing method, while no compression was required for the fabrication of the tablets. Their first layer contained the active compound and the excipients, which consisted of the matrix of the formulation. The deposition of a liquid binder followed for an adequate adhesion between the layers to be obtained (Afsan*a et al*., 2018) (Norman *et al.*, 2017) (Beg *et al.*, 2020) (West and Bradbury, 2019) (Lin*d et al*., 2017) (Ani Jose and Christopher GV, 2018) (Kotta, Nair and Alsabeelah, 2018) (Ha*n et al*., 2018) (Liang, Brambilla and Leroux, 2019) (Dumitrescu *et al.*, 2018).

Therefore, the approval of that 3D printed dosage form has strongly demonstrated the potential of AM on the production of cost-effective formulations with improved characteristics, such as with dose flexibility, more complex but accurate structure, spatial drug distribution and even customized drug release profiles that cannot be fabricated with the conventional pharmaceutical processing techniques (Sandler and Preis, 2016) (Acosta-Vélez and Wu, 2016) (Kotta, Nair and Alsabeelah, 2018) (Trivedi *et al.*, 2018) (Ha*n et al*., 2018).

1.4.2. Types of 3D Printing Processes

There are several 3D printing technologies available today with various energy sources, different principles of operation that are based on –the fashion that the layers of the manufactured object are deposited on the building stage and finally, fused together– and various types of materials that can be used in them, such as waxes, thermoplastics, photopolymers, metals, ceramics, liquids, pastes, powders, or even living cells (Ju *et al.*, 2019) (Kyle *et al.*, 2017) (Chia and Wu, 2015) (Shende and Agrawal, 2018). Additive manufacturing technologies can be divided into three categories based on their principle of operation: powder solidification, liquid solidification and extrusion (Jamróz, Szafraniec, *et al*., 2018).

Drop-on-solid deposition, including Powder Bed Inkjet 3D printing, Selective Laser Sintering (SLS), Selective Laser Melting (SLM) and Electron Beam Melting (EBM) belong in the powder solidification methods (Zhang *et al.*, 2018) (Lepowsky and Tasoglu, 2018) (Jamróz, Szafraniec, *et al*., 2018). Stereolithography (SLA) and drop-on-drop deposition belong in the liquid solidification methods (Dehghanghadikolaei, Namdari and Mohammadian, 2018) (Jamróz, Szafraniec, *et al.*, 2018). Pressure-assisted microsyringe (PAM) and Fused Deposition Modelling (FDM) belong in the extrusion based methods (Sadi*a et al*., 2018) (Shende and Agrawal, 2018) (Lepowsky and Tasoglu, 2018) (Jamróz, Szafraniec, *et al.*, 2018) (Dumitrescu *et al.*, 2018) (Algahtani, Mohammed and Ahmad, 2019) (Vaz and Kumar, 2021). Nevertheless, they all follow the same basic 3D printing steps (***Figure 1.9***) (Ventola, 2014) (Haris *et al.*, 2020) (Palo *et al.*, 2017) (Eshkalak *et al.*, 2020).

More specifically, the first step involves the design of the desired object using CAD software and the optimization of its geometry based on the selected 3D printer. Afterwards, this design is converted to an appropriate format, .stl file, that contains all the information regarding the geometry of the 3D part. The next stage is the loading of this file to the printer software, the "slicing" of the 3D design in several cross-sections of specific thickness and the generation of a file type readable by the printer, .gcode file or other file extensions according to the used printer (Vithani *et al*., 2019b) (Khatri, Shah and Vora, 2018) (Ani Jose and Christopher GV, 2018) (Eshkalak *et al.*, 2020) (Capel *et al.*, 2018) (Jamró*z et al*., 2018). Then, the materials that will be used for the fabrication of the predetermined object are processed into the proper type of intermediate that is required for the loading to the equipment if necessary; granules, filaments,

pastes, hydrogels, solids, liquids, binder inks (Palo *et al.*, 2017) (Khatri, Shah and Vora, 2018). 3D printing of the desired structure follows in a layer-wise way; the printhead is usually capable of moving in two directions, X and Y, while the building stage is moving upwards or downwards, in the Z axis. Each layer most often solidifies quickly after its deposition on the printing platform, which, then, moves in the Z axis according to the predetermined layer height to be created space for the deposition of the next layer. This process is repeated until the manufacture of the desired architecture (Jamróz, Szafraniec, *et al*., 2018) (Vithani, Goyanes, Jannin, Abdul W Basit, *et al*., 2019b). The final step includes post-processing of the fabricated part, such as drying, sintering or polishing. However, this step is depending on the printing process, the materials used and the required properties of the produced structure (Shende and Agrawal, 2018) (Khatri, Shah and Vora, 2018) (Palo *et al.*, 2017) (Haris *et al.*, 2020). Consequently, three factors should be considered before the beginning of the 3D printing process: the printer's hardware, the printer's software –it is used for the communication with the hardware and for the slicing of the CAD file- as well as the materials that will be used (Zhang *et al.*, 2018).

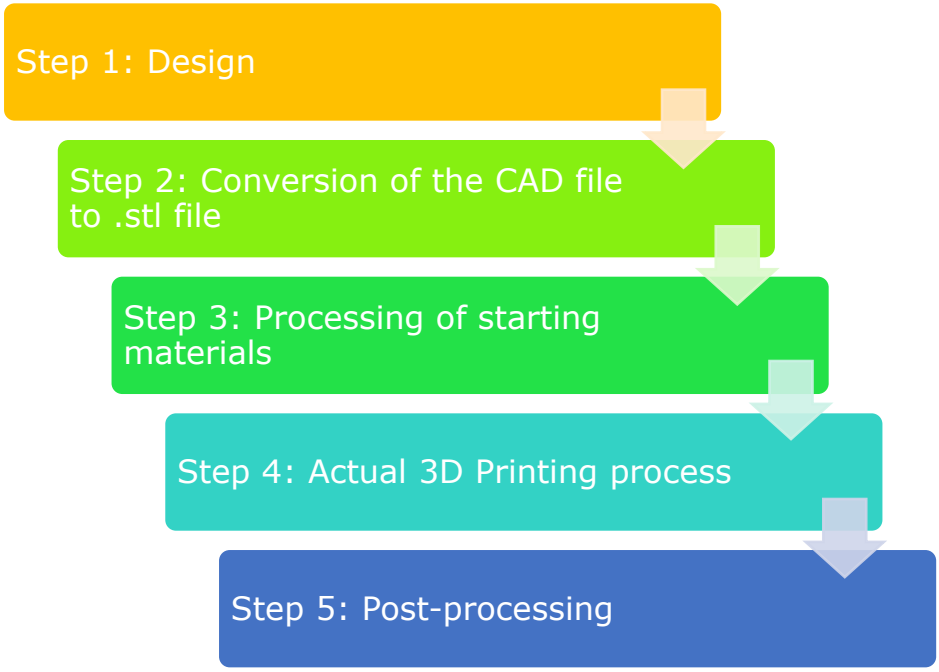

Figure 1.9: *Basic Steps in a 3D Printing Process.*

3D printing technologies that seem promising for the manufacture of solid dosage forms are divided into the following groups: inkjet-based systems, nozzle-based deposition systems and laser-based systems. All the inkjet 3D printing methods, including the Powder Bed Inkjet 3D printing, belong in the first group, Pressure-assisted microsyringe (PAM) and Fused Deposition Modelling (FDM) in the second one, while Stereolithography (SLA), Selective Laser Sintering (SLS), Selective Laser Melting (SLM) and Electron Beam Melting (EBM) in the last one (Ju *et al.*, 2019) (Khatri, Shah and Vora, 2018) (Peng *et al.*, 2017) (Ani Jose and Christopher GV, 2018) (Tian *et al.*, 2019).

Table 1.5: *Advantages and disadvantages of different types of liquid based additive manufacturing technologies.*

3D Printing technologies	Advantages	Disadvantages	References
Stereolithography (SLA) divided into two categories according to the position of the UV light source: ▪ ***Bottom up*** ▪ ***Top down***	▪ high spatial resolution, accuracy, precision, speed of printing ▪ capability of fabrication micron- and submicron-sized parts and complex structures	▪ only a few resins are biocompatible, biodegradable and FDA approved ▪ low drug loaded formulations are usually fabricated ▪ degradation of the active compounds after their exposure to UV light ▪ high cost of the equipment ▪ mandatory post-processing of the manufactured structures (polishing or sanding) ▪ high likelihood of cross-contamination (nature of the vat)	*(Lamichhane, Bashyal, et al., 2019)* *(Hofinger, 2011)* (Dietmar W. Hutmacher, Sittinger and Risbud, 2004) *(Rahman et al., 2018)*
Digital Light Processing (DLP)	▪ whole layer can be strengthened at once ▪ freedom of selecting the light intensity and exposure time based on the polymerization attributes of the used resin	▪ high cost of the equipment ▪ potential toxicity of the used materials and their breakdown products	*(Bahnini et al., 2018)* *(Mathew, Pitzanti and Larrañeta, 2020)*

Vat photopolymerization is a 3D printing method in which a photopolymer in a liquid form (resin) contained in a vat is selectively cured through the application of light which triggers its polymerization. Stereolithography (SLA) and Digital Light Processing (DLP) are liquid based additive manufacturing technologies that belong in this category (***Table 1.5***) (Dumitrescu *et al.*, 2018) (Vithani *et al*., 2019b) (Beg *et al.*, 2020) (Ligon *et al.*, 2017) (Ramya, 2016) (Bahnini *et al.*, 2018) (Awad *et al.*, 2018). Their only differences are the initiation process and the light source; ultraviolet radiations (UV) or other high energy light are applied in SLA 3D printing, while in DLP, the energy applied for the curing of a photopolymersible resin is dynamically developed by an integrated circuit, which is called digital micro-mirror device (Jamróz, Szafraniec, *et al*., 2018) (Eshkalak *et al.*, 2020) (Bahnini *et al.*, 2018) (Mathew, Pitzanti and Larrañeta, 2020) (Sanghavi *et al.*, 2016) (Vithani, Goyanes, Jannin, Abdul W Basit, *et al*., 2019b) (Sadia, Alhnan, *et al.*, 2018) (Pandey *et al.*, 2020).

Table 1.6: *Advantages and disadvantages of Selective Laser Sintering (SLS).*

3D Printing technology	Advantages	Disadvantages	References
Selective Laser Sintering (SLS)	▪ highly porous structures can be obtained ▪ high reproducibility and resolution ▪ high printing speed ▪ manufacture of objects with high mechanical strength ▪ no use of solvents ▪ any powder that was not used during a 3D printing session can be used in the next one	▪ post-processing of the printed part is necessary and time-consuming ▪ the high-energy applied beam can lead to the degradation of the selected materials ▪ the printing speed is lower contrasted with other manufacturing technologies ▪ high cost of the equipment	*(Rahman et al., 2018)* *(Babu and Devaprakasam, 2019)* *(Katstra et al., 2000)* *(Placone and Engler, 2018)*

Table 1.7: *Advantages and disadvantages of Inkjet 3D printing technologies.*

3D Printing technologies	Advantages	Disadvantages	References
Inkjet 3D printing	▪ high precision and spatial resolution (droplets in micron sizes) ▪ fabrication of formulations loaded with several active ingredients with each one exhibiting a specific drug release profile ▪ high production rate	▪ post-processing (drying) ▪ low drug loading ▪ inadequate hardness and rough surface of printed formulations	*(Haris et al., 2020)* *(Ligon et al., 2017)* *(Beg et al., 2020)*
Categories of Inkjet 3D printers based on the method of formation and deposition of the small drops			
Continuous Inkjet 3D printing (CIJ)	▪ quick production of droplets ▪ nozzle is not easily blocked	▪ ink waste (continuous generation of droplets) ▪ low printing resolution ▪ high cost of maintenance of the equipment	*(Daly et al., 2015)* *(Prasad and Smyth, 2016)*
Drop-on-Demand Inkjet 3D printing (DoD)	▪ elimination of ink wastage ▪ simplicity ▪ high precision and accuracy ▪ low cost of the equipment	▪ high cost of maintenance of the equipment	*(Tian et al., 2019)* *(Khatri, Shah and Vora, 2018)*
Categories of Drop-on-Demand Inkjet 3D printers based on the printhead type			
Piezoelectric Inkjet 3D printing	▪ suitable for heat sensitive materials (no heat is applied)		*(Zhang et al., 2018)*
Thermal (Bubble) Inkjet 3D printing		▪ high temperatures applied, (up to 300 ºC) ▪ not suitable for thermal sensitive active agents or excipients	*(Babu and Devaprakasam, 2019)* *(Ani Jose and Christopher GV, 2018)*
Categories of Drop-on-Demand Inkjet 3D printers based on the substrate used for the deposition of the droplets			
Drop-on-Drop Inkjet 3D printing	▪ high drug loading	▪ hard to be used for the manufacture of drug dosage forms	*(Afsana et al., 2018)* *(Lamichhane, Park, et al., 2019)*
Drop-on-Solid Inkjet 3D printing (binder jetting / powder bed inkjet 3D printing / drop-on-powder)	▪ various materials can be loaded ▪ no heat applied ▪ highly porous structures ▪ excellent reproducibility ▪ high printing resolution ▪ precise dosing ▪ fabrication of well-distinct compartments with various materials compositions and drug release profiles	▪ post-processing (drying step can last for up to 9 hours) ▪ high waste of powder ▪ residual solvent is sometimes above the acceptable limit ▪ no hollow parts can be fabricated	*(Lepowsky and Tasoglu, 2018)* *(Trivedi et al., 2018)* *(Dumitrescu et al., 2018)* *(Sadia, Alhnan, et al., 2018)* *(Shende and Agrawal, 2018)*

Powder bed fusion is a 3D printing method in which the fusion of materials with a high melting point is performed through the application of thermal energy in selected regions of a powder platform. In this way, the powder is moderately melting and that contributes to the binding of the layers; this process is known as sintering. The heat source is a laser or an electron beam and contributes to the fusion of the powder particles (Zhang *et al.*, 2018) (Shende and Agrawal, 2018) (Ramya, 2016) (Awad *et al.*, 2018) (Pandey *et al.*, 2020) (Eshkala*k et al*., 2020) (Dumitresc*u et al*., 2018) (Ligon *et al.*, 2017). Selective Laser Sintering (SLS), Selective Laser Melting (SLM) and Electron Beam Melting (EBM) belong in this group (***Table 1.6***) (Awad *et al.*, 2018) (Al-Maliki and Al-Maliki, 2015) (Beg *et al.*, 2020) (Vithani *et al*., 2019b) (Dumitrescu *et al.*, 2018) (Bahnini *et al.*, 2018).

Selective Laser Melting (SLM) and Electron Beam Melting (EBM) are similar processes to SLS (Chia and Wu, 2015) (Liaw and Guvendiren, 2017). In both techniques, metal powders are used for the fabrication of the predetermined architecture. With EBM, a more homogeneous thermal field distribution is attained compared to SLS, since particularly high temperatures are applied. However, its printing accuracy and the surface quality of the printed object are decreased (Awad *et al.*, 2018) (J*u et al*., 2019).

In material jetting, the deposition of the selected material is performed in droplets form at high speed through a nozzle with a small diameter on a surface (Ligo*n et al*., 2017) (Dumitrescu *et al.*, 2018) (Ramya, 2016) (Vithani *et al*., 2019b) (Awad *et al.*, 2018) (Pandey *et al.*, 2020). These materials drops solidify instantly or UV light or another heat source can further be applied for the strengthening of the deposited layer (Al-Maliki and Al-Maliki, 2015) (Awad *et al.*, 2018). Inkjet 3D printing belongs in this additive manufacturing process (Beg *et al.*, 2020) (Dumitrescu *et al.*, 2018).

Inkjet 3D printers are divided into two categories, according to the method of formation and deposition of the small drops; continuous inkjet printers (CIJ) and drop-on-demand inkjet printers (DoD) (***Table 1.7***) (Ani Jose and Christopher GV, 2018) (Vaz and Kumar, 2021) (Pandey *et al.*, 2020) (J*u et al*., 2019) (Afsana *et al.*, 2018) (Algahtani, Mohammed and Ahmad, 2019) (Haris *et al*., 2020) (Daly *et al.*, 2015). DoD is further classified into two groups, according to the printhead type, piezoelectric printers and thermal –also known as bubble– inkjet printers (***Table 1.7***) (Algahtani, Mohammed and Ahmad, 2019) (Lepowsky and Tasoglu,

2018) (Khatri, Shah and Vora, 2018) (Vithani *et al*., 2019b) (Afsana *et al.*, 2018) (Prasad and Smyth, 2016). DoD can also be divided into two other categories, according to the substrate that is used for the deposition of the droplets; drop-on-drop and drop-on-solid (***Table 1.7***) (Vaz and Kumar, 2021) (Afsana *et al.*, 2018) (Ani Jose and Christopher GV, 2018).

Nozzle-based deposition technologies are promising alternatives to address the limitations of inkjet 3D printers. In the material extrusion method, the solid materials are mixed with the binder solution prior to their loading to the equipment and then, they are passing through a small orifice in a molten or semi-liquid phase for the fabrication of the desired 3D structure (Trivedi *et al.*, 2018) (Ju *et al.*, 2019) (Awa*d et al*., 2018) (Dumitresc*u et al*., 2018) (Lepowsky and Tasoglu, 2018) (Ligo*n et al*.2017) (Khatri, Shah and Vora, 2018) (Ani Jose and Christopher GV, 2018) (Ramya, 2016). This process is independent of the substrate, unlike the powder bed inkjet 3D printing (Shende and Agrawal, 2018). Extrusion-based 3D printing and Fused Deposition Modelling are subcategories of nozzle-based deposition techniques (Tia*n et al*., 2019) (Liaw and Guvendiren, 2017) (Beg *et al.*, 2020) (Ani Jose and Christopher GV, 2018) (Khatri, Shah and Vora, 2018) (Awad *et al.*, 2018) (Ju *et al.*, 2019).

In Extrusion-Based 3D Printing, also termed semi-solid extrusion (SSE), pressure assisted microsyringe (PAM), robocasting or robotic material extrusion, cold extrusion-based printing, hydrogel-forming extrusion, melting extrusion, thermal extrusion, soft-material extrusion, melting solidification printing process, direct ink writing, hot-melt ram extrusion, hot melt pneumatic extrusion and micro-extrusion, viscous semi-solid or solid materials are loaded in a metallic or plastic syringe or cartridge based printhead. The loaded materials are extruded through a nozzle onto a glass slide, petri dish or straight onto the printing stage for the manufacture of the predetermined structure in a layer fashion through the application of consistent and low pressure (Vaz and Kumar, 2021) (Seoane-Viano *et al.*, 2021) (Ani Jose and Christopher GV, 2018) (Pandey *et al.*, 2020) (Afsana *et al.*, 2018) (Ju *et al.*, 2019). The printing platform, then, descends to be created space for the deposition of the next layer. This process is repeated until the manufacture of the predetermined architecture (Palo *et al.*, 2017). The fabricated structure solidifies either at room temperature or in an oven to obtain adequate mechanical strength (Pandey *et al.*, 2020) (Aita, Breitkreutz and Quodbach, 2020) (Wen *et al.*, 2019).

A continuous flow of extrusion can be achieved with minimum heating of the nozzle or even at room temperature (Aita, Breitkreutz and Quodbach, 2020) (Khatri, Shah and Vora, 2018) (Trivedi *et al.*, 2018) (Kyle *et al.*, 2017). Mechanical, pneumatic or solenoid pistons are applied for the extrusion of the loaded materials (Seoane-Viano *et al.*, 2021) (Palo *et al.*, 2017) (Afsana *et al.*, 2018) (Tappa and Jammalamadaka, 2018). The driving force for the materials extrusion is, thus, either a rotating screw, compressed air, or a syringe plunge, respectively (***Figure 1.10***). A UV light source is also available in this printer type and can be applied if cross-linking of the extruded materials is required (Algahtani, Mohammed and Ahmad, 2019) (Placone and Engler, 2018) (Tian *et al.*, 2019) (Ju *et al.*, 2019) (Jamróz, Szafraniec, *et al*., 2018) (Zhang *et al.*, 2018) (Trivedi *et al.*, 2018) (Cheng *et al.*, 2021). Pneumatic extrusion is usually applied for highly viscous melted polymers, while piston-driven and screw-controlled extrusion are used for highly viscous hydrogels (Afsana *et al.*, 2018) (Seoane-Viano *et al.*, 2021). The instrumentation of PAM 3D printers will be discussed in more detail in ***Chapter 2.***

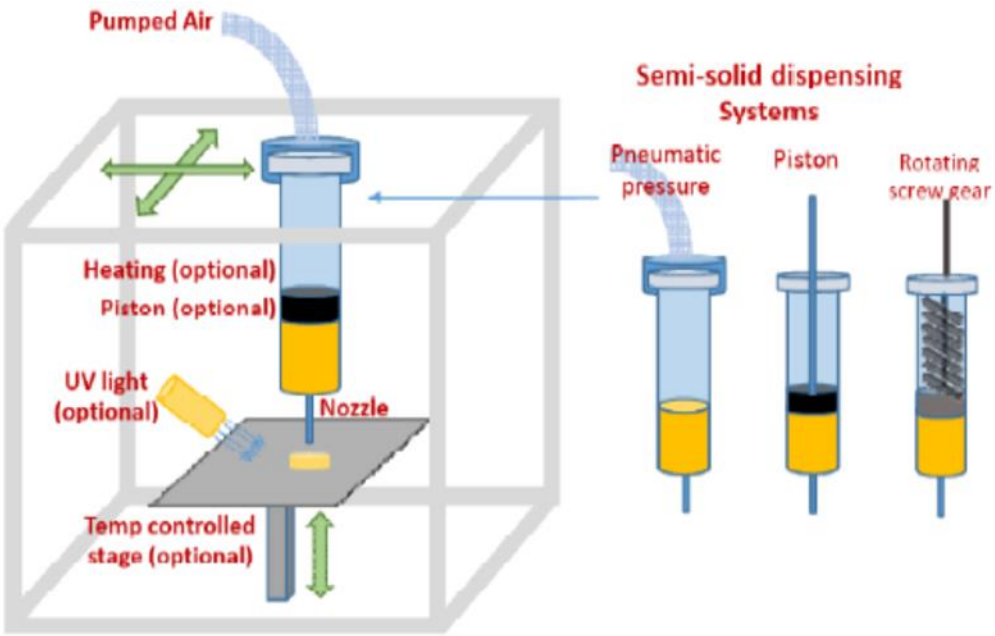

Figure 1.10: *Pressure assisted Microsyringe 3D Printing Process. This figure is reproduced from Algahtani, Mohammed and Ahmad (Algahtani, Mohammed and Ahmad, 2019).*

The main benefit of this technique that led to its selection for the current project is the fact that low temperatures are applied for the fabrication of the final objects and therefore, the usage of a wide range of thermally labile active ingredients and excipients is feasible (Wen *et al.*, 2019) (Ju *et al.*, 2019) (Dumitrescu *et al.*, 2018) (Algahtani, Mohammed and Ahmad, 2019) (Trived*i et al*., 2018) (Seoane-Viano *et al*., 2021) (El Aita *et al.*, 2020) (Vithani *et al*., 2019b) (Awad *et al.*, 2018) (Tian *et al.*, 2019) (Norman *et al.*, 2017). Formulations with high drug loading, up to 90%, can successfully be produced, while they can also be loaded with various active substances with each one demonstrating a specific release profile (Tian *et al.*, 2019) (Vithani, Goyanes, Jannin, Abdul W Bas*it, et al*., 2019b) (Dumitrescu *et al.*, 2018) (Algahtani, Mohammed and Ahmad, 2019) (Jamróz, Szafraniec, *et al*., 2018). The latter can be achieved through the fabrication of different compartments in one dosage form that will allow the loading of even incompatible active compounds in just one formulation with various drug release profiles. Complex structures, such as core and shell formulations can be built with PAM 3D printers, by first manufacturing the shell without its top, then filling it with the selected core and finally printing the top for the completion of the predesigned architecture (Elbadawi *et al.*, 2021) (Awad *et al.*, 2018) (Vithani et al., 2019b) (Algahtani, Mohammed and Ahmad, 2019) (Trivedi *et al.*, 2018) (Sadi*a et al*., 2018) (J*u et al*., 2019) (Cu*i et al*., 2020). An additional advantage of this technology is that the end objects present adequate mechanical strength compared to other 3D printing techniques. PAM printers are, also, low cost and easy to operate. These attributes make PAM 3D printing an excellent and versatile method for the fabrication of personalized medicines (Cui, Li, *et al*., 2019) (Awad *et al.*, 2018).

Shortcomings of this technology are the degradation of thermolabile active ingredients or excipients only when a high temperature is applied for the melting and the final extrusion of the loaded materials; potential post-processing of the produced formulations, such as drying, that might affect their integrity and the materials physicochemical properties (Shende and Agrawal, 2018) (Dumitrescu *et al.*, 2018) (Vithani *et al*., 2019b) (Khatri, Shah and Vora, 2018) (Algahtani, Mohammed and Ahmad, 2019) (Jamróz, Szafraniec, *et al*., 2018) (Zhang *et al.*, 2018) (Tian *et al.*, 2019).

Fused Deposition Modelling (FDM), also known as Fused Filament Fabrication (FFF) or Fused Filament Modelling, was developed to overcome the weaknesses of inkjet 3D printing (Pandey *et al.*, 2020) (Prasad and Smyth, 2016). In this

manufacturing process, thermoplastic materials are loaded in the equipment in a form of a filament that has been prepared through Hot Melt Extrusion (Lamichhane, Bash*yal, et al*., 2019) (Palo *et al.*, 2017) (Mathew, Pitzanti and Larrañeta, 2020) (Ligo*n et al*., 2017) (Vaz and Kumar, 2021) (Nasereddi*n et al*., 2018). Therefore, there is freedom regarding the materials that can be used for the manufacture of the desired object (Prasad and Smyth, 2016). Thermoplastic materials become pliable and moldable above a certain temperature and stiffen upon cooling. They can thus be heated, cooled down, and then, heated again to compose other shapes without any degradation occurring (Drumright, Gruber and Henton, 2000).

During the 3D printing process, the filament, which is fabricated with a predetermined diameter, is rolled up on a coil usually placed outside the printer. It is reaching the nozzle with the aid of two wheels that are pulling the filament inside the instrument towards the nozzle in an inward flow. The wheels are not rotating when no material needs to be deposited on the printing platform for the manufacture of an object. The nozzle is surrounded by a heating system adjusted at an appropriate temperature –close to the substances melting point- for the melting of the loaded materials and their final extrusion in the form of beads of heated plastic (Araujo *et al.*, 2019) (Sanghav*i et al*., 2016) (Ventola, 2014) (Dehghanghadikolaei, Namdari and Mohammadian, 2018) (Palo *et al.*, 2017) (Zhan*g et al*., 2018) (Vithan*i et al*., 2019) (Ramya, 2016) (Algahtani, Mohammed and Ahmad, 2019) (Haris *et al.*, 2020). The deposition of the semi-liquid material on the printing stage is performed based on the design included in the CAD file (Aita, Breitkreutz and Quodbach, 2020) (Ani Jose and Christopher GV, 2018) (Tian *et al.*, 2019) (Chia and Wu, 2015). The filament rapidly solidifies after it goes out of the nozzle, while the bed descends to be created space for the deposition of the subsequent layer according to the CAD file. These steps are repeated until the manufacture of the desired object (Lamichhane, Bashyal, *et al*., 2019) (Bahnin*i et al*., 2018) (El Aita *et al.*, 2020) (Afsana *et al.*, 2018) (Al-Maliki and Al-Maliki, 2015) (Hofinger, 2011) (Haris *et al.*, 2020) (Ramya, 2016) (Vaz and Kumar, 2021).

The printhead in the FDM printers is similar to the one used in inkjet printers (Ventola, 2014). The solid filament behaves like a piston and pushes the semi-molten filament through the nozzle. The nozzle in the FDM is moving in two directions, X and Y, for the building of the predesigned structure, while the building stage is moving in one direction, Z, for the adjustment of the height of each layer of the final product (***Figure 1.11***) (Vaz and Kumar, 2021) (Ramya, 2016) (Trivedi

et al., 2018) (Algahtani, Mohammed and Ahmad, 2019) (Al-Maliki and Al-Maliki, 2015). The instrumentation of the FDM 3D printers will extensively be presented in ***Chapter 2.***

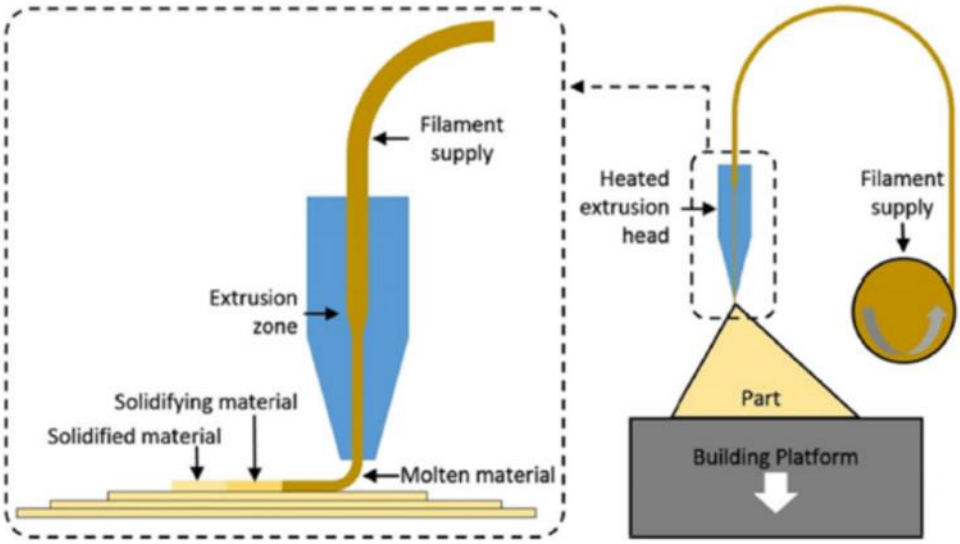

Figure 1.11: *Fused Deposition Modelling 3D Printing Process. This figure is reproduced from Vaz and Kumar (Vaz and Kumar, 2021).*

The main advantage of FDM technology that contributed to its selection for this study is that the layer thickness, size, porosity and weight of the produced object are accurately regulated and that makes the printing process highly reproducible (Pandey *et al.*, 2020) (Tappa and Jammalamadaka, 2018) (Chia and Wu, 2015). The loaded active agent is homogeneously distributed in the end formulation, while high resolution, mechanical strength and dosing accuracy are attained as well (Algahtani, Mohammed and Ahmad, 2019) (Ani Jose and Christopher GV, 2018) (Vitha*ni et al*., 2019b). Therefore, the FDM 3D printing method demonstrates remarkable properties for its application in the pharmaceutical field for the manufacture of personalized medicines (Zhang *et al.*, 2018) (Chia and Wu, 2015) (Pal*o et al*., 2017). Moreover, no addition of solvents is necessary for the formation of the desirable filament (Shende and Agrawal, 2018) (Dumitrescu *et al.*, 2018) (Palo *et al.*, 2017) (Vaz and Kumar, 2021).

The fabrication of dosage forms with complex geometries and well-distinct parts is feasible with these 3D printers, enabling the loading of various active

compounds in one drug delivery device exhibiting various drug release profiles (Zhang *et al.*, 2018) (Algahtani, Mohammed and Ahmad, 2019) (Awad *et al.*, 2018) (Trived*i et al*., 2018) (Dumitrescu *et al.*, 2018) (Ani Jose and Christopher GV, 2018) (Palo *et al.*, 2017) (Pandey *et al.*, 2020) (J*u et al*., 2019). Hollow structures can be fabricated and later loaded with liquid, semi-solid or solid materials, such as the active compounds to avoid their degradation due to the application of high temperatures during the printing process (Algahtani, Mohammed and Ahmad, 2019) (Trivedi *et al.*, 2018) (Vithani, Goyanes, Jannin, Abdul W *Basit, et al*., 2019b) (Dumitrescu *et al.*, 2018). Additional benefits of this technology are the fact that only very low amounts of the starting material are wasted, while no post-printing processing is required since the final structure is dry and can be used immediately (Dehghanghadikolaei, Namdari and Mohammadian, 2018) (V*ithani et al*., 2019b) (Palo *et al.*, 2017) (Algahtani, Mohammed and Ahmad, 2019) (Zhang *et al.*, 2018). Furthermore, this printer type is a compact size, cheaper and easier to operate contrasted with other 3D printers (Ventola, 2014) (Eshkala*k et al*., 2020) (Afsan*a et al*., 2018) (Hoque, Chuan and Pashby, 2011) (Awad *et al.*, 2018) (Haris *et al.*, 2020).

Nevertheless, the main weakness of this technology is the high temperature applied for the melting of the filament, which is not suitable for heat-sensitive active agents or living cells (Linares, Casas and Caraballo, 2019) (Sadi*a et al*., 2018) (Chia and Wu, 2015) (Awad *et al.*, 2018) (Araujo *et al.*, 2019) (Trivedi *et al.*, 2018) (Vithani *et al*., 2019b) (Algahtani, Mohammed and Ahmad, 2019) (Pandey *et al.*, 2020) (El Aita *et al.*, 2020). Moreover, there is not a wide variety of materials that demonstrate sufficient viscosity in order to be used in this technology, while the materials need to be in a filament form to be loaded to the FDM printers (Ju *et al.*, 2019) (Ani Jose and Christopher GV, 2018) (Vithani, Goyanes, Jannin, Abdul W Basit, *et al*., 2019b) (Eshkalak *et al.*, 2020) (Awad *et al.*, 2018) (Chia and Wu, 2015).

Hot Melt Extrusion (HME) is the technology used for the fabrication of the drug loaded filaments that will be later loaded to the FDM 3D printers. In this technique, the active agent is initially blended with a polymer, the chosen active substance and excipients. The next stage involves the loading of the mixture to the hot melt extruder; the final step is the production of the desired filament with a predetermined shape, density and dimensions through a screw-based extrusion system placed in a barrel by the application of elevated temperature. A motor is used for the screw operation, while heat and shear are applied for a homogeneous

mixture to be obtained without agglomerations. The produced filament solidifies either at room temperature or with the use of air, while it is packed in a coil (Moulton and Wallace, 2014) (Vaz and Kumar, 2021) (Vithan*i et al*., 2019) (Araujo *et al.*, 2019) (Censi *et al.*, 2018). The instrumentation of Hot Melt Extruders, which is one of the instruments used in the current study, will extensively be presented in ***Chapter 2***.

Hot Melt Extrusion is also a solvent-free method and its main advantage is that it condenses many steps into one consecutive process, which enhances considerably the manufacturing efficiency (Greha*n et al*., 2014). By fabricating filaments that will later be loaded to the FDM 3D printers, higher drug loading and improved solubility of poorly soluble active compounds are easily achieved (Palo *et al.*, 2017) (Vit*hani et al*., 2019b). The combination of Hot Melt Extrusion with FDM 3D Printing is also recommended by the FDA (Zhang *et al.*, 2018).

1.4.3. Regulatory Aspects of 3D Printing

Additive Manufacturing is particularly promising for the manufacture of dosage forms and especially, personalized ones, as previously mentioned. The variety of the available 3D printing technologies could facilitate the fabrication of a range of formulation types with unique characteristics, based on patient needs and characteristics. Nevertheless, this method is still in its initial stages and no substantive regulatory framework has been issued yet by any regulatory agency regarding the safety and efficacy of on-demand 3D printed medicines (Vaz and Kumar, 2021) (Zema *et al.*, 2017) (Lamichhane, Bashyal, *et al.*, 2019) (G. Chen *et al.*, 2020) (Gioumouxouzis, Karavasili and Fatouros, 2019) (Araujo *et al.*, 2019) (Seoane-Viano *et al.*, 2021).

The FDA published in 2017, guidance for the fabrication of printed medical devices entitled "Technical Considerations for Additive Manufactured Medical Devices" (FDA, 2017). Software and hardware requirements, device design, material controls, post-processing, quality control, process validation, acceptance criteria cleaning and sterilization requirements are some elements of additive manufacturing that were considered and guidelines were issued for them (FDA, 2017) (Zema *et al.*, 2017) (Jamróz, Szafraniec, *et al.*, 2018) (Preis and Öblom, 2017).

To date, more than 200 3D printed medical devices with the aim to fit individuals anatomy have been approved by the FDA, contrasted with only one 3D printed solid dosage form, Spritam® (by Aprecia Pharmaceuticals), for the treatment of epilepsy in adults and children (West and Bradbury, 2019) (Vaz and Kumar, 2021) (Gioumouxouzis, Karavasili and Fatouros, 2019) (Han *et al.*, 2018) (Lamichhane, Bashyal, *et al.*, 2019). The printed formulations should meet the requirements described in the current manufacturing and control guidelines for medicines and medical devices in order to be approved today (Jamróz, Szafraniec, *et al.*, 2018). For example in the case of Spritam®, excipients contained in conventional tablets were used for its fabrication, while the ZipDose® technology applied demonstrates more similarities with the traditionally used powder compaction and mass manufacturing procedures of conventional tablets, unlike the other printing techniques. The approval of this 3D printed formulation, thus, was referring more to a new mass production of equivalent medicine, rather than that of a precision medicinal formulation and it could be approved with the current regulations (Araujo *et al.*, 2019) (Han *et al.*, 2018) (Seoane-Viano *et al.*, 2021) (Preis and Öblom, 2017).

Additive manufacturing is different from the widely applied pharmaceutical processing methods regarding its principles, operation and processing of the materials for the production of the medicines (Lamichhane, Bashyal*, et al*., 2019). Consequently, regulatory guidelines specifically applied to the manufacture of 3D printed formulations are required, while their design and manufacturing procedures, as well as, their quality testing are major aspects that should be considered; crucial settings having an impact on the printability of the materials used for the fabrication of the formulations, crucial process settings for each 3D printing technique, evaluation of the performance of the printed dosage forms, selection of a suitable *in vitro* drug release method, sterilization issues and crucial attributes of intermediate products (such as filaments or inks used for printing) (Lamichhane, Bashyal, *et al.*, 2019) (Jamróz, Szafraniec*, et al*., 2018). As mentioned in the FDA guidance issued for the manufacture of medical devices, though, each 3D printing technique has a unique principle with a different set of parameters being critical for the production of the desired object, as well as, different types of post-processing are required. Guidelines, thereby, for each printing technology used for the production of dosage forms seem more suitable to be issued separately (Jamróz, Szafraniec, *et al.*, 2018) (Ha*n et al*., 2018).

Apart from the technical aspects of this pharmaceutical processing method, the properties of the selected active agent, such as amorphicity/crystallinity, its stability (due to the application of high temperatures), potential incompatibilities, interactions with the other materials used, before and after the printing procedure should also be considered and specified in the guidelines, as they could have a considerable impact on the final medicinal product (Jamróz, Szafraniec*, et al.*, 2018) (Zema *et al.*, 2017).

Additional concerns are raised by the application of additive manufacturing in personalized medicine, enabling the fabrication of medicines not only in the pharmaceutical industry, but also at the point of care, such as community pharmacy and hospital pharmacy (G. Chen *et al.*, 2020) (Araujo *et al*., 2019) (Zema *et al.*, 2017) (Trived*i et al*., 2018). The regulatory guidance that should be followed in each production site should, hence, be specifically applied to each one of them. However, the quality of the product and the patients safety are factors that cannot be compromised and they need to be ensured that are covered by the guidelines (Zem*a et al*., 2017) (Trivedi *et al.*, 2018) (Preis and Öblom, 2017). The printing of QR codes on the surface of the formulations as a means of track-and-trace could particularly contribute to the achievement of the previously mentioned crucial goal (Seoane-Viano *et al*., 2021).

In the UK, the Medicines and Healthcare products Regulatory Agency (MHRA) is planning to issue a regulatory framework for the Point Of Care (POC) manufacturing in which the use of 3D printers for the fabrication of medicines could fit. For this purpose, MHRA had published a relevant proposal open to consultation from the beginning of August 2021 until the end of September 2021 (MHRA, 2021). Several aspects of the production of the POC products were covered in this initial proposal considering the differences that exhibit with the conventional dosage forms. This framework will be the first regulation issued in the world for this rapidly evolving field of innovation.

The short shelf life of the POC medicines due to their immediate administration creates the necessity of their fabrication at a large number of sites, in close proximity to the patient, rather than their mass production (scale-up approach). Control measures, preferably during the manufacturing process and prior to the medicines use, will, thus, be considered in the new legislation for this scale-out approach. Specifications regarding the traceability, as well as, the comparability between the different batches and the products among the wide range of the

manufacturing sites are planned to be established for the quality, safety and efficacy of the final medicinal products to be assured. Guidelines for the requirements that the manufacturing sites need to meet for their authorisation and subsequent inspection will also be considered since, as previously mentioned, various locations are promising candidates for POC manufacture, such as primary healthcare facilities, pharmacies, operating theatres, ambulances, clinics, military field hospitals or even patients homes. Specific criteria that will need to be met regarding the qualification of the used equipment, the validation of the process and the quality attributes of the starting materials are under discussion in the POC manufacturing proposal (MHRA, 2021).

Consequently, the fact that the application of additive manufacturing in the pharmaceutical area could considerably improve patient treatment, compliance and hence, quality of life with the production of bespoke medicines indicates that the next step of this development process is the issue of a regulatory framework. Healthcare regulatory agencies seem to be targeting this direction.

1.4.4. Applications in drug loaded formulations

3D printing technologies, as previously mentioned, have gained much popularity the recent years for the fabrication of various dosage forms and their potential to address the limitations of traditional drug delivery systems (Musazzi *et al.*, 2018). Different types of 3D printing techniques have been explored regarding their printing capabilities; the fabrication of complex internal and external architectures, such as doughnut-shaped, multi-layered, hollow structures; the impact of the formulation shape, such as sphere, torus, cube, disc, oval, pyramid, cylinder, on the release rate of the loaded active ingredient; the production of drug delivery devices containing various active compounds in different compartments or layers; the manufacture of formulations demonstrating controlled drug release mechanisms, such as immediate release tablets, delayed-release tablets, capsules, polypills, hydrogels, implants, patches, microneedles, enteric release tablets, zero order release tablets, fast disintegrating tablets, biphasic release tablets, monolithic sustained release tablets, and pulsatile drug release tablets (Economidou, Lamprou and Douroumis, 2018) (Cui *et al.*, 2020) (Ju *et al.*, 2019) (Khatri, Shah and Vora, 2018) (Shende and Agrawal, 2018) (Yu

et al., 2009) (Jamróz, Szafraniec, *et al.*, 2018) (Martinez *et al.*, 2017) (Katstra *et al.*, 2000) (Martinez *et al.*, 2018) (G. Chen *et al*., 2020).

Various types of dosage forms have been fabricated through different additive manufacturing processes demonstrating their versatility; tablets, hydrogels, and microneedles have been produced through SLA; SLS has been applied for the fabrication of orally disintegrating tablets, immediate release tablets, sustained release tablets, small oral dosage forms, named miniprintlets, printed with bespoke release profiles, various internal and external geometries, such as cylinders, torus, gyroid lattices or bilayer architectures or/and containing multiple active substances with each one having a well-defined drug release mechanism; modified-release tablets have been manufactured by using DPL technology (Kadry *et al.*, 2019) (Fina, Madla, *et al.*, 2018) (Martinez *et al.*, 2017) (Hamed *et al.*, 2021) (Pissinato Pere *et al*., 2018) (Fina *et al.*, 2017) (Healy *et al.*, 2019) (Sarah J Trenfield *et al.*, 2018) (Awad *et al.*, 2019) (G. Chen *et al*., 2020) (Fina, Goyanes, *et al.*, 2018) (Wang *et al.*, 2016) (Yang *et al.*, 2021).

Inkjet 3D printing is one of the additive manufacturing technologies that has been broadly explored for its applications in the pharmaceutical field and it has exhibited attractive outcomes for the manufacture of personalized dosage forms, such as tablets and oral films (Buanz *et al.*, 2015) (Sandler *et al.*, 2011) (Hirshfield *et al.*, 2014). Tablets without the addition of toxic organic solvents, but only with the use of water have been produced using inkjet 3D printing; tablets with predictable and controlled drug release mechanisms have been investigated; medical-graded orodispersible formulations have been studied regarding the delivery of active and non-active ingredients (Scoutaris *et al.*, 2011) (Planchette *et al.*, 2016) (Cader *et al.*, 2019) (Clark *et al.*, 2017) (Hammud *et al.*, 2013) (Zhang, Willis-fox and Daly, 2021). Various infill percentages have been applied during the fabrication of beeswax tablets through a solvent-free inkjet printing method showing that formulations with tunable drug release profiles can successfully be produced (Kyobula *et al.*, 2017). The fabrication of tablets using powder bed-based inkjet 3D printing has also been performed, while the printability of various types of binder inks has been investigated (Infanger *et al.*, 2019).

The production of data-enriched edible pharmaceuticals (DEEP) has been shown to be feasible with a desktop inkjet 3D printer. These formulations had on their surface 3D printed Quick Response (QR) code patterns that contained information related to the dosage form enabling the more effective drug-labelling and

traceability, as well as, safer treatment therapies. In this way, package labelling can be replaced, while the printed information can be read by the patient using a standard smartphone (Öblo*m et al*., 2020) (Trenfield *et al.*, 2019) (Edinger *et al.*, 2018).

Hot Melt Extrusion and FDM 3D printing have been combined in several studies for the manufacture of mainly oral dosage forms, such as sustained release tablets, floating tablets, controlled release tablets, capsular devices, pulsatile release tablets, zero order release tablets, immediate release tablets, but also multi-layered films and intravaginal rings. The fabrication of various types of architectures has also been explored, such as shell-core structures and hollow cylinders (Okwuosa *et al.*, 2017) (Melocchi *et al.*, 2015) (Zhang, Yang, *et al.*, 2017) (Lang, Mcginity and Williams III, 2014) (Genina *et al.*, 2017) (Tan, Maniruzzaman and Nokhodchi, 2018) (Stanković, Frijlink and Hinrichs, 2015) (Nashed, Lam and Nokhodchi, 2021) (Korte *et al.*, 2018) (Weisman *et al.*, 2015) (Fu, Yu and Jin, 2018) (Chai *et al.*, 2017). In most studies, more than one polymer has been used to facilitate their extrusion; HPMCAS, PCL, PLA, PEO, PVP, PVA, polyvinylpyrrolidone-vinyl acetate copolymer (PVP-VAc), hydroxypropyl cellulose (HPC), ethylene vinyl acetate (EVA), ethylcellulose (EC), and thermoplastic polyurethane (TPU) (Fanous *et al.*, 2020) (Fuenmayo*r et al*., 2018) (Tiboni *et al.*, 2021) (Kimura *et al.*, 2019) (Okwuosa *et al.*, 2017) (Goyanes *et al.*, 2018) (Genin*a et al*., 2016) (Öblom *et al.*, 2019) (Ilyés *et al.*, 2019) (Kempin, Domsta, Grathoff, *et al*., 2018) (Zhan*g et al*., 2020) (Martin *et al.*, 2021) (Chai *et al.*, 2017). Various combinations of polymers or polymer-drug mixtures with or without the addition of plasticizers have been investigated regarding their extrudability, printability, drug loading capability with the final aim of fabricating drug loaded formulations demonstrating the desired drug release profiles (Henry *et al.*, 2021) (Verstraete *et al.*, 2016) (Zhang, Feng, *et al.*, 2017) (Isreb *et al.*, 2019) (Melocchi *et al.*, 2016) (Saviano *et al.*, 2019) (Boetker *et al.*, 2016) (Solanki *et al.*, 2018) (Sandler *et al.*, 2014) (Wei *et al.*, 2020). Filaments without the addition of any excipients with high drug loading have successfully been manufactured (Đuranovic *et al.*, 2021) (Goyanes, Fina, *et al.*, 2017) (Kadry *et al.*, 2018). The use of HME for the production of the proper material form that will be loaded to the FDM was proven to be especially beneficial for poorly soluble active agents or drugs with a narrow therapeutic index (Arafat, Qinna, *et al.*, 2018) (Huang *et al.*, 2016) (Jamróz, Kurek, Łyszczarz, Szafraniec, *et al.*, 2017).

FDM 3D printing studies have also been performed with the use of commercially available filaments for the manufacture of different types of dosage forms, such as tablets, microneedles, capsules, gastrofloating tablets, multi-layered tablets and suppositories, incorporating one or several active ingredients and printed with various internal and external structural attributes, such as size, shape –cube, pyramid, torus, cylinder, sphere, cone-, and printing parameters. The release of the loaded active agent, immediate, enteric, pulsatile, sustained or zero order, was shown to be a function of these parameters and therefore, demonstrated the capability of this printing method to be used for the fabrication of dosage forms based on the biological, physical and medical needs of each patient (Goyanes *et al.*, 2014) (Tagam*i et al*., 2018) (Sadia, Isreb, *et al.*, 2018) (Tan *et al.*, 2020) (Luzuriaga *et al.*, 2018) (Goyanes, Chang, *et al.*, 2015) (Lim *et al.*, 2016) (Arafat, Qinna, *et al.*, 2018) (Maroni *et al.*, 2017) (D. Smith *et al*., 2018) (Goyane*s et al*., 2015) (Tagami *et al.*, 2017). Commercially available polymers used in previous studies were PVA, ABS and PLA (Jie *et al.*, 2021) (Huanbutta and Sangnim, 2019) (Skowyra, Pietrzak and Alhnan, 2015) (Jamróz, Kurek, *et al.*, 2018) (Sun and Soh, 2015) (F*u et al*., 2018) (Linares, Casas and Caraballo, 2019) (Tagami, Hayashi, *et al.*, 2019).

Physical features of the produced formulations, as well as, printing parameters, such as print temperature, infill density/percentage, infill pattern, layer, shell, wall or formulation thickness/height, have been explored regarding their influence on the release of the loaded active substances (Lamichhane, Park, *et al.*, 2019) (Chai *et al.*, 2017) (Okwuosa *et al.*, 2017) (Fanous *et al.*, 2020) (Bec*k et al*., 2017) (Fuenmayor *et al.*, 2019) (Zhang, Yang, *et al.*, 2017) (Korte and Quodbach, 2018) (Kimura *et al.*, 2019). In previous research works, it has been demonstrated that with the FDM technology, the drug release rate of the 3D printed tablets can easily be adjusted and mimic the release rate of the commercially available dosage forms without the addition of any filling or disintegrant excipients. That has been achieved by modifying the printing parameters and the physical attributes of the printed formulation, such as the shape, size, infill percentage, infill pattern, tablet thickness or by creating channels of various width, lengths and in various positions in the fabricated dosage forms (Sadia, Arafat*, et al*., 2018) (Gültekin, Tort and Acartürk, 2019) (Ayyoubi *et al.*, 2021) (Y. Yan*g et al*., 2018) (Goyanes, Buanz*, et al*., 2015) (Nukala *et al.*, 2019) (Chai *et al.*, 2017) (Eleftheriadis *et al.*, 2021) (Palekar *et al.*, 2019) (Verstraete *et al.*, 2016) (Öblom *et al.*, 2019). Bilayer tablets containing in each layer (of predetermined thickness) one specific active ingredient that was released with a distinct release mechanism have been

produced with FDM 3D printing (Tabriz *et al*., 2021) (Sadia, Isreb, *et al*., 2018). The manufacture of immediate release tablets at low temperatures demonstrated that the FDM technique can be used even for the printing of formulations incorporating thermally sensitive active agents (Kollamaram *et al.*, 2018) (Kempin, Domsta, Grathoff, *et al.*, 2018) (Kollamaram *et al.*, 2018) (Okwuosa *et al.*, 2016) (Patel and Serajuddin, 2021). Taste-masking of multi-layered tablets has successfully been achieved through HME and FDM 3D printing showing the capability of these technologies to be used for the fabrication of paediatric dosage forms (Ehtezazi *et al.*, 2018) (Tiwari, Patil and Repka, 2016) (Scoutaris, Ross and Douroumis, 2018).

Complex internal geometries can easily be manufactured using an FDM 3D printer; the fabrication of dosage forms with several compartments, with each one containing a specific polymer or active compound, for better control of drug release has been shown to be feasible (Gioumouxouzis *et al.*, 2017) (Jamróz *et al*., 2020) (D. Chen *et al.*, 2020) (Genina *et al*., 2017) (Gioumouxouzis, Baklavaridis, *et al.*, 2018) (Maroni *et al*., 2017). Double-chamber dosage forms, termed DuoTablets, where a tablet was encapsulated in another larger tablet have been printed using an FDM printer. In this way, more efficient control of the drug release mechanism was obtained (Li *et al.*, 2018) (Goyanes, Wang, *et al.*, 2015). Shell-core tablets with various shell thicknesses have been investigated for the impact of the coating-shell on the release of the encapsulated active substance (Kempin, Domsta, Brecht, *et al.*, 2018) (Dumpa, Bandari and Repka, 2020). Shell-core structures can be filled with either solid or liquid drug loaded formulations (D. M. Smith *et al*., 2018) (Gioumouxouzis, Chatzitaki, *et al.*, 2018). Tablets with interconnected blocks have successfully been produced with this additive manufacturing process. The size of the block, the number of the bridges, as well as, the gap between the blocks played a significant role in the release rate of the incorporated active agent (Arafat, Wojsz, *et al*., 2018). The impact of the shape of the printed dosage form on the drug release has been studied, as well, while it has been presented that the surface area/volume ratio was the factor that mainly affected the release of the loaded active compound (Goyanes *et al*., 2015) (Obeid *et al.*, 2021). The above studies, therefore, make FDM an attractive additive manufacturing process for the production of bespoke medicines that is difficult to be done with the conventional pharmaceutical methods. Tablets printed by an FDM 3D printer in various shapes, sizes and colours have also been investigated regarding their selection and ease of swallowing by the patients. Patients' good

acceptability was indicative of the potential of additive manufacturing to be applied for individualized therapies (Goyane*s et al*., 2017).

PAM 3D printing has been proven to be a promising alternative method of the conventional pharmaceutical processing technologies, such as powder compression tabletting; tablets with high drug loading have successfully been manufactured; multi-layered tablets containing different active ingredients in each layer with each one having a distinct drug release mechanism have been produced without the application of high temperature, but at room temperature; the fabrication of controlled release tablets, such as sustained release, as well as, immediate release, orodispersible films, chewable printlets, biodegradable patches, gastrofloating tablets, solid self-emulsifying formulations have been investigated (Conceição *et al.*, 2019) (Khale*d et al*., 2018) (Aita, Breitkreutz and Quodbach, 2019) (Tagami, Ando, *et al*., 2019) (Vithani, Goyanes, Jannin, Abdul W *Basit, et al*., 2019a) (Seoane-Viano *et al.*, 2021) (Khaled *et al.*, 2014) (Cheng *et al.*, 2021) (Pereira *et al.*, 2021) (Cui *et al.*, 2020) (Elbadawi *et al.*, 2021) (El Aita *et al.*, 2020) (Yi *et al.*, 2016). Tablets without the addition of any organic solvent, but only water, have successfully been fabricated with pressure-assisted microsyringe 3D printing (Aita, Breitkreutz and Quodbach, 2020).

In other studies of PAM 3D printing, the impact of the selected materials, the printing parameters, as well as, the design features of the produced devices on the release of the incorporated active compounds have been explored (Zidan, Alayoubi, Coburn, *et al.*, 2019) (Vithani, Goyanes, Jannin, Abdul W Basit, *et al*., 2019a) (Cui, Yang, *et al.*, 2019) (Zidan, Alayoubi, Asfari, *et al.*, 2019). The fabrication of tablets with different internal and external geometry have been demonstrated to play a significant role in the release of the loaded active compound (Shaban A Khaled *et al.*, 2018) (We*n et al*., 2019). The infill percentage in gastrofloating tablets has been shown to affect the period that the formulations were remaining in the gastric juice (Li *et al.*, 2018). In another work, the infill percentage has been demonstrated as an attractive printing parameter for the control of the release rate of the encapsulated active agent (Cu*i et al*., 2020). The printing patterns and the grid width of 3D printed tablets had a considerable impact on the release rate of the incorporated active ingredient (Cui, Yang, *et al.*, 2019). The surface area/mass ratio was another parameter that has been shown to affect the delivery of the active compound (Cui, Li, *et al.*, 2019). These applications indicated, as well, that the fabrication of bespoke medicines is feasible with additive manufacturing even for thermally labile active agents.

Materials mostly selected for the manufacture of drug delivery devices with PAM 3D printers were polymers, such as PLA, PCL, PVP, PVA, PEG, polyvinylpyrrolidone-vinyl acetate copolymer (PVP-VAc), hydroxypropyl methylcellulose (HPMC) (Aita, Breitkreutz and Quodbach, 2019) (Aita, Breitkreutz and Quodbach, 2020). Lipid excipients have recently been investigated for their potential to be used as matrices for the fabrication of solid lipid tablets for the delivery of highly hydrophobic active substances. The printing process has been performed at room temperature, suggesting that heat-sensitive active agents can be used in PAM 3D printers (Johannesson *et al.*, 2021). Food pastes have also been used for the production of chocolate based paediatric-friendly oral dosage forms loaded with both hydrophobic and hydrophilic active ingredients (Karavasil*i et al*., 2020). The use of food pastes for the production of dosage forms through semi-solid extrusion highlighted, thus, the remarkable capabilities of the investigated additive manufacturing process.

One of the most revolutionary applications of 3D printing technologies and more specifically of pressure assisted microsyringe, was the manufacture of a polypill that contained three different active agents in separate parts of the formulation. The loaded active substances have successfully been delivered through two different release mechanisms; drug release by osmosis via the shell which exhibited controlled porosity and drug release by diffusion via the gel layers (Shaban A Khaled *et al.*, 2015). Another polypill has been produced demonstrating the potential of additive manufacturing to be applied in personalized medicine to meet the needs and characteristics of each patient. In this study, five different active agents were loaded in well-distinct compartments of a tablet. Two independent release profiles, sustained and immediate, have been managed to be included in just one dosage form, while a series of elevated dots were printed on the top of the polypill to enable its easier visual identification, as well as by touch (Khale*d et al*., 2015). These two polypills were only the beginning for the manufacturing of other polypills by exploring various combinations of materials used as matrix, as well as, active agents that can be printed and subsequently loaded to the desired dosage form (Siyawamway*a et al*., 2019) (Pereir*a et al*., 2019) (Goh *et al.*, 2021). A polypill has also been fabricated with SLA where a multi-layered tablet has been printed and contained six different active compounds (Robles-Martinez *et al.*, 2019).

A small scale clinical trial has recently been conducted in hospitalised paediatric patients using chewable dosage forms with different flavours and colours produced by a PAM 3D printer. Patients' acceptability was good, even though they exhibited different preferences regarding the formulations colour and flavours. This study, thereby, indicated that additive manufacturing can successfully be applied in hospitals for the fabrication of patient-centric oral dosage forms in a simple, fast and automated way (Go*yanes et al*., 2019).

Additive manufacturing has recently drawn considerable interest in the fabrication of drug-eluting implants, while PLA, PLGA and PLLA are the most widely selected materials (Yang *et al.*, 2020) (Wang *et al.*, 2020) (Water *et al.*, 2015) (W*u et al*., 2009) (Salim*i et al*., 2020). An FDM 3D printer has been used for the production of PLA implants of slender bullet shape with a hollow structure available for drug loading and a porous surface; HME and FDM have been combined for the initial production of a polymeric filament which would later be used for the manufacture of hollow implants with PVA "windows" on their surface; inkjet 3D printing has been applied for the manufacture of implants with complex drug release profiles; powder bed-based inkjet 3D printing has been used for the fabrication of implants composed of PLLA in various shapes, a multi-layered concentric cylinder, doughnut shaped (Huang *et al.*, 2007) (Yan*g et al*., 2018) (Wu *et al.*, 2016) (Stewart, Dom, Mcilorum, Mancuso, *et al.*, 2020) (Wu *et al.*, 2014) (Katstra *et al.*, 2000).

1.4.5. Applications of FDM and PAM 3D Printing in Implants Containing Lidocaine and Polycaprolactone

Polycaprolactone has recently gained much popularity in the manufacture of 3D printed dosage forms. One of the main reasons that this material was not selected for further research for approximately two decades was its extended degradation time that can not be applied in the production of immediate release formulations that were mostly investigated in the past. Nevertheless, this property is the most desirable one for the fabrication of sustained release dosage forms and polycaprolactone exceeded in that compared with the most commonly used polymers (Woodruff and Hutmacher, 2010a) (Dash and Konkimalla, 2012) (Azimi *et al.*, 2014). Only a few studies have previously been conducted using PCL for

the production of implantable devices through either HME and FDM or pressure assisted microsyringe, which are the selected 3D printing technologies for the current work.

In most studies, though, PCL has been mixed with other polymers or solvents for the enhancement of its rheological and thermal properties. Hot Melt Extrusion has been used for the fabrication of implants at a low temperature, 55 ºC. The matrix of that formulation consisted of a multiblock copolymer PEG-PCL, while lysozyme was incorporated in the matrix (Stankovic *et al.*, 2013). PEG-PCL blend has, also, been used in the production of praziquantel loaded implants via Hot Melt Extrusion (Cheng, Lei and Guo, 2010). The latter process has been applied in another work for the fabrication of polymeric implants consisted of polycaprolactone and pluronic F68 and loaded with levonorgestrel (Sun *et al.*, 2006) (Ma *et al.*, 2006). Polymeric filaments composed of PCL, mannitol, PEG, triethyl citrate (TEC), microcrystalline cellulose (MCC) and dexamethasone have been extruded, as well, using the same technique (dos Santos *et al.*, 2021). In another study, PCL filaments loaded with a fluorescent dye, quinine, have been produced using HME technology, for their subsequent use in an FDM 3D printer for the manufacture of implants. In this case, though, organic solvents were used for the materials mixing; the polymer was mixed with methylene chloride, while quinine was dissolved in ethanol. Then, the mixing of the polymeric and drug solutions followed and that blend was later loaded to the extruder (Kempin *et al.*, 2017). HME and FDM have also been combined for the extrusion of doxycycline loaded PCL filaments at a relatively low temperature, 70 ºC, and the final fabrication of femoral implants (Benmassaoud *et al.*, 2019). T-shaped polycaprolactone prototypes of an intrauterine system (IUS) loaded with indomethacin have been produced by using FDM 3D printing as an extension of the HME technology (with an extrusion temperature of 100 ºC) (Holländer *et al.*, 2016).

Pressure assisted microsyringe 3D printing was another additive manufacturing process explored for the manufacture of polycaprolactone implants. Nevertheless, processing of the selected compounds to obtain a more suitable for extrusion form has been performed; PCL and valproate have been mixed for a paste to finally be attained. This semi-solid form has been loaded into the syringe for the subsequent fabrication of drug loaded polymeric implants (Kammerer *et al.*, 2011).

The impact of PCL coating on the prolonged release of the encapsulated active compounds has only recently been investigated. Polymeric hollow implants made

of PLA and PVA have been produced using an FDM 3D printer in which a PLA-PVA filament fabricated through Hot Melt Extrusion has been loaded. Polycaprolactone has been mixed in various concentrations with PEG and has been used for the coating of the 3D printed devices that have been loaded with ibuprofen sodium or methylene blue (Stewart, Dom, Mcilorum, Gonzalez, *et al.*, 2020).

Lidocaine, though, has not extensively been used in 3D printing applications. Lidocaine extrudability has initially been investigated by blending it with hydroxypropyl cellulose and hydroxypropyl methyl cellulose (Repka *et al.*, 2005). Lidocaine loaded polycaprolactone filaments have later been manufactured through Hot Melt Extrusion. Nevertheless, the salt state of lidocaine has been used in that case (Perale *et al.*, 2010). In another work, pneumatic extrusion-based 3D printing was the chosen method for the fabrication of polycaprolactone scaffolds loaded with Ag_3PO_4 and lidocaine. However, an organic solvent, dichloromethane, has been used for the effective blending and preparation of the slurry that has been loaded to the microsyringe of the 3D printer (Shao *et al.*, 2018).

1.5. AIMS AND OBJECTIVES

The aim of this study is the 3D printing of polymeric drug-eluting implants at the lowest temperature possible using a solvents-free and excipients-free method for the production of sustained drug release formulations that can be used in personalized therapies. The selected polymer is polycaprolactone because of its properties, namely, low melting point, ease of processability and prolonged degradation rate, while lidocaine is the chosen model drug as its melting point is close to PCL's. As previously discussed, only very few studies have been conducted using these materials under the suggested conditions of the current project. More specifically, PCL has not been used in a solvent-free or excipient-free system for hot melt extrusion-based 3D printing. Lidocaine base form has been selected for the present study different from the majority of the previously conducted studies and the commercially available formulations. The objectives of this research will be presented below.

The printability of two different molecular weight PCL was explored using two additive manufacturing technologies, Fused Deposition Modelling (FDM) and Pressure Assisted Microsyringe (PAM) 3D printing, as well as the application of

several combinations of printing parameters for the production of a simple geometrical shape. The filament loaded to the FDM 3D printer will be fabricated through Hot Melt Extrusion (HME), while its extrudability will be investigated by using various extrusion settings without the addition of any solvents. Physical and chemical characterizations (DSC, XRD) on the manufactured filaments and objects will follow to study the impact of extrusion and 3D printing on the physical state and thermal properties of polycaprolactone. Based on the initial assessment of the polymer extrusion and the subsequent evaluation of the printing resolution of the produced architectures, the most promising manufacturing method, parameters and molecular weight polymer will be selected for the next stage of the research.

Polymeric implants loaded with different concentrations of the selected model drug will be printed in different geometries (discs and core-shell structures) after optimization of the printing parameters for homogeneous and compact formulations able to lead to prolonged drug release to be obtained. The latter will be achieved by the application of various combinations of printing settings for implants without any surface defects (apertures) to be manufactured. Process parameters that will result in the fabrication of formulations with the desired characteristics will be selected for the production of lidocaine loaded polycaprolactone dosage forms for the subsequent *in vitro* drug release studies. Any modifications in the physical, chemical or thermal properties of the used materials or any chemical interactions occurred after their mixing and 3D printing will be explored with various techniques (SEM, DSC, XRD, FTIR, Raman). The distribution of the incorporated lidocaine in the polymeric formulations will also be assessed.

To conclude, the effectiveness of polycaprolactone both as a barrier-shell and as a matrix for the achievement of sustained drug release will be investigated. Physical and chemical characterizations (SEM, Raman) will follow to explore any changes occurred on the implants after the lidocaine release, as well as, the polymer degradation. The mechanism of drug release will be indicated through the application of kinetics models.

CHAPTER 2: MATERIALS AND METHODS

The principles of the 3D printing technologies applied in this study, as well as, the experimental methods used for the manufacture, characterization and assessment of the *in vitro* drug release profiles and kinetics of drug release from the printed formulations are presented in this chapter.

2.1. MATERIALS

Polycaprolactone (PCL) with Molecular Weight of 25 kDa (LMW PCL) and 50 kDa (HMW PCL) were purchased from Polysciences Europe GmbH, (Hirschberg, Germany). Triethyl Citrate ≥99% (TEC) and Polyethylene Terephthalate (PET) sheet were purchased from Sigma–Aldrich (Gillingham, UK). Lidocaine (LDC) 97.5%, Sodium Chloride 99.5% (NaCl) and Sodium Phosphate Dibasic Anhydrous ≥99% (Na_2HPO_4) were purchased from Fisher Scientific UK Ltd (Loughborough, UK). Potassium phosphate monobasic, ACS Reagent, ≥99% (KH_2PO_4) was purchased from Honeywell Fluka (Loughborough, UK).

The materials selection for this study, polycaprolactone and lidocaine, has been performed based on their properties and the aim of this study which was, as previously mentioned in ***Chapter 1***, the manufacture of 3D printed polymeric implants for sustained drug release without the addition of any solvents at the lowest temperature possible.

2.1.1. Polycaprolactone (PCL)

Poly (ε-caprolactone) (PCL) is an FDA approved, biocompatible, biodegradable, bioresorbable, non-toxic, hydrophobic, thermoplastic and semicrystalline polymer. Its crystallinity is decreasing as its molecular weight is increasing and it can reach up to 69% (Jenkins and Harrison, 2006) (Christen and Vercesi, 2020) (Woodruff and Hutmacher, 2010a) (Cabedo *et al.*, 2006) (Labet and Thielemans, 2009) (Guarino *et al.*, 2017) (Stewart *et al.*, 2018) (Azimi *et al.*, 2014) (Mohamed and Yusoh, 2016) (Kenny *et al.*, 2013) (Thi and Lee, 2010) (Tiptipakorn *et al.*, 2015). This aliphatic polyester is included in the group of poly-α-hydroxy acids, similarly

to PLA and PGA (Sahoo *et al.*, 2010) (Christen and Vercesi, 2020) (Patrício *et al.*, 2014) (Díaz, Sandonis and Valle, 2014) (Navarro-Beana *et al.*, 2016) (Ferreira *et al.*, 2017). It is available at various molecular weights, from 3000 to 90,000 g/mol, with its grades, as well as, its physical, mechanical and chemical properties to be dependent on its molecular weight and crystallinity (Middleton and Tipton, 2000) (Mohamed and Yusoh, 2016) (Christen and Vercesi, 2020) (Guarino *et al.*, 2017) (Labet and Thielemans, 2009). This polymer is highly compatible and permeable by various active substances enabling their incorporation and uniform distribution in the polymeric matrix, while it is fully excreted by the human body after it is bioresorbed without causing any cytotoxic effects (Woodruff and Hutmacher, 2010a) (Mohamed and Yusoh, 2016) (Dash and Konkimalla, 2012) (Guarino *et al.*, 2017) (Christen and Vercesi, 2020) (Ferreira *et al.*, 2017) (Azimi *et al.*, 2014).

Polycaprolactone is among the first polymers synthesized by the Carothers group at the beginning of the 1930s. It consists of a chain of repeated single-unit sequences of ε-caprolactone $(C_6H_{10}O_2)_n$. The chain length (n) and the final molecular weight of this polymer have a considerable impact on its degradation period (Christen and Vercesi, 2020) (Dash and Konkimalla, 2012). More specifically, various anionic, cationic and co-ordination catalysts are used for its synthesis which is happening either via ring opening of the cyclic monomer ε-caprolactone or through free radical ring-opening polymerization of 2-methylene-1-3-dioxepane or via condensation of 6-hydroxycaproic acid (***Figure 2.1***) (Guarino *et al.*, 2017) (Mohamed and Yusoh, 2016) (Cabedo *et al.*, 2006) (Ayyoubi *et al.*, 2021) (Azimi *et al.*, 2014) (Gunatillake and Adhikari, 2003) (Labet and Thielemans, 2009) (Díaz, Sandonis and Valle, 2014). Low molecular weight alcohols can also be used for better control of the molecular weight of the synthesized polymer. Each method of polymerization has a different impact on the molecular weight of the final polymer, as well as, the molecular weight distribution, the end group composition and the chemical structure of the resulting copolymers (Woodruff and Hutmacher, 2010a) (Mohamed and Yusoh, 2016) (Azimi *et al.*, 2014).

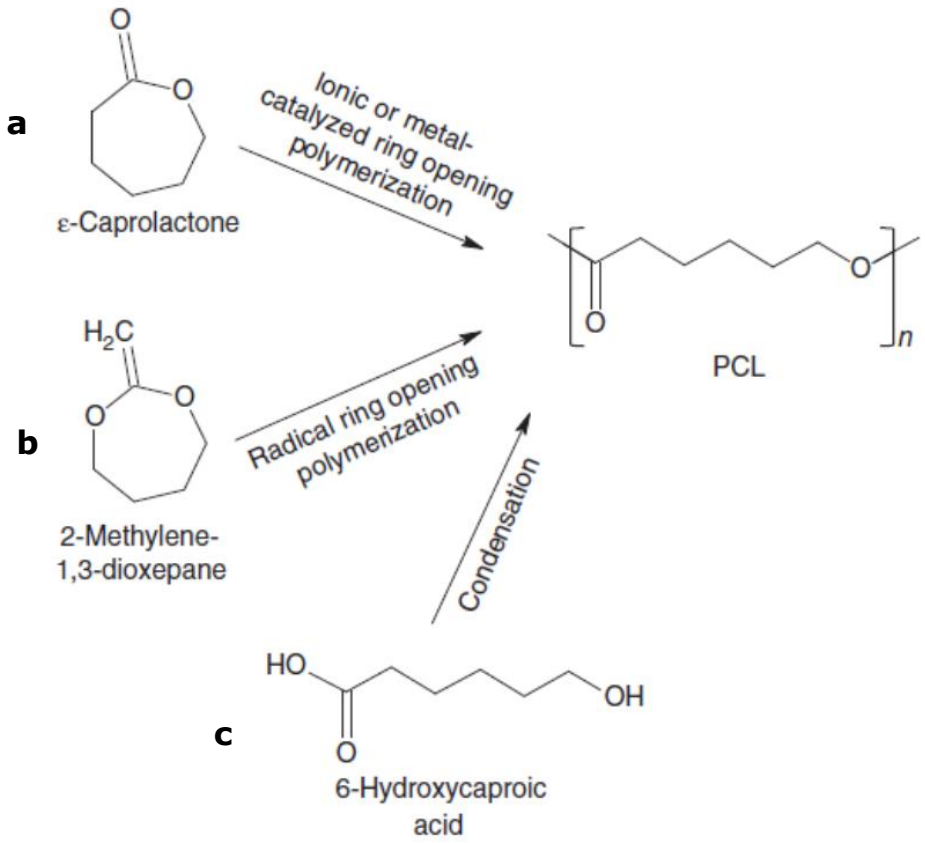

Figure 2.1: *Synthesis of PCL via:* ***(a):*** *ring opening of the cyclic monomer ε-caprolactone,* ***(b):*** *free radical ring-opening polymerization of 2-methylene-1-3-dioxepane and* ***(c):*** *condensation of 6-hydroxycaproic acid. This figure is reproduced from Guarino et al. (Guarino et al., 2017).*

The main properties that made this polymer gain much popularity in the pharmaceutical field and also, led to its selection for the current study are its low melting point (50 – 75 ºC), its particularly slow degradation rate and its outstanding blend compatibility not only with other polymers, but also with various active agents (Peracchia *et al.*, 1997) (Valle, Camps and Díaz, 2011) (De Kesel *et al.*, 1999) (Middleton and Tipton, 2000) (Speranza *et al.*, 2014) (Simao, Bellani and Branciforti, 2017) (Vanessa Azevedo de Mello, 2011) (Cheng, Lei and Guo, 2010) (Jeong, Lee and Cho, 2003) (Sudhakar *et al.*, 2014) (Xue *et al.*, 2014) (Zhang and Ã, 2005) (Rusu, Ursu and Rusu, 2006). The melting point of PCL is influenced by its crystalline nature which contributes to the ease of its processing at low temperatures (Middleton and Tipton, 2000) (Mohamed and Yusoh, 2016)

(Guarino *et al.*, 2017) (Sahoo *et al.*, 2010). This material is in an amorphous rubbery state at its glass transition temperature, ranging from -55 to -68 ºC, while its decomposition temperature is particularly high, 350 ºC (Patrício *et al.*, 2014) (Fortelny *et al.*, 2019) (Major *et al.*, 2020) (Christen and Vercesi, 2020) (Osta *et al.*, 2015) (Azim*i et al*., 2014) (Mohamed and Yusoh, 2016) (Labet and Thielemans, 2009) (Gunatillake and Adhikari, 2003).

PCL is a particularly versatile polymer, which is compatible and can be effectively and homogeneously mixed with many polymers for its mechanical, physical and chemical properties, such as ionic properties, crystallinity, solubility and degradation pattern to be properly adjusted, based on the required attributes of the final product (Gumede, Luyt and Müller, 2018) (Mohamed and Yusoh, 2016) (Park *et al.*, 2018) (Matzino*s et al*., 2002) (Gunatillake and Adhikari, 2003) (Christen and Vercesi, 2020) (Azimi *et al.*, 2014) (Dash and Konkimalla, 2012) (Wachirahuttapong, Thongpin and Sombatsompop, 2016) (Todo *et al.*, 2007). These modifications can lead to the enhancement of stress crack resistance, dyeability, adhesion, hydrophilicity and permeability of the fabricated formulations for the improvement of the cell responses (Guarin*o et al*., 2017) (Mohamed and Yusoh, 2016). Polymers that have already been blended with PCL in previously performed research studies are cellulose propionate, cellulose acetate butyrate, nitrocellulose, ethyleneoxide, PEG, polyvinylchloride, chloroprene, polystyrene, polyurethanes (PU), diisocyanates, oxazolines, polyethylene oxide (PEO), polyethylene, polypropylene, natural rubber, poly (vinyl acetate), poly(ethylene–propylene), poly(styrene–acrylonitrile), poly(acrylonitrile butadiene styrene), poly(bisphenol-A), diglycolide, dilactide, valerlactone, substituted caprolactones, 4-vinyl anisole, styrene, methyl methacrylate, vinyl acetate, chitosan, hydroxyl apatite (HA), starch, gelatin, collagen, polylactic acid and polylactic acid-co-glycolic acid (Patrício *et al*., 2014) (Park *et al.*, 2018) (Peng *et al.*, 2018) (Saho*o et al*., 2010) (Liu *et al.*, 2007) (Woodruff and Hutmacher, 2010a) (Cabedo *et al.*, 2006) (Ma *et al.*, 2007) (Patrício *et al.*, 2013) (Thi and Lee, 2010) (Matta *et al.*, 2014) (Kalambur and Rizvi, 2006) (Przybysz-Romatowska, Haponiuk and Formela, 2020).

Polycaprolactone demonstrates good solubility in several organic solvents at room temperature, such as chloroform, dichloromethane, carbon tetrachloride, benzene, toluene, cyclohexanone and 2-nitropropane. However, its solubility is decreased in acetone, 2-butanone, ethyl acetate, dimethyl formamide and acetonitrile, while PCL is insoluble in alcohol, petroleum ether, diethyl ether and

water (Woodruff and Hutmacher, 2010a) (Mohamed and Yusoh, 2016) (Azimi *et al.*, 2014) (Labet and Thielemans, 2009).

Furthermore, this polymer demonstrates adjustable degradation kinetics and mechanical properties, while it can, also, offer controlled and targeted release of the active ingredient incorporated in its matrix. Its outstanding rheological and viscoelastic properties compared with other biodegradable polymers, as well as, its relatively low cost and ease of shaping and processability under mild conditions enabled its application and further use in the manufacture of various types of pharmaceuticals, such as microspheres, microcapsules, sutures, wound dressings, scaffolds, hydrogels, dendrimers, micelles, contraceptive devices, micro and nanofibers, nanoparticles, pellets, implants and films (Kim *et al.*, 2016) (Middleton and Tipton, 2000) (Dash and Konkimalla, 2012) (Azimi *et al.*, 2014) (Fortelny *et al.*, 2019) (Peng *et al.*, 2018) (Mohamed and Yusoh, 2016) (Christen and Vercesi, 2020) (Ferreira *et al.*, 2017) (Cheng, Guo and Wu, 2009) (Gv *et al.*, 2017) (Kasinathan *et al.*, 2016) (Kenny *et al*., 2013). The exceptional compatibility of polycaprolactone with various active agents is proven by the different types of drugs that have already been encapsulated in polymeric formulations, such as anticancer, antipsychotic, non-steroidal antiinflammatory and anti-hypertensive active substances and contraceptive hormones (Dhanaraju *et al.*, 2003) (Medlicott *et al.*, 1992) (Dhanaraju, Jayakumar and Vamsadhara, 2004) (Goyanes *et al.*, 2016) (Ma *et al.*, 2006) (Christen and Vercesi, 2020) (Kammerer *et al.*, 2011) (Serrano *et al.*, 2009).

Another interesting property of the selected material, that made it an ideal polymer for the present work, is its very slow degradation rate which can last from several months up to 4 years (Stewart *et al.*, 2018) (Gunatillake and Adhikari, 2003) (Azimi *et al.*, 2014) (Labet and Thielemans, 2009) (Dash and Konkimalla, 2012) (Major *et al.*, 2020). This property makes, therefore, polycaprolactone the perfect polymer for the fabrication of sustained release dosage forms compared to other polyesters, such as PLA, PGA or PLGA that exhibit shorter degradation time, since the frequency of drugs administration will be reduced, the therapeutic efficacy and efficiency will be enhanced and the development of unwanted side effects will be eliminated (Guarino *et al.*, 2017) (Chavalitpanya and Phattanarudee, 2013) (Höglund, Hakkarainen and Albertsson, 2007) (Christen and Vercesi, 2020) (Mohamed and Yusoh, 2016).

The degradation time is not only affected by the molecular weight, the nature of polymer backbone, hydrophobicity, crystallinity and length of the polymeric chain of the initial material, but also by the formulation characteristics, such as particle size, surface area volume and porosity, method of manufacture and morphology, as well as, other environmental conditions, such as temperature, pH and presence or absence of enzymes (Azimi *et al.*, 2014) (Dash and Konkimalla, 2012) (Guarino *et al.*, 2017) (Labet and Thielemans, 2009). More specifically, as the molecular weight increases, the degradation period increases; with the increase of the molecular weight, the polymeric chain is becoming longer and consequently, the number of the ester bonds required to be cleaved for the generation of monomers and oligomers is higher. The fact that PCL is a strongly hydrophobic molecule makes difficult the water intrusion in its internal compartments and that, therefore, prolongs its degradation time. This is also influenced by the material's glass transition temperature and crystallinity. When the glass transition temperature is high, the molecular motion is low, as well as, the available volume within the polymer for water penetration. On the contrary, if the glass transition temperature and the crystallinity are low, hydrolytic degradation will occur faster (Höglund, Hakkarainen and Albertsson, 2007) (Patrício *et al.*, 2014) (Guarino *et al.*, 2017) (Dash and Konkimalla, 2012). The degradation conditions or modifications in the chemical structure of the polymer can also play an essential role in the rate of hydrolysis or the ester bonds cleavage. Furthermore, copolymerisation of PCL with other polymers, such as lactones, glycolides, lactides, can result in a different degradation mechanism and hydrolysis rate -faster- compared with the polymer alone. The blending of PCL with hydrophilic polymers, such as PEO, results in an increased rate of water penetration and thus, shorter degradation period (Gunatillake and Adhikari, 2003) (Woodruff and Hutmacher, 2010a) (Guarino *et al.*, 2017) (Dash and Konkimalla, 2012) (Stewart *et al.*, 2018).

Biodegradation of this material occurs in the environment by outdoor living organisms, bacteria and fungi. Enzymatic degradation can occur, as well, with esterase and other types of lipase. Hydrolytic degradation is another degradation mechanism that is happening *in vivo* when the appropriate enzymes are not available (Guarin*o et al*., 2017) (Ferreira *et al.*, 2017) (Labet and Thielemans, 2009) (Dash and Konkimalla, 2012). Hydrolytic degradation of poly (α-hydroxy) esters is feasible due to the unstable aliphatic ester bonds in the initial polymer and it occurs via several mechanisms, either through surface or bulk degradation mechanisms (***Figure 2.2***) (Woodruff and Hutmacher, 2010a) (Patrício *et al.*,

2014) (Mohamed and Yusoh, 2016). However, these procedures in most cases are happening at the same time (Woodruff and Hutmacher, 2010a) (Stewart *et al.*, 2018) (Guarino *et al.*, 2017) (Azim*i et al*., 2014).

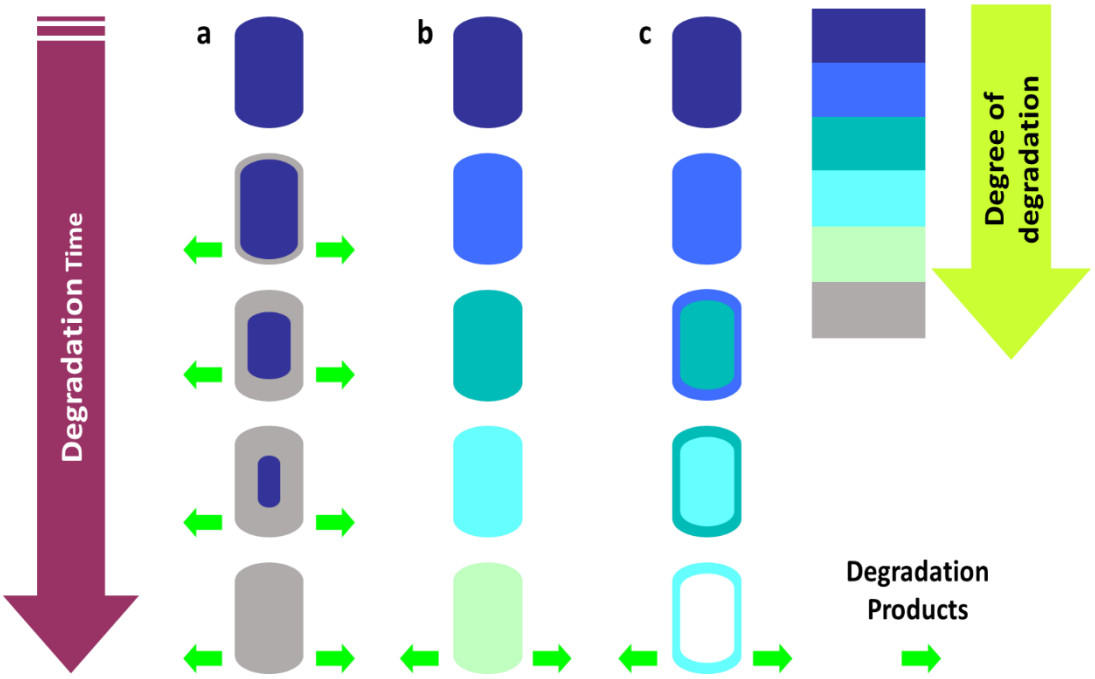

Figure 2.2: *Degradation mechanisms of PCL:* ***(a):*** *Surface erosion,* ***(b):*** *Bulk degradation and* ***(c):*** *Bulk degradation with autocatalysis.*

The process of degradation is, generally, controlled by the diffusion-reaction phenomenon and is happening in two stages, non-enzymatic cleavage and enzymatic fragmentation. In the first phase, the water is penetrating in the amorphous areas of the materials triggering the hydrolytic scission of the ester bonds in these areas and then, continues in the crystalline regions. PCL degradation is performed through end chain scission at higher temperatures and via random chain scission at lower temperatures (Dash and Konkimalla, 2012) (Woodruff and Hutmacher, 2010a) (Labet and Thielemans, 2009) (Christen and Vercesi, 2020) (Guarino *et al.*, 2017). The second phase of the degradation procedure is happening when the molecular weight of the polymer decreases to less than 3000 – 5000 Da, where the material exhibits high crystallinity. Nevertheless, mass loss is usually observed after 3 – 4 months of degradation. Intracellular degradation, then, occurs, and the breakdown products, caproic acid,

penetrate the polymeric matrix and are metabolised through the tricarboxylic acid cycle; either they are catalyzed by enzymes or they are excreted from the human body via the kidneys. Grooves and cracks are often observed on the surface of the polymeric formulation at this stage of the degradation process (Stewart *et al.*, 2018) (Patrício *et al.*, 2014) (Labet and Thielemans, 2009) (Dash and Konkimalla, 2012) (Christen and Vercesi, 2020) (Díaz, Sandonis and Valle, 2014) (Azimi *et al.*, 2014).

In the case that the principle mechanism of biodegradation is surface degradation or erosion, hydrolytic cleavage of the polymer backbone occurs only on the surface. This process is triggered when the rate of hydrolytic chain scission and the generation of oligomers and monomers -that are diffused in the areas around the location of the polymeric device- is considerably faster compared with the rate that the water is penetrating the polymer bulk (Guarin*o et al*., 2017) (Ferreira *et al.*, 2017). As a result, the device is becoming thinner while this process is happening; the molecular weight of the internal bulk of the polymer, though, is not altered during the PCL degradation (***Figure 2.2.a***) (Woodruff and Hutmacher, 2010a) (Ferreira *et al.*, 2017). The benefit of this procedure of erosion in the drug carriers is that the rate of degradation is highly reproducible and can effectively be predicted. The latter, therefore, enables an easier adjustment of the release of the incorporated active ingredients by modifying the available surface area of the formulation. Zero-order release kinetics can be obtained when the degradation is solely controlled by surface erosion (Woodruff and Hutmacher, 2010a) (Guarino *et al.*, 2017).

When bulk degradation is the main process of PCL biodegradation, water intrusion is happening in the whole polymer bulk and that leads to the hydrolysis of the whole polymeric matrix rather than only on its surface. The surface erosion mechanism occurs slower in this case. Hydrolytic chain scission randomly occurs in this case, resulting in a reduction of the molecular weight (***Figure 2.2.b***) (Woodruff and Hutmacher, 2010a) (Guarin*o et al*., 2017) (Christen and Vercesi, 2020) (Azimi *et al.*, 2014) (Ferreira *et al.*, 2017). If the water penetration is happening in the polymer bulk, chain hydrolysis is triggered; the length and the molecular weight of the polymeric chain decrease, while the mass, volume and shape of the formulation do not exhibit any alterations. Then, the produced monomers or oligomers diffuse out (Ferreira *et al.*, 2017) (Christen and Vercesi, 2020). Gradual erosion is happening, while an equilibration of the diffusion-reaction phenomenon will be obtained. If the equilibrium is not maintained for the

entire degradation period or it is interrupted, the biodegradation procedure can activate internal autocatalysis through the carboxyl and hydroxyl end group by-products. In bulk surface erosion mechanisms, the surface oligomers and carboxyl groups are moving to the areas around the polymer; in the bulk degradation process, the internal concentration of autocatalysis products can lead to the generation of an acidic gradient (Guarin*o et al*., 2017). The latter occurs due to the accumulation of the carboxyl end group produced during the ester bond cleavage. In this way, the internal degradation is happening faster contrasted with the surface degradation; a lower molecular weight layer is surrounded by a higher molecular weight one (***Figure 2.2.c***). Bimodal molecular weight distribution controls, hence, the degradation procedure. When the size of the oligomers is considerably decreased, they are able to quickly diffuse through the external layer and that is associated with the reduction of the molecular weight, as well as, the rate with which the chain scission leads to the generation of a hollow structure consisting of an outer layer with high molecular weight (Woodruff and Hutmacher, 2010a).

The disadvantages of the bulk erosion procedure are associated with the fact that drug release kinetics cannot easily be predicted and the fact that the encapsulated active compounds are not protected from possible degradation due to water intrusion (Guarin*o et al*., 2017).

2.1.2. Lidocaine

Lidocaine [2-(diethylamino)-N-(2,6-dimethyl phenyl)-acetamide], also termed lignocaine and xylocaine, is the selected model drug for this study (***Figure 2.3***) (Repka *et al.*, 2005) (Weinberg *et al.*, 2015). It consists of a tertiary amine and an amide group derived from xylene, while it belongs to the Caine Family. It was firstly synthesized by Nils Löfgren, Holger Erdtman and Bengt Lundquist in 1942 and it became available in the market a few years later, in 1948 (Hermanns *et al.*, 2019) (Weinberg *et al.*, 2015) (Gudin and Nalamachu, 2020). The main reason that this active substance was selected for loading to the 3D printed polymeric implants of the current work is its low melting point, which is ranging between 66 to 79 ºC (Ribeiro *et al.*, 2016) (Umeda *et al.*, 2009) (Zhang and Michniak-kohn, 2011) (Chun *et al.*, 2012) (Repka *et al.*, 2005) (Chen *et al.*, 2004) (Kang, Jun and Mccall, 2000) (Cui and Frank, 2006) (Nagarsenker and Joshi, 1997) (Bakonyi *et al.*, 2018) (Peracchia *et al.*, 1997). It is, therefore, close to the melting point of

the studied polymer, PCL (50 – 75 ºC). The decomposition temperature of lidocaine is 196 ºC, while its glass transition temperature is similar to PCL's, -60 ºC (Gala *et al.*, 2015) (Liu *et al.*, 2018). This active ingredient is soluble in water, chloroform, dichloromethane, methanol, ethanol and benzene, but is insoluble in diethyl ether (Groningsson, Lindgren and Lundberg, 1985) (Kumpugdee-Vollrath, Krause and Bürk, 2014).

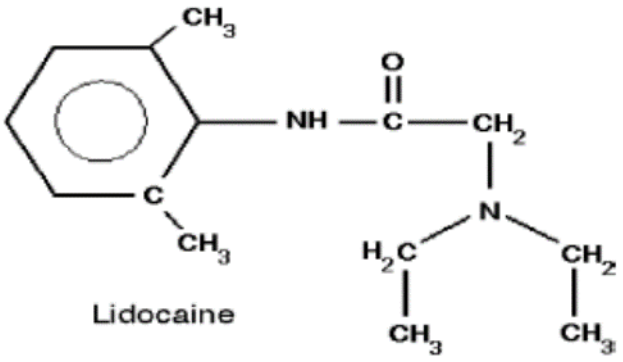

Figure 2.3: *Molecular structure of lidocaine. This figure is reproduced from Repka et al. (Repka et al., 2005).*

Lidocaine is an effective and reliable active compound and one of the most widely used topical anaesthetics. It exhibits rapid onset (45 – 90 sec), intermediate duration of action (90 – 240 min) and low systemic toxicity. This active substance demonstrates faster onset and longer action, as well as, improved patient tolerance and safety compared with other amino ester anaesthetics. Only very rare cases of adverse reactions have been reported (Holgado *et al.*, 2008) (Gudin and Nalamachu, 2020) (Trellakis, Lautermann and Lehnerdt, 2007) (Estebe and Consultant, 2017) (Golzari *et al.*, 2014) (Puglia *et al.*, 2011) (Masic *et al.*, 2018) (Pathak and Nagarsenker, 2009a) (Na *et al.*, 2018) (Bakonyi *et al.*, 2018). This active ingredient is, also, administered as an antiarrhythmic agent for the control of ventricular arrhythmias from myocardial infarction or cardiac manipulation, such as surgery. This amino-amide can also be administered to relieve pain and discomfort usually after surgery, trauma or medical procedures, such as tracheal intubation, for the management of acute and chronic pain, such as chronic neuropathic pain, allodynia, post-herpetic neuralgia (PHN), nerve injury pain from shingles (herpes zoster), headache, hyperalgesia, postherpetic neuralgia, centrally mediated pain, infiltrative malignant neurological lesions or spontaneous

pain. Moreover, lidocaine exhibits antinociceptive, antithrombotic, intiinflammatory, proconvulsant and anticonvulsant properties, while it can be used for the treatment of allergies since it is a selective inverse peripheral histamine H1-receptor agonist (Hermanns *et al.*, 2019) (Masic *et al.*, 2018) (Trellakis, Lautermann and Lehnerdt, 2007) (Weinberg *et al.*, 2015) (Gudin and Nalamachu, 2020) (Estebe and Consultant, 2017) (Golzari *et al.*, 2014).

The mechanism of action of the selected model drug is the blockage of sodium ion channels associated with the initiation and conduction of neuronal impulses (Puglia *et al.*, 2011) (Gudin *et al.*, 2020) (Golzar*i et al*., 2014) (Masic *et al.*, 2018) (Estebe and Consultant, 2017) (Gudin and Nalamachu, 2020) (Chun *et al.*, 2012). The amide group can, generally, behave as an amino acid by interacting with the active regions in the areas of the sodium channel and ultimately, preventing the passage of the sodium ions via the voltage gate channels located on the internal surface or nerve cell membranes. More specifically, neutral uncharged lidocaine molecules diffuse through neural sheaths into the axoplasm. They, subsequently, become ionized in that area through their merge with hydrogen ions. Lidocaine cations are, then, generated and they can reversibly bind to the sodium channels in an open state from the inside, causing a deformation of the channels and blocking in this way, the sodium influx and the nerve depolarization. Consequently, the local neurons are barred from transferring a signal to the brain and that results in the end of the production of new pain signals. Lidocaine's analgesic properties are also linked with an antiinflammatory process through which the circulating inflammatory cytokines, interleukines IL-4 and IL-6 and tumour necrosis factor-alpha (TNF- α), are decreased (Masic *et al.*, 2018) (N*a et al*., 2018) (Weinberg *et al.*, 2015) (Hermanns *et al.*, 2019) (Puglia *et al*., 2011) (Gudin and Nalamachu, 2020).

Lidocaine does not only act in the peripheral nervous system, but also the central nervous system and cardiovascular system. After its administration, it stimulates the central nervous system and then, leads to its depression. Its action in the cardiovascular system is associated with the myocardium where it contributes to the elimination of electrical excitability, conduction rate, and force of contraction. Lidocaine's antinociceptive effect is associated with the blockage of neuronal sodium channels, potassium currents, as well as, presynaptic muscarinic and dopamine receptors (N*a et al*., 2018) (Weinberg *et al.*, 2015) (Hermanns *et al.*, 2019) (Puglia *et al*., 2011).

Lidocaine is mainly metabolized by the cytochrome P450 system in the liver via N-dealkylation to the pharmacologically active metabolite, monoethylglycine xylidide (MEGX) and then, to glycinexylidide (GX), 2,6-xylidine and N-ethylglycine (EG), amongst others. This active substance is removed from the body through the urine (Hermann*s et al*., 2019) (Weinberg *et al.*, 2015) (Masic *et al.*, 2018).

Lidocaine is a stable, crystalline, colourless solid that can be found in two forms; in a base state: lidocaine; and a salt state: lidocaine hydrochloride hydrate (Li*u et al*., 2018) (Gudin and Nalamachu, 2020) (Kumpugdee-Vollrath, Krause and Bürk, 2014) (Weinberg *et al.*, 2015) (Mofenson *et al.*, 1983). The base form, which is unionised, demonstrates enhanced lipophilicity and that contributes to the improvement of the penetration properties of this molecule through the lipophilic cell membranes and stratum corneum, as well as, its ability to create a depot in the hydrophilic dermis. The free base is not very stable and demonstrates lower water solubility contrasted with the hydrochloride salt (Bakony*i et al*., 2018) (Trellakis, Lautermann and Lehnerdt, 2007) (Gudin and Nalamachu, 2020) (Hermanns *et al.*, 2019). The melting point of lidocaine base ranges between 66 to 69 ºC, while the melting point of lidocaine hydrochloride hydrate ranges between 75 to 79 ºC (Groningsson, Lindgren and Lundberg, 1985) (Gala *et al.*, 2015). The base form of lidocaine has been used in the present study contrasted with the majority of the previously performed studies and the commercially available formulations (Preda *et al.*, 2016) (Lidoderm, 2018) (Kau *et al.*, 2014) (ZTLido, 2018).

Lidocaine can be administered through various routes; by injection (intravenous or subcutaneously), inhalation, topical application. Its intravenous administration is considered an effective alternative to opioids when they are proven to be inefficient or cause unwanted complications. It can be combined with other anaesthetics or analgesics for enhanced effectiveness (Golzari *et al.*, 2014) (Masic *et al.*, 2018). It is available in the market in various dosage forms, such as patches, lozenges, suppositories, topical ointments, creams, sprays, gels, emulsions and solutions in various concentrations (Lidoderm, 2018) (Pathak and Nagarsenker, 2009a) (Wonneman*n et al*., 2007) (Gudin *et al.*, 2020) (Mofenson *et al.*, 1983) (ZTLido, 2018) (Umed*a et al*., 2009) (Gudin and Nalamachu, 2020) (Anodesyn, 2013).

2.2. 3D PRINTING TECHNIQUES

In the current work, extrusion based techniques have been used for the PCL printability studies and the manufacture of drug loaded polymeric implants. Hot Melt Extrusion (HME) has been combined with a Fused Deposition Modelling (FDM) 3D printer; a polymeric filament produced by the HME was loaded to an FDM printer for the polymer printability investigation. Pressure Assisted Microsyringe (PAM) 3D printing was also used for the polymer printability explorations and afterwards, for the implants fabrication.

2.2.1. Hot Melt Extrusion

Hot Melt Extrusion (HME) has recently gained a lot of attention in the field of pharmaceuticals due to its compact size, relatively low cost and its capability to effectively produce solid dispersions (Tiwari, Patil and Repka, 2016) (Moulton and Wallace, 2014) (Jamróz, Szafr*aniec, et al*., 2018). It is, basically, a method in which raw materials are mixed and forwarded through a heated barrel to a die at an increased controlled temperature and pressure for the fabrication of a product with a homogeneous shape and density. The hot melt extrusion process can be summarized in four steps (***Figure 2.4***) (Maniruzzaman *et al.*, 2012) (Cunha-Filho *et al.*, 2017):

1) The materials are firstly loaded to the extruder through the feed hopper.
2) Materials blending and grinding, as well as, particle size reduction, removal of the trapped air between the particles and kneading follow.
3) The mixed compounds are, then, pumped into the die.
4) Finally, the molten materials are extruded through the die and downstream processing is performed in the fabricated product.

Each one of the above stages can be regulated for the manufactured extrudate to have the desired attributes (Stanković, Frijlink and Hinrichs, 2015).

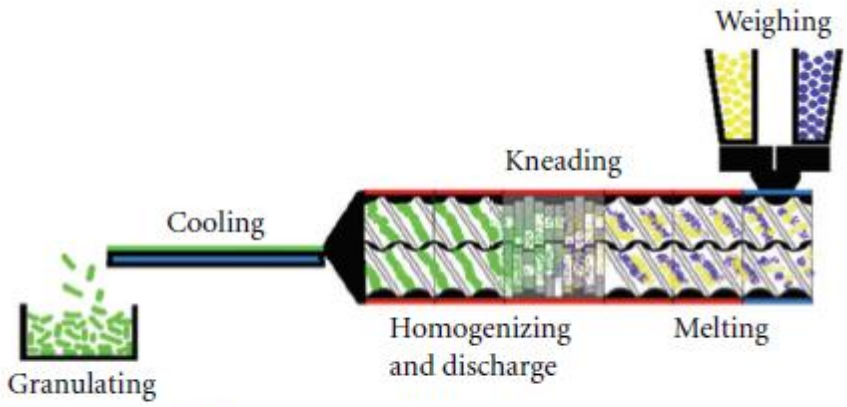

Figure 2.4: *Schematic diagram of the several stages of the Hot Melt Extrusion process. This figure is reproduced from Maniruzzaman et al. (Maniruzzaman et al., 2012).*

Extrusion processes are divided into two categories based on the part that controls the materials pumping through the die; screw extrusion and ram extrusion. In the former, one or several screws are rotating in a heated barrel, while in the latter, a ram or a piston is producing high pressures for the loaded materials to be forwarded to the die. Ram extrusion presents an important disadvantage; lower process temperatures can only be applied which lead to a lower mixture uniformity. Consequently, that might significantly affect the attributes of the manufactured product (Crowley *et al.*, 2007) (Censi *et al.*, 2018).

The extrusion method selected for this study is screw extrusion. In this technology, an intense mixing of the active compound and the material, which will be used as a matrix, is performed. The shear stress applied by the extruder leads to the production of the required frictional energy to overcome the crystal lattice energy of the material used as a drug carrier (Crowley *et al.*, 2007) (Tiwari, Patil and Repka, 2016) (Cunha-Filho *et al.*, 2017). As a result the polymer, which is the material most widely used as a matrix-carrier, becomes softer and enables the active agent to be mixed and included in the matrix. A physical blend of the active agent and the matrix is finally obtained. The quality characteristics of the final product, shape, size, content, are affected by the selected extrusion parameters: feed rate, screw speed, barrel temperature and screw configuration (Tiwari, Patil and Repka, 2016) (Aita, Breitkreutz and Quodbach, 2019).

Nevertheless, the extruder capability of rotating the screw at a pre-established speed and compensating for the torque and shear produced by both the materials extrusion and screws rotation should be independent of the instrument type or the intricacy of the extrusion process and the operation (Maniruzzaman *et al.*, 2012).

The main parts of a screw extruder, irrespective of the screws number, are a motor which is the drive unit, a feed hopper, a temperature controlled barrel which is usually divided into different compartments bolted or clamped together, one or multiple rotating screws (either co-rotating or counter-rotating) located inside the barrel, a die through which the molten materials are ejected at a predetermined throughput rate, as well as, heating and cooling systems (***Figure 2.5***) (Maniruzzaman *et al.*, 2012) (Censi *et al.*, 2018) (Patil, Tiwari and Repka, 2016) (Stanković, Frijlink and Hinrichs, 2015) (Cunha-Filho *et al.*, 2017).

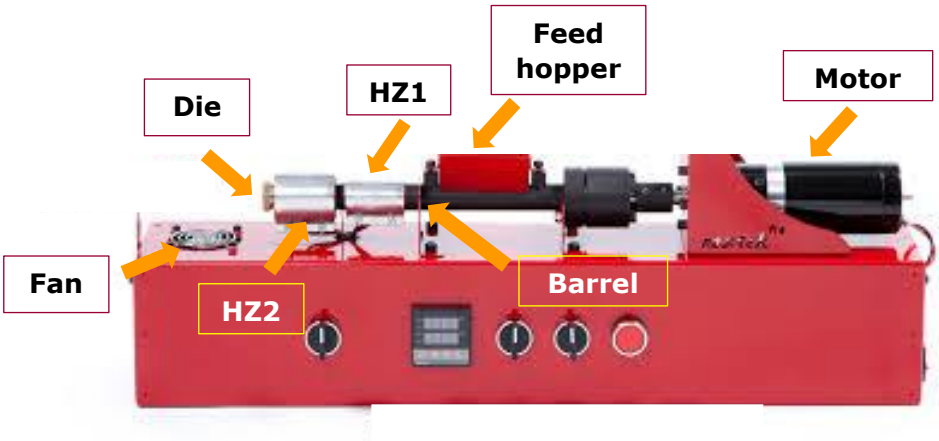

Figure 2.5: *Hot Melt Extruder, Desktop Extruder, Noztek Pro,* ***HZ_1:*** *Heating Zone 1 and* ***HZ_2:*** *Heating Zone 2. The main parts of the extruder (fan, die, feed hopper, heating zones, barrel, motor) are labelled. This figure is reproduced from Noztek Pro manual (Noztek Pro, 2018).*

A single screw extruder (Desktop Extruder, Noztek Pro, Shoreham-by-Sea, UK), was selected for the fabrication of a polymeric filament and is the most frequently used extruder type, due to its low cost and mechanical simplicity. Its three main operations, which are happening continuously, are materials transfer, melting and pumping through the die. Such extruders generate particularly high pressures

during the materials melting and mixing and hence, extrusion of viscous compounds, such as polycaprolactone, can successfully be achieved (Censi *et al.*, 2018). The screw speed (rpm) regulates the output rate of the extrudate (Crowley *et al*., 2007). The screw speed, the pressure and the process temperature along the heating zones of the barrel and the die are adjusted in an electronic control unit for the optimization of the extrusion procedure (Censi *et al.*, 2018) (Patil, Tiwari and Repka, 2016).

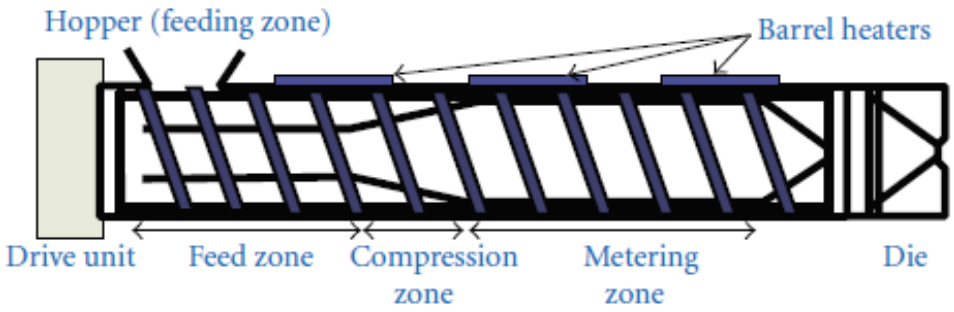

Figure 2.6: *Schematic diagram of the compartments of a single screw extruder. This figure is reproduced from Maniruzzaman et al. (Maniruzzaman et al., 2012).*

The surface of the screws is, in most instruments, coated with stainless steel to reduce material friction or chemical reactions. The temperature controlled barrel consists of three compartments: feeding, melting or compression and metering, as depicted in ***Figure 2.6*** (Maniruzzaman *et al*., 2012) (Censi *et al.*, 2018). The feeding part is used for materials loading and their conveyance from the feed hopper to the barrel. The channel depth in this part is wider compared to the following, while the pressure is relatively low to enable a better mass flow. A constant screw speed is regulated by the pitch and helix angles (***Figure 2.7***) (Patil, Tiwari and Repka, 2016). Then, the depth in the compression area is reduced to give a higher pressure and remove air trapped between the particles. These conditions facilitate an effective mixing and compression of the compounds. Apart from these considerations, the processing in this compartment contributes to material pumping to the next zone in a suitable physical phase; the polymer usually becomes softer and especially the thermoplastic ones, are in a molten phase. The materials mixture is forwarded to the metering area in a helical path,

through transverse flow, drag flow, pressure flow and leakage (Crowley *et al.*, 2007). The role of the metering section is to decrease pulsating flow to give a constant delivery rate through the die aperture; the ultimate goal is the fabrication of an extrudate with a homogeneous composition, thickness, shape and size. The channel depth and the length of the metering zone control the mass flow rate of the extrudate (Maniruzzaman *et al.*, 2012) (Censi *et al.*, 2018).

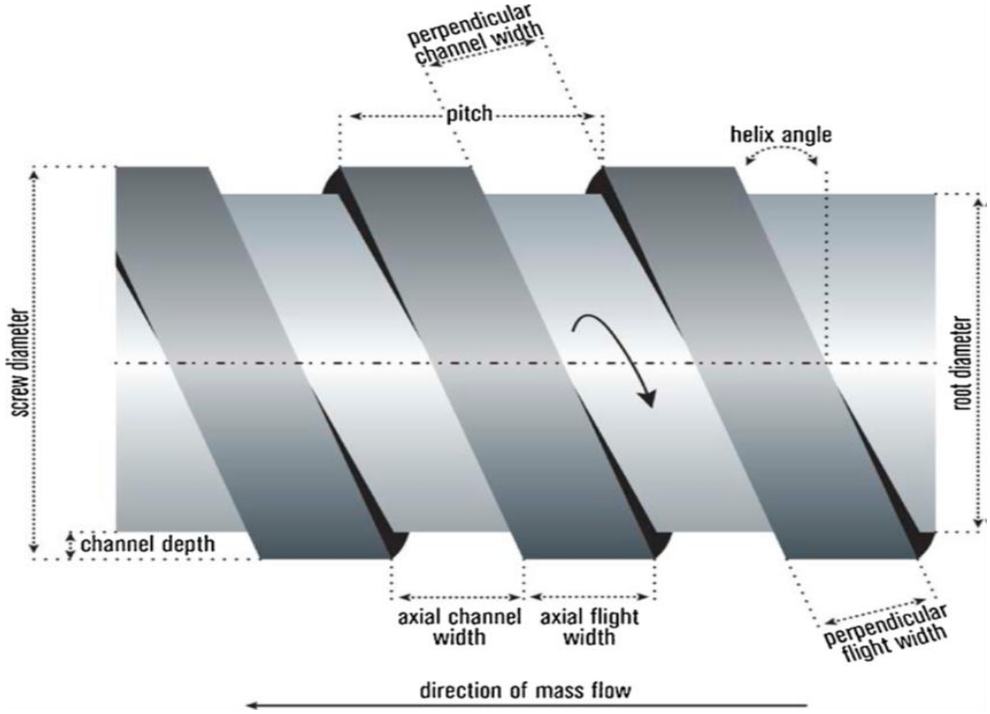

Figure 2.7: *Schematic diagram of the extruder screw geometry. This figure is reproduced from Patil, Tiwari and Repka (Patil, Tiwari and Repka, 2016).*

The die, through which the compounds mixture is pumped, is connected at the end of the heated barrel and depending on its shape and dimensions, a product with the desired characteristics will be manufactured (***Figure 2.6***). In this step, the molten materials are shaped as they are forwarded through the die by the screw (Moulton and Wallace, 2014). The diameter of the final extrudate will be larger than the cavity size of the die due to the die swell or extrudate swelling effect. This comes from the viscoelastic properties of the polymers since the rotating screw leads to deformation and relaxation of the polymeric chains and consequently, to an entropy decrease. After the production of the extrudate, the polymer recovers its initial structure and its entropy is maximized (Crowley *et al*.,

2007) (Koopmans, 1999) (Patil, Tiwari and Repka, 2016) (Aho *et al*., 2019). Extrusion dies are available in various configurations for the fabrication of diverse-shaped products depending on the subsequent application; strands, films, sheets and granules (Patil, Tiwari and Repka, 2016) (Cunha-Filho *et al*., 2017). In the present study, an appropriate sized die for the production of a polycaprolactone filament that would fit in the Fused Deposition Modelling 3D printer was selected.

It is quite common for the extruders to have additional downstream accessories for the fabricated product cooling, cutting and collection (Maniruzzaman *et al*., 2012). The extruder used in this work was equipped with a fan for the faster cooling of the filament (***Figure 2.5***). An extrudate can also be cooled down by water or by contact with a cold surface apart from the air (Stanković, Frijlink and Hinrichs, 2015).

2.2.2. Fused Deposition Modelling 3D Printer

2.2.2.1. Principle

PCL filaments produced by HME were loaded in a Fused Deposition Modelling (FDM) 3D printer (Ultimaker 2+, Geldermalsen, The Netherlands) for their printability to be investigated. Successful extrusion of drug loaded filaments at the applied printing parameters was an indication of the materials printability. The low cost of this printing technique, the ease of use and the relatively easy and inexpensive production or supply of the filament (raw material) needed for the printing are the main reasons that FDM is one of the most widely used Additive Manufacturing (AM) technology. Recently, it has attracted considerable attention for the fabrication of various drug dosage forms (Schmitz *et al.*, 2018) (Wang, Gramlich and Gardner, 2017) (Ventola, 2014) (Lim *et al.*, 2018) (Norman *et al.*, 2017) (Hoque, Chuan and Pashby, 2011) (Tappa and Jammalamadaka, 2018). Moreover, an additional advantage is that no solvents are required for filament production or during the printing process (Verstraete *et al.*, 2018) (Sadia, Alhnan, *et al*., 2018) (Cunha-Filho *et al.*, 2017) (Zema *et al.*, 2017).

FDM is based on a computer controlled material extrusion process where a filament fabricated with one or more materials is fed through a heated nozzle by two gear wheels and is deposited on a building stage for the manufacture of the desired object in a layer by layer fashion. The layers are fused since they are in a semi-molten phase and the final product solidifies on the printing platform (Lamichhane, Bashyal, *et al*., 2019) (Genina *et al.*, 2016) (Goole and Amighi, 2016) (Nasereddin *et al.*, 2018) (Ligon *et al.*, 2017) (Zhang *et al.*, 2018) (Lepowsky and Tasoglu, 2018) (Tappa and Jammalamadaka, 2018). The principle of the FDM 3D printing process is similar to the one of the HME since the loaded material is extruded through a precisely controlled heated nozzle (Jamróz, Kurek, Łyszczarz, Brniak, *et al.*, 2017). The material properties, such as heat conductivity and transfer, and especially material rheological properties, play a significant role in the efficiency of the extrusion. Instruments set up, such as the nozzle diameter, as well as, the printing parameters selection, such as the print speed and the print temperature, may affect the quality attributes of the product (Prasad and Smyth, 2016) (Vithani *et al.*, 2019b) (Acosta-Vélez and Wu, 2016).

The compartments of which a typical FDM 3D printer consist, are a spool, a printer enclosure, a heater/liquefier, a print head, an extrusion nozzle, a building bed and a motor, as depicted in ***Figure 2.8*** (Araujo *et al*., 2019) (Dietmar W Hutmacher, Sittinger and Risbud, 2004). Nozzles are available in various diameters and geometries, similarly to the dies of the HME (Verstraete *et al.*, 2018) (Saaidah *et al.*, 2010). FDM 3D printers with higher complexity or cost have multiple print heads with one extrusion nozzle each (Ventola, 2014) (Vithani *et al*., 2019b) (Mwema and Akinlabi, 2020) (Patterson, Collopy and Messimer, 2015) (Chia and Wu, 2015). In this way, the fabrication of objects with a more complicated shape or geometry or even with various materials with different melting points and physical properties is feasible (Stansbury and Idacavage, 2016) (Katstra *et al.*, 2000) (Khatri, Shah and Vora, 2018) (Jamróz *et al*., 2017) (Acosta-Vélez and Wu, 2016) (Konta, García-Piña and Serrano, 2017). Additionally, depending on the cost of the printer one or several materials can be used; the majority of low-cost 3D printers can only be loaded with one polymer type, normal polylactic acid (PLA). This has an impact, though, on how effective the extrusion will be and consequently, on the printing resolution of the final product (Mwema and Akinlabi, 2020).

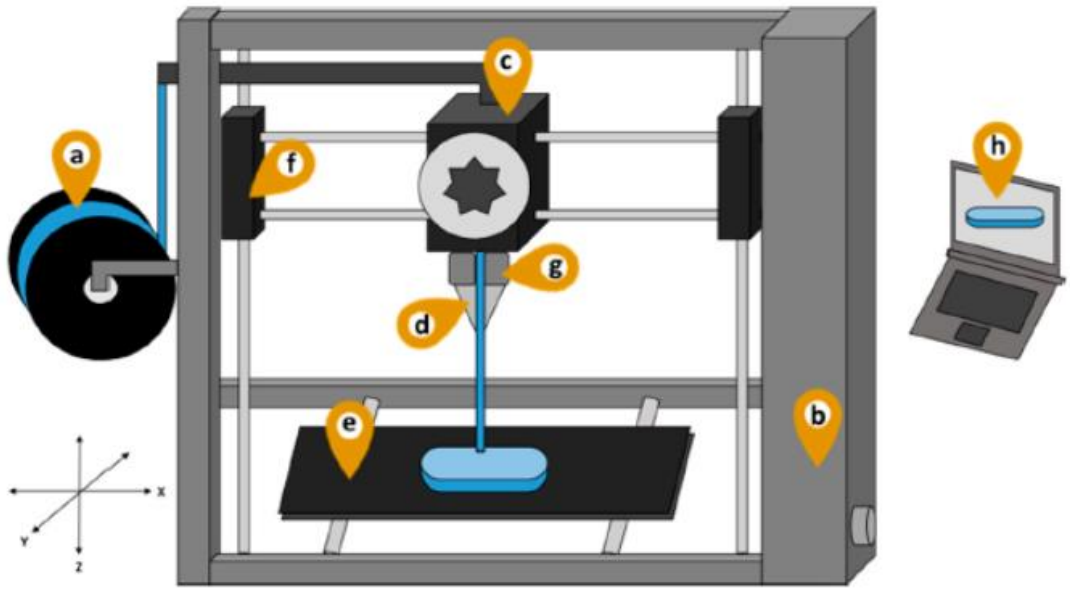

Figure 2.8: *Schematic diagram of the basic compartments of the Fused Deposition Modelling 3D Printer:* ***(a):*** *Spool,* ***(b):*** *Printer enclosure,* ***(c):*** *Print head,* ***(d):*** *Extrusion nozzle,* ***(e):*** *Building plate,* ***(f):*** *Motor,* ***(g):*** *Heater and* ***(h):*** *3D design software. This figure is reproduced from Araujo et al. (Araujo et al., 2019).*

The printer enclosure is often enclosed for the printed model to not be contaminated or exposed to external humidity or dust particles; a laminar flow hood may also be used. In addition, an inert material, often stainless steel, is used for the printer compartments, such as the print head, the extrusion nozzle and the printing plate, as these are in direct contact with the loaded material and the final product. Moreover, mechanical parts of the printer, such as motors, that are covered with lubricant oil should not come into contact with the manufactured object (Araujo *et al.*, 2019).

The process for the fabrication of a structure using the FDM 3D printer is divided into several designing/parameters adjustments and printing steps. The designing/parameters adjustments are the following (Vithani *et al*., 2019b) (Azad *et al.*, 2020) (Masood, 1996) (Mwema and Akinlabi, 2020):

1) Creation of a Computer Aided Design (CAD) file using relevant design software.
2) Production of a Stereolithography (.stl) format file.
3) Loading of the .stl file to the printer slicing software.
4) Adjustment of the printing parameters.
5) Production of a .gcode format file.
6) Uploading of the .gcode format file to the printer.

The printing steps briefly include (Vithan*i et al*., 2019) (Dietmar W Hutmacher, Sittinger and Risbud, 2004) (Zema *et al.*, 2017) (Tian *et al.*, 2019) (Aza*d et al*., 2020):

1) Extrusion of the molten material on the building platform.
2) Deposition of the next layers on top of each other.
3) Solidification of the printed layers.

More specifically, the first step of the printing process includes the loading of a filament with a well-defined and uniform diameter to the instrument (Verstraete *et al.*, 2018) (Lamichhane *et al*., 2019). Depending on the printer type a specific diameter of the filament is required (usually 1.75 – 3 mm) (Tia*n et al*., 2019) (Ligo*n et al*., 2017) (Hoque, Chuan and Pashby, 2011) (Babu and Devaprakasam, 2019) (Jamró*z et al*., 2018).

After the filament is loaded to the printer, it is, then, fed through a tube to the extrusion nozzle by two wheels with an inward flow, while it is unwinding from a spool usually attached on the outer side of the printer (***Figure 2.8***) (Stansbury and Idacavage, 2016) (Araujo *et al*., 2019) (Mwema and Akinlabi, 2020). The wheels are not rotating when no material deposition occurs (Sadia, Alh*nan, et al*., 2018).

When the filament reaches the nozzle, it is softened to facilitate its shaping in the next stage. The print head, which includes the extrusion nozzle, is heated at a temperature either above the melting point for semicrystalline polymers or above the glass transition temperature for amorphous polymers (Ligon *et al.*, 2017) (Algahtani, Mohammed and Ahmad, 2019) (Vithan*i et al*., 2019) (Aho *et al.*, 2019) (Economidou, Lamprou and Douroumis, 2018). Afterwards, the semi-molten material is deposited in a thin ribbon form on the printing platform based on the

predesigned architecture included in the CAD file (Wang, Gramlich and Gardner, 2017) (Dietmar W Hutmacher, Sittinger and Risbud, 2004) (Verstraete *et al.*, 2018) (Saaidah *et al.*, 2010). The continuous filament loading behaves like a piston for the extrusion of the semi-molten material (Aho *et al.*, 2019) (Hoque, Chuan and Pashby, 2011). For a better extrusion through the nozzle, a temperature high enough should be selected to effectively melt the thermoplastic filament. The nozzle moves into different XY positions depositing a precise amount of material on the bed for the formation of each layer according to the pre-adjusted settings in the computer software of the printer (Ventola, 2014) (Lamichhane, Bashyal, *et al*., 2019) (Aho *et al*., 2019) (Algahtani, Mohammed and Ahmad, 2019). The available area for the printing of the desired object is restricted by the minimum and maximum position of the nozzle in the XYZ directions with respect to the building plate (Jamróz, Kurek, Łyszczarz, Brniak, *et al.*, 2017).

The thin layer of material first deposited on the base immediately becomes cooler and then, the mechanical piston, which controls the movement and position of the building platform, moves the bed downwards (Z direction) to be created space for the next layer (***Figure 2.8***) (Saaidah *et al.*, 2010) (Dietmar W Hutmacher, Sittinger and Risbud, 2004) (J*u et al*., 2019) (Zema *et al.*, 2017). The distance between the heated nozzle and the upper surface of the manufactured structure always remains constant (Aho *et al*., 2019). The second layer is, hence, extruded on top of a solidified layer, where it is first fused and then, starts to solidify (Aho *et al.*, 2019).

The above steps are repeated until the fabrication of the desired object with a predefined geometry and shape in a layer by layer way is completed. The manufactured parts generally do not require post-processing since they are already solid and can be used immediately (Verstraete *et al.*, 2018) (Sadia, Alhna*n, et al*., 2018) (Lamichhane, Bashyal, *et al.*, 2019) (Azad *et al.*, 2020).

Supports for the final structure, especially overhangs, can also be fabricated to enhance the structural integrity of the fabricated part, which can easily be detached after the completion of the printing process by either breaking it or using appropriate solvents to dissolve it (Zema *et al.*, 2017) (Tappa and Jammalamadaka, 2018) (Mwema and Akinlabi, 2020). Nevertheless, in the FDM 3D printing, this is only needed for large and more complicated parts but not for smaller ones (Dumitresc*u et al*., 2018). Alternatively, for the first layer to provide

better support to the rest of the fabricated object, the printing plate can be heated to enhance the adhesion (Goole and Amighi, 2016).

2.2.2.2. Filament properties

Filament properties, such as rheology, thermal conductivity, density or glass transition temperature, as well as, its quality characteristics, such as constant dimension, elasticity, stiffness, uniform distribution of the active agent play a significant role in the printing resolution of the fabricated objects (Zhang *et al*., 2018) (Jamróz, Szafraniec*, et al*., 2018) (Chia and Wu, 2015) (Ani Jose and Christopher GV, 2018) (Ligon *et al*., 2017).

Filament stiffness is a critical property for an efficient extrusion to be conducted. The filament needs to be ductile enough to allow some bending in the feeding system, but it also needs to be hard enough to not break or be particularly deformed due to the compression forces generated by the gear wheels (Aho *et al.*, 2019) (Jamróz, Szafr*aniec, et al*., 2018).

The brittleness, the diameter and the shape uniformity of the filaments are essential for the subsequent printing process as they can affect the feeding rate by either clogging the tube of the FDM in which the filament is loaded or by resulting in a decreased feeding rate (Araujo *et al.*, 2019) (Dumitresc*u et al*., 2018).

The filaments that can be loaded in the FDM for the manufacture of pharmaceuticals usually consist of thermoplastic polymers; polylactic acid or polylactide (PLA), polyvinyl alcohol (PVA), polycaprolactone (PCL), hydroxyl propyl cellulose (HPC), ethylene-vinyl acetate (EVA), hydroxypropyl methylcellulose (HPMC), hypromellose acetate succinate (HPMCAS), acrylonitrile-butadiene-styrene copolymers (ABS), aliphatic polyamides, such as nylon, thermoplastic polyurethane (TPU), high impact polystyrene (HIPS), polyethylene terephthalate glycol-modified (PET-G), polycarbonate (PC), polyphenylsulfone (PPSF), polyethylene, propylene (Zhang *et al.*, 2018) (Jamró*z et al*., 2018) (Algahtani, Mohammed and Ahmad, 2019) (Bahnin*i et al*., 2018) (Al-Maliki and Al-Maliki, 2015) (Prasad and Smyth, 2016) (Lepowsky and Tasoglu, 2018) (Capel *et al.*, 2018) (Ramya, 2016) (Vithan*i et al*., 2019) (Dumitrescu *et al.*, 2018) (Ligon *et al.*, 2017) (Hari*s et al*., 2020) (Tappa and Jammalamadaka, 2018).

An ideal material used for filament fabrication should be thermally stable, non-volatile and non-aerosolizing (Lamichhane, Bashyal, *et al*., 2019).

2.2.2.3. Process Parameters

The printing resolution of the manufactured structure can be controlled by the selection of a combination of parameters in the printer software; print speed, layer height, infill density and temperature of both the nozzle and the building stage (Aza*d et al*., 2020) (Sadia, Alhnan, *et al*., 2018) (Goole and Amighi, 2016) (Ligo*n et al*., 2017) (Zhang *et al.*, 2018) (Mwema and Akinlabi, 2020). Optimization of these parameters can result in accurate material deposition and an object with good mechanical properties without any voids (Babu and Devaprakasam, 2019) (Prasad and Smyth, 2016) (Chia and Wu, 2015) (Tappa and Jammalamadaka, 2018) (Khatri, Shah and Vora, 2018).

The print speed is regulated depending on the FDM type, the complexity of the desired structure, the required final printing resolution and the material properties. Low print speed is needed for particularly viscous materials for the necessary amount of material to be extruded and objects with the predesigned shape and geometry to eventually be built (Azad *et al.*, 2020). When the material solidification on the building plate is slow, a low print speed setting is more suitable for the printed layer to have adequate time to become dry enough and consequently, enable the deposition of the next layers on top of it without destroying it (Jamróz, Kurek, Łyszczarz, Brniak, *et al*., 2017) (Sadi*a et al*., 2018).

Layer height is largely associated with the print speed, as according to the selection of the latter setting, the thickness of the deposited layer is affected, as well as, the external appearance of the final structure; the higher the layer, the lower the quality of the manufactured part (Jamró*z et al*., 2017) (Zem*a et al*., 2017). Longer printing times are needed for the manufacture of a part with very thin layers. The nozzle diameter is another factor that can have an impact on the layer height and this printing setting should, thus, be adjusted according to the selected nozzle size; the higher the nozzle size, the higher the printed layer (Dietmar W Hutmacher, Sittinger and Risbud, 2004) (Goole and Amighi, 2016) (Mwema and Akinlabi, 2020) (Jamróz, Szafraniec, *et al*., 2018).

The infill density controls the amount of the material which will be used for the filling of the fabricated product and consequently, its porosity and mechanical strength. The infill density range is from 0% to 100%, where 0% corresponds to a hollow structure and 100% to a solid one with high mechanical strength (Goole and Amighi, 2016) (Vithani *et al*., 2019b). Various geometries can also be selected for the infill, such as concentric, rectilinear, honeycomb or hexagonal, which will affect the quality and the properties of the final part (Jamró*z et al*., 2017) (Jamróz, Szafraniec, *et al.*, 2018) (Aza*d et al*., 2020).

The temperature of the nozzle and the bed are adjusted based on the nature and the properties of the selected thermoplastic polymer. The filament is heated during the extrusion at a temperature above its melting point for a better flow through the nozzle to be achieved. However, the filament remains for a very short time in the nozzle and hence, the applied nozzle temperature must be higher than the one used for the filament production; this difference can be even larger than 100 °C (Cunha-Filh*o et al*., 2017) (Jamró*z et al*., 2017) (Ah*o et al*., 2019). Polymer viscosity is another material property that will affect the selection of the print temperature, similarly to the print speed setting; the more viscous the material, the higher the temperature needed (Azad *et al.*, 2020) (Chia and Wu, 2015) (Goole and Amighi, 2016) (Mwema and Akinlabi, 2020). If the printed layers on the platform are not fused efficiently, poor surface adhesion will lead to poor mechanical properties of the final part, the creation of cavities and eventually, the failure of the printing process. These issues can be addressed by adjusting the bed temperature for the deposited material to remain longer at or above the glass transition temperature. Consequently, a more gradual solidification will occur which will lead to the manufacture of a more uniform structure (Ligo*n et al*., 2017) (Jamróz, Kurek, Łyszczarz, Brniak, *et al*., 2017) (Prasad and Smyth, 2016) (Mwema and Akinlabi, 2020).

The phenomenon of "die swell" or "extrudate swell" is also observed in objects printed by the FDM. This can be controlled by properly adjusting the nozzle temperature or the ratio between the print speed and the feeding speed. If the filament feeding occurs at a slower rate than the motion of the print head, the swelling of the extruded material can be eliminated due to filament stretching. The effect of gravity might also have an impact on the swelling under specific conditions. Nevertheless, the material deposition is generally fast enough and the distance between the nozzle tip and the bed is short enough to neutralize the impact of gravitational forces (Aho *et al*., 2019).

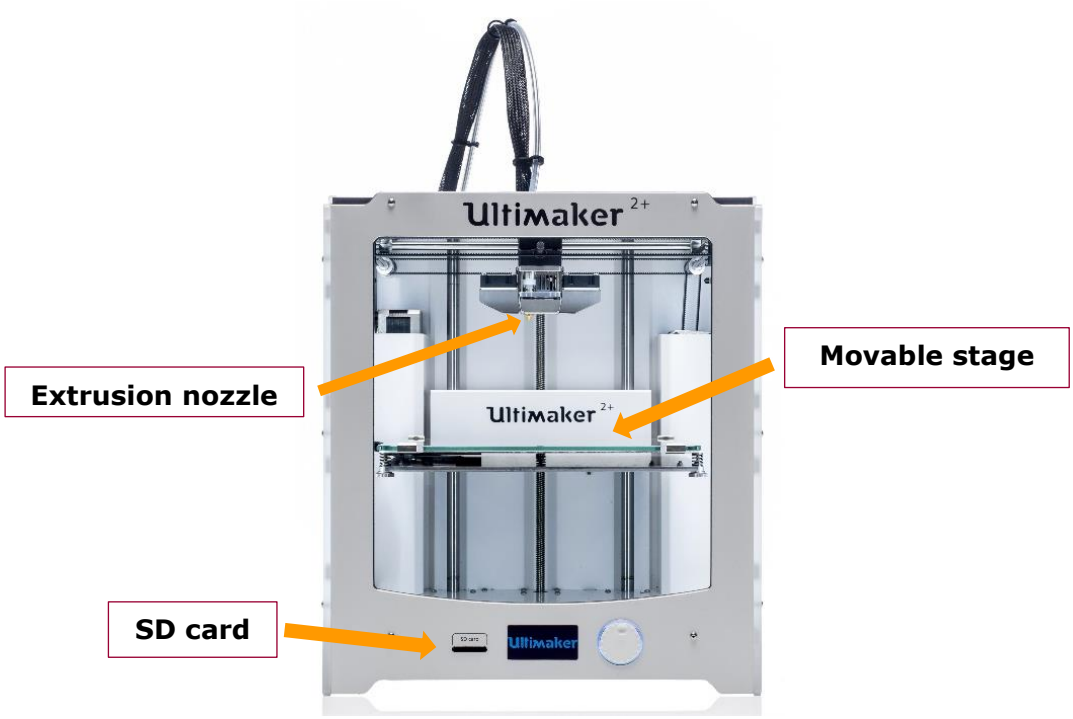

Figure 2.9: *Fused Deposition Modelling 3D printer, Ultimaker 2+. The main parts of the 3D printer (extrusion nozzle, movable stage, SD card) are labelled. This figure is reproduced from Ultimaker 2+ Manual (Ultimaker 2+, 2015).*

A Fused Deposition Modelling (FDM) 3D printer (Ultimaker 2+, Geldermalsen, The Netherlands) was used for the materials printability study (***Figure 2.9***). HMW PCL and LMW PCL filaments produced by the HME were loaded in this printer type. Various printing setups (nozzles) and parameters were initially explored to establish the most promising combinations for the subsequent manufacture of a test shape. Different printing settings were also applied during the fabrication of the selected shape, while its further characterization revealed which ones could be used for future implants printing.

2.2.3. Pressure Assisted Microsyringe 3D printer

Pressure Assisted Microsyringe (PAM) 3D printing from a sometimes heated reservoir is a widely used additive manufacturing technique and has recently drawn considerable interest in the pharmaceutical area for the fabrication of novel dosage forms (Kyle *et al.*, 2017) (Norman *et al.*, 2017) (Shende and Agrawal, 2018) (Cui, Li, *et al*., 2019). This versatile technology demonstrates significant advantages, such as easy operation, compact size, continuous material flow, accurate and precise printing of complex geometries, as well as, various solidification methods even though only materials with particular printability characteristics can be used (Placone and Engler, 2018) (Zidan, Alayoubi, Coburn, *et al.*, 2019) (Zhang *et al.*, 2018) (Ju *et al.*, 2019).

Similarly to the FDM printing process, the desired architecture is initially designed in a relevant design software and a Computer Aided Design (CAD) file (.stl file) is then produced. Afterwards, it is loaded to the printer software, where the printing parameters are adjusted and the CAD architecture is sliced into printable layers. In the end, a .gcode file, suitable for loading to the printer, is created (Placone and Engler, 2018) (Algahtani, Mohammed and Ahmad, 2019).

During slicing, the distance between the layers is essential for sufficient contact between the extruded layers to be obtained and delamination to be avoided. Layers overlap adjustment is particularly depending on the material used each time and the Z height set by the user during the calibration procedure. The latter controls the distance between the nozzle tip and the building platform or between the nozzle tip and the already printed layers on the bed. Mechanical properties of the extruded material play a significant role in the printing accuracy of the final product, while layers overlap might have an impact on them; layers spacing needs to properly be adjusted for no layer sagging to occur, particularly in areas without any support (Placone and Engler, 2018).

Extrudate diameter, also termed thread diameter and strand diameter, is the main way with which the layers distance can be effectively adjusted. Nevertheless, the thread diameter is also affected by a series of other printing parameters, such as nozzle diameter, extrusion rate, pressure, print speed, material viscosity and temperature of the print head (Placone and Engler, 2018) (Algahtani, Mohammed and Ahmad, 2019) (Zidan, Alayoubi, Asfari, *et al*., 2019) (Zhang *et al.*, 2018). When the extrusion rate or pressure decreases, the extrudate diameter decreases.

An increase in the applied pressure might be needed in this case, though, for a continuous flow to be achieved. If the print speed increases, a smaller diameter thread will be deposited on the building stage, while the pressure might also need to be increased for a homogeneous extrusion. Print head temperature is closely associated with the material viscosity, but these parameters also influence the diameter of the strand and consequently, the printing accuracy; the higher the temperature the lower the viscosity of the compounds (Placone and Engler, 2018). Viscous materials can result in nozzle blockage (Aita, Breitkreutz and Quodbach, 2019). In the case of a low viscous material, rapid extrusion will occur, which will affect the diameter consistency of the strand and after its deposition, it will most probably flatten. Proper adjustment of these parameters, thereby, will significantly contribute to a high printing accuracy and structural integrity of the manufactured part (Placone and Engler, 2018) (Aita, Breitkreutz and Quodbach, 2019) (Zhang *et al.*, 2018).

During the printing process, the material loaded in the cartridge is pumped to the nozzle either with pneumatic extrusion or mechanical forces (Tappa and Jammalamadaka, 2018) (Kyle *et al.*, 2017) (Peng *et al.*, 2017) (Konta, García-Piña and Serrano, 2017). The material is, then, deposited on the building stage and it is allowed to cool down. Each extruded layer needs to have adequate time to mostly solidify before the next layer is deposited so as to not result in its collapse. These steps are repeated until the fabrication of the desired object in a layer-by-layer manner (Algahtani, Mohammed and Ahmad, 2019) (Sadia, Alhnan, *et al*., 2018).

There are PAM 3D printers where the building stage can be heated, but this parameter is optional to be set, similarly to the print head temperature, and is adjusted according to the material properties (Algahtani, Mohammed and Ahmad, 2019). Depending on the printer type, materials with different physical, chemical and biological properties, such as rheology, can be loaded and extruded under various conditions. 3D printers with more than one print head allow the production of more complex multimaterial objects (Placone and Engler, 2018) (Kyle *et al.*, 2017) (Vithani *et al*., 2019b). It is noteworthy that printing using especially viscous materials, such as polycaprolactone, is feasible with a PAM 3D printer (Kyl*e et al*., 2017) (Dumitresc*u et al*., 2018).

A disadvantage of this technique, though, is that often post-printing processing is required for the complete solidification of the manufactured object; drying, heating, or desiccation (Cu*i et al*., 2019) (Tian *et al.*, 2019) (Norman *et al.*, 2017) (Sadia, Alhnan, *et al*., 2018) (Ju *et al.*, 2019) (Aita, Breitkreutz and Quodbach, 2020).

PAM 3D printers consist of two main compartments, the printer and the extruder. The former is responsible for the nozzle movement and position, while the latter is for the material flow. Based on the printer type, extrusion is performed using three different systems; a stepper motor driven piston, a conveying screw or pneumatic extrusion (***Figure 2.10***) (Huang, 2018) (Kyle *et al.*, 2017) (Tia*n et al*., 2019) (Placone and Engler, 2018) (Ju *et al.*, 2019) (Sadia, Alhnan, *et al*., 2018) (Algahtani, Mohammed and Ahmad, 2019) (Placone and Engler, 2018) (Peng *et al.*, 2017).

The pneumatic extrusion design, also named pressure-assisted microsyringe method or syringe method, is the selected one for the current study. Compressed gas is applied in this case as the driving force and it forwards the loaded material to the nozzle (***Figure 2.10.b***) (Huang, 2018) (Lim *et al.*, 2018) (Goole and Amighi, 2016) (Pandey *et al.*, 2020) (Sadia, Alhnan, *et al*., 2018) (J*u et al*., 2019) (Aita, Breitkreutz and Quodbach, 2020). The most widely used gas is air, but nitrogen is also used for sterility purposes, such as when biological inks are printed. In this type of extrusion, a wide range of viscoelastic inks can be applied (Huang, 2018). One of its benefits is the faster response time compared with the other two methods, while the cartridge can be pressurized and depressurized rapidly. Therefore, better printing accuracy is obtained (Algahtani, Mohammed and Ahmad, 2019). Nevertheless, its disadvantage relates to its set-up, which is more complex than the motor driven design, as a gas provider and a compressor are required (Huang, 2018). Additionally, solvents are usually mixed with the materials loaded to the cartridge and therefore, post-processing, drying, of the manufactured part is required (Aita, Breitkreutz and Quodbach, 2019).

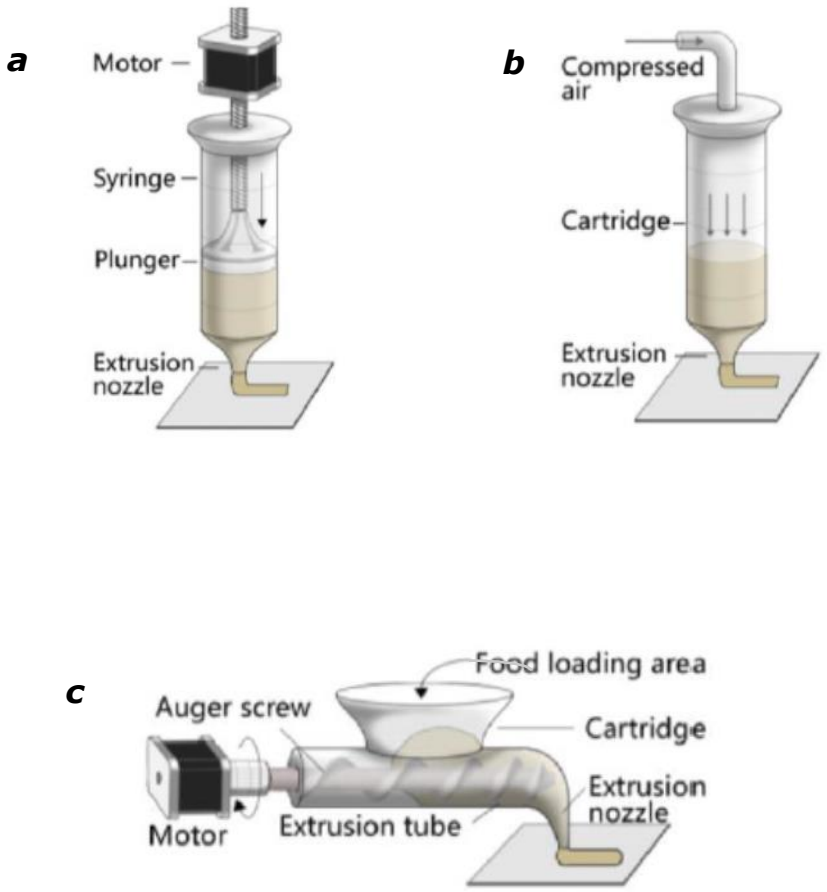

Figure 2.10: *Schematic diagram of the extrusion designs:* ***(a):*** *Stepper motor driven piston system,* ***(b):*** *Pneumatic extrusion and* ***(c):*** *Conveying screw extrusion system. This figure is reproduced from Huang (Huang, 2018).*

For the ink extrusion, three techniques are generally applied: gel-forming extrusion, cold extrusion and hot-melt extrusion. Cold extrusion is at room temperature and no phase transition of the ink occurs, while the latter is observed in the other two approaches (Huang, 2018) (Konta, García-Piña and Serrano, 2017).

In gel-forming extrusion, no heating is involved; only chemical or physical crosslinking of the ink occurs to form the solid (Peng *et al.*, 2017) (Placone and Engler, 2018) (Kyle *et al.*, 2017). The gelation is, thus, activated by ionic species added in the extruded materials or by UV processing of the fabricated objects (Huang, 2018) (Algahtani, Mohammed and Ahmad, 2019) (Zhang *et al.*, 2018).

Cold extrusion or room temperature extrusion is entirely depending on the ink rheology. No heating is used (Tian *et al.*, 2019) (Kyle *et al.*, 2017) (Zhang *et al.*, 2018) (Goole and Amighi, 2016) (Sadia, Alhna*n, et al*., 2018) (Ju *et al.*, 2019) (Aita, Breitkreutz and Quodbach, 2020). The materials extrudability and capability of assembling self-supporting layers rely solely on the ink properties. Ink rheology can be altered, though, by adding thickeners or changing its composition (Huang, 2018). Materials printed generally require a drying step, sometimes promoted by a heating stage or post-processing.

In hot-melt extrusion 3DP, which is the technology applied in the current work, the ink is heated to allow its flow out of the nozzle and hence, its extrusion before it cools down and solidifies in the syringe and nozzle (Huang, 2018) (Pandey *et al.*, 2020) (Tian *et al.*, 2019).

Materials loaded in this 3D printer type can be in a molten, semi-solid or paste form and therefore, no melting is required for their extrusion. Colloidal suspensions, solutions, hydrogels, organic and inorganic pastes, gels, powders, polyurethanes, silicones, polymer latex, plastisols, biomaterials, various molten synthetic polymers, such as polycaprolactone (PCL), polyvinyl alcohol (PVA), polyethylene glycol (PEG), poly (lactic-co-glycolic) acid (PLGA) and hydroxypropyl methylcellulose (HPMC), natural polymers, such as collagen, gelatin, alginate, chitosan, starch and hyaluronic acid, even biologically active ingredients and living cells can be used for the fabrication of objects through pressure assisted microsyringe 3D printing (Shende and Agrawal, 2018) (Jamróz, Szafraniec, *et al*., 2018) (Zhang *et al.*, 2018) (Ligo*n et al*., 2017) (Awa*d et al*., 2018) (Liaw and Guvendiren, 2017) (Palo *et al.*, 2017) (Tappa and Jammalamadaka, 2018) (Lepowsky and Tasoglu, 2018) (Zhang *et al.*, 2018). The starting materials are blended before their loading to the printer. Their physical, chemical and mechanical properties, such as rheological properties, viscosity and miscibility of materials are tested prior to the start of the printing process since they can have a significant impact on their processing –more viscous materials compared to the other 3D printing technologies can be loaded and finally extruded with PAM printers (Zhang *et al.*, 2018) (Vithani *et al*., 2019b) (Dumitresc*u et al*., 2018). Various solvents can be used to decrease the materials viscosity in order for smooth and homogeneous materials forms to be obtained that will not block the nozzle (Sadi*a et al*., 2018). The solvent can be removed from the final product through a post-processing step which will include drying in an oven or a desiccator

(Cui, Li, *et al*., 2019). It is required for the material mixtures to be free of large particulates for the nozzle to not be blocked during the 3D printing process (Sadia, Alhnan*, et al*., 2018).

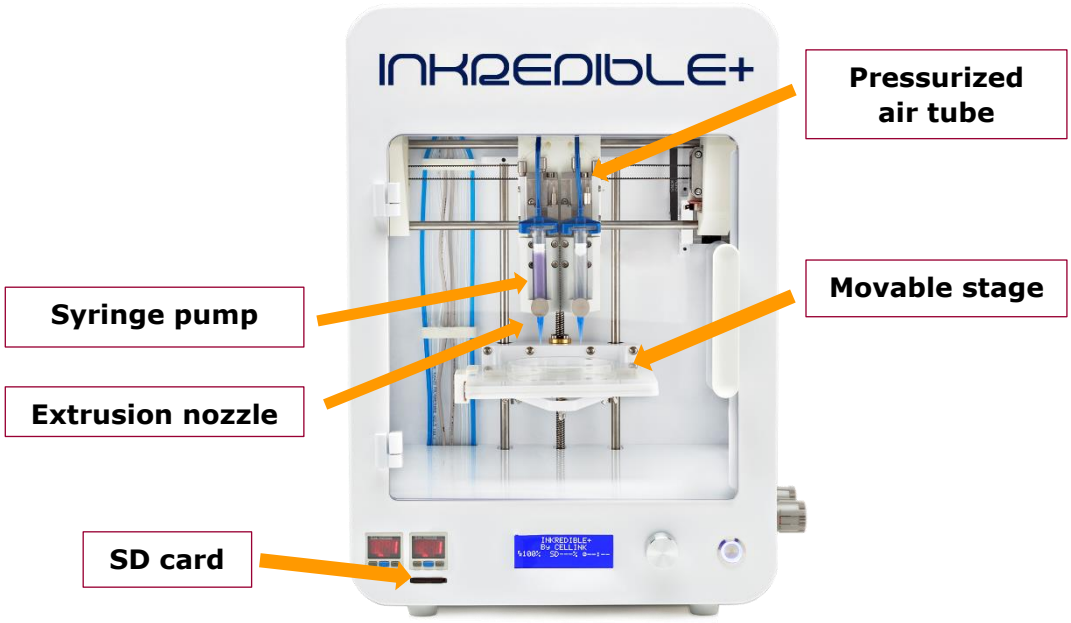

Figure 2.11: *Pressure Assisted Microsyringe 3D printer, Inkredible+, Cellink. The main parts of the 3D printer (pressurized air tube, syringe pump, extrusion nozzle, movable stage, SD card) are labelled. This figure is reproduced from Inkredible+ Manual (Inkredible+, 2019).*

A Pressure Assisted Microsyringe 3D printer (Inkredible +, Cellink, Gothenburg, Sweden) has been used for the manufacture of drug loaded and drug free implants. Several steps of printing tests and optimizations have been conducted for the fabrication of the final formulations with the desired properties (***Figure 2.11***).

Firstly, the printability (successful extrusion of the loaded materials) of LMW and HMW PCL was investigated with various printing setups (cartridges, nozzles) and parameters. The production of a test shape, with dimensions as close as possible to the dimensions of the predesigned shape, followed by characterization of the prints indicated the most promising combinations of materials and settings for the

next stage of the study, the manufacture of implants. Disc-shaped HMW PCL implants loaded with 30% w/w lidocaine or 5% w/w lidocaine or drug free implants were printed.

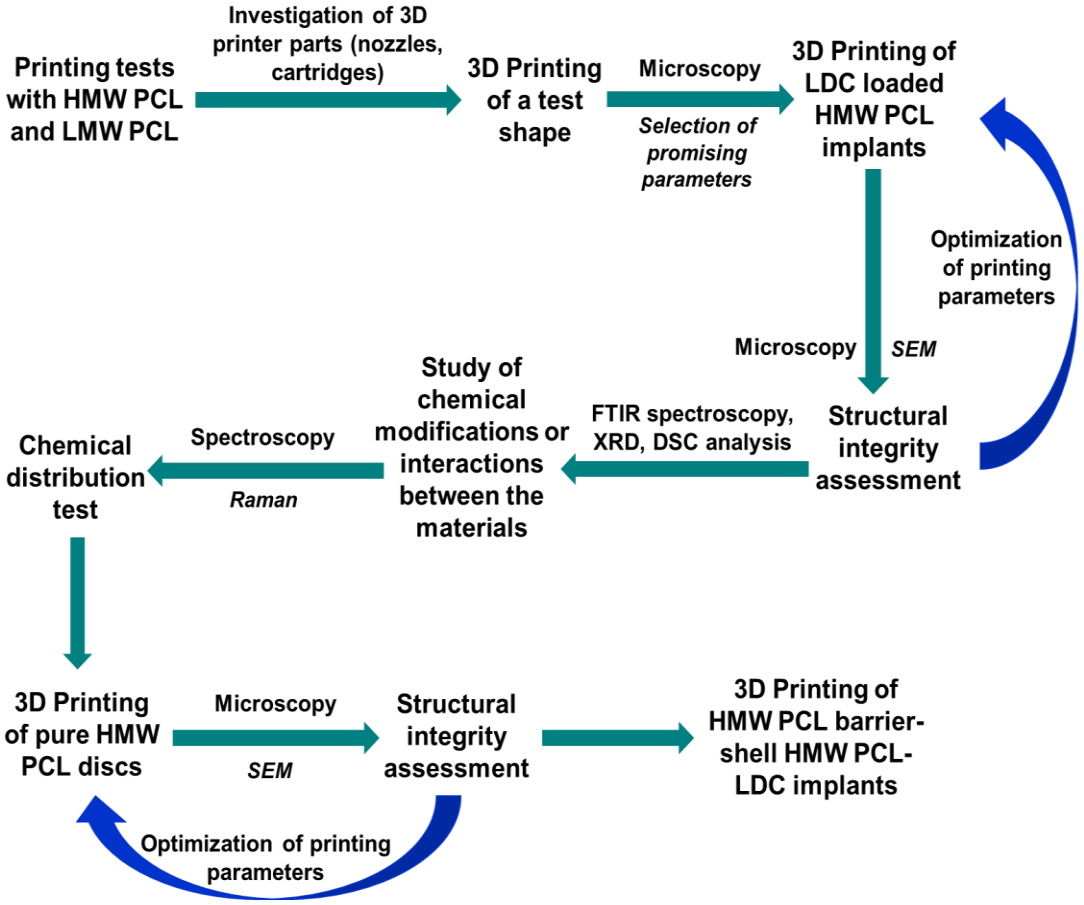

Figure 2.12: *Schematic diagram of the optimization procedure for the establishment of the 3D printing parameters for the manufacture of the lidocaine loaded HMW PCL implants and their characterization procedures.*

Finally, implants with an HMW PCL barrier-shell were manufactured based on the established settings. Characterization of the compounds before and after their mixing and extrusion was conducted to explore potential changes in their properties or any chemical interactions or modifications occurred during the 3D printing process. The process flow of manufacture and characterisation are summarised in ***Figure 2.12.***

2.3. 3D PRINTING METHODS

2.3.1. Filament production through Hot Melt Extrusion

A Hot Melt Extruder (Desktop Extruder, Noztek Pro, Shoreham-by-Sea, UK) was used for the production of LMW PCL and HMW PCL filaments by applying different settings. The size of the steel die used for the production of the filament was 3 mm.

The material used for the filament production was loaded in the extruder and was allowed to equilibrate for 10 min to the desired temperature to allow a homogeneous distribution of the molten mass to be created. Different combinations of extrusion speeds (30 - 40 rpm) and temperatures (45 - 215 ^{o}C) at the two heating zones of the barrel were explored for the production of both HMW PCL and LMW PCL filaments with and without the addition of the plasticiser Triethyl Citrate (***Table 2.1*** and ***Table 2.2***). All the combinations in the HME were tested twice.

Mixing for both HMW PCL and LMW PCL with 1% w/w Triethyl Citrate (TEC) was performed using a mortar and pestle for 3 min.

Table 2.1: *Combinations of temperatures and extrusion speeds for the HMW PCL and LMW PCL filament production tests in the HME (n=2).*

Temperature for heating zone 1 (°C)	Temperature for heating zone 2 (°C)	Extrusion speed (rpm)	HMW PCL	LMW PCL
45	45	30	•	
45	45	35	•	
45	45	40	•	
50	50	30	•	
50	50	35	•	
50	50	40	•	
60	60	30	•	
60	60	35	•	
60	60	40	•	
70	70	30	•	
70	70	35	•	
70	70	40	•	
80	80	30	•	•
80	80	35	•	•
80	80	40	•	•
90	90	30	•	•
90	90	35	•	•
90	90	40	•	•
100	100	30	•	•
100	100	35	•	•
100	100	40	•	•
100	115	30	•	
150	150	30	•	•
150	150	35	•	•
150	150	40	•	•
180	180	30	•	•
180	180	35		•
180	180	40		•
200	200	30	•	•
200	200	35		•
200	200	40	•	•
215	215	40	•	

Table 2.2: *Combinations of temperatures and extrusion speeds for the HMW PCL – TEC and LMW PCL-TEC filament production tests in the HME (n=2).*

		Temperature for heating zone 2					
		45 °C	**50 °C**	**55 °C**	**60 °C**	**65 °C**	**70 °C**
Temperature for heating zone 1 / Extrusion speed	**45 °C/ 30 rpm**	•	•				
	45 °C/ 35 rpm	•	•				
	45 °C/ 40 rpm	•	•				
	50 °C/ 30 rpm	•	•	•			
	50 °C/ 35 rpm	•	•	•			
	50 °C/ 40 rpm	•	•	•			
	55 °C/ 30 rpm		•	•	•		
	55 °C/ 35 rpm		•	•	•		
	55 °C/ 40 rpm		•	•	•		
	60 °C/ 30 rpm			•	•	•	
	60 °C/ 35 rpm			•	•	•	
	60 °C/ 40 rpm			•	•	•	
	65 °C/ 30 rpm				•	•	•
	65 °C/ 35 rpm				•	•	•
	65 °C/ 40 rpm				•	•	•
	70 °C/ 30 rpm					•	•
	70 °C/ 35 rpm					•	•
	70 °C/ 40 rpm					•	•

2.3.2. Printing tests in an FDM 3D printer

The printability of the LMW PCL-TEC and HMW PCL-TEC filaments were investigated using temperatures from 60 to 190 °C and steel nozzles with different diameters (0.4 mm and 0.8 mm). All the combinations were tested twice.

Successful extrusion of the loaded filament at the applied printing parameters was an indication of the materials printability.

2.3.3. 3D Printing of a simple object with LMW PCL-TEC and HMW PCL-TEC filaments in an FDM 3D printer

A test shape was selected to assess the printing resolution of different settings. The selected object was a triangle, as it consists of a combination of lines and angles. The printing of a shape with dimensions close to the ones of the predesigned shape would indicate the most promising printing parameters for the fabrication of the drug loaded formulations.

A test triangle shape was designed using TinkerCAD online software (Autodesk Inc.), where the dimensions of the object were adjusted (25 mm length x 22 mm width x 1 mm height and 60^{o} internal angle). The .stl file was then uploaded to Ultimaker Cura software where the printing settings were adjusted and the files were saved in a .gcode format. Different combinations of temperatures (180, 190 ^{o}C) and print speeds (5 - 20 mm/s) were examined with other parameters kept constant, as presented in ***Table 2.3***. The build plate temperature was used at Room Temperature, which was measured to be 23 ^{o}C. A steel nozzle with a diameter of 0.8 mm was used for the 3D printing on a PET substrate.

Table 2.3: *Settings for the 3D printing of HMW PCL-TEC and LMW PCL-TEC triangles in the FDM 3D printer.*

Printing Parameters	
Build Plate Temperature	23 ^{o}C
Layer Height	0.60 mm
Infill Density	100 %
Infill Pattern	Lines

2.3.4. Printing tests in a PAM 3D printer

The printability (successful extrusion of the loaded materials) of PCL (LMW:25 kDa and HMW:50 kDa) were investigated using a plastic and an aluminium cartridge at different printing settings. The polymer was loaded in the cartridge at room temperature (the Room Temperature was measured to be 23 °C) and was allowed to equilibrate for 10 min at the studied temperature each time in the printer to melt completely.

The highest temperature that could be used in this 3D printer type was 130 °C and the highest pressure 400 kPa.

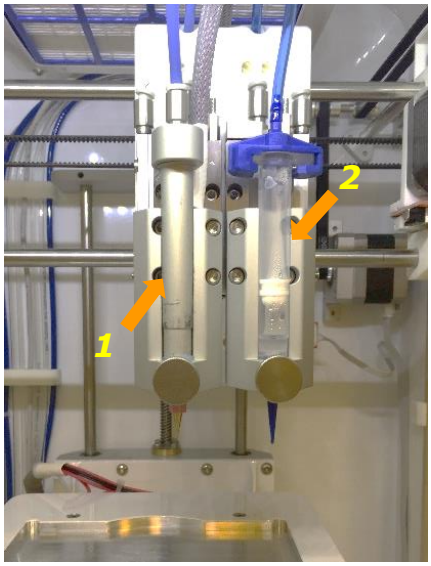

Figure 2.13: *Pressure Assisted Microsyringe 3D printer with* ***(1):*** *aluminum cartridge and steel nozzle and* ***(2):*** *plastic cartridge and plastic nozzle.*

Different combinations of temperatures (80 - 130 °C), pressure (300 – 400 kPa), and nozzle types (plastic nozzles with a diameter of 0.20 - 0.41 mm and steel nozzle with a diameter of 0.41 mm) were studied. A plastic cartridge has been used for the printing tests, which were performed twice (***Figure 2.13.2***).

Different combinations of temperatures (80 - 130 °C), nozzle sizes (0.34, 0.61 mm) at a pressure of 400 kPa were examined. An aluminium cartridge has been used for the printing tests, which were conducted twice (***Figure 2.13.1***).

2.3.5. 3D Printing of a simple object with LMW PCL and HMW PCL in a PAM 3D printer

Firstly, a test shape was chosen to assess the printing resolution achieved in different settings. The printing of a shape with dimensions close to the ones of the predesigned shape will indicate the most promising printing parameters for the fabrication of the drug loaded formulations. As previously, the selected object was a triangle, designed in TinkerCAD online software (Autodesk Inc.), where the dimensions of the object were adjusted. Triangles with different layer heights (25 mm length x 22.93 mm width x 0.82 mm height and 60° internal angle for a nozzle diameter of 0.61 mm, 25 mm length x 22.93 mm width x 0.45 mm height and 60° internal angle for a nozzle diameter of 0.34 mm) have been designed as the printing of just 1 layer was the desired outcome.

Table 2.4: *Settings for the 3D printing of HMW PCL and LMW PCL triangles in the PAM 3D printer with nozzle diameters of 0.61 mm and 0.34 mm.*

Printing Parameters		
	0.61 mm	***0.34 mm***
Bed Temperature	30 °C	30 °C
Pressure	400 kPa	400 kPa
Layer Height	0.82 mm	0.45 mm
Infill Density	30 %	30 %
Extrusion width	100 %	100 %
Infill Pattern	rectilinear	rectilinear

Afterwards, the .stl files were uploaded to the Cellink Heartware software where the printing parameters were adjusted and the files were saved in a .gcode format. The polymer was loaded in the cartridge at room temperature (the Room Temperature was measured to be 23 °C) and was allowed to equilibrate for 10 min at the studied temperature each time in the printer to melt completely. Different combinations of temperatures (100 - 130 °C), print speeds (1 - 6 mm/s) and nozzle sizes (0.34, 0.61 mm) were examined with other parameters kept constant, as can be seen in ***Table 2.4***. An aluminium cartridge and steel nozzles were used for the printing of the triangles on a PET substrate.

The temperature on the movable stage was selected to be higher than the room temperature to enhance the adhesion of the printed object.

2.3.6. 3D Printing of HMW PCL-LDC implants in a PAM 3D printer with different printing settings and drug loading

The implants were decided to be fabricated in a disc shape of dimensions 10 mm diameter and 2 mm height for ease of handling. The discs were designed in TinkerCAD online software (Autodesk Inc.), as in the case of the triangles (***Figure 2.14***). The .stl files were, then, uploaded to the Cellink Heartware software where the printing parameters were adjusted and the files were saved in a .gcode format.

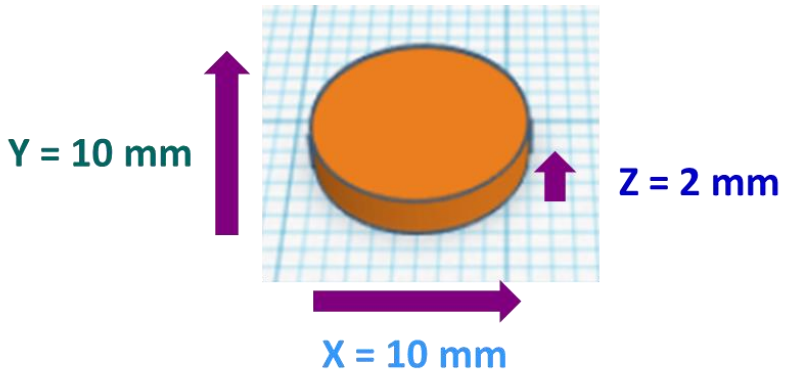

Figure 2.14: *Disc designed in TinkerCAD for the printing of lidocaine loaded HMW PCL implants in the PAM 3D printer with a nozzle diameter of 0.61 mm. The dimensions of the triangles are labelled.*

2.3.6.1. HMW PCL-LDC powder preparation for 3D printing

HMW PCL and LDC powders were first weighed and then, mixed using a mortar and a pestle for 3 min for a powder mixture (HMW PCL-LDC 30%) containing 70% w/w HMW PCL and 30% w/w LDC to be obtained (***Figure 2.15***). The same procedure was followed for the preparation of a mixture (HMW PCL-LDC 5%) containing 95% w/w HMW PCL and 5% w/w LDC.

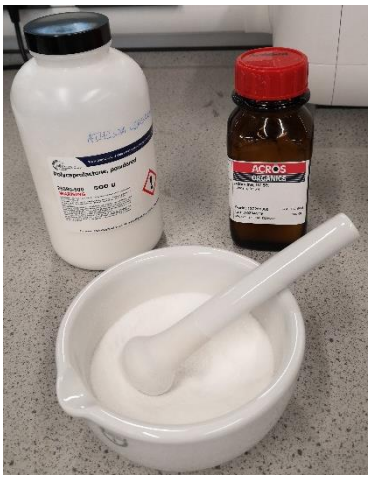

Figure 2.15: *HMW PCL and LDC powders mixed with a mortar and a pestle.*

2.3.6.2. 3D Printing of LDC loaded and free HMW PCL implants

The printing settings for the manufacture of polycaprolactone encased and non-encased implants with two different LDC loading, 30% and 5% w/w, are presented in the following sections.

2.3.6.2.1. 3D Printing of HMW PCL-LDC 30% implants

The previously prepared polymer-drug mixture was loaded in the aluminium cartridge at room temperature and was allowed to equilibrate for 10 min at the studied temperature each time in the printer to melt completely. Different combinations of temperatures (70 - 130 °C), print speeds (1 – 1.5 mm/s), extrusion widths (50 – 100 %), line spacing (distance between the centre of the printed lines) (0.305 – 0.610 mm) and pressure (75 – 400 kPa) were examined. A temperature of 24 °C in the building stage was attributed to the measured room temperature. Other parameters were kept constant (***Table 2.5***). An aluminium cartridge and a steel nozzle with a diameter of 0.61 mm were used for the printing of the implants on a PET substrate.

Table 2.5: *Settings for the 3D printing of HMW PCL-LDC 30% implants in the PAM 3D printer with a nozzle diameter of 0.61 mm.*

Printing Parameters	
Layer Height	0.82 mm
First Layer Height	1.3 mm
Infill Density	30 %
Infill Pattern	concentric

2.3.6.2.2. 3D Printing of HMW PCL-LDC 5% implants

The previously prepared polymer-drug mixture was loaded in the aluminium cartridge at room temperature and was allowed to equilibrate for 10 min at the studied temperature each time in the printer to melt completely. Different combinations of temperatures (70 – 110 °C), extrusion widths (50 – 60 %), line spacing (distance between the centre of the printed lines) (0.305 – 0.366 mm), pressure (125 – 400 kPa) and bed temperatures (24 – 40 °C) were explored. A temperature of 24 °C in the building stage was attributed to the measured room temperature. Other parameters were kept constant, as can be seen in ***Table 2.6***. An aluminium cartridge and a steel nozzle with a diameter of 0.61 mm were used for the printing of the implants on a PET substrate.

Table 2.6: *Settings for the 3D printing of HMW PCL-LDC 5% implants in the PAM 3D printer with a nozzle diameter of 0.61 mm.*

Printing Parameters	
Layer Height	0.82 mm
Print Speed	1 mm/s
First Layer Height	1.3 mm
Infill Density	30 %
Infill Pattern	concentric

2.3.6.2.3. 3D Printing of HMW PCL implants

The as-received polycaprolactone powder was loaded in the aluminium cartridge at room temperature (Room Temperature was measured to be 24 °C) and was allowed to equilibrate for 10 min at 110 °C in the printer to melt completely. Discs with dimensions of 10 mm length x 10 mm width x 2 mm height were printed with different extrusion widths (40 – 50 %) and line spacing (distance between the centre of the printed lines) (0.244 - 0.305 mm). Other parameters were kept constant, as can be seen in ***Table 2.7***.

Table 2.7: *Settings for the 3D printing of HMW PCL implants in the PAM 3D printer with a nozzle diameter of 0.61 mm.*

Printing Parameters	
Layer Height	0.82 mm
Print Speed	1 mm/s
First Layer Height	1.3 mm
Infill Density	30 %
Infill Pattern	concentric
Pressure	400 kPa
Bed temperature	40 °C
Print temperature	110 °C

An aluminium cartridge and a steel nozzle with a diameter of 0.61 mm were used for the printing of the implants on a PET substrate.

2.3.7. 3D Printing of HMW PCL barrier-shell HMW PCL-LDC 30% implants in a PAM 3D printer

Disc-shaped polycaprolactone barrier-shell HMW PCL-LDC 30% (HMW PCL – HMW PCL-LDC 30%) implants were printed in several stages starting with the HMW PCL base and shell, followed by the printing of the drug loaded polymeric formulation and the HMW PCL cap in the end (***Figure 2.16***).

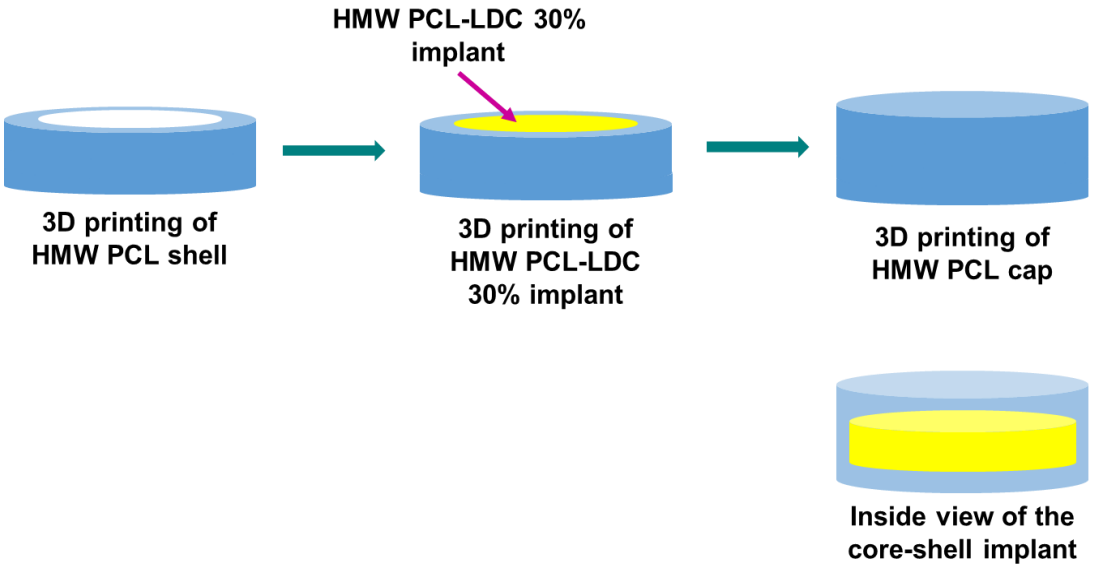

Figure 2.16: *Schematic diagram of 3D printing of Polycaprolactone barrier-shell HMW PCL-LDC 30% implants in several stages. The white circle represents the gap inside the HMW PCL shell and the yellow circle the HMW PCL-LDC 30% implant.*

The dimensions of this formulation were 11 mm length x 11 mm width x 4 mm height. The number of the printed layers was 4 with a layer thickness of 1 mm. The thickness of the HMW PCL barrier was 1 mm. The dimensions of the HMW PCL-LDC 30% implant printed as a core were 9 mm length x 9 mm width x 2 mm height. The number of the printed layers was 2 with a layer thickness of 1 mm.

The geometry of the produced core-shell implant was designed in TinkerCAD online software (Autodesk Inc.).

The previously prepared polymer-drug mixture or the as-received PCL powder was loaded in the aluminium cartridge at room temperature (Room Temperature was measured to be 24 °C) and was allowed to equilibrate for 10 min at 110 °C in the printer to melt completely. The printing settings for each part are presented in ***Table 2.8***. An aluminium cartridge and a steel nozzle with a diameter of 0.61 mm were used for the printing of the implants on a PET substrate.

Table 2.8: *Settings for the 3D printing of each part of the HMW PCL barrier-shell HMW PCL-LDC 30% implant in the PAM 3D printer with a nozzle diameter of 0.61 mm.*

Printing Parameters	**Implant part**	
	HMW PCL barrier - shell	***HMW PCL-LDC 30% core***
Layer Height	0.82 mm	0.82 mm
Print Speed	1 mm/s	1 mm/s
First Layer Height	1.3 mm	1.3 mm
Infill Density	30 %	30 %
Infill Pattern	concentric	concentric
Pressure	400 kPa	125 kPa
Bed temperature	40 °C	40 °C
Print temperature	110 °C	110 °C
Extrusion width	40%	60%

2.4. CHARACTERIZATION TECHNIQUES

2.4.1. Differential Scanning Calorimetry (DSC)

DSC was conducted to study the thermal properties of PCL and lidocaine before and after their mixing, hot melt extrusion and 3D printing using a Differential Scanning Calorimeter, DSC 8000, Perkin Elmer (Waltham, Massachusetts, USA) (***Figure 2.17.a***). Pyris Manager software was used for the data analysis.

Before the running of the samples, empty sample pans were placed in the DSC for the background to be checked in case substances from previous measurements have remained in the bases. The temperature program was the same as the samples. The temperature in the Intercooler was –105 °C. The selected gas was Nitrogen with a flow rate of 20 ml/min. One heating-cooling cycle was run (***Figure S.1***).

a  ***b*** 

Figure 2.17: (a): *Differential Scanning Calorimeter, DSC 8000, Perkin Elmer and* ***(b):*** *Closed aluminium sample pans.*

Approximately 15 mg (analytical balance ABT, 100-5NM, KERN & SOHN GmbH, Balingen, Germany) amounts of pure LMW and HMW PCL powders, HMW PCL-LDC powder mixtures, LMW and HMW drug free and drug loaded 3D printed objects were weighed and then, sealed in aluminium pans (***Figure 2.17.b***). The temperature programme was adjusted from -10 to 110 °C at a rate of 10 °C/min

and two heating-cooling cycles were run. The temperature in the Intercooler was –105 °C. The selected gas was Nitrogen with a flow rate of 20 ml/min.

Three heating-cooling cycles were run for the HMW PCL powder with the above mentioned settings.

Three heating-cooling cycles were run for the HMW PCL-LDC 30% powder mixture from -10 to 110 °C at a rate of 1 °C/min.

An empty sealed aluminium pan was used as a reference.

Approximately 15 mg amounts of lidocaine were weighed and then, sealed in aluminium pans. The temperature programme was adjusted from 25 to 100 °C at a rate of 10 °C/min and two heating-cooling cycles were run. The temperature in the Intercooler was –105 °C. The selected gas was Nitrogen with a flow rate of 20 ml/min. An empty sealed aluminium pan was used as a reference.

The crystallinity degree (X_C %) of PCL before and after its mixing with lidocaine and 3D printing was calculated using the following equation:

$$X_c\,\% = \frac{\Delta H_f}{\Delta H_{f0}} * 100 \qquad \textbf{(1)}$$

Where ΔH_f is the enthalpy of fusion of the sample measured at the melting point and ΔH_{f0} is the enthalpy of fusion of 100% crystalline PCL. According to the literature data, the value used for the ΔH_{f0} was 139.5 J/g (Ferreira *et al*., 2017) (Taylor *et al.*, 2007) (Rychter *et al*., 2018a) (Sravanthi, 2009).

2.4.2. X-Ray Diffraction (XRD)

To reveal the crystal forms of HMW PCL, LMW PCL and lidocaine before and after their mixing, hot melt extrusion and 3D printing, XRD analysis was performed using a PANalytical X'Pert Pro diffractometer (Royston, United Kingdom) in reflection mode using Cu Ka_1 (lambda = 1.54 Å) (***Figure 2.18***). X'Pert Data software was used for data analysis.

Figure 2.18: (a): *PANalytical X'Pert Pro diffractometer.* ***(b):*** *PANalytical X'Pert Pro diffractometer for sample analysis.*

Before the samples scan, an empty brass sample holder was run at the same program as the samples for the holder's background to be checked (***Figure S.2***).

Approximately 100 mg amounts of each sample were placed in a brass zero background holder. The scan was operated at a voltage of 40 kV and a current of 40 mA. The scan range was from 5 to 40 (2θ degrees) with 51 sec step time and 0.02 degrees/min scan rate.

The crystallinity percentage of PCL and LDC before and after their mixing and 3D printing was calculated by firstly assuming that the experimentally obtained crystalline and amorphous intensities are proportional to the theoretical crystalline and amorphous fractions of the samples. A Gaussian fit was, then, used for the calculation of the area under each peak in the CASA XPS software. The following equation was used to estimate the crystallinity degree (X_C %):

$$X_c\,\% = \frac{A_c}{A_c + A_a} * 100 \qquad \textbf{(2)}$$

Where A_c and A_a correspond to the areas related to the crystalline and amorphous phases of the sample to the diffractograms, respectively (Monteiro, Inês and

Tavares, 2018a) (Zidan *et al*., 2012) (Rumondor and Taylor, 2010) (Lopez-rubio *et al.*, 2008).

2.4.3. Optical Microscopy

The side width and the angles of the 3D printed polymeric triangles were measured using an optical microscope (Nikon Eclipse LV100ND, Nikon Metrology UK Ltd, Derby, UK) (***Figure 2.19***), as well as, the NIS-Elements and Image J software to determine which ones of the investigated different printing settings were the most promising ones for the subsequent manufacture of the drug loaded polymeric implants.

Figure 2.19: *Optical microscope Nikon Eclipse LV100ND.*

2.4.4. Scanning Electron Microscopy (SEM)

SEM analysis was performed on the pure HMW PCL and LDC powders to determine their particles size and morphology. The lidocaine loaded PCL implants printed with different parameters were also characterized. HMW PCL encased and non-encased formulations were characterized, as well, after *in vitro* drug release studies to detect the early stages of PCL degradation.

A small amount of the as-received HMW PCL and LDC powders was placed on sticky metallic round discs (***Figure 2.20.c***). The excess powder was removed for a better gold coating to be achieved.

The 3D printed implants were stuck on metallic round discs.

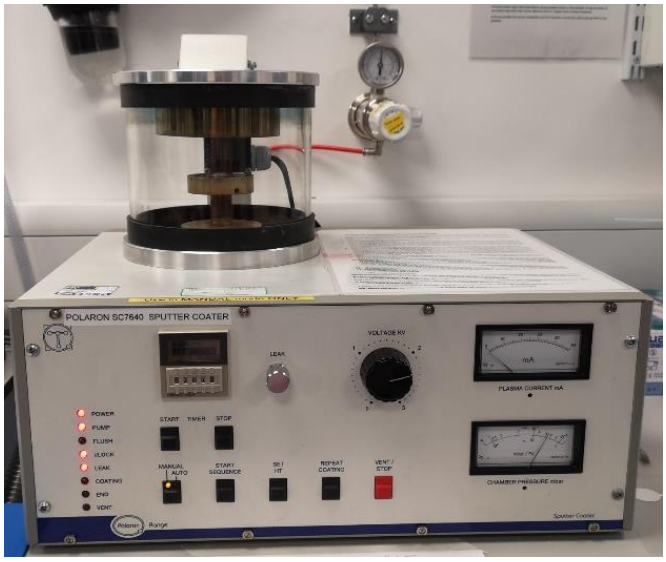

a

b

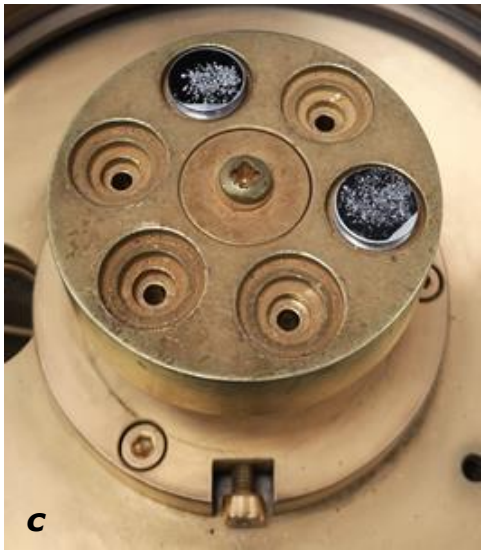

c

Figure 2.20: (a): *Gold Coater Polaron SC7640 Sputter Coater,* ***(b):*** *Implants before gold coating,* ***(c):*** *HMW PCL and LDC powders before gold coating.*

The metal round discs were, then, placed in the base of the gold coating machine (Polaron SC7640 Sputter Coater, Quorum Technologies Ltd, Kent, UK) (***Figure 2.20.b***). The gold coating was performed for 90 sec at a voltage of 2.2 kV, chamber pressure of 4 x 10^{-2} mbar, and plasma current of 20 mA (***Figure 2.20.a***). A thin and even layer of conductive gold coating (10-15 nm) is required to not affect the imaging of the samples due to charging that would occur on an insulator (***Figure 2.21.a***).

a

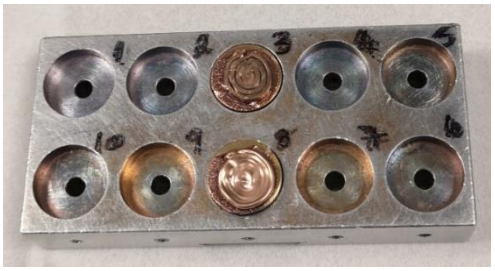

b

Figure 2.21: (a): *Implants after gold coating on the SEM sample holder,* ***(b):*** *JEOL 6060LV SEM instrument.*

The gold coated samples were placed in the SEM holder (***Figure 2.21.a***) and inserted into the SEM base (Scanning Electron Microscope JEOL 6060LV, Field Emission Gun SEM with Tungsten Electron Filament as an electron source, JEOL UK Ltd, Welwyn Garden City, UK) (***Figure 2.21.b***). The SEM parameters were adjusted to optimize image quality; accelerating voltage of 10 kV, Working Distance (WD) of 21 mm, Z height of 20 mm and spotsize of 43 nm. Images from

different areas (top and bottom side for the non-encased lidocaine loaded and free HMW PCL implants, top and bottom side and outside layers-side view for the HMW PCL core-shell implants) of the samples were then taken, with various magnifications adjusting the focus, contrast, and brightness when needed. Image J software was used for further analysis of the SEM images.

2.4.5. Fourier-Transform Infrared Spectroscopy (FTIR)

FTIR analysis was performed to investigate potential chemical modifications or interactions between PCL and lidocaine after their mixing and 3D printing. A Diamond Attenuated Total Reflectance (ATR) accessory was used for all the characterizations. ATR-FTIR spectra were obtained using an Agilent Cary 630 FTIR spectrometer (Stockport, UK) (***Figure 2.22***).

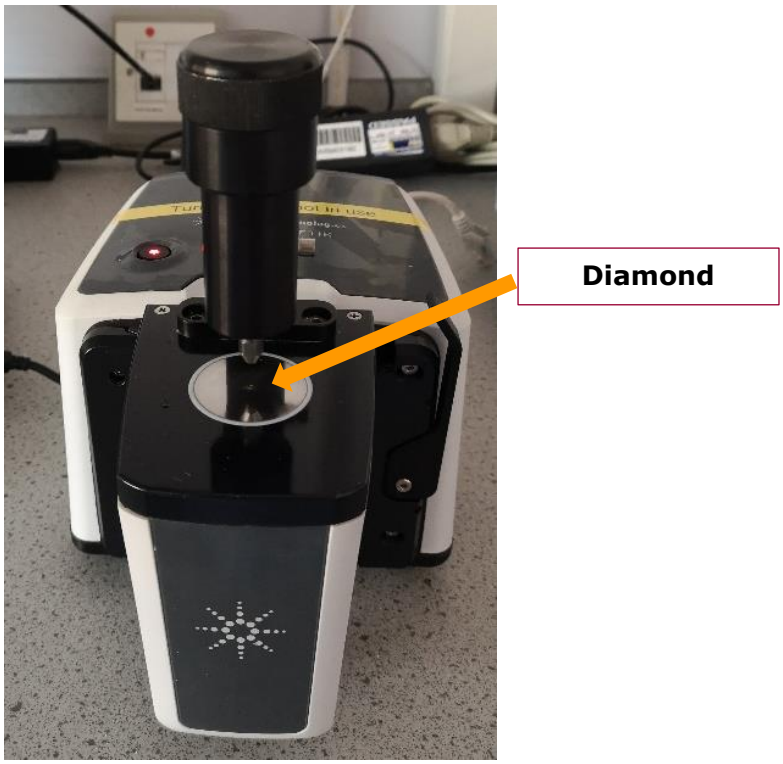

Figure 2.22: *Agilent Cary 630 FTIR spectrometer.*

A small amount of the pure HMW PCL and LDC powders, as well as, of the HMW PCL-LDC 30% and HMW PCL-LDC 5% powders was placed on top of the ATR crystal.

3D printed lidocaine loaded and free polycaprolactone implants were placed on top of the ATR crystal.

The sample recording was operated at room temperature (room temperature was measured to be 23 ^{o}C) in the region of 3500 – 420 cm^{-1} with a resolution of 4 cm^{-1} using 100 scans. The sampling surface was 200 μm with a 2 μm depth of penetration of the infrared energy. Before the sample analysis, an empty ATR cell without any sample was recorded as a background spectrum with the same settings to be checked that no substances from previous measurements have remained on the crystal. Agilent Resolutions Pro software was used for data analysis.

2.4.6. Raman Spectroscopy

Raman analysis was conducted on the pure HMW PCL and lidocaine powders, as well as, on the 3D printed HMW PCL loaded implants before and after the dissolution studies to investigate the polymer and drug distribution on their surface.

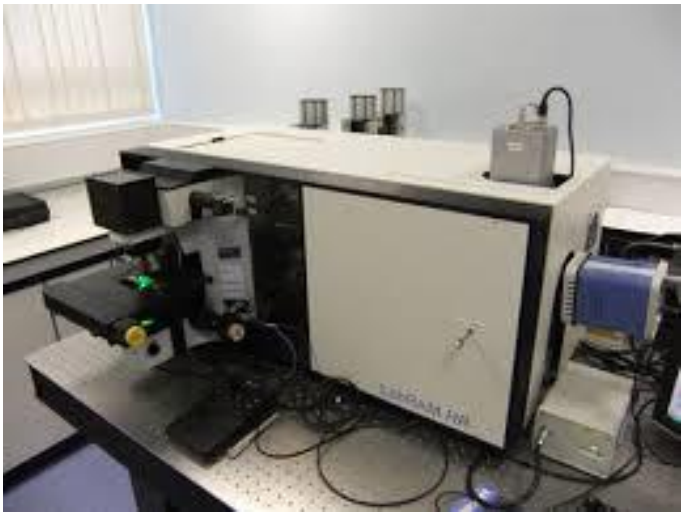

Figure 2.23: *Horiba LabRAM HR Confocal Raman microscope.*

Single-point Raman spectra were acquired using a Horiba LabRAM HR Confocal Raman microscope (Northampton, UK) with an automated xyz stage (Märzhäuser) (***Figure 2.23***).

A small amount of the pure HMW PCL and LDC powders was placed on glass slides for their analysis in the microscope.

3D printed HMW PCL – LDC 30% implants before and after dissolution were placed on glass slides for their analysis in the microscope.

The collection of the spectra was performed with a 785 nm laser adjusted to a power of 20 mW, a 100x objective lens, a 200 μm confocal pinhole and a 300 lines mm^{-1} grating. The measurements were carried out in the region of 400 – 1800 cm^{-1} with an acquisition time of 30 sec after 2 accumulations for the noise spikes due to cosmic rays to be automatically removed and the signal to noise ratio to be improved. The beam spot size was 1 μm, while the depth of analysis 5-10 μm.

2.5. STATISTICAL ANALYSIS

All the data were presented, where appropriate, as a mean ± standard deviation (SD). One-way analysis of variance (ANOVA) was employed using GraphPad Software (GraphPad Software, LLC) to analyse the size of the 3D printed implants and define whether there are any significant differences among the formulations printed with different printing parameters. Differences below the probability level ($p \leq 0.05$) were considered statistically significant, while differences above the probability level ($p > 0.05$) were considered not statistically significant.

2.6. DRUG RELEASE STUDIES

2.6.1. Dissolution medium preparation

A Phosphate Buffered Saline (PBS) dissolution medium with a concentration of 2.3 mM and 0.14 M NaCl was prepared by dissolving 0.063 g KH_2PO_4, 0.261 g Na_2HPO_4

and 8.4 g NaCl in 1000 ml dH_2O at 120 °C under 400 rpm magnetic stirring (RCT basic, IKA England LTD, Oxford, UK) for 1 hour.

In case of water evaporation, dH_2O was added for the final volume of the PBS solution to be 1000 ml. The pH value of the final solution was measured to be 7.4 using a pH meter (FiveEasy pH meter F20, Mettler-Toledo Ltd., Leicester, UK) (***Figure 2.24***).

Figure 2.24: *FiveEasy pH meter F20, Mettler-Toledo Ltd.*

The phosphates and NaCl concentrations were corresponding to the physiological phosphates (1.8 – 2.3 mM) and sodium chloride concentrations (0.135 – 0.147 M) in the blood (Song, 2017) (Heer *et al.*, 2000). In most body fluids, except for urine, the ratio of the phosphates concentration is $[HPO_4^{2-}]:[H_2PO_4^-] \sim 4:1$ (Bansal, 1990).

2.6.2. Lidocaine solubility in aqueous solutions

The solubility of lidocaine in aqueous solutions was investigated in various concentrations, 1 – 4 mg/ml, to determine the saturation concentration of the selected model drug in dH_2O and the dissolution medium.

Lidocaine solutions with concentrations of 1, 2, 3 and 4 mg/ml were prepared by dissolving a proper amount of the drug powder in dH_2O or PBS under magnetic stirring of 300 rpm at various temperatures, 70 – 100 °C, until a clear solution was obtained, indicative of complete solubilisation.

Bath sonication (Ultrasonic Cleaning Bath, FB15051, Fisherbrand, Loughborough, UK) was also used for the solutions with the highest investigated lidocaine concentrations, 3 and 4 mg/ml, for 30, 60 and 105 min.

2.6.3. In vitro drug release studies using a Flow-Through Cell Apparatus (USP Apparatus IV)

Dissolution studies were performed to investigate lidocaine release from the differently printed implants, as well as, the effectiveness of the HMW PCL barrier-shell, using a SOTAX CE7 smart USP 4 "flow-through" dissolution tester (Foston, UK) equipped with 7 tablet cells of a diameter of 22.6 mm, each one connected with a glass bottle placed on a magnetic stirrer (RT 10, IKA England LTD, Oxford, UK) (***Figure 2.25***). The tests were conducted in a closed-system configuration at 37 °C. A 5 mm diameter ruby bead was placed in the apex of each flow-through cell for a laminar flow of the dissolution medium to be obtained. Phosphate Buffered Saline (PBS, 2.3 mM) with a pH of 7.4 was the dissolution medium, while the pulse action was adjusted to 120 pulses/minute. Each glass bottle connected with a tablet cell was filled with 100 ml of PBS, while the temperature in the magnetic stirrer was adjusted at 37 °C and the magnetic stirring at 300 rpm.

Two different flow rates were applied, 35 ml/min, which is attributed to the blood flow rate in the coronary vessels and a lower one, 8 ml/min, according to the United States Pharmacopeia (USP) recommendations (Seidlitz and Weitschies, 2012) (US Pharmacopeia, 2016).

The drug release tests for the HMW PCL-LDC 30% implants printed at 70 °C and 110 °C, HMW PCL-LDC 5% and HMW PCL – PCL-LDC 30% implants were done in triplicates, while a pure HMW PCL disc was used as a control. Each 100 ml bottle was under continuous stirring and heating for the duration of the study for a homogeneous solution to be obtained. Samples of 5 ml were collected at predetermined time points and the medium was, then, replenished with an equal

volume of fresh preheated PBS; for the HMW PCL-LDC 30% implants at 15, 30, 45 min and 1, 2, 3, 4, 5, 6, 7, 24, 28, 31, 48, 52, 55, 72, 76, 79 hr and for the HMW PCL-LDC 5% and HMW PCL – HMW PCL-LDC 30% implants at 15, 30, 45 min and 1, 2, 3, 4, 5, 6, 7, 19, 20, 22, 24, 25, 28, 31, 43, 44, 46, 48, 49, 52, 55, 67, 68, 70, 72, 73, 76, 79 hr.

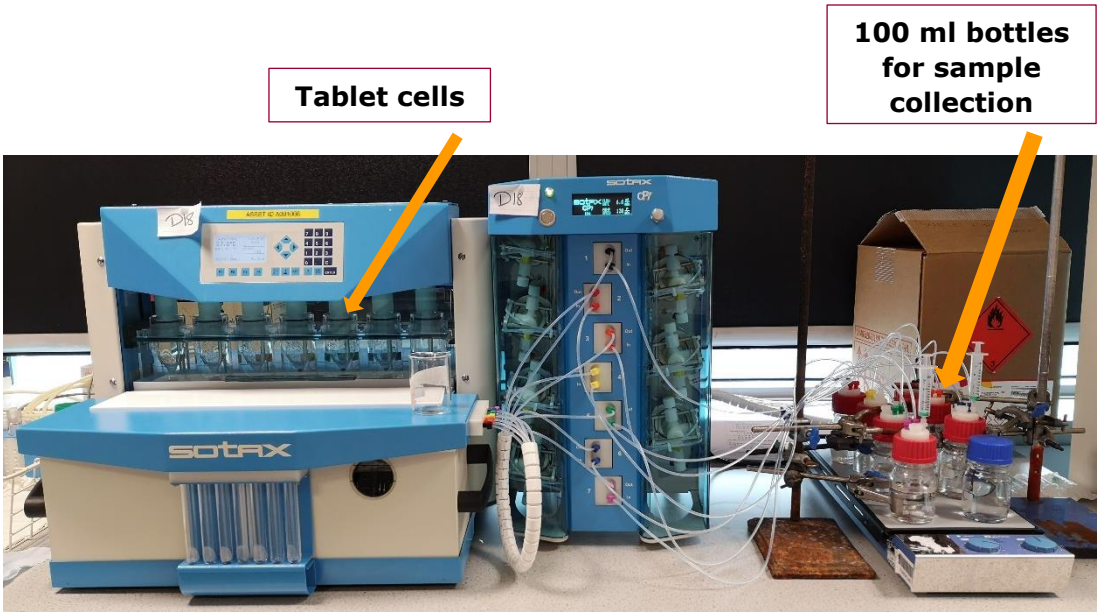

Figure 2.25: *SOTAX CE7 smart USP 4 "flow-through" dissolution tester (Foston, UK) equipped with 7 tablet cells of a diameter of 22.6 mm, each one connected with a glass bottle placed on a magnetic stirrer (RT 10, IKA England LTD, Oxford, UK).*

2.6.4. UV-Vis Spectroscopy

Lidocaine concentration was measured in an Agilent Cary 50 Bio UV-Visible Spectrophotometer (Stockport, UK) (***Figure 2.26***) at a λ max of 262 nm using a quartz cuvette, while PBS was used as a blank solution (***Figure S.16***).

Calibration standard solutions were also prepared by, first, diluting in PBS accurately weighed lidocaine powder at 100 °C for 40 min in a magnetic stirrer and then, proceeding to serial dilutions.

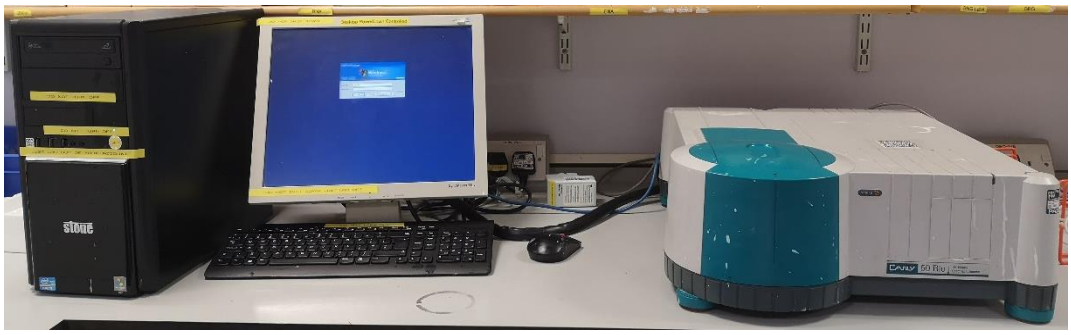

Figure 2.26: *Agilent Cary 50 Bio UV-Visible Spectrophotometer (Stockport, UK).*

A calibration curve was produced by measuring the absorbance of the standards in the UV-Vis spectrophotometer at the characteristic peak of lidocaine, 262 nm (***Figure S.17***) (Wiberg *et al*., 2001) (Perale *et al.*, 2010). The amount of the released drug was calculated through the application of the Beer-Lambert law defined by the following equation:

$$A = \varepsilon\, b\, c \qquad \textbf{(3)}$$

Where A is the absorbance of the solution (no units), ε is the molar extinction coefficient or molar absorptivity (units of 1 mol^{-1} cm^{-1}), which depends on the nature of the chemical and the wavelength of the applied light, b is the length of the path radiation that must travel through the absorbing medium (units of cm), which is typically 1 cm, and c is the concentration of the analyzed solution (units of M or mol l^{-1}) (Worsfold, 2005) (Colthup, 2003).

The average percentage of cumulative drug release was plotted as a function of time.

2.6.5. In vitro release kinetics and mathematical modelling

To investigate the drug release mechanism from the 3D printed implants, the drug release data were fitted to four mathematical models of drug release: zero-order, first-order, Higuchi and Korsmeyer-Peppas. To determine which model demonstrated the best fit, a linear regression was assessed using the squared correlation coefficient, R^2.

Zero-order model

The release of a drug that follows zero-order kinetics can be expressed with the following equation:

$$Q_t = Q_0 + K_0 t \qquad \textbf{(4)}$$

where Q_t is the cumulative amount of drug released at time t, Q_0 is the initial amount of drug in the solution before release (usually t=0) and K_0 is the zero-order release rate constant (Gouda, Baishya and Qing, 2017).

Zero-order kinetics defines the process of a constant release of an active ingredient from the formulation, which is independent of the active agent and is only a function of time (Tomic *et al.*, 2016).

First-order model

The release of a drug that follows first-order kinetics can be represented with the following equation:

$$dC_t / dt = K_1 C_t \qquad \textbf{(5)}$$

where C_t is the remaining amount of drug in the formulation at time t and K_1 is the first-order release rate constant (Gouda, Baishya and Qing, 2017).

Eq. (5) can also be expressed as follows:

$$\log C_t = \log C_0 - K_1 t/2.303 \qquad \textbf{(6)}$$

where C_t is the remaining amount of drug in the formulation at time t, C_0 is the initial amount of drug in the formulation before release and K_1 is the first-order release rate constant (Gouda, Baishya and Qing, 2017).

First-order kinetics demonstrates that the amount of the active agent released is directly proportional to the amount of the active agent remaining in the matrix. The amount of the drug released is, therefore, decreasing as a function of time (Vanessa Azevedo de Mello, 2011).

Higuchi model

The release of a drug expressed by the Higuchi model can be represented with the following equation:

$$Q_t = K_H \, t^{1/2} \qquad \textbf{(7)}$$

where Q_t is the cumulative amount of drug released at time t and K_H is the release rate constant of Higuchi (Higuchi, 1961).

The drug release mechanism of an active ingredient from the matrix, as described in the Higuchi model, is based on Fick's law and it is, thus, controlled by diffusion (Higuchi, 1961).

Korsmeyer-Peppas model

The release of a drug expressed by the Korsmeyer-Peppas model can be represented with the following equation:

$$Q_t / Q_\infty = K_{K\text{-}P} \, t^n \qquad \textbf{(8)}$$

where Q_t / Q_∞ is a fraction of drug released at time t, $K_{K\text{-}P}$ is the release rate constant of Korsmeyer-Peppas and n is the drug release exponent (Ritger and Peppas, 1987a).

Eq. (8) can also be expressed as follows:

$$\log Q_t / Q_\infty = \log K_{K\text{-}P} + n \log t \qquad \textbf{(9)}$$

A limitation of this model is that only 60% of the cumulative amount of the released drug can be plotted (Ritger and Peppas, 1987a).

The value of the release exponent, n, is used in this model to determine the release mechanism of the drug from the studied formulation. For cylindrical tablets, $n \leq 0.45$ indicates Fickian's diffusion, which means that the drug release is diffusion related; $0.45 < n < 1$ corresponds to anomalous (non-Fickian) transport mechanism, where the drug release is controlled by two processes occurring simultaneously, diffusion and polymeric relaxation or swelling; $n = 1$ suggests zero-order release or Case II transport, where the mechanism of transport is led by swelling or relaxation of the polymeric chains (Ritger and Peppas, 1987a) (Ritger and Peppas, 1987b).

CHAPTER 3: POLYCAPROLACTONE CHARACTERIZATION AND PRINTABILITY

3.1. INTRODUCTION

This chapter focuses on the investigation of the printability of polycaprolactone, with two different molecular weights, 25 kDa (LMW PCL) and 50 kDa (HMW PCL), in two types of extrusion-based 3D printers. It also investigates the most promising printing parameters for future implants manufacture through the printing of a test shape. Successful extrusion of the loaded material was an indication of the PCL printability in the investigated 3D printer.

Poly(ε-caprolactone) (PCL) was the chosen material for the fabrication of sustained release implants as it is considered non-toxic and is FDA approved (Woodruff and Hutmacher, 2010b) (Azimi *et al*., 2014). Its potential for long term degradation also contributed to its selection, as it can be used for the release of an active substance for up to several months or even years (Luong-van et al., 2006) (Mavis and Demirtas, 2009) (Sahoo *et al.*, 2010). PCL can be processed without difficulty due to the low melting temperature, 50 – 75 ºC (C. S. Wu, 2005) (Shen, Lu and Liang, 2013b) (Valle, Camps and Díaz, 2011) (De Kesel *et al.*, 1999) (Middleton and Tipton, 2000) (Simao, Bellani and Branciforti, 2017) (Cheng, Lei and Guo, 2010) (Sudhakar *et al.*, 2014) (Rusu, Ursu and Rusu, 2006). It is compatible with many different drugs and that makes feasible the uniform distribution of the active agent in a matrix (Liu *et al.*, 2007) (Ma *et al.*, 2007).

The extrusion-based 3D printers used for this study used Fused Deposition Modelling (FDM) and Pressure Assisted Microsyringe (PAM) approaches. In the latter 3D printer, no pre-processing of the materials used for the printing was required; the as-received material could be loaded to the printer's cartridge. Various settings were applied for the evaluation of PCL printability. In the former printer type, though, a polymeric filament was required to be produced using a Hot Melt Extruder (HME). The addition of a plasticiser, Triethyl Citrate (TEC), was necessary for the extrusion of a PCL filament in both molecular weights from the HME due to the high viscosity of the studied material. For the production of the polymeric filament, as well as, for its printability assessment various parameters and setups have been explored.

Afterwards, a test shape, triangle, was selected to evaluate the printing resolution of each material in each investigated 3D printer by applying various printing settings; optical microscopy has been used to assess how close the dimensions of the printed shape were to the ones of the predesigned shape. Pure LMW PCL and HMW PCL have been used for the manufacture of triangles in the PAM 3D printer, while LMW PCL-TEC and HMW PCL-TEC filaments have been loaded to the FDM for the triangles fabrication. Printing settings resulting in the production of the test shape with a high printing accuracy were selected as the ones that could be applied for future implants manufacture.

The thermal properties and the physical state of the polymer before and after testing it in 3D printers have also been examined and presented in the current Chapter.

3.2. RESULTS AND DISCUSSION

3.2.1. Polycaprolactone Printability

The production of LMW PCL and HMW PCL filaments with and without the addition of plasticiser using an HME are presented in this section. The printability of the produced filaments in the FDM, as well as, of the raw LMW PCL and HMW PCL in the PAM were, afterwards, evaluated through the application of various printing parameters. The printing resolution of a test shape was assessed, as well, for the most promising parameters to be selected for the next stages of this study.

3.2.1.1. Filament production through Hot Melt Extrusion

An HME (Desktop Extruder, Noztek Pro, Shoreham-by-Sea, UK) was used for the production of LMW PCL and HMW PCL filaments by applying various settings.

Different combinations of extrusion speeds (30, 35, 40 rpm) and temperatures (80, 90, 100, 150, 180, 200 ^{o}C), higher than the melting point of PCL of 56-65 ^{o}C, but below its decomposition temperature of 350 ^{o}C were explored for the production of a filament suitable for subsequent FDM 3DP using the LMW PCL (***Table 3.1***) (Labet and Thielemans, 2009).

For the production of HMW PCL filaments, low and higher temperatures (45, 50, 60, 70, 80, 100, 115, 150, 180, 200, 215 ^{o}C) were explored in combination with various extrusion speeds (30, 35, 40 rpm) (***Table 3.1***). Temperatures lower than the melting point of the studied polymer (45, 50 ^{o}C) have been selected in these tests, as the material in the HME needs to be in a semi-molten phase and not necessarily completely molten in order to be extruded. Furthermore, it was observed that the HMW PCL powder was reaching a semi-molten stage in the extruder at a lower temperature compared to the LMW PCL pellets.

The PCL filament production was unsuccessful with all the combinations of temperatures, extrusion speeds and different molecular weights of polymer presented in ***Table 3.1,*** as the material was very viscous under all conditions. It was indeed melting inside the extruder but due to its high viscosity, it could not be extruded through the die at the extrusion speeds that could be applied.

The PCL, thus, needed to be mixed with another material designed to decrease its viscosity and enhance its poor flow from the die. The selected material was triethyl citrate (TEC), an FDA approved plasticizer that can contribute to the continuous flow of the polymer through the die (FDA, 2018). Only a small amount (1% w/w) of TEC was required for this purpose.

Polycaprolactone was mixed with 1% w/w TEC using a mortar and pestle for 3 min. The blend was loaded to the feeding hopper of the Hot Melt Extruder and several combinations of temperatures and pressures were examined for both mixtures, HMW PCL-TEC and LMW PCL-TEC, as displayed in ***Table 3.2*** and ***Table 3.3***.

Table 3.1: *Combinations of temperatures (for heating zones 1 and 2) and extrusion speeds for the HMW PCL and LMW PCL filament production tests in the HME (n=2).*

Temperature for heating zone 1 (°C)	Temperature for heating zone 2 (°C)	Extrusion speed (rpm)	HMW PCL	LMW PCL
45	45	30	X	
45	45	35	X	
45	45	40	X	
50	50	30	X	
50	50	35	X	
50	50	40	X	
60	60	30	X	
60	60	35	X	
60	60	40	X	
70	70	30	X	
70	70	35	X	
70	70	40	X	
80	80	30	X	X
80	80	35	X	X
80	80	40	X	X
90	90	30	X	X
90	90	35	X	X
90	90	40	X	X
100	100	30	X	X
100	100	35	X	X
100	100	40	X	X
100	115	30	X	
150	150	30	X	X
150	150	35	X	X
150	150	40	X	X
180	180	30	X	X
180	180	35		X
180	180	40		X
200	200	30	X	X
200	200	35		X
200	200	40	X	X
215	215	40	X	

X : no filament production

Table 3.2: *Combinations of temperatures (for heating zones 1 and 2) and extrusion speeds for the LMW PCL - TEC filament production tests in the HME (n=2).*

		Temperature for heating zone 2 (T_2)					
		45 °C	**50 °C**	**55 °C**	**60 °C**	**65 °C**	**70 °C**
Temperature for heating zone 1 (T_1) / Extrusion speed	**45 °C/ 30 rpm**	X	X				
	45 °C/ 35 rpm	X	X				
	45 °C/ 40 rpm	X	X				
	50 °C/ 30 rpm	X	X	X			
	50 °C/ 35 rpm	X	X	X			
	50 °C/ 40 rpm	X	X	X			
	55 °C/ 30 rpm		X	X	X		
	55 °C/ 35 rpm		X	X	X		
	55 °C/ 40 rpm		X	?	X		
	60 °C/ 30 rpm			X	X	X	
	60 °C/ 35 rpm			√	√	X	
	60 °C/ 40 rpm			?	?	X	
	65 °C/ 30 rpm				X	X	X
	65 °C/ 35 rpm				X	X	X
	65 °C/ 40 rpm				X	X	X
	70 °C/ 30 rpm					X	X
	70 °C/ 35 rpm					X	X
	70 °C/ 40 rpm					X	X

√ : successful filament production

? : promising filament production

X : no filament production

a  ***b*** 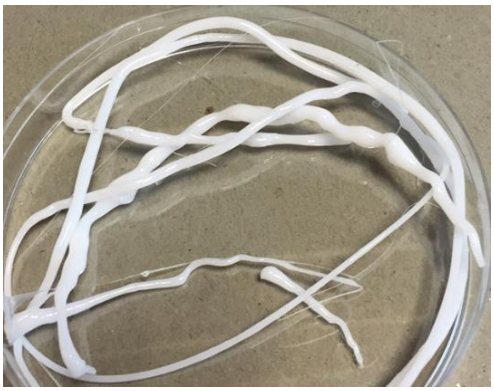

Figure 3.1: *LMW PCL-TEC filaments produced with extrusion temperatures of T_1: 60 °C, T_2: 55 °C, and an extrusion speed of* ***(b):*** *35 rpm and* ***(b):*** *40 rpm.*

No LMW PCL-TEC 1% filament production was feasible when temperatures lower than 50 °C were applied even at the highest extrusion speed investigated (***Table 3.2***). The first indication of the production of an LMW PCL-TEC filament was at 55 °C (in both heating zones) and the highest extrusion speed, 40 rpm, where some small filament pieces were slowly produced. When the temperature in the first heating zone was set at 60 °C and in the second one at 55 °C, a homogeneous filament production was achieved with an extrusion speed of 35 rpm (***Figure 3.1.a***). In the lowest extrusion speed, no filament was extruded, whilst in the highest investigated extrusion speed a filament with a varying diameter was fabricated (***Figure 3.1.b***). At some parts of the filament, the surface appeared uneven and had a diameter higher than 3 mm, which was the die diameter used in the HME. A filament with such dimension and characteristics could not be loaded into the FDM 3D printer. The above observation could be attributed to the parameter that changed in this test, the extrusion speed, which was pushing the loaded material in the HME faster out of the die. When the temperature in both heating zones was adjusted at 60 °C similar observations were found. At temperatures higher than 60 °C, no filament was extruded. An explanation for that could be that the polymer with the plasticizer were completely molten and they could not be, thus, shaped to the desired product. The applied extrusion speed did not seem to enhance the extrudability of the loaded mixture.

Table 3.3: *Combinations of temperatures (for heating zones 1 and 2) and extrusion speeds for the HMW PCL - TEC filament production tests in the HME (n=2).*

		Temperature for heating zone 2 (T_2)					
		45 °C	**50 °C**	**55 °C**	**60 °C**	**65 °C**	**70 °C**
Temperature for heating zone 1 (T_1) / Extrusion speed	**45 °C/ 30 rpm**	X	X				
	45 °C/ 35 rpm	X	X				
	45 °C/ 40 rpm	X	X				
	50 °C/ 30 rpm	X	X	X			
	50 °C/ 35 rpm	X	X	√			
	50 °C/ 40 rpm	X	X	?			
	55 °C/ 30 rpm		X	√	X		
	55 °C/ 35 rpm		X	√	X		
	55 °C/ 40 rpm		X	?	X		
	60 °C/ 30 rpm			X	X	X	
	60 °C/ 35 rpm			X	X	X	
	60 °C/ 40 rpm			X	X	X	
	65 °C/ 30 rpm				X	X	X
	65 °C/ 35 rpm				X	X	X
	65 °C/ 40 rpm				X	X	X
	70 °C/ 30 rpm					X	X
	70 °C/ 35 rpm					X	X
	70 °C/ 40 rpm					X	X

√ : successful filament production

? : promising filament production

X : no filament production

As can be seen in ***Table 3.3***, HMW PCL-TEC 1% filaments were successfully produced at temperatures close to the melting point of the studied polymer. Similarly, as in the case of the LMW PCL-TEC mixture, no filament was extruded at the lowest investigated temperature, 45 ^{o}C. The high applied extrusion speed did not have any effect on the mixture extrudability.

A homogeneous and continuous HMW PCL-TEC filament was manufactured for 50 ^{o}C for heating zone 1 and 55 ^{o}C for heating zone 2 with an extrusion speed of 35 rpm (***Figure 3.2***). With the highest extrusion speed, a non-homogeneous filament was produced, as in the case of the LMW PCL-TEC filament (***Figure 3.1.b***). HMW PCL-TEC filaments were successfully produced at an extrusion temperature of 55 ^{o}C (in both heating zones) and the lowest extrusion speeds, 30 rpm and 35 rpm. At the highest extrusion speed, 40 rpm, the same effect was observed as in the previously investigated combination of temperatures; the filament was not produced with a stable diameter, while some bubbles appeared on its surface. No filament was extruded when higher temperatures were explored, since the loaded mixture was not in the required softened semi-molten phase, but in a completely molten one. In this state, it seemed impossible for the extruder to push it through the nozzle. No filaments were obtained at temperatures lower than 50 ^{o}C since these temperatures were not high enough for the sufficient melting of the loaded materials.

Figure 3.2: *HMW PCL-TEC filament produced with an extrusion speed of 35 rpm and extrusion temperatures of T_1: 50 ^{o}C, T_2: 55 ^{o}C.*

The production of the HMW PCL-TEC filament was achieved at a lower temperature than the LMW PCL-TEC one, which confirmed the previously mentioned observation; the HMW PCL powder was reaching the semi-molten stage at a lower temperature than the LMW PCL pellets.

3.2.1.2. Printing tests in an FDM 3D printer with LMW PCL-TEC and HMW PCL-TEC filaments

The printability of the optimally produced LMW PCL-TEC and HMW PCL-TEC filaments were investigated at various temperatures (60, 70, 80, 90, 100, 110, 120, 130, 140, 150, 160, 170, 180, 190 ^{o}C) in an FDM 3D printer (Ultimaker 2+, Geldermalsen, The Netherlands); from low temperatures, close to the filament production temperature and polymer's melting point, to high, but still lower than its decomposition temperature (***Table 3.4***) (Labet and Thielemans, 2009).

The filaments that were used for these tests were the ones manufactured at the lowest extrusion temperatures, since the aim of this project is the fabrication of filaments and implants at the lowest temperatures possible to avoid possible degradation of the active agent. The LMW PCL-TEC filament used was produced at temperatures of T_1: 60 ^{o}C, T_2: 55 ^{o}C and an extrusion speed of 35 rpm, whereas for the HMW PCL-TEC at temperatures of T_1: 50 ^{o}C, T_2: 55 ^{o}C and an extrusion speed of 35 rpm. Steel nozzles, rather than plastic, with two different diameters (0.4 mm and 0.8 mm) were used for these tests to ensure good thermal conduction to the filament throughout contact with the printer parts.

No filament melting was observed at any of the applied temperatures for any material for the 0.4 mm nozzle. When the 0.8 mm nozzle was used, it was observed that both filaments, LMW PCL-TEC and HMW PCL-TEC, could successfully be extruded at the higher studied temperatures of 180 and 190 ^{o}C (***Table 3.4***). Therefore, the latter settings were used for the next printing tests.

Table 3.4: *Combinations of printing temperatures and nozzle sizes for the initial printing tests of the HMW PCL – TEC and LMW PCL – TEC filaments in the FDM (n=2).*

Printing Temperature (°C)	Nozzle size (mm)	
	0.4	0.8
60	X	X
70	X	X
80	X	X
90	X	X
100	X	X
110	X	X
120	X	X
130	X	X
140	X	X
150	X	X
160	X	X
170	X	X
180	X	√
190	X	√

√ : successful extrusion

X : no extrusion

3.2.1.3. Printing of test triangles with LMW PCL-TEC filament in an FDM 3D printer

A triangle test shape was printed using the LMW PCL-TEC filament in the FDM 3D printer to assess the printing resolution. The dimensions of the triangle designed using TinkerCAD online software (Autodesk Inc.) were 25 mm length x 22 mm width x 1 mm height and 60° internal angle, as displayed in ***Figure 3.3***. The

printing of a shape close to the predesigned one will indicate the most promising printing parameters for the fabrication of future drug loaded formulations.

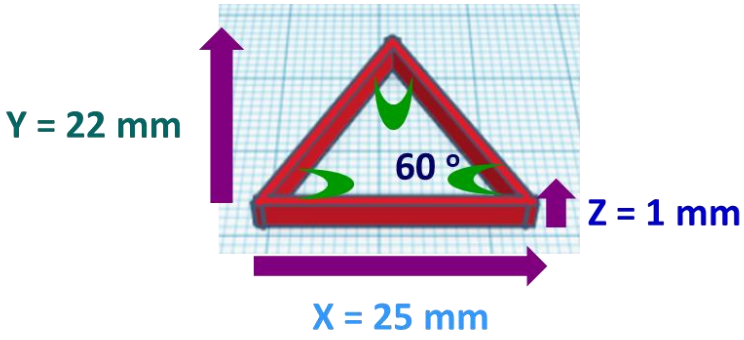

Figure 3.3: *Triangle designed in TinkerCAD for the printing assessments in the FDM 3D printer. The dimensions of the triangle are as labelled.*

3D printing of triangle test shapes using the produced LMW PCL-TEC filament was explored at different combinations of temperatures (180, 190 °C) and print speeds (5, 10, 15, 20 mm/s) in the FDM 3D printer with a steel nozzle with a diameter of 0.8 mm (***Figure 3.4***).

a 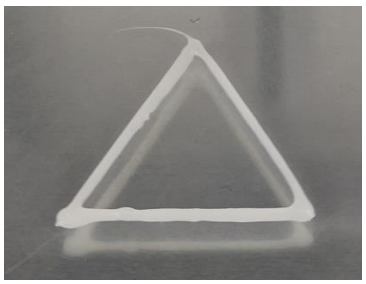 ***b*** 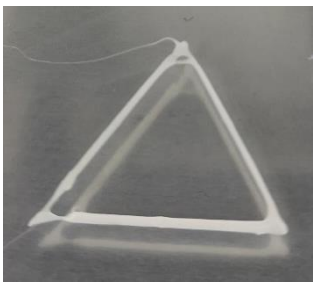

Figure 3.4: (a): *3D printed LMW PCL-TEC triangle with a nozzle diameter of 0.8 mm, print temperature of 180 °C and print speed of 10 mm/s,* ***(b):*** *3D printed HMW PCL-TEC triangle with a nozzle diameter of 0.8 mm, print temperature of 190 °C and print speed of 15 mm/s. The bottom triangle is a reflection of the printed triangle on the printing platform.*

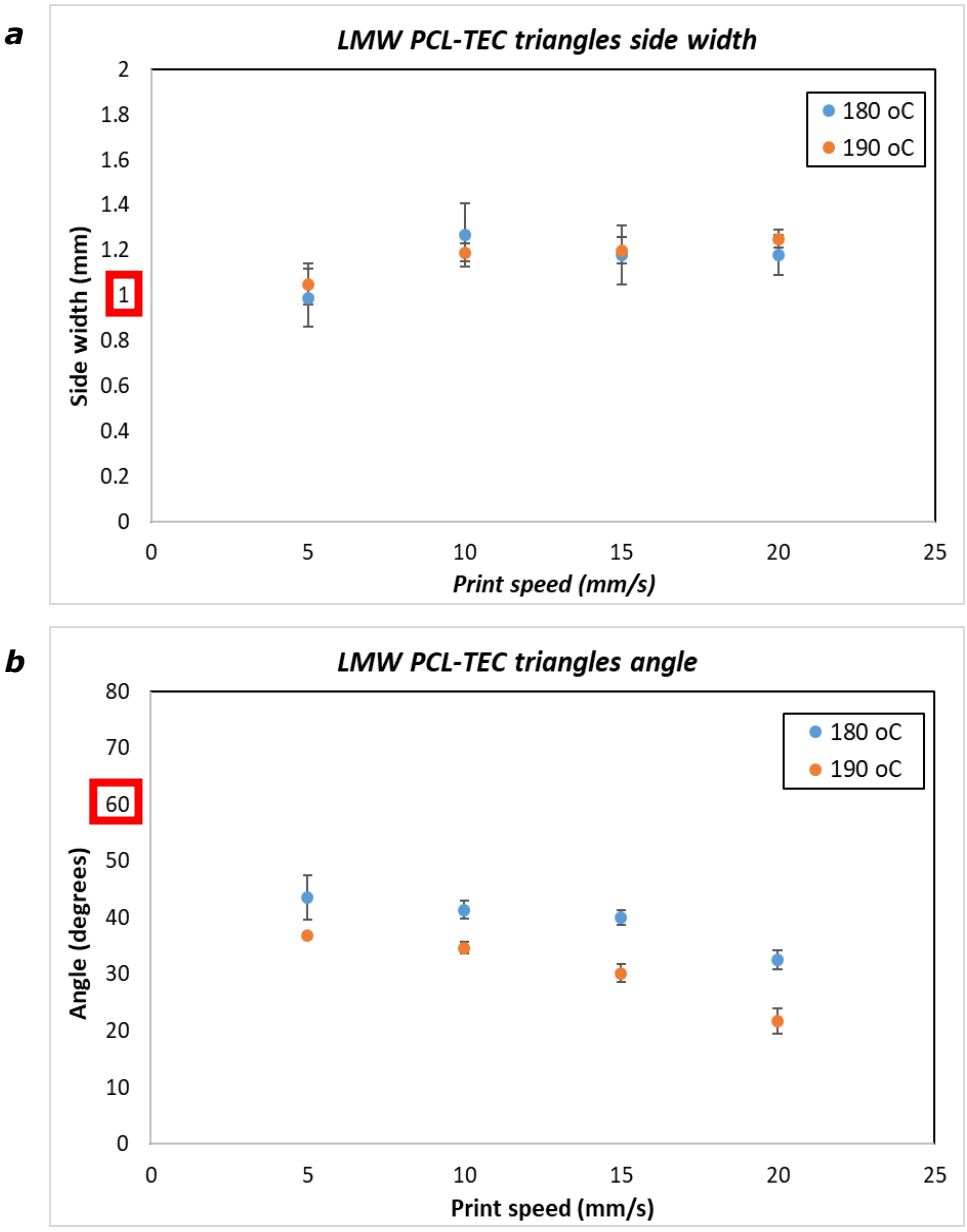

Figure 3.5: (a): *Side width of the 3D printed LMW PCL-TEC triangles with a nozzle diameter of 0.8 mm at different temperatures and print speeds,* ***(b):*** *Angle of the 3D printed LMW PCL-TEC triangles with a nozzle diameter of 0.8 mm at different temperatures and print speeds. Red boxed figures represent the theoretical dimensions of the printed triangle as in the CAD file.*

According to ***Figure 3.5***, not all the printed triangles had the predetermined dimensions (25 mm length x 22 mm width x 1 mm height and 60^{o} angle) as observed in the optical microscope. More PCL was extruded from the nozzle at the higher temperatures examined, which had, as a result, the printing of triangles with sides of a width larger than designed (***Figure 3.5.a***). The triangles' internal angle was also affected by this; as the side width increased the angle decreased (***Figure 3.5.b***). The same trend was also noticed when the print speed increased. Combining the results from ***Figure 3.5.a*** and ***Figure 3.5.b***, the most promising printing settings for the LMW PCL-TEC filament in the FDM are at the lowest temperature, 180 ^{o}C and with print speeds of 5, 10 and 15 mm/s (***Figure 3.4.a***).

3.2.1.4. Printing of test triangles with HMW PCL-TEC filament in an FDM 3D printer

The same settings as in the case of the LMW PCL-TEC filaments were also applied for the printing of triangles with HMW PCL-TEC filaments, ie. different combinations of temperatures (180, 190 ^{o}C) and print speeds (5, 10, 15, 20 mm/s) with a nozzle diameter of 0.8 mm (***Figure 3.6***).

a 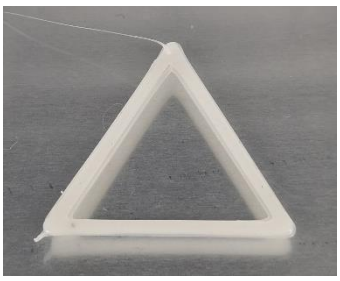 ***b*** 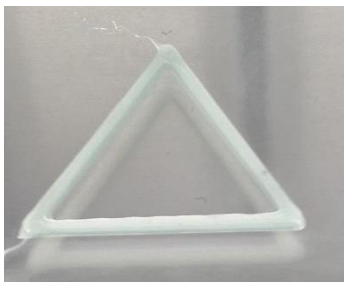

Figure 3.6: (a): *3D printed LMW PCL-TEC triangle with a nozzle diameter of 0.8 mm, print temperature of 180 ^{o}C and print speed of 15 mm/s,* ***(b):*** *3D printed HMW PCL-TEC triangle with a nozzle diameter of 0.8 mm, print temperature of 190 ^{o}C and print speed of 15 mm/s. The bottom triangle is a reflection of the printed triangle on the printing platform.*

a

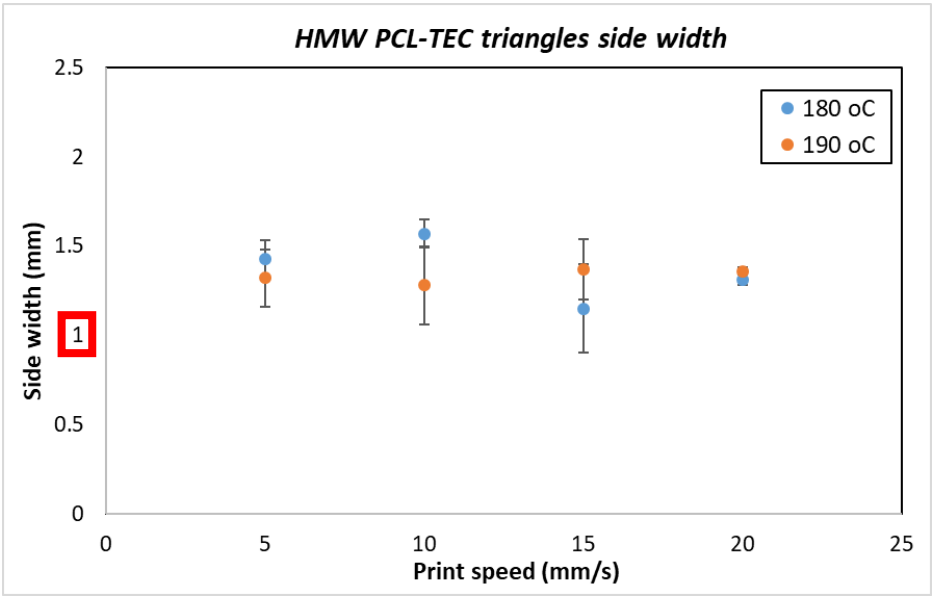

b

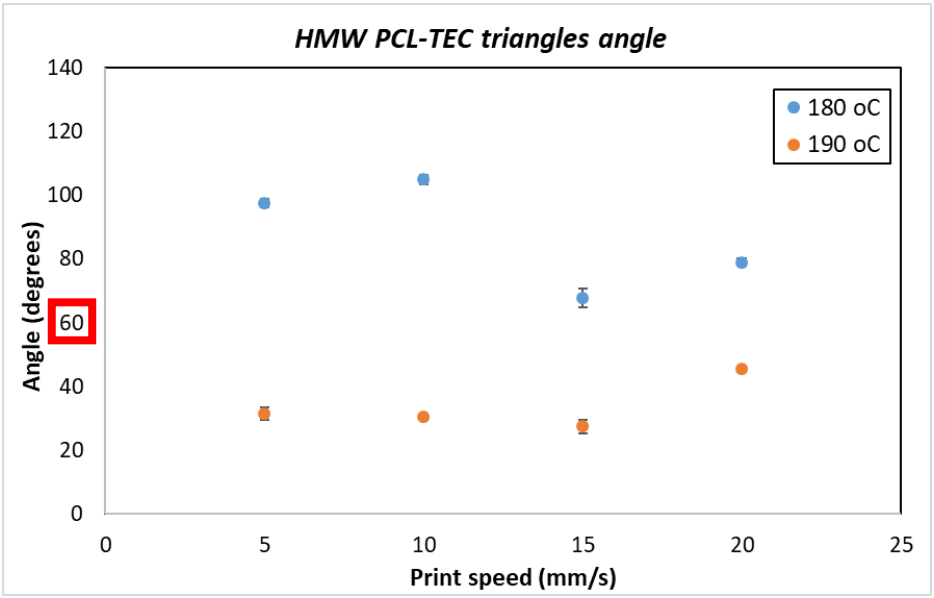

Figure 3.7: (a): *Side width of the 3D printed HMW PCL-TEC triangles with a nozzle diameter of 0.8 mm at different temperatures and print speeds,* ***(b):*** *Angle of the 3D printed HMW PCL-TEC triangles with a nozzle diameter of 0.8 mm at different temperatures and print speeds. Red boxed figures represent the theoretical dimensions of the printed triangle as in the CAD file.*

Figure 3.7 depicts the dimensions of the printed triangles with increasing print speeds and temperature. It is clear that not all of the triangles had the predetermined expected dimensions (25 mm length x 22 mm width x 1 mm height and 60° internal angle). More PCL extruded from the nozzle as the temperature

increased, which resulted in the fabrication of triangles with a larger side width than designed (***Figure 3.7.a***). This factor again, also, influenced the triangles' angle; the larger the side width the smaller the angle (***Figure 3.7.b***). Another parameter that affected the angle of the printed triangles was the print speed. As the print speed increased, the angle of the produced objects decreased.

According to the data in ***Figure 3.7.a*** and ***Figure 3.7.b***, the HMW PCL-TEC filament could better be printed at the lowest applied temperature (180 ^{o}C) and the highest print speeds (15, 20 mm/s) (***Figure 3.6.b***). Therefore, these printing settings could further be investigated for the fabrication of polymeric implants using the FDM 3D printer.

3.2.1.5. Printing tests in a PAM 3D printer with Low and High Molecular Weight Polycaprolactone powders with a plastic cartridge

The printability of Polycaprolactone with Molecular Weights of 25 kDa (LMW PCL) and 50 kDa (HMW PCL) were investigated in a PAM 3D printer (Inkredible +, Cellink, Gothenburg, Sweden) using initially a plastic cartridge.

As shown in ***Table 3.5***, different temperatures, pressure and the use of plastic nozzles with different diameters have been applied in the PAM 3D printer to investigate the printability of the LMW PCL loaded in a plastic cartridge.

Table 3.5: *Combinations of temperatures, pressure and nozzle sizes for the LMW PCL printing tests in the PAM 3D printer with a plastic cartridge (n=2).*

Temperature (^{o}C)	Pressure (kPa)	Nozzle diameter (mm)
80	400	0.41
80	400	0.20
80	400	0.25
100	400	0.25
130	400	0.20
130	300	0.41

Printing tests with the HMW PCL using a plastic cartridge and combinations of temperatures, pressure and different nozzle types and sizes have also been performed in the PAM 3D printer, as demonstrated in ***Table 3.6***.

Table 3.6: *Combinations of temperatures, pressure, nozzle types and sizes for the HMW PCL printing tests in the PAM 3D printer with a plastic cartridge (n=2).*

Temperature (°C)	*Pressure (kPa)*	*Nozzle type*	*Nozzle diameter (mm)*
80	300	plastic	0.20
80	335	plastic	0.20
100	335	plastic	0.20
100	300	plastic	0.25
100	400	plastic	0.25
120	400	plastic	0.20
120	400	plastic	0.25
120	400	plastic	0.41
120	400	steel	0.41
130	400	plastic	0.41

The printing attempts in the PAM 3D printer using a plastic cartridge were unsuccessful for both the high and the low molecular weight PCL even though many different combinations of temperatures, nozzle types and sizes were applied. The problem was that the polymer solidified quickly at room temperature. Therefore, as long as the polymer was inside the cartridge that was heated, it was molten but when it was forwarded into the (unheated) nozzle (***Figure 3.8***), it solidified and blocked the nozzle. Use of a metal nozzle, as for the previous printer, allowed heat transfer to occur between the cartridge and the nozzle and maintained the liquid state of the polymer.

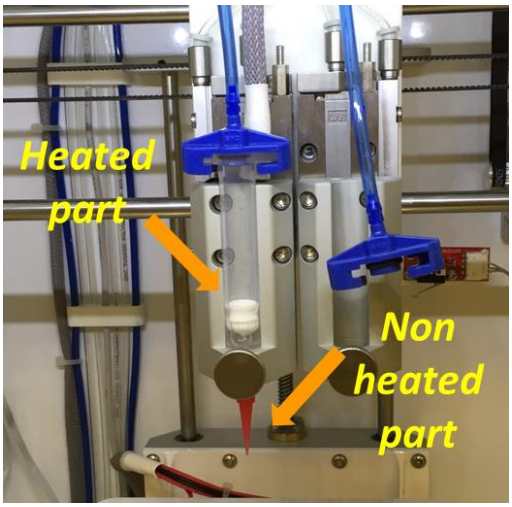

Figure 3.8: *Pressure Assisted Microsyringe 3D printer with a plastic cartridge and a plastic nozzle.*

3.2.1.6. Printing tests in a PAM 3D printer with Low and High Molecular Weight Polycaprolactone with an aluminium cartridge

As mentioned above, PCL without TEC could not be extruded out of the nozzle because there was not sufficient heat transfer between the parts containing the polymer. Therefore, an aluminium cartridge was decided to be used in combination with steel nozzles in order to help address this issue.

Different printing settings were investigated for both molecular weights PCL with two different nozzle sizes, 0.34 and 0.61 mm. A range of temperatures, from low to high (80, 90, 100, 110, 120, 130 ^{o}C), were applied to the PAM 3D printer with each nozzle. A pressure of 400 kPa was selected for all the printing tests.

The extrusion of PCL was only feasible at the highest studied temperatures (100, 110, 120, 130 ^{o}C) for both HMW and LMW PCL and nozzles. Nevertheless, LMW PCL seemed to be less viscous compared to HMW PCL as it was extruded faster from the nozzle, which is consistent with the literature (Kasaai, 2007). Consequently, these settings were used for further printing studies.

3.2.1.7. Printing of test triangles with LMW PCL in a PAM 3D printer

Similarly, as in the printing attempts with the FDM 3D printer, the chosen test shape was a one-layer triangle. The dimensions of the designed triangle were adjusted according to the nozzle size; for a nozzle diameter of 0.61 mm, the dimensions of the triangle were 25 mm length x 22.93 mm width x 0.82 mm height and 60º internal angle, ***Figure 3.9.a,*** where for a nozzle diameter of 0.34 mm the dimensions of the triangle were 25 mm length x 22.93 mm width x 0.45 mm height and 60º internal angle, ***Figure 3.9.b***.

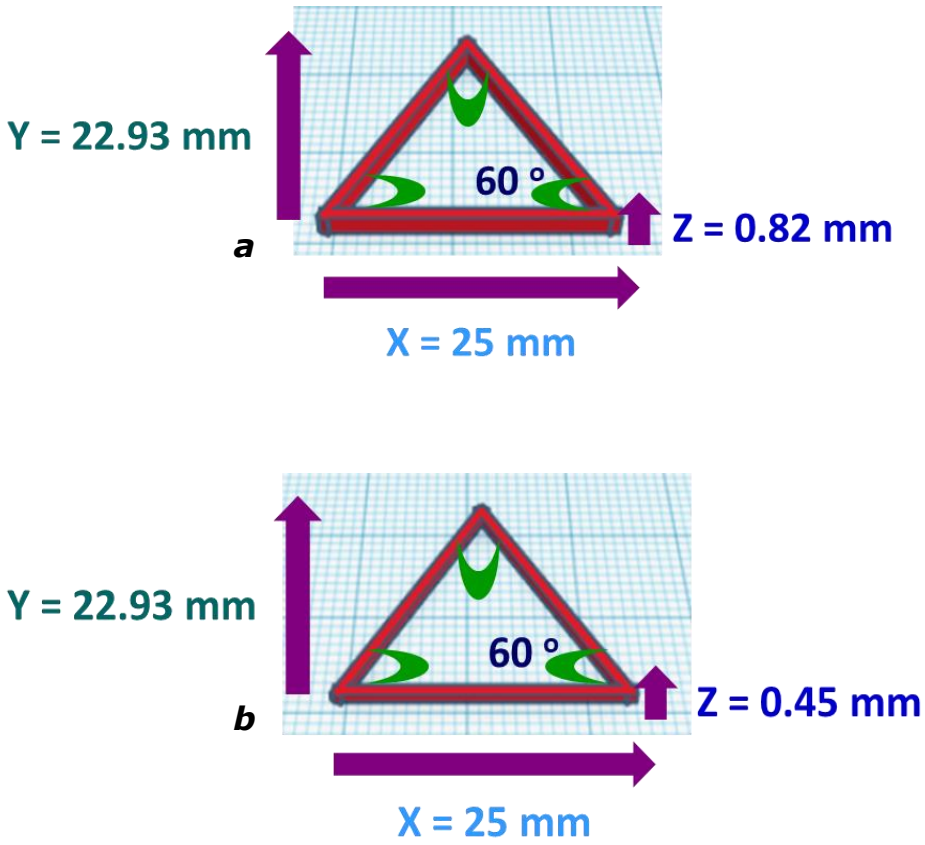

Figure 3.9: *Triangles designed in TinkerCAD for the printing assessments in the PAM 3D printer with a nozzle diameter of* ***(a)*** *0.61 mm and* ***(b)*** *0.34 mm. The dimensions of the triangles are labelled.*

Printing of test triangles using the LMW PCL was explored by applying different combinations of temperatures (100, 110, 120, 130 °C), print speeds (1, 1.5, 3, 6 mm/s) and nozzle sizes (0.34, 0.61 mm) in the PAM 3D printer (***Figure 3.10***).

a 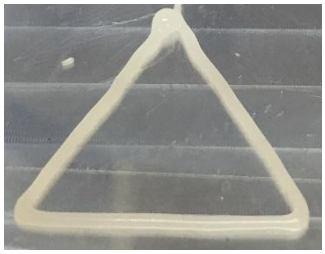 ***b*** 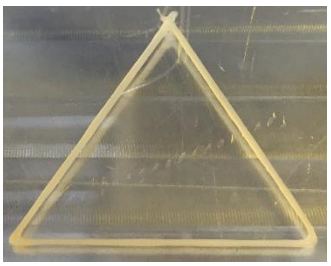

Figure 3.10: (a): *3D printed LMW PCL triangle with a nozzle diameter of 0.61 mm, print temperature of 120 °C and print speed of 6 mm/s,* ***(b):*** *3D printed LMW PCL triangle with a nozzle diameter of 0.34 mm, print temperature of 130 °C and print speed of 1 mm/s. The bottom triangle is a reflection of the printed triangle on the printing platform.*

According to ***Figure 3.11***, the 3D printing of the LMW PCL with an aluminium cartridge and a steel nozzle with a diameter of 0.61 mm was possible at all the studied temperatures and print speeds. Nevertheless, not all the printed triangles had the predesigned dimensions (25 mm length x 22.93 mm width x 0.82 mm height and 60° angle).

In general, as the temperature increased, a greater flow rate of PCL from the nozzle was achieved, which resulted in an increased side width (***Figure 3.11.a***). At the lowest print speeds (1, 1.5 mm/s), this impact was much greater. The triangles' angle was also affected by this effect; the bigger the side width the smaller the angle (***Figure 3.11.b***). Combining the results from ***Figure 3.11.a*** and ***Figure 3.11.b***, the best printing settings for the LMW PCL using the 0.61 mm nozzle were at the highest applied temperatures (110, 120, 130 °C) and print speed (6 mm/s) (***Figure 3.10.a***).

a

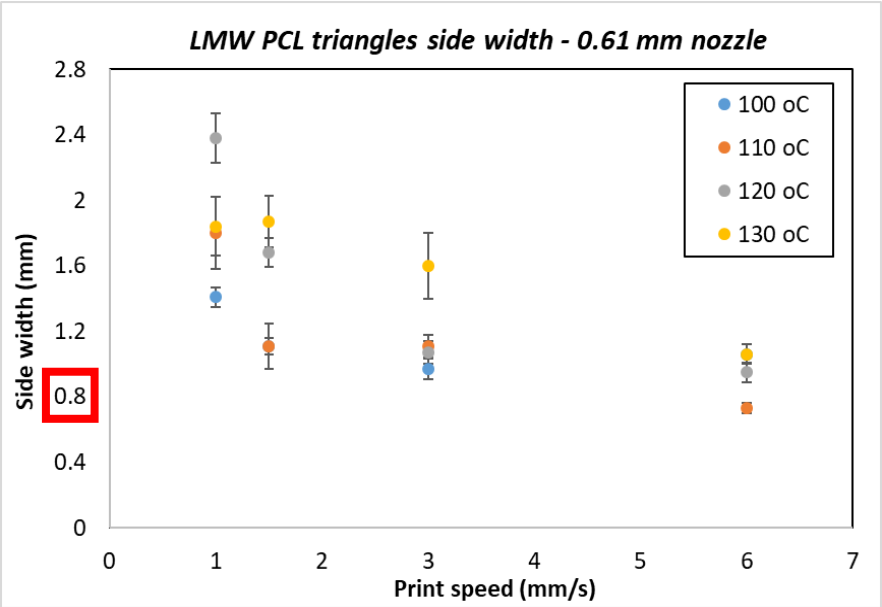

b

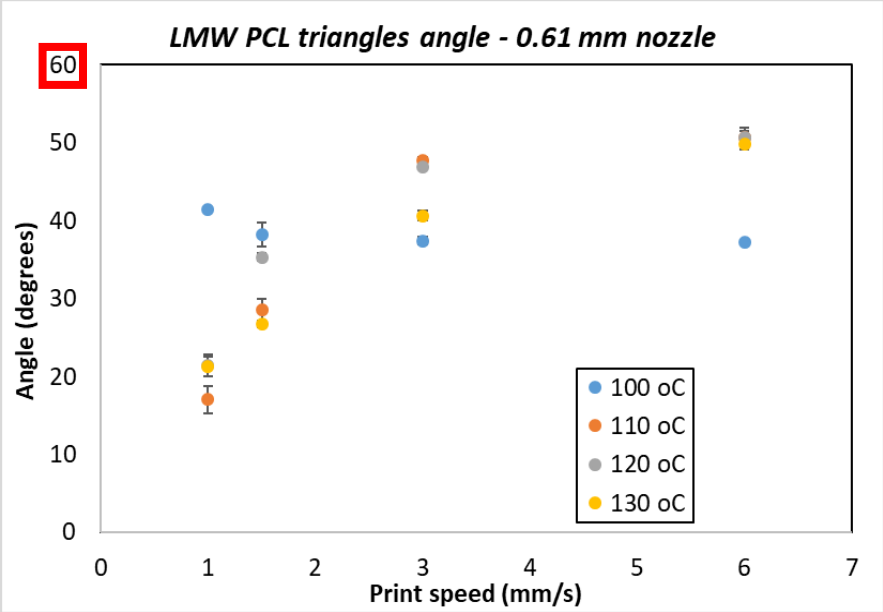

Figure 3.11: (a): *Side width of the 3D printed LMW PCL triangles with a nozzle diameter of 0.61 mm,* ***(b):*** *Angle of the 3D printed LMW PCL triangles with a nozzle diameter of 0.61 mm. Red boxed figures represent the theoretical dimensions of the printed triangle as in the CAD file.*

When the nozzle with a smaller diameter (0.34 mm) was used for the printing of the triangles with the LMW PCL, the attempts were not as successful compared to the larger nozzle (0.61 mm). One explanation is that the studied polymer is quite viscous and when a small diameter nozzle is used its extrusion becomes slower

and much more difficult. Only at the highest temperatures (120, 130 °C) and the lowest print speed (1 mm/s) was the printing feasible. Even though the side width was relatively well defined in both triangles (0.41±0.03 mm at 120 °C and 0.47±0.01 mm at 130 °C), the accuracy of the angle was different (19.0±0.8° at 120 °C and 44.6±0.9° at 130 °C). Therefore, only one of these printing combinations (130 °C, 1 mm/s) could further be investigated for the printing of implants (***Figure 3.10.b***).

3.2.1.8. Printing of test triangles with HMW PCL in a PAM 3D printer

HMW PCL has also been investigated in the PAM 3D printer for the fabrication of triangles using the same settings applied during the printing of the LMW PCL triangles; temperatures: 100, 110, 120, 130 °C, print speeds: 1, 1.5, 3, 6 mm/s and nozzles diameters: 0.34, 0.61 mm (***Figure 3.12***).

a ***b***

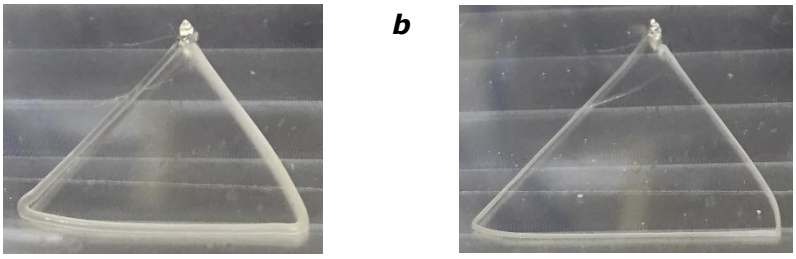

Figure 3.12: (a): *3D printed HMW PCL triangle with a nozzle diameter of 0.61 mm, print temperature of 110 °C and print speed of 1.5 mm/s,* ***(b):*** *3D printed HMW PCL triangle with a nozzle diameter of 0.34 mm, print temperature of 130 °C and print speed of 1 mm/s. The bottom triangle is a reflection of the printed triangle on the printing platform.*

Generally, the printability of the HMW PCL was not as easy as the LMW PCL, even though an aluminium cartridge and steel nozzles were used. An explanation for this is that the viscosity of the polymer increases with molecular weight (Kasaai, 2007). This was also indicated by the fact that the HMW PCL could only be used for the printing of triangles with a nozzle diameter of 0.61 mm at the lowest studied print speeds (1, 1.5 mm/s) (***Figure 3.13***).

a

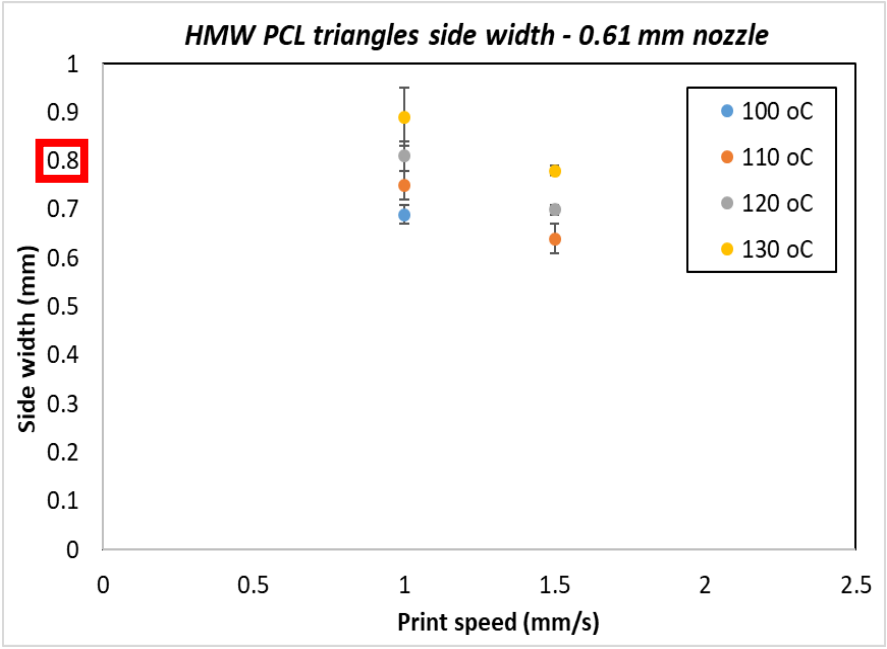

b

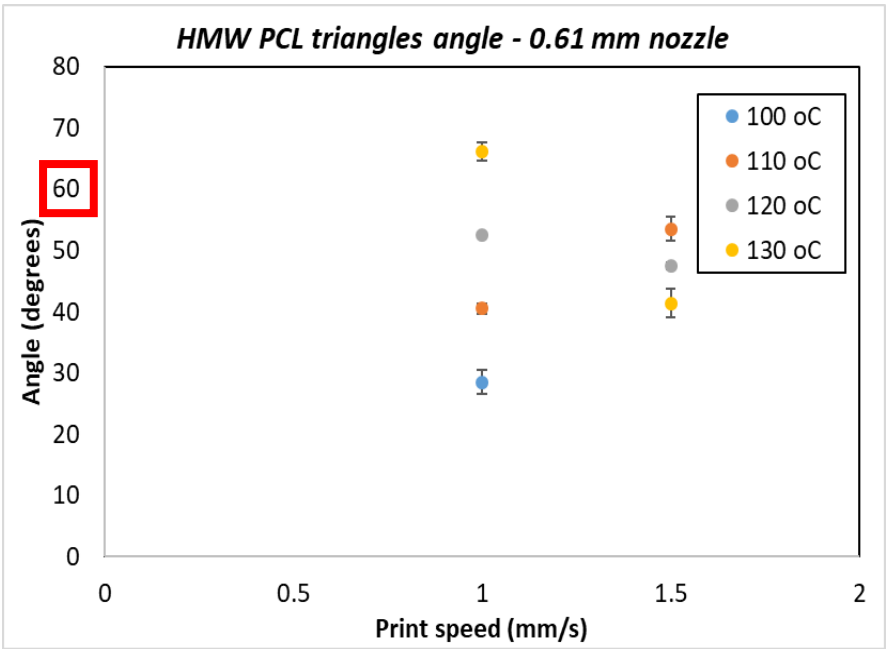

Figure 3.13: (a): *Side width of the 3D printed HMW PCL triangles with a nozzle diameter of 0.61 mm,* ***(b):*** *Angle of the 3D printed HMW PCL triangles with a nozzle diameter of 0.61 mm. Red boxed figures represent the theoretical dimensions of the printed triangle as in the CAD file.*

After the characterization of the printed triangles in an optical microscope, it was noticed that the side width of the triangles increased with the applied printing temperature and the print speed remaining low, similar to the LMW PCL (***Figure 3.13.a***). The angles of the printed triangles were also influenced in this case by the printing temperature and speed and consequently, by the side width (***Figure 3.13.b***). When the print speed was 1.5 mm/s, the angles of the printed triangles were closer to the desired 60°. According to the data in ***Figure 3.13.a*** and ***Figure 3.13.b***, the most promising printing parameters for the HMW PCL when it was used with a nozzle of diameter 0.61 mm were those at the highest temperatures (110, 120, 130 °C) and lower print speeds (1, 1.5 mm/s) (***Figure 3.12.a***).

The printing of the HMW PCL using a steel nozzle with a diameter of 0.34 mm was the most difficult. The only successful attempt of printing a triangle was at the highest investigated temperature (130 °C) and lowest print speed (1 mm/s). The reason is as before; the relatively high viscosity of the polymer. At this setting, the side width of the printed triangles was reasonable (0.31±0.01 mm) and the printing of the angles (60.82±0.01°) was precise to the predesigned object (***Figure 3.12.b***). This printing setting could be applied in future printing of implant studies.

3.2.2. Characterizations of 3D printed LMW PCL and HMW PCL triangles

Pure Low and High Molecular Weight Polycaprolactone powders were characterized before and after their mixing with the plasticizer, TEC, their extrusion and 3D printing to investigate if their thermal and physical properties have been affected by all these processes.

3.2.2.1. DSC Characterization

Figure 3.14.a and ***Figure 3.14.c*** display DSC thermograms of the pure HMW PCL and LMW PCL powders before extrusion and printing, respectively. The DSC curves of both types of PCL were obtained from two heat-cool cycles and exhibit a similar melting temperature, T_m and crystallization temperature, T_c; both as expected (Valle, Camps and Díaz, 2011) (Simao, Bellani and Branciforti, 2017)

(Guang-*Mei et al*., 2010). According to the data summarized in ***Table 3.7,*** LMW PCL and HMW PCL crystallize at 20.8 °C and 28.2 °C respectively, both very close to room temperature. This might be the reason that both types of PCL solidified in the non-heated plastic nozzles during the printing checks in the PAM 3D printer after they were molten in the cartridge.

In the DSC thermograms of both the HMW PCL and LMW PCL powders, a slight decrease of the peak for the melting point to lower temperatures was observed during the second cycle, but no shift in the crystallization peak. Therefore, it was decided to run the HMW PCL polymer in 3 cycles (***Figure 3.14.b***) under the same conditions to check if after the second cycle the melting point stabilised. As anticipated, the peak for the melting point in the third cycle was identical to the peak of the second cycle. The difference in the melting points of the first and the second cycle may be related to the different "thermal history" between the pure PCL and the polymer after the first heating-cooling cycle in the DSC. The latter procedure could also be considered as quite extreme, since it stresses the substance with the application of low and high temperatures. This change in the DSC thermogram of the pure PCL is also in accordance with the literature (Murphy, 2011).

DSC has also been performed on selected polymeric triangles from both 3D printers. For this purpose, from the FDM fabricated triangles: the LMW PCL triangle printed at 190 °C and a print speed of 10 mm/s (***Figure 3.15***) was analysed, and from the PAM 3D printed objects: the LMW PCL triangle printed at 100 °C, with a print speed of 3 mm/s and a nozzle diameter of 0.61 mm (***Figure 3.16***), the HMW PCL triangle printed at 110 °C, with a print speed of 1.5 mm/s and a nozzle diameter of 0.61 mm (***Figure 3.17.a***), the HMW PCL triangle printed at 130 °C, with a print speed of 1 mm/s and a nozzle diameter of 0.34 mm (***Figure 3.17.b***) and the LMW PCL triangle printed at 100 °C, with a print speed of 3 mm/s and a nozzle diameter of 0.61 mm were examined.

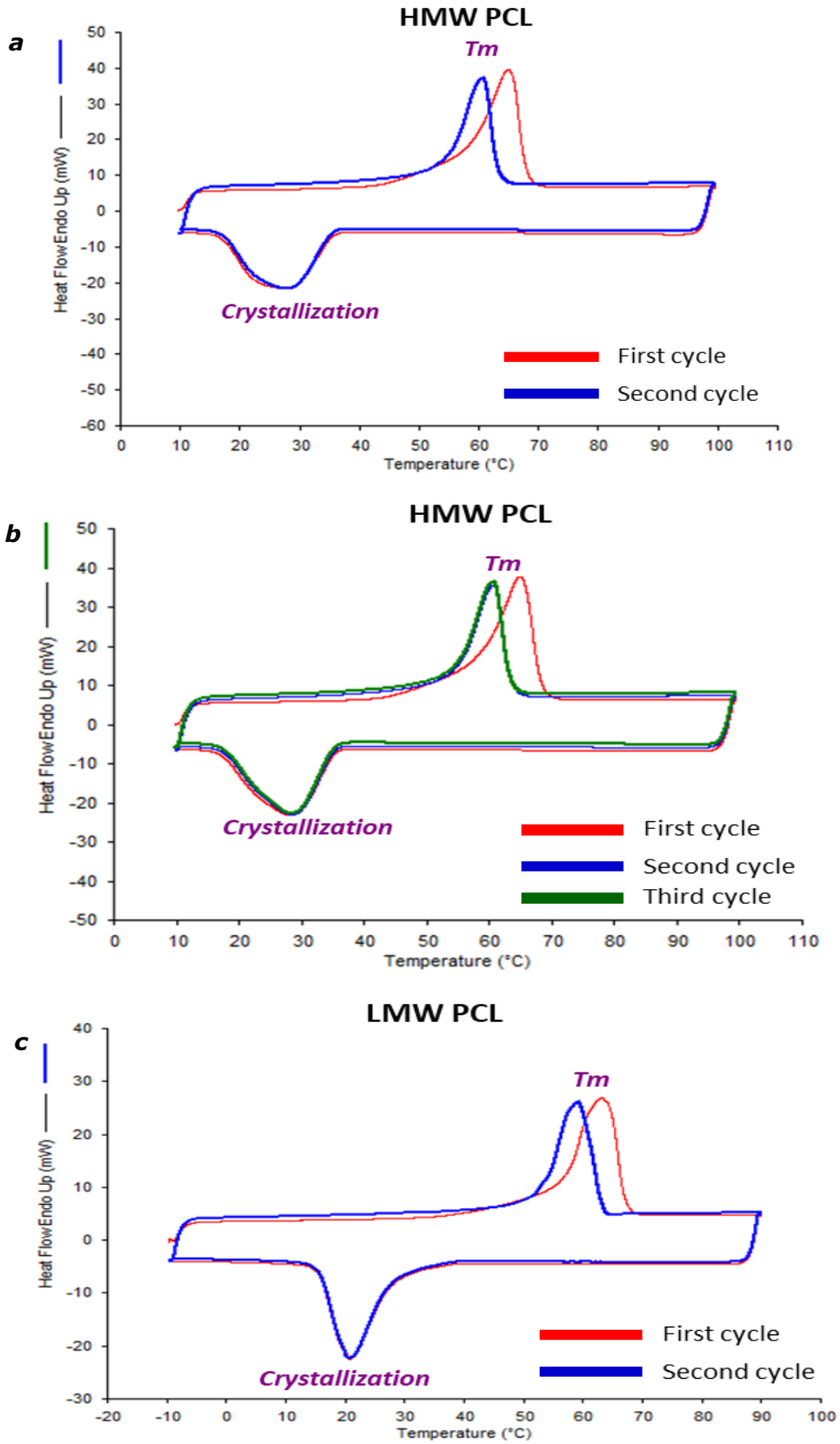

Figure 3.14: *DSC thermograms of* ***(a):*** *pure HMW PCL powder after 2 heating-cooling cycles,* ***(b):*** *pure HMW PCL powder after 3 heating-cooling cycles,* ***(c):*** *pure LMW PCL powder. The red line represents the first heating-cooling cycle, the blue line the second cycle and the green line the third cycle.*

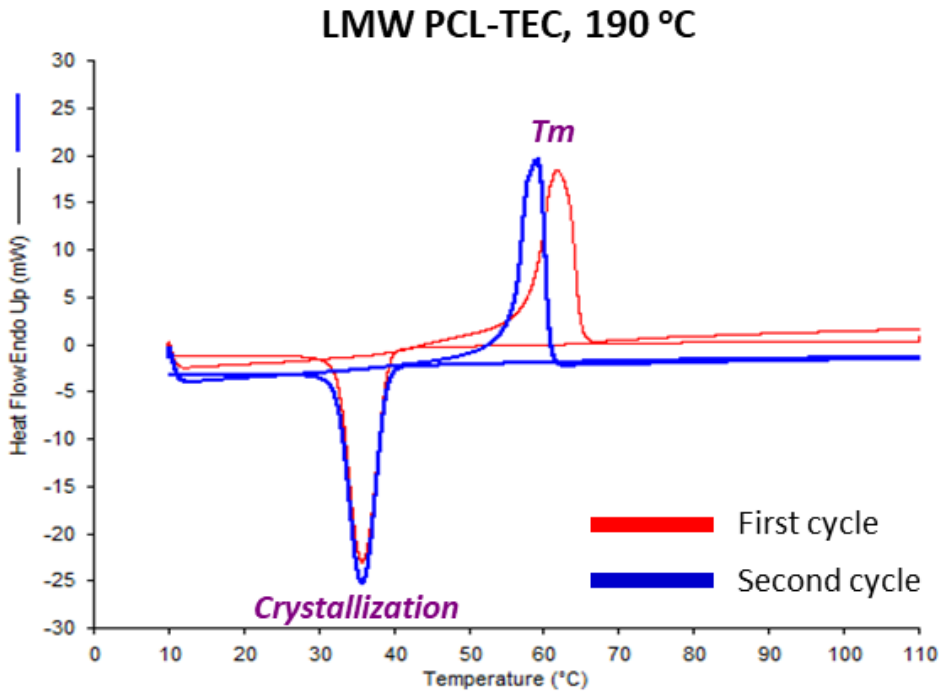

Figure 3.15: *DSC thermogram of LMW PCL-TEC triangle printed at 190 °C and a print speed of 10 mm/s from the FDM. The red line represents the first heating-cooling cycle and the blue line the second cycle.*

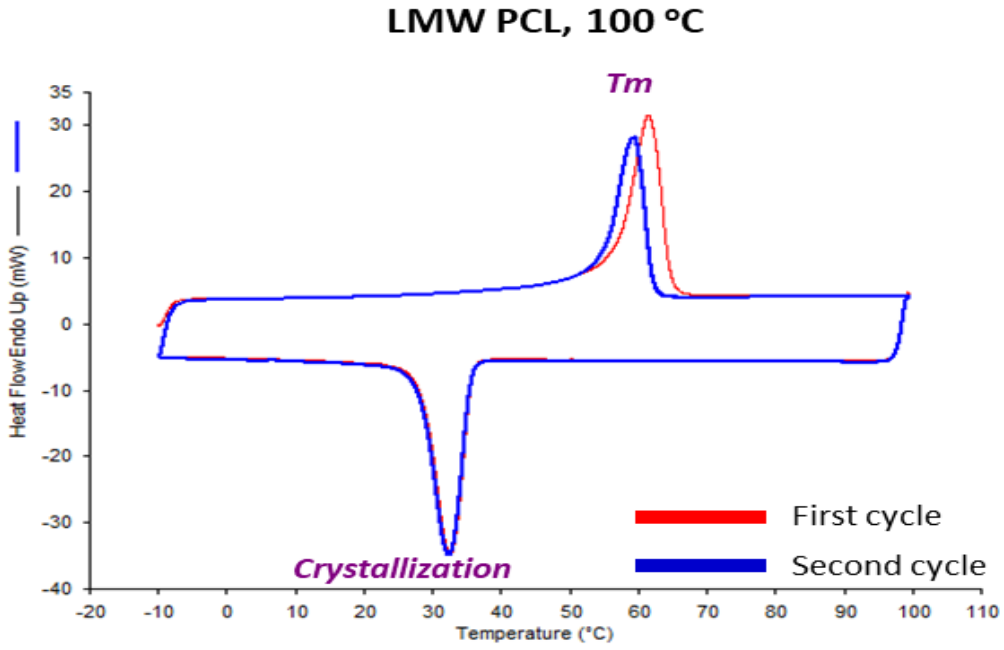

Figure 3.16: *DSC thermogram of LMW PCL triangle printed at 100 °C, with a print speed of 3 mm/s and a nozzle diameter of 0.61 mm from the PAM 3D printer. The red line represents the first heating-cooling cycle and the blue line the second cycle.*

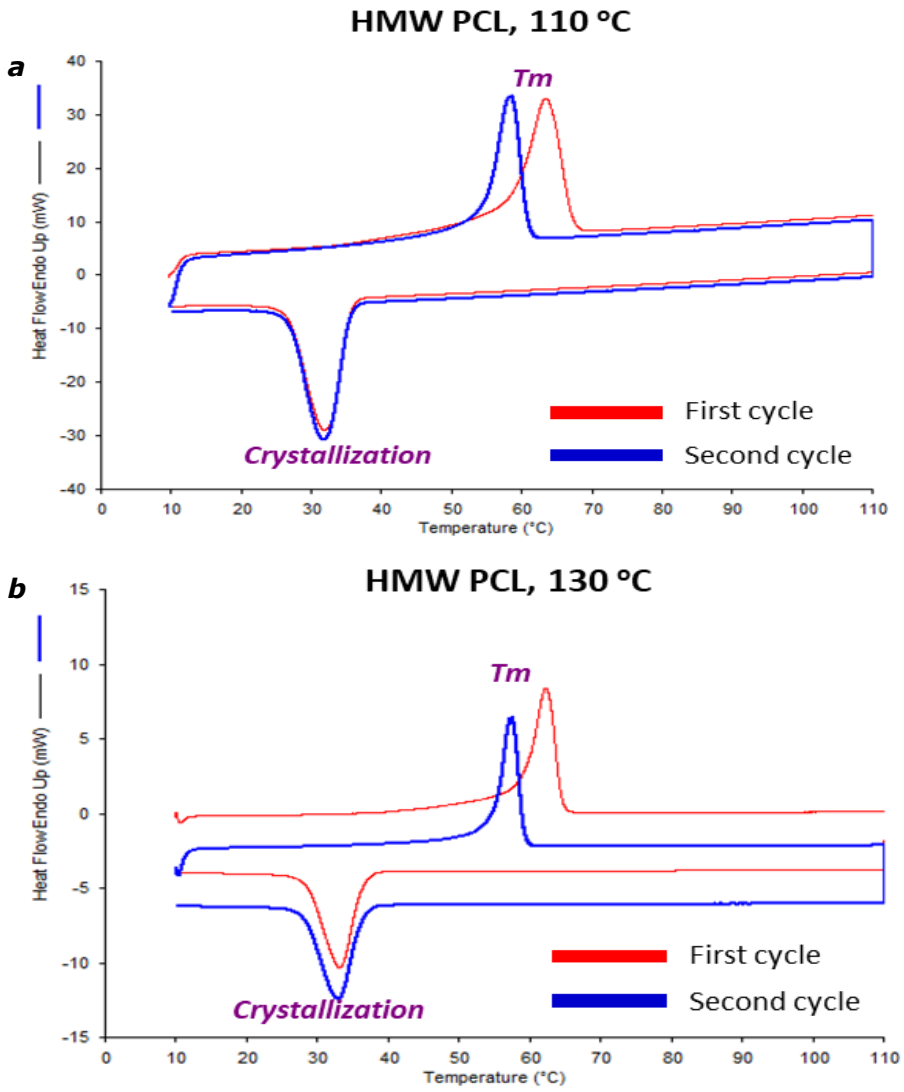

Figure 3.17: *DSC thermograms of* ***(a):*** *HMW PCL triangle printed at 110 °C, with a print speed of 1.5 mm/s and a nozzle diameter of 0.61 mm from the PAM 3D printer,* ***(b):*** *HMW PCL triangle printed at 130 °C, with a print speed of 1 mm/s and a nozzle diameter of 0.34 mm from the PAM 3D printer. The red line represents the first heating-cooling cycle and the blue line the second cycle.*

The mixing of polycaprolactone with the plasticizer, TEC, did not seem to have any impact on the thermal properties of the studied polymer, according to its DSC thermogram in ***Figure 3.15***. The peaks for the melting and the crystallization of PCL appeared at the same temperatures as in the case of the pure polymer; the melting point in the second heating cycle was detected at a lower temperature

compared to the one of the first heating program similarly to the raw material. These observations indicated, therefore, that no significant interaction between the used materials had occurred and neither hot melt extrusion, nor 3D printing altered PCL's thermal properties.

Table 3.7: *DSC data of pure LMW PCL powder (N=2), pure HMW PCL powder (N=4), and LMW PCL-TEC 3D printed triangle at 190 °C and a print speed of 10 mm/s from the FDM (N=2), LMW PCL triangle printed at 100 °C, a print speed of 3 mm/s and a nozzle diameter of 0.61 mm from the PAM 3D printer (N=2), HMW PCL triangle printed at 110 °C, with a print speed of 1.5 mm/s and a nozzle diameter of 0.61 mm from the PAM 3D printer (N=2), HMW PCL triangle printed at 130 °C, with a print speed of 1 mm/s with a nozzle diameter of 0.34 mm from the PAM 3D printer (N=2) obtained by two heating-cooling scans and pure HMW PCL powder (N=2) obtained by three heating-cooling scans.*

	T_m (°C)			T_c (°C)
	1st cycle	***2nd cycle***	***3rd cycle***	
LMW PCL	65.4 ± 3.5	61.3 ± 2.3		20.8 ± 0.1
HMW PCL	64.1 ± 1.1	60.1 ± 3.2		28.6 ± 0.6
HMW PCL	64.9 ± 0.04	60.4 ± 0.3	60.4 ± 0.3	28.4 ± 0.2
LMW PCL-TEC 190 °C (FDM)	61.7 ± 0.01	59.1 ± 0.01		35.8 ± 0.04
LMW PCL 100 °C (PAM 3D printer)	63.9 ± 0.03	58.8 ± 0.01		32.9 ± 0.03
HMW PCL 110 °C (PAM 3D printer)	63.4 ± 0.01	58.5 ± 0.02		31.9 ± 0.04
HMW PCL 130 °C (PAM 3D printer)	62.3 ± 0.01	57.4 ± 0.01		32 ± 0.1

According to the data presented in ***Table 3.7,*** the extrusion and the relatively high temperatures applied during the 3D printing process led to a slight decrease in the melting temperature of the analysed polymer and a slight increase in its detected crystalline temperature compared with the raw material. An explanation could be that during the extrusion and printing of the analysed triangles a heating-cooling cycle has occurred at an uncontrolled rate compared to DSC analysis, with the solidification of the printed triangles occurring at room temperature. PCL crystals were, thereby, forming after the PCL triangles fabrication, with crystals with different growth defects, degree of order or crystals habits formed during the cooling phase compared with the crystals present in the as-received polymer (Shekunov *et al*., 1996) (Ferreira *et al.*, 2017) (Simao, Bellani and Branciforti, 2017) (Tiptipakorn *et al.*, 2015). The different nozzle sizes and print speeds used during the printing studies did not show any effect on the melting point, nor the crystallization temperature of the PCL, as expected (***Figure 3.15, Figure 3.16, Figure 3.17***). To note, a lower melting point in the second heating-cooling cycle was also observed in all the studied triangles, as with the raw polymer.

The crystallinity percentage (X_c %) of the polymer in the as-received materials, as well as, in the 3D printed triangles was calculated from the DSC thermograms. As shown in ***Table 3.8,*** the crystallinity degree of the LMW PCL and HMW PCL is similar and consistent with the literature data (Kotula, Snyder and Migler, 2017) (Monteiro, Inês and Tavares, 2018b) (Sato *et al*., 2012). However, it was observed that in the second heating-cooling cycle the crystallinity percentage in the pure polymer decreased. This is because the area under the curve of the melting point, that was used for the calculation of the enthalpy of fusion, ΔH_f, which was, then, used for the calculation of the crystallinity degree, differed between the first two heating programs.

Table 3.8: *Crystallinity percentage (X_c %) of pure LMW PCL (N=2), pure HMW PCL (N=4), and LMW PCL-TEC 3D printed triangle at 190 °C and a print speed of 10 mm/s from the FDM (N=2), LMW PCL triangle printed at 100 °C, a print speed of 3 mm/s and a nozzle diameter of 0.61 mm from the PAM 3D printer (N=2), HMW PCL triangle printed at 110 °C, with a print speed of 1.5 mm/s and a nozzle diameter of 0.61 mm from the PAM 3D printer (N=2), HMW PCL triangle printed at 130 °C, with a print speed of 1 mm/s with a nozzle diameter of 0.34 mm from the PAM 3D printer (N=2) obtained by two heating-cooling scans and pure HMW PCL powder (N=2) obtained by three heating-cooling scans.*

% Crystallinity degree			
	1st cycle	*2nd cycle*	*3rd cycle*
LMW PCL	55.7 ± 0.9	36.8 ± 2.5	
HMW PCL	52.2 ± 4.8	32.4 ± 3.3	
HMW PCL	44.5 ± 4.7	27.4 ± 2.3	27 ± 1.7
LMW PCL-TEC 190 °C (FDM)	42.1 ± 1	31.1 ± 0.7	
LMW PCL 100 °C (PAM 3D printer)	40.7 ± 0.02	26.9 ± 2.5	
HMW PCL 110 °C (PAM 3D printer)	38.6 ± 1.5	26.8 ± 1.3	
HMW PCL 130 °C (PAM 3D printer)	35.4 ± 1.7	30.9 ± 1.7	

As can be seen in the DSC thermograms of the raw polymer and the 3D printed polymeric triangles, ***Figure 3.14, Figure 3.15, Figure 3.16, Figure 3.17,*** the peak for the melting point during the first heating-cooling cycle is broader compared to the peak appearing in the second and third heating programs, even though all the curves for the peaks started at similar temperatures. Nevertheless, it could be observed in the DSC thermograms of the polymer that in the first heating cycle a smaller peak located in the temperature of the T_m of the second and third cycles could be hidden and integrated into the curve of the T_m of the first cycle. Consequently, the area under the peak of the melting point of the first heating-cooling program was larger compared to the one of the subsequent cycles,

resulting in the calculation of a higher crystallinity degree. It was, thus, indicated that there was a double melting peak for PCL in the first heating cycle. In most cases, the reason for this is that two crystal populations co-exist in the investigated sample and hence, two melting points (Nunez, 2004) (López *et al.*, 2016). These peaks, though, are usually gradually merged after the melting of the crystals and their recrystallization will lead to a different crystal (and single) rearrangement and formation. More stable crystals are, therefore, obtained during the controlled cooling cycle and the double melting point peaks disappear in the next heating programs, as also happened in the studied polymer. This is an attribute of the thermal behaviour of PCL displayed in its DSC thermograms and is in good correspondence with the already published data (López *et al.*, 2016) (Nunez, 2004) (Sakurai and Nojima, 2011).

The crystallinity degree of all the 3D printed triangles was reduced compared to the raw polymer. This might have happened due to the cooling rate of the 3D printed triangles that was not controlled as in the DSC characterizations. When the PCL was extruded from the 3D printers, it was in a molten phase in order to be arranged in the desired shape. When it solidified at room temperature this has resulted in the formation of fewer crystals in the freshly printed material compared to the as-provided PCL. It is noteworthy that the crystallinity percentage decreased even more in the second heating program, which could be associated with the presence of different types of crystals in the 3D printed material, similarly to the raw polymer.

The various applied temperatures and print speeds did not show to have any impact on the crystallinity percentage of the used materials, though (***Table 3.8***). The mixing of the polymer with triethyl citrate did not lead to any further decrease of the crystallinity degree, at the very low concentration employed; neither the combination of hot melt extrusion for the filament production and the 3D printing with the FDM for the manufacture of the triangles.

3.2.2.2. XRD Characterization

XRD data were collected on the pure high and low molecular weight polycaprolactone before extrusion and printing, the produced LMW and HMW PCL-TEC filaments, and the 3D printed polymeric objects from the PAM and the FDM 3D printers in order to identify their physical nature.

Figure 3.18.a. and ***Figure 3.18.b.*** show the XRD patterns of the two studied PCL molecular weights, which from a visual inspection are identical. More specifically, the characteristic peaks of the LMW PCL are at 21.60 and 24.12° 2θ and of the HMW PCL are at 21.45 and 23.89° 2θ, related to the crystalline component of the polymer. These data match well with those reported in the literature (Monteiro, Inês and Tavares, 2018b) (Shoja *et al*., 2015) (Shkarina *et al.*, 2018) (Aliah and Ansari, 2017).

Figure 3.19.a and ***Figure 3.19.b*** depict the XRD diffractograms of LMW PCL and HMW PCL, respectively, before and after the production of the filament, as well as, their triangles printed in the FDM. The objects used for this characterization are the LMW PCL triangle printed at 180 °C with a print speed of 5 mm/s, the LMW PCL triangle printed at 190 °C with a print speed of 20 mm/s, the HMW PCL triangle printed at 180 °C with a print speed of 15 mm/s and the HMW PCL triangle printed at 190 °C with a print speed of 10 mm/s.

According to the XRD patterns in ***Figure 3.19***, the intensity for both the HMW and LMW PCL peaks after the extrusion and 3D printing processes demonstrated a slight decrease compared to the peaks of the raw materials. This indicated a change in the crystallinity of the investigated polymer, which could be explained by the uncontrolled heat-cool cycle occurring during the extrusion and 3D printing leading to the formation of fewer crystals with various degrees of order, crystal defects, shape and orientation, as mentioned previously. The various print speeds used did not cause any changes in the crystalline nature of the polymer, nor its mixing with the plasticizer, TEC.

a

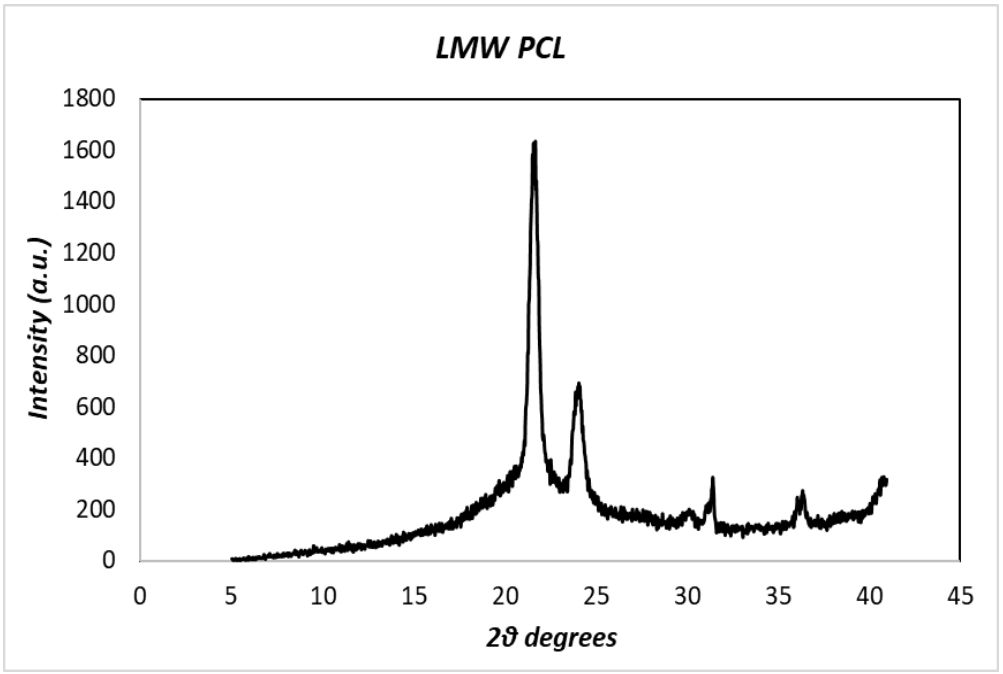

b

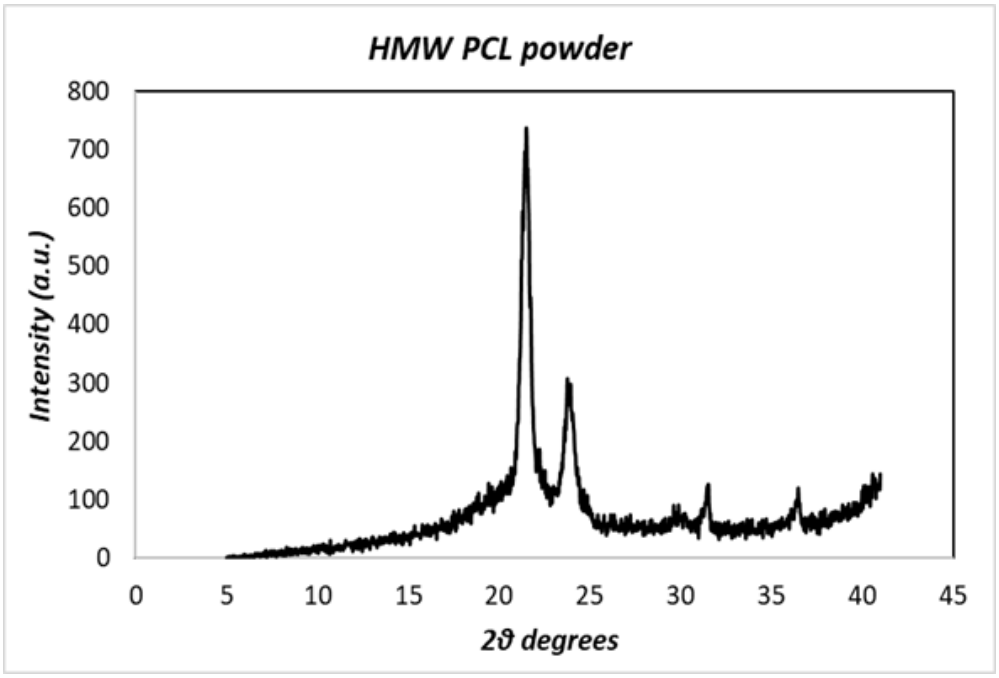

Figure 3.18: *XRPD diffractograms of* ***(a):*** *LMW PCL and* ***(b):*** *HMW PCL powder. All materials before extrusion and printing.*

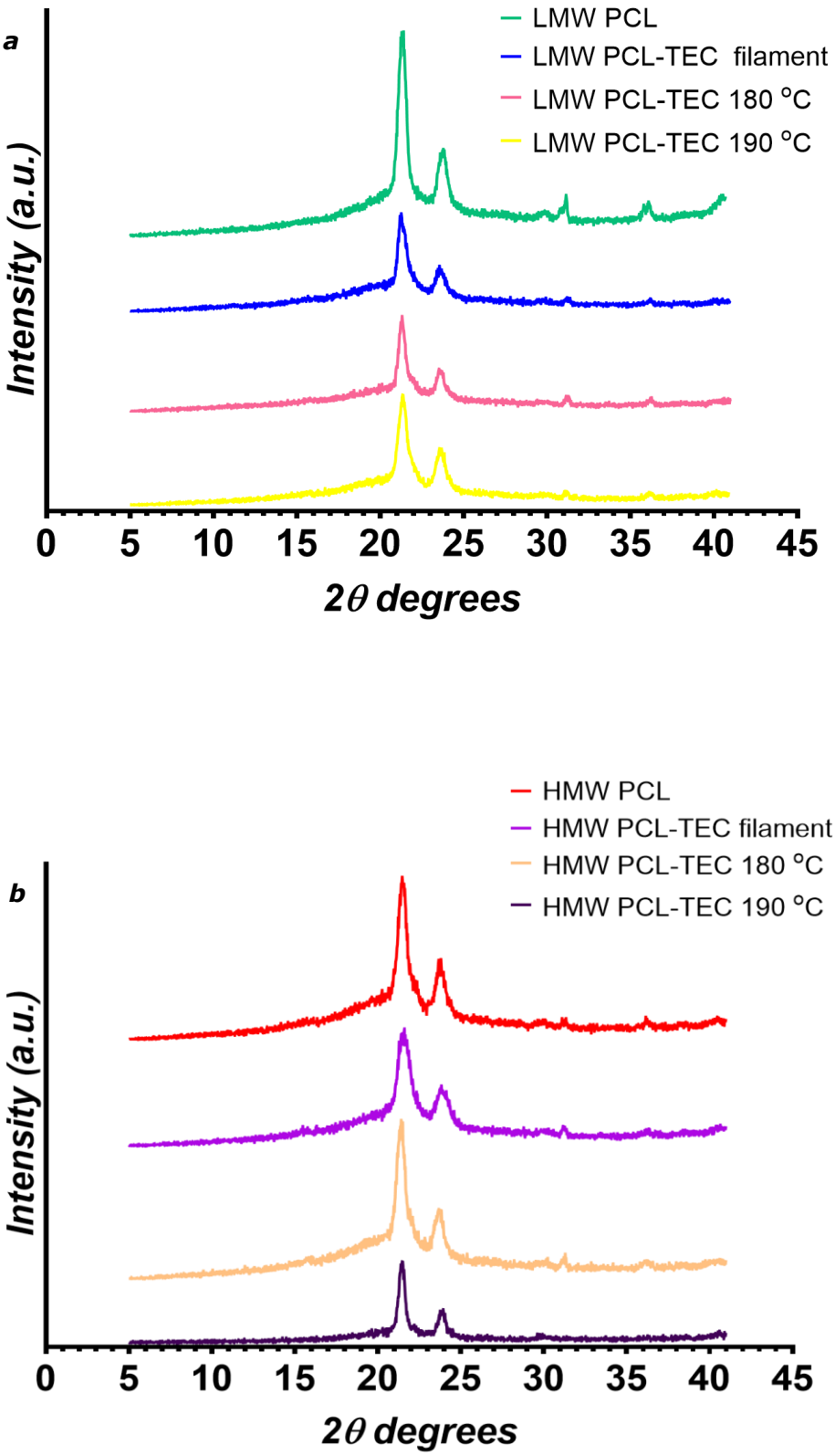

Figure 3.19: *XRD diffractograms of* ***(a):*** *LMW PCL before and after extrusion and 3D printing in the FDM 3D printer,* ***(b):*** *HMW PCL before and after extrusion and 3D printing in the FDM 3D printer.*

The crystallinity percentage (X_c %) of the different molecular weights polycaprolactone in the as-received materials, as well as, in the produced filaments from the HME and the 3D printed triangles was calculated from the XRD diffractograms. According to ***Table 3.9,*** the crystallinity degree of the polymer before extrusion and 3D printing was similar for both molecular weights. The extrusion for the filament production and the subsequent 3D printing processing of the polymeric material led, though, to a slight decrease of the crystallinity percentage of the material of interest. An explanation for that could be, as also mentioned in the discussion of the DSC results, that the cooling of the extruded material was happening in an uncontrolled way and therefore, fewer crystals were formed under these circumstances compared to the crystals present in the raw material. Nevertheless, the different applied settings, temperature, print speed, during the printing of the triangles in the FDM 3D printer demonstrated no impact on the calculated PCL crystallinity degree.

Table 3.9: *Crystallinity percentage (X_c %) of pure LMW PCL powder (N=2), pure HMW PCL powder (N=2), and LMW PCL-TEC filament (N=2), LMW PCL-TEC 3D printed triangle at 180 °C and a print speed of 5 mm/s from the FDM (N=2), LMW PCL-TEC 3D printed triangle at 190 °C and a print speed of 20 mm/s from the FDM (N=2), HMW PCL-TEC filament (N=2), HMW PCL-TEC 3D printed triangle at 180 °C and a print speed of 15 mm/s from the FDM (N=2), HMW PCL-TEC 3D printed triangle at 190 °C and a print speed of 10 mm/s from the FDM (N=2).*

% Crystallinity degree		
	LMW PCL	***HMW PCL***
Before extrusion and 3D printing	32.7 ± 0.5	34.8 ± 3.3
Filament	30.1 ± 1.2	33.2 ± 2.6
180 °C	31.6 ± 0.7	31.2 ± 2.5
190 °C	29.7 ± 2.3	30.3 ± 3.7

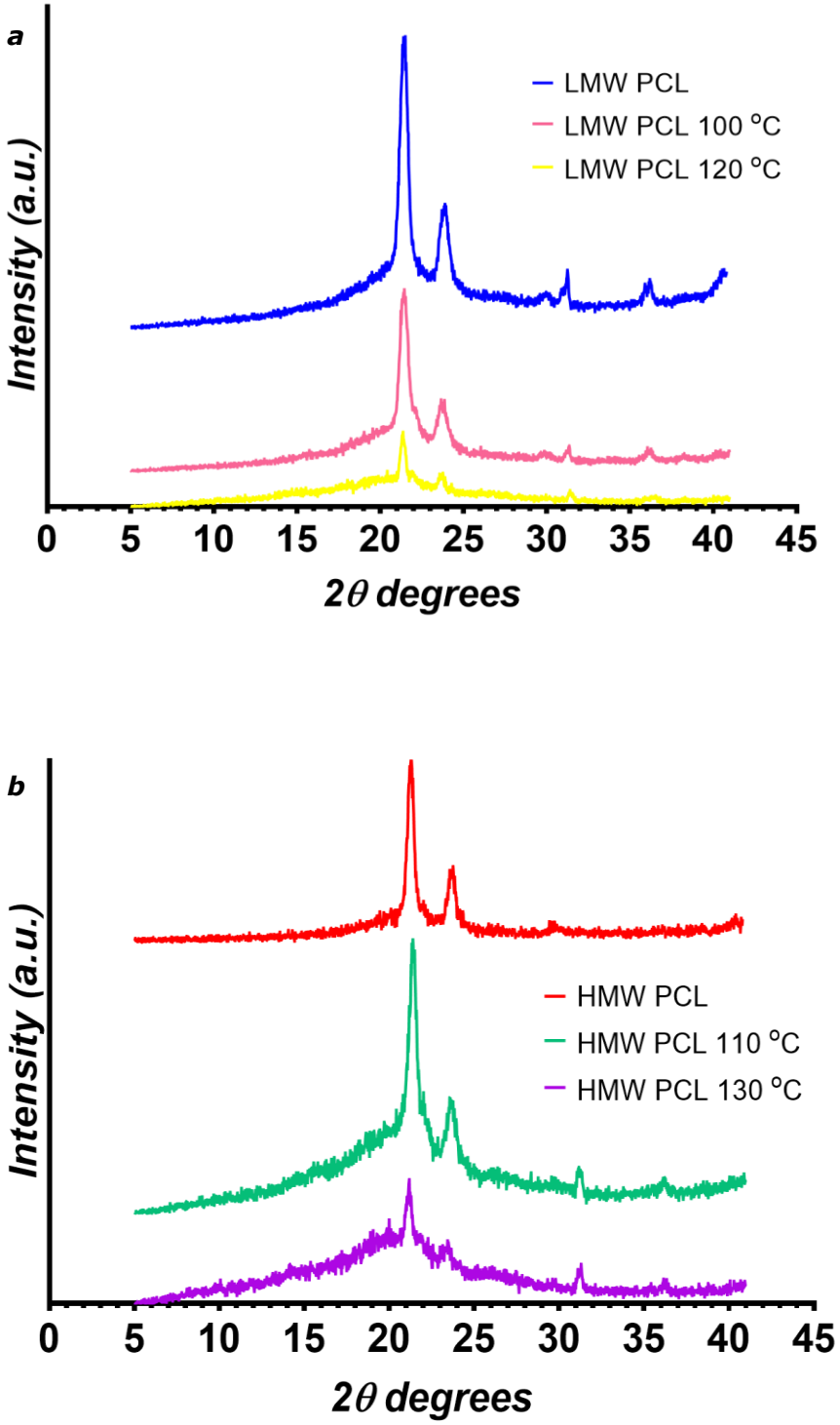

Figure 3.20: *XRD diffractograms of* ***(a):*** *LMW PCL before and after 3D printing in the PAM 3D printer,* ***(b):*** *HMW PCL before and after 3D printing in the PAM 3D printer.*

These results are generally consistent with the crystallinity percentage calculated by the DSC thermograms in the second heating-cooling cycle, where the thermal properties of the polymer have been stabilised and are summarized in ***Table 3.11***; a further discussion will follow.

However, no direct comparisons should be done for the crystallinity degree calculated with these two techniques, since their sensitivity level and their principles of operation are different; XRD analysis was performed at room temperature measured at 24 ^{o}C (Buckton and Darcy, 1995) (Hogan and Buckton, 2001) (Shah, Kakumanu and Bansal, 2006).

XRD patterns of the LMW PCL and HMW PCL before and after the printing of triangles in the PAM 3D printer are demonstrated in ***Figure 3.20.a*** and ***Figure 3.20.b,*** respectively. The samples analysed in the XRD are the LMW PCL triangle printed at 100 ^{o}C, with a print speed of 3 mm/s and a nozzle diameter of 0.61 mm, the LMW PCL triangle printed at 120 ^{o}C, with a print speed of 1 mm/s and a nozzle diameter of 0.34 mm, the HMW PCL triangle printed at 110 ^{o}C, with a print speed of 1 mm/s and a nozzle diameter of 0.61 mm, the HMW PCL triangle printed at 130 ^{o}C, with a print speed of 1 mm/s and a nozzle diameter of 0.34 mm.

A slight drop in the intensity of the characteristic peaks of both HMW and LMW PCL was observed after the manufacture of the triangles with the PAM 3D printer (***Figure 3.20***). This is associated, as described above, with the uncontrolled rate of the solidification phase of the printed objects resulting in the formation of fewer crystals with different shapes and orientations contrasted with the as-received polymers. The two molecular weights polycaprolactone demonstrated similar behaviour, as for their physical state, in all the print temperatures, speeds and nozzle sizes applied during the fabrication of the test shape.

Table 3.10: *Crystallinity percentage (X_c %) of pure LMW PCL powder (N=2), pure HMW PCL powder (N=2), and LMW PCL 3D printed triangle at 100 °C, with a print speed of 3 mm/s and a nozzle diameter of 0.61 mm from the PAM 3D printer (N=2), and LMW PCL 3D printed triangle at 120 °C, with a print speed of 1 mm/s and a nozzle diameter of 0.34 mm from the PAM 3D printer (N=2), HMW PCL 3D printed triangle at 110 °C, with a print speed of 1 mm/s and a nozzle diameter of 0.61 mm from the PAM 3D printer (N=2), and HMW PCL 3D printed triangle at 130 °C, with a print speed of 1 mm/s and a nozzle diameter of 0.34 mm from the PAM 3D printer (N=2).*

% Crystallinity degree		
	LMW PCL	**HMW PCL**
Before extrusion and 3D printing	32.7 ± 0.5	34.8 ± 3.3
100 °C	31.9 ± 1.4	
110 °C		31.7 ± 2.6
120 °C	25.1 ± 3.9	
130 °C		27.8 ± 4.9

Based on the XRD diffractograms of the pure LMW and HMW PCL powder, as well as, their 3D printed triangles, the crystallinity degree of the polymer was calculated. As presented in ***Table 3.10,*** the crystallinity of the polymer was not considerably affected by the different temperatures and print speeds applied during the manufacture of the triangles. It was noticed though, that for both molecular weights of PCL, the crystallinity percentage decreased after 3D printing, similarly to the crystallinity degree calculated in the extruded filaments and the triangles fabricated by the FDM 3D printer. The uncontrolled cooling of the manufactured parts could potentially have influenced the formation of polymeric crystals, as mentioned above.

Table 3.11: *Summary of the crystallinity degree of HMW and LMW PCL before and after their processing in the HME, the FDM 3D printer and the PAM 3D printer.*

% Crystallinity degree				
	DSC results			XRD results
	1st cycle	2nd cycle	3rd cycle	
LMW PCL	55.7 ± 0.9	36.8 ± 2.5		32.7 ± 0.5
HMW PCL	52.2 ± 4.8	32.4 ± 3.3		34.8 ± 3.3
HMW PCL	44.5 ± 4.7	27.4 ± 2.3	27 ± 1.7	
LMW PCL filament				30.1 ± 1.2
HMW PCL filament				33.2 ± 2.6
LMW PCL-TEC 180 °C (FDM)				31.6 ± 0.7
LMW PCL-TEC 190 °C (FDM)	42.1 ± 1	31.1 ± 0.7		29.7 ± 2.3
HMW PCL-TEC 180 °C (FDM)				31.2 ± 2.5
HMW PCL-TEC 190 °C (FDM)				30.3 ± 3.7
LMW PCL 100 °C (PAM 3D printer)	40.7 ± 0.02	26.9 ± 2.5		31.9 ± 1.4
HMW PCL 110 °C (PAM 3D printer)	38.6 ± 1.5	26.8 ± 1.3		31.7 ± 2.6
HMW PCL 120 °C (PAM 3D printer)				25.1 ± 3.9
HMW PCL 130 °C (PAM 3D printer)	35.4 ± 1.7	30.9 ± 1.7		27.8 ± 4.9

Summarizing the results of the crystallinity degree detected and calculated from the XRD diffractograms and DSC thermograms in ***Table 3.11***, it is observed that the crystallinity percentage based on the XRD data is similar to the one corresponding to the second (and third) heating cycle of the DSC thermograms. This could be attributed to the presence of two crystal populations in the polymeric samples demonstrating different thermal behaviour and resulting in the appearance of broader peaks for the melting point which were used for the calculation of the crystallinity degree, as mentioned earlier. Hot melt extrusion and 3D printing processes demonstrated to have an effect on the rearrangement of the crystals since, as previously discussed, the heating and cooling cycles performed during these technologies are not controlled and could not be considered equivalent with the controlled heating and cooling occurring during the DSC analysis. That was, thereby, leading to a slight decrease of the crystallinity percentage of PCL after hot melt extrusion and 3D printing as derived by the XRD diffractograms.

3.3. CONCLUSIONS

This chapter demonstrates that the printing of PCL in extrusion-based 3D printers is feasible. PCL is a viscous material, which solidifies quickly at room temperature. For this purpose, all the parts participating in the printing need to be heated and therefore, metal parts are needed, where heat transfer is more effectively performed. The most suitable print temperatures for both the LMW PCL and the HMW PCL were at the highest studied ones. Pure LMW PCL was better printed at the highest print speeds, while the HMW PCL at the lowest ones (***Table 3.12***).

The difficulties in the HME filament production using pure PCL have been solved by mixing the polymer with a plasticizer, TEC. Only a very small amount of the latter was required, 1% w/w, for the extrusion of quite fine PCL filaments at a low temperature, close to the polymer's melting point. Nevertheless, the printing of LMW PCL-TEC and HMW PCL-TEC filaments in the FDM was better achieved at higher temperatures and low print speeds for the LMW PCL and higher print speeds for the HMW PCL (***Table 3.12***).

Table 3.12: *Summary of the best settings (temperature, print speed, nozzle size) for 3D printing with the HMW and LMW PCL in the PAM 3D printer and the FDM.*

Material	***PAM 3D printer***		***FDM***
Nozzle diameter	***0.34 mm***	***0.61 mm***	***0.8 mm***
LMW PCL	130 °C, 1 mm/s	110 °C, 6 mm/s	180 °C, 5 mm/s
		120 °C, 6 mm/s	180 °C, 10 mm/s
		130 °C, 6 mm/s	180 °C, 15 mm/s
HMW PCL	130 °C, 1 mm/s	110 °C, 1 mm/s	180 °C, 15 mm/s
		120 °C, 1 mm/s	180 °C, 20 mm/s
		130 °C, 1 mm/s	
		110 °C, 1.5 mm/s	
		120 °C, 1.5 mm/s	
		130 °C, 1.5 mm/s	

According to the DSC and XRD analysis, both HMW and LMW PCL were crystalline after the extrusion and 3D printing, while this property was not affected by the various applied printing settings. However, a few differences were observed in the post printed polymers compared with the raw materials; a slight decrease in the melting temperature, a slight increase in the crystallization temperature, as well as, a slight decrease in the intensity of the polymer peaks in the XRD patterns. These changes were attributed to the uncontrolled heat-cool cycle occurring during the extrusion and 3D printing processes.

Based on the crystallinity degree calculation from both the XRD diffractograms and the DSC thermograms, it was demonstrated that this property of the different molecular weights PCL decreased in the hot melt extruded filaments and 3D printed triangles. Nevertheless, the polymer crystallinity percentage was not affected by its mixing with a plasticiser, nor by the different applied temperatures and print speeds in the two studied 3D printers, the FDM and the PAM 3D printer.

For the next steps of my research, it was decided to focus on one material and 3D printing process for the manufacture of lidocaine loaded polycaprolactone implants. The selected polymer was the HMW PCL and the selected printer the PAM 3D printer. This combination seemed to be the most promising in order to achieve the aim of my project; the fabrication of drug loaded polymeric implants at the lowest temperature possible using a solvent-free and excipients-free method. An excipient was not required in this 3D printing process for the successful material extrusion and fabrication of the predesigned object, contrasted with the HME and the FDM. Therefore, the nozzle with a diameter of 0.61 mm will be the one that will be used for future experiments, since the printing of PCL objects is feasible at temperatures closer to the melting point of the studied polymer and drug with this nozzle than with the smallest one.

CHAPTER 4: 3D PRINTING OF LIDOCAINE LOADED AND FREE HMW PCL IMPLANTS IN A PRESSURE-ASSISTED MICROSYRINGE 3D PRINTER AND CHARACTERIZATION OF THE PRINTED FORMULATIONS

4.1. INTRODUCTION

The manufacture of HMW PCL encased and non-encased polymeric implants with different drug loading, as well as, drug free HMW PCL implants using a PAM 3D printer (Inkredible +, Cellink, Gothenburg, Sweden) is presented in this Chapter. The selection of the model drug that was loaded in the polymeric implants has been made in part based on its melting temperature, which was needed to be lower than the melting point of PCL, 50 – 75 ºC. Lidocaine was the chosen drug as its decomposition temperature (196 ºC) is higher than the melting point of the studied polymer (Gala *et al*., 2015). Its melting point (66 – 79 ºC) is, however, relatively close to PCL's melting point, and therefore, a similar temperature is needed for the melting and extrusion of the blended compounds (Pathak and Nagarsenker, 2009b) (Umeda *et al.*, 2009) (Repka *et al.*, 2005) (Chen *et al.*, 2004) (Kang, Jun and Mccall, 2000) (Cui and Frank, 2006) (Bakonyi *et al.*, 2018) (Peracchia *et al.*, 1997).

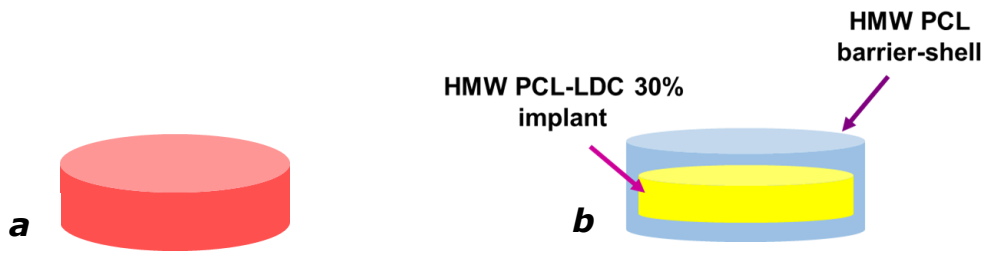

Figure 4.1: *Disc-shaped* ***(a):*** *lidocaine loaded and free polycaprolactone implants and* ***(b)*** *HMW PCL barrier-shell lidocaine loaded polycaprolactone implants.*

More specifically, the implants were printed in a disc shape for ease of handling (***Figure 4.1.a***). The manufacture of implants with various drug loading (5% and 30% w/w), as well as, the production of a core-shell formulation were performed to demonstrate the versatility of PAM 3D printing technique and its potential application in personalized therapy. The dosage forms fabricated for this study are the following:

- HMW PCL implants loaded with 30% w/w lidocaine (HMW PCL-LDC 30%)
- HMW PCL implants loaded with 5% w/w lidocaine (HMW PCL-LDC 5%)
- HMW PCL barrier-shell implants loaded with HMW PCL-LDC 30% discs (HMW PCL – HMW PCL-LDC 30%) (***Figure 4.1.b***)
- HMW PCL implants (drug free)

Different settings have been applied during the 3D printing process (print speed, print temperature, extrusion width, bed temperature, pressure) in order for homogeneous and compact dosage forms to be manufactured and sustained drug release to be achieved (***Figure 4.2***). The overall aim was the fabrication of implants without any apertures or surface defects that could lead to an uncontrolled and faster release of the enclosed drug. Additionally, printing accuracy was assessed and presented in the current Chapter, since implants with dimensions as close as possible to the dimensions of the predesigned object needed to be produced. Printing accuracy regarding the size of the implants is a particularly important attribute since the volume and the weight of the manufactured formulation is associated with the amount of the drug contained in it and hence, the overall dose. The final settings for the fabrication of each formulation presented in this Chapter after several steps of optimization are summarized in ***Table 4.1.***

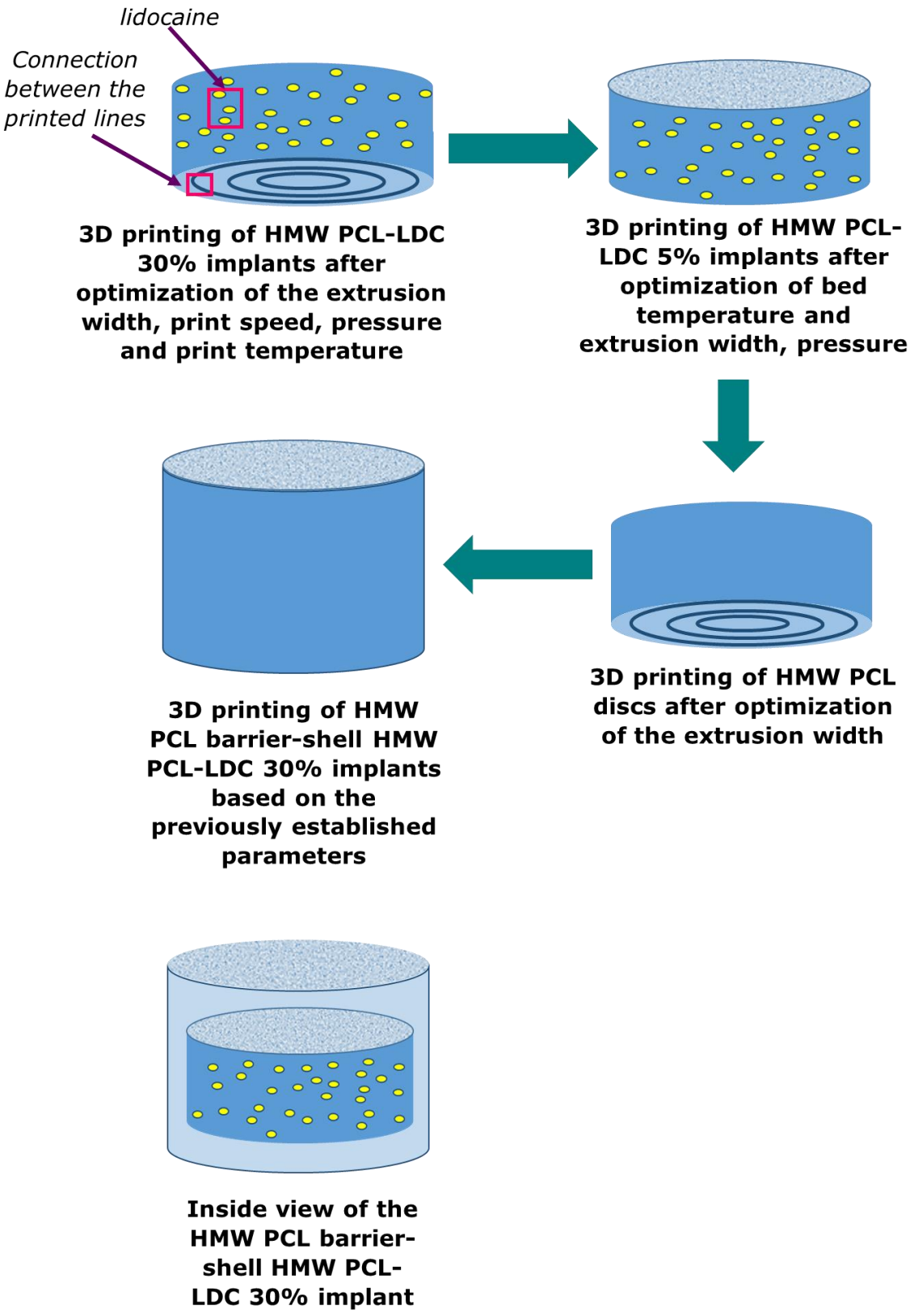

Figure 4.2: *Schematic diagram of the optimization procedure for the establishment of the printing parameters for the manufacture of HMW PCL-LDC 30%, HMW PCL-LDC 5%, HMW PCL and HMW PCL barrier-shell HMW PCL-LDC 30% implants. The darker blue lines represent the connection between the printed lines and the yellow dots the lidocaine.*

Table 4.1: *Summary of printing settings for the manufacture of HMW PCL implants (HMW PCL barrier-shell), HMW PCL-LDC 30% implant-core (shell-core implant), HMW PCL-LDC 30% implants and HMW PCL-LDC 5% implants after optimization of the printing parameters.*

Printing Settings	Implant type			
	HMW PCL implant (HMW PCL barrier-shell)	***HMW PCL-LDC 30% implant - core (shell-core implant)***	***HMW PCL-LDC 30% implant***	***HMW PCL-LDC 5% implant***
Print Speed (mm/s)	1	1	1	1
Infill Pattern	concentric	concentric	concentric	concentric
Pressure (kPa)	400	125	125	400
Bed temperature (°C)	40	40	24	40
Print temperature (°C)	110	110	110	110
Extrusion width (%)	40	60	60	50

Physical and chemical characterization (SEM, DSC, XRD, FTIR, Raman) has been carried out before and after implant fabrication to investigate whether material properties have been affected by the printing and if any interactions or chemical modifications occurred between the polymer and the drug.

A part of this Chapter has been published (***Appendix 2***) (Liaskoni, Wildman and Roberts, 2021).

4.2. RESULTS AND DISCUSSION

4.2.1. PAM 3D Printing of Lidocaine loaded HMW PCL implants

The selected model drug, lidocaine, was mixed with different concentrations of the polymer powder for formulations with different drug loading (5% and 30%) to be produced. Optimization of the printing parameters was performed for implants suitable for sustained drug release to be fabricated. A core-shell implant has been manufactured to illustrate the versatility of PAM 3D printing in the production of personalised formulations.

4.2.1.1. 3D Printing of HMW PCL-LDC 30% implants

HMW PCL-LDC 30% implants were printed with different printing settings in order for the best ones to be selected. Each setting was independently altered and appropriate characterizations were carried out to select the most suitable.

For the printing of the implants, HMW PCL powder was mixed with 30% w/w Lidocaine (LDC) powder using a mortar and a pestle for 3 min.

Disc-shaped implants with dimensions of 10 mm length x 10 mm width x 2 mm height were printed.

4.2.1.1.1. 3D Printing of HMW PCL-LDC 30% implants with different print speeds

According to the printing tests described in ***Chapter 3***, on which triangles have been printed with a nozzle diameter of 0.61 mm and a pressure of 400 kPa, the most promising printing settings were at 110, 120 and 130 ^{o}C with low print speeds, 1 and 1.5 mm/s. Nevertheless, after loading the HMW PCL-LDC 30% powder mixture in the aluminium cartridge and after heating to 110 ^{o}C in the PAM 3D printer, the materials extrudability was initially assessed before the implant production (by applying a pressure of 400 kPa).

The loaded compounds were indeed extruded, as anticipated, but this by observation happened at a faster rate than with the pure polymer. An explanation for that could be that the mixing of lidocaine with polycaprolactone contributed to the decrease of the viscosity of the polymer-drug mixture, in accordance with the previously reported data (de Melo and Marijnissen-Hofste, 2012). The extrudability of the mixture was then investigated at lower temperatures (70 - 100 °C), but still above the melting point of the polymer and the drug and also, at higher ones (110 - 130 °C) (***Table 4.2***).

Table 4.2: *Combinations of temperatures and pressure for the extrudability assessment of the HMW PCL-LDC 30% powder mixture.*

Temperature (°C)	*Pressure (kPa)*
70	400
80	400
90	400
100	400
110	400
120	400
130	400

HMW PCL mixed with 30% w/w LDC was successfully extruded at all the examined combinations (***Table 4.2***). Therefore, all these temperatures could be used for the manufacture of implants.

The next stage of this study was to explore the fabrication of implants with two different print speeds, 1 and 1.5 mm/s. For this study, different combinations of temperature: 70 – 130 °C and print speeds: 1 – 1.5 mm/s were applied, while the rest of the parameters remained the same, namely: pressure of 400 kPa, extrusion width of 100% (suggested value in the Heartware software), line spacing of 0.61 mm (distance between the centre of the printed lines) and concentric infill pattern.

The discs adhesiveness on the building stage was sufficient and thus, no higher temperature than the RT (measured to be 24 °C) was needed for the stage, as for the printing of pure PCL triangles.

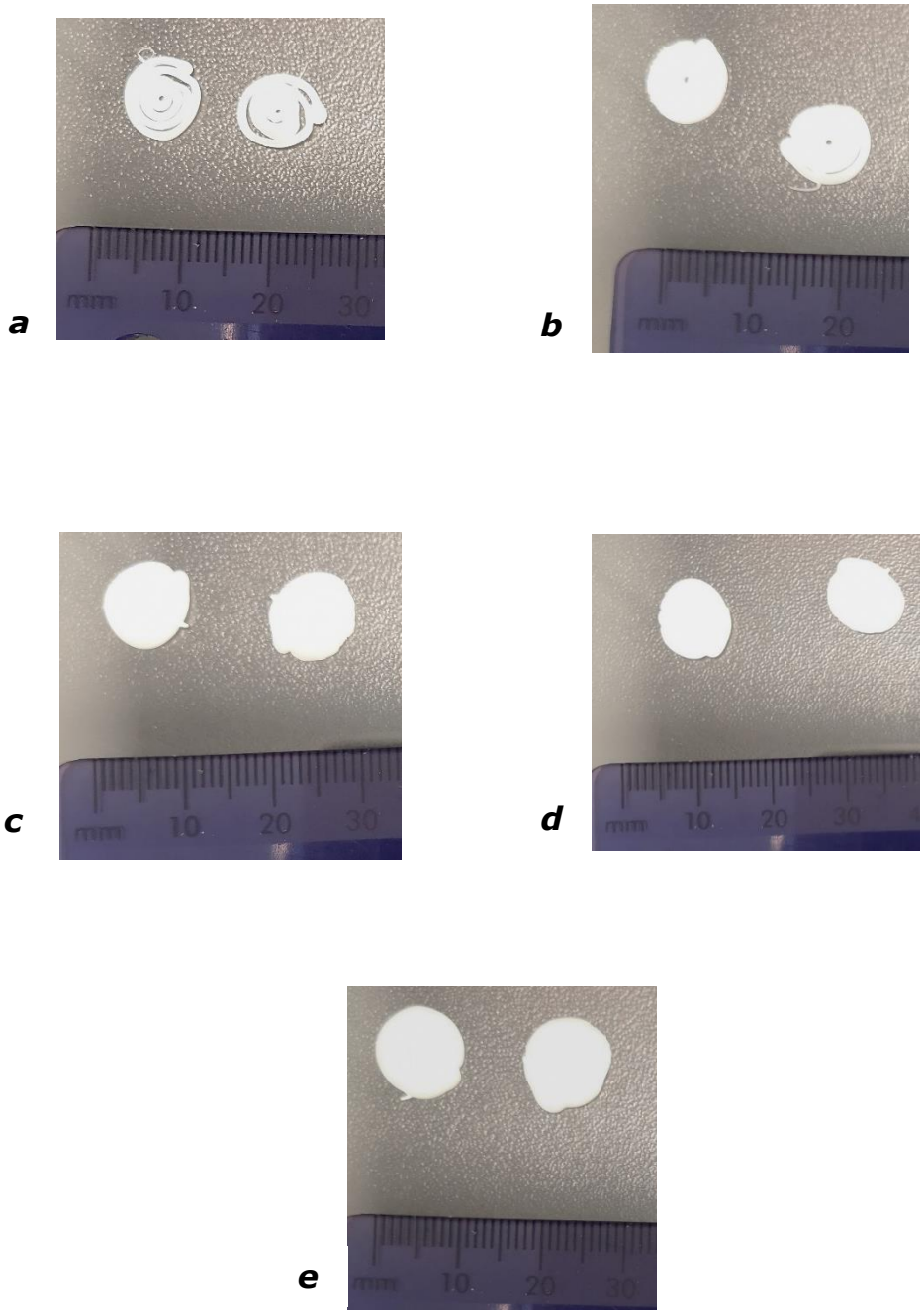

Figure 4.3: *HMW PCL-LDC 30% implants printed with a print speed of 1.5 mm/s at* ***(a):*** *70 °C,* ***(b)*** *80 °C,* ***(c)*** *90 °C,* ***(d)*** *100 °C and* ***(e)*** *110 °C.*

It was observed that there were some gaps between the printed lines of the implants printed at 70 °C. This trait was more evident, though, when the implants were printed with a print speed of 1.5 mm/s (***Figure 4.3.a***) than with the lower print speed (***Figure 4.4.a***). As the temperature increased, more material extruded which resulted in an elimination of these gaps (***Figure 4.3.a-e, Figure 4.4.a-c***). For the implants fabricated with a print speed of 1.5 mm/s, no gaps were visible after printing at 90 °C (***Figure 4.3.c***), while this was noticed at a lower temperature, 80 °C, in the implants manufactured with a print speed of 1 mm/s (***Figure 4.4.b***).

a 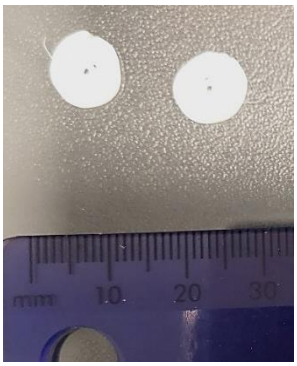 ***b*** 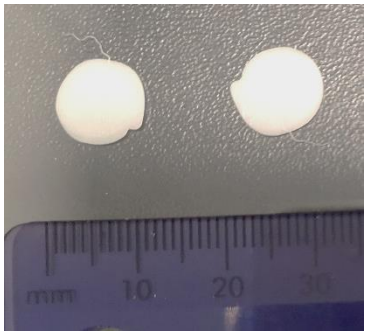

c 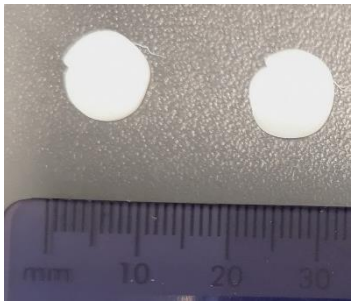

Figure 4.4: *HMW PCL-LDC 30% implants printed with a print speed of 1 mm/s.* ***(a):*** *70 °C,* ***(b)*** *80 °C and* ***(c)*** *90 °C.*

The size of the produced implants (n=5 for each print speed/temperature combination) was then measured in two different parallels (horizontally and vertically) using Image J software (measurement in Image J was performed twice for each implant) and their mean values calculated.

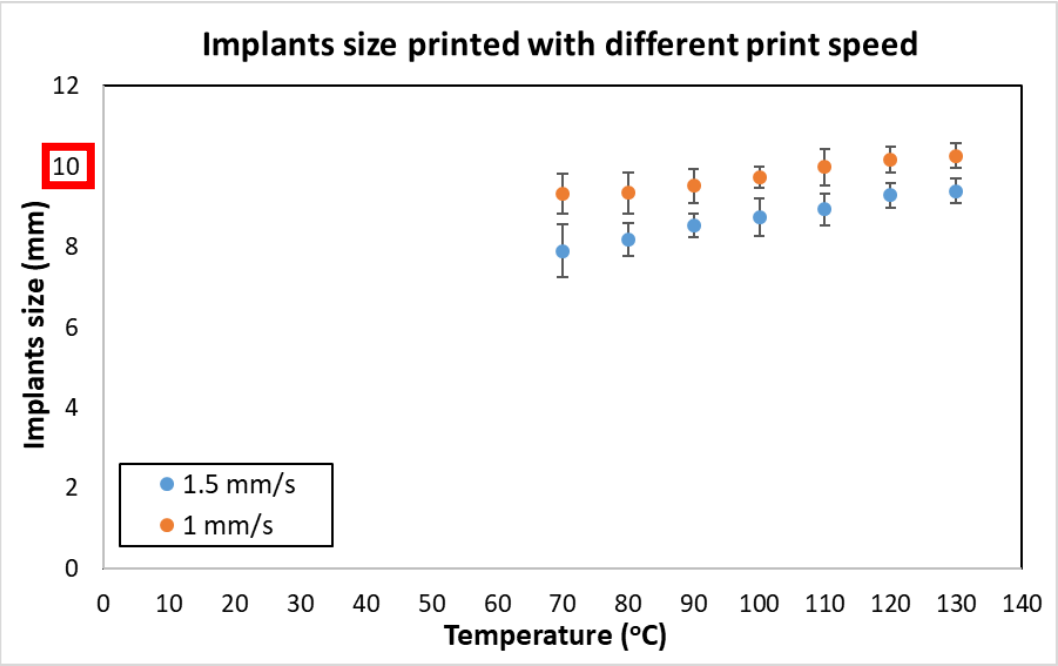

Figure 4.5: *Size of the HMW PCL-LDC 30% implants printed with print speeds of 1 and 1.5 mm/s at different temperatures, as measured in Image J (n=5 implants were measured at each temperature/print speed combination). Red boxed figure represents the theoretical dimensions of the printed disc-shaped implant as in the CAD file.*

Figure 4.5 depicts the size of the lidocaine loaded PCL implants printed at the two investigated print speeds plotted against increasing temperature. The formulations manufactured with the highest print speed resulted in discs with dimensions considerably smaller than the desired ones (10 mm length x 10 mm width x 2 mm height). When the lowest print temperatures were applied, the fabricated discs were even smaller than 8 mm. The powder mixture was still quite viscous, though and in combination with the fact that temperatures closer to the melting point of the used compounds were applied resulted in slower materials extrusion and consequently, slower materials deposition on the printing platform. This could also be verified by the gaps appearing in the implants in ***Figure 4.3.a*** and ***Figure 4.3.b.*** Higher than 70 °C print temperature could lead to a better melting of both the polymer and the drug and thus, faster materials extrusion from the nozzle. This was indicated, as well, by a feature observed in both sample groups; as the temperature increased the size of the discs also increased.

In the case of the implants printed with the lowest print speed, 1 mm/s, far higher accuracy in their size was achieved, even when the lowest temperature was applied, as displayed in ***Figure 4.5.*** It should be noted that even the formulation printed at 70 °C was closer to 10 mm than the one printed with the highest temperature and print speed.

Printing of implants with dimensions as close as possible to the ones of the predesigned object is particularly important since the volume of the manufactured formulation is associated with the amount of the drug contained in it and thereby, the overall dose.

Based on the above observations and implants size measurements, it was concluded that the most promising print speed for the fabrication of the disc-shaped lidocaine loaded polycaprolactone implants was the lowest applied one, 1 mm/s, in all the examined temperatures.

4.2.1.1.2. 3D Printing of HMW PCL-LDC 30% implants with different extrusion width

The next printing study was associated with the investigation of the impact of the extrusion width on the printing resolution. This was the next parameter that was explored since it was regulating the lines distancing and as previously noticed, there were some gaps between the printed lines. The selected print temperature was 70 °C -where the formulations presented the most gaps- as it was the temperature closest to the melting point of the used compounds and the lowest temperature in which drug loaded polymeric implants could be manufactured.

Extrusion width settings of 50, 60, 70, 80 and 100% were used. This parameter was calculated according to the nozzle diameter and it was adjusting the distance between the centres of each printed line horizontally (***Table 4.3***). The diameter of the nozzle used in these printing tests was 0.61 mm. The remaining printing settings were kept constant, as presented in ***Table 4.4.***

Table 4.3: *Interpretation of extrusion width setting in distance between the centres of each printed line.*

Extrusion width (%)	*Distance (μm)*
50	305
60	366
70	427
80	488
100	610

Table 4.4: *Settings for the assessment of the printing resolution with different extrusion width applied.*

Printing Parameters	
Temperature	70 °C
Print Speed	1 mm/s
Pressure	400 kPa
Bed Temperature	24 °C
Infill pattern	concentric

As shown in ***Figure 4.6***, as the distance between the centres of the printed lines decreased, the dimensions of the disc-shaped implants were closer to the predesigned ones (10 mm length x 10 mm width x 2 mm height). Nonetheless, an ANOVA test performed using the data depicted in ***Figure 4.6*** demonstrated that they are not significantly different since the P value was 0.3249 ($P > 0.05$).

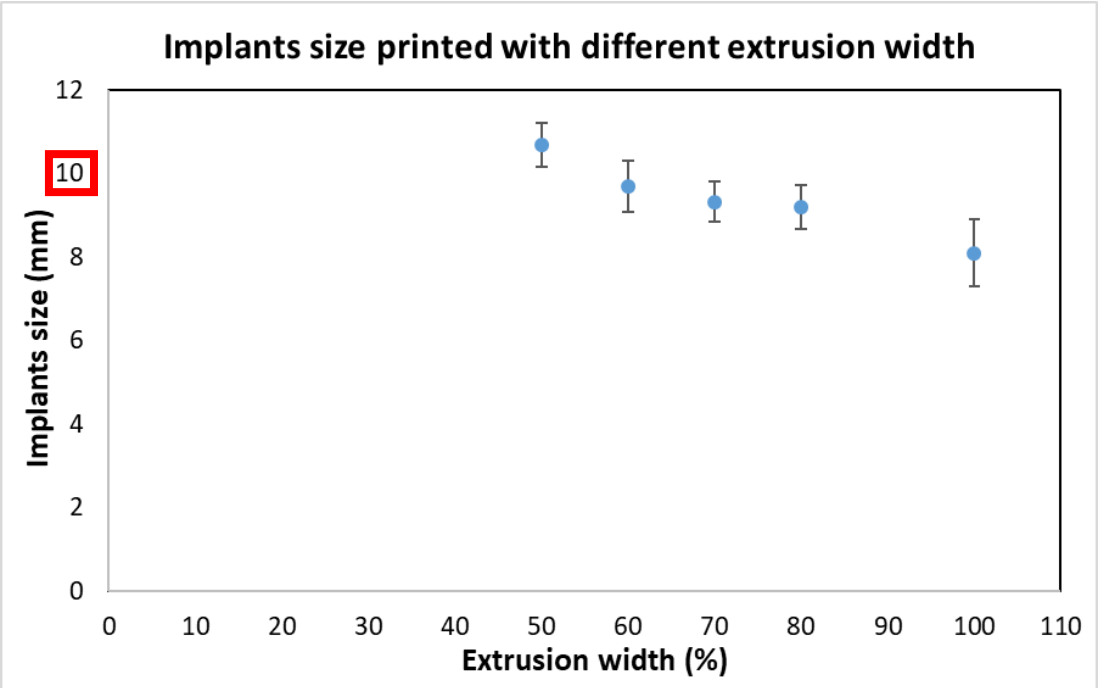

Figure 4.6: *Size of the HMW PCL-LDC 30% implants printed with different extrusion widths, 50-100%, and a print speed of 1 mm/s at 70 °C, as measured in Image J (n=5 implants were measured at each extrusion width). Red boxed figure represents the theoretical dimensions of the printed disc-shaped implant as in the CAD file.*

The fabricated implants didn't seem to differ much visually as can be seen in ***Figure 4.7***. No gaps have been observed and a homogeneous printing was assumed to have been achieved.

Nevertheless, further characterizations on the implant surface were needed to confirm these observations.

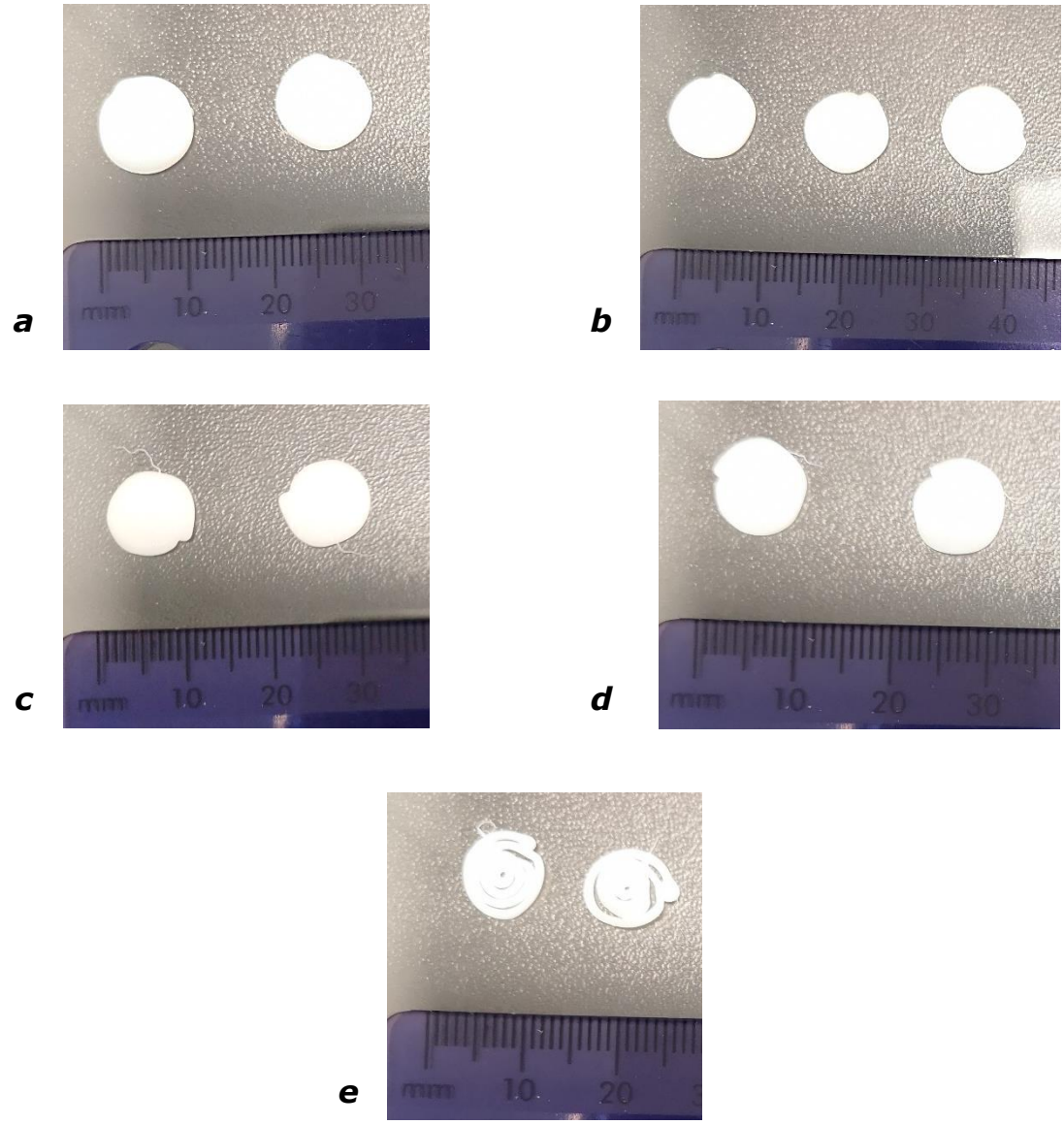

Figure 4.7: *HMW PCL-LDC 30% implants printed with an extrusion width setting of* ***(a):*** *50%,* ***(b):*** *60%,* ***(c)*** *70%,* ***(d)*** *80% and* ***(e)*** *100%.*

4.2.1.1.2.1. SEM Characterization

SEM characterization on the PCL implants loaded with 30% lidocaine and fabricated with different extrusion widths followed for a more in-depth analysis of their printing resolution.

As demonstrated in ***Figure 4.8***, the implants surface differed based on the selected extrusion width setting. According to the SEM image of the implant printed with an extrusion width setting of 100% (***Figure 4.8.e***), there were some gaps on its surface. The gap size between the printed lines decreased towards zero as the extrusion width decreased (***Figure 4.9.a***). Less material was extruded in the connection between the printed lines and that could explain the discussed observation. To note, the apertures appeared in parallel concentric cycles, which was the selected infill pattern. No gap was visible, though, on the surface of the implants printed with extrusion width settings of 50% and 60% (***Figure 4.8.a, Figure 4.8.b***).

The distance of the centres of the printed lines for the implants printed with extrusion width settings of 60% to 100% was measured in Image J. The measurement of the centres distance for the implants printed with an extrusion width setting of 50% was not feasible, since the connection of the printed lines was not visible in the SEM image (***Figure 4.8.a***).

As shown in ***Figure 4.9.b,*** the centres distance was approximately 1.6 times higher than expected. This could be attributed to the materials swelling after their extrusion from the nozzle. This phenomenon usually happens during polymer processing and is called die or extrudate swelling or Barus effect. It is associated with entropy and polymer relaxation within the flow stream. When the polymer is loaded in the cartridge and the compressed air is slowly pushing it forward, a constant rate of flow stream is achieved with the material entropy being maximized. When the loaded compound is extruded through the die or nozzle, the flow rate is increased. While this is happening, the polymer is staying for some time inside the nozzle, which results in the change of its shape and the relaxation of the polymeric chain. When the polymer is going out of the die, the physical entanglements that are left, result in the formation of the materials initial shape. That leads, similarly as before, to maximum entropy (Koopmans, 1999).

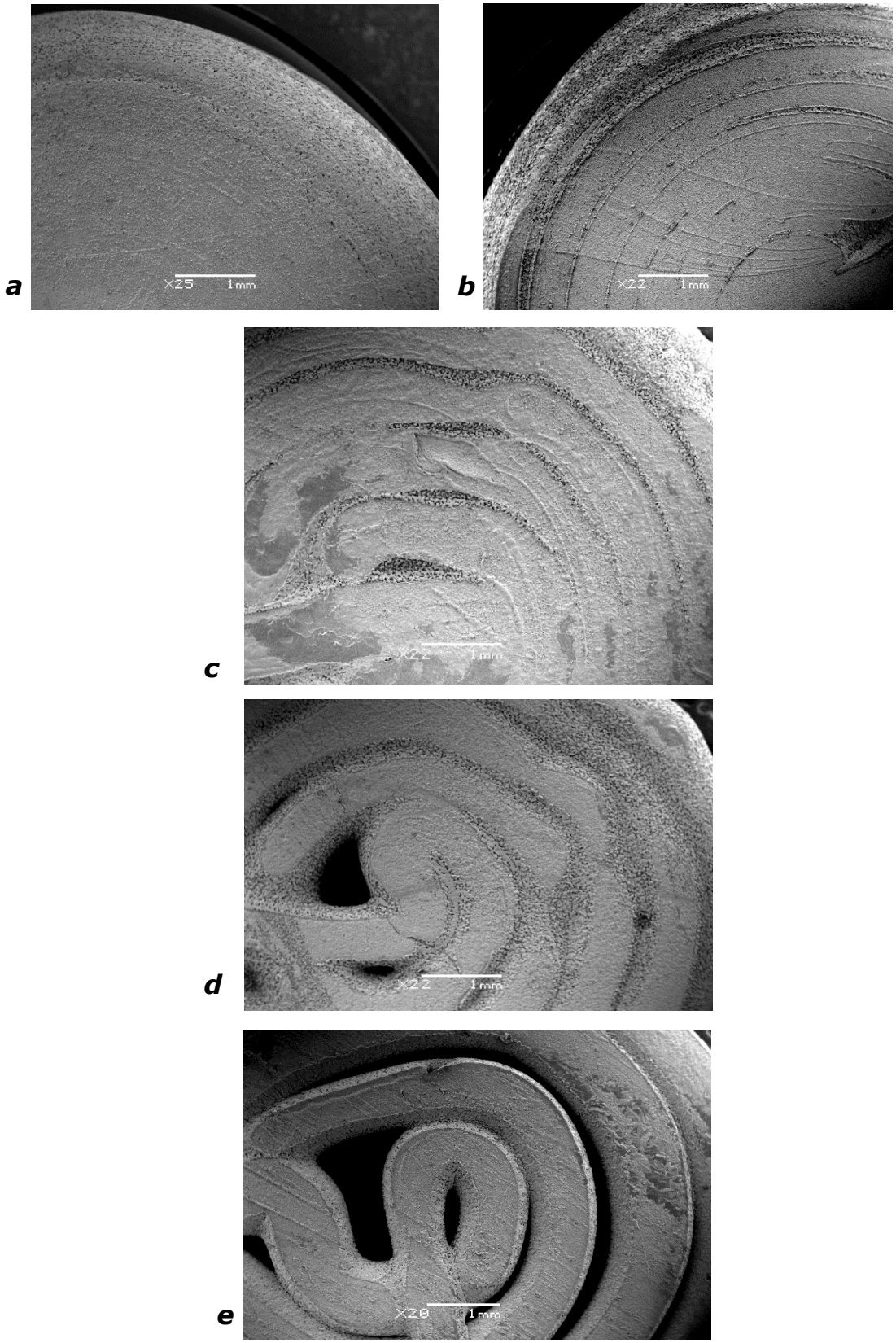

Figure 4.8: *SEM images of the bottom side of HMW PCL-LDC 30% implants printed at 70 °C with an extrusion width setting of* ***(a):*** *50%,* ***(b):*** *60%,* ***(c)*** *70%,* ***(d)*** *80% and* ***(e)*** *100%. The scale bars are 1 mm and the magnification is labelled on each SEM image separately.*

a

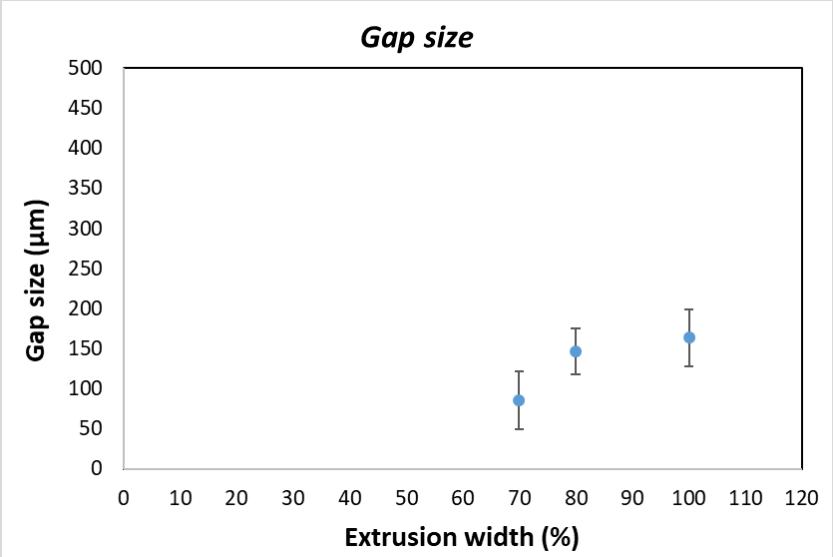

b

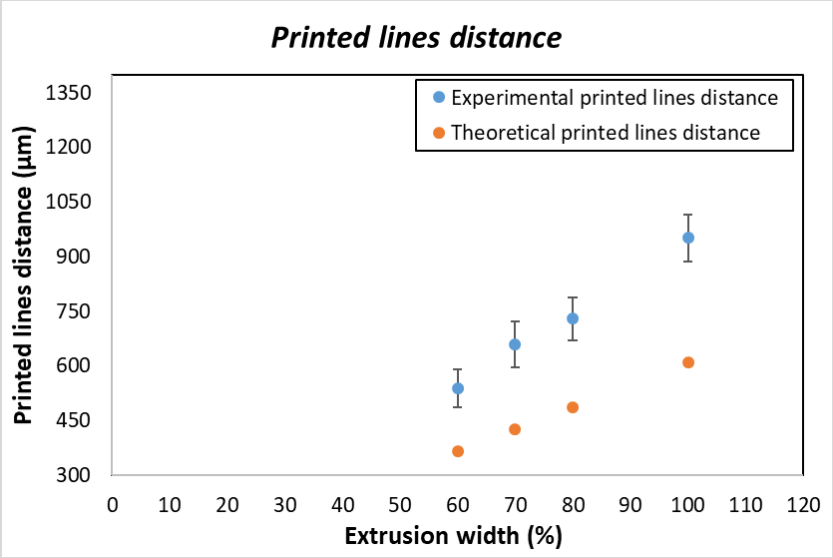

Figure 4.9: (a): *Gap size on the HMW PCL-LDC 30% implants surface printed with different extrusion widths, 50-100%, and a print speed of 1 mm/s at 70 °C, as measured in Image J.* ***(b):*** *Distance of the centres of the printed lines on the HMW PCL-LDC 30% implants surface printed with different extrusion widths, 60-100%, and a print speed of 1 mm/s at 70 °C, as measured in Image J.*

Consequently, the most promising implants from this study were the ones printed with extrusion width settings of 50% and 60%. The gaps between the printed lines detected in the implants printed with a higher extrusion width could enhance the lidocaine release and the polymer degradation and thus, compact formulations were the most desired ones for the purpose of this study.

4.2.1.1.3. 3D Printing of HMW PCL-LDC 30% implants with different print temperatures

Based on the previous printing tests and the explored parameters, the settings which demonstrated the most positive signs were the print speed of 1 mm/s and the extrusion widths of 50% and 60%. 60% extrusion width was preferred as no gaps were present on the surface of the implants and their fabrication was faster (7 min and 24 sec) than with the 50% extrusion width (9 min and 43 sec).

The investigated temperature range was, as in the case of the print speed tests, 70– 130 °C. However, it was observed that the fabricated discs exceeded the target dimensions. Therefore, another parameter in this case needed to be altered according to the applied temperature each time; pressure was the selected setting (***Table 4.5***). The remaining printing settings were fixed: bed temperature at room temperature (measured to be 24 °C) and concentric infill pattern.

Table 4.5: *Combinations of temperatures and pressure applied in the PAM 3D printer after pressure tuning.*

Temperature (°C)	*Pressure before adjustment (kPa)*	*Pressure after adjustment (kPa)*
80	400	300
90	300	200
100	200	150
110	150	125
120	125	100
130	100	75

Figure 4.10 depicts the size of the implants printed with different pressure, whereas high pressure corresponds to the one before adjustment. According to this graph, before the pressure adjustment, the size of the printed disc-shaped implants was higher than 10 mm which were the predesigned dimensions.

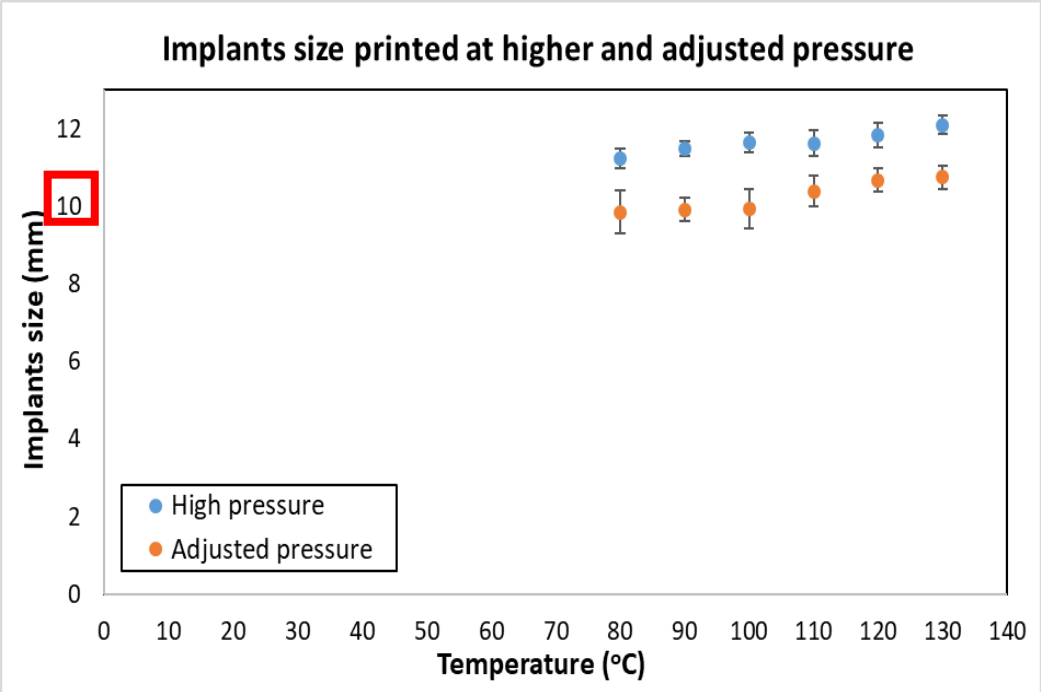

Figure 4.10: *Size of the HMW PCL-LDC 30% implants printed with different temperature and pressure, a print speed of 1 mm/s and an extrusion width setting of 60%, as measured in Image J (n=5 implants were measured at each temperature/pressure combination). High pressure corresponds to the pressure applied before adjustment. Red boxed figure represents the theoretical dimensions of the printed disc-shaped implant as in the CAD file.*

Implants printed at 70 °C with a pressure of 400 kPa were also printed in order to be used for characterization (***Figure S.3***). The size of these formulations is not shown in ***Figure 4.10*** since their printing pressure didn't need to be adjusted. Additionally, their size has already been presented in ***Figure 4.6*** (implant printed with an extrusion width setting of 60%).

4.2.1.1.3.1. SEM Characterization of 3D printed HMW PCL-LDC 30% implants, pure HMW PCL and LDC powders

HMW PCL-LDC 30% implants printed with an adjusted pressure were visually the same, without any apertures between the printed lines, as depicted in ***Figure 4.11***. Their printing resolution was further explored on the SEM in order for the absence of the gaps to be verified.

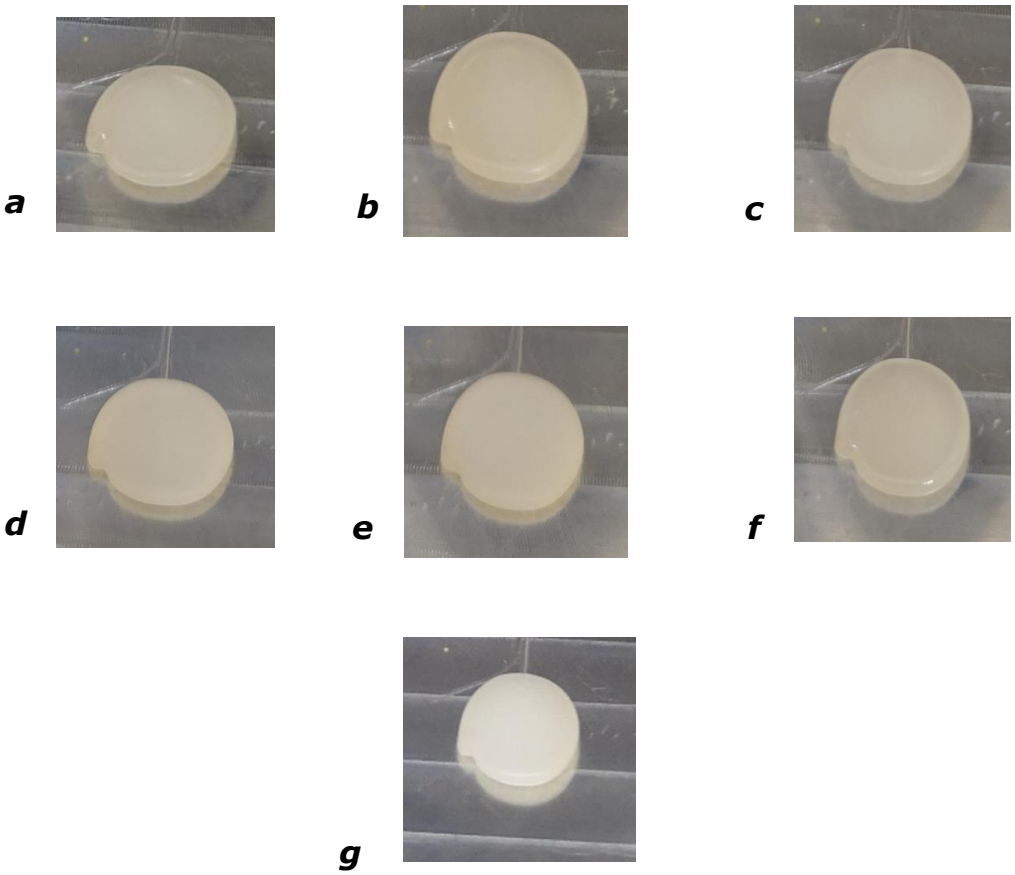

Figure 4.11: *HMW PCL-LDC 30% implants printed with an extrusion width setting of 60% at* ***(a):*** *70 °C,* ***(b):*** *80 °C,* ***(c)*** *90 °C,* ***(d)*** *100 °C,* ***(e)*** *110 °C,* ***(f)*** *120 °C and* ***(g)*** *130 °C. The bottom disc is a reflection of the printed disc on the printing platform.*

According to the SEM images (***Figure 4.12***) of the implants printed at various temperatures, there are no gaps present on their surface. It was, thus, verified that the extrusion width setting of 60% was correctly selected for the manufacture of the drug loaded polymeric implants. Nevertheless, the surface of the produced formulations looked highly featured at this scale of observation. This trait was more intense when the print temperature used was closer to the melting point of the used compounds. Higher magnification was applied during the SEM characterization of the 3D printed samples for this attribute to be better illustrated (***Figure 4.13, Figure 4.14***).

Figure 4.13.a depicts the SEM image of the HMW PCL-LDC 30% implant printed at 70 ^{o}C. It was observed that its surface was indeed relatively rough with some small particles on it. These particles could be attributed to either the polymer or the drug, since temperatures very close to their melting point have been used for the 3D printing of the implants. Therefore, 70 ^{o}C or even slightly higher temperatures might have not been sufficient for the complete melting of the materials used. As a result, the non-molten powder particles could have been mixed with the molten phase while they were extruded leading to the formation of small clusters on the implants surface (***Figure 4.14***). As the print temperature increased, the size of the particles decreased, as can be seen in ***Figure 4.13, Figure 4.14*** and ***Figure 4.15.*** Implants printed at 110 ^{o}C and higher had a smoother surface.

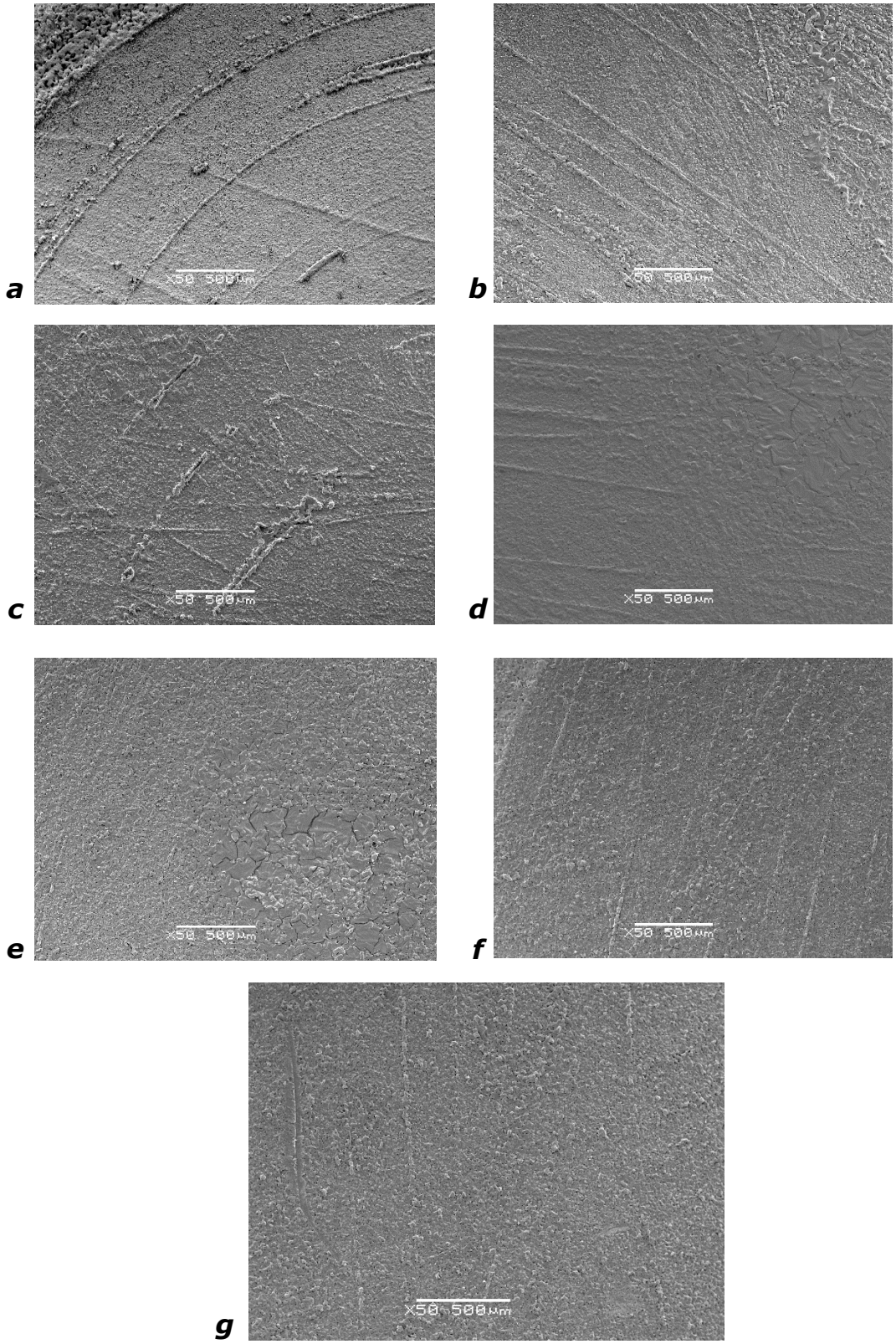

Figure 4.12: *SEM images of the top side of HMW PCL-LDC 30% implants printed with an extrusion width setting of 60% at* ***(a):*** *70 °C,* ***(b):*** *80 °C,* ***(c)*** *90 °C,* ***(d)*** *100 °C,* ***(e)*** *110 °C,* ***(f)*** *120 °C and* ***(g)*** *130 °C. The magnification is x50 and the scale bars are 500 µm.*

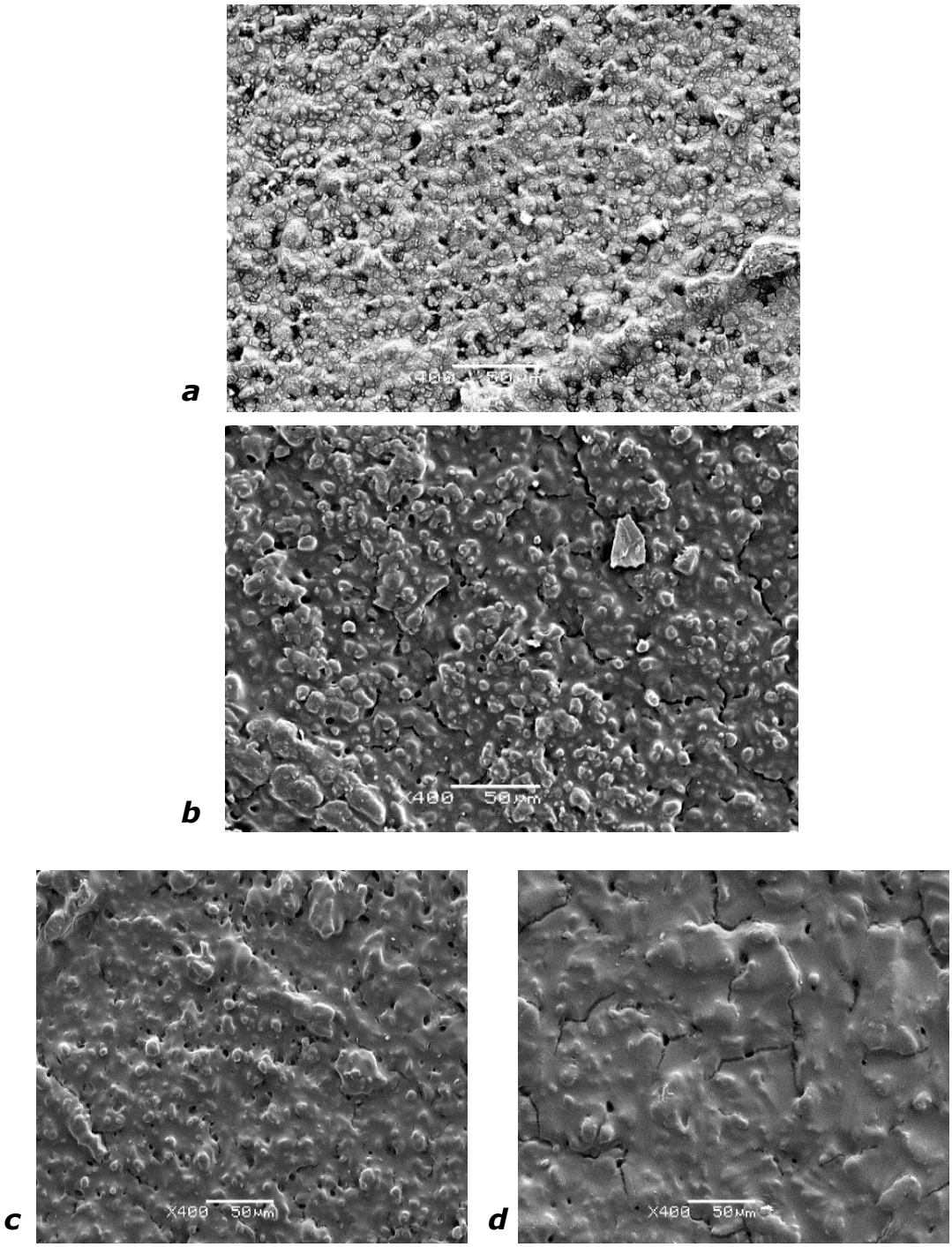

Figure 4.13: *SEM images of the top side of HMW PCL-LDC 30% implants printed with an extrusion width setting of 60% at* ***(a):*** *70 °C,* ***(b):*** *80 °C,* ***(c)*** *90 °C and* ***(d)*** *100 °C. The magnification is x400 and the scale bars are 50 µm.*

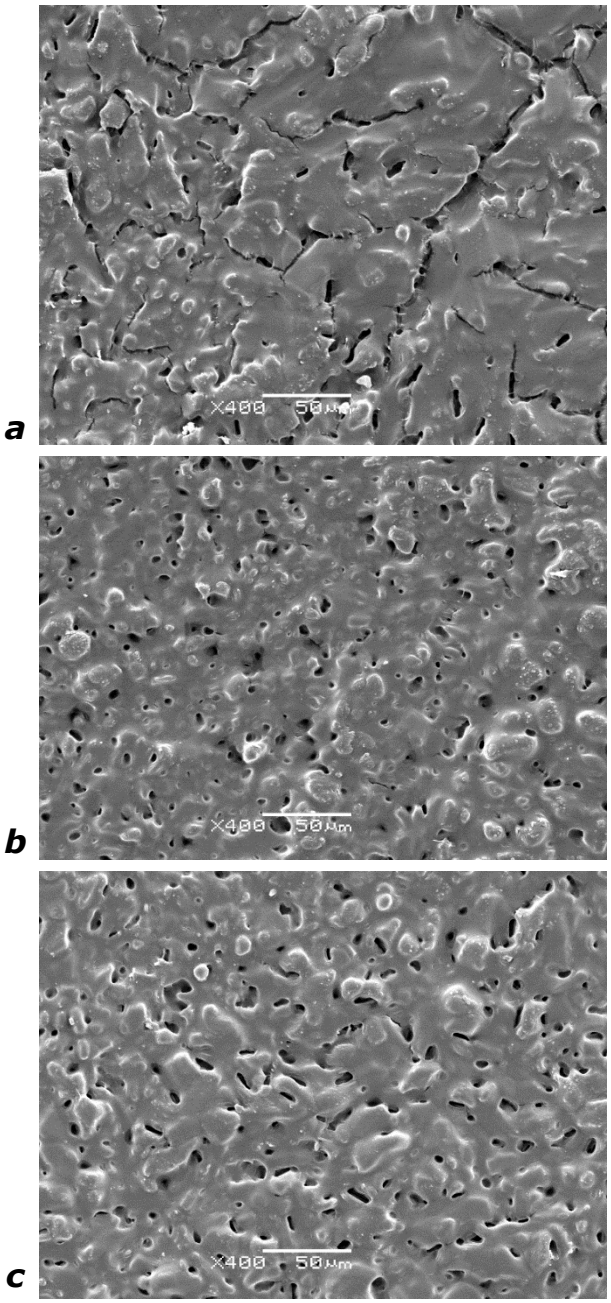

Figure 4.14: *SEM images of the top side of HMW PCL-LDC 30% implants printed with an extrusion width setting of 60% at* ***(a):*** *110 °C,* ***(b):*** *120 °C and* ***(c)*** *130 °C. The magnification is x400 and the scale bars are 50 µm.*

Figure 4.15 demonstrates that the size of the particles on the surface of the 3D printed implants was becoming more uniform at around 7 μm when the printing temperature was 110 °C.

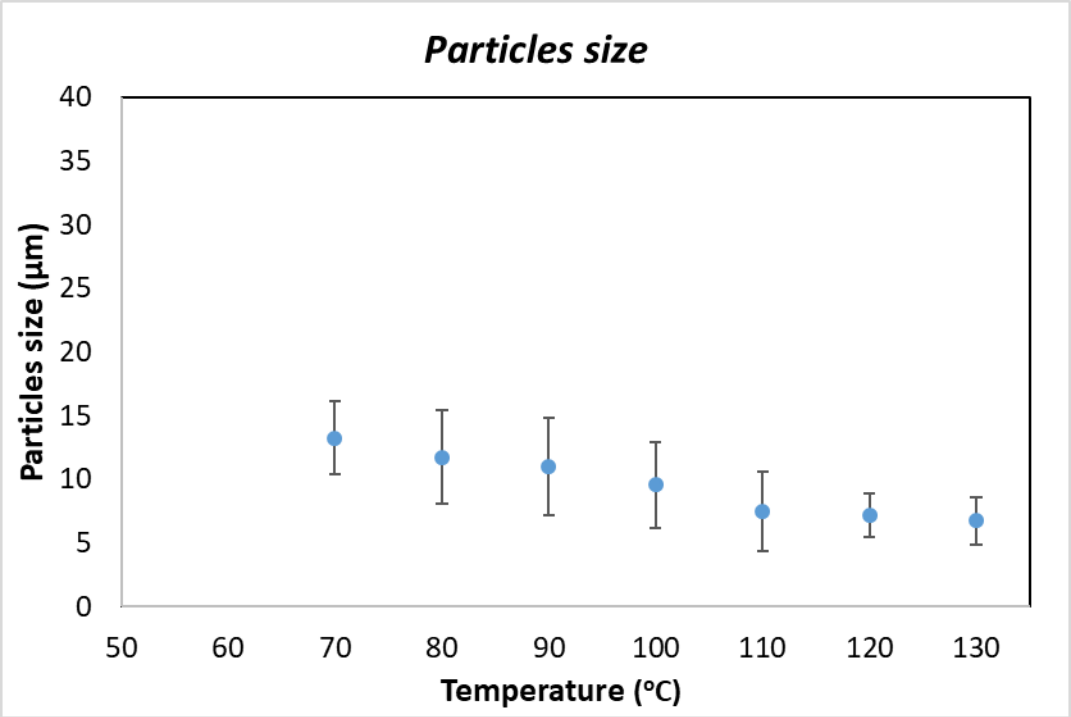

Figure 4.15: *Size of the particles on the surface of the HMW PCL-LDC 30% implants printed with different temperatures, a print speed of 1 mm/s and an extrusion width setting of 60%, as measured in Image J.*

SEM characterization on the pure HMW PCL and lidocaine powders was performed to investigate the particles size of the raw materials and possibly identify the origin of the clusters on the implants surface. This step was necessary since, if lidocaine particles were not completely molten before their extrusion and were remaining on the surface of the implants, their release from the polymeric matrix could occur faster than anticipated.

a

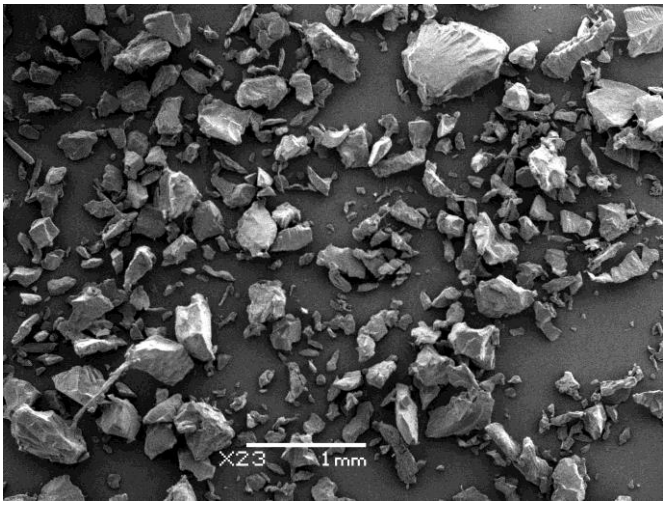

b

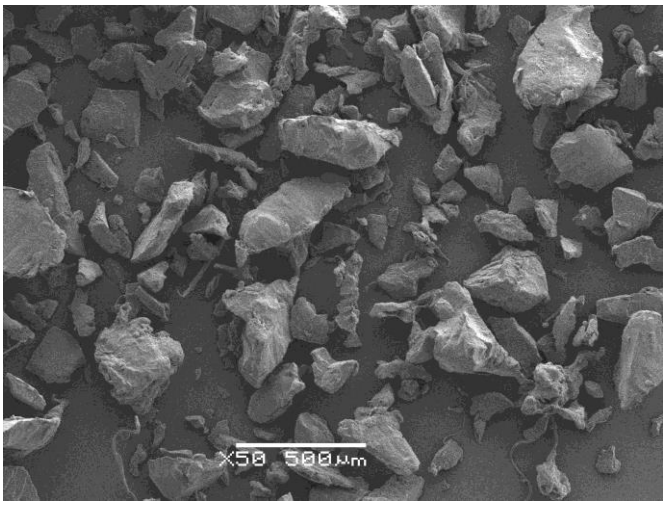

Figure 4.16: *SEM images of pure HMW PCL powder* ***(a):*** *x23 magnification and* ***(b):*** *x50 magnification. The magnification and the scale bar are labelled on each SEM image separately.*

As presented in ***Figure 4.16,*** HMW PCL powder consisted of relatively large particles with an average size of 379 ± 44 μm; smaller particles were also detected in the SEM images with an average size of 159 ± 29 μm. Therefore, PCL particles were, in general, much bigger than the particles that appeared on the implants surface, (approximately 6 – 13 μm) which means that the polymer particles could not be responsible for the surface roughness of the printed formulations.

a

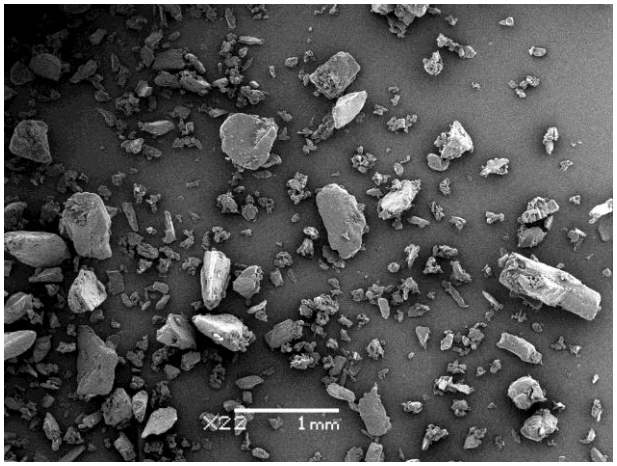

b

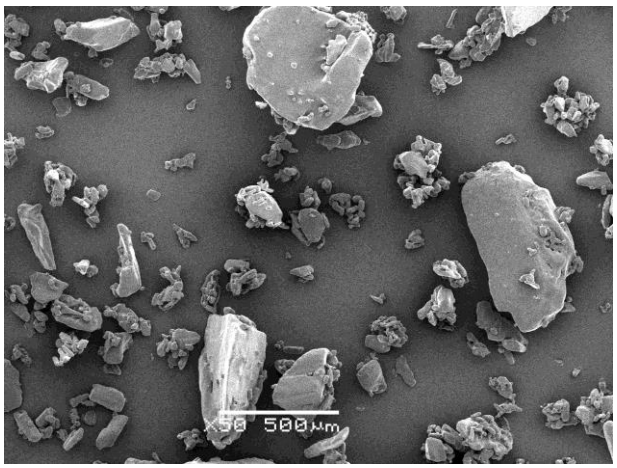

Figure 4.17: *SEM images of pure lidocaine powder* ***(a):*** *x22 magnification,* ***(b):*** *x50 magnification. The scale bar is labelled on each SEM image separately.*

According to ***Figure 4.17,*** lidocaine powder demonstrated a particularly heterogeneous morphological structure and degree of disorder, since particles of various orientations and sizes, larger, smaller, as well as intermediate, appeared in the as-received material. Nevertheless, the presence of crystals is evident, exhibiting the shape of needles (Larsen and Jensen, 2011) (Anacleto *et al*., 2018). The size of the particles was measured using Image J; the larger particles were 600 to 700 μm in their longest dimension, while the smaller substantive ones (fines) around 150 to 250 μm. Moreover, smaller (fine) particles were residing on the surface of the needle-shaped crystals and these could have an impact on the crystallinity degree of the drug (Briggner *et al.*, 1994) (Saleki-Gerhardt, Ahlneck and Zografi, 1994) (Shah, Kakumanu and Bansal, 2006).

LDC powder could be milled or sieved before further use to obtain a more homogeneous sample. However, with these methods, crystallinity can be decreased, as disorder is potentially caused in the crystals, which might result in the formation of amorphous regions on the crystal surface (Briggner *et al*., 1994) (Saleki-Gerhardt, Ahlneck and Zografi, 1994).

Similarly, to the particles size of the PCL powder, LDC particles were generally much larger than the detected particles on the surface of the implants (approximately 6 – 13 μm). Furthermore, some of the LDC particles were almost twice in size compared to the PCL particles.

Nevertheless, the HMW PCL-LDC 30% powder blend was prepared using a mortar and pestle. This mixing method might act as a milling process since both methods result in a more homogeneous sample consisting of fine powder particles. However, no SEM imaging on the powder blend has been performed to reveal the particles size of the materials included in the final HMW PCL-LDC 30% powder mixture.

SEM characterization, though, of the printed implants and their raw materials, did not show to significantly contribute to the detection of the origin of the surface particles. Raman analysis was, then, selected for further study of the implants surface since its spectra are characteristics of the investigated materials.

4.2.1.1.3.2. Raman Characterization of 3D printed HMW PCL-LDC 30% implants, pure HMW PCL and LDC powders

Raman spectra of the pure HMW PCL and lidocaine powders before mixing and 3D printing were initially acquired. Raman characterization was, then, conducted on the 30% w/w lidocaine loaded implants to investigate their near surface composition since from SEM some small particles appeared on their surface (***Figure 4.13, Figure 4.14***). This analysis was necessary as it could indicate whether sustained drug release could be achieved; if the surface particles consisted of lidocaine, its release from these areas could initially be enhanced.

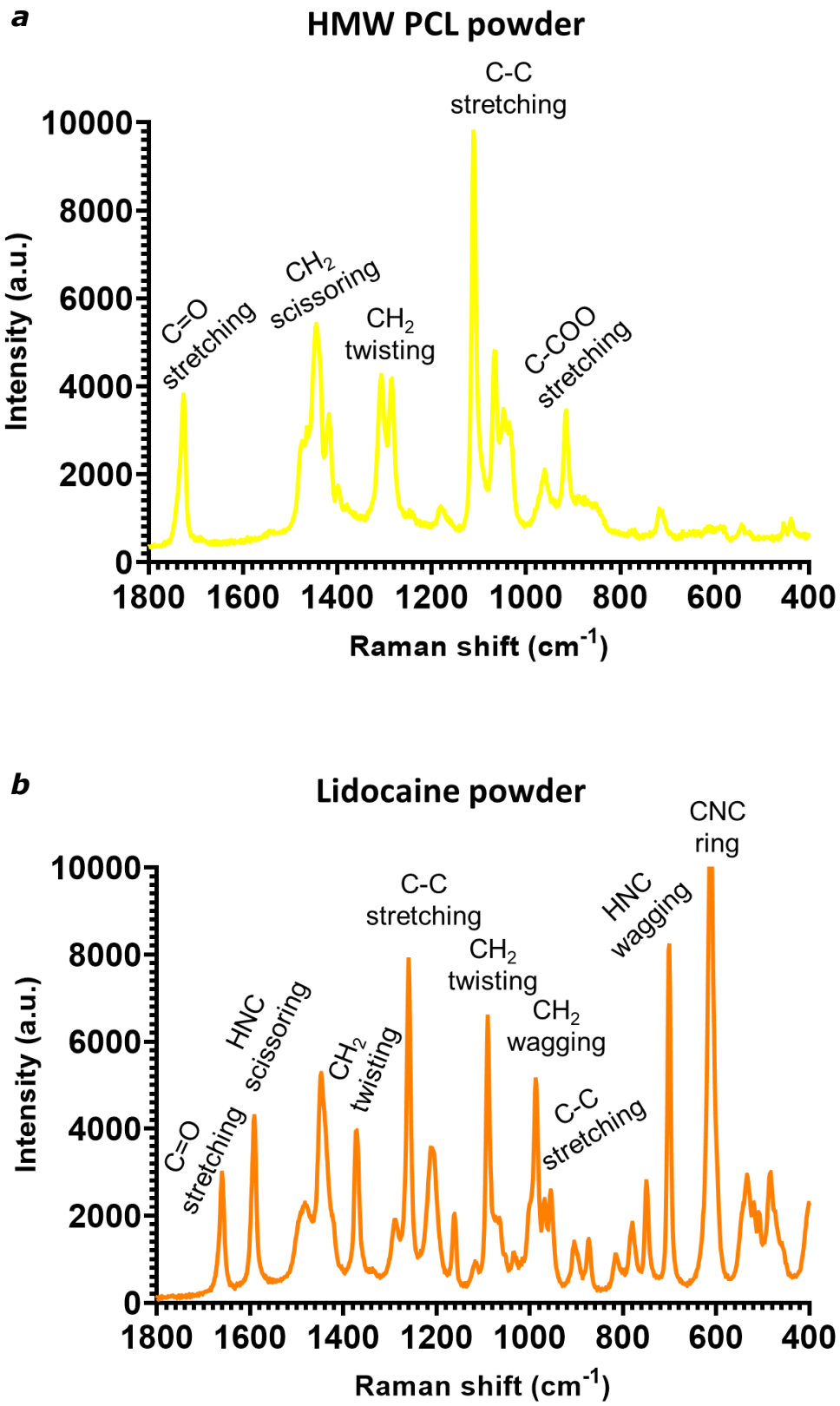

Figure 4.18: *Raman spectra of pure* ***(a):*** *HMW PCL powder and* ***(b):*** *lidocaine powder.*

The Raman spectrum of pure HMW PCL powder in ***Figure 4.18.a*** presented characteristic peaks at 1725 cm^{-1} corresponding to C=O stretching and at 1442 and 1419 cm^{-1} to CH_2 scissoring. Bands detected at 1307 and 1283 cm^{-1} are attributed to CH_2 twisting, while the ones at 1111, 1066 and 1045 cm^{-1} to C-C skeletal stretching. A C-COO stretching is indicated by a peak at 916 cm^{-1}. These are in good correspondence with the published data (Sayya*r et al.*, 2012) (Kotula, Snyder and Migler, 2017) (Smith *et al.*, 2017).

Many sharp peaks appeared in the Raman spectrum of the raw lidocaine powder in ***Figure 4.18.b***; a peak at 1664 cm^{-1} is assigned to C=O stretching, while a peak at 1589 cm^{-1} to HNC scissoring vibration, N-C amide stretching and CH_2 asymmetric deformation. Bands detected at 1482 and 1450 cm^{-1} correspond to CH_2 asymmetric deformation and CH_2 scissor deformation, respectively. CH_2 twisting and ring stretching deformation are indicated by a peak at 1374 cm^{-1}, whereas CH bending and C-C symmetric stretching by a peak at 1261 cm^{-1}. A band at 1211 cm^{-1} is related to amide N-N stretching and C-C stretching, while the one at 1164 cm^{-1} to NC_2 asymmetric stretching, CH_2 twisting, C-H bending and ring stretching deformation. Furthermore, a peak at 1094 cm^{-1} corresponds to CH_2 twisting and peaks at 991 and 974 cm^{-1} to CH_2 wagging. C-C stretching and NCO scissoring deformation are attributed to a peak at 958 cm^{-1} and C-C stretching at 907 cm^{-1}. A band observed at 876 cm^{-1} indicates ring bending, while the one at 752 cm^{-1} HNC wagging and ring torsional deformation. HNC wagging, CNC ring, ring torsional deformation and ring bending correspond to peaks detected at 703, 613, 536, and 488 cm^{-1}, respectively. These are in agreement with the literature data (Bakony*i et al*., 2018) (Liu *et al.*, 2018) (Shende *et al.*, 2014).

For the analysis of the surface of the fabricated implants, particles on the surface of the formulations were separately investigated, as well as, the implant matrix. The sampling area was approximately 1 micron.

The Raman spectra of the surface particles and the matrix of the implant printed at 70 ºC were identical and exhibited peaks related to the loaded drug, as displayed in ***Figure 4.19***. It is, thus, suggested that the composition of the studied areas was the same. Furthermore, it was demonstrated that the 3D printing process did not lead to any detectable changes in the chemical structure of the compounds.

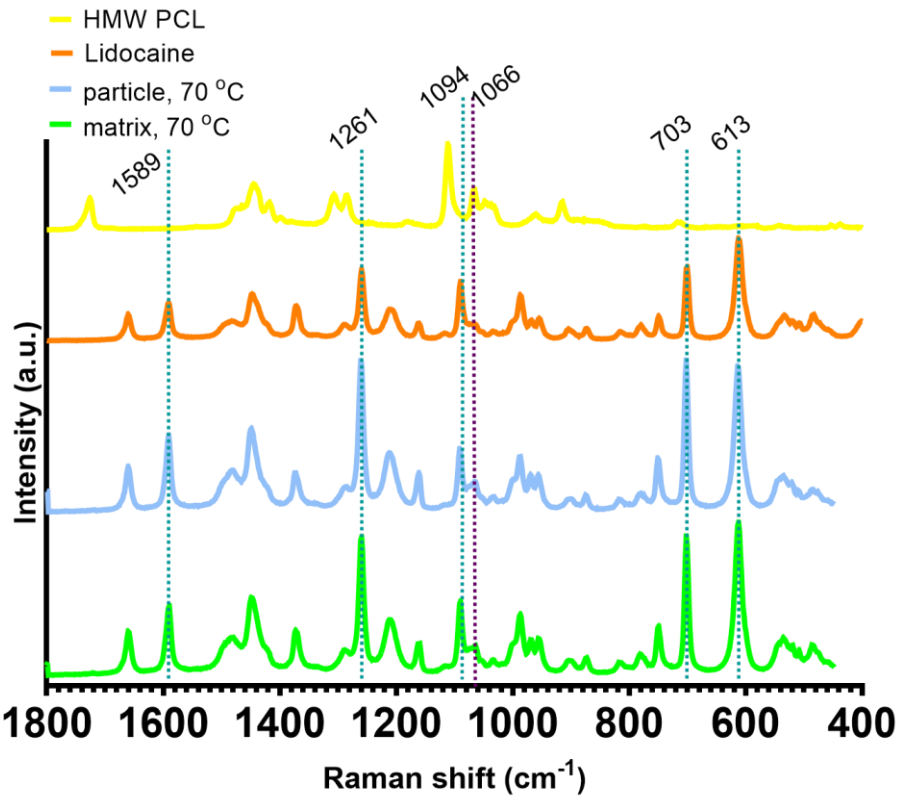

Figure 4.19: *Raman spectra of pure HMW PCL and lidocaine powders and surface particles and matrix of HMW PCL-LDC 30% implant printed at 70 °C with an extrusion width setting of 60%. LDC peaks are highlighted with the blue dot-line and HMW PCL peaks with the purple dot-line.*

Further analysis on the surface of the implants printed at higher temperatures, where the surface particles were observed to be smaller than the ones in the implants printed at 70 ºC (***Figure 4.13, Figure 4.14, Figure 4.15***) showed that the spectra for the surface particles and the matrix of the implants produced at higher temperatures were identical with the spectra of the implants fabricated with the lowest temperature, as depicted in ***Figure 4.19***. This indicates that both PCL and lidocaine were present in the matrix and the surface particles. The different temperature applied during the extrusion was illustrated to not have any impact on the chemical structure of the materials used.

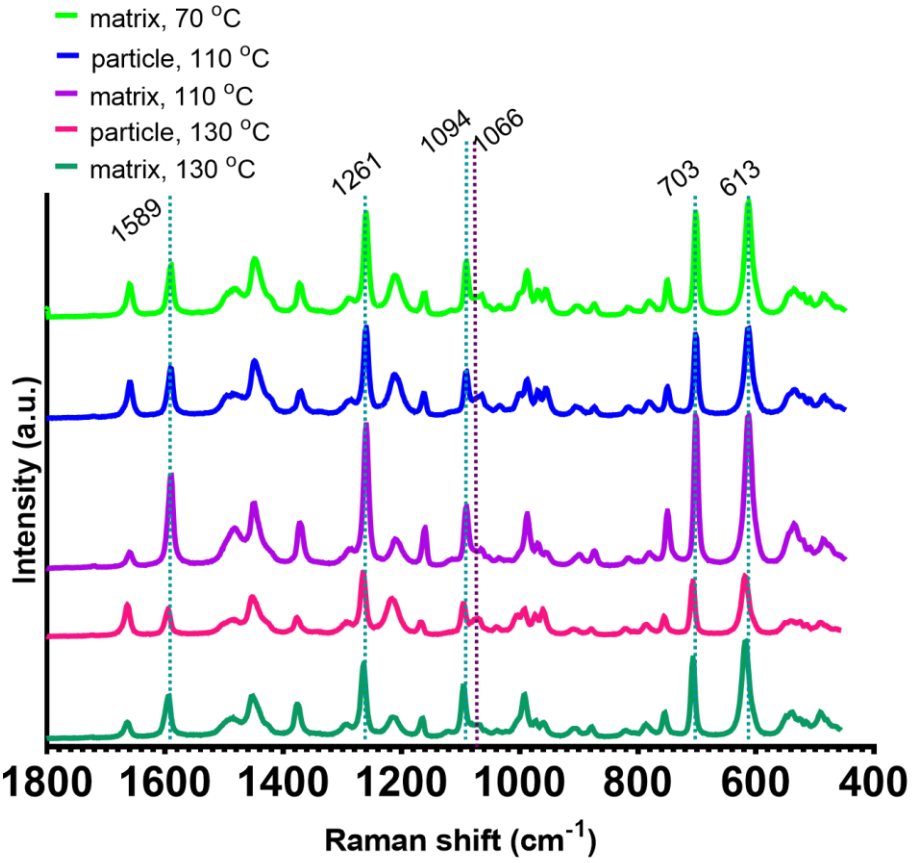

Figure 4.20: *Raman spectra of pure HMW PCL and lidocaine powders and surface particles and matrix of HMW PCL-LDC 30% implants printed at 70 °C, 110 °C and 130 °C with an extrusion width setting of 60%. LDC peaks are highlighted with the blue dot-line and HMW PCL peaks with the purple dot-line.*

Raman analysis was performed in a single point (with a spot size of approximately 1 μm and depth of analysis of approximately 5 – 10 μm) of the matrix/particle and it could not, thus, provide any information regarding the homogeneity of the materials in the printed formulations.

In general, the Raman spectra of the fabricated discs (***Figure 4.19, Figure 4.20***) confirmed that no detectable interaction has occurred between the polymer and the drug in any printing temperature, even when very high ones have been applied.

Since the origin of the surface particles could not be verified through the SEM and Raman characterization of the raw materials and the produced implants, other experimental methods were applied to eliminate the appearance of clusters; sieving of the powder mixture prior to its loading to the 3D printer did not demonstrate any effect on the appearance of the particles on the surface of the implants. A sieve with a pores size of 180 μm was used for this purpose.

Since similar data were obtained before and after powder sieving, it could be proposed that this feature was characteristic of the materials and concentration used rather than related to particle sizes and size distributions. During the sieving process, particles that had the proper size were collected. For their extrusion through the nozzle, they were completely molten in the cartridge in order to be extruded. Therefore, these processes could not have a significant impact on the creation of the particles. The stage that might have contributed the most was the solidification of the printed implants at room temperature. This was not a controlled process and it could result in an uneven surface.

4.2.1.2. 3D Printing of HMW PCL-LDC 5% implants

The fabrication of another formulation with a lower drug loading, 5%, was done in order to compare its LDC release rate with the higher drug loading, 30% w/w.

Different concentrations of the polymer and the drug investigated in this implant type resulted in a different extrudability of the materials mixture during the 3D printing process (***Figure S.4, Table S.1***). Similar optimization protocols of the previously established parameters have been followed in order to obtain a compact drug dosage form with the desired shape (disc) and dimensions (10 mm length x 10 mm height x 2 mm width) (***Table 4.6, Figure S.6, Figure S.8, Figure S.9***).

More specifically, in this implant type, the temperature of the printing platform was required to be increased compared to the room temperature applied during the manufacture of the 30% w/w lidocaine loaded polycaprolactone implants (***Figure S.5***). In this approach, better disc adhesion was obtained, resulting in the enhancement of the accuracy of the printed object with the predesigned disc.

Table 4.6: *Parameters explored for the manufacture of HMW PCL-LDC 5% implants fit for purpose.*

Temperature (°C)	*Extrusion width setting (%)*	*Pressure (kPa)*	*Bed Temperature (°C)*	*3D Printed implant*
70	60	400	24	X
70	60	400	30	X
70	60	400	40	X
70	50	400	40	X
110	60	400	24	X
110	60	400	30	X
110	60	400	40	X
110	60	300	40	X
110	60	200	40	X
110	60	125	40	X
110	50	400	40	√
110	50	300	40	X
110	50	200	40	X
110	50	125	40	X

X : implant demonstrating surface defects or not meeting the predetermined size

√ : implant appearing suitable for further studies

4.2.1.2.1. SEM Characterization

SEM characterization was particularly useful, as previously, to explore the impact of the selected printing parameters on the printing accuracy and resolution of the final object. That analysis revealed that the most optimal printing resolution was achieved with the lowest studied extrusion width (50%) and the highest pressure (400 kPa) (***Figure 4.21.b***). All the other combinations of these two investigated

parameters resulted in the creation of apertures on the surface of the produced discs (***Figure 4.21.a, Figure S.7, Figure S.10***).

a

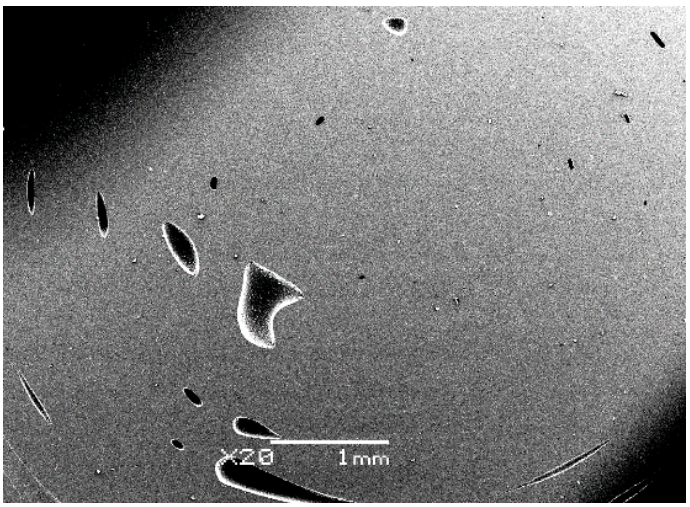

b

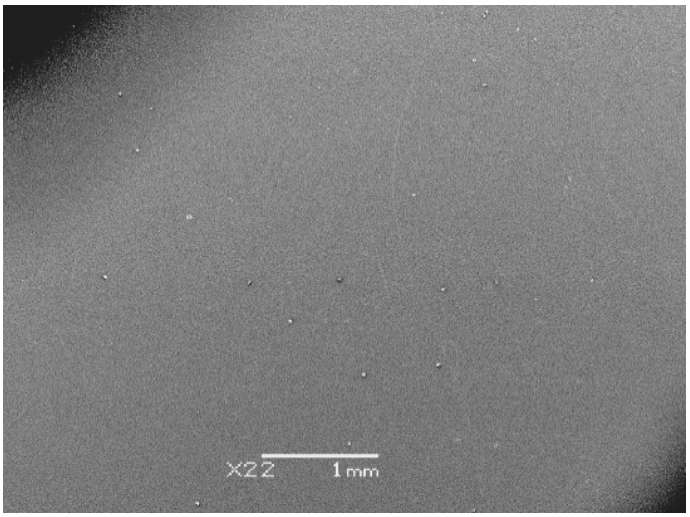

Figure 4.21: *SEM images of the bottom side of PCL-LDC 5% implants printed at 110 ºC with* ***(a):*** *an extrusion width setting of 60%, pressure of 200 kPa and* ***(b):*** *an extrusion width setting of 50%, pressure of 400 kPa. The magnification and the scale bar are labelled on each SEM image separately.*

4.2.1.3. 3D Printing of HMW PCL implants

The manufacture of pure HMW PCL implants was next since they would be needed as control samples for the subsequent dissolution studies. As previously observed, the extrudability of the polymer was affected by the amount of lidocaine that was added to the powder mixture used for the production of the implants.

Therefore, the fabrication of polymeric discs has been conducted in a similar fashion as for the drug loaded formulations; optimization of the printing parameters has been performed after the assessment of the size and structure integrity (***Table 4.7***). The printed implants needed to have the same characteristics as the lidocaine loaded polycaprolactone implants; a compact and smooth surface without any apertures, in order to be effectively compared. Disc-shaped implants with dimensions of 10 mm length x 10 mm width x 2 mm height were printed.

Table 4.7: *Parameters explored for the manufacture of HMW PCL implants fit for purpose.*

Temperature (°C)	*Extrusion width setting (%)*	*Pressure (kPa)*	*Bed Temperature (°C)*	*3D Printed implant*
110	50	400	40	X
110	40	400	40	√

X : implant demonstrating surface defects or not meeting the predetermined size

√ : implant appearing suitable for further studies

Even though the produced implants were visually the same (***Figure S.11***) and did not seem to have any holes on their surface, a more in-depth analysis was needed to verify that. SEM was performed for this purpose, as in the previously produced drug loaded delivery systems (***Figure S.12***). It was, thus, suggested that the lowest applied extrusion width (40%) was the most appropriate one for the production of polycaprolactone discs with similar characteristics as the drug loaded

formulations (***Figure S.12.a***). A comparison, hence, between them would be feasible in the next stages of the study.

4.2.1.4. 3D Printing of HMW PCL barrier-shell HMW PCL-LDC 30% implants

The final fabricated formulation was an HMW PCL barrier-shell HMW PCL-LDC 30% implant designed to explore the effectiveness of the polymeric barrier on the release of the drug since PCL has a very slow degradation rate (Fernández, Etxeberria and Sarasua, 2015) (Domingos *et al.*, 2010). The printing parameters of all of its compartments have previously been established and no further optimization was needed (***Figure 4.22***). The printing settings for the HMW PCL parts were as follows; print temperature of 110 ^{o}C, extrusion width of 40%, pressure of 400 kPa, print speed of 1 mm/s, bed temperature of 40 ^{o}C and concentric as the infill pattern. The parameters for the lidocaine loaded compartment were print temperature of 110 ^{o}C, extrusion width of 60%, pressure of 125 kPa, print speed of 1 mm/s, bed temperature of 40 ^{o}C and concentric as the infill pattern. Two aluminium cartridges and two steel nozzles with a diameter of 0.61 mm, one for each powder mixture, were used.

The manufacture of the core-shell formulation occurred in several stages, starting with the HMW PCL base and shell, followed by the printing of the drug loaded polymeric implant and the HMW PCL cap. The shape of this formulation was a disc with dimensions 11 mm diameter x 4 mm height with 4 printed layers. The thickness of the HMW PCL barrier was 1 mm. The dimensions of the HMW PCL-LDC 30% implant printed as a core were 9 mm diameter x 2 mm height.

As displayed in ***Figure 4.23***, the core-shell implants seemed to have been evenly printed, as no holes on the PCL shell were visible. Even though good accuracy has been achieved for the implants diameter, 11.1 ± 0.6 mm, the layers thickness did not follow the same trend with the implants height measured to be 5.6 ± 0.6 mm, approximately 1.6 times higher than the designed 4 mm (***Figure 4.23.b***). This can be attributed as before to the die swelling effect, which was also observed during the printing of the HMW PCL-LDC 30% implants.

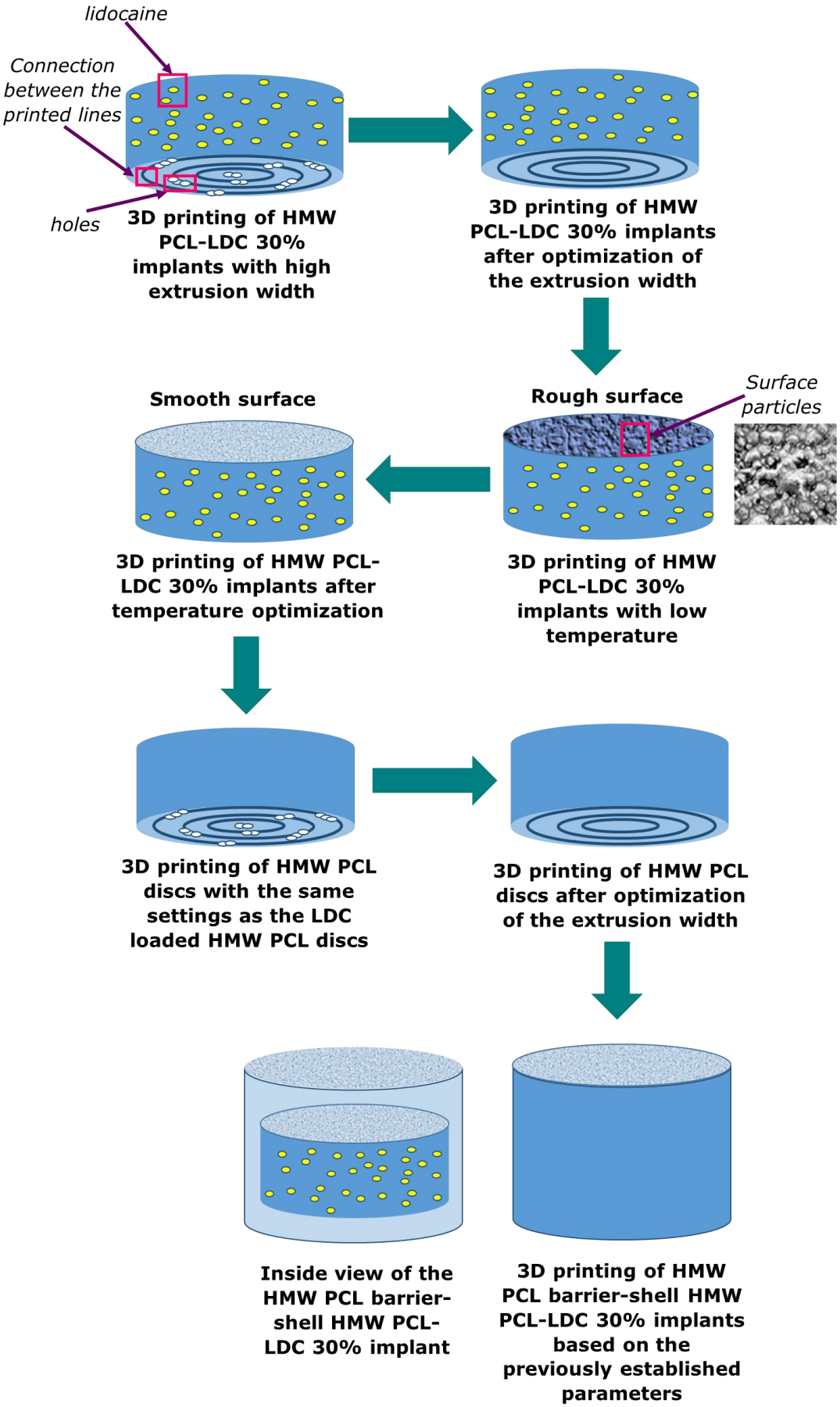

Figure 4.22: *Schematic diagram of the optimization procedure for the establishment of the printing parameters for the manufacture of the HMW PCL barrier-shell HMW PCL-LDC 30% implants. The deep blue lines represent the connection between the printed lines, the white dots the holes/gaps on the implants surface and the yellow dots the lidocaine.*

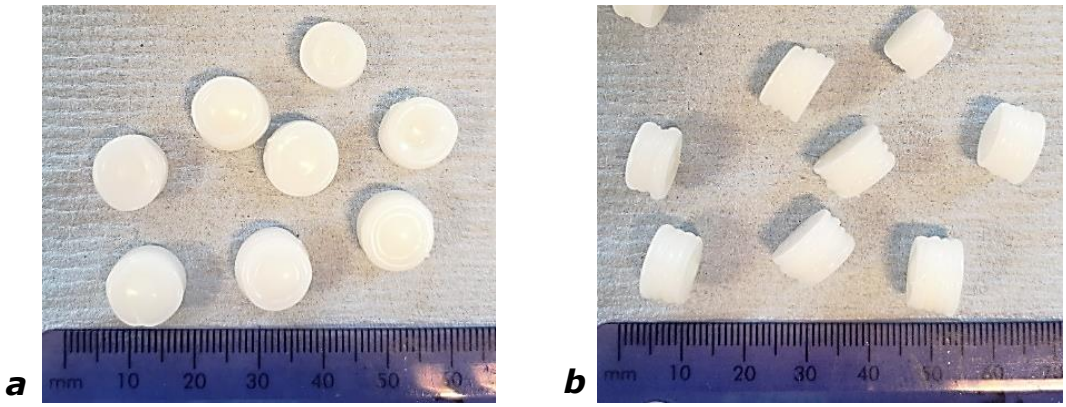

Figure 4.23: *3D printed HMW PCL barrier-shell HMW PCL-LDC 30% implants* ***(a):*** *top side and* ***(b):*** *cross section.*

4.2.1.4.1. SEM Characterization

SEM analysis was particularly important to be conducted in the HMW PCL barrier-shell lidocaine loaded formulation not only to reveal potential extrudate swelling, but also to investigate the printing resolution and the effective layer alignment and integration since the manufacture was performed in several stages.

According to the SEM images in ***Figure 4.24,*** both the top and the bottom side of the core-shell implants have been printed quite homogeneously, since no cavities appeared on their surface. The polymeric base and cap were, therefore, providing an effective barrier to the HMW PCL-LDC 30% implant printed in the inner part of the studied formulation. This verified again that the applied printing parameters were the most suitable ones for the fabrication of a compact HMW PCL disc.

The connection between the printed layers of the core-shell implant was also explored by SEM (***Figure 4.25***). The printed layers were well integrated with no gaps detected, and hence, the shell, which is required to control drug release, appears fit for purpose.

a

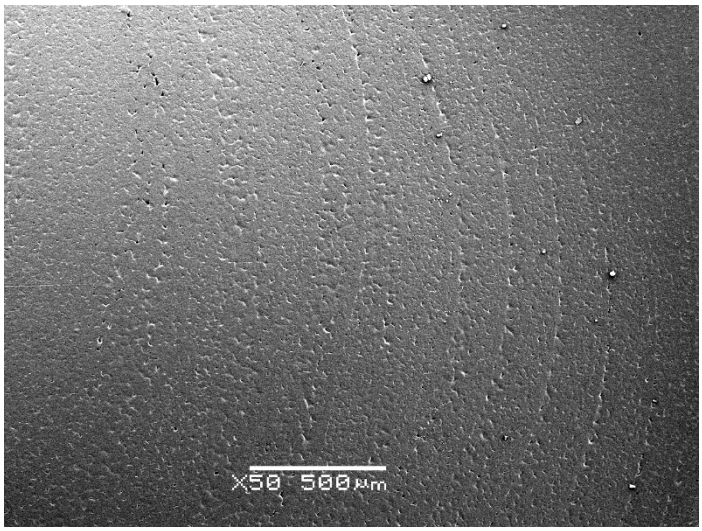

b

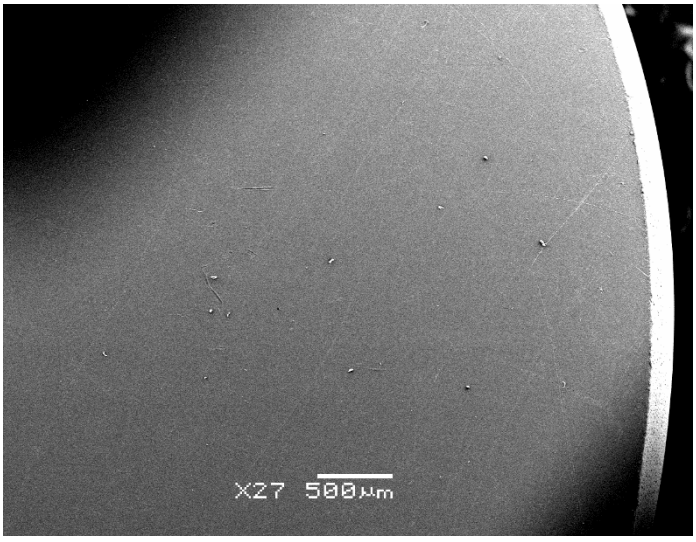

Figure 4.24: *SEM images of the HMW PCL – HMW PCL-LDC 30% implants* ***(a):*** *top side and* ***(b):*** *bottom side. The magnification and the scale bar are labelled on each SEM image separately.*

A misalignment between the printed layers was observed, though, in ***Figure 4.25.a.*** This could be associated with the fact that the printing of this formulation was performed in several stages compared to the non-encased fabricated discs. A single nose configuration was used for the extrusion of different composition mixtures since only one head of the employed 3D printer was heated.

The individual layer height was designed to be 1 mm; however, SEM images (***Figure 4.25.a***) indicated that the phenomenon of die swelling occurring during the printing of the implants layers, leading to these being approximately 1.6 times larger than expected. Measurements in Image J showed that the layers size was 1.6 ± 0.2 mm.

a

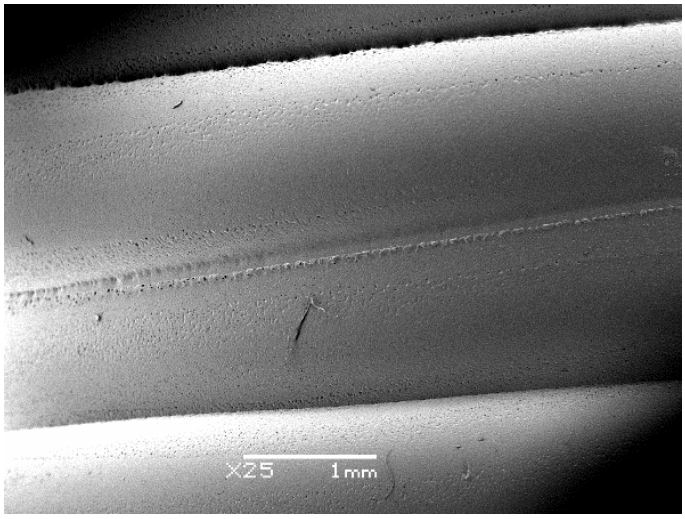

b

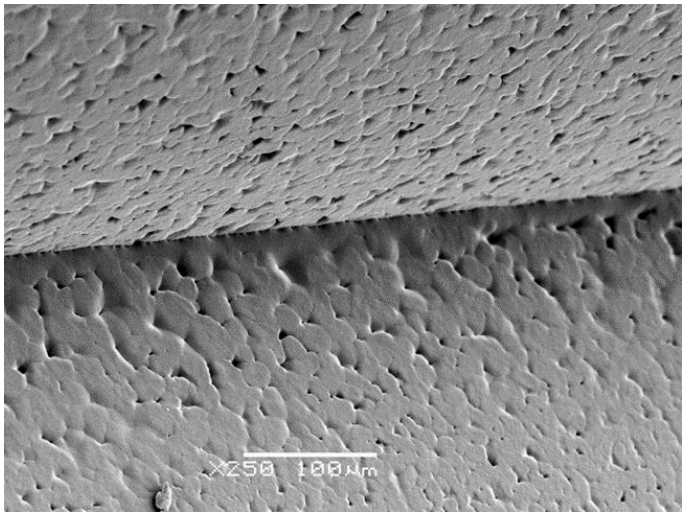

Figure 4.25: *SEM images of the outside layers of the 3D printed HMW PCL barrier-shell HMW PCL-LDC 30% implants with a magnification* ***(a):*** *x25 and* ***(b):*** *x250. The magnification and the scale bar are labelled on each SEM image separately.*

4.2.2. Polycaprolactone implant characterization

Physical and chemical characterization of pure HMW PCL implants, as well as, non-encased implants loaded with lidocaine with various concentrations, will be presented in the following sections. These were performed to investigate the impact of mixing and 3D printing on material properties. The core-shell implants were not analyzed with the following techniques since their compartments consisted of materials that were already characterized.

4.2.2.1. DSC Characterization

Pure lidocaine powder was initially analysed in DSC before being mixed with PCL and 3D printed. ***Figure 4.26*** depicts the DSC thermogram of lidocaine. The DSC curves obtained from two heating programs exhibit similar T_m and crystallization temperature and match well with the data found in the literature (Pathak and Nagarsenker, 2009b) (Chun *et al*., 2012) (Na *et al.*, 2018). The melting point of lidocaine was measured as 73.1 ± 1.9 ^oC and its crystallization temperature as 33.8 ± 1.7 ^oC.

HMW PCL powder mixed with 30% w/w lidocaine powder was subsequently analysed in DSC before their loading to the printer and their extrusion. As depicted in ***Figure 4.27.a,*** in the first heating cycle two melting point peaks were detected; a broad peak at 62.4 ^oC and a narrow one at 71.5 ^oC. The detection of these two peaks could be attributed to the presence of more than one polymeric crystal forms having slightly different thermal behaviour, as previously discussed in ***Chapter 3***.

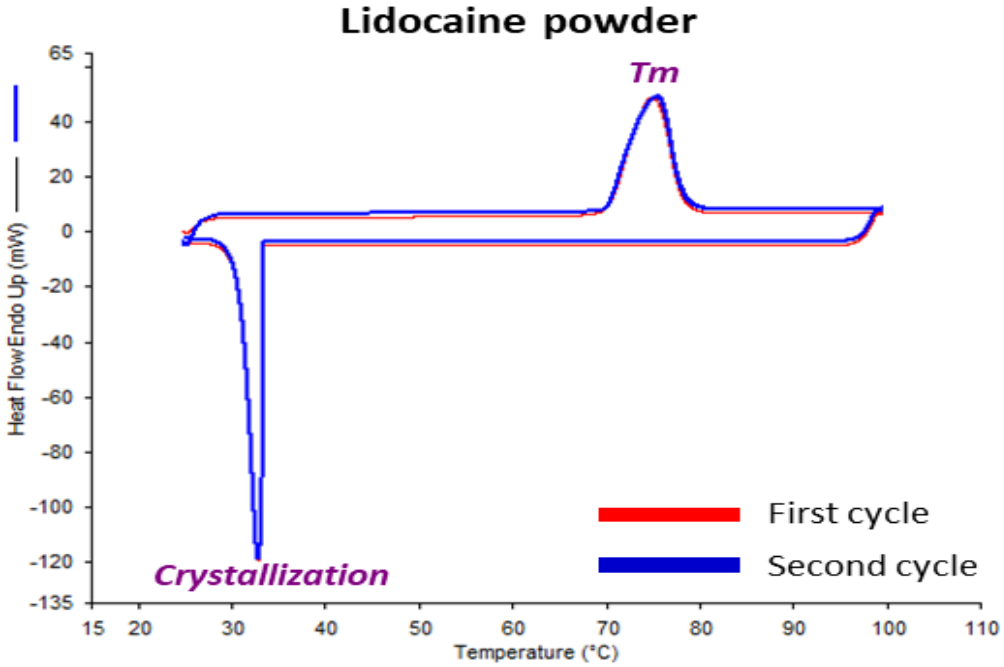

Figure 4.26: *DSC thermogram of pure lidocaine after 2 heating-cooling cycles, before extrusion and 3D printing. The red line represents the first heating-cooling cycle and the blue line the second cycle.*

As for the recrystallization point, a quite broad peak appeared at 18.5 °C (first cycle) and 8.9 °C (second cycle), but these do not correspond to the characteristic peaks of any of HMW PCL or lidocaine. The detection of a broad crystallization peak was an indication of the fact that the polymer and the drug molecules were hindering each other's segmental motion and consequently, crystal growth processes (C. S. Wu, 2005) (Sato *et al.*, 2012) (Monteiro, Inês and Tavares, 2018b) (Valle, Camps and Díaz, 2011).

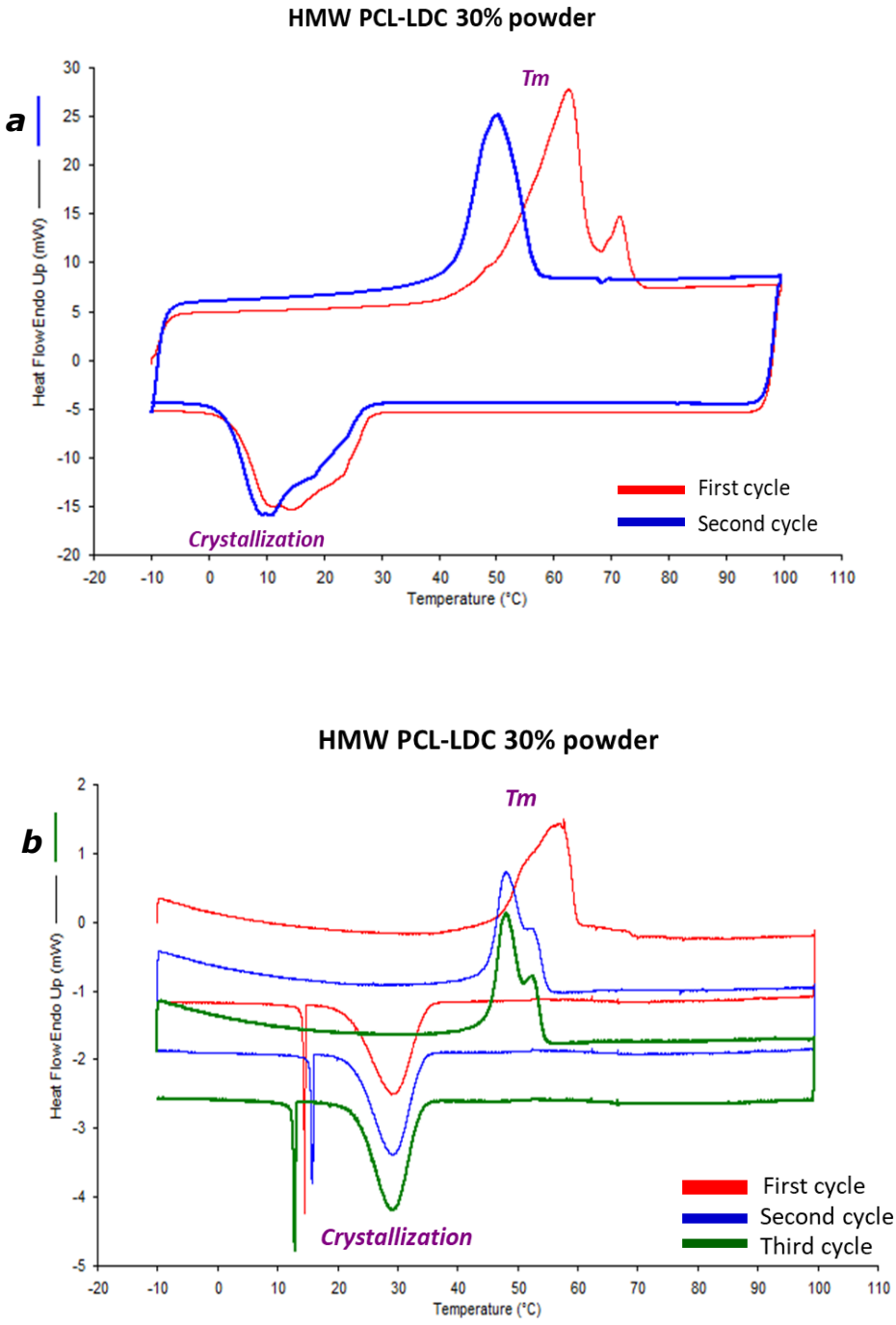

Figure 4.27: *DSC thermograms of HMW PCL-LDC 30% powder before 3D printing after* ***(a):*** *two heating-cooling cycles and a heating rate of 10 °C/min and* ***(b):*** *three heating-cooling cycles and a heating rate of 1 °C/min. The red line represents the first heating-cooling cycle, the blue line the second cycle and the green line the third cycle.*

In the second heating cycle, only one T_m was observed at 50.2 °C, assigned to the HMW PCL, suggesting that the different crystal populations are merged after their controlled melting and recrystallization. The fact that no characteristic peak for the melting point of lidocaine was detected could be attributed to the effective molecular dispersion of the drug within the amorphous polymer matrix – meaning that a solid dispersion has been formed - or its concentration was below the detection limit of this technique (Mackin *et al.*, 2002) (Hogan and Buckton, 2001). An alternative explanation could be the co-crystallization of lidocaine with PCL occurring after the first heating-cooling cycle leading to the creation of a new crystal phase (Garbacz *et al.*, 2020) (Sekhon, 2009) (Khan, Ahmad and Idrees, 2020) (ter Horst and Cains, 2009) (Kumar and Nanda, 2017).

Further analysis of the polymer-drug mixture was performed with a slower heating-cooling rate, 1 °C/min, compared to the 10 °C/min to examine whether a better distinction of the characteristic peaks could be achieved. As can be seen in ***Figure 4.27.b,*** in the first heating cycle one broad peak was detected at 57.7 °C. However, this peak did not seem to be centred at the measured temperature since a smaller peak was slightly visible at around 50 °C. Similarly to the DSC thermogram of the powder mixture depicted in ***Figure 4.27.a,*** the fact that another peak seemed to be included in the detected melting point peak could be associated with different polymeric crystal populations (as previously observed in ***Figure 3.14.a***) or with the presence of more than one material. No clear characteristic peak for lidocaine was detected in the DSC thermogram suggesting that the concentration of this material was below the sensitivity limit of the current analysis (Ry*chter et al*., 2018b).

In the first cooling cycle, two separate peaks were detected at 29.1 °C and 14.5 °C indicating that the materials recrystallization was affected by each other's presence by decreasing their molecular mobility and consequently, their recrystallization temperature (Sayyar *et al.*, 2012) (Priselac *et al.*, 2017) (Benjamin Ho *et al*., 2017) (Cui and Frank, 2006) (Shen, Lu and Liang, 2013a) (Simao, Bellani and Branciforti, 2017).

In the second heating cycle, as demonstrated in ***Figure 4.27.b,*** two melting point peaks were detected, at 48.1 °C and 52.6 °C. These melting points appeared at around similar temperatures to the melting point peak of the first heating cycle. Moreover, the onset and the end of these peaks was approximately at 45 °C and 55 °C, respectively; these temperatures were particularly close to the onset and end of the melting point peak appearing in the second heating cycle in the DSC thermogram depicted in ***Figure 4.27.a*** when a higher heating-cooling rate was applied. The presence of two peaks in the second heating cycle of the slower heating rate DSC thermogram of the polymer-drug powder mixture was indicative of two crystal populations co-existing in the investigated sample. These crystal forms could be associated either with PCL or with the presence of more than one material; lidocaine and PCL could have formed a co-crystal after the first heating-cooling cycle and their recrystallization could lead to the appearance of the two melting point peaks. The slower heating-cooling rate applied during the DSC run in ***Figure 4.27.b*** compared to the one in ***Figure 4.27.a*** may have contributed to more effective detection of the thermal behaviour of the polymeric crystal forms, since less broad peaks are generally detected at lower heating rates compared to higher ones (Wang and Harrison, 1994). The fact that a melting point peak appeared at a lower temperature than in the first heating cycle was due to the different "thermal history" of the material, as previously discussed in ***Chapter 3.***

The HMW PCL melting point in the DSC thermogram of the powder mixture with the slower heating-cooling rate (***Figure 4.27.b***) appeared at a slightly lower temperature than when the higher temperature rate was applied (***Figure 4.27.a***), as can be seen in ***Table 4.8.*** This could be associated with the applied settings, heating-cooling rate of 1 °C/min and 10°C/min. It has previously been reported in the literature that as the heating rate increased, the peak broadened, while the melting point of the investigated material was detected at a higher temperature (Wang and Harrison, 1994).

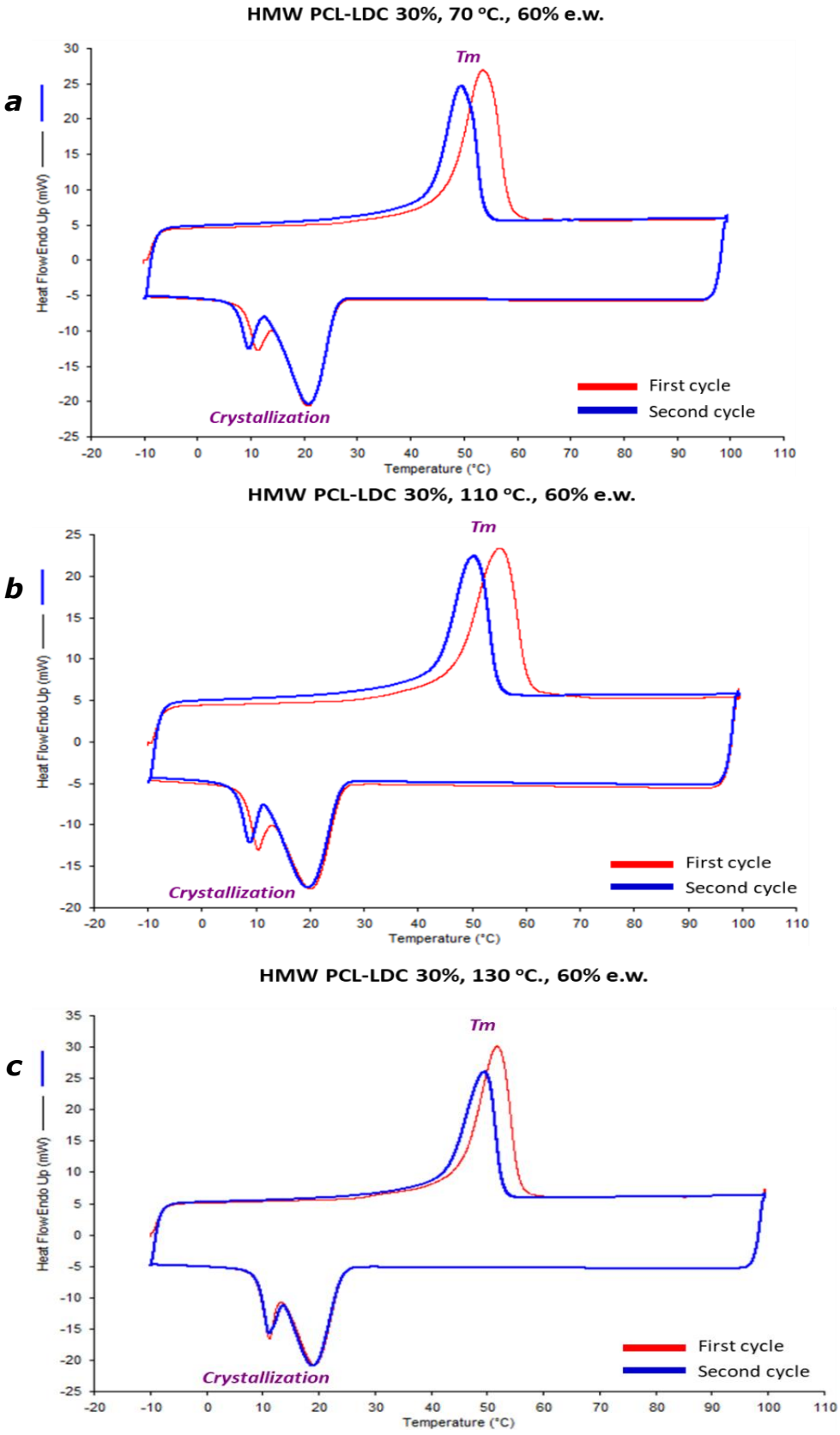

Figure 4.28: *DSC thermograms of HMW PCL-LDC 30% implants printed with an extrusion width (e.w.) setting of 60% at* ***(a):*** *70 °C,* ***(b):*** *110 °C and* ***(b):*** *130 °C. The red line represents the first heating-cooling cycle and the blue line the second cycle.*

In the second cooling cycle, two distinct peaks (broad peak at 29.1 °C and narrow peak at 15.7 °C) for the materials crystallization appeared, similarly to the first cycle, as shown in ***Figure 4.27.b***. These peaks were indicative of the presence of more than one material in the analysed sample. These peaks, though, were detected at temperatures lower than the characteristic crystallization temperatures of HMW PCL and lidocaine (***Figure 3.14.a, Figure 4.26***) and could be attributed to confined mobility of the molecules inhibiting their recrystallization.

The third heating-cooling cycle was exactly the same as the second one, as anticipated. A similar observation has previously been discussed for the thermal analysis of the raw polymer in ***Chapter 3***, where it has also been shown that the melting point and the crystallization temperature were stabilised after the second heating-cooling cycle.

Based on ***Figure 4.27,*** the mixing of the polymer and the drug did not considerably affect their thermal properties. The fact that the crystallization temperature for both materials was close to room temperature could explain the fast solidification of the printed implants when the building platform was not heated leading to poor disc adhesiveness.

3D printed lidocaine loaded and free polycaprolactone implants were, then, analysed in DSC to investigate the impact of the extrusion on the materials properties. According to ***Figure 4.28, Figure 4.29, Figure 4.30.b, Figure S.13, Figure S.14*** and ***Figure S.15,*** no peaks for the melting point of lidocaine were detected in any of the drug loaded printed formulations, indicating a largely amorphous state of the drug within the amorphous polymer matrix after printing and likely formation of a solid dispersion (Rychter *et al.*, 2018b). Furthermore, the low quantity of lidocaine incorporated in the 3D printed implants could be below the detection limit of this technique (Mackin *et al.*, 2002) (Hogan and Buckton, 2001).

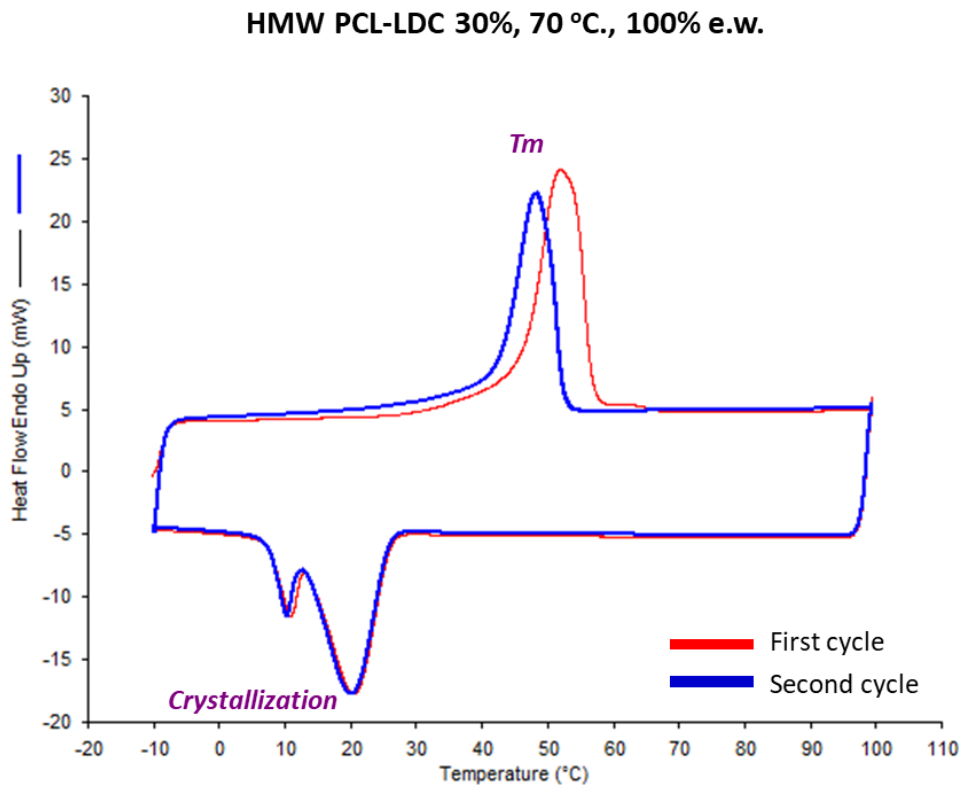

Figure 4.29: *DSC thermogram of HMW PCL-LDC 30% implant printed at 70 °C with an extrusion width (e.w.) setting of 100%. The red line represents the first heating-cooling cycle and the blue line the second cycle.*

Similarly to the DSC thermograms of the HMW PCL-LDC 30% powder, ***Figure 4.27,*** two recrystallization peaks at around 10 °C and 20 °C appeared in the thermograms of the 3D printed implants in ***Figure 4.28*** and ***Figure 4.29,*** consistent with the presence of two materials in the examined samples. The latter indicated the formation of a new crystal phase through co-crystallization of lidocaine with PCL or a solid dispersion consisting of a few crystalline particles of the investigated materials.

Table 4.8: *DSC data of pure HMW PCL powder (N=4), HMW PCL-LDC 30% powder before 3D printing (N=2), HMW PCL-LDC 30% implants printed with an extrusion width (e.w.) setting of 60% at 70 °C (N=2), 80 °C (N=2), 90 °C (N=2), 100 °C (N=2), 110 °C (N=2), 120 °C (N=2) and 130 °C (N=2).*

PCL data				
	T_m (°C)			T_c (°C)
	1st cycle	2nd cycle	3rd cycle	
HMW PCL powder	64.1 ± 1.1	60.1 ± 3.2		28.6 ± 0.6
HMW PCL-LDC 30% powder	62.4 ± 0.1	50.2 ± 0.4		
HMW PCL-LDC 30% powder (heating/cooling rate: 1 °C/min)	57.7 ± 0.3	48.1 ± 0.1	48.1 ± 0.1	29.1 ± 0.1
HMW PCL-LDC 30% 70 °C, 60% e.w.	53.6 ± 0.2	49.9 ± 0.1		
HMW PCL-LDC 30% 80 °C, 60% e.w.	53.9 ± 0.2	49.8 ± 0.1		
HMW PCL-LDC 30% 90 °C, 60% e.w.	53.2 ± 0.3	49.3 ± 0.2		
HMW PCL-LDC 30% 100 °C, 60% e.w.	54.5 ± 0.8	49.1 ± 0.6		
HMW PCL-LDC 30% 110 °C, 60% e.w.	54.2 ± 1.1	49.7 ± 0.6		
HMW PCL-LDC 30% 120 °C, 60% e.w.	53.1 ± 1.1	49.6 ± 0.2		
HMW PCL-LDC 30% 130 °C, 60% e.w.	52.9 ± 1.3	49.7 ± 0.2		

Only one peak for the melting point was detected, though, in all the printed discs, which was assigned to the polymer, similarly to the powder mixture DSC analysis (***Figure 4.27***). This observation suggested that lidocaine was molecularly dispersed in the amorphous polymeric matrix or that it was predominantly amorphous after the 3D printing process with very few crystalline particles in a concentration lower than the sensitivity limit of this technique. However, the

melting point peak of the HMW PCL in the second heating cycle appeared at a lower temperature than in the first one due to the different "thermal history" of the analysed compounds (***Table 4.9***), which was also previously seen (***Table 4.8***). In general, the HMW PCL melting point of the fabricated formulations shifted to relatively lower temperatures than in the powder mixture indicating that the drug was well-dispersed in the amorphous polymer phase or that a new crystal phase has been created through the co-crystallization of the lidocaine with the HMW PCL (Valle, Camps and Díaz, 2011) (ter Horst and Cains, 2009) (Garbacz *et al.*, 2020) (Kumar and Nanda, 2017). The glass transition temperature of the materials used for the manufacture of the implants could not be detected with the current technique and equipment used as it was appearing at below -60 °C (Cui and Frank, 2006) (Liu *et al.*, 2018) (Rusu, Ursu and Rusu, 2006) (Govor *et al.*, 2014) (Priselac *et al.*, 2017) (De Kesel *et al.*, 1999) (Shen, Lu and Liang, 2013b).

Table 4.9: *DSC data of pure HMW PCL powder (N=4), HMW PCL-LDC 30% powder before 3D printing, HMW PCL-LDC 30% implants printed at 70 °C with an extrusion width (e.w.) setting of 50% (N=2), 60% (N=2), 70% (N=2), 80% (N=2) and 100% (N=2).*

PCL data			
	T_m (°C)		T_c (°C)
	1st cycle	*2nd cycle*	
HMW PCL powder	64.1 ± 1.1	60.1 ± 3.2	28.6 ± 0.6
HMW PCL-LDC 30% powder	62.4 ± 0.1	50.2 ± 0.4	
HMW PCL-LDC 30% 70 °C, 50% e.w.	53.4 ± 0.1	49.4 ± 0.3	
HMW PCL-LDC 30% 70 °C, 60% e.w.	53.6 ± 0.2	49.9 ± 0.1	
HMW PCL-LDC 30% 70 °C, 70% e.w.	53.1 ± 0.1	49.1 ± 0.1	
HMW PCL-LDC 30% 70 °C, 80% e.w.	53.1 ± 0.5	49.3 ± 0.1	
HMW PCL-LDC 30% 70 °C, 100% e.w.	52.1 ± 0.3	48.5 ± 0.2	

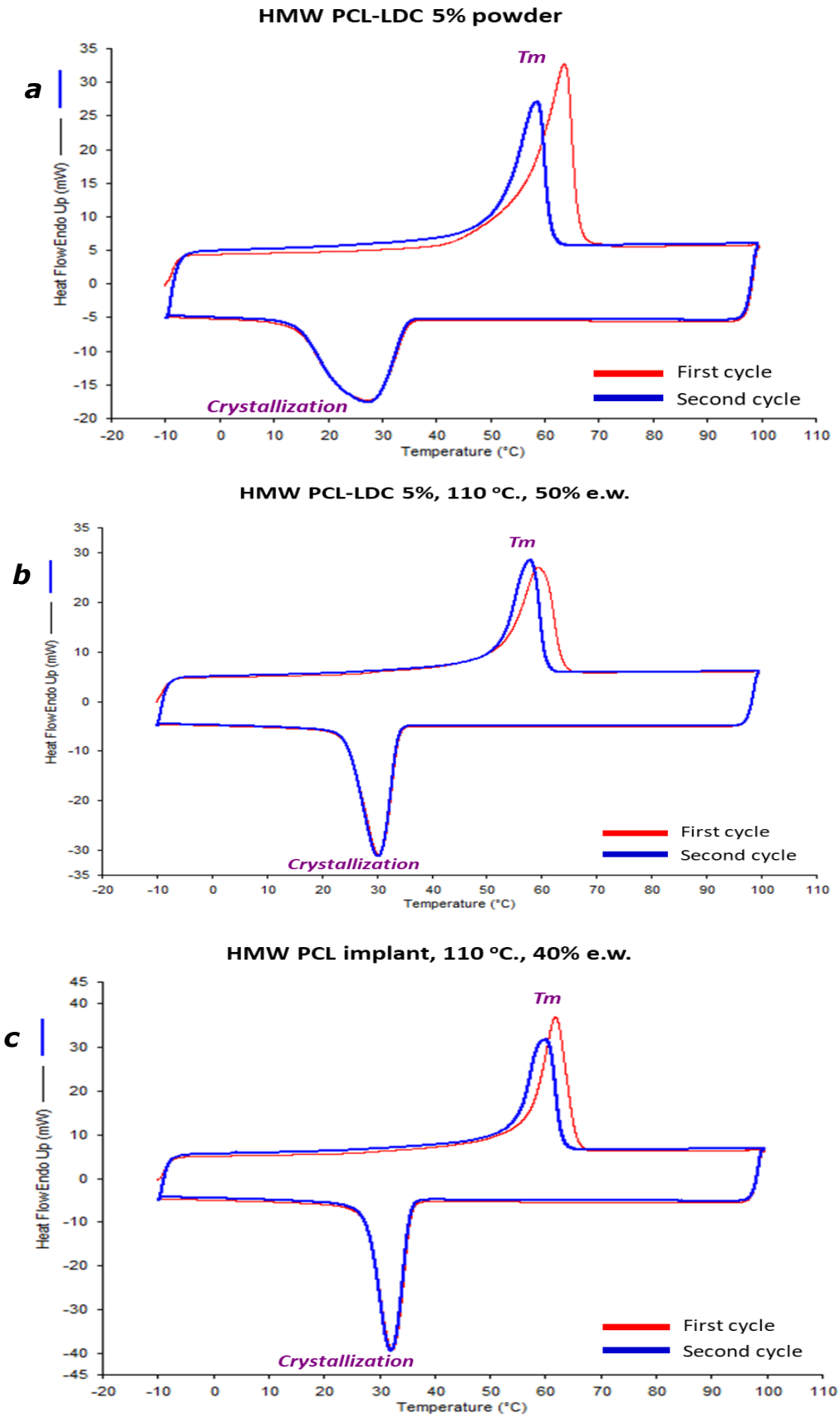

Figure 4.30: *DSC thermograms of* ***(a):*** *HMW PCL-LDC 5% powder before 3D printing,* ***(b):*** *HMW PCL-LDC 5% implant printed at 110 °C with an extrusion width (e.w.) setting of 50% and* ***(c):*** *HMW PCL implant printed at 110 °C with an extrusion width (e.w.) setting of 40%. The red line represents the first heating-cooling cycle and the blue line the second cycle.*

As presented in ***Table 4.8, Table 4.9, Figure 4.28*** and ***Figure 4.29,*** the mixing and the PAM printing processes did not considerably affect the thermal properties of the polymer. The different settings applied during the 3D printing, extrusion width and print temperature, did not demonstrate any effect on the melting point, neither the crystallization temperature of the HMW PCL.

The next formulation analysed in the DSC was the one with 5% w/w lidocaine loading. Initially, the polymer-drug mixture was characterized showing only one peak for the melting point and one for the crystallization temperature (***Figure 4.30.a***). A similar thermogram was acquired for the HMW PCL-LDC 5% implant, as demonstrated in ***Figure 4.30.b.*** There was no evidence, though, of drug crystallisation, as seen for the higher drug loaded samples.

The lower melting point detected in the second heating cycle at 57.8 ^{o}C compared to the one in the first cycle at 63.1 ^{o}C of the HMW PCL-LDC 5% powder in ***Figure 4.30.a***, was an attribute also observed in the pure HMW PCL powder (***Figure 3.12.a***). The recrystallization peak in the thermogram of the powder mixture was significantly broader than in the thermogram of the as-received polymer, indicating the presence of another material apart from the polymer, ie. the drug. The low drug concentration was in this case below the limits of detection of this technique, 5% w/w, and hence, there being no peaks for lidocaine is likely a result of this (Hogan and Buckton, 2001) (Mackin *et al.*, 2002). It was also indicated that a solid dispersion was formed during the manufacture of this dosage form.

After the printing of the HMW PCL-LDC 5% implants, it was observed in ***Figure 4.30.b*** and ***Table 4.10*** that the temperature applied during the 3D printing process did not have any significant impact on the HMW PCL thermal properties similar to the thermograms of the formulations with a higher drug loading.

Table 4.10: *DSC data of pure HMW PCL powder (N=4), HMW PCL implants printed with an extrusion width (e.w.) setting of 40% at 110 °C (N=2), HMW PCL-LDC 5% powder before 3D printing (N=2) and HMW PCL-LDC 5% implants printed with an extrusion width (e.w.) setting of 50% at 110 °C (N=2).*

PCL data			
	T_m (°C)		T_c (°C)
	1st cycle	2nd cycle	
HMW PCL powder	64.1 ± 1.1	60.1 ± 3.2	28.6 ± 0.6
HMW PCL 110 °C, 40% e.w.	65.1 ± 3.6	62.6 ± 3.1	31.2 ± 1.1
HMW PCL-LDC 5% powder	63.1 ± 0.8	57.8 ± 0.6	28.6 ± 1.1
HMW PCL-LDC 5% 110 °C, 50% e.w.	61.5 ± 1.8	58.7 ± 1.1	30.2 ± 0.5

A polymeric implant printed without any drug loaded was also characterized in the DSC, as demonstrated in ***Figure 4.30.c***. The thermogram of this sample was nearly identical with the thermogram of the pure HMW PCL powder, also verifying that the extrusion and the settings, print temperature and extrusion width, applied did not have any effect on the thermal properties of the examined compound.

Table 4.11: *PCL Crystallinity percentage (X_c %) of pure HMW PCL powder (N=4), HMW PCL-LDC 30% powder before 3D printing (N=2), HMW PCL-LDC 30% implants printed with an extrusion width (e.w.) setting of 60% at 70 °C (N=2), 80 °C (N=2), 90 °C (N=2), 100 °C (N=2), 110 °C (N=2), 120 °C (N=2) and 130 °C (N=2).*

PCL data		
	% Crystallinity degree	
	1st cycle	2nd cycle
HMW PCL powder	52.2 ± 4.8	32.4 ± 3.3
HMW PCL-LDC 30% powder	43.7 ± 5.3	27.9 ± 2.2
HMW PCL-LDC 30% 70 °C, 60% e.w.	40.3 ± 0.8	28.8 ± 0.4
HMW PCL-LDC 30% 80 °C, 60% e.w.	38.2 ± 1.2	30.7 ± 0.6
HMW PCL-LDC 30% 90 °C, 60% e.w.	41.1 ± 1.1	29.7 ± 0.7
HMW PCL-LDC 30% 100 °C, 60% e.w.	40.1 ± 1.6	29.8 ± 1.1
HMW PCL-LDC 30% 110 °C, 60% e.w.	39.5 ± 1.1	30.4 ± 1.1
HMW PCL-LDC 30% 120 °C, 60% e.w.	41.8 ± 1.1	32.6 ± 0.7
HMW PCL-LDC 30% 130 °C, 60% e.w.	39.5 ± 0.4	30.9 ± 0.7

The crystallinity percentage (X_c %) of the HMW PCL was calculated from the DSC thermograms of the polymer-drug powder mixture and the 3D printed lidocaine loaded and free polycaprolactone implants (***Table 4.11, Table 4.12***).

The crystallinity degree of the selected model drug was calculated from the XRPD diffractogram only and not from the DSC thermogram. The enthalpy of fusion of 100% crystalline LDC (ΔH_{f0}) was needed for the LDC crystallinity calculation based

on the DSC thermogram. This information, though, could not be found in the literature or the DSC data library.

Table 4.12: *PCL Crystallinity percentage (X_c %) of pure HMW PCL powder (N=4), HMW PCL-LDC 30% powder before 3D printing (N=2), HMW PCL-LDC 30% implants printed at 70 °C with an extrusion width (e.w.) setting of 50% (N=2), 60% (N=2), 70% (N=2), 80% (N=2) and 100% (N=2).*

PCL data		
	% Crystallinity degree	
	1st cycle	2nd cycle
HMW PCL powder	52.2 ± 4.8	32.4 ± 3.3
HMW PCL-LDC 30% powder	43.7 ± 5.3	27.9 ± 2.2
HMW PCL-LDC 30% 70 °C, 50% e.w.	39.8 ± 0.4	30.2 ± 0.7
HMW PCL-LDC 30% 70 °C, 60% e.w.	40.3 ± 0.8	28.8 ± 0.4
HMW PCL-LDC 30% 70 °C, 70% e.w.	38.9 ± 1.5	29.8 ± 0.7
HMW PCL-LDC 30% 70 °C, 80% e.w.	39.4 ± 1.1	30.1 ± 0.5
HMW PCL-LDC 30% 70 °C, 100% e.w.	39.4 ± 0.9	29.2 ± 0.4

According to ***Table 4.11*** and ***Table 4.12,*** PCL crystallinity degree in the HMW PCL-LDC 30% powder mixture was lower than the pure polymer powder. A potential explanation could be that the polymer-drug mixture acquired after blending the materials with a mortar and pestle led to a reduction in the crystalline order. This mixing method could be compared with a milling process as they both result in a more homogeneous sample consisting of fine powder particles. Surface molecular damage may occur leading to a disruption of the crystal structure; various degrees of disorder in the form of crystal defects and/or amorphous

regions are appearing to primarily reside on the crystal surface (Sheokand, Modi and Bansal, 2016) (Young *et al.*, 2007).

PCL crystallinity in the polymer-drug mixtures was further decreased in the second heating-cooling cycle. This was also observed in the pure polymer and as previously discussed in ***Chapter 3,*** is related to the presence of more than one type of crystal.

Table 4.13: *PCL Crystallinity percentage (X_c %) of pure HMW PCL powder (N=4), HMW PCL implants printed with an extrusion width (e.w.) setting of 40% at 110 ^oC (N=2), HMW PCL-LDC 5% powder before 3D printing (N=2) and HMW PCL-LDC 5% implants printed with an extrusion width (e.w.) setting of 50% at 110 ^oC (N=2).*

PCL data		
	% Crystallinity degree	
	1st cycle	2nd cycle
HMW PCL powder	52.2 ± 4.8	32.4 ± 3.3
HMW PCL 110 °C, 40% e.w.	47.5 ± 4.2	31.6 ± 1.9
HMW PCL-LDC 5% powder	45.4 ± 4.5	30.8 ± 2.2
HMW PCL-LDC 5% 110 °C, 50% e.w.	43.7 ± 4.1	27.7 ± 3.6

Thermal analysis in the 3D printed polycaprolactone implants loaded with 30% w/w (***Table 4.11, Table 4.12***) or 5% w/w lidocaine (***Table 4.13***) revealed that the polymer crystallinity degree was slightly reduced compared to the one measured in the polymer-drug mixture prior to printing. During the manufacture of the implants a heating-cooling cycle also occurred, but at an uncontrolled rate in this case; the solidification of the produced object occurred at room temperature. Various forms of crystals with different morphologic characteristics (crystal habits, growth defects, density, degree of order) were, therefore, formed

compared to the ones present in the raw polymer, resulting in a crystallinity degree drop (Shekunov *et al*., 1996). This could also explain the decreased percentage of crystallinity detected in the pure polycaprolactone implants. However, the polymer's crystallinity degree in the first heating-cooling cycle was higher than in the drug loaded formulations, verifying the impact of the blending method on this property.

As presented in ***Table 4.11*** and ***Table 4.12,*** the different settings, print temperature and extrusion width, applied during the fabrication of the lidocaine loaded HMW PCL implants did not affect the crystallinity degree of the polymer. Neither the different drug loading had any impact (***Table 4.11, Table 4.12, Table 4.13***), which was an indication that no chemical interaction or modification had occurred between the used compounds after their blending and extrusion.

4.2.2.2. XRD Characterization

Pure lidocaine powder was initially analysed in the XRPD before its mixing with PCL and 3D printing. As can be seen in ***Figure 4.31,*** many peaks appeared which verify the crystalline nature of this compound. More specifically, the characteristic peaks of lidocaine in the XRPD pattern are at 10.11, 12.76, 13.71, 14.34, 14.94, 16.12, 16.71, 19.12, 19.81, 21.16, 22.21, 22.87, 25.08, 27.44, 28.96 ^{o} 2θ and they are in accordance with the literature data (Powell, 1986a) (Leng *et al*., 2012) (Ribeiro *et al.*, 2016).

XRD analysis was subsequently conducted on the polymer-drug powder mixture, as well as, on the lidocaine loaded polycaprolactone implants printed with different settings, extrusion width and temperature, to investigate whether the crystalline nature of the used compounds has changed after the mixing and the extrusion.

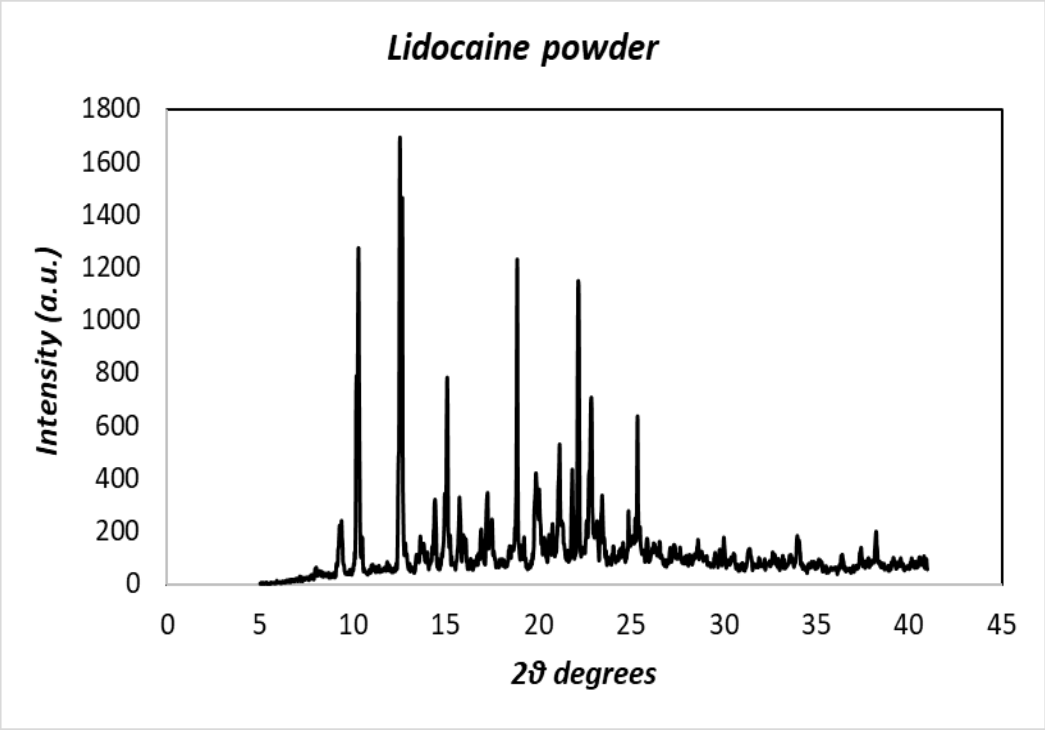

Figure 4.31: *XRPD diffractogram of pure lidocaine before extrusion and 3D printing.*

After mixing of 30% w/w lidocaine powder with 70% w/w HMW PCL powder, the crystalline form of these materials was not affected since peaks for both the polymer and the drug have been detected in the XRD diffractogram, as depicted in ***Figure 4.32.*** Characteristic peaks of HMW PCL appeared at 21.45 and 23.89° 2θ, while peaks at 10.11, 12.76, 14.94, 19.12 and 19.81° 2θ correspond to lidocaine (Pichayakorn *et al.*, 2014) (Powell, 1986b) (Gupta *et al.*, 2012) (Boonme *et al.*, 2013) (Leng *et al.*, 2012) (M. Shoja *et al.*, 2015) (Bae *et al.*, 2006) (Nelson *et al.*, 2012). Similar diffractograms have been obtained after the characterization of the implants printed with different extrusion width and temperatures, indicating that 3D printing and the different settings applied did not have any significant impact on the physical nature of the materials (***Figure 4.32***). The formation of HMW PCL-lidocaine co-crystals, though, could not be supported by XRD (Kumar and Nanda, 2017) (ter Horst and Cains, 2009) (Khan, Ahmad and Idrees, 2020) (Garbacz *et al.*, 2020).

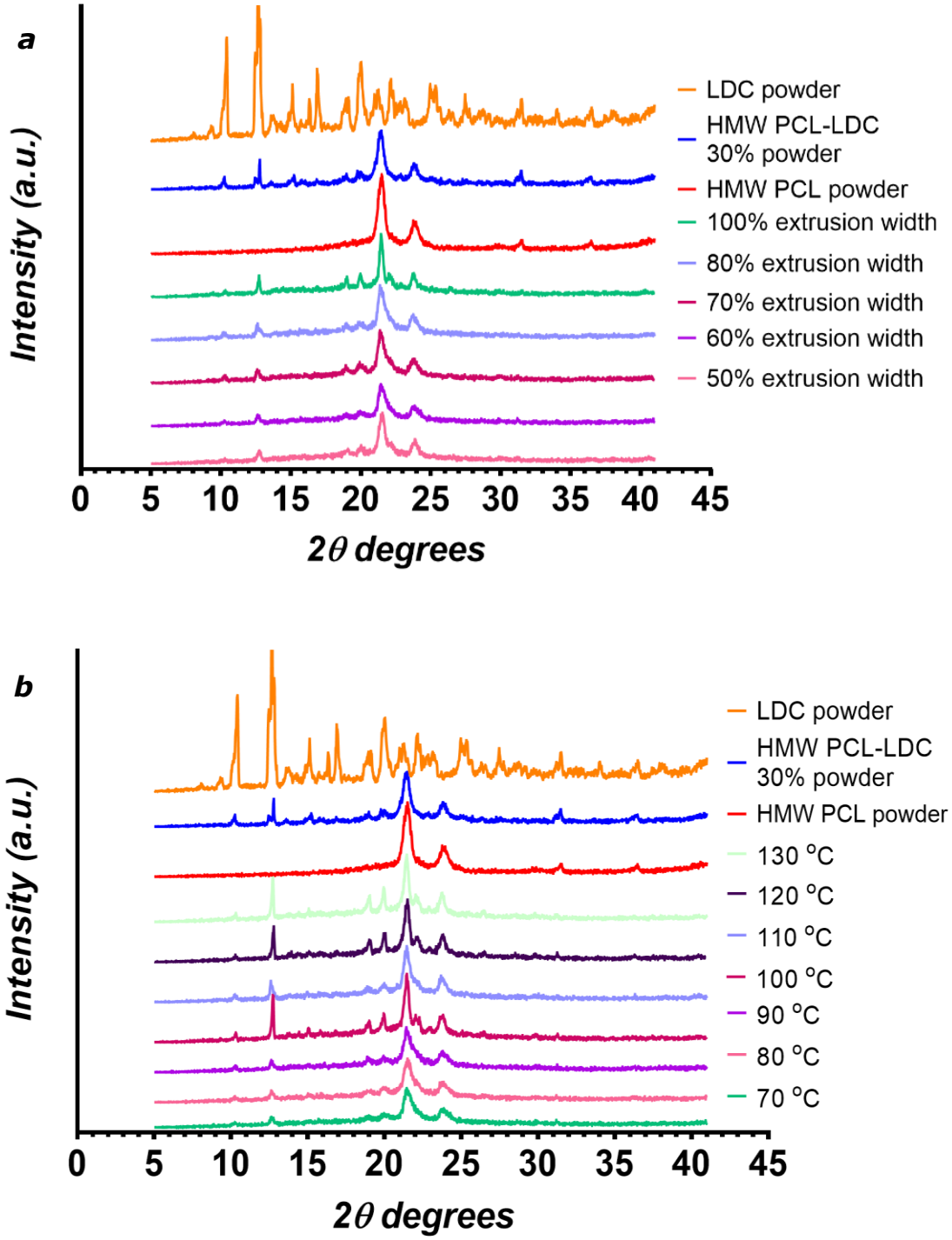

Figure 4.32: *XRD Diffractograms of pure HMW PCL and lidocaine powders, HMW PCL-LDC 30% powder and implants printed* ***(a):*** *with different extrusion width at 70 °C,* ***(b):*** *at different temperatures with an extrusion width setting of 60%.*

There are, hence, some differences in the DSC and XRD data for the 30% loaded samples, as DSC did not detect the presence of drug crystallinity whereas XRD has. This can be rationalised when considering the relative sensitivity of the two approaches (Newman *et al*., 2015) (Venkatesh *et al.*, 2001). Whilst both are bulk techniques, XRD is known to be more sensitive to the presence of crystallinity than DSC, at least on their standard forms as used here, with broad detection limits for XRD as low as 1% w/w, whereas for DSC 5% w/w is more typical (Briggner *et al.*, 1994) (Sheokand, Modi and Bansal, 2016) (Sebhatu, Angberg and Ahlneck, 1994). It is proposed that for the 30% drug loaded system, that whilst the drug is largely in an amorphous or discorded state, sufficient crystallinity remains to be detected by XRD but not DSC.

However, fewer characteristic peaks of lidocaine and lower intensity HMW PCL peaks were detected in the XRD diffractograms of the HMW PCL-LDC 30% powder and implants indicating that the active agent was well dispersed in the amorphous polymeric matrix being in a largely amorphous state. Nevertheless, the crystal peaks observed were characteristic of the materials incorporated in the printed implants, while no distinct peaks appeared suggesting the formation of a new crystal phase corresponding to HMW PCL-lidocaine co-crystals (Khan, Ahmad and Idrees, 2020) (ter Horst and Cains, 2009) (Sekhon, 2009) (Garbacz *et al.*, 2020).

The polymeric and drug crystals contained in the analysed samples seemed to have been influenced by the mixing process, where small disorder (amorphous) areas could have been created on the surface of the crystals (Hogan and Buckton, 2001) (Young *et al.*, 2007) (Saleki-Gerhardt, Ahlneck and Zografi, 1994). Additionally, the heating and cooling procedures occurring during the 3D printing could result in the formation of crystals with different degrees of order or defects (***Figure 4.32***). Therefore, both compounds, polycaprolactone and lidocaine consisted of more amorphous areas after their processing compared to their starting materials.

When the 5% w/w lidocaine loaded polycaprolactone implant and powder were characterized in the XRD, it was observed in ***Figure 4.33*** that the obtained diffractograms only presented the characteristic peaks of the polymer and not of the loaded drug, similarly to the DSC thermograms. This could be related to a quite low amount of the drug used in this case and the formation of the solid drug dispersion after the extrusion. Clearly, for the 5% loaded sample the amount of

crystallinity, if any, falls below the detection limit of both techniques (Shah, Kakumanu and Bansal, 2006).

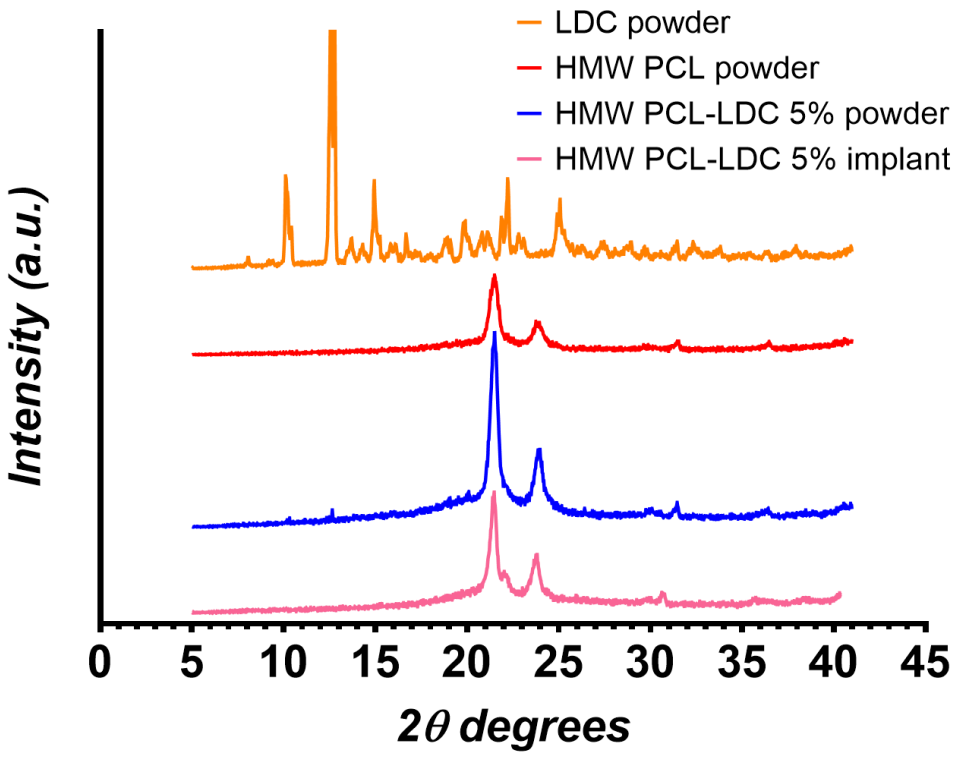

Figure 4.33: *XRD Diffractograms of pure HMW PCL and lidocaine powders, HMW PCL-LDC 5% powder and implant printed at 110 °C with an extrusion width setting of 50%.*

As observed in ***Figure 4.32*** and ***Figure 4.33,*** lower intensity peaks were detected for both PCL and lidocaine in the mixed and 3D printed samples. This trait in combination with the fewer characteristic peaks detected for the drug indicated that even though the crystalline nature of the materials was not affected by the mixing and extrusion, the degree of crystallinity has been decreased. A further investigation of this was, hence, needed to examine the impact of the pre-printing and printing processes on material properties.

Table 4.14: *PCL and Lidocaine Crystallinity percentage (X_c %) of pure HMW PCL (N=4) and LDC (N=4) powder, HMW PCL-LDC 30% powder before 3D printing (N=2), HMW PCL-LDC 30% implants printed with an extrusion width (e.w.) setting of 60% at 70 °C (N=2), 80 °C (N=2), 90 °C (N=2), 100 °C (N=2), 110 °C (N=2), 120 °C (N=2) and 130 °C (N=2).*

	% Crystallinity degree	
	PCL	LDC
HMW PCL powder	34.8 ± 3.3	
LDC powder		74.4 ± 1.4
HMW PCL-LDC 30% powder	32.6 ± 4.8	30.8 ± 4.4
HMW PCL-LDC 30% 70 °C, 60% e.w.	31.1 ± 1.5	14.5 ± 1.1
HMW PCL-LDC 30% 80 °C, 60% e.w.	30.8 ± 4.6	14.8 ± 0.2
HMW PCL-LDC 30% 90 °C, 60% e.w.	31.4 ± 2.1	16.1 ± 2.3
HMW PCL-LDC 30% 100 °C, 60% e.w.	31.6 ± 0.6	16.7 ± 0.1
HMW PCL-LDC 30% 110 °C, 60% e.w.	31.5 ± 4.1	14.1 ± 0.2
HMW PCL-LDC 30% 120 °C, 60% e.w.	30.5 ± 2.5	16.5 ± 0.6
HMW PCL-LDC 30% 130 °C, 60% e.w.	30.8 ± 3.1	16.8 ± 2.3

Table 4.15: *Summary of the crystallinity percentage (X_c %) of PCL in pure HMW PCL powder, HMW PCL-LDC 30% powder before 3D printing, HMW PCL-LDC 30% implants printed with an extrusion width (e.w.) setting of 60% at 70 °C, 80 °C, 90 °C, 100 °C, 110 °C, 120 °C and 130 °C.*

% Crystallinity degree			
	DSC results		XRD results
	1st cycle	2nd cycle	
HMW PCL powder	52.2 ± 4.8	32.4 ± 3.3	34.8 ± 3.3
HMW PCL-LDC 30% powder	43.7 ± 5.3	27.9 ± 2.2	32.6 ± 4.8
HMW PCL-LDC 30% 70 °C, 60% e.w.	40.3 ± 0.8	28.8 ± 0.4	31.1 ± 1.5
HMW PCL-LDC 30% 80 °C, 60% e.w.	38.2 ± 1.2	30.7 ± 0.6	30.8 ± 4.6
HMW PCL-LDC 30% 90 °C, 60% e.w.	41.1 ± 1.1	29.7 ± 0.7	31.4 ± 2.1
HMW PCL-LDC 30% 100 °C, 60% e.w.	40.1 ± 1.6	29.8 ± 1.1	31.6 ± 0.6
HMW PCL-LDC 30% 110 °C, 60% e.w.	39.5 ± 1.1	30.4 ± 1.1	31.5 ± 4.1
HMW PCL-LDC 30% 120 °C, 60% e.w.	41.8 ± 1.1	32.6 ± 0.7	30.5 ± 2.5
HMW PCL-LDC 30% 130 °C, 60% e.w.	39.5 ± 0.4	30.9 ± 0.7	30.8 ± 3.1

In the beginning, the crystallinity percentage of the raw materials was calculated and was found to be 34.8 ± 3.3 % for HMW PCL and 74.4 ± 1.4 % for lidocaine (***Table 4.14***). HMW PCL crystallinity degree was similar to that measured in the second cycle of the DSC analysis, as displayed in ***Table 4.15***. This was already discussed in ***Chapter 3***; it could be associated with the presence of different types of polymeric crystals that influence the shape of the peak of the melting point in the first heating program in the DSC thermogram and thereby, the area under the peak which was used for the subsequent calculation of the crystallinity percentage.

The crystallinity percentage of the pure powder from XRPD was 74 ± 1 %. This value is significant since XRD has a detection limit as low as 1% w/w and its accuracy at this level of crystallinity is considered good (Buckton and Darcy, 1995) (Hogan and Buckton, 2001) (Shah, Kakumanu and Bansal, 2006) (Sheokand, Modi and Bansal, 2016) (Young *et al*., 2007) (Lehto *et al.*, 2006) (Briggner *et al.*, 1994) (Sebhatu, Angberg and Ahlneck, 1994). However, it does suggest that about 25% of the as supplied drug is in a disordered or amorphous state; it possibly contains microcrystallites but without sufficient long range order to cause detectable diffraction. Lidocaine crystallinity percentage was not available by the supplier, neither its preparation method.

The heterogeneous morphological structure, degree of disorder and particles of various orientations and sizes observed in the SEM images of the as-received material (***Figure 4.17***) could explain the lower than 100% crystallinity calculated by the XRD diffractograms, where the signal is affected by the size or orientation of the crystals (Shah, Kakumanu and Bansal, 2006). Moreover, smaller (fine) particles were residing on the surface of the needle-shaped crystals and these could also affect the XRD analysis and consequently, the measured crystallinity percentage; a lower crystallinity degree was calculated in this way.

As demonstrated in ***Table 4.14, Table 4.16*** and ***Table 4.18***, the crystallinity percentage of the polymer in the polymer-drug mixture was slightly affected by the blending process, but it was independent of the concentration of the drug. Lidocaine crystallinity degree was greatly decreased, as well, after its mixing with 70% w/w HMW PCL powder with a mortar and pestle (***Table 4.14, Table 4.16***).

This blending method, as previously discussed, could lead to the creation of more amorphous regions or defects on the crystal surface (Sheokand, Modi and Bansal, 2016) (Saleki-Gerhardt, Ahlneck and Zografi, 1994) (Mackin *et al.*, 2002).

Table 4.16: *PCL and Lidocaine Crystallinity percentage (X_c %) of pure HMW PCL (N=4) and LDC (N=4) powder, HMW PCL-LDC 30% powder before 3D printing (N=2), HMW PCL-LDC 30% implants printed at 70 °C with an extrusion width (e.w.) setting of 50% (N=2), 60% (N=2), 70% (N=2), 80% (N=2) and 100% (N=2).*

	% Crystallinity degree	
	PCL	**LDC**
HMW PCL powder	34.8 ± 3.3	
LDC powder		74.4 ± 1.4
HMW PCL-LDC 30% powder	32.6 ± 4.8	30.8 ± 4.4
HMW PCL-LDC 30% 70 °C, 50% e.w.	31.7 ± 5.4	14.5 ± 0.8
HMW PCL-LDC 30% 70 °C, 60% e.w.	30.1 ± 1.5	14.5 ± 1.1
HMW PCL-LDC 30% 70 °C, 70% e.w.	31.8 ± 4.7	14.8 ± 0.4
HMW PCL-LDC 30% 70 °C, 80% e.w.	31.1 ± 3.2	13.1 ± 5.2
HMW PCL-LDC 30% 70 °C, 100% e.w.	30.7 ± 5.1	14.1 ± 4.1

The implants fabricated using the 70% w/w HMW PCL- 30% w/w LDC powder presented similar crystallinity percentages to the used materials in all the parameter combinations; various temperatures and extrusion widths have been applied (***Table 4.14, Table 4.16***).

Table 4.17: *Summary of the crystallinity percentage (X_c %) of PCL in pure HMW PCL powder, HMW PCL-LDC 30% powder before 3D printing, HMW PCL-LDC 30% implants printed at 70 °C with an extrusion width (e.w.) setting of 50%, 60%, 70%, 80% and 100%.*

% Crystallinity degree			
	DSC results		XRD results
	1st cycle	2nd cycle	
HMW PCL powder	52.2 ± 4.8	32.4 ± 3.3	34.8 ± 3.3
HMW PCL-LDC 30% powder	43.7 ± 5.3	27.9 ± 2.2	32.6 ± 4.8
HMW PCL-LDC 30% 70 °C, 50% e.w.	39.8 ± 0.4	30.2 ± 0.7	31.7 ± 5.4
HMW PCL-LDC 30% 70 °C, 60% e.w.	40.3 ± 0.8	28.8 ± 0.4	30.1 ± 1.5
HMW PCL-LDC 30% 70 °C, 70% e.w.	38.9 ± 1.5	29.8 ± 0.7	31.8 ± 4.7
HMW PCL-LDC 30% 70 °C, 80% e.w.	39.4 ± 1.1	30.1 ± 0.5	31.1 ± 3.2
HMW PCL-LDC 30% 70 °C, 100% e.w.	39.4 ± 0.9	29.2 ± 0.4	30.7 ± 5.1

The amount of crystallinity for the polymer demonstrated a further decrease after the extrusion, similar to the results obtained on the DSC analysis (***Table 4.15, Table 4.17***). The uncontrolled heating-cooling process occurring during the extrusion printing procedure, as previously discussed, could result in the formation

of crystals with different orientations, degree of order or habits contrasted with the as-received material, leading to the observed decrease in crystallinity.

The crystallinity percentage of the drug was considerably affected, as well, by the formation of a drug dispersion in the polymeric matrix. It was indicated, thus, by the XRD diffractograms that the active ingredient was in a largely amorphous state within the polymeric phase, while only a few crystalline particles being present in the printed formulation leading to a drop of its crystallinity degree. This reduction is consistent with another study performed on lidocaine where the amorphous content was calculated after repeated heating-cooling cycles. It was found that a 100% crystalline sample of lidocaine has become more than 90% amorphous after three cycles (Pava*n et al*., 2013).

Since no peaks for lidocaine have been detected in the XRD diffractograms of PCL implants containing 5% w/w lidocaine and the powder prepared for their printing (***Figure 4.33***), the crystallinity percentage of the polymer was the only one calculated (***Table 4.18***). The obtained results were as anticipated, considering the previously analysed implants with higher drug loading (***Table 4.14, Table 4.16***); HMW PCL crystallinity degree decreased after the mixing process, while a further crystallinity drop was observed after the extrusion.

Table 4.18: *PCL and Lidocaine Crystallinity percentage (X_c %) of pure HMW PCL powder (N=4), HMW PCL-LDC 5% powder before 3D printing (N=2) and HMW PCL-LDC 5% implants printed with an extrusion width (e.w.) setting of 50% at 110 °C (N=2).*

	% Crystallinity degree	
	PCL	***LDC***
HMW PCL powder	34.8 ± 3.3	
LDC powder		74.4 ± 1.4
HMW PCL-LDC 5% powder	32.2 ± 1.2	
HMW PCL-LDC 5% 110 °C, 50% e.w.	30.2 ± 4.9	

Table 4.19: *Summary of the crystallinity percentage (X_c %) of PCL in pure HMW PCL powder, HMW PCL-LDC 5% powder before 3D printing and HMW PCL-LDC 5% implants printed with an extrusion width (e.w.) setting of 50% at 110 °C.*

% Crystallinity degree			
	DSC results		*XRD results*
	1st cycle	*2nd cycle*	
HMW PCL powder	52.2 ± 4.8	32.4 ± 3.3	34.8 ± 3.3
HMW PCL-LDC 5% powder	45.4 ± 4.5	30.8 ± 2.2	32.2 ± 1.2
HMW PCL-LDC 5% 110 °C, 50% e.w.	43.7 ± 4.1	27.7 ± 3.6	30.2 ± 4.9

Summarizing from the crystallinity degree of HMW PCL as calculated by the DSC and XRD analyses in ***Table 4.15, Table 4.17*** and ***Table 4.19***, it was observed that the crystallinity percentage derived from the XRD diffractograms was in accordance with the one observed in the second heating cycle of the DSC thermograms, similarly to the results of the 3D printed polymeric triangles as discussed in ***Chapter 3***. More than one crystal population was indicated to be present in the polymeric sample and consequently, that could have an impact on the shape and the area under the peak of the melting point during the first heating-cooling program. The area under the characteristic peaks in the obtained DSC and XRD graphs were subsequently used for the calculation of the crystallinity degree of the material of interest.

According to the DSC and XRD characterizations of the HMW PCL-LDC 30% implants printed with different extrusion widths, no impact of this parameter has been detected on the materials properties. Consequently, these implants did not need to be further characterized, while the formulations printed at different temperatures would be used in the next stages of this study. Furthermore, these were shown to be the most promising formulations for the achievement of sustained drug release.

Another common trait in all the polymeric formulations, based on the DSC and XRD analyses, is that a drug dispersion within the amorphous polymeric phase has been achieved with the hot melt extrusion based 3D printing method. The active agent was in a largely amorphous state resulting in the detection of low lidocaine crystallinity degree in the XRD diffractograms.

Therefore, it is suggested that the investigated printing technology can be used for the formation of solid dispersions for the improvement of the bioavailability of poorly soluble active compounds, enhancing their solubility and release rate or even for the achievement of sustained drug release formulations since the material properties of the matrix dictate the dissolution rate of the encapsulated active ingredient (Vasconcelos, Sarmento and Costa, 2007) (Allawadi *et al.*, 2014) (Sharma *et al.*, 2019) (Chiou and Riegelman, 1971) (Huang and Dai, 2014) (Tran *et al.*, 2019). The latter could be attained since a variety of materials could be loaded to the investigated 3D printing technology (Jamróz, Szafr*aniec, et al*., 2018) (Shende and Agrawal, 2018) (Ligo*n et al*., 2017) (Awa*d et al*., 2018) (Liaw and Guvendiren, 2017) (Palo *et al.*, 2017) (Zhang *et al.*, 2018).

4.2.2.3. FTIR Characterization

Spectra of the as-received PCL and lidocaine powders were recorded using FTIR-ATR. Powder physical mixtures and the implants printed with different settings and drug loading were, then, analysed to explore potential interactions between

the polymer and the drug and whether the extrusion and the parameters applied led to detectable modifications on their chemical structure.

The detected peaks for PCL were in good correspondence with the published data (Rychte*r et al*., 2018) (Xue *et al.*, 2014) (Shkarina *et al.*, 2018). As displayed in the spectrum of HMW PCL in ***Figure 4.34.a***, its characteristic peaks detected at 2943 and 2872 cm^{-1} correspond to C-H stretching and at 1724 cm^{-1} to C=O stretching. Smaller peaks at 1471, 1412 and 1364 cm^{-1} are assigned to CH_2 bending, while at 1293 cm^{-1} to C-O and C-C stretching in the crystalline phase. Bands at 1237 and 1166, 1114 cm^{-1} indicate asymmetric C-O-C stretching and symmetric C-O-C stretching, respectively. A peak of the raw polymer appeared at 1055, 952 cm^{-1} is attributed to C-O stretching and at 731 cm^{-1} to C-H bending vibration.

Lidocaine powder analysis in the FTIR resulted in the spectrum depicted in ***Figure 4.34.b***. Characteristic bands detected at 3255 cm^{-1} are indicating N-H stretching and at 3021, 2968, 2921 and 2799 cm^{-1} aromatic C-H stretching. A sharp peak at 1655 cm^{-1} is assigned to C=O stretching, while a broader peak centred at 1496 cm^{-1} corresponds to C-N stretching of the amide group. A C-H bending vibration is indicated by a band at 770 cm^{-1}. These bands were consistent with the literature data (Anacleto *et al.*, 2018) (Na *et al.*, 2018) (Pichayakorn *et al.*, 2014).

As demonstrated in the FTIR spectrum of the HMW PCL-LDC 30% powder physical mixture, ***Figure 4.35***, peaks for both the polymer and the drug have been detected unchanged indicating no significant interaction has occurred during the mixing process that could lead to the formation of co-crystals (ter Horst and Cains, 2009) (Garbacz *et al.*, 2020) (Khan, Ahmad and Idrees, 2020).

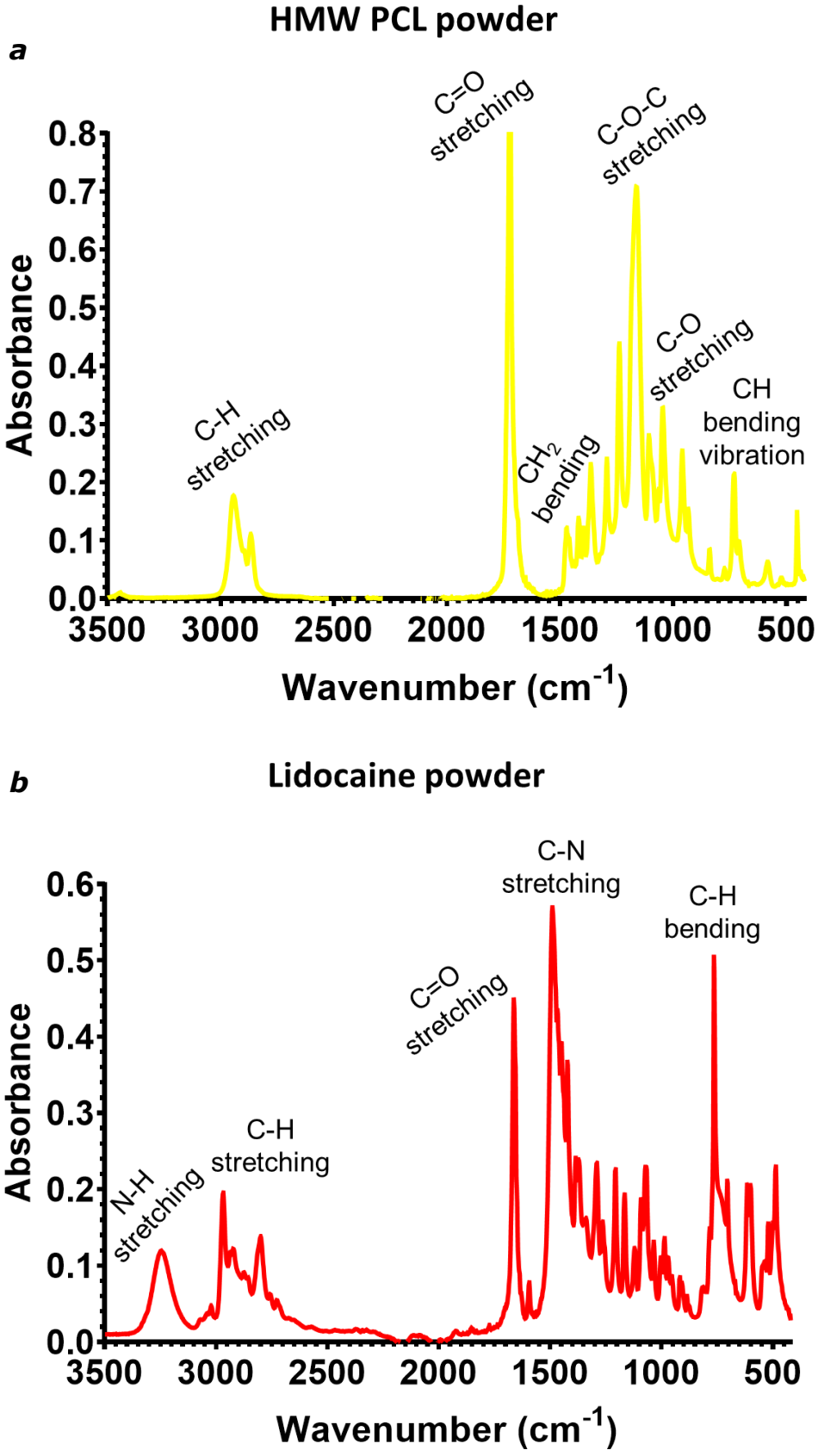

Figure 4.34: *FTIR spectra of pure* ***(a):*** *HMW PCL powder and* ***(b):*** *lidocaine powder.*

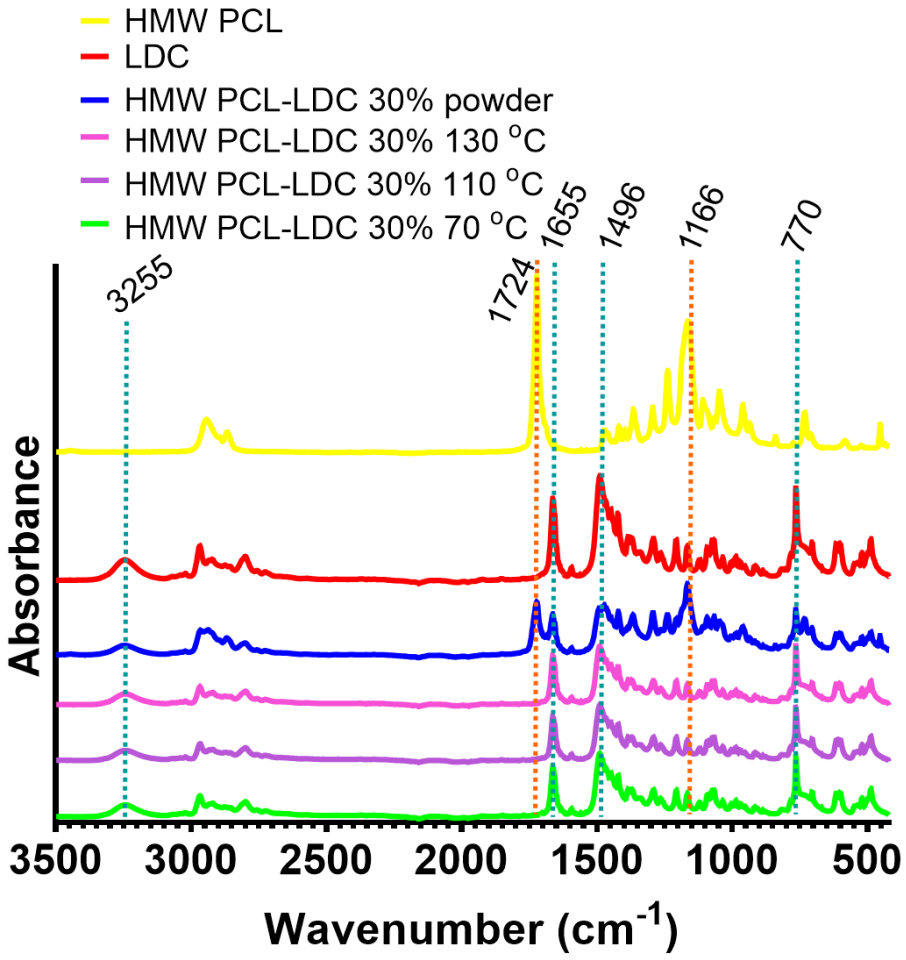

Figure 4.35: *FTIR spectra of pure HMW PCL and lidocaine powders, HMW PCL-LDC 30% powder and HMW PCL-LDC 30% implants printed at 70 °C, 110 °C and 130 °C with an extrusion width setting of 60%. LDC peaks are highlighted with the blue dot-line and HMW PCL peaks with the orange dot-line.*

The temperature applied during the printing process did not significantly affect the properties of the used compounds based on the results of the previously performed characterizations, DSC and XRD. Consequently, only three types of HMW PCL implants loaded with 30% w/w lidocaine were selected for the FTIR analysis to investigate the impact of the print temperature on the chemical structure of the materials used; formulations printed with a low, intermediate and high temperature, 70, 110 and 130 ºC, respectively.

In the FTIR spectra of the HMW PCL-LDC 30% implants shown in ***Figure 4.35***, display of the characteristic peaks of the polymer and the loaded drug did not present any shifts or changes indicating that the temperature applied for the manufacture of the drug formulations using 3D printing did not have any detectable impact on the chemical structure of the used compounds. According to these observations, the creation of a new crystal phase through the chemical interaction of lidocaine and polycaprolactone was not apparent (Kumar and Nanda, 2017) (Sekhon, 2009) (Garbacz *et al.*, 2020).

However, as depicted in ***Figure 4.35***, there are fewer peaks in the spectra of the fabricated implants compared to the spectrum of the powder mixture, such as the characteristic peak of HMW PCL at 1724 cm^{-1}. A possible explanation could be that only one specific area was analyzed in the FTIR; the sampling surface was 200 μm wide with a 2 μm depth (Helmy *et al.*, 2003) (Lebon *et al.*, 2016). Therefore, if a not fully homogenized powder mixture was loaded to the printer for the manufacture of the desired formulations, then the polymer and the drug would not be so well distributed on the discs. The latter could result in one material mainly being detected in the analyzed area and then, displayed in the acquired spectrum.

The spectra of the HMW PCL-LDC 5% powder mixture and printed implant are shown in ***Figure 4.36***; they were identical with each other, as well as, with the HMW PCL powder spectrum. Characteristic bands of the polymer were only detected in these spectra, as the drug loading is below the sensitivity of the technique, 10% w/w (Lebo*n et al*., 2016) (Helmy *et al.*, 2003). It has been illustrated, though, that the different printing settings did not cause any modifications or interactions between the polymer and the drug; the extrusion width applied for the manufacture of the HMW PCL-LDC 5% implants was 50%, while for the HMW PCL-LDC 30% implants was 60%.

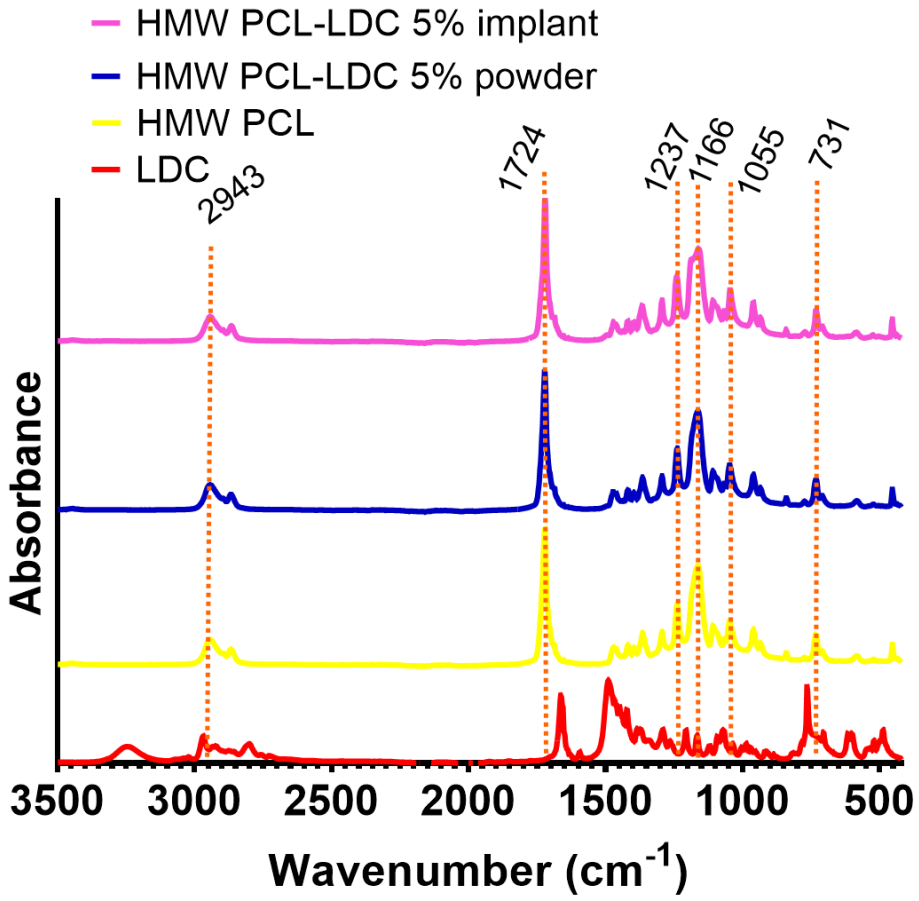

Figure 4.36: *FTIR spectra of pure HMW PCL and lidocaine powders, HMW PCL-LDC 5% powder and HMW PCL-LDC 5% implants printed at 110 °C with an extrusion width setting of 50%. HMW PCL peaks are highlighted with the orange dot-line.*

The final formulation analysed in the FTIR was the 3D printed pure HMW PCL control implant. Its spectrum (***Figure 4.37***) was identical to the as-received polymer powder, as expected and consistent with the previously characterized implants. It was, hence, shown that extrusion did not lead to any shifts or changes in the peaks of the HMW PCL.

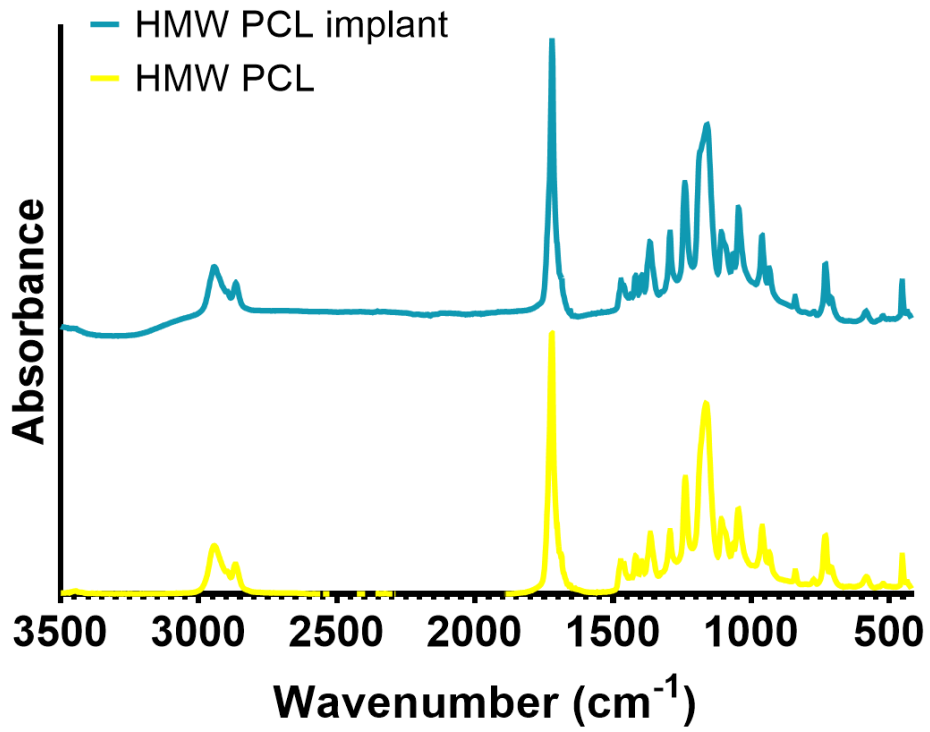

Figure 4.37: *FTIR spectra of pure HMW PCL powder and HMW PCL implant printed at 110 °C with an extrusion width setting of 40%.*

4.3. CONCLUSIONS

This chapter demonstrates that polycaprolactone encased and non-encased implants with different drug loading using a PAM 3D printer at relatively low printing temperatures have successfully been fabricated. Even though powder mixture viscosity was affected by the concentrations of the polymer and the drug, proper selection of the printing parameters allowed the manufacture of formulations suitable for sustained drug release. No excipients or solvents were needed to be added to the powder mixture, prior to its loading to the printer.

More specifically, it has been shown that polycaprolactone viscosity significantly decreased on the addition of lidocaine. When 30% w/w lidocaine was mixed with the polymer, the manufacture of implants at relatively low temperatures, close to

the melting points of the used compounds, was feasible. However, SEM analysis presented a highly featured surface at the lowest applied printing temperature, 70 ^{o}C. As the temperature increased, these surface characteristics (particulates) were reduced.

Raman characterizations on the implants fabricated after powder mixing demonstrated that both polycaprolactone and lidocaine were present in the matrix, as well as, the surface particles of the implants observed by SEM. No shifts or changes were detected in the characteristic peaks of the polymer and the drug after their mixing and extrusion, even when the highest studied temperatures were applied. That was, also, good evidence that the chemical structure of the used compounds was not modified.

Physical gaps appearing between the printed lines needed to be eliminated since this could affect polymer degradation and drug release. Extrusion width was the setting found to most effectively address this problem, as it was regulating the distance of the centres of the printed lines. The larger the extrusion width the larger the distance between the centres of the printed lines and hence, the larger the line width. Printing pressure was another important parameter exhibiting to have an impact on the printing resolution and accuracy. When more pressure was applied, more material was extruded and thereby, more evenly the formulations were fabricated.

During the manufacture of the HMW PCL-LDC 5% implants, the lower lidocaine concentration was demonstrated to influence the printing efficiency, while further optimization of the printing parameters was required to be performed. Lower extrusion width, compared to the one used for the fabrication of the HMW PCL-LDC 30% implants, was required to be applied for compact formulations without any cavities to be produced. This effect was even more intense when no lidocaine was added for the fabrication of pure HMW PCL discs.

The final manufactured formulation was an HMW PCL barrier-shell lidocaine loaded polymeric implant which illustrated the versatility of the PAM 3D printer in the production of sustained release systems. The printing of a core-shell formulation was shown to be achieved quite fast and without any special preparation of the materials loaded to the printer or any after-printing processing.

DSC and XRD data revealed that both polycaprolactone and lidocaine were crystalline after their mixing and extrusion even when different printing settings were applied. The amount of the loaded drug did not have any impact on the materials properties. Nevertheless, a few differences were observed in the printed drug loaded polymeric implants compared with the as-received materials; a slight decrease in the melting temperature of HMW PCL, fewer characteristic LDC peaks in the XRD diffractograms, as well as, a slight decrease in the intensity of the polymer peaks in the XRD patterns. These changes were attributed to the uncontrolled heat-cool cycle occurring during the 3D printing process.

However, the crystallinity degree of the polymer and the drug was reduced after their mixing, as calculated from the DSC thermograms and XRD diffractograms. A further decrease in the materials crystallinity amount was acquired after the manufacture of the lidocaine loaded polycaprolactone implants. This indicated that a solid drug dispersion has been formed where the active agent was in a largely amorphous phase and well dispersed in the amorphous polymeric matrix, maintaining at the same time a few crystalline particles. The different drug loading and printing parameters used, though, did not illustrate to have any further influence on that.

The formation of a solid dispersion clearly exhibited the capability of the studied hot melt extrusion based 3D printing technology to be applied in more areas of the pharmaceutical field. In this way, the effective delivery of poorly water soluble active substances enclosed in a polymeric matrix could be achieved; their solubility, dissolution rate and bioavailability would be enhanced. Not only immediate release formulations, but also sustained release ones could successfully be manufactured since the solubility and the degradation rate of the selected carrier regulate the dissolution rate of the molecularly dispersed active compound. The latter could successfully be attained as a wide range of materials could be used in the investigated printing technique.

According to the FTIR spectra, no detectable chemical interactions or modifications occurred between the polymer and the drug before and after their mixing and 3D printing. Similarly, to the other characterization, the different drug loading and the various applied printing settings did not result in any changes in the chemical structure of neither the HMW PCL, either the lidocaine.

In the next stages of this work, drug release studies will investigate the lidocaine release rate and the effectiveness of the polymeric barrier. The most promising fabricated implants will be used for this purpose, while the impact of the various applied printing settings and drug loading on the release of the selected model drug will be assessed.

CHAPTER 5: DISSOLUTION STUDIES ON LIDOCAINE LOADED HMW PCL IMPLANTS

5.1. INTRODUCTION

Lidocaine release profiles from the HMW PCL encased and non-encased polymeric implants will be demonstrated in this Chapter. The effectiveness of PCL, both as a barrier-shell and as a matrix, towards the achievement of sustained drug release has been investigated. Differently printed formulations with various lidocaine loading were studied for their potential impact on drug release:

- HMW PCL implants loaded with 30% w/w lidocaine (HMW PCL-LDC 30%) printed at 70 °C
- HMW PCL implants loaded with 30% w/w lidocaine (HMW PCL-LDC 30%) printed at 110 °C
- HMW PCL implants loaded with 5% w/w lidocaine (HMW PCL-LDC 5%) printed at 110 °C
- HMW PCL barrier-shell implants loaded with HMW PCL-LDC 30% discs (HMW PCL – HMW PCL-LDC 30%) printed at 110 °C

Pure HMW PCL implants (drug free) printed at 110 °C were used as control samples to explore whether polymer degradation had occurred after the four-day-long *in vitro* drug dissolution study.

Physical and chemical characterizations (SEM, Raman) have been performed on the HMW PCL encased and non-encased drug loaded and drug free implants after their dissolution tests to explore potential changes on their surface, related to the release of the drug and polymer degradation. The mechanism of lidocaine release was investigated by the fitting of the dissolution data to four established mathematical models: zero-order, first-order, Higuchi and Korsmeyer-Peppas.

A part of this Chapter has been published (***Appendix 2***) (Liaskoni, Wildman and Roberts, 2021).

5.2. RESULTS AND DISCUSSION

5.2.1. Lidocaine solubility in aqueous solutions

The solubility of lidocaine in aqueous solutions was investigated in various concentrations to establish the saturation concentration of the active ingredient. This was necessary to determine the lowest volume of medium which could be used for the subsequent dissolution studies; not all the amount of the drug loaded in the implants was expected to be released in the four-day-long release tests due to the slow PCL degradation rate and hence, sink conditions could be expected to be maintained. Using the lowest medium volume allowable contributes to the improved detection of even very small amounts of the released drug within the limit of detection, especially during the first hours of the study.

Aqueous solutions were used, since according to the previously published data lidocaine solubility in dH_2O was 4 mg/ml (Kumpugdee-Vollrath, Krause and Bürk, 2014). As PBS also contains salts, this could affect the drug solubility.

Initially, the solubility of lidocaine in concentrations of 1 and 2 mg/ml in dH_2O was tested at 70 ^oC under magnetic stirring for 40 min. That temperature was selected since it was the melting temperature of the active agent based on its thermal analysis (***Figure 4.26***). The obtained solutions were clear and all the drug powder was effectively dissolved (***Figure 5.1.a, Figure 5.1.b***). When the same experimental procedure was followed for the solutions with concentrations of 3 and 4 mg/ml, lidocaine powder was not effectively dissolved, but a suspension was formed (***Figure 5.1.c, Figure 5.1.d***). The latter was more obvious in the lidocaine solution with the highest explored concentration, 4 mg/ml, where large lidocaine particles appeared in the dH_2O (***Figure 5.1.d***).

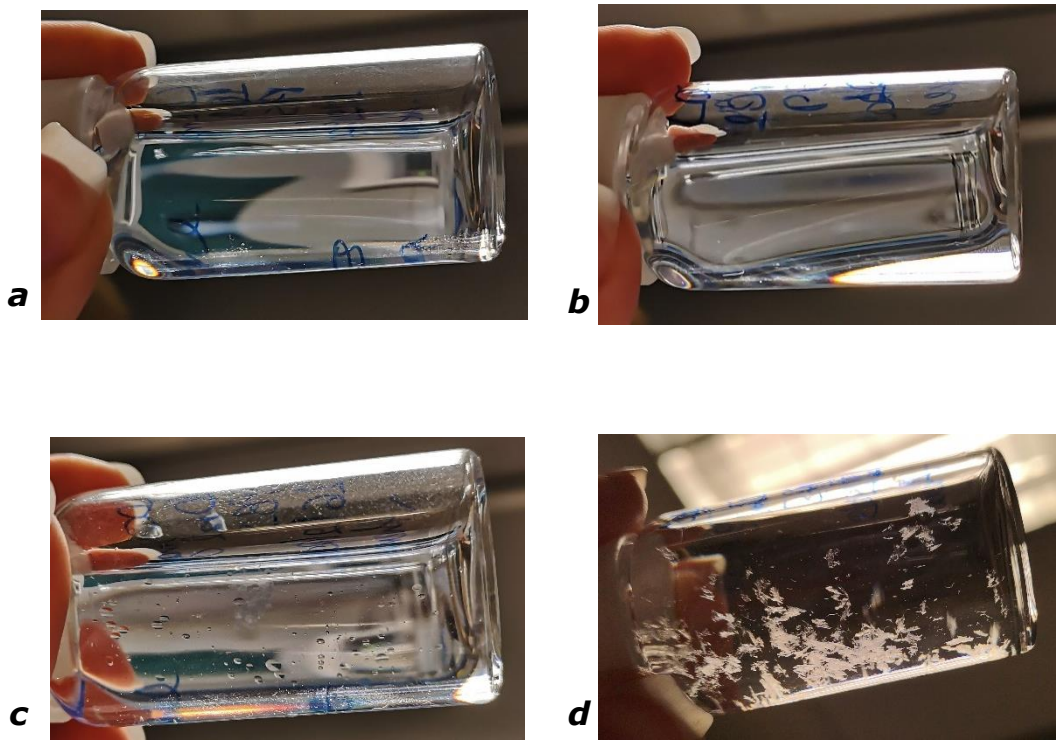

Figure 5.1: *Lidocaine solutions in dH_2O after magnetic stirring at 300 rpm and 70 °C for 40 min with a concentration of* ***(a):*** *1 mg/ml,* ***(b):*** *2 mg/ml,* ***(c):*** *3 mg/ml and* ***(d):*** *4 mg/ml.*

A higher temperature was then adjusted at the hot plate, 100 °C, and after 30 min of magnetic stirring, clear solutions containing 3 and 4 mg/ml of lidocaine were obtained (***Figure 5.2***), similar to those of the lower concentrations (***Figure 5.1.a, Figure 5.1.b***). This is in good agreement with the literature (Kumpugdee-Vollrath, Krause and Bürk, 2014).

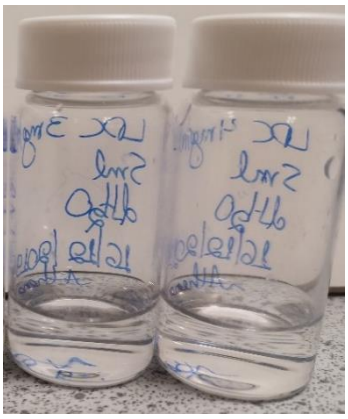

Figure 5.2: *Lidocaine solutions in dH_2O after magnetic stirring at 300 rpm and 100 °C for 30 min with a concentration of 3 mg/ml (left glass vial) and 4 mg/ml (right glass vial).*

The solubility of the drug in the dissolution medium, PBS, was determined to be lower than dH_2O. Firstly, lidocaine solutions of the same concentrations, 1, 2, 3 and 4 mg/ml, were placed on the hot plate at 70 °C, but after 40 min of magnetic stirring, no drug was dissolved in any solution. Only suspensions were formed; the higher the concentration the larger the lidocaine particles which were observed in the solutions. At a higher temperature, 100 °C, and after 30 min of magnetic stirring, clear lidocaine solutions of 1 and 2 mg/ml were acquired (***Figure 5.3***). This did not happen in the highly concentrated solutions, as seen previously; further processing was needed for all the lidocaine particles to be effectively dissolved and a clear solution to be obtained.

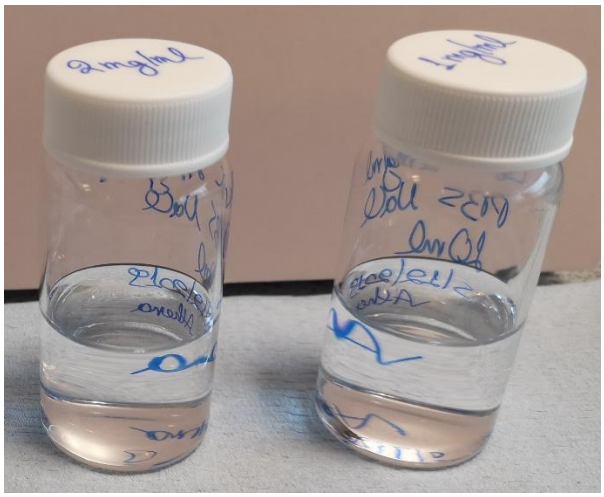

Figure 5.3: *Lidocaine solutions in PBS after magnetic stirring at 300 rpm and 100 °C for 30 min with a concentration of 1 mg/ml (right glass vial) and 2 mg/ml (left glass vial).*

Bath sonication was, then, applied to the lidocaine solutions with the highest investigated concentrations, 3 and 4 mg/ml, for 30, 60 and 105 min. However, no change in the large white lidocaine particles was observed (***Figure 5.4***). It was, thereby, indicated that the presence of salts in the dissolution medium was reducing the lidocaine solubility in concentrations closer to its saturation (in dH_2O).

a  ***b*** 

Figure 5.4: *Lidocaine solutions in PBS after bath sonication for 105 min with a concentration of* ***(a):*** *3 mg/ml and* ***(b):*** *4 mg/ml.*

Consequently, since the saturation lidocaine concentration was 2 mg/ml in PBS and each 3D printed HMW PCL-LDC 30% implant, which was the implant with the highest drug loading, contained 98.54 ± 2.98 mg of the drug, the lowest medium volume that could be used for the dissolution studies was determined to be 50 ml.

5.2.2. In vitro drug release studies

Dissolution data from HMW PCL encased and non-encased implants printed at various temperatures and with different drug loadings demonstrated, in general, sustained drug release, even when a relatively high dissolution media flow rate was applied (***Figure 5.5***).

PCL core-shell implants presented a particularly prolonged release; less than 6% of the drug was released after 4 days, suggesting that the studied polymer provided an effective barrier to the release of the active ingredient and the potential to achieve sustained release for periods of months based on the slow degradation of the studied polymer (***Figure 5.5***). This is in good agreement with the published data where combinations of different molecular weight PCL were used for the coating of 3D printed PVA-PLA implants (Stewart, Dom, Mcilorum, Gonzalez, *et al*., 2020). Such PCL coated formulations demonstrated sustained drug release compared to the uncoated ones, while the higher molecular weight of PCL used for the coating contributed to a more extended release of the active agent.

In the HMW PCL implants without a barrier-shell, no burst release was observed, indicating that whilst lidocaine was potentially detected on their surface, it, nevertheless, remained sufficiently physically associated with the polymer (or poorly soluble as in a crystalline state) to slow the release. This led to a sustained release of the active compound illustrating the effectiveness of the selected polymer on the prolongation of the drug release when used as a matrix and not only as a barrier, with 55 – 65 % of the loaded drug released after four days.

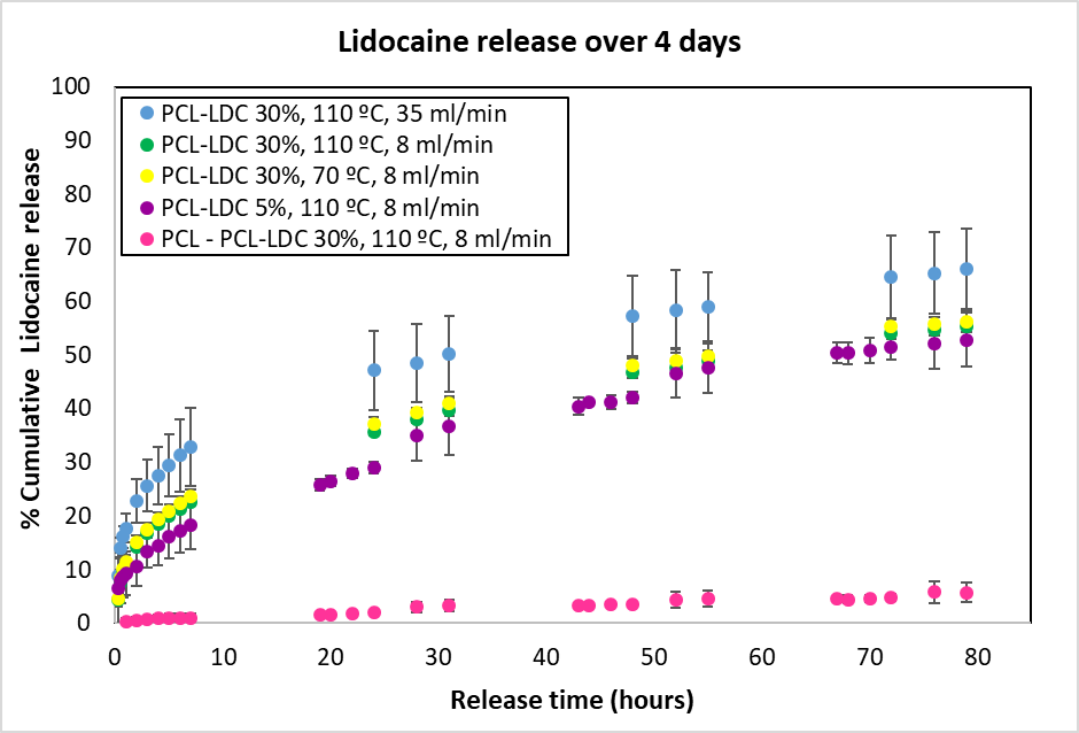

Figure 5.5: *Dissolution profiles of differently printed polycaprolactone non-encased implants with various lidocaine loadings (PCL-LDC 30% implants printed at 70 °C, PCL-LDC 30% implants printed at 110 °C, PCL-LDC 5% implants printed at 110 °C) and core-shell implants (PCL - PCL-LDC 30% implants printed at 110 °C) over 4 days. Two flow rates, 35 ml/min and 8 ml/min, have been investigated during the dissolution studies of 3D printed lidocaine loaded PCL implants.*

The various printing settings applied during the manufacture of the investigated formulations or the different drug loadings did not exhibit any observable impact on the release rate of the active ingredient. The dissolution settings, though, slightly affected the amount of the released lidocaine released after a four-day-long study. More specifically, *in vitro* drug release tests with two different flow rates, 35 ml/min and 8 ml/min, where HMW PCL-LDC 30% implants printed at 110 ºC were tested, illustrated a 10% difference in the cumulative amount of the released lidocaine; 65% for 35 ml/min flow rate and 55% for 8 ml/min flow rate.

The error bars in the dissolution study with the 35 ml/min flow rate were larger than with the slower flow rate which could be assigned to the applied dissolution parameter. The drug, thus, dissolved faster in the closed system due to more rapid replenishment of the buffer solution when the flow rate of 35 ml/min was used.

The impact of printing temperature on drug release was investigated, since in the SEM images of the fabricated implants it was observed that their surface characteristics were different (***Figure 4.13, Figure 4.14***). For this purpose, HMW PCL-LDC 30% implants printed at two different temperatures, 70 and 110 ºC, were examined, but showed no differences. More precisely, as depicted in ***Figure 5.5***, lidocaine release from the polymeric implants was not affected by the nature of surface particles (***Figure 4.13, Figure 4.14***). No burst release has been detected in the first hours of the study, on the contrary, the drug was slowly released over time. This was verified by the very short intervals of the sample time points, especially during the first day (***Figure 5.5***)***.***

Therefore, it was demonstrated that sustained drug release could be achieved with PCL implants printed at a relatively low temperature close to the melting point of the used compounds, 70 ºC. Consequently, this temperature is the most promising for the manufacture of HMW PCL formulations loaded with other active substances that are not particularly heat resistant.

HMW PCL implants with a lower drug loading, 5% w/w, were also tested; as displayed in ***Figure 5.5***, lidocaine was released in a similar way to the 30% w/w LDC loaded samples, which means that no burst release had occurred in the first day and extended drug release has been achieved in both cases. Thereby, the amount of the drug incorporated in the formulation did not affect its release rate from the polymeric systems.

Table 5.1: *Amount of lidocaine released (mg) per day over four days of dissolution per implant: HMW PCL – LDC 30% implants printed at 110 °C over dissolution with a flow rate of 35 ml/min (N=3), HMW PCL – LDC 30% implants printed at 110 °C over dissolution with a flow rate of 8 ml/min (N=3), HMW PCL – LDC 30% implants printed at 70 °C over dissolution with a flow rate of 8 ml/min (N=3), HMW PCL – LDC 5% implants printed at 110 °C over dissolution with a flow rate of 8 ml/min (N=3), HMW PCL - HMW PCL–LDC 30% implants printed at 110 °C over dissolution with a flow rate of 8 ml/min (N=3).*

Lidocaine released (mg)				
Release day				
Implant, print temperature, flow rate	***1***	***2***	***3***	***4***
HMW PCL – LDC 30%, 110 °C, 35 ml/min	48.33 ± 7.51	10.47 ± 7.65	7.47 ± 7.88	1.52 ± 7.79
HMW PCL – LDC 30%, 110 °C, 8 ml/min	32.19 ± 2.66	10.11 ± 0.76	6.59 ± 0.91	2.03 ± 1.16
HMW PCL – LDC 30%, 70 °C, 8 ml/min	33.12 ± 0.17	9.92 ± 0.42	6.36 ± 0.23	2.08 ± 1.25
HMW PCL – LDC 5%, 110 °C, 8 ml/min	5.68 ± 1.11	1.96 ± 0.59	1.05 ± 0.32	0.74 ± 0.95
HMW PCL - HMW PCL–LDC 30%, 110 °C, 8 ml/min	1.71 ± 0.53	0.80 ± 0.20	0.69 ± 0.27	0.52 ± 0.48

The drug release rate was, in general, faster during the first day of the dissolution study in all the differently fabricated formulations and then, it slowed on the second day, according to ***Figure 5.5*** and ***Table 5.1***. However, this effect was less intense in the HMW PCL encased implants indicating that the polymeric shell was degrading over time and allowing the release of the loaded drug for a prolonged period.

The higher flow rate applied during the four-day-long dissolution study had a significant impact on the amount of the active substance released from the 30% w/w lidocaine loaded PCL implants compared to the lower flower rate (***Table 5.1***). The enhanced release of the drug was more evident during the first day (***Figure 5.5***); the amount of the drug released from the tested formulations after one day of dissolution with a flow rate of 35 ml/min was 48.33 ± 7.51 mg compared to the 32.19 ± 2.66 mg for the 8 ml/min flow rate. This is presumably related to the faster flow rate promoting PCL degradation and more rapid removal (and hence, diffusion) of the drug. In contrast, in regard to the various printing settings used for implant manufacture, there was no impact on the amount of the released drug.

Comparison of the lidocaine release data from the 3D printed formulations with the dosage forms already in the market demonstrated the potential effectiveness of the printed implants. In the present study, the active ingredient released over the first 24 hours from the 30% w/w lidocaine loaded polymeric implants was almost double the amount of the drug delivered from the commercially available lidocaine adhesive patches, Lidoderm® and ZTLido® and below the recommended maximum total dose, 300 mg or 4.5 mg/kg for a healthy adult in 24 hours; lidocaine effective dose range in plasma is between 1 to 5 μg/ml/kg (Gudin and Nalamachu, 2020) (G*udin et al*., 2020). In contrast, the HMW PCL-LDC 5% implants and HMW PCL barrier-shell HMW PCL-LDC 30% implants under the conditions tested here released less drug than the commercial products. Hence, here for the 3D printed PCL dosage forms therapeutic lidocaine levels can be achieved when higher than 5% drug loading was applied (Kau *et al.*, 2014) (Shao *et al.*, 2018).

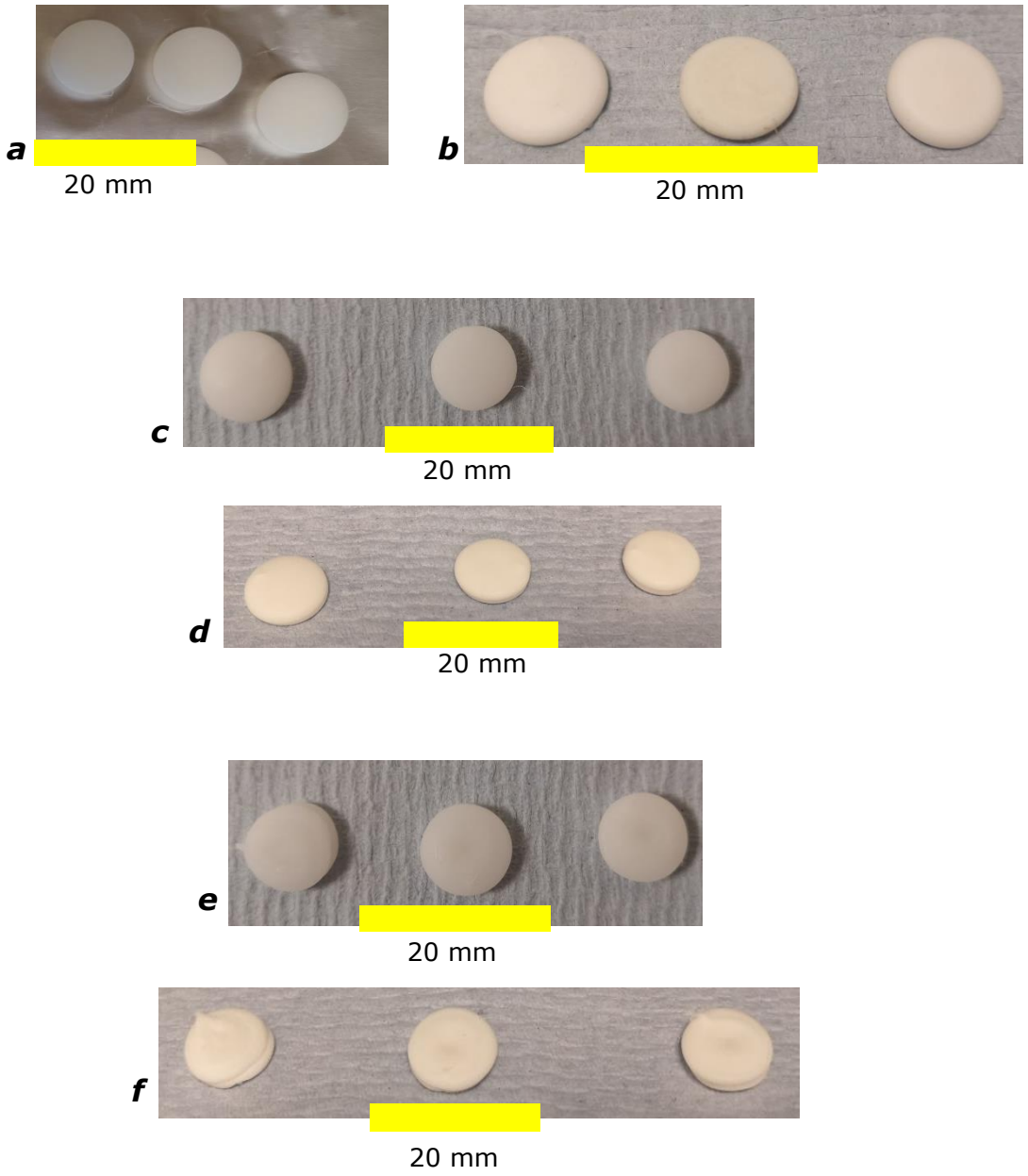

Figure 5.6: *HMW PCL-LDC 30% implants printed at* ***(a):*** *110 °C before dissolution,* ***(b):*** *110 °C after dissolution with a 35 ml/min flow rate,* ***(c):*** *110 °C before dissolution,* ***(d):*** *110 °C after dissolution with an 8 ml/min flow rate,* ***(e):*** *70 °C before dissolution and* ***(f):*** *70 °C after dissolution with an 8 ml/min flow rate. The scale bar is 20 mm and is labelled on each image separately.*

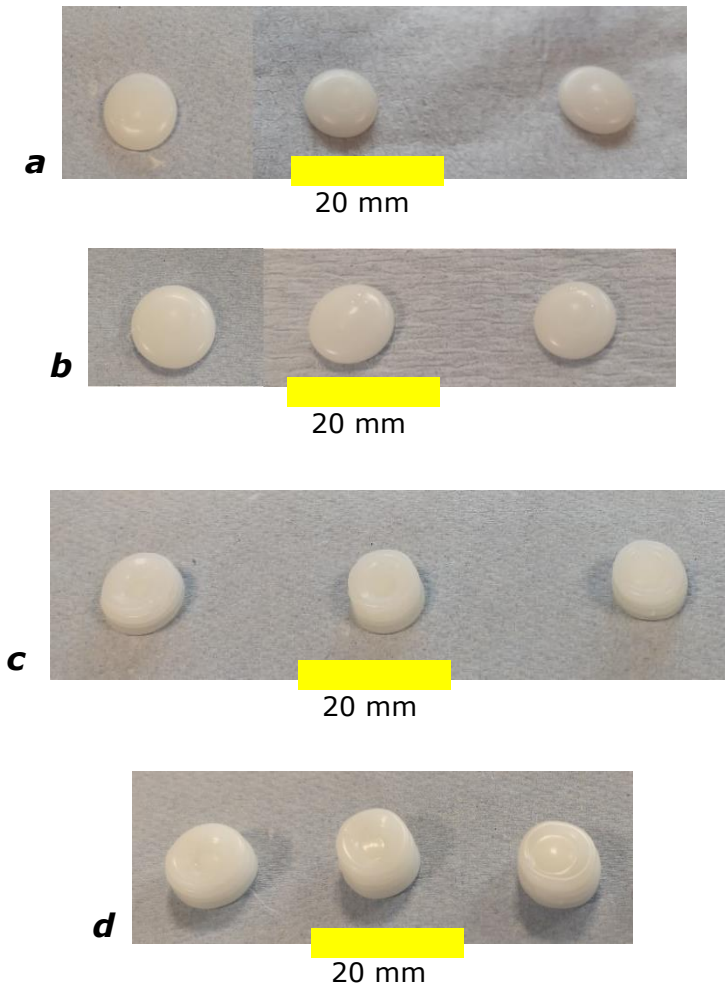

Figure 5.7:(a): *HMW PCL-LDC 5% implants printed at 110 °C before dissolution,* ***(b):*** *HMW PCL-LDC 5% implants printed at 110 °C after dissolution with an 8 ml/min flow rate,* ***(c):*** *HMW PCL - HMW PCL-LDC 30% implants printed at 110 °C before dissolution and* ***(d):*** *HMW PCL - HMW PCL-LDC 30% printed at 110 °C after dissolution with an 8 ml/min flow rate. The scale bar is 20 mm and is labelled on each image separately.*

The implants before and after the four-day dissolution studies were visually unchanged, as demonstrated in ***Figure 5.6*** and ***Figure 5.7***. In fact, no significant changes were expected to occur in the implants since the PCL degradation is very slow and the dissolution medium did not enhance this process (Fernández, Etxeberria and Sarasua, 2015) (Domingos *et al.*, 2010). Further analysis is needed to detect any surface modifications of the implants after the completion of the drug release tests.

Table 5.2: *Average weight of HMW PCL – LDC 30% implants printed at 110 °C before and after dissolution with a flow rate of 35 ml/min (N=3), HMW PCL – LDC 30% implants printed at 110 °C before and after dissolution with a flow rate of 8 ml/min (N=3), HMW PCL – LDC 30% implants printed at 70 °C before and after dissolution with a flow rate of 8 ml/min (N=3), HMW PCL – LDC 5% implants printed at 110 °C before and after dissolution with a flow rate of 8 ml/min (N=3), HMW PCL - HMW PCL–LDC 30% implants printed at 110 °C before and after dissolution with a flow rate of 8 ml/min (N=3), pure HMW PCL implants printed at 110 °C before and after dissolution with a flow rate of 8 ml/min (N=3) and average weight of lidocaine released after four days of dissolution (N=3 for each lidocaine loaded implant type).*

Implant type, print temperature, flow rate	***Implants weight before dissolution (mg)***	***Implants weight after dissolution (mg)***	***Implants weight difference before and after dissolution (mg)***	***Lidocaine released after dissolution (mg)***
HMW PCL – LDC 30%, 110 °C, 35 ml/min	332.03 ± 6.32	242.82 ± 4.62	89.21 ± 6.86	73.06 ± 7.83
HMW PCL – LDC 30%, 110 °C, 8 ml/min	321.05 ± 7.24	266.24 ± 5.99	54.81 ± 6.27	49.86 ± 1.95
HMW PCL – LDC 30%, 70 °C, 8 ml/min	317.05 ± 8.17	261.56 ± 8.33	55.49 ± 1.24	50.26 ± 2.84
HMW PCL – LDC 5%, 110 °C, 8 ml/min	328.24 ± 4.22	314.16 ± 3.77	14.08 ± 1.42	7.88 ± 1.44
HMW PCL - HMW PCL–LDC 30%, 110 °C, 8 ml/min	731.75 ± 2.34	708.12 ± 5.77	23.63 ± 6.57	3.07 ± 0.88
HMW PCL, 110 °C, 8 ml/min	285.54 ± 3.85	276.85 ± 3.83	8.69 ± 2.04	

However, by weighing the lidocaine loaded polycaprolactone implants before and after the completion of the *in vitro* drug release tests, the total mass loss for each implant type was more than the amount of the released drug (***Table 5.2***). Since the 3D printed formulations consisted of only lidocaine and HMW PCL, this weight difference indicated that polymer erosion whilst slow had occurred enough to show a weight change following dissolution. This was also verified by the fact that the weight of the pure HMW PCL implants after four days of dissolution decreased by 3.04% ± 1.01.

The two different medium flow rate settings, as well as, the drug loading had an impact on the total mass loss from the investigated discs. At the highest flow rate, 35 ml/min, a 26.87% ± 1.73 mass loss for the HMW PCL–LDC 30% implants was measured, compared to 17.07% ± 0.46 for the same implants at 8 ml/min. This shows that the higher flow rate enhanced polymer degradation, as proposed earlier.

Even though the formulations printed at higher temperatures closer to the melting point of the used compounds demonstrated a different surface nature (***Figure 4.13, Figure 4.14***), no significant variation was detected in their mass loss or lidocaine release profiles (***Figure 5.5***).

As demonstrated in ***Table 5.2***, the weight of the formulations with 5% w/w lidocaine loading exhibited a smaller percentage weight decrease of 4.29% ± 0.39 compared to 17.07% ± 0.46 of the implants with 30% w/w drug. An explanation could be that the higher drug loading corresponds to a larger API quantity in the implant and as the release rates of the low and high loadings are similar, the total drug amount released is higher for the 30% w/w drug loaded implants. The particles of the drug were the ones that mostly contributed to the weight change of the discs, since they were released from the polymeric carrier. Furthermore, the degradation rate of the HMW PCL is very slow (Gunatillake and Adhikari, 2003) (Middleton and Tipton, 2000). The latter is in good correspondence with the mass loss data calculated for the HMW PCL core-shell drug loaded polymeric implants, as well as, the pure HMW PCL discs after the dissolution test; 3.23% ± 0.48 and 3.04% ± 0.01 respectively. In these cases, it was also observed that the amount of the released active substance contributed to a relatively higher reduction in the formulations weight compared to the drug free polymeric dosage forms.

5.2.3. Characterization of the lidocaine loaded polycaprolactone implants before and after dissolution studies

Based on the dissolution studies performed in the USP4 – flow-through cell apparatus and the released lidocaine measured in a UV-Vis spectrometer, sustained drug release has been achieved with the HMW PCL encased and non-encased 3D printed implants. However, due to the slow PCL degradation rate, no obvious surface changes could visually be seen, even though the weight of the formulations before and after the *in vitro* drug release tests indicated that a small amount of polymer erosion had occurred. Consequently, SEM and Raman analyses were conducted to investigate the implants integrity, the materials distribution and the first stages of PCL degradation.

5.2.3.1. SEM Characterization

PCL implants printed with various settings and different drug loading were characterized by SEM to explore whether any modifications had occurred on their surface after the four-day-long dissolution studies.

SEM images (***Figure 5.8-12***) after dissolution for all samples showed a small number of pits on their surface consistent with a slow PCL degradation rate and consequent slow lidocaine release (***Figure 5.5***) and small mass loss (***Table 5.2***), especially in the case of the HMW PCL barrier-shell HMW PCL – LDC 30% formulations. Small cavities on the surface of the other PCL formulations have also been detected after several days of dissolution in previously published studies (Díaz, Sandonis and Valle, 2014) (Ferreira *et al.*, 2017) (Wang *et al.*, 2010).

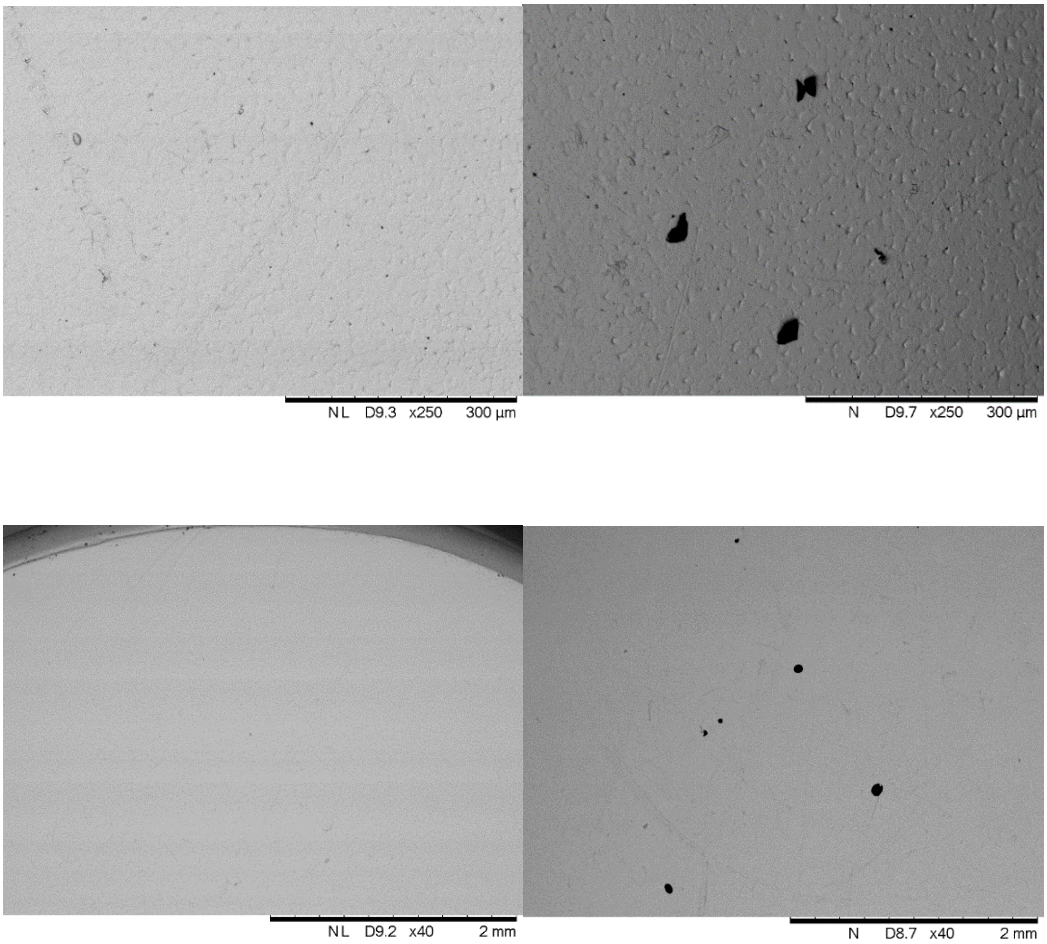

Figure 5.8: *SEM images of pure HMW PCL implants printed at 110 °C before (left image) and after (right image) dissolution with a flow rate of 8 ml/min* ***(a):*** *top side and* ***(b):*** *bottom side. The magnification and the scale bar are labelled on each SEM image separately.*

SEM images of the HMW PCL non-encased lidocaine loaded implants after four days of dissolution, exhibited some irregular shaped holes in the range of 25 - 45 µm on the surface of the discs (***Figure 5.9, Figure 5.10, Figure 5.11***), consistent with the release of the drug, the decrease of the implants weight and the beginning of PCL degradation (Perale *et al*., 2010) (Cheng, Guo and Wu, 2009) (Campbell *et al.*, 2009). The latter has likely led to the smoother surface revealed after the release of the active ingredient (***Figure 5.10***). These observations indicated that the release of the drug occurs from the core parts of the discs through these open channels as water penetrated the degrading PCL matrix.

a

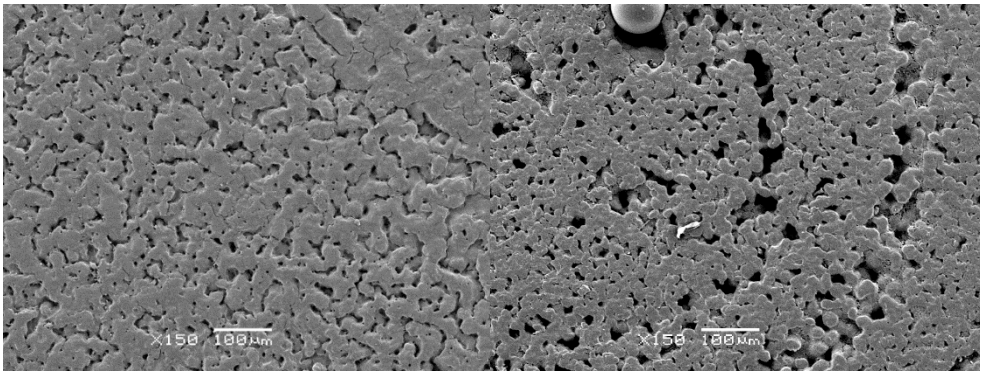

b

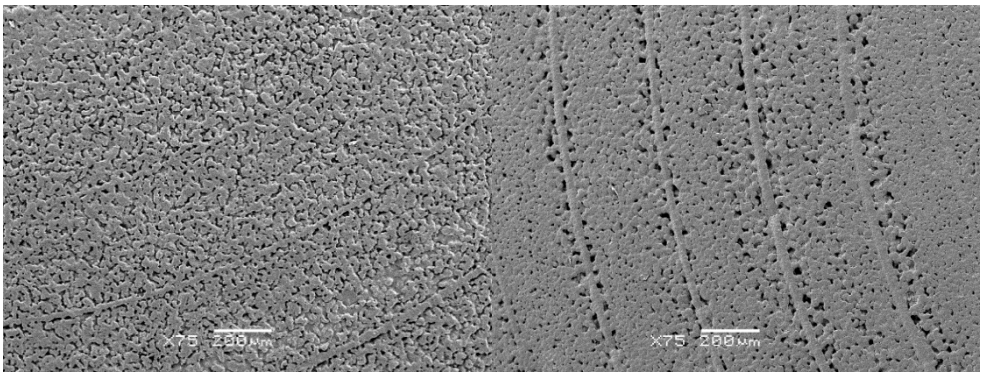

c

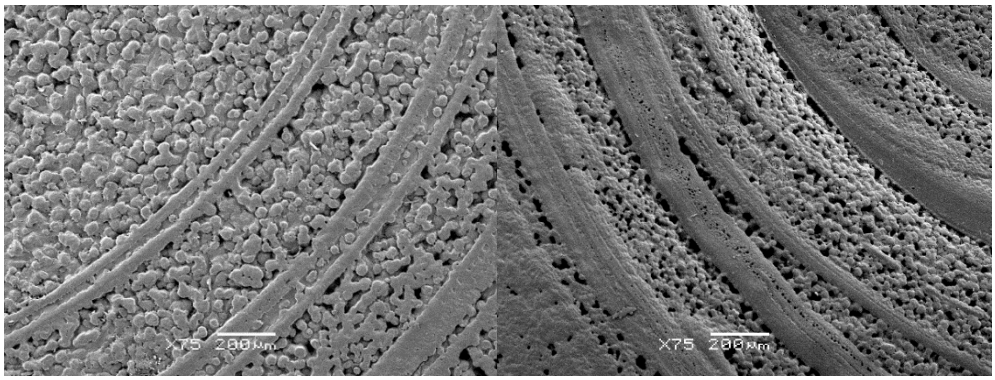

<u>Figure 5.9:</u> *SEM images of the top side of HMW PCL-LDC 30% implants* ***<u>(a):</u>*** *printed at 110 °C before (left image) and after (right image) dissolution with a flow rate of 35 ml/min,* ***<u>(b):</u>*** *printed at 110 °C before (left image) and after (right image) dissolution with a flow rate of 8 ml/min and* ***<u>(c):</u>*** *printed at 70 °C before (left image) and after (right image) dissolution with a flow rate of 8 ml/min. The magnification and the scale bar are labelled on each SEM image separately.*

a

b

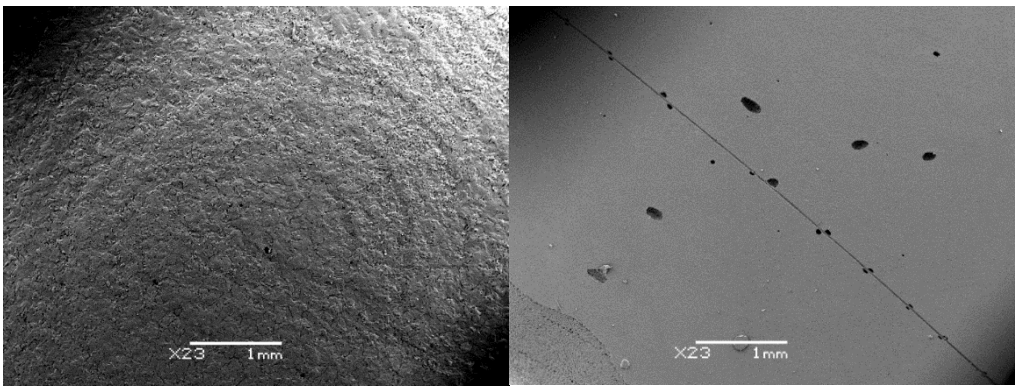

c

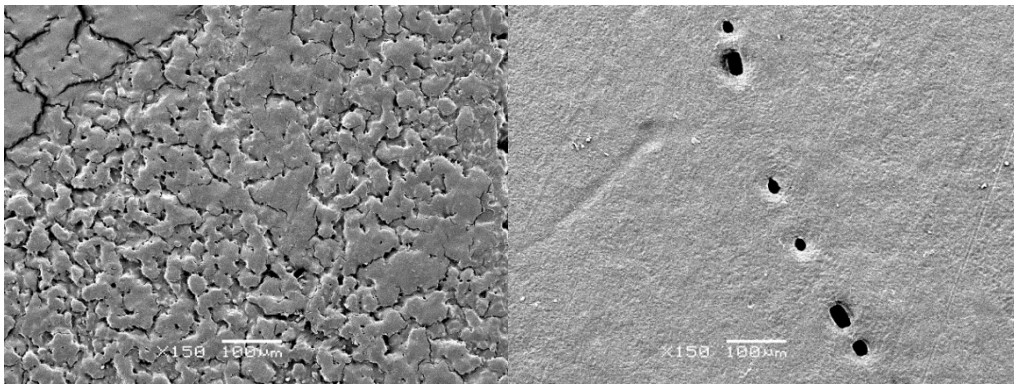

Figure 5.10: *SEM images of the bottom side of HMW PCL-LDC 30% implants* ***(a):*** *printed at 110 °C before (left image) and after (right image) dissolution with a flow rate of 35 ml/min,* ***(b):*** *printed at 110 °C before (left image) and after (right image) dissolution with a flow rate of 8 ml/min and* ***(c):*** *printed at 70 °C before (left image) and after (right image) dissolution with a flow rate of 8 ml/min. The magnification and the scale bar are labelled on each SEM image separately.*

As displayed in the SEM images of the top side of the 30% w/w and 5% w/w lidocaine loaded PCL implants, ***Figure 5.9*** and ***Figure 5.11.a***, the apertures mainly appeared at the interfaces of the printed lines, indicating that the polymer in these areas was more susceptible to erosion, possibly due to an increased surface area. A similar pattern, though, was not observed in the bottom side of the drug loaded polymeric formulations (printed onto the flat substrates), as presented in the SEM images in ***Figure 5.10*** and ***Figure 5.11.b***, where holes in random locations of the discs occur.

a

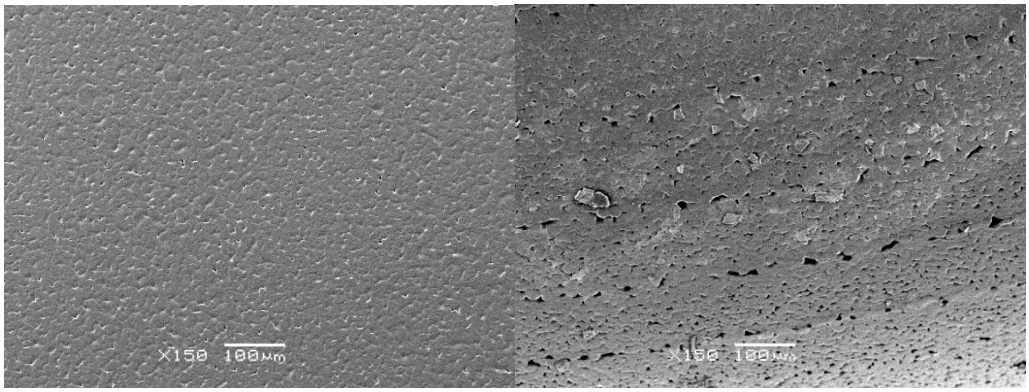

b

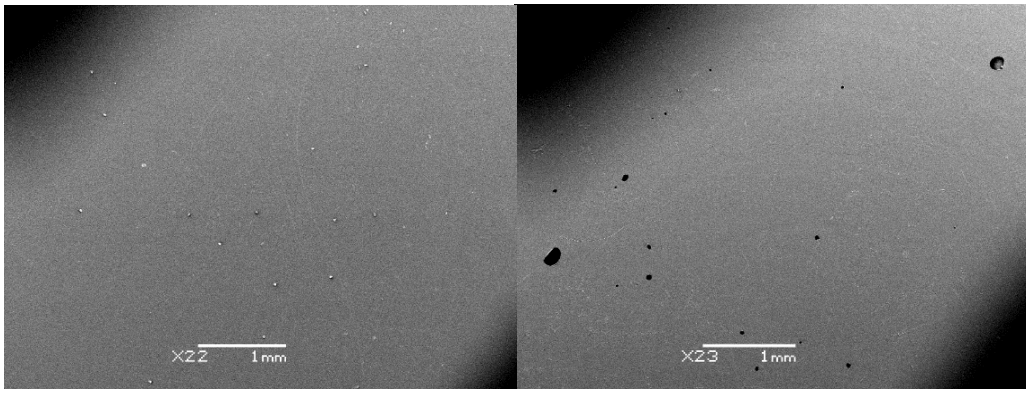

Figure 5.11: *SEM images of HMW PCL-LDC 5% implants printed at 110 °C before (left image) and after (right image) dissolution with a flow rate of 8 ml/min* ***(a):*** *top side and* ***(b):*** *bottom side. The magnification and the scale bar are labelled on each SEM image separately.*

a

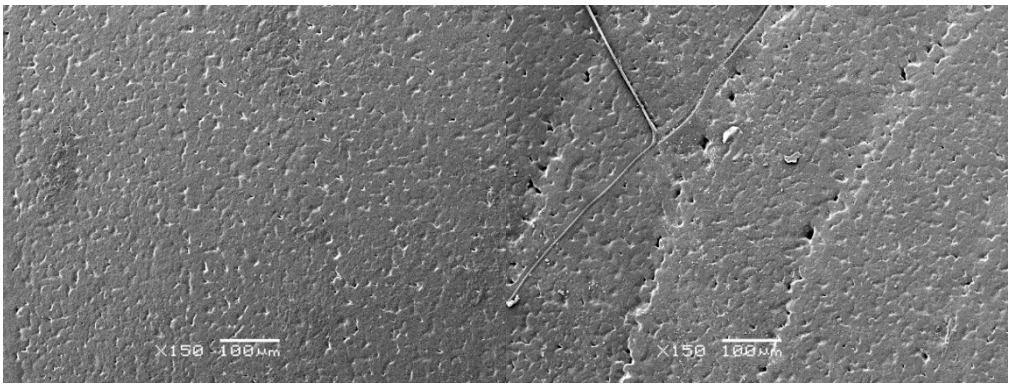

b

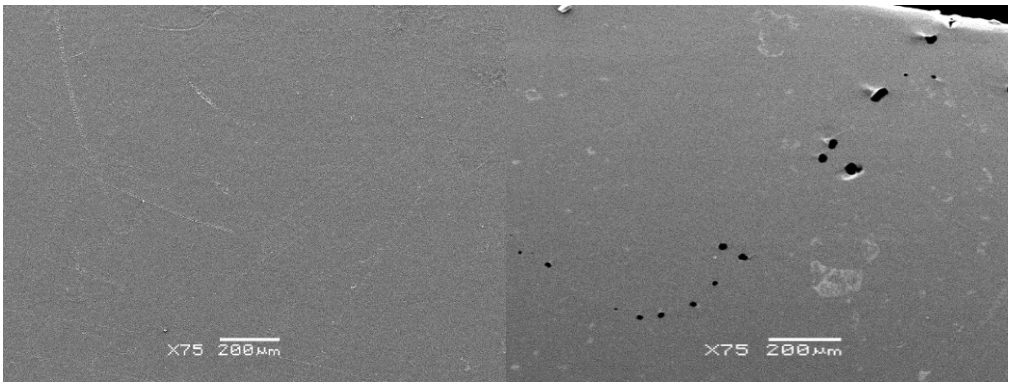

c

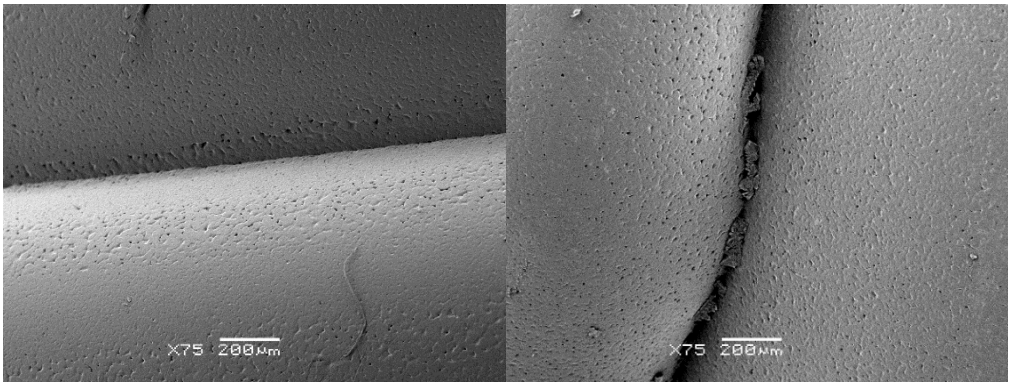

Figure 5.12: *SEM images of HMW PCL - HMW PCL-LDC 30% implants printed at 110 °C before (left image) and after (right image) dissolution with a flow rate of 8 ml/min* ***(a):*** *top side,* ***(b):*** *bottom side and* ***(c):*** *outside layers. The magnification and the scale bar are labelled on each SEM image separately.*

Lidocaine loaded PCL implants printed with different settings showed the same surface characteristics after the dissolution. The media flow rate was the only investigated parameter that had an impact on the creation of cavities as might be expected given its impact on weight loss and drug release. When the flow rate was 35 ml/min more holes were detected (***Figure 5.10.a***) compared to a flow rate of 8 ml/min (***Figure 5.10.b, Figure 5.10.c, Figure 5.11***).

In the case of the HMW PCL barrier-shell HMW PCL-LDC 30% implants, the outer surface consisted of pure HMW PCL and only a few small pores with an average size of around 20 μm were visible after dissolution (***Figure 5.12.a, Figure 5.12.b***). Furthermore, some gaps were detected between the printed layers, as can be seen in ***Figure 5.12.c***. The polymer in these areas seemed to be more susceptible to degradation similarly to the connection between the printed lines. Collectively, these would have contributed to the release of the drug from the internal compartments of the manufactured implants at a rate consistent with the long-term release.

Consequently, based on the dissolution profiles of the differently printed formulations (***Figure 5.5***) and their SEM images after drug release studies, it was suggested that a solid dispersion has been formed, where the encapsulated active agent was slowly released by the polymeric matrix based on the material properties of polycaprolactone, its low degradation rate (***Figure 5.8, Figure 5.9, Figure 5.10, Figure 5.11, Figure 5.12***).

5.2.3.2. Raman Characterization

Raman analysis has been performed on the surface of the 30% w/w lidocaine loaded PCL implants printed at 70 and 110 ^{o}C after their dissolution studies with a medium flow rate of 8 ml/min to investigate the materials distribution both in the matrix and the apertures detected during the SEM characterization.

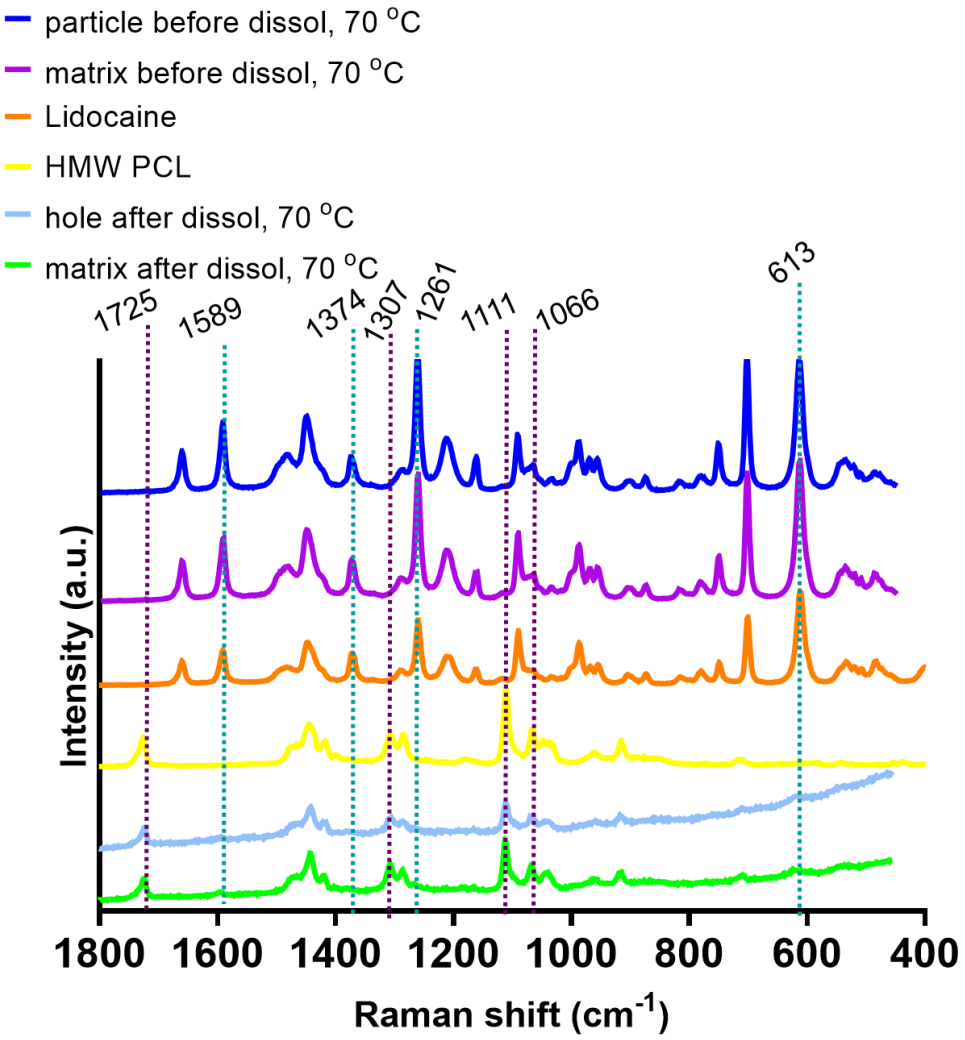

Figure 5.13: *Raman spectra of surface particles, matrix and holes of HMW PCL-LDC 30% implants printed at 70 °C before and after dissolution with a flow rate of 8 ml/min. Lidocaine peaks are highlighted with the blue dot-line and Polycaprolactone peaks with the purple dot-line.*

As depicted in ***Figure 5.13*** and ***Figure 5.14***, the spectra recorded from the holes and the matrix of the implants after the dissolution were identical with each other at each print temperature, similarly to the spectra of the surface particles and the matrix of the implants before the dissolution. Nevertheless, the Raman spectra of the surface attributes of the implants after the drug release test were considerably different from the spectra of the surface particles and the matrix before that test. Fewer peaks were detected in the spectra of the formulations after the release of lidocaine and these peaks were mainly assigned to the characteristic peaks of the polymer; 1725, 1442, 1421, 1307, 1111, 1066, 1043, 917 and 714 cm^{-1}.

Furthermore, the intensity of some of these peaks demonstrated a small increase in the after dissolution samples, while the intensity of the few lidocaine bands in the same spectra decreased, indicating the successful release and hence, depletion of the drug from the implants surface region.

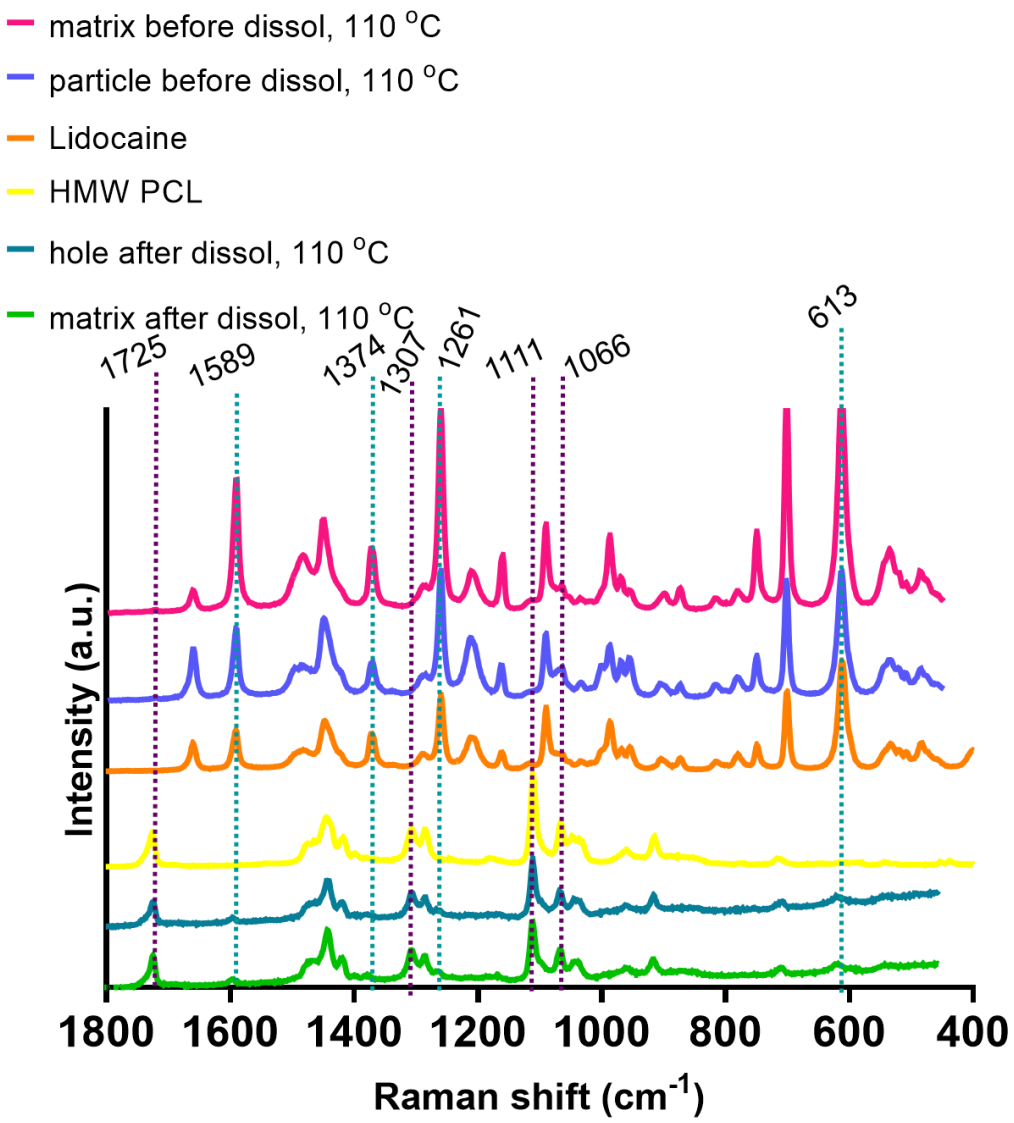

Figure 5.14: *Raman spectra of surface particles, matrix and holes of HMW PCL-LDC 30% implants printed at 110 °C before and after dissolution with a flow rate of 8 ml/min. Lidocaine peaks are highlighted with the blue dot-line and Polycaprolactone peaks with the purple dot-line.*

In the spectra of the implants printed at 70 ºC, according to ***Figure 5.13***, peaks at 1589, 1374, 1261 and 613 cm^{-1} can be attributed to lidocaine, while the peak intensity for the matrix after the dissolution was 11.6 , 25.6 , 10.4 and 14.6 % of the peak intensity before the dissolution, respectively. The opposite effect was observed in the case of the characteristic bands of the polymer at 1066 and 1043 cm^{-1}, where the peak intensity for the matrix after the drug release study was 111.3 and 129.3 % of the peak intensity before that study, respectively. This is consistent with the depletion of the drug from the near surface region leaving behind predominantly polymer.

The intensities of the bands of the polymer and the drug after the dissolution, as presented in the Raman spectra of the formulations printed at 110 ºC (***Figure 5.14***) exhibited similar behaviour with the peaks of the implants printed at a lower temperature. More specifically, the intensity for the lidocaine peaks 1589, 1374, 1261 and 613 cm^{-1} detected in the sample matrix after the drug release was 6.2, 18.5 , 8.0 and 10.7 % of the band intensity before the drug release, respectively. As for the PCL peaks at 1066 and 1043 cm^{-1}, the percentage of the intensity ratio after/before the dissolution was 122.5 and 149.1 %, respectively.

Even though the intensity of the LDC peaks in the samples after the dissolution was significantly lower than in the initial samples, it did not represent the percentage of the released drug as measured in the UV-Vis spectroscopy; based on the peaks intensity ratio, more than 55 % of lidocaine has been released from the polymeric formulations. This could be explained by the fact that Raman is a near-surface measurement, which means that the obtained spectra reflect the composition of the samples surface only, while for the calculation of the released drug the total amount of the loaded drug was compared with the measured drug in the solutions collected during the dissolution study (Bumbrah and Sharma, 2016).

Similarly, the fact that the intensity of the peaks corresponding to the polymer has been increased and was higher than 100%, did not mean that higher quantities of polymer were present on the implants surface after the dissolution compared to the as-printed samples. Lidocaine was mainly released from the implants surface in the first days of the dissolution and hence, less lidocaine was remaining in this area. As mentioned previously, Raman is a near-surface measurement, while the sampling area was 1 μm with a depth of analysis of 5-10 μm. Therefore, it was highly likely that the analyzed area had PCL in a relatively

higher concentration than the active compound leading to higher intensity peaks for the polymer and lower intensity peaks for the active substance appearing in the Raman spectra, respectively (Cleveland *et al.*, 2007).

5.2.4. Drug Release Kinetics

The drug release mechanism of the 3D printed implants was further investigated by plotting the dissolution data in different mathematical models: Zero-order, First-order, Higuchi model and Korsmeyer-Peppas model. Linear regression was applied and the squared correlation coefficient (R^2) was compared among the models to indicate potential transportation mechanisms of lidocaine from the HMW PCL matrix.

As presented in ***Table 5.3***, the Korsmeyer-Peppas model was found to be the best fit for all the printed formulations. More specifically, for the implants printed without the HMW PCL barrier-shell after 4 days of dissolution, the release exponent value was $n < 0.45$, indicating that the drug release mechanism was diffusion related partially through the polymeric matrix and partially through holes on the formulation surface (Ritger and Peppas, 1987a) (Ritger and Peppas, 1987b). This is consistent with the SEM and Raman characterization, where apertures were detected on the surface of the formulations after the four-days long dissolution study, suggesting that the active agent was initially released from the surface. These openings would then facilitate the penetration of the medium through the matrix reaching the active agent that was enclosed in the internal compartments.

The different printing settings, drug loading and the medium flow rates used during the dissolution study did not affect the lidocaine transportation mechanism, as depicted in ***Figure 5.15, Figure 5.17, Figure 5.18, Figure 5.19***.

Table 5.3: *Release kinetics parameters of different formulations over 4 days of dissolution: HMW PCL – LDC 30% implants printed at 110 °C after dissolution with a flow rate of 35 ml/min, HMW PCL – LDC 30% implants printed at 110 °C after dissolution with a flow rate of 8 ml/min, HMW PCL – LDC 30% implants printed at 70 °C after dissolution with a flow rate of 8 ml/min, HMW PCL – LDC 5% implants printed at 110 °C after dissolution with a flow rate of 8 ml/min, HMW PCL - HMW PCL–LDC 30% implants printed at 110 °C after dissolution with a flow rate of 8 ml/min.*

Kinetics models									
Formulation, print temperature, flow rate	***Zero-order***		***First-order***		***Higuchi***		***Korsmeyer-Peppas***		
	R^2	K_0	R^2	K_1	R^2	K_H	R^2	K_{K-P}	n
HMW PCL – LDC 30%, 110 °C, 35 ml/min	0.118	0.0173	0.9504	-0.00008	0.82	1.0796	0.9893	4.682	0.3163
HMW PCL – LDC 30%, 110 °C, 8 ml/min	0.5495	0.0142	0.9593	-0.00007	0.9567	0.8682	0.9902	1.953	0.4002
HMW PCL – LDC 30%, 70 °C, 8 ml/min	0.511	0.0145	0.9555	-0.00007	0.9468	0.8906	0.9867	2.120	0.3933
HMW PCL – LDC 5%, 110 °C, 8 ml/min	0.7001	0.0135	0.9805	-0.00006	0.9852	0.7964	0.9856	1.7065	0.3898
HMW PCL - HMW PCL– LDC 30%, 110 °C, 8 ml/min	0.9211	0.0012	0.9268	-0.00006	0.9186	0.0705	0.9728	39.228	0.6234

R^2: squared correlation coefficient, K_0: zero-order release constant, K_1: first-order release constant, K_H: release rate constant of Higuchi, K_{K-P}: release rate constant of Korsmeyer-Peppas and n: drug release exponent.

According to the dissolution data of the HMW PCL-LDC 30% implant when a medium flow rate of 35 ml/min was applied (***Figure 5.5***), the total lidocaine release after four days was 66.08%. There is a limitation, though, in the Korsmeyer-Peppas model regarding the plotting of the data; only 60% of the cumulative amount of the released drug can be plotted (Ritger and Peppas, 1987a). Therefore, three-days-dissolution data could only be plotted in this mathematical model; the cumulative percentage of the released drug was detected to be 59.02% after three days of *in vitro* drug release test. For comparison, three days data should be plotted in the other three investigated models, as well, to effectively compare the squared correlation coefficient (R^2) among them with the aim to establish the transportation mechanism of lidocaine from the PCL matrix; the relevant graphs are depicted in ***Figure 5.16.*** The limitation of the Korsmeyer-Peppas model allows the four days dissolution data in the rest formulations studied to be plotted when a lower medium flow rate was applied (***Figure 5.17, Figure 5.18, Figure 5.19, Figure 5.20***).

Data of the released active substance from the 30% w/w lidocaine loaded polycaprolactone implants after a three days long drug release test with a medium flow rate of 35 ml/min were fitted to the four explored kinetics models (***Figure 5.16***)***.*** The Korsmeyer-Peppas model still exhibited the best fit similarly to the four days data presented in ***Figure 5.15.*** The release exponent value was in both cases $n < 0.45$, indicating that the drug release mechanism was controlled by Fickian diffusion; $n = 0.3208$ for the three days dissolution study and $n = 0.3163$ for the four-day dissolution study. Since no significant differences have been observed between the three and four days obtained data and the indications for the drug transport mechanism, it was preferred for consistency purposes the four days data to be used for the comparisons with the other formulations and dissolution studies. Consequently, in ***Table 5.3***, the squared correlation coefficients, release constants and drug release exponents correspond to the four days modelling data acquired from ***Figure 5.15, Figure 5.17, Figure 5.18, Figure 5.19, Figure 5.20***.

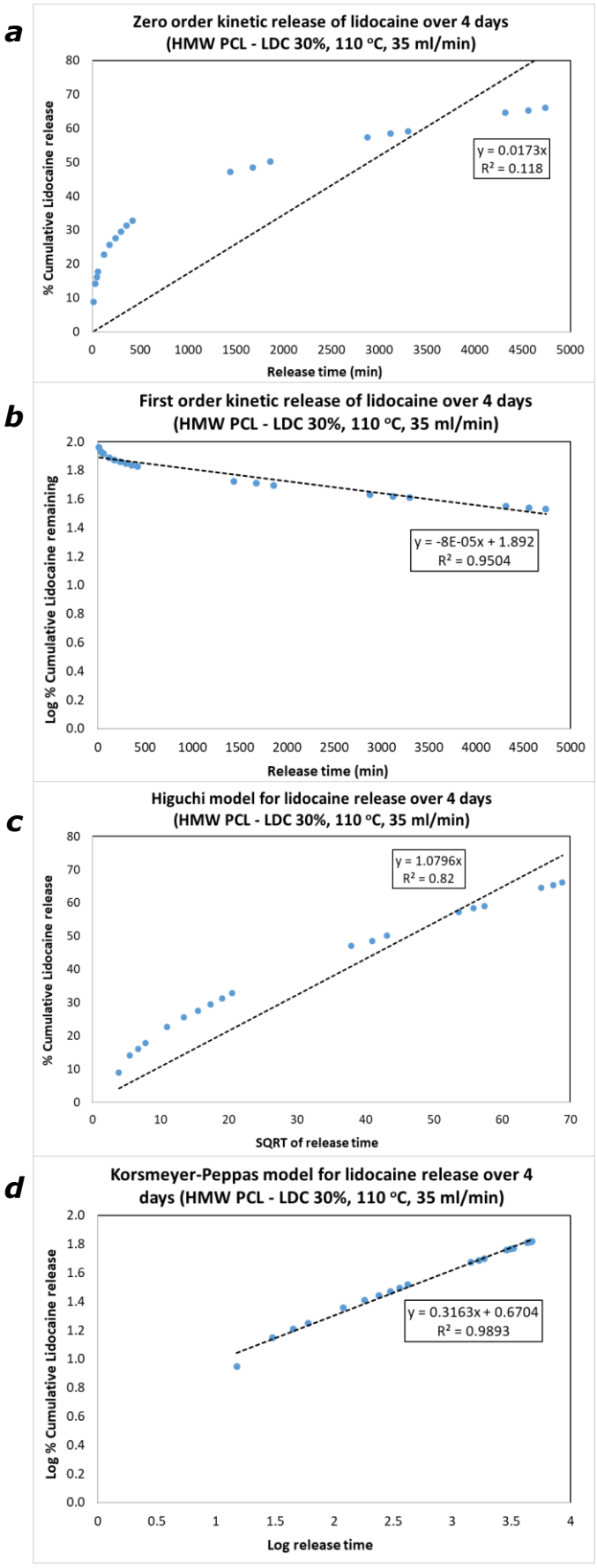

Figure 5.15: (a): *Zero-order,* ***(b):*** *First-order,* ***(c):*** *Higuchi and* ***(d):*** *Korsmeyer-Peppas model kinetic release for lidocaine from HMW PCL-LDC 30% implants printed at 110 °C over 4 days of dissolution with a flow rate of 35 ml/min.*

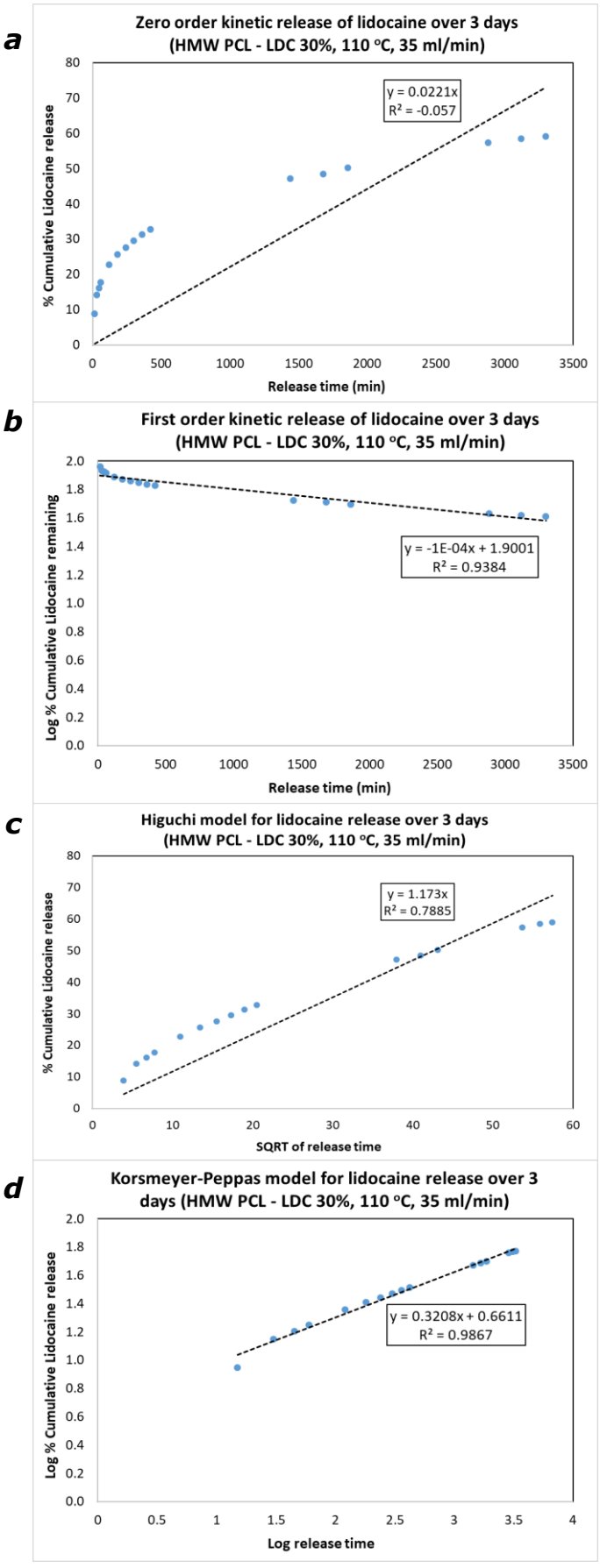

Figure 5.16: (a): *Zero-order,* ***(b):*** *First-order,* ***(c):*** *Higuchi and* ***(d):*** *Korsmeyer-Peppas model kinetic release for lidocaine from HMW PCL-LDC 30% implants printed at 110 °C over 3 days of dissolution with a flow rate of 35 ml/min.*

In the zero-order model fitting, though, ***Figure 5.15.a, Figure 5.16.a, Figure 5.17.a, Figure 5.18.a, Figure 5.19.a***, ***Figure 5.20.a,*** it is shown that the lidocaine release rate was faster during the first day, while after the second day it became slower and the same pattern was followed in the next days of the dissolution study for all the printed formulations, as previously observed (***Table 5.1, Figure 5.5***). This was also in good correspondence with the SEM observations where the holes formed by the lidocaine release from the implants surface and the beginning of the PCL degradation indicated that the release of the encapsulated active compound was initially happening from the external area of the formulation that was in direct contact with the dissolution medium. This was followed by the release of the active agent from the internal parts; dependent on the slow degradation rate of the polymeric matrix.

Based on the above observation, fitting of the drug release data to the four mathematic models was divided into two release periods, day 1 and days 2 – 4, for a more effective representation and investigation of the drug release mechanism. As displayed in ***Table 5.4*** and ***Table 5.5*** and ***Figure S.18, Figure S.19, Figure S.21, Figure S.22, Figure S.23, Figure S.24, Figure S.25, Figure S.26, Figure S.27, Figure S.28,*** the Korsmeyer-Peppas model was shown to have the closest to value of 1 for the squared correlation coefficient, R^2, compared to the other three examined models for the entire dissolution data. However, the release exponent value indicative of the drug release mechanism did not follow the same pattern in all the explored combinations of formulations-release period, as it was previously observed in ***Table 5.3*** for the 3D printed implants without a PCL barrier-shell. More specifically, for the HMW PCL-LDC 30% implant printed at 110 °C after a dissolution study with a 35 ml/min medium flow rate the release exponent value was $n < 0.45$ for both the first day and the rest of the period of the drug release study, similarly to the fitting of the data in the same graph (***Figure 5.15, Figure 5.16, Figure S.18, Figure S.19, Figure S.20***). It was, thereby, suggested a diffusion-related drug release mechanism was occurring to a certain extent through the polymeric matrix, as well as, through apertures on the formulation surface.

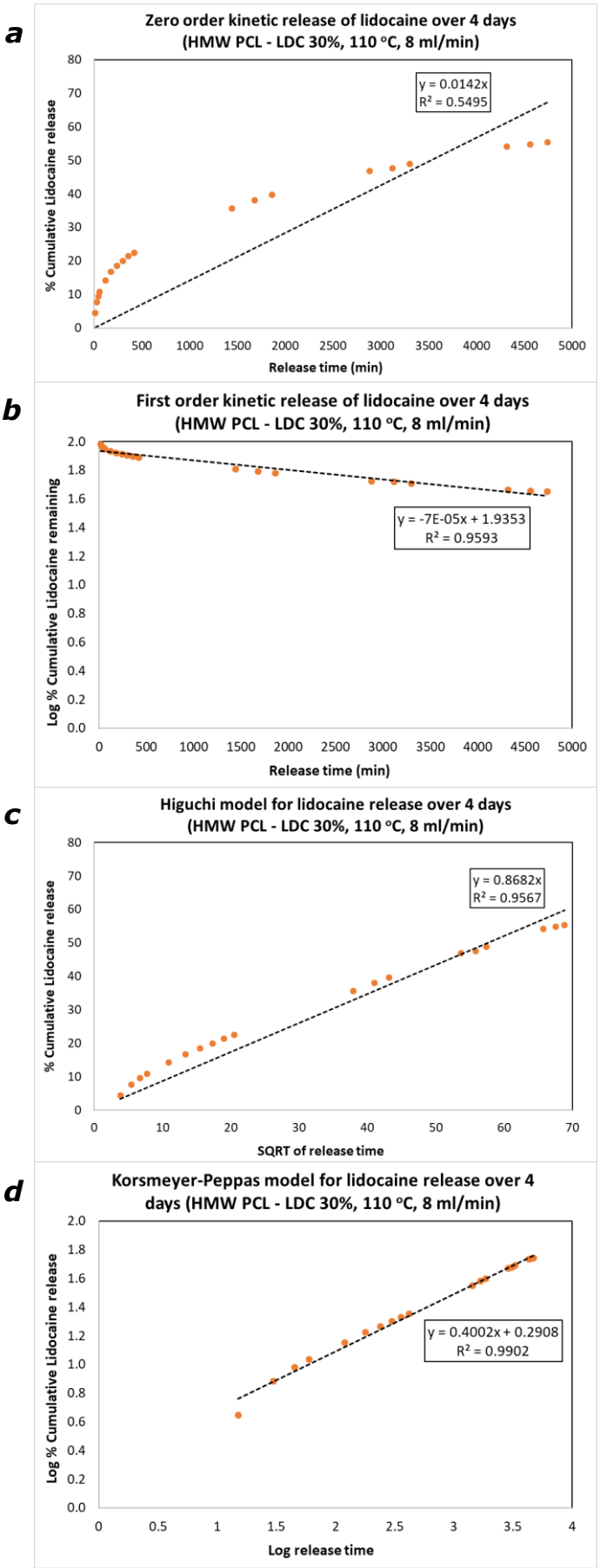

Figure 5.17: (a): *Zero-order,* ***(b):*** *First-order,* ***(c):*** *Higuchi and* ***(d):*** *Korsmeyer-Peppas model kinetic release for lidocaine from HMW PCL-LDC 30% implants printed at 110 °C over 4 days of dissolution with a flow rate of 8 ml/min.*

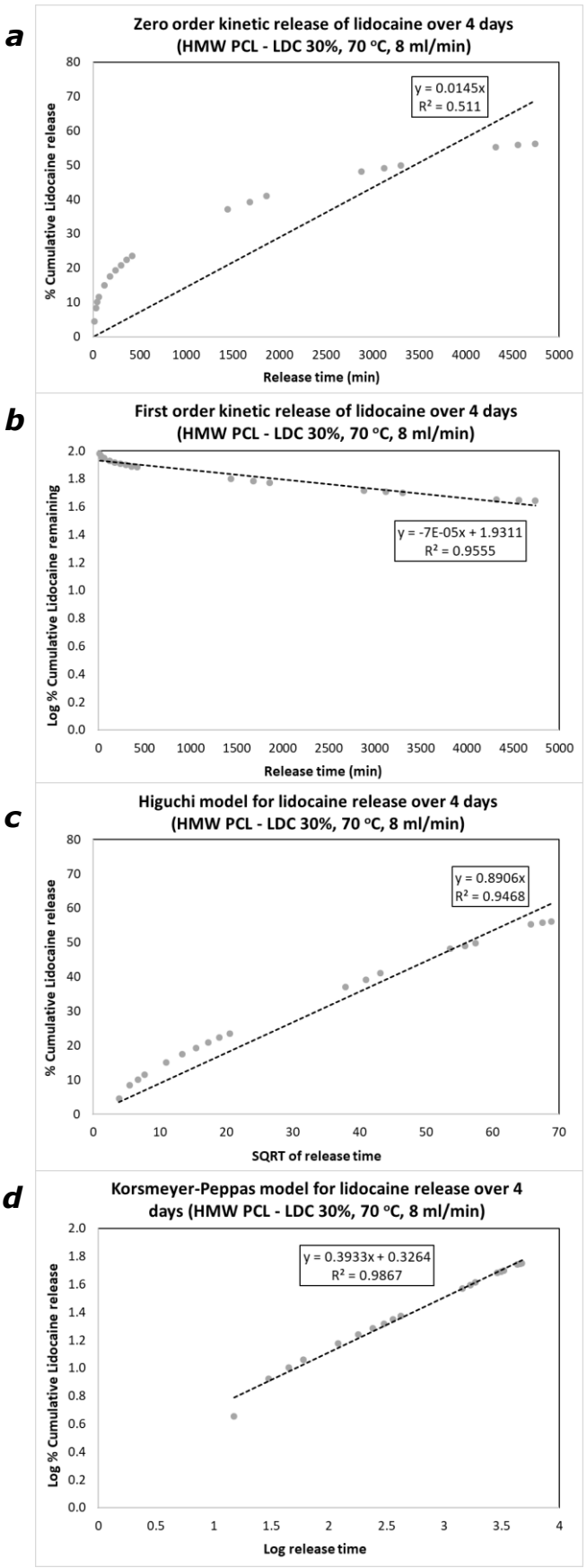

Figure 5.18: (a): *Zero-order,* ***(b):*** *First-order,* ***(c):*** *Higuchi and* ***(d):*** *Korsmeyer-Peppas model kinetic release for lidocaine from HMW PCL-LDC 30% implants printed at 70 °C over 4 days of dissolution with a flow rate of 8 ml/min.*

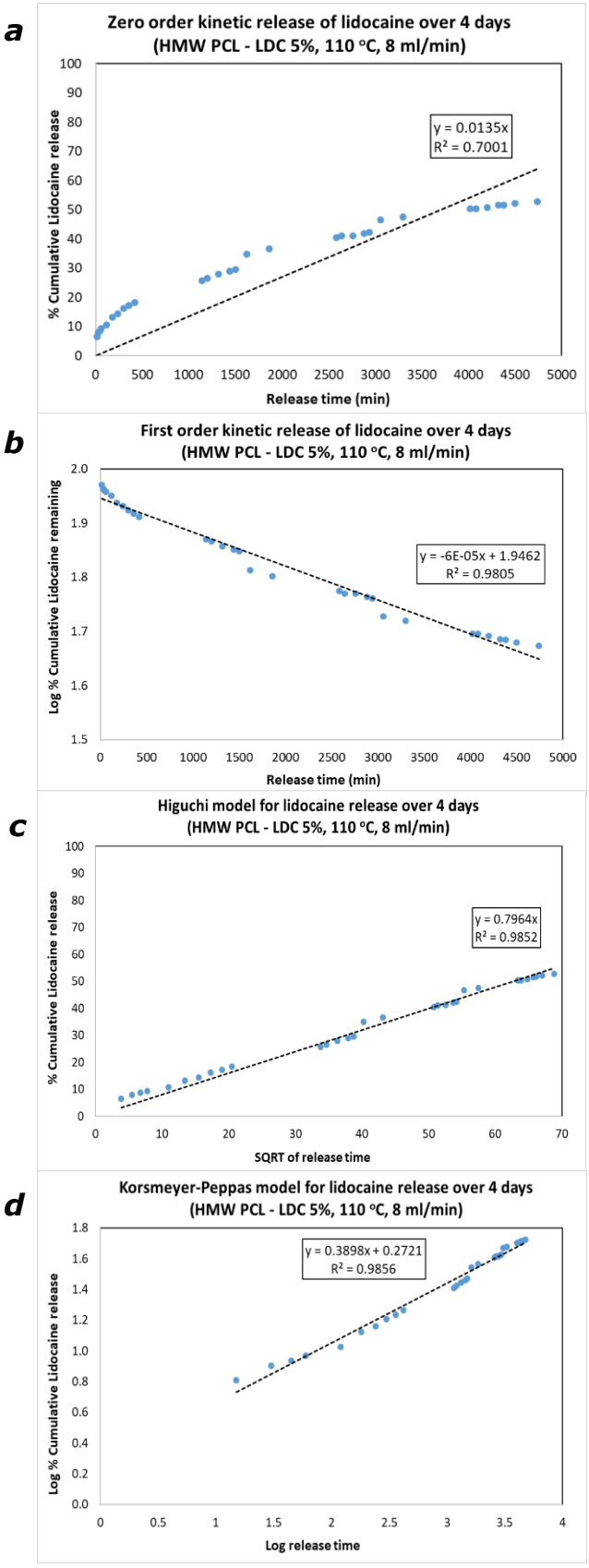

Figure 5.19: (a): *Zero-order,* ***(b):*** *First-order,* ***(c):*** *Higuchi and* ***(d):*** *Korsmeyer-Peppas model kinetic release for lidocaine from HMW PCL-LDC 5% implants printed at 110 °C over 4 days of dissolution with a flow rate of 8 ml/min.*

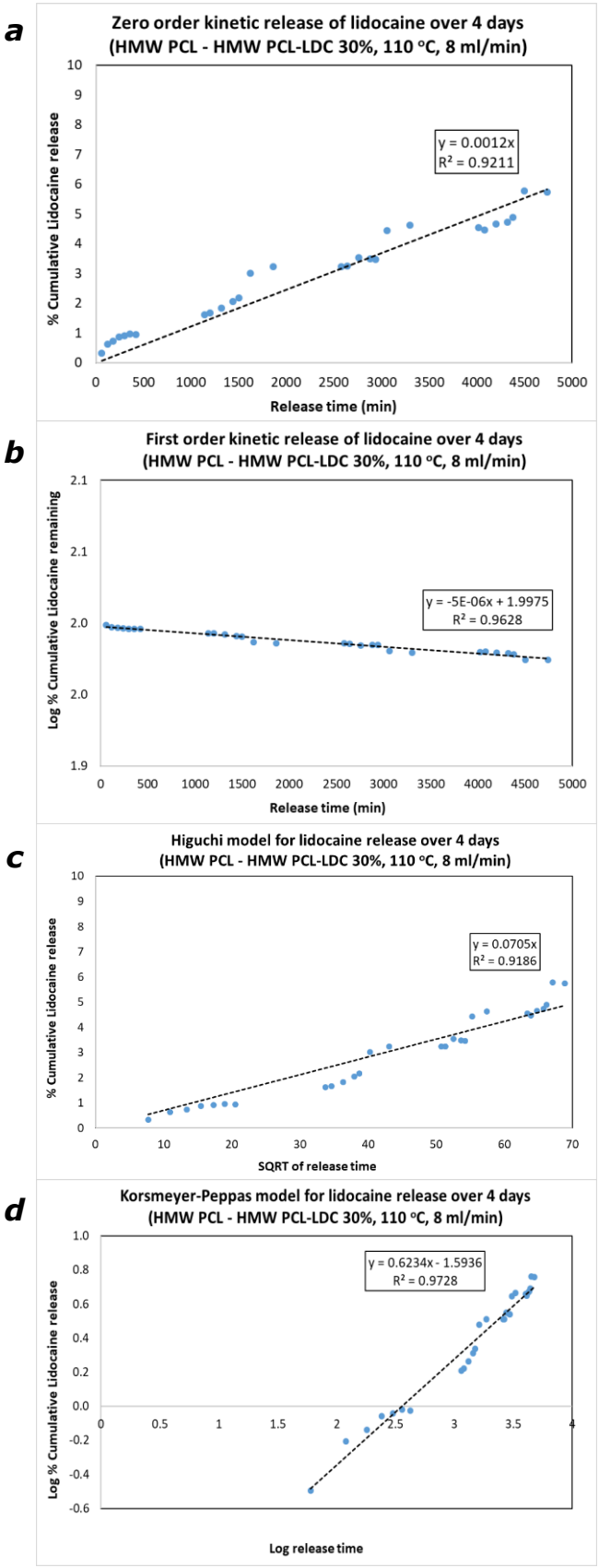

Figure 5.20: (a): *Zero-order,* ***(b):*** *First-order,* ***(c):*** *Higuchi and* ***(d):*** *Korsmeyer-Peppas model kinetic release for lidocaine from HMW PCL - HMW PCL-LDC 30% implants printed at 110 °C over 4 days of dissolution with a flow rate of 8 ml/min.*

For the dissolution study of the HMW PCL-LDC 30% implants printed at 110 °C and 70 °C with the lower medium flow rate, 8 ml/min, the release exponent value was $0.45 < n < 1$ during the first day of the study, but it was lower, $n < 0.45$ for the remaining period (***Table 5.4, Table 5.5, Figure S.21, Figure S.22, Figure S.23, Figure S.24***). Consequently, the suggested drug release mechanism for the first part of these *in vitro* drug release studies is the so-called "anomalous" transport, while for the second part, it is indicating diffusion through pores, similarly to the dissolution study where a higher medium flow rate was applied. In the "anomalous" transport, the release of the active ingredient is controlled by two mechanisms that might be happening simultaneously; here, diffusion and relaxation of polymeric chains (Ritger and Peppas, 1987a) (Ritger and Peppas, 1987b). The latter is caused by hydrolytic chain scission due to the temperature applied during the four-day-long *in vitro* drug release test. This results in PCL degradation and the creation of pores in the polymeric matrix. The dissolution medium could, then, gain access to the internal compartments via these holes to facilitate drug release through diffusion (Monte*iro et al*., 2016). Accordingly, the release of the enclosed lidocaine in the next days of the dissolution could occur through diffusion via the newly formed apertures.

In contrast, the release exponent value after the first day of dissolution of the HMW PCL-LDC 5% implant was $n < 0.45$, while it was $0.45 < n < 1$ for the remaining days of the study (***Table 5.4, Table 5.5, Figure S.25, Figure S.26***). These values mean that diffusion partially through the matrix and partially through pores was the suggested drug release mechanism based on the Korsmeyer-Peppas model during the first hours of the *in vitro* drug release test, followed by "anomalous" transport with two mechanisms occurring at the same time. The fact that the order of appearance of these mechanisms was reversed for the formulation with the lower drug loading could be explained by less of the active agent being resided on the surface of this formulation compared to the 30% lidocaine loaded implants and thus, less mass of lidocaine being released resulting in the slower creation of apertures on the implants surface. This is in agreement with the dissolution data in ***Table 5.2***. The holes on the surface were associated with the relaxation of the polymeric chains and they were promoting in this way, the PCL degradation, which was more intensively happening after the second day, while a diffusion related drug release was also occurring simultaneously.

Table 5.4: *Release kinetics parameters of different formulations during day 1 of dissolution for the following formulations: HMW PCL – LDC 30% implants printed at 110 °C after dissolution with a flow rate of 35 ml/min, HMW PCL – LDC 30% implants printed at 110 °C after dissolution with a flow rate of 8 ml/min, HMW PCL – LDC 30% implants printed at 70 °C after dissolution with a flow rate of 8 ml/min, HMW PCL – LDC 5% implants printed at 110 °C after dissolution with a flow rate of 8 ml/min, HMW PCL - HMW PCL–LDC 30% implants printed at 110 °C after dissolution with a flow rate of 8 ml/min.*

Kinetics models									
Formulation, print temperature, flow rate	***Zero-order***		***First-order***		***Higuchi***		***Korsmeyer-Peppas***		
	R^2	K_0	R^2	K_1	R^2	K_H	R^2	K_{K-P}	n
HMW PCL – LDC 30%, 110 °C, 35 ml/min	-0.263	0.099	0.9241	-0.0003	0.8455	1.7823	0.9767	3.833	0.362
HMW PCL – LDC 30%, 110 °C, 8 ml/min	0.3165	0.0664	0.9313	-0.0002	0.9608	1.1783	0.976	1.555	0.4524
HMW PCL – LDC 30%, 70 °C, 8 ml/min	0.2797	0.0695	0.9283	-0.0002	0.9532	1.2354	0.9649	1.637	0.4519
HMW PCL – LDC 5%, 110 °C, 8 ml/min	-0.031	0.0251	0.952	-0.00008	0.8878	0.8292	0.9894	2.464	0.3307
HMW PCL - HMW PCL– LDC 30%, 110 °C, 8 ml/min	0.4402	0.0015	0.9563	-0.000004	0.9821	0.0495	0.9844	16.542	0.4704

R^2: squared correlation coefficient, K_0: zero-order release constant, K_1: first-order release constant, K_H: release rate constant of Higuchi, K_{K-P}: release rate constant of Korsmeyer-Peppas and n: drug release exponent.

Table 5.5: *Release kinetics parameters of different formulations during days 2 – 4 of dissolution for the following formulations: HMW PCL – LDC 30% implants printed at 110 °C after dissolution with a flow rate of 35 ml/min, HMW PCL – LDC 30% implants printed at 110 °C after dissolution with a flow rate of 8 ml/min, HMW PCL – LDC 30% implants printed at 70 °C after dissolution with a flow rate of 8 ml/min, HMW PCL – LDC 5% implants printed at 110 °C after dissolution with a flow rate of 8 ml/min, HMW PCL - HMW PCL–LDC 30% implants printed at 110 °C after dissolution with a flow rate of 8 ml/min.*

Kinetics models									
Formulation, print temperature, flow rate	***Zero-order***		***First-order***		***Higuchi***		***Korsmeyer-Peppas***		
	R^2	K_0	R^2	K_1	R^2	K_H	R^2	K_{K-P}	n
HMW PCL – LDC 30%, 110 °C, 35 ml/min	-3.188	0.0169	0.9976	-0.00006	0.551	1.035	0.9984	5.642	0.2906
HMW PCL – LDC 30%, 110 °C, 8 ml/min	-1.117	0.0139	0.994	-0.00005	0.8825	0.8486	0.9987	2.466	0.3684
HMW PCL – LDC 30%, 70 °C, 8 ml/min	-1.442	0.0142	0.992	-0.00005	0.8374	0.8687	0.998	2.877	0.3523
HMW PCL – LDC 5%, 110 °C, 8 ml/min	0.0495	0.0132	0.9676	-0.00005	0.9647	0.7932	0.9704	1.073	0.4629
HMW PCL - HMW PCL– LDC 30%, 110 °C, 8 ml/min	0.7816	0.0012	0.8853	-0.000004	0.8156	0.0724	0.897	78.632	0.7133

R^2: squared correlation coefficient, K_0: zero-order release constant, K_1: first-order release constant, K_H: release rate constant of Higuchi, K_{K-P}: release rate constant of Korsmeyer-Peppas and n: drug release exponent.

Therefore, the fact that the zero-order model fitting indicated that the release of the enclosed active agent was happening at a slower rate after the second day of the study in the non-encased implants is in good correspondence with the above observations. The Korsmeyer-Peppas model, which was the best fit for all the dissolution data of the non-encased formulations, even when plotted in two groups (day 1 and days 2-4), suggests that diffusion was followed by the relaxation of the polymeric chains leading to the polymer degradation, which as previously mentioned is a quite slow process. This was, then, making feasible the release of the encapsulated active substance from the inner parts of the printed dosage form through diffusion.

In the case of the HMW PCL shell-core HMW PCL-LDC 30% implants, the Korsmeyer-Peppas model also provided the highest squared correlation coefficient, R^2, compared to the other three kinetics models, as shown in ***Table 5.3*** and ***Figure 5.20***. The obtained value of the release exponent was $0.45 < n < 1$, not only when the dissolution data of all the days were plotted in the same graph, but also when they were divided into two phases, the initial rapid one and the slower one that followed (***Table 5.4, Table 5.5, Figure 5.20.d, Figure S.27.d, Figure S.28.d***). It is suggested, hence, that so-called 'anomalous' transport was responsible, as well, for the release of lidocaine from these implants, whereby a combination of two mechanisms maybe occurring simultaneously. In this formulation type, no active agent was initially exposed to the medium, but the degradation of the polycaprolactone needed to happen for openings to be created on the polymeric shell facilitating the intrusion of the medium to the drug loaded core.

Based on the Korsmeyer-Peppas model, a prolonged drug release could be achieved not only with the shell-core dosage forms, but also with the investigated non-encased drug loaded polycaprolactone formulations. The printing temperature did not influence the drug release length, while the applied flow rate seemed to have an impact, since it resulted in a slightly faster release of the active agent as previously discussed (***Figure 5.15, Figure 5.17, Figure 5.18***).

Table 5.6: *Number of days needed for the total amount of the loaded lidocaine to be released according to the Korsmeyer-Peppas model from the 3D printed formulations: HMW PCL – LDC 30% implants printed at 110 °C after dissolution with a flow rate of 35 ml/min, HMW PCL – LDC 30% implants printed at 110 °C after dissolution with a flow rate of 8 ml/min, HMW PCL – LDC 30% implants printed at 70 °C after dissolution with a flow rate of 8 ml/min, HMW PCL – LDC 5% implants printed at 110 °C after dissolution with a flow rate of 8 ml/min, HMW PCL - HMW PCL–LDC 30% implants printed at 110 °C after dissolution with a flow rate of 8 ml/min.*

Formulation, print temperature, flow rate	Number of days needed for the total amount of the loaded drug to be released from the implants
HMW PCL – LDC 30%, 110 °C, 35 ml/min	11
HMW PCL – LDC 30%, 110 °C, 8 ml/min	13
HMW PCL – LDC 30%, 70 °C, 8 ml/min	13
HMW PCL – LDC 5%, 110 °C, 8 ml/min	18
HMW PCL - HMW PCL–LDC 30%, 110 °C, 8 ml/min	404

According to the Korsmeyer-Peppas model, the incorporated lidocaine would be completely released from the HMW PCL-LDC 30% implants after approximately 11 days when a 35 ml/min dissolution medium flow rate was applied, and almost after 13 days with the slower media flow rate, 8 ml/min. The total number of days needed for the release of the encapsulated active agent was not affected by the temperature applied for the printing of the polymeric implant, as displayed in ***Table 5.6***.

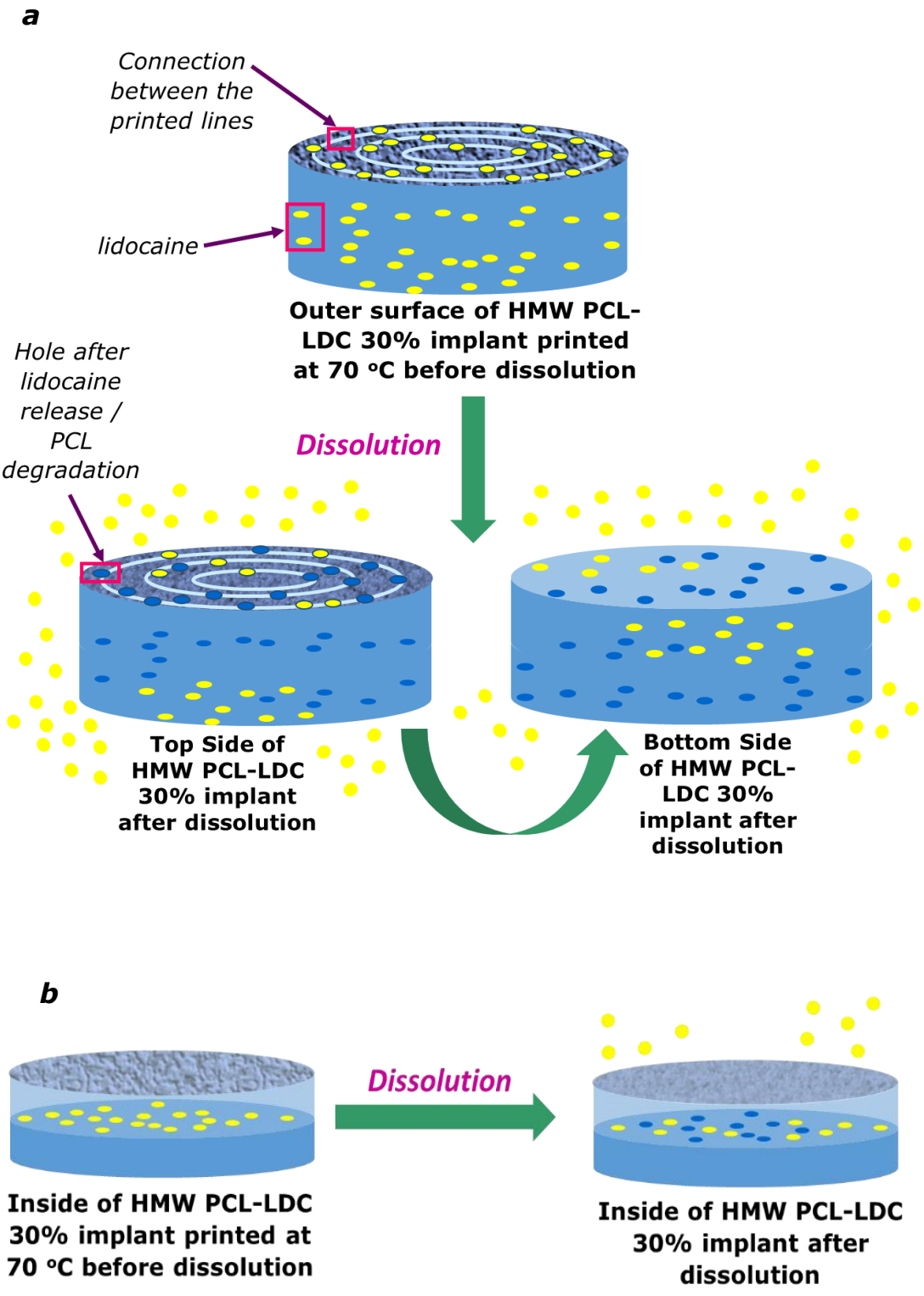

Figure 5.21: (a): *Outer surface and* ***(b):*** *inside of HMW PCL-LDC 30% implant printed at 70 °C before and after dissolution.*

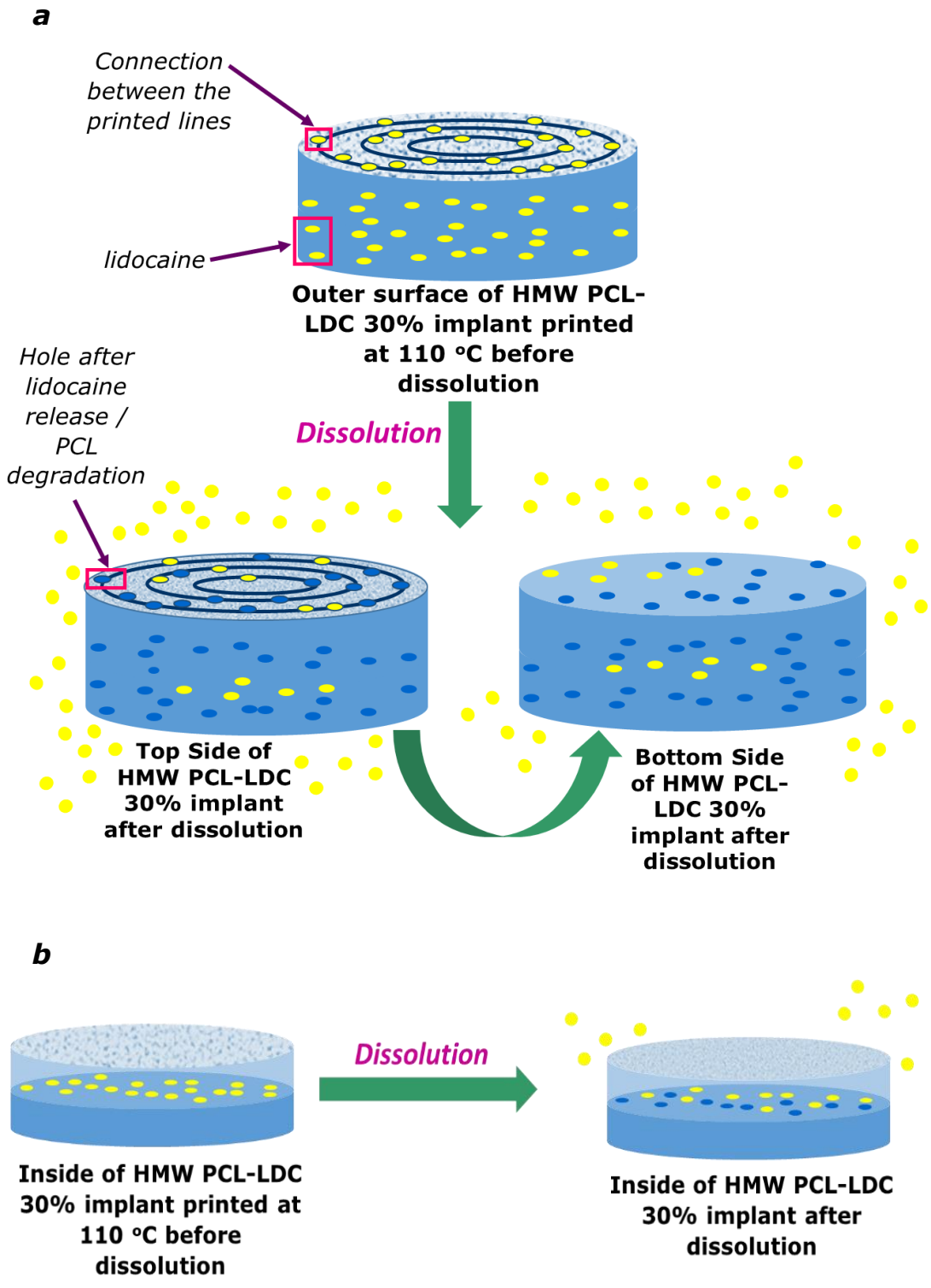

Figure 5.22: (a): *Outer surface and* ***(b):*** *inside of HMW PCL-LDC 30% implant printed at 110 °C before and after dissolution.*

As can be seen in ***Table 5.6,*** different drug loading did not significantly affect the number of days needed for the total amount of the loaded active agent to be released from the polymeric dosage forms printed without a barrier-shell; 18 days would be needed for the HMW PCL-LDC 5% implants to release their whole load compared to the 13 days needed in the case of the HMW PCL-LDC 30% implants. This was meaning that the drug release rate from the 3D printed polymeric formulations was not affected by the drug loading, as previously mentioned (***Figure 5.5***).

According to the dissolution data, the release of the drug occurred at a very slow rate and based on the SEM images, the PCL degradation was also very slow. This is in good correspondence with the Korsmeyer-Peppas model fitting which suggested that the total amount of the loaded drug would be completely released from the HMW PCL shell-core HMW PCL-LDC 30% implants after at least 400 days (***Table 5.6***). The latter, hence, clearly indicated that PCL works as a particularly effective barrier for prolonged drug release in the HMW PCL cased HMW PCL-LDC 30% implants.

Figure 5.21, Figure 5.22, Figure 5.23, Figure 5.24 schematically summarise the general observations and conclusions derived from the dissolution, SEM and Raman analyses, as well as the drug release kinetics models. More specifically, the encapsulated active agent was initially released from the surface of the printed formulations, as derived from the Raman characterization of the after-dissolution implants, leading to the creation of holes. Based on SEM images after the dissolution, gaps were also detected between the printed lines or layers which seemed to be the most susceptible areas for polymer degradation via polymer relaxation and hydrolysis. Consequently, the dissolution medium could easier penetrate the inside compartments of the implants resulting in the release of the drug located in these areas. More precisely, diffusion related drug release occurred in these cases in combination with PCL hydrolysis and polymeric chain relaxation, as indicated by the Korsmeyer-Peppas model. In ***Figure 5.21.b, Figure 5.22.b, Figure 5.23.b, Figure 5.24.b*** a representation of these was demonstrated. Nevertheless, the latter procedures were happening at a slower rate. The reason for that was the polymer degradation rate leading to the creation of holes on the implants surface, as observed above in the SEM images of the drug-free HMW PCL formulations after the four-day-long dissolution studies (***Figure 5.25***).

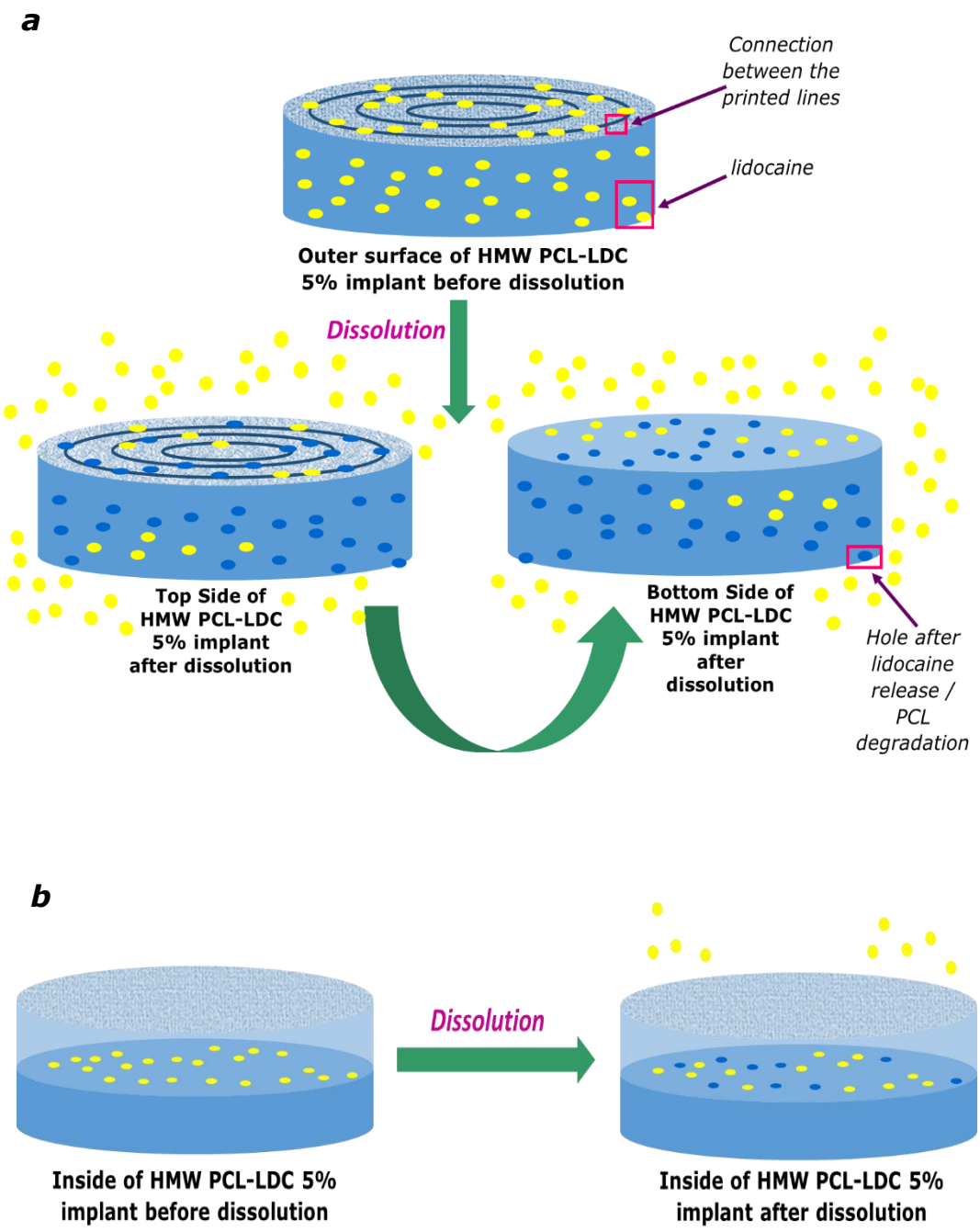

Figure 5.23: (a): *Outer surface and* ***(b):*** *inside of HMW PCL-LDC 5% implant printed at 110 °C before and after dissolution.*

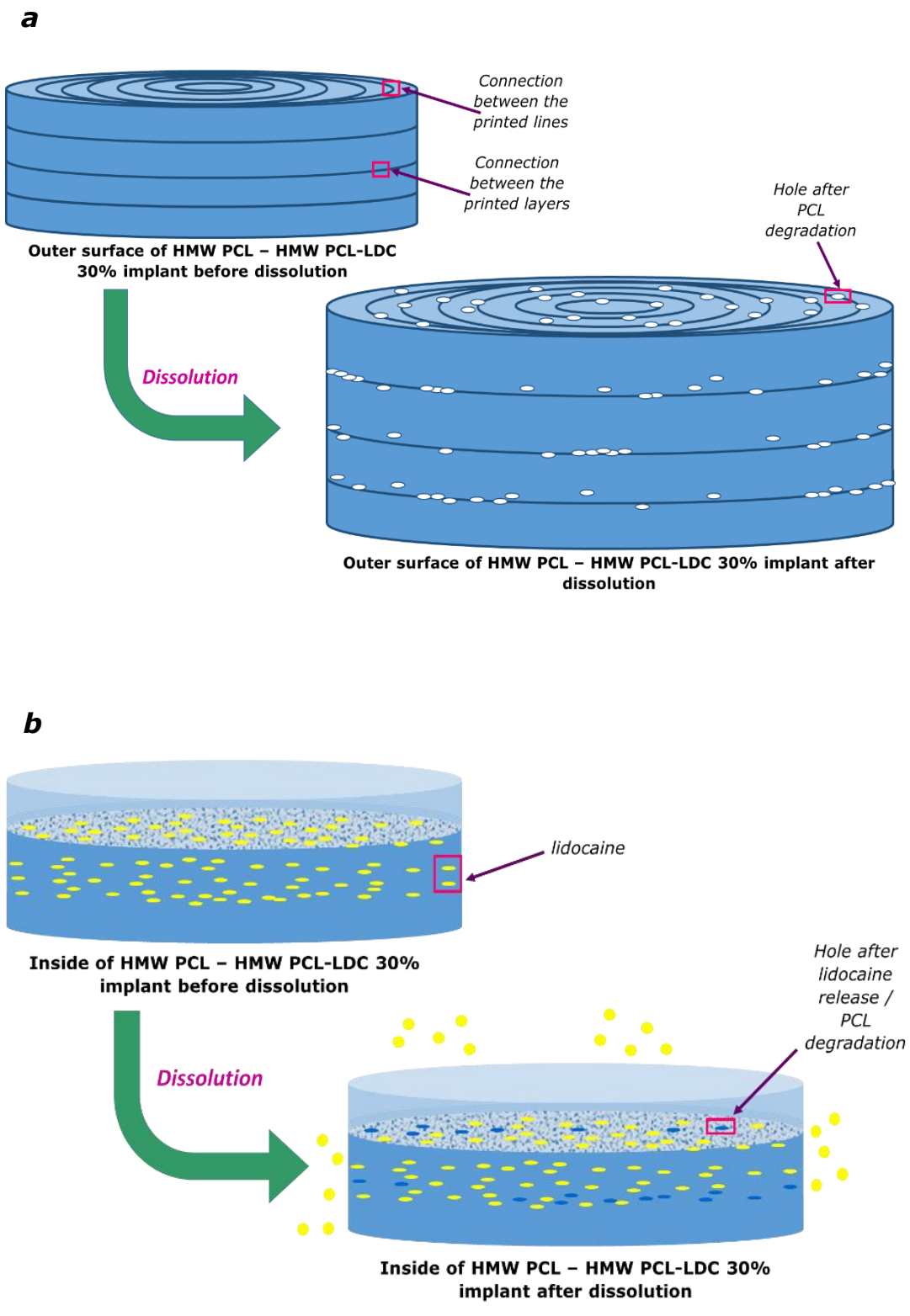

Figure 5.24: (a): *Outer surface and* ***(b):*** *inside of HMW PCL – HMW PCL-LDC 30% implant printed at 110 °C before and after dissolution.*

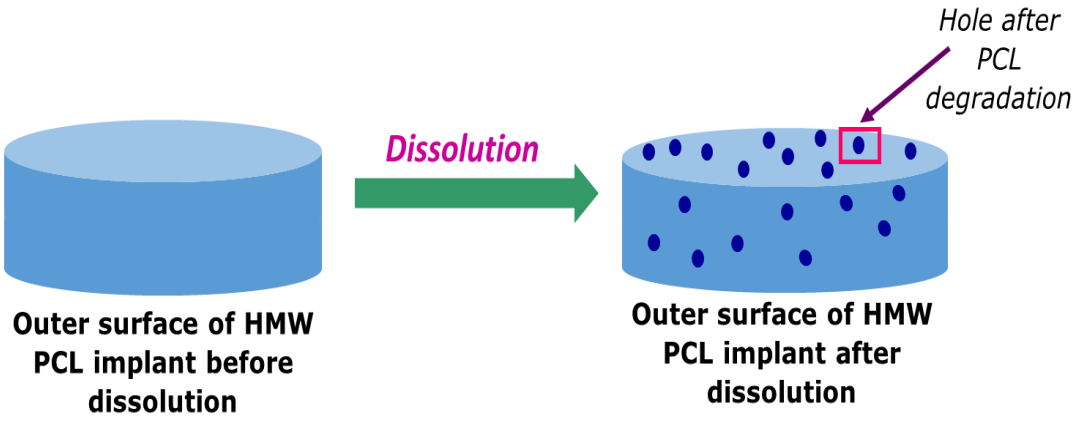

Figure 5.25: *Outer surface of pure HMW PCL implant printed at 110 °C before and after dissolution.*

The impact of the lidocaine release and the PCL degradation is, also, exhibited on the surface of the implants printed at 110 °C and 70 °C that were relatively rough with some surface particles. After the dissolution, the implant surfaces appeared to be smoother (***Figure 5.21.a, Figure 5.22.a***).

5.3. CONCLUSIONS

Lidocaine release profile from differently printed polycaprolactone encased and non-encased implants has been presented. Formulations printed with different drug loading, 30% and 5%, at 70 and 110 °C were used in dissolution tests at media flow rates of 35 and 8 ml/min. Sustained lidocaine release was achieved in all cases, with no burst release during the first day. Particularly prolonged drug release has been obtained with the HMW PCL core-shell implants, where less than 6% of the loaded lidocaine was released within 4 days compared to 55-65% from the non-encased formulations. The drug release rate was faster during the first day of the study, while it was becoming slower on the second day and the remaining days of the test.

According to the Korsmeyer-Peppas model, which demonstrated the best mathematical fit to the dissolution data for all the studied dosage forms, the suggested lidocaine release mechanism was diffusion. More specifically, in the case of the HMW PCL-LDC 30% implants printed at 110 °C, where the higher medium flow rate, 35 ml/min, was applied during the *in vitro* drug release test, the release mechanism for the active agent was indicated to be diffusion related partially through the polymeric matrix and partially through holes on the formulation surface. In the rest non-encased polycaprolactone implants, the two-phased release was more evident. The previously mentioned drug release mechanism was also occurring during the first day of the dissolution, while the next days, Fickian diffusion was happening simultaneously with the relaxation of the polymeric chains and the PCL hydrolysis contributing to the beginning of its degradation process. In the HMW PCL barrier-shell HMW PCL-LDC 30% core implants, the latter mechanisms were indicated, as well, by the Korsmeyer-Peppas model as the main drug release mechanisms for all the days of the dissolution test.

The impact of the early stages of the polymer degradation was also supported by the SEM characterization of the pure HMW PCL control prints after dissolution, where some holes appeared on their surfaces. The lidocaine loaded polymeric implants exhibited gaps preferentially between the printed lines of the formulation, through which the media was reaching the internal compartments resulting in the release of the active agent.

Therefore, the release of the enclosed active compound was occurring in two phases, initially from the surface of the non-encased implants and then, from their inner parts after the formation of openings due to the degradation of the polymeric matrix.

The highly featured surface of the dosage forms printed at 70 °C did not have any impact on the lidocaine release rate compared to the implants printed at a higher temperature, 110 °C. The higher medium flow rate applied, though, led to the creation of more cavities on the discs surfaces and a 10% higher lidocaine release.

Raman analysis on the after-dissolution formulations printed with different temperatures showed that lidocaine residing on their surface was, indeed, largely released; with mostly HMW PCL being present both in the matrix and the detected holes compared to the before-dissolution discs.

Different lidocaine loading, 5% compared to 30%, did not influence the drug release rate or release mechanism or predicted length of complete lidocaine release (based on the Korsmeyer-Peppas model). In the case of the HMW PCL barrier-shell implants, a particularly low drug release rate was exhibited. That could last for several months and hence, this formulation would be a suitable candidate for use as an implant.

The effectiveness of polycaprolactone both as a matrix and as a barrier-shell for the achievement of sustained drug release has been, thus, demonstrated, making it a particularly promising material for the manufacture of sustained release systems.

CHAPTER 6: GENERAL CONCLUSIONS

This study has demonstrated the manufacture of sustained drug release formulations using a solvent-free method at a relatively low printing temperature using a hot melt extrusion-based 3D printer with polycaprolactone, a particularly viscous polymer.

The printability of PCL with two molecular weights (25 kDa and 50 kDa) was shown to be successful without the addition of any other material – excipient – when a pressure assisted microsyringe (PAM) 3D printer was used. Printing issues associated with the viscosity of the polymer, especially of the 50kDa molecular weight were addressed by using only metal parts (aluminium cartridge instead of a plastic one and steel nozzles) that provided a more effective thermal conductivity to the PCL. Appropriate selection of the printing parameters, such as print temperature (100 – 130 ^{o}C), or the nozzle diameter (0.34 – 0.61 mm) could also enhance polymer printability. The printing accuracy and resolution of a predesigned shape were optimised by properly adjusting the applied printing parameters, such as print speed (1 – 6 mm/s) and aforementioned temperature and nozzle diameter.

PCL extrudability in a Hot Melt Extruder (HME) has, also, been demonstrated to be feasible with the addition of 1% w/w plasticizer, triethyl citrate, and by a suitable combination of the temperature in the extruder's heat zones (50 – 60 ^{o}C), as well as, the screw speed (35 rpm). Both molecular weight PCL have been extruded in fine filaments at low temperatures (50 – 60 ^{o}C), close to the polymer's melting point (60 – 65 ^{o}C) (***Figure 6.1***). The printability of the polymeric filaments in a Fused Deposition Modelling (FDM) 3D printer has, subsequently, been achieved at higher temperatures (180 – 190 ^{o}C) compared to the PAM 3D printer (110 – 130 ^{o}C). The printing resolution and accuracy of a predetermined shape were again optimised by an appropriate combination of nozzle diameter (0.8 mm) and printing settings, such as print speed (5 – 20 mm/s) or temperature (180 ^{o}C).

The polymeric thermal and crystalline properties of the filaments, as well as, of the 3D printed test shape were similar to the starting polymer material. No changes in the melting point or the crystalline nature of the polymer have been detected after the application of various extrusion and 3D printing and settings. Nevertheless, a slight decrease in the melting temperature and a slight increase in the crystallization temperature of the polymer post extrusion and printing, as

well as, a slight decrease in the intensity of the polymer peaks in the XRD patterns were observed. These were associated with the uncontrolled heat-cool cycle occurring during the extrusion and 3D printing processes.

Based on the conclusions drawn by the PCL printability study the higher molecular weight PCL was selected to be used in the pressure assisted microsyringe 3D printer for the manufacture of sustained release dosage forms using a solvent and additive free method at a relatively low temperature. Successful fabrication of encased and non-encased drug loaded formulations was achieved (***Figure 6.2***). Some further optimization of the printing settings, such as print temperature, speed, bed temperature, extrusion width and pressure, was required to accommodate the impact of formulation changes. For example, the manufacture of polymeric implants with 30% w/w lidocaine loading has been performed at a lower temperature (70 ^{o}C) – closer to the melting point of the used substances- compared to the implants with 5% w/w drug loading and the drug-free polymeric implants (printed at 110 ^{o}C), as the addition of lidocaine decreased the formulation viscosity and hence, a lower printing temperature could be used with larger amounts of the drug.

Visual defects detected on the surface of the 3D printed polymeric drug loaded and drug-free formulations were reduced by decreasing the printer extrusion width resulting in a reduction in the distance between the centres of the printed lines and an increased printing resolution. Printing pressure was another way to reduce defects in the fabricated discs, as this regulates the amount and speed of material printed; the higher the pressure, the more material was extruded and consequently, the more evenly the formulations could be produced.

The versatility of the selected 3D printing method was proven by the successful manufacture of a PCL barrier–shell lidocaine loaded polymeric implant without any particular materials preparation prior to their loading to the cartridge of the printer or any post–printing processing.

DSC and XRD characterization of the 3D printed PCL lidocaine implants revealed that the blending and extrusion processes did not significantly affect the thermal behaviour of the materials used with PCL, while lidocaine crystals were present in the fabricated formulations. Nevertheless, the low crystallinity degree of the active agent detected in the 3D printed implants indicated the formation of solid dispersion. Lidocaine was in a largely amorphous state within the polymeric

matrix, even though a few crystalline particles of the active compound were still present in the fabricated formulation. The ability to form solid dispersions in the manufacture of dosage forms with poorly soluble active compounds can enhance their solubility, dissolution rate and bioavailability. Moreover, both immediate and sustained drug release formulations could successfully be fabricated with the PAM 3D printing method as several types of materials can be used in this technique and the dissolution rate of the enclosed active agent is dictated by the material properties of the selected carrier.

FTIR and Raman analysis demonstrated that no detectable chemical interactions or modifications occurred between the polymer and the drug before and after their mixing and 3D printing. The chemical structure of the used materials, PCL and lidocaine, was therefore independent of the printing process used. In addition, Raman spectra suggested that both the polymer and the active ingredient were present on the surface of the fabricated formulations. Despite this, no burst drug release occurred during the dissolution studies indicating that the active compound remained sufficiently physically associated with the polymer contributing to more effective control of drug release.

Dissolution studies showed that sustained lidocaine release has been achieved either when PCL was used as a matrix or as a shell of the fabricated dosage forms, due to its slow degradation rate. The use of the PCL barrier enabled delayed and slower drug release.

Drug release was proposed to be controlled by combined transportation mechanisms, diffusion and polymeric chain relaxation, as indicated by the close fit to the Korsmeyer-Peppas model. According to the investigated drug release kinetics, lidocaine was initially released from the surface of the non-encased formulations partially through the matrix and partially through pores, while slow PCL degradation led to the creation of cavities on the implants surface through which the active ingredient was released from the inner parts. Hence, a two-phased drug release has been obtained, with an initial faster phase occurring during the first day.

The early stages of the polymer degradation were also supported by the SEM characterization of the pure PCL control prints after dissolution, where the appearance of some holes has been detected on their surface. The lidocaine loaded polymeric implants demonstrated apertures, as well, on their surface, especially

between the connection of the printed lines that seemed to be more susceptible to polymer relaxation and hydrolysis.

In the case of the PCL barrier-shell lidocaine loaded polymeric implants, the majority of the surface holes were again detected between the printed layers that were more prone to polymer degradation. In this way, the intrusion of the dissolution medium to the inner compartments containing the active substance was facilitated. Consequently, again as indicated by the Korsmeyer-Peppas model, PCL hydrolysis contributed to the polymer degradation and the diffusion of the active substance that were two mechanisms occurring simultaneously resulting in the sustained release of lidocaine from the core.

The fabrication of personalized formulations could in the future be further explored by printing drug loaded polymeric implants with various barrier-shell thicknesses. The latter implants attribute could be applied to investigate its ability to predictably control drug release rate and timing. A more complete understanding of the relationship between PCL degradation and printing parameters would also be helpful. A buffer solution with or without the addition of enzymes, such as lipase, or simulated body fluid (SBF), an acellular, aqueous solution with an ionic composition quite similar to that of human plasma, and buffered to physiological pH 7.25-7.4 could be used for this study. Mass loss, differences in molecular weight, detection of degradation products, morphological analysis for porosity and pores size are the main implant attributes that could be explored during the PCL degradation investigation with characterization technologies, such as size exclusion chromatography or gel permeation chromatography, Gas Chromatography-Mass Spectroscopy (GC-MS), Scanning Electron Microscopy (SEM).

A later phase of this proposed future work would be *in vivo* studies in animals during which the detection and analysis of the drug concentration in plasma after blood collection would verify not only the *in vitro* dissolution data and observations, but also the *in vitro* degradation investigations. The characterization and quantification of the inflammation – mediating cells adjacent to the implant can demonstrate potential inflammation triggered by tissue injury during the implantation process or by prolonged presence of the dosage forms in a predetermined area of the human body. Furthermore, it can indicate the safety of the drug loaded polymeric 3D printed implants in humans.

To conclude, this work has demonstrated that polycaprolactone has a significant potential for the production of prolonged drug release formulations by 3D printing, both as a matrix and as a barrier-shell to enable predictably delayed drug release. Solid drug dispersions can successfully be manufactured with this printing method broadening its applications in the pharmaceutical field. It has also been shown that drug loading can be varied in a bespoke fashion for each implant, showing that personalisable implants can be manufactured by 3D printing.

It seems that precision medicine will soon be feasible to be applied for more effective patient treatment, since new legislation is being issued in Europe to prepare for this. A regulatory framework has been issued in the UK, earlier in 2021, regarding the human use of medicinal products including for the first time guidelines for the manufacture, quality controls and administration of personalized medicines with innovative methods, such as 3D printing. New legislation is also anticipated to be issued by the EU in 2022 covering the same areas. The fact that the current legislations are updated to include regulations for this novel area of patient treatment undoubtedly illustrates that sooner rather than later personalized medicines will be used in the wider population considerably improving their quality of life. This will be the first step of a series of necessary changes in the pharmaceutical area, with the introduction of novel manufacturing technologies, such as 3D printing, to follow. The current study clearly demonstrates that the application of these methods could lead to the achievement of the desired goals, the fabrication of safe and effective medicines.

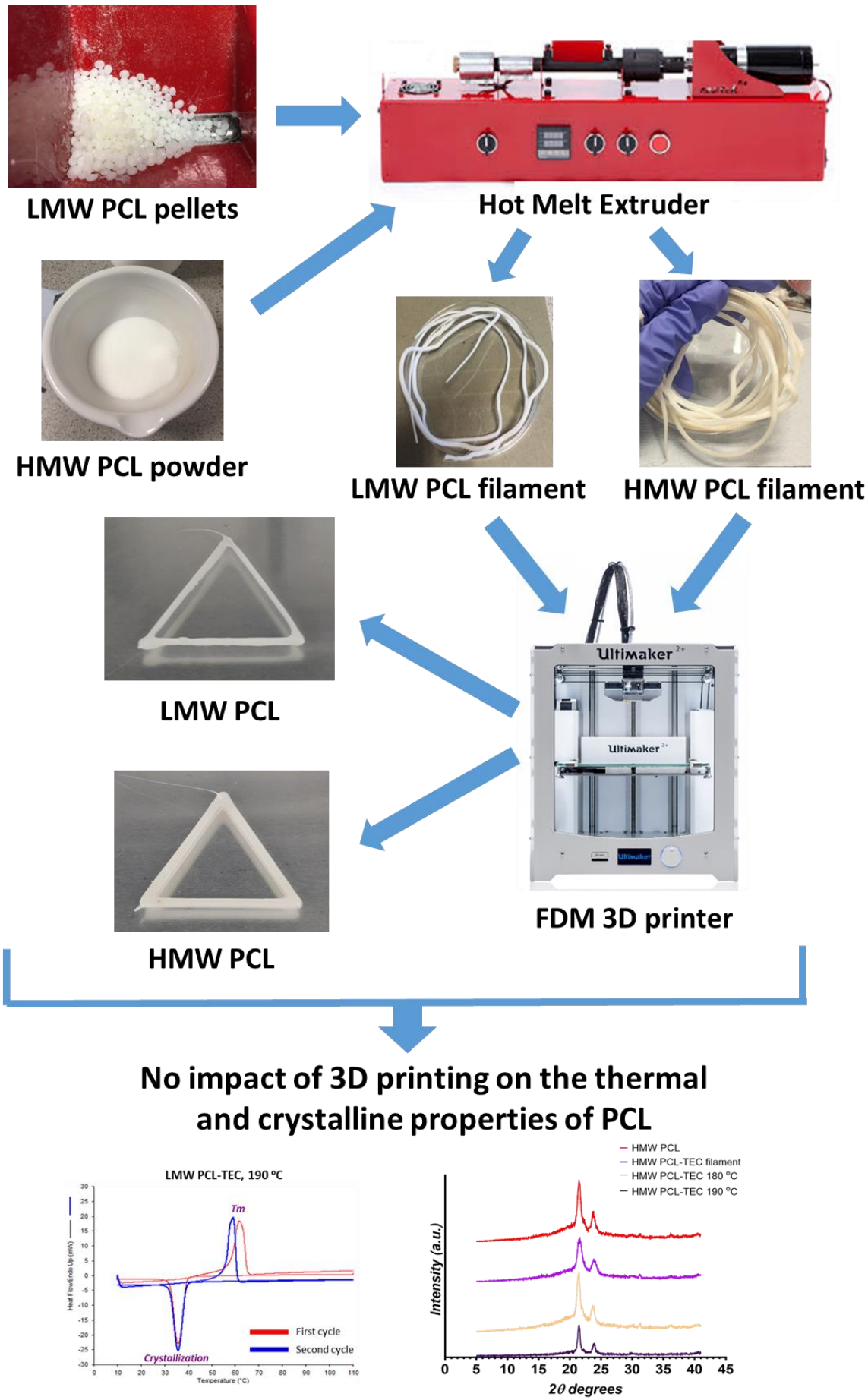

Figure 6.1: *Schematic diagram displaying the main steps and conclusions of the extrudability and printability studies in the Hot Melt Extruder and Fused Deposition Modelling (FDM) 3D printer, respectively, of polycaprolactone with two molecular weights (25kDa – LMW PCL and 50kDa – HMW PCL).*

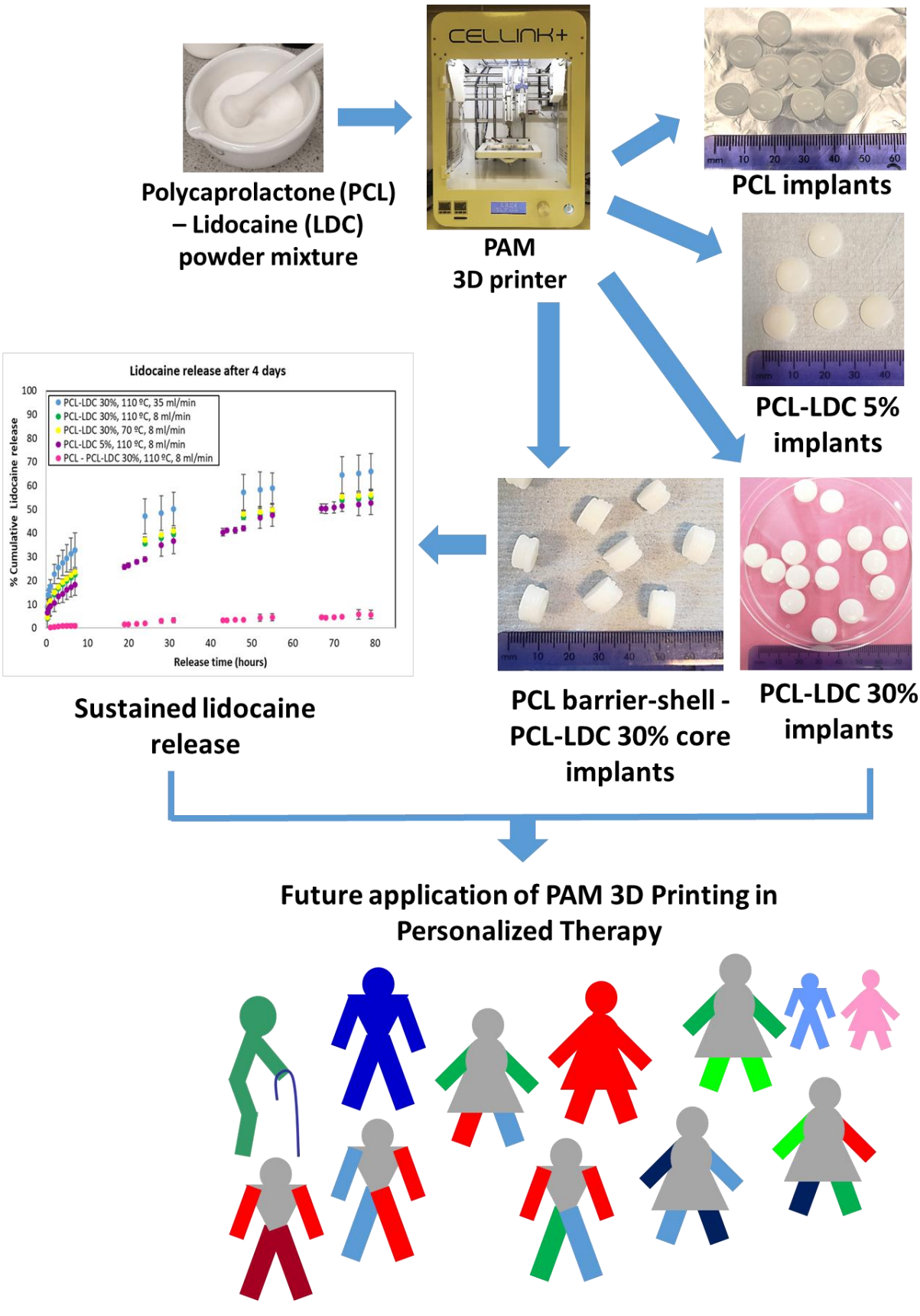

Figure 6.2: *Schematic diagram depicting the main stages and conclusions of the current study: The desired materials are initially loaded to the PAM 3D printer without any pre-printing processing or the addition of any solvents or excipients. The manufacture of formulations with different drug loading and structural attributes (encased and non-encased implants) is feasible. Sustained lidocaine release has been attained with all the printed formulations. Therefore, this technology is promising for future applications in personalized therapy.*

REFERENCES

Abu-thabit, N. Y. and Makhlouf, A. S. H. (2018) *Historical development of drug delivery systems: From conventional macroscale to controlled, targeted, and responsive nanoscale systems*, *Stimuli Responsive Polymeric Nanocarriers for Drug Delivery Applications, Volume 1*. Cairo: Elsevier Ltd. doi: 10.1016/B978-0-08-101997-9.00001-1.

Acosta-Vélez, G. F. and Wu, B. M. (2016) '3D Pharming : Direct Printing of Personalized Pharmaceutical Tablets', *Polymer Sciences*, 1(11), pp. 1–10. doi: 10.4172/2471-9935.100011 Polymer.

Afsana *et al.* (2018) '3D Printing in Personalized Drug Delivery', *Current Pharmaceutical Design*, 24, pp. 5062–5071. doi: 10.2174/1381612825666190215122208.

Aho, J. *et al.* (2019) 'Roadmap to 3D-Printed Oral Pharmaceutical Dosage Forms : Feedstock Filament Properties and Characterization for Fused Deposition Modeling', *Journal of Pharmaceutical Sciences*. Elsevier Ltd, 108(1), pp. 26–35. doi: 10.1016/j.xphs.2018.11.012.

El Aita, I. *et al.* (2020) '3D-Printing with precise layer-wise dose adjustments for paediatric use via pressure-assisted microsyringe printing', *European Journal of Pharmaceutics and Biopharmaceutics*, 157, pp. 59–65. doi: 10.1016/j.ejpb.2020.09.012.

Aita, I. El, Breitkreutz, J. and Quodbach, J. (2019) 'On-demand manufacturing of immediate release levetiracetam tablets using pressure-assisted microsyringe printing', *European Journal of Pharmaceutics and Biopharmaceutics*. Elsevier, 134, pp. 29–36. doi: 10.1016/j.ejpb.2018.11.008.

Aita, I. El, Breitkreutz, J. and Quodbach, J. (2020) 'Investigation of semi-solid formulations for 3D printing of drugs after prolonged storage to mimic real-life applications', *European Journal of Pharmaceutical Sciences*. Elsevier, 146, p. 105266. doi: 10.1016/j.ejps.2020.105266.

Akash, S. *et al.* (2016) 'Rapid Manufacturing Process- 3D Printing Technology Advantages , Disadvantages and Applications', *International Journal for Scientific Research & Development*, 4(11), pp. 16–18.

Akmal, J. S. *et al.* (2018) 'Implementation of Industrial Additive Manufacturing :

Intelligent Implants and Drug Delivery Systems', *Journal of Functional Biomateriala*, 41(9), pp. 1–14. doi: 10.3390/jfb9030041.

Al-Maliki, J. Q. and Al-Maliki, A. J. Q. (2015) 'The Processes and Technologies of 3D Printing', *International Journal of Advances in Computer Science and Technology*, 4(10), pp. 161–165. Available at: http://www.warse.org/IJACST/static/pdf/file/ijacst024102015.pdf.

Algahtani, M. S., Mohammed, A. A. and Ahmad, J. (2019) 'Extrusion-Based 3D Printing for Pharmaceuticals : Contemporary Research and Applications', *Current Pharmaceutical Design*, 24, pp. 1–18. doi: 10.2174/1381612825666190110155931.

Aliah, N. N. and Ansari, M. N. M. (2017) 'Thermal analysis on Characterization of Polycaprolactone (PCL) – Chitosan Scaffold for Tissue Engineering', *International Journal of Scientific Research Engineering & Technology*, 6(2), pp. 2278–882. Available at: www.ijsret.org.

Allawadi, D. *et al.* (2014) 'ChemInform Abstract: Solid Dispersions: A Review on Drug Delivery System and Solubility Enhancement', *ChemInform*, 45(18), p. no-no. doi: 10.1002/chin.201418290.

Alomari, M. *et al.* (2015) 'Personalised dosing: Printing a dose of one's own medicine', *International Journal of Pharmaceutics*. Elsevier B.V., 494(2), pp. 568–577. doi: 10.1016/j.ijpharm.2014.12.006.

Anacleto, S. *et al.* (2018) 'Evaluation of physicochemical properties as supporting information on quality control of raw materials and veterinary pharmaceutical formulations', *Journal of Pharmaceutical Analysis*. Elsevier B.V., 8(3), pp. 168–175. doi: 10.1016/j.jpha.2018.01.001.

Ani Jose, P. and Christopher GV, P. (2018) '3D PRINTING OF PHARMACEUTICALS – A POTENTIAL TECHNOLOGY IN DEVELOPING PERSONALIZED MEDICINE', *Asian Journal of Pharmaceutical and Development*, 6(3), pp. 46–54. doi: 10.22270/ajprd.v6.i3.375.

Anodesyn (2013) 'ANODESYN SUPPOSITORIES'. Huddersfield: Thornton and Ross Ltd., pp. 1–3.

Aquino, R. P. *et al.* (2018) 'Envisioning smart and sustainable healthcare: 3D Printing technologies for personalized medication', *Futures*. Elsevier Ltd,

103(March), pp. 35–50. doi: 10.1016/j.futures.2018.03.002.

Arafat, B., Wojsz, M., *et al.* (2018) 'Tablet fragmentation without a disintegrant : A novel design approach for accelerating disintegration and drug release from 3D printed cellulosic tablets', *European Journal of Pharmaceutical Sciences*, 118, pp. 191–199. doi: 10.1016/j.ejps.2018.03.019.

Arafat, B., Qinna, N., *et al.* (2018) 'Tailored on demand anti-coagulant dosing : An in vitro and in vivo evaluation of 3D printed purpose-designed oral dosage forms', *European Journal of Pharmaceutics and Biopharmaceutics*. Elsevier, 128, pp. 282–289. doi: 10.1016/j.ejpb.2018.04.010.

Araujo, M. R. P. *et al.* (2019) 'The Digital Pharmacies Era : How 3D Printing Technology Using Fused Deposition Modeling Can Become a Reality', *Pharmaceutics*, 128(11), pp. 1–14. doi: 10.3390/pharmaceutics11030128.

Awad, A. *et al.* (2018) 'Reshaping drug development using 3D printing', *Drug Discovery Today*. Elsevier Ltd, 23(8), pp. 1547–1555. doi: 10.1016/j.drudis.2018.05.025.

Awad, A. *et al.* (2019) '3D Printed Pellets (Miniprintlets): A Novel , Multi-Drug , Controlled Release Platform Technology', *Pharmaceutics*, 11(4), pp. 1–17. doi: 10.3390/pharmaceutics11040148.

Ayyoubi, S. *et al.* (2021) '3D printed spherical mini-tablets : Geometry versus composition effects in controlling dissolution from personalised solid dosage forms', *International Journal of Pharmaceutics*, 597, p. 120336. doi: 10.1016/j.ijpharm.2021.120336.

Azad, M. A. *et al.* (2020) 'Polymers for Extrusion-Based 3D Printing of Pharmaceuticals : A Holistic Materials – Process Perspective', *Pharmaceutics*, 12(124), pp. 1–34. doi: 10.3390/pharmaceutics12020124.

Azimi, B. *et al.* (2014) 'Poly (ε -caprolactone) Fiber : An Overview', *Journal of Engineered Fibers and Fabrics*, 9(3), pp. 74–90. doi: 10.1177/155892501400900309.

Babu, R. D. and Devaprakasam, D. (2019) 'A Review on Additive Manufacturing Techniques in Medical Applications', *International Journal of Advanced Science and Engineering*, 5(3), pp. 988–997. doi: 10.29294/IJASE.5.3.2019.988-997.

Bae, S. J. *et al.* (2006) 'Gelation Behavior of Poly (ethylene glycol) and

Polycaprolactone Triblock and Multiblock Copolymer Aqueous Solutions', *Macromolecules*, 39, pp. 4873–4879. doi: 10.1021/ma060153s.

Bahnini, I. *et al.* (2018) 'Additive manufacturing technology: the status, applications, and prospects', *International Journal of Advanced Manufacturing Technology*. The International Journal of Advanced Manufacturing Technology, 97, pp. 147–161. doi: 10.1007/s00170-018-1932-y.

Bakonyi, M. *et al.* (2018) 'Following-up skin penetration of lidocaine from different vehicles by Raman spectroscopic mapping', *Journal of Pharmaceutical and Biomedical Analysis*, 154, pp. 1–6. doi: 10.1016/j.jpba.2018.02.056.

Bansal, V. K. (1990) 'Serum Inorganic Phosphorus', in Walker, H. K., Hall, W. D., and Hurst, J. W. (eds) *Clinical Methods: The History, Physical, and Laboratory Examinations.* 3rd Editio. Boston, pp. 895–899.

Beaman, J. J. and Deckard, C. R. (1990) 'Selective Laser Sinterng With Assisted Powder Handlng', *United States Patent*, (19), pp. 1–17. Available at: https://patents.google.com/patent/US4938816A/en%0Ahttps://patentimages.storage.googleapis.com/bf/cb/03/4cbcb828f78e25/US4938816.pdf.

Beck, R. C. R. *et al.* (2017) '3D printed tablets loaded with polymeric nanocapsules: An innovative approach to produce customized drug delivery systems', *International Journal of Pharmaceutics*. Elsevier B.V., 528(1–2), pp. 268–279. doi: 10.1016/j.ijpharm.2017.05.074.

Beg, S. *et al.* (2020) '3D printing for drug delivery and biomedical applications', *Drug Discovery Today*. Elsevier Ltd, 25(9), pp. 1668–1681. doi: 10.1016/j.drudis.2020.07.007.

Benjamin Ho, C. M. *et al.* (2017) '3D Printed Polycaprolactone Carbon Nanotube Composite Scaffolds for Cardiac Tissue Engineering', *Macromolecular Bioscience*, 17, pp. 1–9. doi: 10.1002/mabi.201600250.

Benmassaoud, M. M. *et al.* (2019) 'Efficacy of eluted antibiotics through 3D printed femoral implants', *Biomedical Devices*. Biomedical Microdevices, 21(51), pp. 1–10. doi: 10.1007/s10544-019-0395-8 Efficacy.

Berman, B. (2012) '3-D printing: The new industrial revolution', *Business Horizons*. 'Kelley School of Business, Indiana University', 55(2), pp. 155–162. doi: 10.1016/j.bushor.2011.11.003.

Bhowmik, D. *et al.* (2012) 'Controlled Release Drug Delivery Systems', *The Pharma Innovation*, 1(10), pp. 24–32. Available at: www.thepharmajournal.com.

Bijukumar, D. *et al.* (2016) 'An electro-conductive fluid as a responsive implant for the controlled stimuli-release of diclofenac sodium', *Pharmaceutical Development and Technology*. Taylor & Francis, 21(7), pp. 875–886. doi: 10.3109/10837450.2015.1073742.

Bikiaris, D., Koutris, E. and Karavas, E. (2007) 'New Aspects in Sustained Drug Release Formulations', *Recent patents on drug delivery & formulation*, 1(3), pp. 201–213. doi: 10.2174/187221107782331629.

Boetker, J. *et al.* (2016) 'Modifying release characteristics from 3D printed drug-eluting products', *European Journal of Pharmaceutical Sciences*. Elsevier B.V., 90, pp. 47–52. doi: 10.1016/j.ejps.2016.03.013.

Boonme, P. *et al.* (2013) 'Characterization of Lidocaine Transdermal Patches from Natural Rubber Latex', *Advanced Materials Research*, 747, pp. 103–106. doi: 10.4028/www.scientific.net/AMR.747.103.

Briggner, L. *et al.* (1994) 'The use of isothermal microcalorimetry in the study of changes in crystallinity induced during the processing of powders', *International Journal of Pharmaceutics*, 105, pp. 125–135. doi: 10.1016/0378-5173(94)90458-8.

Buanz, A. B. M. *et al.* (2015) 'Ink-jet printing versus solvent casting to prepare oral films: Effect on mechanical properties and physical stability', *International Journal of Pharmaceutics*. Elsevier B.V., 494(2), pp. 611–618. doi: 10.1016/j.ijpharm.2014.12.032.

Buckton, G. and Darcy, P. (1995) 'journal of pharmaceutics The use of gravimetric studies to assess the degree of crystallinity of predominantly crystalline powders', *International Journal of Pharmaceutics*, 123, pp. 265–271. doi: 10.1016/0378-5173(95)00083-U.

Bumbrah, G. S. and Sharma, R. M. (2016) 'Raman spectroscopy – Basic principle, instrumentation and selected applications for the characterization of drugs of abuse', *Egyptian Journal of Forensic Sciences*. The International Association of Law and Forensic Sciences (IALFS), 6(3), pp. 209–215. doi: 10.1016/j.ejfs.2015.06.001.

Cabedo, L. *et al.* (2006) 'Optimization of Biodegradable Nanocomposites Based on aPLA / PCL Blends for Food Packaging Applications', *Macromolecular Symposia*, 233, pp. 191–197. doi: 10.1002/masy.200650124.

Cader, H. K. *et al.* (2019) 'Water-based 3D inkjet printing of an oral pharmaceutical dosage form', *International Journal of Pharmaceutics*. Elsevier, 564, pp. 359–368. doi: 10.1016/j.ijpharm.2019.04.026.

Campbell, K. *et al.* (2009) 'Paracetamol-Loaded Poly (e -Caprolactone) Layered Silicate Nanocomposites Prepared Using Hot-Melt Extrusion', *Journal of Pharmaceutical Sciences*, 98(12), pp. 4831–4843. doi: 10.1002/jps.

Capel, A. J. *et al.* (2018) '3D printing for chemical, pharmaceutical and biological applications', *Nature Reviews Chemistry*. Springer US, 2, pp. 422–436. doi: 10.1038/s41570-018-0058-y.

Censi, R. *et al.* (2018) 'Hot Melt Extrusion : Highlighting Physicochemical Factors to Be Investigated While Designing and Optimizing a Hot Melt Extrusion Process', *Pharmaceutics*, 89(10), pp. 1–27. doi: 10.3390/pharmaceutics10030089.

Chai, X. *et al.* (2017) 'Fused Deposition Modeling (FDM) 3D Printed Tablets for Intragastric Floating Delivery of Domperidone', *Scientific Reports*, 7(1), pp. 1–9. doi: 10.1038/s41598-017-03097-x.

Chavalitpanya, K. and Phattanarudee, S. (2013) 'Poly (lactic acid)/ Polycaprolactone Blends Compatibilized with Block Copolymer', *Energy Procedia*. Elsevier B.V., 34, pp. 542–548. doi: 10.1016/j.egypro.2013.06.783.

Chen, D. *et al.* (2020) 'Preparation and In vitro Evaluation of FDM 3D-Printed Ellipsoid-Shaped Gastric Floating Tablets with Low Infill Percentages', *AAPS PharmSciTech*. AAPS PharmSciTech, 21(6), pp. 1–13. doi: 10.1208/s12249-019-1521-x.

Chen, G. *et al.* (2020) 'Pharmaceutical Applications of 3D Printing', *Additive Manufacturing*. Elsevier, 34, p. 101209. doi: 10.1016/j.addma.2020.101209.

Chen, P.-C. *et al.* (2004) 'Injectable microparticle – gel system for prolonged and localized lidocaine release . II . In vivo anesthetic effects', *Journal of Biomedical Materials Research - Part A*, 407, pp. 0–7. doi: 10.1002/jbm.a.30101.

Cheng, L., Guo, S. and Wu, W. (2009) 'Characterization and in vitro release of

praziquantel from poly (e -caprolactone) implants', *International Journal of Pharmaceutics*, 377, pp. 112–119. doi: 10.1016/j.ijpharm.2009.05.007.

Cheng, L., Lei, L. and Guo, S. (2010) 'In vitro and in vivo evaluation of praziquantel loaded implants based on PEG / PCL blends', *International Journal of Pharmaceutics*. Elsevier B.V., 387(1–2), pp. 129–138. doi: 10.1016/j.ijpharm.2009.12.010.

Cheng, Y. *et al.* (2021) 'Development of methylcellulose-based sustained-release dosage by semisolid extrusion additive manufacturing in drug delivery system', *Journal of Biomedical Materials Research*, (109), pp. 257–268. doi: 10.1002/jbm.b.34697.

Chia, H. N. and Wu, B. M. (2015) 'Recent advances in 3D printing of biomaterials', *Journal of Biological Engineering*, 9(4), pp. 1–14. doi: 10.1186/s13036-015-0001-4.

Chiou, W. L. and Riegelman, S. (1971) 'Pharmaceutical applications of solid dispersion systems', *Journal of Pharmaceutical Sciences*, 60(9), pp. 1281–1302. doi: 10.1002/jps.2600600902.

Choonara, Y. E. *et al.* (2016) '3D-printing and the effect on medical costs : a new era ?', *Expert Review of Pharmacoeconomics & Outcomes Research*, 7167. doi: 10.1586/14737167.2016.1138860.

Christen, M.-O. and Vercesi, F. (2020) 'Polycaprolactone : How a Well-Known and Futuristic Polymer Has Become an Innovative Collagen-Stimulator in Esthetics', *Clinical, Cosmetic and Investigational Dermatology*, 13, pp. 31–48. doi: 10.2147/CCID.S229054.

Christoforidis, J. B. *et al.* (2012) 'Systemic treatment of vitreous inflammation', *Mediators of Inflammation*, 2012, pp. 1–8. doi: 10.1155/2012/936721.

Chun, M. K. *et al.* (2012) 'Development of cataplasmic transdermal drug delivery system containing eutectic mixture of lidocaine and prilocaine', *Journal of Pharmaceutical Investigation*, 42(3), pp. 139–146. doi: 10.1007/s40005-012-0023-6.

Clark, E. A. *et al.* (2017) '3D printing of tablets using inkjet with UV photoinitiation', *International Journal of Pharmaceutics*. Elsevier B.V., 529(1–2), pp. 523–530. doi: 10.1016/j.ijpharm.2017.06.085.

Cleveland, D. *et al.* (2007) 'Raman spectroscopy for the undergraduate teaching laboratory: Quantification of ethanol concentration in consumer alcoholic beverages and qualitative identification of marine diesels using a miniature raman spectrometer', *Spectroscopy Letters*, 40(6), pp. 903–924. doi: 10.1080/00387010701525638.

Colthup, N. B. (2003) 'Infrared Spectroscopy', in Meyers, R. A. (ed.) *Encyclopedia of Physical Science and Technology*. Third Edit. Stamford: Elsevier Ltd, pp. 793–816. doi: 10.1016/b0-12-227410-5/00340-9.

Conceição, J. *et al.* (2019) 'Hydroxypropyl- β -cyclodextrin-based fast dissolving carbamazepine printlets prepared by semisolid extrusion 3D printing', *Carbohydrate Polymers*. Elsevier, 221(May), pp. 55–62. doi: 10.1016/j.carbpol.2019.05.084.

Crowley, M. M. *et al.* (2007) 'Pharmaceutical Applications of Hot-Melt Extrusion : Part I', *Drug Development and Industrial Pharmacy*, 33, pp. 909–926. doi: 10.1080/03639040701498759.

Crump, S. S. (1979) 'APPARATUS AND METHOD FOR CREATING THREE-DIMENSIONAL OBJECTS', *United States Patent*, 28(3), pp. 1–15. doi: 10.2116/bunsekikagaku.28.3_195.

Cui, M., Yang, Y., *et al.* (2019) 'Effect of novel internal structures on printability and drug release behavior of 3D printed tablets', *Journal of Drug Delivery Science and Technology*. Elsevier, 49, pp. 14–23. doi: 10.1016/j.jddst.2018.10.037.

Cui, M., Li, Y., *et al.* (2019) 'Exploration and Preparation of a Dose-Flexible Regulation System for Levetiracetam Tablets via Novel Semi-Solid Extrusion Three-Dimensional Printing', *Journal of Pharmaceutical Sciences*. Elsevier Ltd, 108(2), pp. 977–986. doi: 10.1016/j.xphs.2018.10.001.

Cui, M. *et al.* (2020) 'Fabrication of high drug loading levetiracetam tablets using semi-solid extrusion 3D printing', *Journal of Drug Delivery Science and Technology*. Elsevier, 57, p. 101683. doi: 10.1016/j.jddst.2020.101683.

Cui, Y. and Frank, S. G. (2006) 'Characterization of Supersaturated Lidocaine / Polyacrylate Pressure Sensitive Adhesive Systems : Thermal Analysis and FT-IR', *Journal of Pharmaceutical Sciences*, 95(3), pp. 701–713. doi: 10.1002/jps.

Cunha-Filho, M. *et al.* (2017) 'FDM 3D printing of modified drug-delivery systems using hot melt extrusion : a new approach for individualized therapy', *Therapeutic Delivery*, 8(11), pp. 957–966. doi: 10.4155/tde-2017-0067.

Daly, R. *et al.* (2015) 'Inkjet printing for pharmaceutics - A review of research and manufacturing', *International Journal of Pharmaceutics*. Elsevier B.V., 494(2), pp. 554–567. doi: 10.1016/j.ijpharm.2015.03.017.

Danafar, H. *et al.* (2014) 'Biodegradable m-PEG / PCL Core-Shell Micelles : Preparation and Characterization as a Sustained Release Formulation for Curcumin', *Advanced Pharmaceutical Bulletpoint*, 4(Suppl 2), pp. 501–510. doi: 10.5681/apb.2014.074.

Danckwerts, M. and Fassihi, A. (1991) 'Implantable controlled release drug delivery systems: a review', *Drug Development and Industrial Pharmacy*, 17(11), pp. 1465–1502. doi: 10.3109/03639049109026629.

Dash, A. K. and Cudworth II, G. C. (1999) 'Therapeutic Applications of Implantable Drug Delivery Systems', *Journal of Pharmacological and Toxicological Methods*, 40(1), pp. 1–12. doi: 10.1016/s1056-8719(98)00027-6.

Dash, T. K. and Konkimalla, V. B. (2012) 'Poly-ε-caprolactone based formulations for drug delivery and tissue engineering: A review', *Journal of Controlled Release*. Elsevier B.V., 158(1), pp. 15–33. doi: 10.1016/j.jconrel.2011.09.064.

Dehghanghadikolaei, A., Namdari, N. and Mohammadian, B. (2018) 'Additive Manufacturing Methods : A Brief Overview', *Journal of Scientific and Engineering Research*, 5(8), pp. 123–131.

Deshpande, A. A. *et al.* (1996) 'Controlled-Release Drug Delivery Systems for Prolonged Gastric Residence : An Overview', *Drug Development and Industrial Pharmacy*, 22(6), pp. 531–539. doi: 10.3109/03639049609108355.

Dhanaraju, M. D. *et al.* (2003) 'Preparation and characterization of injectable microspheres of contraceptive hormones', *International Journal of Pharmaceutics*, 268(1–2), pp. 23–29. doi: 10.1016/j.ijpharm.2003.08.011.

Dhanaraju, M. D., Jayakumar, R. and Vamsadhara, C. (2004) 'Influence of Manufacturing Parameters on Development of Contraceptive Steroid Loaded Injectable Microspheres', *Chemical & Pharmaceutical Bulletin*, 52(8), pp. 976–

979. doi: 10.1248/cpb.52.976.

Díaz, E., Sandonis, I. and Valle, M. B. (2014) 'In Vitro Degradation of Poly (caprolactone)/ nHA Composites', *Journal of Nanomaterials*, 15(3), pp. 1–8. doi: 10.1155/2014/802435 Research.

Dincer, C. *et al.* (2017) 'Biosensors and personalized drug therapy : what does the future hold ?', *Expert Review of Precision Medicine and Drug Development*. Taylor & Francis, 2(6), pp. 303–305. doi: 10.1080/23808993.2017.1395691.

Domingos, M. *et al.* (2010) 'Evaluation of in vitro degradation of PCL scaffolds fabricated via BioExtrusion . Part 1 : Influence of the degradation environment', *Virtual and Physical Prototyping*, 5(2), pp. 65–73. doi: 10.1080/17452751003769440.

Drumright, R. E., Gruber, P. R. and Henton, D. E. (2000) 'Polylactic acid technology', *Advanced Materials*, 12(23), pp. 1841–1846. doi: 10.1002/1521-4095(200012)12:23<1841::AID-ADMA1841>3.0.CO;2-E.

Dumitrescu, I.-B. *et al.* (2018) 'THE AGE OF PHARMACEUTICAL 3D PRINTING . TECHNOLOGICAL AND THERAPEUTICAL IMPLICATIONS OF ADDITIVE MANUFACTURING .', *Farmacia*, 66(3), pp. 365–389.

Dumpa, N. R., Bandari, S. and Repka, M. A. (2020) 'Novel Gastroretentive Floating Pulsatile Drug Delivery System Produced via Hot-Melt Extrusion and Fused Deposition Modeling 3D Printing', *Pharmaceutics*, 12, p. 52. doi: 10.3390/pharmaceutics12010052.

Đuranovic, M. *et al.* (2021) 'Paracetamol extended release FDM 3D printlets : Evaluation of formulation variables on printability and drug release', *International Journal of Pharmaceutics*, 592, p. 102253. doi: 10.1016/j.ijpharm.2020.120053.

Economidou, S. N., Lamprou, D. A. and Douroumis, D. (2018) '3D printing applications for transdermal drug delivery', *International Journal of Pharmaceutics*. Elsevier, 544(2), pp. 415–424. doi: 10.1016/j.ijpharm.2018.01.031.

Edinger, M. *et al.* (2018) 'QR encoded smart oral dosage forms by inkjet printing', *International Journal of Pharmaceutics*. Elsevier, 536(1), pp. 138–145. doi: 10.1016/j.ijpharm.2017.11.052.

Ehtezazi, T. *et al.* (2018) 'The Application of 3D Printing in the Formulation of Multilayered Fast Dissolving Oral Films', *Journal of Pharmaceutical Sciences*. Elsevier Ltd, 107(4), pp. 1076–1085. doi: 10.1016/j.xphs.2017.11.019.

Elbadawi, M. *et al.* (2021) 'Pressure-assisted microsyringe 3D printing of oral films based on pullulan and hydroxypropyl methylcellulose', *International Journal of Pharmaceutics*. Elsevier B.V., 595, p. 120197. doi: 10.1016/j.ijpharm.2021.120197.

Eleftheriadis, G. K. *et al.* (2021) 'Automated digital design for 3D-printed individualized therapies', *International Journal of Pharmaceutics*. Elsevier B.V., 599, p. 120437. doi: 10.1016/j.ijpharm.2021.120437.

Emmens, C. W. (1941) 'RATE OF ABSORPTION OF ANDROGENS AND', *Endocrinology*, 28(4), pp. 633–642. doi: 10.1210/endo-28-4-633.

Eshkalak, S. K. *et al.* (2020) 'The role of three-dimensional printing in healthcare and medicine', *Materials & Design*. The Author(s), 194, p. 108940. doi: 10.1016/j.matdes.2020.108940.

Estebe, J. and Consultant, S. (2017) 'Best Practice & Research Clinical Anaesthesiology Intravenous lidocaine', *Best Practice & Research Clinical Anaesthesiology*. Elsevier Ltd, 31(4), pp. 513–521. doi: 10.1016/j.bpa.2017.05.005.

EU Legislation (2021) *Personalised medicine*. Brussels. Available at: ec.europa.eu/health/human-use/personalised-medicine_en.

Fanous, M. *et al.* (2020) 'Development of immediate release (IR) 3D-printed oral dosage forms with focus on industrial relevance', *European Journal of Pharmaceutical Sciences*. Elsevier, 155, p. 105558. doi: 10.1016/j.ejps.2020.105558.

FDA (2017) *Technical Considerations for Additive Manufactured Medical Devices*. Rockville. Available at: https://www.fda.gov/regulatory-information/search-fda-guidance-documents/technical-considerations-additive-manufactured-medical-devices.

FDA (2018) 'Code of Federal Regulations', in *Food and Drugs*, pp. 1–2.

Fernández, J., Etxeberria, A. and Sarasua, J.-R. (2015) 'In vitro degradation studies and mechanical behavior of poly (e -caprolactone-co-d-valerolactone)

and poly (e-caprolactone-co-L-lactide) with random and semi-alternating chain microstructures', *European Polymer Journal*. Elsevier Ltd, 71, pp. 585–595. doi: 10.1016/j.eurpolymj.2015.09.001.

Ferreira, J. *et al.* (2017) 'Effect of in vitro enzymatic degradation on 3D printed poly(ε-caprolactone) scaffolds: morphological, chemical and mechanical properties', *Journal of Applied Biomaterials & Functional Materials*, 15(3), pp. 185–195. doi: 10.5301/jabfm.5000363.

Fialho, S. L., Cunha, S. and Cunha, S. (2005) 'Manufacturing Techniques of Biodegradable Implants Intended for Intraocular Application Manufacturing Techniques of Biodegradable Implants Intended for Intraocular Application', *Drug Delivery*, 12(2), pp. 109–116. doi: 10.1080/10717540590921432.

Fina, F. *et al.* (2017) 'Selective laser sintering (SLS) 3D printing of medicines', *International Journal of Pharmaceutics*. Elsevier B.V., 529(1–2), pp. 285–293. doi: 10.1016/j.ijpharm.2017.06.082.

Fina, F., Goyanes, A., *et al.* (2018) '3D printing of drug-loaded gyroid lattices using selective laser sintering', *International Journal of Pharmaceutics*, 547(1–2), pp. 44–52. doi: 10.1016/j.ijpharm.2018.05.044.

Fina, F., Madla, C. M., *et al.* (2018) 'Fabricating 3D printed orally disintegrating printlets using selective laser sintering', *International Journal of Pharmaceutics*. Elsevier, 541(1–2), pp. 101–107. doi: 10.1016/j.ijpharm.2018.02.015.

Folkman, J. and Long, D. M. (1964) 'The Use of Silicone Rubber as a Carrier for Prolonged Drug Therapy', *Journal of Surgical Research*, 4(3), pp. 139–142. doi: 10.1016/S0022-4804(64)80040-8.

Fortelny, I. *et al.* (2019) 'Phase Structure , Compatibility , and Toughness of PLA / PCL Blends':, *Frontiers in Materials*, 6, pp. 1–13. doi: 10.3389/fmats.2019.00206.

Fu, J. *et al.* (2018) 'Combination of 3D printing technologies and compressed tablets for preparation of ribo fl avin fl oating tablet-in-device (TiD) systems', *International Journal of Pharmaceutics*. Elsevier, 549(1–2), pp. 370–379. doi: 10.1016/j.ijpharm.2018.08.011.

Fu, J., Yu, X. and Jin, Y. (2018) '3D printing of vaginal rings with personalized shapes for controlled release of progesterone', *International Journal of*

Pharmaceutics. Elsevier, 539(1–2), pp. 75–82. doi: 10.1016/j.ijpharm.2018.01.036.

Fuenmayor, E. *et al.* (2018) 'Material Considerations for Fused-Filament Fabrication of Solid Dosage Forms', *Pharmaceutics*, 44(10), pp. 1–27. doi: 10.3390/pharmaceutics10020044.

Fuenmayor, E. *et al.* (2019) 'Comparison of fused-filament fabrication to direct compression and injection molding in the manufacture of oral tablets', *International Journal of Pharmaceutics*. Elsevier, 558, pp. 328–340. doi: 10.1016/j.ijpharm.2019.01.013.

Gala, U. *et al.* (2015) 'Characterization and Comparison of Lidocaine-Tetracaine and Lidocaine-Camphor Eutectic Mixtures Based on Their Crystallization and Hydrogen-Bonding Abilities', *AAPS PharmSciTech*, 16(3), pp. 528–536. doi: 10.1208/s12249-014-0242-4.

Garbacz, P. *et al.* (2020) 'Structural characterization of co-crystals of chlordiazepoxide with p-aminobenzoic acid and lorazepam with nicotinamide by dsc, x-ray diffraction, ftir and raman spectroscopy', *Pharmaceutics*, 12(7), pp. 1–17. doi: 10.3390/pharmaceutics12070648.

Genina, N. *et al.* (2016) 'Ethylene vinyl acetate (EVA) as a new drug carrier for 3D printed medical drug delivery devices', *European Journal of Pharmaceutical Sciences*. Elsevier B.V., 90, pp. 53–63. doi: 10.1016/j.ejps.2015.11.005.

Genina, N. *et al.* (2017) 'Anti-tuberculosis drug combination for controlled oral delivery using 3D printed compartmental dosage forms: From drug product design to in vivo testing', *Journal of Controlled Release*. Elsevier, 268, pp. 40–48. doi: 10.1016/j.jconrel.2017.10.003.

Gioumouxouzis, C. I. *et al.* (2017) '3D printed oral solid dosage forms containing hydrochlorothiazide for controlled drug delivery', *Journal of Drug Delivery Science and Technology*. Elsevier Ltd, 40, pp. 164–171. doi: 10.1016/j.jddst.2017.06.008.

Gioumouxouzis, C. I., Baklavaridis, A., *et al.* (2018) 'A 3D printed bilayer oral solid dosage form combining metformin for prolonged and glimepiride for immediate drug delivery', *European Journal of Pharmaceutical Sciences*. Elsevier, 120, pp. 40–52. doi: 10.1016/j.ejps.2018.04.020.

Gioumouxouzis, C. I., Chatzitaki, A., *et al.* (2018) 'Controlled Release of 5-Fluorouracil from Alginate Beads Encapsulated in 3D Printed pH-Responsive Solid Dosage Forms', *AAPS PharmSciTech*. AAPS PharmSciTech, 19(8), pp. 3362–3375. doi: 10.1208/s12249-018-1084-2.

Gioumouxouzis, C. I., Karavasili, C. and Fatouros, D. G. (2019) 'Recent advances in pharmaceutical dosage forms and devices using additive manufacturing technologies', *Drug Discovery Today*. Elsevier Ltd, 24(2), pp. 636–643. doi: 10.1016/j.drudis.2018.11.019.

Goh, W. J. *et al.* (2021) '3D printing of four-in-one oral polypill with multiple release profiles for personalized delivery of caffeine and vitamin B analogues', *International Journal of Pharmaceutics*. Elsevier B.V., 598, p. 120360. doi: 10.1016/j.ijpharm.2021.120360.

Golzari, S. E. J. *et al.* (2014) 'Lidocaine and Pain Management in the Emergency Department : A Review Article', *Anesthesiology and Pain Medicine*, 4(1), pp. 1–6. doi: 10.5812/aapm.15444.

Goole, J. and Amighi, K. (2016) '3D printing in pharmaceutics: A new tool for designing customized drug delivery systems', *International Journal of Pharmaceutics*. Elsevier B.V., 499(1–2), pp. 376–394. doi: 10.1016/j.ijpharm.2015.12.071.

Gouda, R., Baishya, H. and Qing, Z. (2017) 'Journal of Developing Drugs Application of Mathematical Models in Drug Release Kinetics of Carbidopa and Levodopa ER Tablets', 6(2), pp. 1–8. doi: 10.4172/2329-6631.1000171.

Gov.UK (2020) *Impact Assessment (IA) of Medicines and Medical Devices Bill*. London.

Gov.UK (2021) *Regulating Medical Devices from 1st January 2021*. London. Available at: bhta.com/regulating-medical-devices-from-1st-january-2021/.

Govor, E. *et al.* (2014) 'Characterization of Biodegradable Polycaprolactone Containing Titanium Dioxide Micro and Nanoparticles', *International Journal of Chemical, Molecular, Nuclear, Materials and Metallurgical Engineering*, 8(7), pp. 577–581.

Goyanes, A. *et al.* (2014) 'Fused-filament 3D printing (3DP) for fabrication of tablets', *International Journal of Pharmaceutics*, 476(1), pp. 88–92. doi:

10.1016/j.ijpharm.2014.09.044.

Goyanes, A., Wang, J., *et al.* (2015) '3D Printing of Medicines: Engineering Novel Oral Devices with Unique Design and Drug Release Characteristics', *Molecular Pharmaceutics*, 12(11), pp. 4077–4084. doi: 10.1021/acs.molpharmaceut.5b00510.

Goyanes, A., Buanz, A. B. M., *et al.* (2015) '3D printing of modified-release aminosalicylate (4-ASA and 5-ASA) tablets', *European Journal of Pharmaceutics and Biopharmaceutics*. Elsevier B.V., 89, pp. 157–162. doi: 10.1016/j.ejpb.2014.12.003.

Goyanes, A., Robles Martinez, P., *et al.* (2015) 'Effect of geometry on drug release from 3D printed tablets', *International Journal of Pharmaceutics*. Elsevier B.V., 494(2), pp. 657–663. doi: 10.1016/j.ijpharm.2015.04.069.

Goyanes, A., Chang, H., *et al.* (2015) 'Fabrication of controlled-release budesonide tablets via desktop (FDM) 3D printing', *International Journal of Pharmaceutics*. Elsevier B.V., 496(2), pp. 414–420. doi: 10.1016/j.ijpharm.2015.10.039.

Goyanes, A. *et al.* (2016) '3D scanning and 3D printing as innovative technologies for fabricating personalized topical drug delivery systems', *Journal of Controlled Release*. Elsevier B.V., 234, pp. 41–48. doi: 10.1016/j.jconrel.2016.05.034.

Goyanes, A., Fina, F., *et al.* (2017) 'Development of modified release 3D printed tablets (printlets) with pharmaceutical excipients using additive manufacturing', *International Journal of Pharmaceutics*. Elsevier B.V., 527(1–2), pp. 21–30. doi: 10.1016/j.ijpharm.2017.05.021.

Goyanes, A., Scarpa, M., *et al.* (2017) 'Patient acceptability of 3D printed medicines', *International Journal of Pharmaceutics*. Elsevier B.V., 530(1–2), pp. 71–78. doi: 10.1016/j.ijpharm.2017.07.064.

Goyanes, A. *et al.* (2018) 'PET / CT imaging of 3D printed devices in the gastrointestinal tract of rodents', *International Journal of Pharmaceutics*. Elsevier, 536(1), pp. 158–164. doi: 10.1016/j.ijpharm.2017.11.055.

Goyanes, A. *et al.* (2019) 'Automated therapy preparation of isoleucine formulations using 3D printing for the treatment of MSUD : First single-centre ,

prospective , crossover study in patients', *International Journal of Pharmaceutics*. Elsevier, 567, p. 118497. doi: 10.1016/j.ijpharm.2019.118497.

Grehan, L. *et al.* (2014) 'The Development of Hot Melt Extruded Biocompatible Controlled Release Drug Delivery Devices', *International Journal of Polymeric Materials and Polymeric Biomaterials*, 63(9), pp. 476–485. doi: 10.1080/00914037.2013.854218.

Groningsson, K., Lindgren, J. and Lundberg, E. (1985) 'LIDOCAINE BASE AND HYDROCHLORIDE', in *Analytical Profiles of Drug Substances and Excipients*. 14th edn. American Pharmaceutical Association, pp. 209–237.

Guang-Mei, C. *et al.* (2010) 'Crystallization properties of polycaprolactone induced by different hydroxyapatite nano-particles', *Asian Journal of Chemistry*, 22(8), pp. 5902–5912.

Guarino, V. *et al.* (2017) 'POLYCAPROLACTONE: SYNTHESIS, PROPERTIES, AND APPLICATIONS', in *Encyclopedia ofPolymer Science and Technology*. John Wiley & Sons, Inc., pp. 1–36. doi: 10.1002/0471440264.pst658.

Gudin, J. *et al.* (2020) 'A Randomized , Open-Label , Bioequivalence Study of Lidocaine Topical System 1 . 8 % and Lidocaine Patch 5 % in Healthy Subjects', *Journal of Pain Research*, 13, pp. 1485–1496. doi: 10.2147/JPR.S237934.

Gudin, J. and Nalamachu, S. (2020) 'Utility of lidocaine as a topical analgesic and improvements in patch delivery systems', *Postgraduate Medicine*. Taylor & Francis, 132(1), pp. 28–36. doi: 10.1080/00325481.2019.1702296.

Gültekin, H. E., Tort, S. and Acartürk, F. (2019) 'An Effective Technology for the Development of Immediate Release Solid Dosage Forms Containing Low-Dose Drug : Fused Deposition Modeling 3D Printing', *Pharmaceutical Development and Technology*, 36, p. 128. doi: 10.1007/s11095-019-2655-y.

Gumede, T. P., Luyt, A. S. and Müller, A. J. (2018) 'Review on PCL , PBS , and PCL / PBS blends containing carbon nanotubes', *Express Polymer Letters*, 12(6), pp. 505–529. doi: 10.3144/expresspolymlett.2018.43.

Gunatillake, P. A. and Adhikari, R. (2003) 'Biodegradable synthetic polymers for tissue engineering', *European Cells and Materials*, 5, pp. 1–16. doi: 10.22203/eCM.v005a01.

Gupta, K. K. *et al.* (2012) 'Polycaprolactone composites with TiO 2 for potential

nanobiomaterials : tunable properties using different phases w', *Physical Chemistry Chemical Physics*, 14, pp. 12844–12853. doi: 10.1039/c2cp41789h.

Gv, S. *et al.* (2017) '3D printing of PCL / Fluorouracil tablets by selective laser sintering : Properties of implantable drug delivery for cartilage cancer treatment', *Rheumatology and Orthopedic Medicine Research*, 2(3), pp. 1–7. doi: 10.15761/ROM.1000121.

Hamed, R. *et al.* (2021) '3D-printing of lopinavir printlets by selective laser sintering and quantification of crystalline fraction by XRPD-chemometric models', *International Journal of Pharmaceutics*. Elsevier B.V., 592, p. 120059. doi: 10.1016/j.ijpharm.2020.120059.

Hammud, K. K. *et al.* (2013) 'Thermodynamic parameters for phenanthrene interaction with a biological π- acceptor (folic acid) by spectroscopic measurements', *Journal of Chemical and Pharmaceutical Research*, 5(2), pp. 24–28.

Han, S. *et al.* (2018) '3D printed drug delivery and testing systems — a passing fad or the future ?', *Advanced Drug Delivery Reviews*. Elsevier B.V., 132, pp. 139–168. doi: 10.1016/j.addr.2018.05.006.

Handelsman, D. J., Conway, A. J. and Boylan, L. M. (1990) 'Pharmacokinetics and pharmacodynamics of testosterone pellets in man', *Journal of Clinical Endocrinology and Metabolism*, 71(1), pp. 216–222. doi: 10.1210/jcem-71-1-216.

Haris, M. S. *et al.* (2020) '3D-printed Drugs : A Fabrication of Pharmaceuticals towards Personalized Medicine', *Indian Journal of Pharmaceutical Education and Research*, 54(3), pp. 411–422. doi: 10.5530/ijper.54.3s.139.

Healy, A. V *et al.* (2019) 'Additive Manufacturing of Personalized Pharmaceutical Dosage Forms via Stereolithography', *Pharmaceutics*, 11(645), pp. 13–15. doi: 10.3390/pharmaceutics11120645.

Heer, M. *et al.* (2000) 'High dietary sodium chloride consumption may not induce body fluid retention in humans', *American Journal of Physiology-Renal Physiology*, 278(4), pp. 585–595. doi: 10.1152/ajprenal.2000.278.4.f585.

Helmy, R. *et al.* (2003) 'Characterization and Quantitation of Aprepitant Drug Substance Polymorphs by Attenuated Total Reflectance Fourier Transform

Infrared Spectroscopy FT-IR) for the identification and quantitation of two', *Analytical Chemistry*, 75(3), pp. 605–611. doi: 10.1021/ac020538i.

Henry, S. *et al.* (2021) 'Extrusion-based 3D printing of oral solid dosage forms : Material requirements and equipment dependencies', *International Journal of Pharmaceutics*. Elsevier B.V., 598, p. 120361. doi: 10.1016/j.ijpharm.2021.120361.

Hermanns, H. *et al.* (2019) 'Molecular mechanisms of action of systemic lidocaine in acute and chronic pain : a narrative review', *British Journal of Anaesthesia*. Elsevier Ltd, 123(3), pp. 335–349. doi: 10.1016/j.bja.2019.06.014.

Higuchi, T. (1961) 'Rate of Release of Medicaments from Ointment Bases Containing Drugs in Suspension', *Journal of Pharmaceutucal Sciences*, 50(10), pp. 874–875. doi: 10.1002/jps.2600501018.

Hirshfield, L. *et al.* (2014) 'Dropwise additive manufacturing of pharmaceutical products for solvent-based dosage forms', *Journal of Pharmaceutical Sciences*. Elsevier Masson SAS, 103(2), pp. 496–506. doi: 10.1002/jps.23803.

Hofinger, S. (2011) *Master Thesis Rapid Implant Manufacturing by the Adapted Use of an Open Architecture 3D Printer*. University of Applied Sciences Wiener Neustadt, Austria.

Hogan, S. E. and Buckton, G. (2001) 'The Application of Near Infrared Spectroscopy and Dynamic Vapor Sorption to Quantify Low Amorphous Contents of Crystalline Lactose', *Pharmaceutical Research*, 18(1), pp. 112–116. doi: 10.1023/A:1011091113734.

Höglund, A., Hakkarainen, M. and Albertsson, A. C. (2007) 'Degradation Profile of Poly (ϵ - caprolactone)– the Influence of Macroscopic and Macromolecular Biomaterial Design', *Journal of Macromolecular Science*, 44, pp. 1041–1046. doi: 10.1080/10601320701424487.

Holgado, M. A. *et al.* (2008) 'Synthesis of lidocaine-loaded PLGA microparticles by flow focusing Effects on drug loading and release properties', *International Journal of Pharmaceutics*, 358, pp. 27–35. doi: 10.1016/j.ijpharm.2008.02.012.

Holländer, J. *et al.* (2016) 'Three-Dimensional Printed PCL-Based Implantable Prototypes of Medical Devices for Controlled Drug Delivery', *Journal of*

Pharmaceutical Sciences, 105(9), pp. 2665–2676. doi: 10.1016/j.xphs.2015.12.012.

Hoque, M. E., Chuan, Y. L. and Pashby, I. (2011) 'Extrusion Based Rapid Prototyping Technique: An Advanced Platform for Tissue Engineering Scaffold Fabrication', *Biopolymers*, 97(2), pp. 83–93. doi: 10.1002/bip.21701.

Horst, D. J. (2018) '3D Printing of Pharmaceutical Drug Delivery Systems', *Archives of Organic and Inorganic Chemical Sciences*, 1(2), pp. 1–5. doi: 10.32474/AOICS.2018.01.000109.

ter Horst, J. H. and Cains, P. W. (2009) 'Discovering New Co-Crystals', *Crystal Growth and Design*, 9(3), pp. 1531–1537. doi: 10.1021/cg801200h.

Hsiao, W. *et al.* (2018) '3D printing of oral drugs : a new reality or hype ?', *Expert Opinion on Drug Delivery*. Taylor & Francis, 15(1), pp. 1–4. doi: 10.1080/17425247.2017.1371698.

Huanbutta, K. and Sangnim, T. (2019) 'Design and development of zero-order drug release gastroretentive fl oating tablets fabricated by 3D printing technology', *Journal of Drug Delivery Science and Technology*. Elsevier, 52, pp. 831–837. doi: 10.1016/j.jddst.2019.06.004.

Huang, C. Y. (2018) *Extrusion-based 3D Printing and Characterization of Edible Materials*. University of Waterloo.

Huang, S. *et al.* (2016) 'A New Extrudable Form of Hypromellose : AFFINISOL ™ HPMC HME', *AAPS PharmSciTech*, 17(1), pp. 106–119. doi: 10.1208/s12249-015-0395-9.

Huang, W. *et al.* (2007) 'Levofloxacin implants with predefined microstructure fabricated by three-dimensional printing technique', *International Journal of Pharmaceutics*, 339(1–2), pp. 33–38. doi: 10.1016/j.ijpharm.2007.02.021.

Huang, X. and Brazel, C. S. (2001) 'On the importance and mechanisms of burst release in matrix-controlled drug delivery systems', *Journal of Controlled Release*, 73(2–3), pp. 121–136. doi: 10.1016/S0168-3659(01)00248-6.

Huang, Y. and Dai, W.-G. (2014) 'Fundamental aspects of solid dispersion technology for poorly soluble drugs', *Acta Pharmaceutica Sinica B*. Elsevier, 4(1), pp. 18–25. doi: 10.1016/j.apsb.2013.11.001.

Hull, C. W. (1986) 'APPARATUS FOR PRODUCTION OF THREE-DMENSONAL OBJECTS BY STEREO THOGRAPHY', *United States Patent*, (4575330), pp. 1–16.

Hung, C. Y. *et al.* (2013) 'Preparation, Crystallization Behavior, and Morphology of Poly(lactic acid) Clay Hybrids via Wet Kneading Masterbatch Process', *Journal of Inorganic and Organometallic Polymers and Materials*, 23(6), pp. 1389–1396. doi: 10.1007/s10904-013-9941-7.

Hutmacher, Dietmar W., Sittinger, M. and Risbud, M. V. (2004) 'Scaffold-based tissue engineering: Rationale for computer-aided design and solid free-form fabrication systems', *Trends in Biotechnology*, 22(7), pp. 354–362. doi: 10.1016/j.tibtech.2004.05.005.

Hutmacher, Dietmar W, Sittinger, M. and Risbud, M. V (2004) 'Scaffold-based tissue engineering : rationale for computer-aided design and solid free-form fabrication systems', *Trends in Biotechnology*, 22(7), pp. 354–362. doi: 10.1016/j.tibtech.2004.05.005.

Ilyés, K. *et al.* (2019) 'The applicability of pharmaceutical polymeric blends for the fused deposition modelling (FDM) 3D technique : Material considerations – printability – process modulation , with consecutive e ff ects on in vitro release , stability and degradation', *European Journal of Pharmaceutical Sciences*, 129, pp. 110–123. doi: 10.1016/j.ejps.2018.12.019.

Infanger, S. *et al.* (2019) 'Powder bed 3D-printing of highly loaded drug delivery devices with hydroxypropyl cellulose as solid binder', *International Journal of Pharmaceutics*. Elsevier, 555, pp. 198–206. doi: 10.1016/j.ijpharm.2018.11.048.

Inkredible+ (2019) *Inkredible+ User Manual*. Gothenburg.

Isreb, A. *et al.* (2019) '3D printed oral theophylline doses with innovative " radiator-like " design : Impact of polyethylene oxide (PEO) molecular weight', *International Journal of Pharmaceutics*. Elsevier, 564, pp. 98–105. doi: 10.1016/j.ijpharm.2019.04.017.

Jain, K. (2008) 'Drug Delivery System', *Freepatentsonline.Com*. doi: 10.1007/978-1-4939-0363-4.

Jain, K. K. (2008) 'Drug Delivery Systems - An Overview', in Jain, K. K. (ed.) *Drug Delivery Systems*. Totowa, Nj: Humana Press, pp. 1–50.

Jamróz, W., Kurek, M., Łyszczarz, E., Szafraniec, J., *et al.* (2017) '3D printed orodispersible films with Aripiprazole', *International Journal of Pharmaceutics*, 533(2), pp. 413–420. doi: 10.1016/j.ijpharm.2017.05.052.

Jamróz, W., Kurek, M., Łyszczarz, E., Brniak, W., *et al.* (2017) 'Printing techniques: Recent developments in pharmaceutical technology', *Acta Poloniae Pharmaceutica - Drug Research*, 74(3), pp. 753–763.

Jamróz, W., Szafraniec, J., *et al.* (2018) '3D Printing in Pharmaceutical and Medical Applications – Recent Achievements and Challenges', *Pharmaceutical Research*. Pharmaceutical Research, 35(9), p. 176. doi: 10.1007/s11095-018-2454-x.

Jamróz, W., Kurek, M., *et al.* (2018) '3D printing of tablets containing amorphous aripiprazole by fi laments co- extrusion', *European Journal of Pharmaceutics and Biopharmaceutics*. Elsevier, 131, pp. 44–47. doi: 10.1016/j.ejpb.2018.07.017.

Jamróz, W. *et al.* (2020) 'Speed it up , slow it down … An issue of bicalutamide release from 3D printed tablets', *European Journal of Pharmaceutical Sciences*, 143, p. 105169. doi: 10.1016/j.ejps.2019.105169.

Jasiuk, I. *et al.* (2018) 'An Overview on Additive Manufacturing of Polymers', *JOM*. Springer US, 70(3), pp. 275–283. doi: 10.1007/s11837-017-2730-y.

Jenkins, M. J. and Harrison, K. L. (2006) 'The effect of molecular weight on the crystallization kinetics of polycaprolactone', *Polymers for Advanced Technologies*, 17, pp. 474–478. doi: 10.1002/pat.

Jeong, J.-C., Lee, J. and Cho, K. (2003) 'Effects of crystalline microstructure on drug release behavior of poly (q -caprolactone) microspheres', *Journal of Controlled Release*, 92, pp. 249–258. doi: 10.1016/S0168-3659(03)00367-5.

Jie, Y. *et al.* (2021) 'Customizable drug tablets with constant release profiles via 3D printing technology', *International Journal of Pharmaceutics*. Elsevier B.V., 598, p. 120370. doi: 10.1016/j.ijpharm.2021.120370.

Johannesson, J. *et al.* (2021) '3D-printing of solid lipid tablets from emulsion gels', *International Journal of Pharmaceutics*, 597, p. 102304. doi: 10.1016/j.ijpharm.2021.120304.

Johari, A. P. *et al.* (2016) 'Influence of surface modified cellulose microfibrils on

the improved mechanical properties of poly (lactic acid)', *International Journal of Biological Macromolecules*. Elsevier B.V., 84, pp. 329–339. doi: 10.1016/j.ijbiomac.2015.12.038.

Ju, B. *et al.* (2019) 'Pharmaceutical applications of 3D printing technology : current understanding and future perspectives', *Journal of Pharmaceutical Investigation*. Springer Singapore, 49(6), pp. 575–585. doi: 10.1007/s40005-018-00414-y.

Kadry, H. *et al.* (2018) 'Multi-purposable filaments of HPMC for 3D printing of medications with tailored drug release and timed-absorption', *International Journal of Pharmaceutics*. Elsevier, 544(1), pp. 285–296. doi: 10.1016/j.ijpharm.2018.04.010.

Kadry, H. *et al.* (2019) 'Digital light processing (DLP) 3D-printing technology and photoreactive polymers in fabrication of modi fi ed-release tablets', *European Journal of Pharmaceutical Sciences*. Elsevier, 135(April), pp. 60–67. doi: 10.1016/j.ejps.2019.05.008.

Kalambur, S. and Rizvi, S. S. H. (2006) 'Rheological Behavior of Starch – Polycaprolactone (PCL) Nanocomposite Melts Synthesized by Reactive Extrusion', *Polymer Engineering and Science*, 46(5), pp. 650–658. doi: 10.1002/pen.

Kammerer, M. *et al.* (2011) 'Valproate release from polycaprolactone implants prepared by 3D-bioplotting', *Pharmazie*, 66(7), pp. 511–516. doi: 10.1691/ph.2011.0882.

Kang, L., Jun, H. W. and Mccall, J. W. (2000) 'Physicochemical studies of lidocaine – menthol binary systems for enhanced membrane transport', *International Journal of Pharmaceutics*, 206, pp. 35–42. doi: 10.1016/S0378-5173(00)00505-6.

Karavasili, C. *et al.* (2020) 'Pediatric-friendly chocolate-based dosage forms for the oral administration of both hydrophilic and lipophilic drugs fabricated with extrusion-based 3D printing', *European Journal of Pharmaceutical Sciences*. Elsevier, 147(March), p. 105291. doi: 10.1016/j.ejps.2020.105291.

Kasaai, M. R. (2007) 'Calculation of Mark-Houwink-Sakurada (MHS) equation viscometric constants for chitosan in any solvent-temperature system using experimental reported viscometric constants data', *Carbohydrate Polymers*,

68(3), pp. 477–488. doi: 10.1016/j.carbpol.2006.11.006.

Kasinathan, N. *et al.* (2016) 'Polycaprolactone-based in situ implant containing curcumin-PLGA nanoparticles prepared using the multivariate technique', *Artificial Cells, Nanomedicine and Biotechnology*, 44(6), pp. 1520–1528. doi: 10.3109/21691401.2015.1058810.

Katstra, W. . *et al.* (2000) 'Oral dosage forms fabricated by Three Dimensional Printing™', *Journal of Controlled Release*, 66(1), pp. 1–9. doi: 10.1016/S0168-3659(99)00224-2.

Kau, Y. *et al.* (2014) 'Sustained Release of Lidocaine from Solvent-Free Biodegradable Poly[(d,l)-Lactide-co-Glycolide] (PLGA): In Vitro and In Vivo Study', *Materials*, 7, pp. 6660–6676. doi: 10.3390/ma7096660.

Kaurav, H. and Kapoor, D. N. (2017) 'Implantable systems for drug delivery to the brain', *Therapeutic Delivery*, 8(12), pp. 1097–1107. doi: 10.4155/tde-2017-0082.

Kelleher, S. *et al.* (2004) 'Testosterone release rate and duration of action of testosterone pellet implants', *Clinical Endocrinology*, 60(4), pp. 420–428. doi: 10.1111/j.1365-2265.2004.01994.x.

Kempin, W. *et al.* (2017) 'Assessment of different polymers and drug loads for fused deposition modeling of drug loaded implants', *European Journal of Pharmaceutics and Biopharmaceutics*. Elsevier B.V., 115, pp. 84–93. doi: 10.1016/j.ejpb.2017.02.014.

Kempin, W., Domsta, V., Brecht, I., *et al.* (2018) 'Development of a dual extrusion printing technique for an acid- and thermo- labile drug', *European Journal of Pharmaceutical Sciences*. Elsevier, 123, pp. 191–198. doi: 10.1016/j.ejps.2018.07.041.

Kempin, W., Domsta, V., Grathoff, G., *et al.* (2018) 'Immediate Release 3D-Printed Tablets Produced Via Fused Deposition Modeling of a Thermo-Sensitive Drug', *Pharmaceutical Research*. Pharmaceutical Research, 35(124), pp. 1–12. doi: 10.1007/s11095-018-2405-6.

Kenny, E. *et al.* (2013) 'PROCESSING AND CHARACTERISATION OF VARIOUS POLYMER BLENDS TO DEVELOP IMPLANT FOR TISSUE ENGINEERING APPLICATIONS Declan Devine Luke Geever Materials', *Journal of Asian Scientific*

Research, 3(6), pp. 654–669. Available at: http://aessweb.com/journal-detail.php?id=5003.

Kerrels, J. *et al.* (2021) *Medicinal product regulation and product liability in the EU : overview*. Brussels.

De Kesel, C. *et al.* (1999) 'Blends of polycaprolactone with polyvinylalcohol: A DSC, optical microscopy and solid state NMR study', *Polymer*, 40(8), pp. 1969–1978. doi: 10.1016/S0032-3861(98)00253-5.

Khaled, S. A. *et al.* (2014) 'Desktop 3D printing of controlled release pharmaceutical bilayer tablets', *International Journal of Pharmaceutics*. Elsevier B.V., 461(1–2), pp. 105–111. doi: 10.1016/j.ijpharm.2013.11.021.

Khaled, Shaban A. *et al.* (2015) '3D printing of five-in-one dose combination polypill with defined immediate and sustained release profiles', *Journal of Controlled Release*, 217, pp. 308–314. doi: 10.1016/j.jconrel.2015.09.028.

Khaled, Shaban A *et al.* (2015) '3D printing of tablets containing multiple drugs with defined release profiles', *International Journal of Pharmaceutics*, 494, pp. 643–650. doi: 10.1016/j.ijpharm.2015.07.067.

Khaled, Shaban A. *et al.* (2018) '3D extrusion printing of high drug loading immediate release paracetamol tablets', *International Journal of Pharmaceutics*. Elsevier, 538(1–2), pp. 223–230. doi: 10.1016/j.ijpharm.2018.01.024.

Khaled, Shaban A *et al.* (2018) 'Extrusion 3D Printing of Paracetamol Tablets from a Single Formulation with Tunable Release Profiles Through Control of Tablet Geometry', *AAPS PharmSciTech*. AAPS PharmSciTech, 19(8), pp. 3403–3413. doi: 10.1208/s12249-018-1107-z.

Khan, F. M., Ahmad, M. and Idrees, H. A. (2020) 'Simvastatin-nicotinamide co-crystals: Formation, pharmaceutical characterization and in vivo profile', *Drug Design, Development and Therapy*, 14, pp. 4303–4313. doi: 10.2147/DDDT.S270742.

Khan, R. and Gillespie, G. (2013) 'Implantable technology for pain management', *Anaesthesia and Intensive Care Medicine*. Elsevier Ltd, 14(12), pp. 520–523. doi: 10.1016/j.mpaic.2013.09.009.

Khatri, P., Shah, M. K. and Vora, N. (2018) 'Formulation strategies for solid oral dosage form using 3D printing technology : A mini-review', *Journal of Drug*

Delivery Science and Technology. Elsevier, 46, pp. 148–155. doi: 10.1016/j.jddst.2018.05.009.

Kim, J. *et al.* (2016) 'Biocompatibility and pharmacokinetic analysis of an intracameral polycaprolactone drug delivery implant for glaucoma', *Investigative Ophthalmology and Visual Science*, 57(10), pp. 4341–4346. doi: 10.1167/iovs.16-19585.

Kimura, S. *et al.* (2019) 'Fabrication of Zero-Order Sustained-Release Floating Tablets via Fused Depositing Modeling 3D Printer', *Chemical & Pharmaceutical Bulletin*, 67(9), pp. 992–999. doi: 10.1248/cpb.c19-00290.

Kollamaram, G. *et al.* (2018) 'Low temperature fused deposition modeling (FDM) 3D printing of thermolabile drugs', *International Journal of Pharmaceutics*. Elsevier, 545(1–2), pp. 144–152. doi: 10.1016/j.ijpharm.2018.04.055.

Kompbella, U. B., Kadam, R. S. and Lee, V. H. L. (2011) 'Recent advances in ophthalmic drug delivery', *Therapeutic Delivery*, 1(3), pp. 219–263. doi: 10.4155/TDE.10.40.Recent.

Konta, A., García-Piña, M. and Serrano, D. (2017) 'Personalised 3D Printed Medicines: Which Techniques and Polymers Are More Successful?', *Bioengineering*, 4(4), p. 79. doi: 10.3390/bioengineering4040079.

Koopmans, R. J. (1999) 'Die swell or extrudate swell', in Karger-Kocsis, J. (ed.) *Polymer Science and Technology Series, vol 2*. Second Edi. Dordrecht: Springer, pp. 158–162. doi: 10.1007/978-94-011-4421-6_22.

Korte, C. *et al.* (2018) 'Formulation development and process analysis of drug-loaded filaments manufactured via hot-melt extrusion for 3D-printing of medicines manufactured via hot-melt extrusion for 3D-printing of medicines', *Pharmaceutical Development and Technology*. Informa Healthcare USA, Inc, pp. 1–11. doi: 10.1080/10837450.2018.1433208.

Korte, C. and Quodbach, J. (2018) '3D-Printed Network Structures as Controlled-Release Drug Delivery Systems : Dose Adjustment , API Release Analysis and Prediction', *AAPS PharmSciTech*. AAPS PharmSciTech, 19(8), pp. 3333–3342. doi: 10.1208/s12249-018-1017-0.

Kotta, S., Nair, A. and Alsabeelah, N. (2018) '3D Printing Technology in Drug Delivery: Recent Progress and Application', *Current Pharmaceutical Design*, 24,

pp. 5039–5048. doi: 10.2174/138161282566181206123828.

Kotula, A. P., Snyder, C. R. and Migler, K. B. (2017) 'Determining conformational order and crystallinity in polycaprolactone via Raman spectroscopy *', *Polymer*. Elsevier Ltd, 117, pp. 1–10. doi: 10.1016/j.polymer.2017.04.006.

Kumar, A. and Pillai, J. (2018) *Implantable drug delivery systems: An overview*, *Nanostructures for the Engineering of Cells, Tissues and Organs:* Edited by A. M. Grumezescu. Elsevier Inc. doi: 10.1016/B978-0-12-813665-2.00013-2.

Kumar, S. and Nanda, A. (2017) 'Pharmaceutical cocrystals: An overview', *Indian Journal of Pharmaceutical Sciences*, 79(6), pp. 858–871. doi: 10.4172/pharmaceutical-sciences.1000302.

Kumpugdee-Vollrath, M., Krause, J.-P. and Bürk, S. (2014) 'Surfactant-Free o/w Emulsion as Drug Delivery System', *International Journal of Medical, Health, Biomedical, Bioengineering and Pharmaceutical Engineering*, 8(9), pp. 574–577. doi: 10.5281/zenodo.1337451.

Kyle, S. *et al.* (2017) '" Printability " of Candidate Biomaterials for Extrusion Based 3D Printing : State-of-the-Art', *Advanced Healthcare Materials*, 6, pp. 1–16. doi: 10.1002/adhm.201700264.

Kyobula, M. *et al.* (2017) '3D inkjet printing of tablets exploiting bespoke complex geometries for controlled and tuneable drug release', *Journal of Controlled Release*. Elsevier, 261, pp. 207–215. doi: 10.1016/j.jconrel.2017.06.025.

Labet, M. and Thielemans, W. (2009) 'Synthesis of polycaprolactone: a review', *Chemical Society Reviews*, 38(12), p. 3484. doi: 10.1039/b820162p.

Lamichhane, S., Bashyal, S., *et al.* (2019) 'Complex formulations , simple techniques : Can 3D printing technology be the Midas touch in pharmaceutical industry ?', *Asian Journal of Pharmaceutical Sciences*. Elsevier B.V., 14, pp. 465–479. doi: 10.1016/j.ajps.2018.11.008.

Lamichhane, S., Park, J., *et al.* (2019) 'Customized Novel Design of 3D Printed Pregabalin Tablets for Intra-Gastric Floating and Controlled Release Using Fused Deposition Modeling', *Pharmaceutics*, 564(11), pp. 1–14. doi: 10.3390/pharmaceutics11110564.

Lang, B., Mcginity, J. W. and Williams III, R. O. (2014) 'Hot-melt extrusion –

basic principles and pharmaceutical applications', *Drug Development and Industrial Pharmacy*, 9045, pp. 1–23. doi: 10.3109/03639045.2013.838577.

Langer, R. (1983) 'Implantable controlled release systems', *Pharmacology and Therapeutics*, 21(2), pp. 35–51. doi: 10.1016/0163-7258(83)90066-9.

Langer, R. (1990) 'New Methods of Drug Delivery', *Science*, 249(4976), pp. 1527–1533. doi: 10.1126/science.2218494 ARTICLE.

Langer, R. (1993) 'Polymer-Controlled Drug Delivery Systems', *Accounts of Chemical Research*, 26, pp. 537–542. doi: 10.1021/ar00034a004.

Langer, R. S. and Peppas, N. A. (1981) 'Present and future applications of biomaterials in controlled drug delivery systems', *Biomaterials*, 2(4), pp. 201–214. doi: 10.1016/0142-9612(81)90059-4.

Larsen, C. and Jensen, H. (2011) 'Monitoring Lidocaine Single-Crystal Dissolution by Ultraviolet Imaging', *Journal of Pharmaceutical Sciences*, 100(8), pp. 1–6. doi: 10.1002/jps.

Lebon, M. *et al.* (2016) 'RAPID QUANTIFICATION OF BONE COLLAGEN CONTENT BY ATR-FTIR SPECTROSCOPY', *Radiocarbon*, 58(1), pp. 131–146. doi: 10.1017/RDC.2015.11.

Lee, D. (2015) 'Intraocular Implants for the Treatment of Autoimmune Uveitis', *Journal of Functional Biomaterials*, 6(3), pp. 650–666. doi: 10.3390/jfb6030650.

Lee, S. H. *et al.* (2019) 'Implantable multireservoir device with stimulus-responsive membrane for on-demand and pulsatile delivery of growth hormone', *PNAS*, 116(24), pp. 11664–11672. doi: 10.1073/pnas.1906931116.

Lehto, V. *et al.* (2006) 'The comparison of seven different methods to quantify the amorphous content of spray dried lactose', *Powder Technologyology*, 167, pp. 85–93. doi: 10.1016/j.powtec.2006.05.019.

Leng, F. *et al.* (2012) 'Prolongation of Epidural Analgesia Using Solid Lipid Nanoparticles as Drug Carrier for Lidocaine', *Regional Anesthesia and Pain Medicine*, 37(2), pp. 159–165. doi: 10.1097/AAP.0b013e31823fc058.

Lepowsky, E. and Tasoglu, S. (2018) '3D printing for drug manufacturing : A perspective on the future of pharmaceuticals', *International Journal of Bioprinting*, 4(1), pp. 1–13. doi: 10.18063/IJB.v4i1.119.

Li, Q. *et al.* (2018) 'Preparation and investigation of novel gastro-floating tablets with 3D extrusion-based printing', *International Journal of Pharmaceutics*. Elsevier, 535(1–2), pp. 325–332. doi: 10.1016/j.ijpharm.2017.10.037.

Liang, K., Brambilla, D. and Leroux, J. (2019) 'Is 3D Printing of Pharmaceuticals a Disruptor or Enabler?', *Advanced Materials*, 31(1805680), pp. 1–4. doi: 10.1002/adma.201805680.

Liaskoni, A., Wildman, R. D. and Roberts, C. J. (2021) '3D printed polymeric drug-eluting implants', *International Journal of Pharmaceutics*. Elsevier B.V., 597, p. 120330. doi: 10.1016/j.ijpharm.2021.120330.

Liaw, C. and Guvendiren, M. (2017) 'Current and emerging applications of 3D printing in medicine', *Biofabrication*. IOP Publishing, 9, pp. 1–18. doi: 10.1088/1758-5090/aa7279.

Lidoderm (2018) 'LIDODERM □ (Lidocaine Patch 5%) R'. Endo Pharmaceuticals Inc, pp. 1–8.

Liechty, W. B. *et al.* (2010) 'Polymers for Drug Delivery Systems', *Annual Review of Chemical and Biomolecular Engineering*, 1, pp. 149–173. doi: 10.1146/annurev-chembioeng-073009-100847.

Ligon, S. C. *et al.* (2017) 'Polymers for 3D Printing and Customized Additive Manufacturing', *Chemical Reviews*, 117, pp. 10210–10290. doi: 10.1021/acs.chemrev.7b00074.

Lim, S. H. *et al.* (2016) 'Three-Dimensional Printing of Carbamazepine Sustained-Release Scaffold', *Journal of Pharmaceutical Sciences*. Elsevier Ltd, 105(7), pp. 2155–2163. doi: 10.1016/j.xphs.2016.04.031.

Lim, S. H. *et al.* (2018) '3D printed drug delivery and testing systems — a passing fad or the future?', *Advanced Drug Delivery Reviews*. Elsevier B.V., 132, pp. 139–168. doi: 10.1016/j.addr.2018.05.006.

Linares, V., Casas, M. and Caraballo, I. (2019) 'Printfills : 3D printed systems combining fused deposition modeling and injection volume filling. Application to colon-specific drug delivery', *European Journal of Pharmaceutics and Biopharmaceutics*. Elsevier, 134, pp. 138–143. doi: 10.1016/j.ejpb.2018.11.021.

Lind, J. *et al.* (2017) 'Social aspects in additive manufacturing of pharmaceutical products Social aspects in additive manufacturing of pharmaceutical products',

Expert Opinion on Drug Delivery. Taylor & Francis, 14(8), pp. 1–10. doi: 10.1080/17425247.2017.1266336.

Liu, C. B. *et al.* (2007) 'Thermoreversible Gel – Sol Behavior of Biodegradable PCL-PEG-PCL Triblock Copolymer in Aqueous Solutions', *Journal of Biomedical Materials Research Parts B: Applied Biomaterials*, 84(1), pp. 165–175. doi: 10.1002/jbmb.

Liu, D. *et al.* (2016) 'The Smart Drug Delivery System and Its Clinical Potential', *Theranostics*, 6(9), pp. 1306–1323. doi: 10.7150/thno.14858.

Liu, X. *et al.* (2018) 'Influence of lidocaine forms (salt vs . freebase) on properties of drug – Eudragit ® L100-55 extrudates prepared by reactive melt extrusion In fl uence of lidocaine forms (salt vs . freebase) on properties of drug – eudragit ® L100-55 extrudates prepa', *International Journal of Pharmaceutics*. Elsevier, 547(1–2), pp. 291–302. doi: 10.1016/j.ijpharm.2018.06.009.

Lopez-rubio, A. *et al.* (2008) 'Biopolymers Volume 89 / Number 9 761', 89(9), pp. 761–768. doi: 10.1002/bip.21005.

López, J. V. *et al.* (2016) 'The influence of small amounts of linear polycaprolactone chains on the crystallization of cyclic analogue molecules', *RSC Advances*, 6(53), pp. 48049–48063. doi: 10.1039/c6ra04823d.

Luzuriaga, M. A. *et al.* (2018) 'Biodegradable 3D printed polymer microneedles for transdermal drug delivery', *Lab Chip*. Royal Society of Chemistry, 18(8), pp. 1223–1230. doi: 10.1039/c8lc00098k.

Ma, G. *et al.* (2006) 'A biodegradable levonorgestrel-releasing implant made of PCL/F68 compound as tested in rats and dogs', *Contraception*, 74(2), pp. 141–147. doi: 10.1016/j.contraception.2006.02.013.

Ma, Z. *et al.* (2007) 'Micelles of poly (ethylene oxide) - b -poly (e - caprolactone) as vehicles for the solubilization , stabilization , and controlled delivery of curcumin', *Journal of Biomedical Materials Research Parts A*, 86(2), pp. 300–310. doi: 10.1002/jbm.a.31584.

Mackin, L. *et al.* (2002) 'Quantification of low levels (B 10 %) of amorphous content in micronised active batches using dynamic vapour sorption and isothermal microcalorimetry', *International Journal of Pharmaceutics*, 231, pp.

227–236. doi: 10.1016/S0378-5173(01)00881-X.

Maiti, S. and Sen, K. K. (2017) 'Introductory Chapter: Drug Delivery Concepts', in *Advanced Technology for Delivering Therapeutics*. Asansol, pp. 1–13. doi: 10.5772/65245.

Major, I. *et al.* (2020) 'Implantable drug delivery systems', in *Engineering Drug Delivery Systems*. Elsevier LTD., pp. 111–146. doi: 10.1016/B978-0-08-102548-2.00005-6.

Makadia, H. and Siegel, S. J. (2012) 'Poly Lactic-co-Glycolic Acid (PLGA) as Biodegradable Controlled Drug Delivery Carrier', *Polymers (Basel)*, 3(3), pp. 1377–1397. doi: 10.3390/polym3031377.Poly.

Maniruzzaman, M. *et al.* (2012) 'A Review of Hot-Melt Extrusion : Process Technology to Pharmaceutical Products', *International Scholarly Research Newtork ISRN Pharmaceutics*, 2012, pp. 1–9. doi: 10.5402/2012/436763.

Maroni, A. *et al.* (2017) '3D printed multi-compartment capsular devices for two-pulse oral drug delivery', *Journal of Controlled Release*. Elsevier, 268, pp. 10–18. doi: 10.1016/j.jconrel.2017.10.008.

Martin, N. K. *et al.* (2021) 'Fused deposition modelling for the development of drug loaded cardiovascular prosthesis', *International Journal of Pharmaceutics*, 595, p. 120243. doi: 10.1016/j.ijpharm.2021.120243.

Martinez, P. R. *et al.* (2017) 'Fabrication of drug-loaded hydrogels with stereolithographic 3D printing', *International Journal of Pharmaceutics*. Elsevier, 532(1), pp. 313–317. doi: 10.1016/j.ijpharm.2017.09.003.

Martinez, P. R. *et al.* (2018) 'Influence of Geometry on the Drug Release Profiles of Stereolithographic (SLA) 3D-Printed Tablets', *AAPS PharmSciTech*. AAPS PharmSciTech, 19(8), pp. 3355–3361. doi: 10.1208/s12249-018-1075-3.

Masic, D. *et al.* (2018) 'Intraenous Lidocaine for Acute Pain : A Systematic Review', *Pharmacotherapy*, 38(12), pp. 1250–12159. doi: 10.1002/phar.2189.

Masood, S. H. (1996) 'Intelligent rapid prototyping with fused deposition modelling', *Rapid Prototyping Journal*, 2(1), pp. 24–33. doi: 10.1108/13552549610109054.

Mathew, E., Pitzanti, G. and Larrañeta, E. (2020) '3D Printing of Pharmaceuticals

and Drug Delivery Devices', *Pharmaceutics*, 12(3), pp. 1–9. doi: 10.3390/pharmaceutics12030266.

Matta, A. K. *et al.* (2014) 'Preparation and Characterization of Biodegradable PLA / PCL Polymeric Blends', *Procedia Materials Science*. Elsevier B.V., 6, pp. 1266–1270. doi: 10.1016/j.mspro.2014.07.201.

Matzinos, P. *et al.* (2002) 'Processing and characterization of LDPE / starch / PCL blends', *European Polymer Journal*, 38, pp. 1713–1720. doi: 10.1016/S0014-3057(02)00061-7.

Mavis, B. and Demirtas, T. T. (2009) 'Synthesis , characterization and osteoblastic activity of polycaprolactone nanofibers coated with biomimetic calcium phosphate', *Acta Biomaterialia*, 5, pp. 3098–3111. doi: 10.1016/j.actbio.2009.04.037.

Medlicott, N. J. *et al.* (1992) 'Preliminary release studies of chlorhexidine (base and diacetate) from poly(ε{lunate}-caprolactone) films prepared by solvent evaporation', *International Journal of Pharmaceutics*, 84(1), pp. 85–89. doi: 10.1016/0378-5173(92)90218-Q.

de Melo, F. and Marijnissen-Hofste, J. (2012) 'Investigation of Physical Properties of a Polycaprolactone Dermal Filler when Mixed with Lidocaine and Lidocaine / Epinephrine', *Dermatology Therapy*, 13(2), pp. 1–10. doi: 10.1007/s13555-012-0013-7.

Melocchi, A. *et al.* (2015) '3D printing by fused deposition modeling (FDM) of a swellable/erodible capsular device for oral pulsatile release of drugs', *Journal of Drug Delivery Science and Technology*. Elsevier Ltd, 30, pp. 360–367. doi: 10.1016/j.jddst.2015.07.016.

Melocchi, A. *et al.* (2016) 'Hot-melt extruded filaments based on pharmaceutical grade polymers for 3D printing by fused deposition modeling', *International Journal of Pharmaceutics*. Elsevier B.V., 509(1–2), pp. 255–263. doi: 10.1016/j.ijpharm.2016.05.036.

Meng, E. and Hoang, T. (2012) 'Micro- and nano-fabricated implantable drug-delivery systems', *Therapeutic Delivery*, 3(12), pp. 1457–1467. doi: 10.4155/tde.12.132.

MHRA (2021) *Consultation on Point of Care manufacturing*. London. Available at:

https://www.gov.uk/government/consultations/point-of-care-consultation/consultation-on-point-of-care-manufacturing.

Middleton, J. C. and Tipton, A. J. (2000) 'Synthetic biodegradable polymers as orthopedic devices', *Biomaterials*, 21, pp. 2335–2346. doi: 10.1016/S0142-9612(00)00101-0.

Modi, K. *et al.* (2013) 'Oral Controlled Release Drug Delivery System: an Overview', *International Research Journal of Pharmacy*, 4(3), pp. 70–76. doi: 10.7897/2230-8407.04312.

Mofenson, H. C. *et al.* (1983) 'Lidocaine Toxicity from Mucosal Application', *Clinical Pediatrics*, 22(3), pp. 190–192. doi: 10.1177/000992288302200306.

Mohamed, R. M. and Yusoh, K. (2016) 'A Review on the Recent Research of Polycaprolactone (PCL)', *Advanced Materials Research*, 1134, pp. 249–255. doi: 10.4028/www.scientific.net/AMR.1134.249.

Monteiro, M. S. D. S. B., Inês, M. and Tavares, B. (2018a) 'The Development and Characterization of Polycaprolactone and Titanium Dioxide Hybrids', pp. 11–27. doi: 10.4236/anp.2018.71002.

Monteiro, M. S. D. S. B., Inês, M. and Tavares, B. (2018b) 'The Development and Characterization of Polycaprolactone and Titanium Dioxide Hybrids', *Advances in Nanoparticles*, 7, pp. 11–27. doi: 10.4236/anp.2018.71002.

Monteiro, M. S. S. B. *et al.* (2016) 'Evaluation of Nevirapine Release Kinetics from Polycaprolactone Hybrids', *Materials Science and Applications*, 7, pp. 680–701. doi: 10.4236/msa.2016.711055.

Moulton, S. E. and Wallace, G. G. (2014) '3-dimensional (3D) fabricated polymer based drug delivery systems', *Journal of Controlled Release*. Elsevier B.V., 193, pp. 27–34. doi: 10.1016/j.jconrel.2014.07.005.

Murphy, S. (2011) *Melting Point Depression in Biodegradable Polyesters by*. University of Birmingham.

Musazzi, U. M. *et al.* (2018) 'Personalized orodispersible fi lms by hot melt ram extrusion 3D printing', *International Journal of Pharmaceutics*. Elsevier, 551(1–2), pp. 52–59. doi: 10.1016/j.ijpharm.2018.09.013.

Mwema, F. M. and Akinlabi, E. T. (2020) 'Basics of Fused Deposition Modelling (

FDM)', in *Fused Deposition Modeling*. Springer, Cham, pp. 1–15. doi: 10.1007/978-3-030-48259-6.

Na, S. *et al.* (2018) 'Mesoporous silica nanoparticles for enhanced lidocaine skin delivery', *International Journal of Pharmaceutics*, 550, pp. 325–332. doi: 10.1016/j.ijpharm.2018.08.004.

Nagarsenker, M. S. and Joshi, A. A. (1997) 'Preparation , Characterization , and Evaluation of Liposomal Dispersions of Lidocaine', *Drug Development and Industrial Pharmacy*, 23(12), pp. 1159–1165. doi: 10.3109/03639049709146153.

Nagpal, S. (2018) 'From the Patron's Desk Personalized medicine', *Journal of Pharmaceutical Research*, 17(2), p. 131124. doi: 10.18579/jpcrkc/2018/17/2/131124.

Nasereddin, J. M. *et al.* (2018) 'Development of a Simple Mechanical Screening Method for Predicting the Feedability of a Pharmaceutical FDM 3D Printing Filament', *Pharmaceutical Research*. Pharmaceutical Research, 35(151), pp. 1–13. doi: 10.1007/s11095-018-2432-3.

Nashed, N., Lam, M. and Nokhodchi, A. (2021) 'A comprehensive overview of extended release oral dosage forms manufactured through hot melt extrusion and its combination with 3D printing', *International Journal of Pharmaceutics*. Elsevier B.V., 596, p. 120237. doi: 10.1016/j.ijpharm.2021.120237.

Navarro-Beana, I. *et al.* (2016) 'Design of biodegradable blends based on PLA and PCL : From morphological , thermal and mechanical studies to shape memory behavior Iv a', *Polymer Degradation and Stability*, 132, pp. 97–108. doi: 10.1016/j.polymdegradstab.2016.03.037.

Nelson, M. T. *et al.* (2012) 'Electrospun composite polycaprolactone scaffolds for optimized tissue regeneration', *Journal of Nanoengineering and Nanosystems*, 226(3), pp. 111–121. doi: 10.1177/1740349912450828.

Newman, J. A. *et al.* (2015) 'Parts per Million Powder X - ray Diffraction', *Analytical Chemistry*, 87, pp. 10950–10955. doi: 10.1021/acs.analchem.5b02758.

NHS England (2020) 'Structured medication reviews and medicines optimisation: Guidance', *NHS*, September(September), pp. 1–20. Available at:

https://www.england.nhs.uk/wp-content/uploads/2020/09/SMR-Spec-Guidance-2020-21-FINAL-.pdf.

Norman, J. *et al.* (2017) 'A new chapter in pharmaceutical manufacturing: 3D-printed drug products', *Advanced Drug Delivery Reviews*. Elsevier B.V., 108, pp. 39–50. doi: 10.1016/j.addr.2016.03.001.

Noztek Pro (2018) *Noztek Pro User Manual*. Shoreham by Sea.

Nukala, P. K. *et al.* (2019) 'Abuse Deterrent Immediate Release Egg-Shaped Tablet (Egglets) Using 3D Printing Technology : Quality by Design to Optimize Drug Release and Extraction', *AAPS PharmSciTech*. AAPS PharmSciTech, 20, p. 80. doi: 10.1208/s12249-019-1298-y.

Nunez, E. (2004) *CRYSTALLISATION OF STAR POLYESTERS WITH POLY(e-CAPROLACTONE) ARMS - Approaching the Problem of Early Stages in Polymer Crystallisation*. KTH Royal Institute of Technology. Available at: urn.kb.se/resolve?urn=urn:nbn:se:kth:diva-327.

Obeid, S. *et al.* (2021) 'Predicting drug release from diazepam FDM printed tablets using deep learning approach : Influence of process parameters and tablet surface / volume ratio', *International Journal of Pharmaceutics*, 601, p. 120507. doi: 10.1016/j.ijpharm.2021.120507.

Öblom, H. *et al.* (2019) '3D-Printed Isoniazid Tablets for the Treatment and Prevention of Tuberculosis — Personalized Dosing and Drug Release', *AAPS PharmSciTech*. AAPS PharmSciTech, 2, p. 52. doi: 10.1208/s12249-018-1233-7.

Öblom, H. *et al.* (2020) 'Data-enriched edible pharmaceuticals (DEEP) of medical cannabis by inkjet printing', *International Journal of Pharmaceutics*. Elsevier, 589, p. 119866. doi: 10.1016/j.ijpharm.2020.119866.

Okwuosa, T. C. *et al.* (2016) 'A Lower Temperature FDM 3D Printing for the Manufacture of Patient-Specific Immediate Release Tablets', *Pharmaceutical Research*. Pharmaceutical Research, 33(11), pp. 2704–2712. doi: 10.1007/s11095-016-1995-0.

Okwuosa, T. C. *et al.* (2017) 'Fabricating a Shell-Core Delayed Release Tablet Using Dual FDM 3D Printing for Patient-Centred Therapy', *Pharmaceutical Research*. Pharmaceutical Research, 34(2), pp. 427–437. doi: 10.1007/s11095-016-2073-3.

Osta, A. *et al.* (2015) 'Advances Synergistic effects in mechanical properties of PLA / PCL blends with optimized composition, processing, and morphology', *RSC Advances*, 5, pp. 98971–98982. doi: 10.1039/c5ra21178f.

Palekar, S. *et al.* (2019) 'Application of 3D printing technology and quality by design approach for development of age-appropriate pediatric formulation of baclofen', *International Journal of Pharmaceutics*. Elsevier, 556, pp. 106–116. doi: 10.1016/j.ijpharm.2018.11.062.

Palo, M. *et al.* (2017) '3D printed drug delivery devices : perspectives and technical challenges', *Expert Review of Medical Devices*. Taylor & Francis, 14(9), pp. 685–696. doi: 10.1080/17434440.2017.1363647.

Pandey, M. *et al.* (2020) '3D printing for oral drug delivery : a new tool to customize drug delivery', *Drug Delivery and Translational Research*. Drug Delivery and Translational Research, 10, pp. 986–1001. doi: 10.1007/s13346-020-00737-0.

Paolino, D. *et al.* (2006) 'Drug Delivery Systems', in Webster, J. G. (ed.) *Encyclopedia of Medical Devices and Instrumentation*. Second Edi. John Wiley & Sons, Inc., pp. 437–495.

Park, S. A. *et al.* (2018) 'Fabrication of 3D Printed PCL / PEG Polyblend Scaffold Using Rapid Prototyping System for Bone Tissue Engineering Application', *Journal of Bionic Engineering*, 15, pp. 435–442. doi: 10.1007/s42235-018-0034-8.

Parkes, A. S. (1938) 'Effective absorption of hormones', *British Medical Journal*, 1(4024), p. 371. doi: 10.1136/bmj.1.4024.371.

Patel, N. G. and Serajuddin, A. T. M. (2021) 'Development of FDM 3D-printed tablets with rapid drug release , high drug-polymer miscibility and reduced printing temperature by applying the acid-base supersolubilization (ABS) principle', *International Journal of Pharmaceutics*. Elsevier B.V., 600, p. 120524. doi: 10.1016/j.ijpharm.2021.120524.

Pathak, P. and Nagarsenker, M. (2009a) 'Formulation and Evaluation of Lidocaine Lipid Nanosystems for Dermal Delivery', *AAPS PharmSciTech*, 10(3), pp. 985–992. doi: 10.1208/s12249-009-9287-1.

Pathak, P. and Nagarsenker, M. (2009b) 'Formulation and Evaluation of

Lidocaine Lipid Nanosystems for Dermal Delivery', *AAPS PharmSciTech*, 10(3), pp. 985–992. doi: 10.1208/s12249-009-9287-1.

Patil, H., Tiwari, R. V and Repka, M. A. (2016) 'Hot-Melt Extrusion : from Theory to Application in Pharmaceutical Formulation', *AAPS PharmSciTech*, 17(1), pp. 20–42. doi: 10.1208/s12249-015-0360-7.

Patrício, T. *et al.* (2013) 'Characterisation of PCL and PCL / PLA scaffolds for tissue engineering', *Procedia - Social and Behavioral Sciences*. Elsevier B.V., 5, pp. 110–114. doi: 10.1016/j.procir.2013.01.022.

Patrício, T. *et al.* (2014) 'Fabrication and characterisation of PCL and PCL / PLA scaffolds for tissue engineering', *Rapid Prototyping Journal*, 20(2), pp. 145–156. doi: 10.1108/RPJ-04-2012-0037.

Patterson, A. E., Collopy, P. D. and Messimer, S. L. (2015) *State-of-the-Art Survey of Additive Manufacturing Technologies , Methods , and Materials*. Huntsville, Alabama. doi: 10.13140/RG.2.2.33894.47684/1.

Pavan, M. *et al.* (2013) 'Characterization of crystalline and amorphous content in pharmaceutical solids by dielectric thermal analysis', *Journal of Thermal Analysis and Calorimetry*, 111, pp. 1987–1997. doi: 10.1007/s10973-011-2140-2.

Peng, C. *et al.* (2018) 'Response of hPDLSCs on 3D printed PCL / PLGA composite scaffolds in vitro', *Molecular Medicine Reports*, 18, pp. 1335–1344. doi: 10.3892/mmr.2018.9076.

Peng, W. *et al.* (2017) '3D bioprinting for drug discovery and development in pharmaceutics', *Acta Biomaterialia*. Acta Materialia Inc., 57, pp. 26–46. doi: 10.1016/j.actbio.2017.05.025.

Peracchia, M. T. *et al.* (1997) 'PEG-coated nanospheres from amphiphilic diblock and multiblock copolymers : Investigation of their drug encapsulation and release characteristics', *Journal of Controlled Release*, 46, pp. 223–231. doi: 0168-3659/97/$17.00.

Perale, G. *et al.* (2010) 'Lidocaine Release from Polycaprolactone Threads', *Journal of Applied Polymer SciencePolymer Science*, 117, pp. 3610–3614. doi: 10.1002/app.

Pereira, B. C. *et al.* (2019) '" Temporary Plasticiser ": A novel solution to fabricate 3D printed patient- centred cardiovascular " Polypill " architectures',

European Journal of Pharmaceutics and Biopharmaceutics. Elsevier, 135, pp. 94–103. doi: 10.1016/j.ejpb.2018.12.009.

Pereira, B. C. *et al.* (2021) 'Solvent-free temperature-facilitated direct extrusion 3D printing for pharmaceuticals d', *International Journal of Pharmaceutics*, 598, pp. 1–9. doi: 10.1016/j.ijpharm.2021.120305.

Petchey, L. *et al.* (2018) 'More harm than good', *Age UK*, pp. 1–26. doi: 10.3368/jhr.55.1.0416-7839r1.

Pichayakorn, W. *et al.* (2014) 'Physicochemical and Drug Release Characterization of Lidocaine- Loaded Transdermal Patches Prepared from STR-5L Block Rubber', *Industrial and Engineering Chemistry Research*, 53, pp. 1672–1677. doi: 10.1021/ie403529f.

Pissinato Pere, C. P. *et al.* (2018) '3D printed microneedles for insulin skin delivery', *International Journal of Pharmaceutics*. Elsevier, 544(2), pp. 425–432. doi: 10.1016/j.ijpharm.2018.03.031.

Placone, J. K. and Engler, A. J. (2018) 'Recent Advances in Extrusion-Based 3D Printing for Biomedical Applications', *Advanced Healthcare Materials*, 7, pp. 1–11. doi: 10.1002/adhm.201701161.

Planchette, C. *et al.* (2016) 'Printing medicines as orodispersible dosage forms : Effect of substrate on the printed micro-structure', *International Journal of Pharmaceutics*, 509, pp. 518–527. doi: 10.1016/j.ijpharm.2015.10.054.

Powell, M. F. (1986a) 'Lidocaine and Lidocaine Hydrochloride', *Analytical Profiles of Drug Substances and Excipients*, 15, pp. 761–779. doi: 10.1016/S0099-5428(08)60428-1.

Powell, M. F. (1986b) 'Lidocaine and Lidocaine Hydrochloride', *Analytical Profiles of Drug Substances and Excipients*, 15(C), pp. 761–779. doi: 10.1016/S0099-5428(08)60428-1.

Prasad, L. K. and Smyth, H. (2016) '3D Printing technologies for drug delivery: a review', *Drug Development and Industrial Pharmacy*, 42(7), pp. 1019–1031. doi: 10.3109/03639045.2015.1120743.

Preda, G. *et al.* (2016) 'An in vitro study of the release capacity of the local anaesthetics from siloxane matrices', *Romanian Journal of Anaesthesia and Intensive Care*, 23(2), pp. 123–131. doi: 10.21454/rjaic.7518.232.vit.

Preis, M. and Öblom, H. (2017) '3D-Printed Drugs for Children—Are We Ready Yet?', *AAPS PharmSciTech*. AAPS PharmSciTech, 18(2), pp. 303–308. doi: 10.1208/s12249-016-0704-y.

Priselac, D. *et al.* (2017) 'Thermal, surface and mechanical properties of PCL/PLA composites with coconut fibres as an alternative material to photopolymer printing plates', *Tehnički glasnik*, 11(3), pp. 111–116. Available at: https://hrcak.srce.hr/index.php?show=clanak&id_clanak_jezik=275277.

Prodanov, D. and Delbeke, J. (2016) 'Mechanical and Biological Interactions of Implants with the Brain and Their Impact on Implant Design', *Frontiers in Neuroscience*, 10(11), pp. 1–20. doi: 10.3389/fnins.2016.00011.

Przybysz-Romatowska, M., Haponiuk, J. and Formela, K. (2020) 'Compatibilized by Peroxide Initiators : Comparison of Two Strategies', *Polymers*, 228, p. 12. doi: 10.3390/polym12010228.

Puglia, C. *et al.* (2011) 'Development , Characterization , and In Vitro and In Vivo Evaluation of Benzocaine- and Lidocaine-Loaded', *Journal of Pharmaceutical Sciences*, 100(5), pp. 1892–1899. doi: 10.1002/jps.

Qian, S. *et al.* (2016) 'Poly(lactic acid) biocomposites reinforced with ultrafine bamboo-char: Morphology, mechanical, thermal, and water absorption properties', *Journal of Applied Polymer Science*, 133(20). doi: 10.1002/app.43425.

Rahman, Z. *et al.* (2018) 'Additive Manufacturing with 3D Printing : Progress from Bench to Bedside', *The AAPS Journal*. The AAPS Journal, 20(101), pp. 1–14. doi: 10.1208/s12248-018-0225-6.

Ramya, A. (2016) '3D PRINTING TECHNOLOGIES IN VARIOUS APPLICATIONS', *International Journal of Mechanical Engineering and Technology (IJMET)*, 7(3), pp. 396–409. Available at: http://www.iaeme.com/IJMET/issues.asp?JType=IJMET&VType=7&IType=3.

Ranade, V. V. (1990) 'Drug Delivery Systems in Drug Delivery', *Journal of Clinical Pharmacology*, 30(10), pp. 871–889. doi: 10.1111/j.1525-1594.1988.tb02766.x.

Ranade, V. V. and Hollinger, M. A. (2015) 'Drug delivery systems', in Bruschi, M. L. (ed.) *Strategies to Modify the Drug Release from Pharmaceutical Systems,*.

Second Edi. Woodhead Publishing, pp. 87–194. doi: 10.9774/gleaf.9781315302317-14.

Rawle, M. J. *et al.* (2018) 'The prevalence and determinants of polypharmacy at age 69: A British birth cohort study', *BMC Geriatrics*. BMC Geriatrics, 18(1), pp. 1–12. doi: 10.1186/s12877-018-0795-2.

Repka, M. A. *et al.* (2005) 'Characterization of cellulosic hot-melt extruded films containing lidocaine', *European Journal of Pharmaceutics and Biopharmaceutics*, 59, pp. 189–196. doi: 10.1016/j.ejpb.2004.06.008.

Ribeiro, L. N. M. *et al.* (2016) 'Nanostructured lipid carriers as robust systems for topical lidocaine-prilocaine release in dentistry', *European Journal of Pharmaceutical Sciences*. Elsevier B.V., 93, pp. 192–202. doi: 10.1016/j.ejps.2016.08.030.

Ritger, P. L. and Peppas, N. A. (1987a) 'A SIMPLE EQUATION FOR DESCRIPTION OF SOLUTE RELEASE I. FICKIAN AND NON-FICKIAN RELEASE FROM NON-SWELLABLE DEVICES IN THE FORM OF SLABS, SPHERES, CYLINDERS OR DISCS', *Journal of Controlled Release*, 5, pp. 23–36. doi: 10.1016/0168-3659(87)90034-4.

Ritger, P. L. and Peppas, N. A. (1987b) 'A SIMPLE EQUATION FOR DESCRIPTION OF SOLUTE RELEASE II. FICKIAN AND ANOMALOUS RELEASE FROM SWELLABLE DEVICES', *Journal of Controlled Release*, 5, pp. 37–42. doi: https://doi.org/10.1016/0168-3659(87)90035-6.

Robles-Martinez, P. *et al.* (2019) '3D Printing of a Multi-Layered Polypill Containing Six Drugs Using a Novel Stereolithographic Method', *Pharmaceutics*, 274(11), pp. 1–16. doi: 10.3390/pharmaceutics11060274.

Rodríguez Villanueva, J., Rodríguez Villanueva, L. and Guzmán Navarro, M. (2017) 'Pharmaceutical technology can turn a traditional drug, dexamethasone into a first-line ocular medicine. A global perspective and future trends', *International Journal of Pharmaceutics*, 516(1–2), pp. 342–351. doi: 10.1016/j.ijpharm.2016.11.053.

Rothen-Weinhold, A. *et al.* (1999) 'Injection-molding versus extrusion as manufacturing technique for the preparation of biodegradable implants', *European Journal of Pharmaceutics and Biopharmaceutics*, 48, pp. 113–121. doi: s0939-6411(99)00034-x.

Rumondor, A. C. F. and Taylor, L. S. (2010) 'Application of Partial Least-Squares (PLS) modeling in quantifying drug crystallinity in amorphous solid dispersions', *International Journal of Pharmaceutics*. Elsevier B.V., 398(1–2), pp. 155–160. doi: 10.1016/j.ijpharm.2010.07.049.

Rusu, M., Ursu, M. and Rusu, D. (2006) 'Poly(vinyl chloride) and poly(e-caprolactone) blends for medical use', *Journal of Thermoplastic Composite Materials*, 19(2), pp. 173–190. doi: 10.1177/0892705706056463.

Rychter, M. *et al.* (2018a) 'Cilostazol-Loaded Poly (ε -Caprolactone) Electrospun Drug Delivery System for Cardiovascular Applications'.

Rychter, M. *et al.* (2018b) 'Cilostazol-Loaded Poly (ε -Caprolactone) Electrospun Drug Delivery System for Cardiovascular Applications', *Pharmaceutical Research*, 35(32). doi: 10.1007/s11095-017-2314-0.

Saaidah, N. *et al.* (2010) 'Analysis on fused deposition modelling performance', *Journal of Zhejiang University-SCIENCE A (Applied Physics & Engineering)*, 11(12), pp. 972–977. doi: 10.1631/jzus.A1001365.

Sachs, E. M. *et al.* (1993) 'THREE-DIMENSIONAL PRINTING TECHNIQUES', *United States Patent*, (19), pp. 1–14.

Sadia, M., Alhnan, M. A., *et al.* (2018) '3D Printing of Pharmaceuticals', in Jackson, M. J. and Ahmed, W. (eds) *Micro and Nanomanufacturing*. Springer International Publishing AG 2018, pp. 467–498. doi: 10.1007/978-3-319-67132-1.

Sadia, M., Arafat, B., *et al.* (2018) 'Channelled tablets : An innovative approach to accelerating drug release from 3D printed tablets', *Journal of Controlled Release*. Elsevier, 269, pp. 355–363. doi: 10.1016/j.jconrel.2017.11.022.

Sadia, M., Isreb, A., *et al.* (2018) 'From " fixed dose combinations " to " a dynamic dose combiner " : 3D printed bi-layer antihypertensive tablets', *European Journal of Pharmaceutical Sciences*. Elsevier, 123, pp. 484–494. doi: 10.1016/j.ejps.2018.07.045.

Sahoo, S. *et al.* (2010) 'Synthesis and Characterization of Chitosan-Polycaprolactone Blended with Organoclay for Control Release of Doxycycline', *Journal of Applied Polymer Science*, 118, pp. 3167–3175. doi: 10.1002/app.

Sakurai, T. and Nojima, S. (2011) 'Significant increase in the melting

temperature of poly(ε- caprolactone) blocks confined in the crystallized lamellar morphology of poly(ε-caprolactone)-block-polyethylene copolymers', *Polymer Journal*. Nature Publishing Group, 43(4), pp. 370–377. doi: 10.1038/pj.2011.4.

Saleki-Gerhardt, A., Ahlneck, C. and Zografi, G. (1994) 'Assessment of disorder in crystalline solids', *International Jpournal of Pharmaceutics*, 101, pp. 237–247. doi: 10.1016/0378-5173(94)90219-4.

Salimi, S. *et al.* (2020) 'A 3D printed drug delivery implant formed from a dynamic supramolecular polyurethane', *Polymer Chemistry*. Royal Society of Chemistry, 11(20), pp. 3453–3464. doi: 10.1039/d0py00068j.

Sandler, N. *et al.* (2011) 'Inkjet Printing of Drug Substances and Use of Porous Substrates-Towards Individualized Dosing', *Journal of Pharmaceutical Sciences*, 100(3), pp. 3386–3395. doi: 10.1002/jps.

Sandler, N. *et al.* (2014) 'Towards fabrication of 3D printed medical devices to prevent biofilm formation', *International Journal of Pharmaceutics*. Elsevier B.V., 459(1–2), pp. 62–64. doi: 10.1016/j.ijpharm.2013.11.001.

Sandler, N. and Preis, M. (2016) 'Printed Drug-Delivery Systems for Improved Patient Treatment', *Trends in Pharmacological Sciences*. Elsevier Ltd, 37(12), pp. 1070–1080. doi: 10.1016/j.tips.2016.10.002.

Sanghavi, A. *et al.* (2016) 'DIFFERENT GENERATIONS OF MANUFACTURING PROCESSES : A CRITICAL REVIEW', *International Journal of Mechanical Engineering and Technology (IJMET)*, 7(5), pp. 250–271. Available at: www.iaeme.com/ijmet/issues.asp?JType=IJMET&VType=7&IType=5.

Santos, A. *et al.* (2014) 'Drug-releasing implants: current progress, challenges and perspectives', *Journal of Materials Chemistry B*. Royal Society of Chemistry, 2, pp. 6157–6182. doi: 10.1039/c4tb00548a.

dos Santos, J. *et al.* (2021) 'Multiple variable effects in the customisation of fused deposition modelling 3D-printed medicines : A design of experiments (DoE) approach', *International Journal of Pharmaceutics*. Elsevier B.V., 597, p. 120331. doi: 10.1016/j.ijpharm.2021.120331.

Sato, M. *et al.* (2012) 'Inorganic-Organic Hybrids Based on Poly (ε - Caprolactone) and Silica Oxide and Characterization by Relaxometry Applying Low-field NMR 3 . Preparation of PCL / silica Oxide Hybrids 4 . Characterization

Techniques', *Materials Research*, 15(6), pp. 825–832. doi: 10.1590/S1516-14392012005000121.

Saviano, M. *et al.* (2019) 'Poly (vinyl alcohol) 3D printed tablets : The effect of polymer particle size on drug loading and process efficiency', *International Journal of Pharmaceutics*, 561, pp. 1–8. doi: 10.1016/j.ijpharm.2019.02.025.

Sayyar, S. *et al.* (2012) 'Covalently linked biocompatible graphene / polycaprolactone composites for tissue engineering', *Carbon*. Elsevier Ltd, 52, pp. 296–304. doi: 10.1016/j.carbon.2012.09.031.

Schmitz, D. P. *et al.* (2018) 'Electromagnetic interference shielding effectiveness of ABS carbon-based composites manufactured via fused deposition modelling', *Materials Today Communications*. Elsevier, 15, pp. 70–80. doi: 10.1016/j.mtcomm.2018.02.034.

Scoutaris, N. *et al.* (2011) 'Inkjet printing as a novel medicine formulation technique', *Journal of Controlled Release*. Elsevier B.V., 156(2), pp. 179–185. doi: 10.1016/j.jconrel.2011.07.033.

Scoutaris, N., Ross, S. A. and Douroumis, D. (2018) '3D Printed "Starmix" Drug Loaded Dosage Forms for Paediatric Applications', *Pharmaceutical Research*. Pharmaceutical Research, 35, p. 34. doi: 10.1007/s11095-017-2284-2.

Sebhatu, T., Angberg, M. and Ahlneck, C. (1994) 'Assessment of the degree of disorder in crystalline solids by isothermal microcalorimetry', *International Journal of Pharmaceutics*, 104, pp. 135–144. doi: 10.1016/0378-5173(94)90188-0.

Seidlitz, A. and Weitschies, W. (2012) 'In-vitro dissolution methods for controlled release parenterals and their applicability to drug-eluting stent testing', *Journal of Pharmacy and Pharmacology*, 64, pp. 969–985. doi: 10.1111/j.2042-7158.2011.01439.x.

Sekhon, B. (2009) 'Pharmaceutical co-crystals - a review', *ARS Pharmaceutica*, 50(3), pp. 99–117. Available at: http://farmacia.ugr.es/ars/.

Seoane-Viano, I. *et al.* (2021) 'Semi-solid extrusion 3D printing in drug delivery and biomedicine : Personalised solutions for healthcare challenges', *Journal of Controlled Release*, 332, pp. 367–389. doi: 10.1016/j.jconrel.2021.02.027.

Seoane-Viaño, I. *et al.* (2021) 'Translating 3D printed pharmaceuticals : From

hype to real-world clinical applications', *Advanced Drug Delivery Reviews*, 174, pp. 553–575. doi: 10.1016/j.addr.2021.05.003.

Serrano, M. C. *et al.* (2009) 'Nitric oxide production by endothelial cells derived from blood progenitors cultured on NaOH-treated polycaprolactone films: A biofunctionality study', *Acta Biomaterialia*, 5(6), pp. 2045–2053. doi: 10.1016/j.actbio.2009.02.034.

Shafiee, A. and Atala, A. (2016) 'Printing Technologies for Medical Applications', *Trends in Molecular Medicine*, 22(3), pp. 254–265. doi: 10.1016/j.molmed.2016.01.003.

Shah, B., Kakumanu, V. K. and Bansal, A. K. (2006) 'Review Analytical Techniques for Quantification of Amorphous / Crystalline Phases in Pharmaceutical Solids', *Journal of Pharmaceutical Sciences*, 95(8), pp. 1641–1665. doi: 10.1002/jps.

Shaik, M. R., Korsapati, M. and Panati, D. (2012) 'Polymers in Controlled Drug Delivery Systems', *International Journal of Pharma Sciences*, 2(4), pp. 112–116.

Shaikh, R. *et al.* (2018) 'The development of a pharmaceutical oral solid dosage forms', in Singh, R. and Zhihong, Y. (eds) *Computer Aided Chemical Engineering*. Volume 41. Elsevier, pp. 27–65. doi: 10.1016/B978-0-444-63963-9.00002-6.

Shao, J. *et al.* (2018) 'Three-Dimensional Printing of Drug-Loaded Scaffolds for Antibacterial and Analgesic Applications', *Tiussue Engineering: Part C*, 25(1), pp. 1–10. doi: 10.1089/ten.TEC.2018.0293.

Sharma, K. S. *et al.* (2019) 'Solid dispersions: A technology for improving bioavailability', *Journal of Analytical & Pharmaceutical Research*, 8(4), pp. 127–133. doi: 10.15406/japlr.2019.08.00326.

Shekunov, B. Y. *et al.* (1996) 'Effect of temperature on crystal growth and crystal properties of paracetamol', *Journal of the Chemical Society, Faraday Transactions*, 92(24), pp. 439–444. doi: 10.1039/FT9969200439.

Shen, T., Lu, M. and Liang, L. (2013a) 'Modification of the properties of polylactide/ polycaprolactone blends by incorporation of blocked polyisocyanates', *Journal of Macromolecular Science, Part A: Pure and Applied Chemistry*, 50(5), pp. 547–554. doi: 10.1080/10601325.2013.781463.

Shen, T., Lu, M. and Liang, L. (2013b) 'Modification of the Properties of Polylactide / Polycaprolactone Blends by Incorporation of Blocked Modification of the Properties of Polylactide / Polycaprolactone Blends by Incorporation of Blocked Polyisocyanate', *Journal of Macromolecular Science*, 50, pp. 37–41. doi: 10.1080/10601325.2013.781463.

Shende, C. *et al.* (2014) 'Drug Stability Analysis by Raman Spectroscopy', *Pharmaceutics*, 6, pp. 651–662. doi: 10.3390/pharmaceutics6040651.

Shende, P. and Agrawal, S. (2018) 'Integration of 3D printing with dosage forms : A new perspective for modern healthcare', *Biomedicine & Pharmacotherapy*, 107, pp. 146–154. doi: 10.1016/j.biopha.2018.07.167.

Sheokand, S., Modi, S. R. and Bansal, A. K. (2016) 'Quantification of low levels of amorphous content in crystalline celecoxib using dynamic vapor sorption (DVS)', *European Journal of Pharmaceutics and Biopharmaceutics*. Elsevier B.V., 102, pp. 77–86. doi: 10.1016/j.ejpb.2016.03.006.

Shkarina, S. *et al.* (2018) '3D biodegradable scaffolds of polycaprolactone with silicate-containing hydroxyapatite microparticles for bone tissue engineering: High-resolution tomography and in vitro study', *Scientific Reports*, 8(1), pp. 1–13. doi: 10.1038/s41598-018-27097-7.

Shoja, M *et al.* (2015) 'PREPARATION AND CHARACTERIZATION OF POLY (ε-CAPROLACTONE)/TiO 2 MICRO-COMPOSITES', *Digest Journal of Nanomaterials and Biostructures*, 10(2), pp. 471–477.

Shoja, M. *et al.* (2015) 'Preparation and characterization of poly (ε-caprolactone)/TioO2 micro-composites', *Digest Journal of Nanomaterials and Biostructures*, 10(2), pp. 471–477.

Siegel, R. A. and Rathbone, M. J. (2012) 'Chapter 2 - Overview of Controlled Release Mechanisms', in Siepmann, J. (ed.) *Advances in Delivery Science and Technology*. Controlled Release Society, pp. 19–44. doi: 10.1007/978-1-4614-0881-9.

Simao, A. J., Bellani, C. F. and Branciforti, M. C. (2017) 'Thermal properties and crystallinity of PCL / PBSA / cellulose nanocrystals grafted with PCL chains', *Journal of Applied Polymer Science*, 44493, pp. 1–9. doi: 10.1002/app.44493.

Siyawamwaya, M. *et al.* (2019) '3D printed , controlled release , tritherapeutic

tablet matrix for advanced anti-HIV-1 drug delivery', *European Journal of Pharmaceutics and Biopharmaceutics*. Elsevier, 138, pp. 99–110. doi: 10.1016/j.ejpb.2018.04.007.

Skowyra, J., Pietrzak, K. and Alhnan, M. A. (2015) 'Fabrication of extended-release patient-tailored prednisolone tablets via fused deposition modelling (FDM) 3D printing', *European Journal of Pharmaceutical Sciences*. Elsevier B.V., 68, pp. 11–17. doi: 10.1016/j.ejps.2014.11.009.

Smith, D. *et al.* (2018) '3D printed capsules for quantitative regional absorption studies in the GI tract', *International Journal of Pharmaceutics*, 550, pp. 418–428. doi: 10.1016/j.ijpharm.2018.08.055.

Smith, D. M. *et al.* (2018) 'Pharmaceutical 3D printing: Design and qualification of a single step print and fill capsule', *International Journal of Pharmaceutics*, 544(1), pp. 21–30. doi: 10.1016/j.ijpharm.2018.03.056.

Smith, G. P. S. *et al.* (2017) 'Raman microscopic imaging of electrospun fi bers made from a polycaprolactone and polyethylene oxide blend', *Vibrational Spectroscopy*. Elsevier B.V., 92, pp. 27–34. doi: 10.1016/j.vibspec.2017.05.002.

Solanki, N. G. *et al.* (2018) 'Formulation of 3D Printed Tablet for Rapid Drug Release by Fused Deposition Modeling: Screening Polymers for Drug Release, Drug-Polymer Miscibility and Printability', *Journal of Pharmaceutical Sciences*. Elsevier Ltd, 107(1), pp. 390–401. doi: 10.1016/j.xphs.2017.10.021.

Song, L. (2017) 'Calcium and Bone Metabolism Indices', in *Advances in Clinical Chemistry*. 1st edn. Elsevier Inc., pp. 1–46. doi: 10.1016/bs.acc.2017.06.005.

Speranza, V. *et al.* (2014) 'Characterization of the polycaprolactone melt crystallization: Complementary optical microscopy, DSC, and AFM studies', *The Scientific World Journal*, p. 720157. doi: 10.1155/2014/720157.

Sravanthi, R. (2009) 'Preparation and characterization of poly (ε -caprolactone) PCL scaffolds for tissue engineering applications Preparation and characterization of poly (ε -caprolactone) PCL scaffolds for tissue engineering applications', 769008(207), p. 41.

Stankovic, M. *et al.* (2013) 'Low temperature extruded implants based on novel hydrophilic multiblock copolymer for long-term protein delivery', *European Journal of Pharmaceutical Sciences*, 49, pp. 578–587. doi:

10.1016/j.ejps.2013.05.011.

Stanković, M., Frijlink, H. W. and Hinrichs, W. L. J. (2015) 'Polymeric formulations for drug release prepared by hot melt extrusion: application and characterization', *Drug Discovery Today*, 20(7), pp. 812–823. doi: 10.1016/j.drudis.2015.01.012.

Stansbury, J. W. and Idacavage, M. J. (2016) '3D printing with polymers: Challenges among expanding options and opportunities', *Dental Materials*. The Academy of Dental Materials, 32(1), pp. 54–64. doi: 10.1016/j.dental.2015.09.018.

Stewart, S. A. *et al.* (2018) 'Implantable Polymeric Drug Delivery Devices : Clinical Applications', *Polymers*, 10, pp. 1–24. doi: 10.3390/polym10121379.

Stewart, S. A., Dom, J., Mcilorum, V. J., Mancuso, E., *et al.* (2020) 'Development of a Biodegradable Subcutaneous Implant for Prolonged Drug Delivery Using 3D Printing', *Pharmaceutics*, 12(2), pp. 1–16. doi: 10.3390/pharmaceutics12020105.

Stewart, S. A., Dom, J., Mcilorum, V. J., Gonzalez, Z., *et al.* (2020) 'Poly (caprolactone) -Based Coatings on 3D-Printed Biodegradable Implants : A Novel Strategy to Prolong Delivery of Hydrophilic Drugs', *Molecular pharmaceutics*, 17(9), pp. 3487–3500. doi: 10.1021/acs.molpharmaceut.0c00515.

Sudhakar, K. *et al.* (2014) 'Development of pH-sensitive polycaprolactone-based microspheres for in vitro release studies of Triprolidine Hydrochloride', *Designed Monomers and Polymers*. Taylor & Francis, 17(7), pp. 617–623. doi: 10.1080/15685551.2014.907614.

Sun, H. *et al.* (2006) 'The in vivo degradation, absorption and excretion of PCL-based implant', *Biomaterials*, 27(9), pp. 1735–1740. doi: 10.1016/j.biomaterials.2005.09.019.

Sun, Y. and Soh, S. (2015) 'Printing Tablets with Fully Customizable Release Profiles for Personalized Medicine', *Advanced Materials*, 27(47), pp. 7847–7853. doi: 10.1002/adma.201504122.

Tabriz, A. G. *et al.* (2021) '3D printed bilayer tablet with dual controlled drug release for tuberculosis treatment', *International Journal of Pharmaceutics*. Elsevier B.V., 593, p. 120147. doi: 10.1016/j.ijpharm.2020.120147.

Tagami, T. *et al.* (2017) '3D Printing Factors Important for the Fabrication of Polyvinylalcohol Filament-Based Tablets', *Biological and Pharmaceutical Bulletin*, 40(3), pp. 357–364. doi: 10.1248/bpb.b16-00878.

Tagami, T. *et al.* (2018) 'Defined drug release from 3D-printed composite tablets consisting of drug-loaded polyvinylalcohol and a water-soluble or water-insoluble polymer filler', *International Journal of Pharmaceutics*. Elsevier, 543(1–2), pp. 361–367. doi: 10.1016/j.ijpharm.2018.03.057.

Tagami, T., Hayashi, N., *et al.* (2019) '3D printing of unique water-soluble polymer-based suppository shell for controlled drug release', *International Journal of Pharmaceutics*. Elsevier, 568, p. 118494. doi: 10.1016/j.ijpharm.2019.118494.

Tagami, T., Ando, M., *et al.* (2019) 'Fabrication of Naftopidil-Loaded Tablets Using a Semisolid Extrusion-Type 3D Printer and the Characteristics of the Printed Hydrogel and Resulting Tablets', *Journal of Pharmaceutical Sciences*. Elsevier Ltd, 108(2), pp. 907–913. doi: 10.1016/j.xphs.2018.08.026.

Talebian, S. *et al.* (2018) 'Biopolymers for Antitumor Implantable Drug Delivery Systems : Recent Advances and Future Outlook', *Advanced Materials*, 30(1706665), pp. 1–31. doi: 10.1002/adma.201706665.

Tan, D. K., Maniruzzaman, M. and Nokhodchi, A. (2018) 'Advanced Pharmaceutical Applications of Hot-Melt Extrusion Coupled with Fused Deposition Modelling (FDM) 3D Printing for Personalised Drug Delivery', *Pharmaceutics*, 10, p. 203. doi: 10.3390/pharmaceutics10040203.

Tan, Y. J. N. *et al.* (2020) 'On-demand fully customizable drug tablets via 3D printing technology for personalized medicine', *Journal of Controlled Release*. Elsevier, 322(February), pp. 42–52. doi: 10.1016/j.jconrel.2020.02.046.

Tappa, K. and Jammalamadaka, U. (2018) 'Novel Biomaterials Used in Medical 3D Printing Techniques', *Journal of Functional Biomaterials*, 17(9), pp. 1–16. doi: 10.3390/jfb9010017.

Taylor, P. *et al.* (2007) 'Degradation Profile of Poly (ϵ - caprolactone)– the Influence of Macroscopic and Macromolecular Biomaterial Design Degradation Profile of Poly (1 -caprolactone) – the Influence of Macroscopic and Macromolecular Biomaterial Design', (November 2014), pp. 37–41. doi: 10.1080/10601320701424487.

Tee, Y. B. *et al.* (2013) 'Thermally Grafting Aminosilane onto Kenaf-Derived Cellulose and Its Influence on the Thermal Properties of Poly(Lactic Acid) Composites', *BioResources*, 8(3), pp. 4468–4483. doi: 10.15376/biores.8.3.4468-4483.

Theeuwes, F. and Yum, S. I. (1976) 'Principles of the design and operation of generic osmotic pumps for the delivery of semisolid or liquid drug formulations', *Annals of Biomedical Engineering*, 4(4), pp. 343–353. doi: 10.1007/BF02584524.

Thi, N. and Lee, H. B. (2010) 'Electro-spinning of PLGA / PCL blends for tissue engineering and their biocompatibility', *Journal of Materials Science: Materials in Medicine*, 21, pp. 1969–1978. doi: 10.1007/s10856-010-4048-y.

Thom, M. H., Collins, W. P. and Studd, J. W. W. (1981) 'Hormonal Profiles in Postmenopausal Women After Therapy With Subcutaneous Implants', *BJOG: An International Journal of Obstetrics & Gynaecology*, 88(4), pp. 426–433. doi: 10.1111/j.1471-0528.1981.tb01008.x.

Tian, Y. *et al.* (2019) 'Oromucosal films : from patient centricity to production by printing techniques', *Expert Opinion on Drug Delivery*. Taylor & Francis, 16(9), pp. 981–993. doi: 10.1080/17425247.2019.1652595.

Tiboni, M. *et al.* (2021) '3D printed clotrimazole intravaginal ring for the treatment of recurrent vaginal candidiasis', *International Journal of Pharmaceutics*. Elsevier B.V., 596, p. 120290. doi: 10.1016/j.ijpharm.2021.120290.

Tiptipakorn, S. *et al.* (2015) 'Effects of polycaprolactone molecular weights on thermal and mechanical properties of polybenzoxazine', *Journal of Applied Polymer Science*, 41915, pp. 1–11. doi: 10.1002/app.41915.

Tiwari, R. V., Patil, H. and Repka, M. A. (2016) 'Contribution of hot-melt extrusion technology to advance drug delivery in the 21st century', *Expert Opinion on Drug Delivery*. Informa Healthcare, 13(3), pp. 451–464. doi: 10.1517/17425247.2016.1126246.

Todo, M. *et al.* (2007) 'Fracture micromechanisms of bioabsorbable PLLA / PCL polymer blends', *Engineering Fracture Mechanics*. Elsevier Ltd, 74(12), pp. 1872–1883. doi: 10.1016/j.engfracmech.2006.05.021.

Tomic, I. *et al.* (2016) 'Setting accelerated dissolution test for PLGA microspheres containing peptide , investigation of critical parameters affecting drug release rate and mechanism', *International Journal of Pharmaceutics*. Elsevier B.V., 505(1–2), pp. 42–51. doi: 10.1016/j.ijpharm.2016.03.048.

Tran, P. *et al.* (2019) 'Overview of the manufacturing methods of solid dispersion technology for improving the solubility of poorly water-soluble drugs and application to anticancer drugs', *Pharmaceutics*, 11(3), pp. 1–26. doi: 10.3390/pharmaceutics11030132.

Trellakis, S., Lautermann, J. and Lehnerdt, G. (2007) 'Lidocaine : neurobiological targets and effects on the auditory system', *Progress in Brain Research*, 166, pp. 303–322. doi: 10.1016/S0079-6123(07)66028-2.

Trenfield, Sarah J *et al.* (2018) '3D printed drug products : Non-destructive dose veri fi cation using a rapid point-and-shoot approach', *International Journal of Pharmaceutics*, 549, pp. 283–292. doi: 10.1016/j.ijpharm.2018.08.002.

Trenfield, Sarah J. *et al.* (2018) '3D Printing Pharmaceuticals: Drug Development to Frontline Care', *Trends in Pharmacological Sciences*, 39(5), pp. 440–451. doi: 10.1016/j.tips.2018.02.006.

Trenfield, S. J. *et al.* (2019) 'Track-and-trace : Novel anti-counterfeit measures for 3D printed personalized drug products using smart material inks', *International Journal of Pharmaceutics*, 567, p. 118443. doi: 10.1016/j.ijpharm.2019.06.034.

Trivedi, M. *et al.* (2018) 'Additive manufacturing of pharmaceuticals for precision medicine applications : A review of the promises and perils in implementation', *Additive Manufacturing*. Elsevier, 23(May), pp. 319–328. doi: 10.1016/j.addma.2018.07.004.

Uhrich, K. E. *et al.* (1999) 'Polymeric Systems for Controlled Drug Release', *Chemical Reviews*, 99(11), pp. 3181–3198. doi: 10.1021/cr940351u.

UK Legislation (2021) *Medicines and Medical Devices Act 2021 Medicines and Medical Devices Act 2021*. London: Department of Health and Social Care. Available at: legislation.gov.uk/ukpga/2021/3 PART.

Ultimaker 2+ (2015) *Ultimaker 2+ User Manual*.

Umeda, Y. *et al.* (2009) 'Characterization of multicomponent crystal formed

between indomethacin and lidocaine', *Drug Development and Industrial Pharmacy*, 35(7), pp. 843–851. doi: 10.1080/03639040802660489.

Ummadi, S. *et al.* (2013) 'Overview on controlled release dosage forms', *International Journal of Pharma Sciences*, 3(4), pp. 258–269.

US Pharmacopeia (2016) '711 DISSOLUTION', in *US Pharmacopeia*. USP 39–NF. Available at: http://www.usppf.com/pf/pub/index.html.

Vadlapudi, A. D. *et al.* (2014) 'Implants', in Mitra, A. K., Lee, C. H., and Cheng, K. (eds) *Advanced Drug Delivery*. First Edit. John Wiley & Sons, Inc., pp. 183–200.

Valle, L. J., Camps, R. and Díaz, A. (2011) 'Electrospinning of polylactide and polycaprolactone mixtures for preparation of materials with tunable drug release properties', *Journal of Polymer Research*, 18, pp. 1903–1917. doi: 10.1007/s10965-011-9597-3.

Vanessa Azevedo de Mello, E. R.-J. (2011) 'ENCAPSULATION OF NAPROXEN IN NANOSTRUCTURED SYSTEM: STRUCTURAL CHARACTERIZATION AND IN VITRO RELEASE STUDIES', *Química Nova*, 34(6), pp. 933–939. doi: https://doi.org/10.1590/S0100-40422011000600004.

Vasconcelos, T., Sarmento, B. and Costa, P. (2007) 'Solid dispersions as strategy to improve oral bioavailability of poor water soluble drugs', *Drug Discovery Today*, 12(23–24), pp. 1068–1075. doi: 10.1016/j.drudis.2007.09.005.

Vaz, V. M. and Kumar, L. (2021) '3D Printing as a Promising Tool in Personalized Medicine', *AAPS PharmSciTech*. AAPS PharmSciTech, 22(49), pp. 1–20. doi: 10.1208/s12249-020-01905-8.

Venkatesh, G. M. *et al.* (2001) 'Detection of Low Levels of the Amorphous Phase in Crystalline Pharmaceutical Materials by Current Spectrometry 1', *Pharmaceutical Research*, 18(1), pp. 98–103. doi: 10.1023/a:1011087012826.

Ventola, C. L. (2014) 'Medical Applications for 3D Printing: Current and Projected Uses.', *P & T*, 39(10), pp. 704–711. doi: 10.1016/j.infsof.2008.09.005.

Verstraete, G. *et al.* (2016) 'A comparative study between melt granulation/compression and hot melt extrusion/injection molding for the manufacturing of oral sustained release thermoplastic polyurethane matrices',

International Journal of Pharmaceutics. Elsevier B.V., 513(1–2), pp. 602–611. doi: 10.1016/j.ijpharm.2016.09.072.

Verstraete, G. *et al.* (2018) '3D printing of high drug loaded dosage forms using thermoplastic polyurethanes', *International Journal of Pharmaceutics*. Elsevier, 536(1), pp. 318–325. doi: 10.1016/j.ijpharm.2017.12.002.

Vithani, K. *et al.* (2019a) 'A Proof of Concept for 3D Printing of Solid Lipid-Based Formulations of Poorly Water-Soluble Drugs to Control Formulation Dispersion Kinetics', *Pharmaceutical Research*. Pharmaceutical Research, 36, p. 102. doi: 10.1007/s11095-019-2639-y.

Vithani, K. *et al.* (2019b) 'An Overview of 3D Printing Technologies for Soft Materials and Potential Opportunities for Lipid-based Drug Delivery Systems', *Pharmaceutical Research*. Pharmaceutical Research, 36(4), pp. 1–20. doi: 10.1007/s11095-018-2531-1.

Wachirahuttapong, S., Thongpin, C. and Sombatsompop, N. (2016) 'Effect of PCL and compatibility contents on the morphology , crystallization and mechanical properties of PLA / PCL blends', *Energy Procedia*. The Author(s), 89, pp. 198–206. doi: 10.1016/j.egypro.2016.05.026.

Wang, D. *et al.* (2019) 'Non-Magnetic Injectable Implant for Magnetic Field-Driven Thermochemotherapy and Dual Stimuli-Responsive Drug Delivery: Transformable Liquid Metal Hybrid Platform for Cancer Theranostics', *Small*, 15(16), pp. 1–11. doi: 10.1002/smll.201900511.

Wang, G. and Harrison, I. R. (1994) 'Polymer melting: heating rate effects on DSC melting peaks', *Thermochimica Acta*, 231(C), pp. 203–213. doi: 10.1016/0040-6031(94)80023-5.

Wang, J. *et al.* (2013) 'Drug Delivery Implants in the Treatment of Vitreous Inflammation', *Mediators of Inflammation*, 2013(780634), pp. 1–8. doi: 10.1155/2013/780634.

Wang, J. *et al.* (2016) 'Stereolithographic (SLA) 3D printing of oral modi fi ed-release dosage forms', *International Journal of Pharmaceutics*. Elsevier B.V., 503(1–2), pp. 207–212. doi: 10.1016/j.ijpharm.2016.03.016.

Wang, L., Gramlich, W. M. and Gardner, D. J. (2017) 'Improving the impact strength of Poly(lactic acid) (PLA) in fused layer modeling (FLM)', *Polymer*

(United Kingdom). Elsevier Ltd, 114, pp. 242–248. doi: 10.1016/j.polymer.2017.03.011.

Wang, Y. *et al.* (2010) 'Micro-CT in drug delivery', *European Journal of Pharmaceutics and Biopharmaceutics*. Elsevier B.V., 74(1), pp. 41–49. doi: 10.1016/j.ejpb.2009.05.008.

Wang, Y. *et al.* (2020) '3D printed biodegradable implants as an individualized drug delivery system for local chemotherapy of osteosarcoma', *Materials & Design*. Elsevier Ltd, 186, p. 108336. doi: 10.1016/j.matdes.2019.108336.

Water, J. J. *et al.* (2015) 'Three-dimensional printing of drug-eluting implants: Preparation of an antimicrobial polylactide feedstock material', *Journal of Pharmaceutical Sciences*. Elsevier Masson SAS, 104(3), pp. 1099–1107. doi: 10.1002/jps.24305.

Wei, C. *et al.* (2020) 'Development of 3D Printed Tablets by Fused Deposition Modeling Using Polyvinyl Alcohol as Polymeric Matrix for Rapid Drug Release', *Journal of Pharmaceutical Sciences*. Elsevier Ltd, 109(4), pp. 1558–1572. doi: 10.1016/j.xphs.2020.01.015.

Weinberg, L. *et al.* (2015) 'Pharmacokinetics and pharmacodynamics of lignocaine: A review', *World Journal of Anesthesiology*, 4(2), pp. 17–29. doi: 10.5313/wja.v4.i2.17.

Weisman, J. A. *et al.* (2015) 'Antibiotic and chemotherapeutic enhanced three-dimensional printer filaments and constructs for biomedical applications', *International Journal of Nanomedicine*, 10, pp. 357–370. doi: 10.2147/IJN.S74811.

Wen, H. *et al.* (2019) 'Structure-Based Gastro-Retentive and Controlled-Release Drug Delivery with Novel 3D Printing', *AAPS PharmSciTech*. AAPS PharmSciTech, 20(68), pp. 1–12. doi: 10.1208/s12249-018-1237-3.

West, T. G. and Bradbury, T. J. (2019) '3D Printing : A Case of ZipDose Technology – World 's First Pharmaceutical Product 3D Printing Platform to Obtain FDA Approval for a Pharmaceutical Product', in Maniruzzaman, M. (ed.) *3D and 4D Printing in Biomedical Applications: Process Engineering and Additive Manufacturing*. First Edit. Wiley-VCHVerlag GmbH& Co. KGaA. 53, pp. 53–79.

Wiberg, K. *et al.* (2001) 'Determination of the content and identity of lidocaine

solutions with UV–visible spectroscopy and multivariate calibration', *Analyst*, 126, pp. 1142–1148. doi: 10.1039/b102545g.

Wiring, R. (2020) *With the introduction of a new Pharmaceutical Strategy for Europe , the EU Commission initiates widespread reforms*. Hamburg.

Wonnemann, M. *et al.* (2007) 'Lidocaine 8 mg Sore Throat Lozenges in the Treatment of Acute Pharyngitis', *Arzneimittel-Forschung (Drug Research)*, 57(11), pp. 689–697. doi: 10.1055/s-0031-1296669.

Woodruff, M. A. and Hutmacher, D. W. (2010a) 'The return of a forgotten polymer—Polycaprolactone in the 21st century', *Progress in Polymer Science*. doi: 10.1016/j.progpolymsci.2010.04.002.

Woodruff, M. A. and Hutmacher, D. W. (2010b) 'The return of a forgotten polymer - Polycaprolactone in the 21st century', *Progress in Polymer Science (Oxford)*, 35(10), pp. 1217–1256. doi: 10.1016/j.progpolymsci.2010.04.002.

Worsfold, P. J. (2005) 'Spectrophotometry / Overview', in Worsfold, P. J., Townshend, A., and Poole, C. (eds) *Encyclopedia of Analyticals Science*. Second Edi. Plymouth: Elsevier Ltd, pp. 318–321. doi: 10.1016/B0-12-369397-7/00714-7.

Wu, C. (2005) 'A comparison of the structure , thermal properties , and biodegradability of polycaprolactone / chitosan and acrylic acid grafted polycaprolactone / chitosan', *Polymer*, 46, pp. 147–155. doi: 10.1016/j.polymer.2004.11.013.

Wu, C. S. (2005) 'A comparison of the structure, thermal properties, and biodegradability of polycaprolactone/chitosan and acrylic acid grafted polycaprolactone/chitosan', *Polymer*, 46(1), pp. 147–155. doi: 10.1016/j.polymer.2004.11.013.

Wu, G. *et al.* (2014) 'Experimental study of PLLA / INH slow release implant fabricated by three dimensional printing technique and drug release characteristics in vitro', *BioMedical Engineering OnLine*, 13(97), pp. 1–11. doi: 10.1186/1475-925X-13-97.

Wu, W. *et al.* (2009) 'A programmed release multi-drug implant fabricated by three-dimensional printing technology for bone tuberculosis therapy', *Biomedical Materials*, 4(6). doi: 10.1088/1748-6041/4/6/065005.

Wu, W. *et al.* (2016) 'A therapeutic delivery system for chronic osteomyelitis via a multi-drug implant based on three-dimensional printing technology', *Journal of Biomaterials Applications*, 31(2), pp. 250–260. doi: 10.1177/0885328216640660.

Xue, J. *et al.* (2014) 'Drug loaded homogeneous electrospun PCL/gelatin hybrid nano fi ber structures for anti-infective tissue regeneration membranes', *Biomaterials*. Elsevier Ltd, 35(34), pp. 9395–9405. doi: 10.1016/j.biomaterials.2014.07.060.

Yang, N. *et al.* (2018) '3D printing and coating to fabricate a hollow bullet-shaped implant with porous surface for controlled cytoxan release', *International Journal of Pharmaceutics*. Elsevier, 552(1–2), pp. 91–98. doi: 10.1016/j.ijpharm.2018.09.042.

Yang, W. W. and Pierstorff, E. (2012) 'Reservoir-based polymer drug delivery systems', *Journal of Laboratory Automation*, 17(1), pp. 50–58. doi: 10.1177/2211068211428189.

Yang, Y. *et al.* (2018) '3D printed tablets with internal scaffold structure using ethyl cellulose to achieve sustained ibuprofen release', *European Journal of Pharmaceutical Sciences*. Elsevier, 115, pp. 11–18. doi: 10.1016/j.ejps.2018.01.005.

Yang, Y. *et al.* (2020) 'Biomaterials E-jet 3D printed drug delivery implants to inhibit growth and metastasis of orthotopic breast cancer', *Biomaterials*. Elsevier, 230, p. 119618. doi: 10.1016/j.biomaterials.2019.119618.

Yang, Y. *et al.* (2021) 'Oral preparations with tunable dissolution behavior based on selective laser sintering technique', *International Journal of Pharmaceutics*. Elsevier B.V., 593, p. 120127. doi: 10.1016/j.ijpharm.2020.120127.

Yasin, M. N. *et al.* (2014) 'Implants for drug delivery to the posterior segment of the eye : A focus on stimuli-responsive and tunable release systems', *Journal of Controlled Release*. Elsevier B.V., 196, pp. 208–221. doi: 10.1016/j.jconrel.2014.09.030.

Yasukawa, T. *et al.* (2006) 'Drug delivery from ocular', *Expert Opinion Drug Delivery*, 3(2), pp. 261–273. doi: 10.1517/17425247.3.2.261.

Yi, H. *et al.* (2016) 'A 3D-printed local drug delivery patch for pancreatic cancer

growth suppression', *Journal of Controlled Release*. Elsevier B.V., 238, pp. 231–241. doi: 10.1016/j.jconrel.2016.06.015.

Young, P. M. *et al.* (2007) 'The Use of Organic Vapor Sorption to Determine Low Levels of Amorphous Content in Processed', *Drug Development and Industrial Pharmacy*, 44(20), pp. 91–97. doi: 10.1080/03639040600969991.

Yu, D. G. *et al.* (2009) 'Novel drug delivery devices for providing linear release profiles fabricated by 3DP', *International Journal of Pharmaceutics*, 370(1–2), pp. 160–166. doi: 10.1016/j.ijpharm.2008.12.008.

Zaki Aj., M. *et al.* (2012) 'Implantable Drug Delivery System : A Review', *International Journal of PharmTech Research*, 4(1), pp. 280–292.

Zema, L. *et al.* (2017) 'Three-Dimensional Printing of Medicinal Products and the Challenge of Personalized Therapy', *Journal of Pharmaceutical Sciences*. Elsevier Ltd, 106(7), pp. 1697–1705. doi: 10.1016/j.xphs.2017.03.021.

Zhang, J., Feng, X., *et al.* (2017) 'Coupling 3D printing with hot-melt extrusion to produce controlled-release tablets', *International Journal of Pharmaceutics*. Elsevier B.V., 519(1–2), pp. 186–197. doi: 10.1016/j.ijpharm.2016.12.049.

Zhang, J., Yang, W., *et al.* (2017) 'Hydroxypropyl methylcellulose-based controlled release dosage by melt extrusion and 3D printing: Structure and drug release correlation', *Carbohydrate Polymers*. Elsevier, 177, pp. 49–57. doi: 10.1016/j.carbpol.2017.08.058.

Zhang, J. *et al.* (2018) 'Pharmaceutical Additive Manufacturing : a Novel Tool for Complex and Personalized Drug Delivery Systems', *AAPS PharmSciTech*. AAPS PharmSciTech, 19(8), pp. 3388–3402. doi: 10.1208/s12249-018-1097-x.

Zhang, J. *et al.* (2020) 'Structure-function correlation and personalized 3D printed tablets using a quality by design (QbD) approach', *International Journal of Pharmaceutics*. Elsevier B.V., 590, p. 119945. doi: 10.1016/j.ijpharm.2020.119945.

Zhang, J. and Michniak-kohn, B. (2011) 'Investigation of microemulsion microstructures and their relationship to transdermal permeation of model drugs : Ketoprofen , lidocaine , and caffeine', *International Journal of Pharmaceutics*. Elsevier B.V., 421(1), pp. 34–44. doi: 10.1016/j.ijpharm.2011.09.014.

Zhang, Q., Willis-fox, N. and Daly, R. (2021) 'Capturing the value in printed pharmaceuticals – A study of inkjet droplets released from a polymer matrix', *International Journal of Pharmaceutics*. Elsevier B.V., 599, p. 120436. doi: 10.1016/j.ijpharm.2021.120436.

Zhang, Y. and Ã, R. Z. (2005) 'Synthesis and in vitro drug release behavior of amphiphilic triblock copolymer nanoparticles based on poly (ethylene glycol) and polycaprolactone', *Biomaterials*, 26, pp. 6736–6742. doi: 10.1016/j.biomaterials.2005.03.045.

Zidan, A., Alayoubi, A., Asfari, S., *et al.* (2019) 'Development of mechanistic models to identify critical formulation and process variables of pastes for 3D printing of modified release tablets', *International Journal of Pharmaceutics*. Elsevier, 555, pp. 109–123. doi: 10.1016/j.ijpharm.2018.11.044.

Zidan, A., Alayoubi, A., Coburn, J., *et al.* (2019) 'Extrudability analysis of drug loaded pastes for 3D printing of modified release tablets', *International Journal of Pharmaceutics*. Elsevier, 554, pp. 292–301. doi: 10.1016/j.ijpharm.2018.11.025.

Zidan, A. S. *et al.* (2012) 'Crystallinity evaluation of tacrolimus solid dispersions by chemometric analysis ', *International Journal of Pharmaceutics*. Elsevier B.V., 423(2), pp. 341–350. doi: 10.1016/j.ijpharm.2011.11.003.

ZTLido (2018) 'LIDODERM PATCHES LIDODERM PATCHES', pp. 1–3.

APPENDIX 1

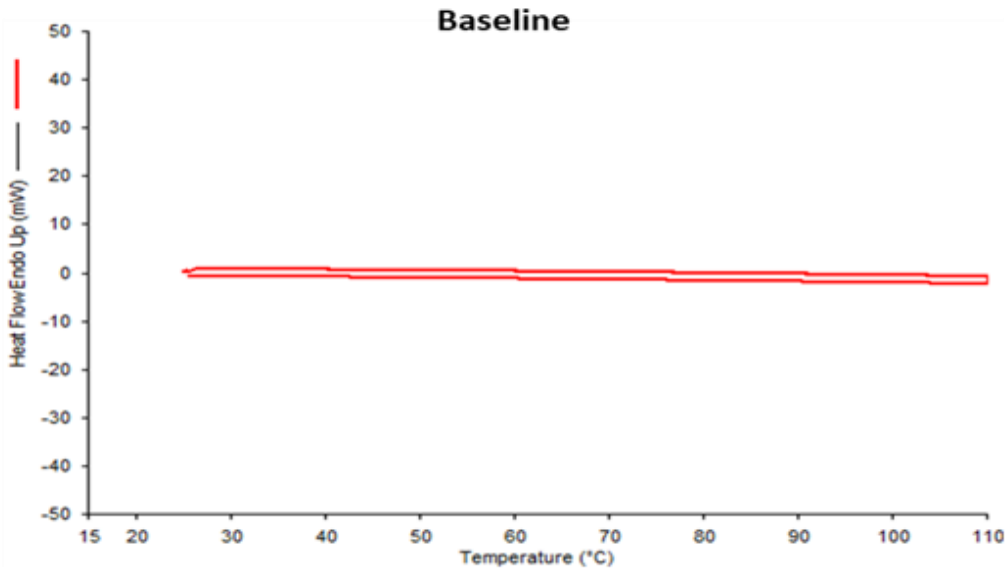

Figure S.1: *Baseline for DSC analysis of samples with a temperature program from -10 to 110 °C at a rate of 10 °C/min, Intercooler temperature –105 °C, Nitrogen flow rate of 20 ml/min.*

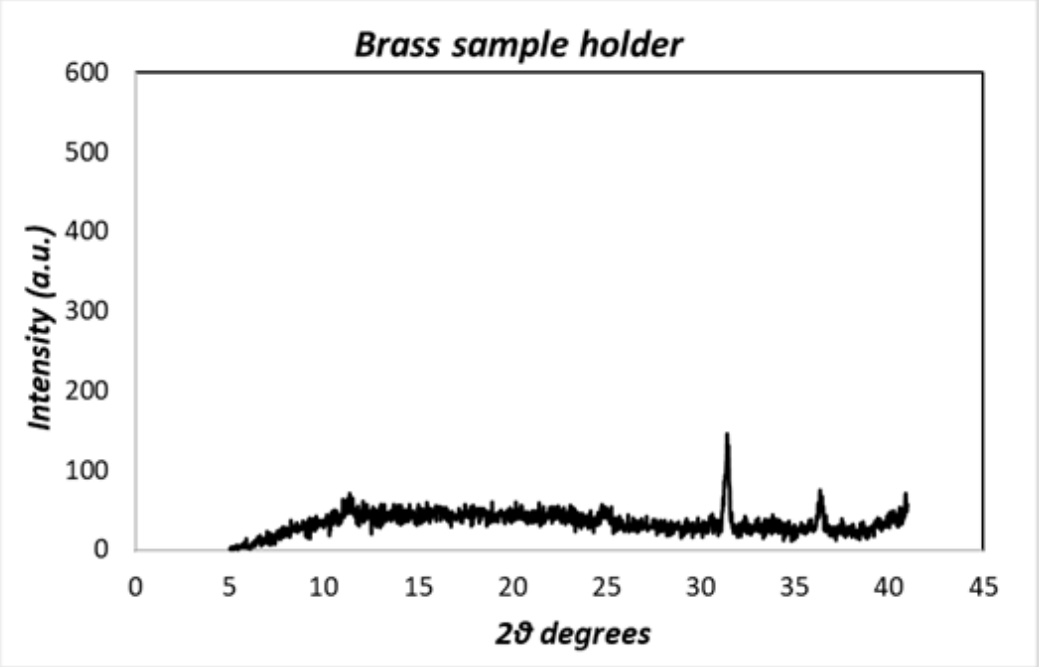

Figure S.2: *XRD difractogram of an empty brass sample holder.*

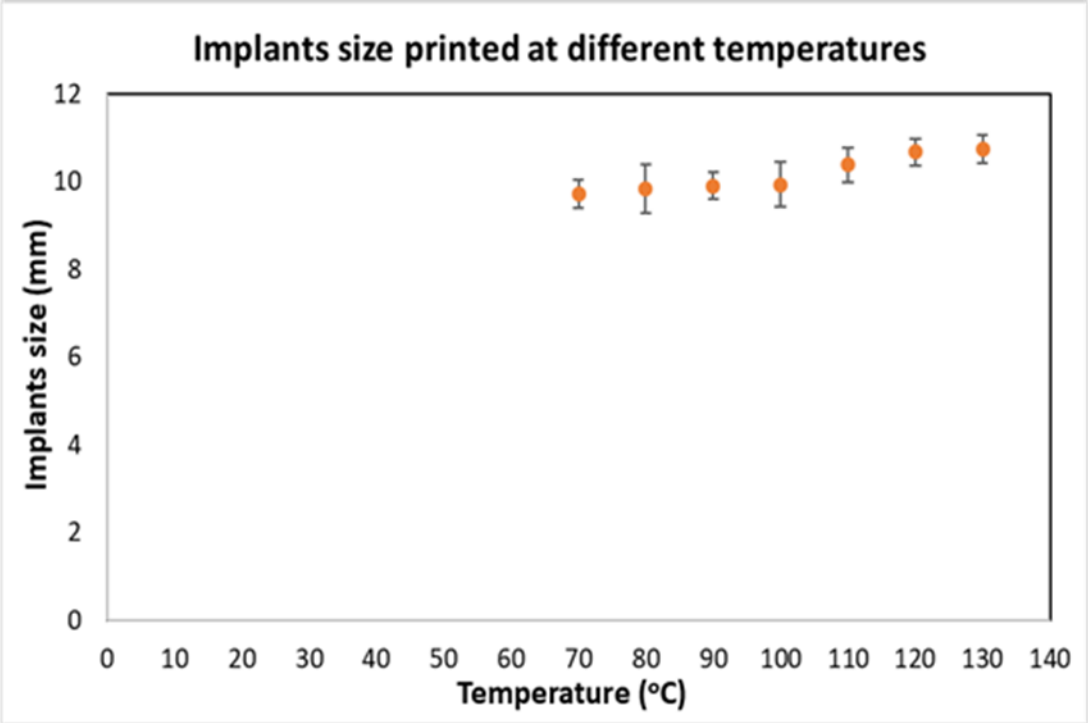

Figure S.3: *Size of the HMW PCL-LDC 30% implants printed with different temperature and pressure, a print speed of 1 mm/s and an extrusion with setting of 60%, as measured in Image J.*

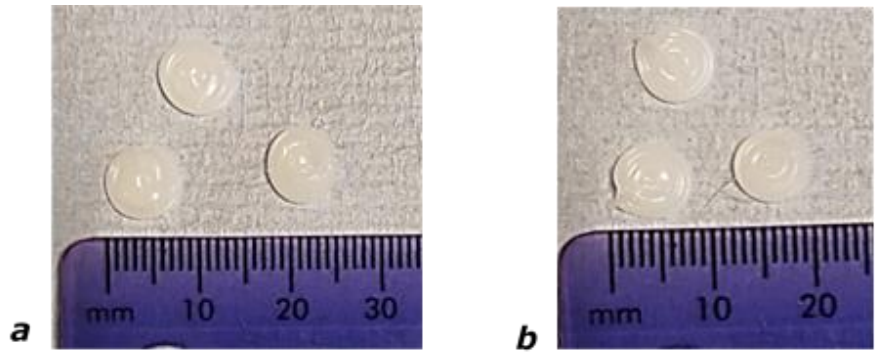

Figure S.4: *HMW PCL-LDC 5% implants printed at 70 °C, bed temperature of 40 °C and an extrusion width setting of* ***(a):*** *50% and* ***(b):*** *60%.*

The fabrication of polycaprolactone implants loaded with 5% w/w lidocaine was initially attempted at 70 °C, as this was the lowest temperature at which successful printing of HMW PCL-LDC 30% has been achieved. The rest settings were as before: pressure of 400 kPa, extrusion width of 60%, print speed of 1 mm/s and bed temperature of 24 °C, corresponding to room temperature.

No adequate adhesion of the produced formulation to the building platform could be reached at room temperature and the nozzle was moving the disc during the 3D printing process. An explanation for that was that the solidification of the extruded materials was happening quite fast and it was, hence, easier for the disc to be detached from the printing platform. Consequently, the fabricated implant did not have the shape and dimensions of the predesigned object.

A higher bed temperature was, then, applied, 30 °C. Nevertheless, the disc adhesion to the printing platform was not sufficiently enhanced for the manufacture of the desired formulation.

Table S.1: *HMW PCL-LDC 5% disc size printed at 70 °C and bed temperature of 40 °C with different extrusion width settings.*

Extrusion width setting (%)	*Printed disc size (mm)*
50	7.8 ± 0.1
60	7.1 ± 0.3

When a bed temperature of 40 °C was used, the extruded material on the building platform was not solidifying very fast, but it was remaining in a semi-molten phase until at least the completion of the printing of the implant. A great adhesion of the produced discs has, thus, been achieved with this temperature. Their size, though, was smaller than 10 mm (***Figure S.4.b***), which could be attributed to the slower extrusion of the loaded materials from the nozzle (***Table S.1***). To address this issue, a lower extrusion width, 50%, was adjusted since the line width was smaller in this case and less material was needed to be extruded. Even though a larger disc has been printed (***Figure S.4.a***), its size did not reach the predesigned dimensions, 10 mm (***Table S.1***). A reason for that was the different concentrations of the polymer and the drug used for the manufacture of this formulation. The lower the lidocaine concentration, the more viscous the PCL mixture was becoming (de Melo and Marijnissen-Hofste, 2012). A similar observation was mentioned at the beginning of this chapter, where the HMW PCL-LDC 30% powder mixture was extruded faster than the pure polymer at the same temperature.

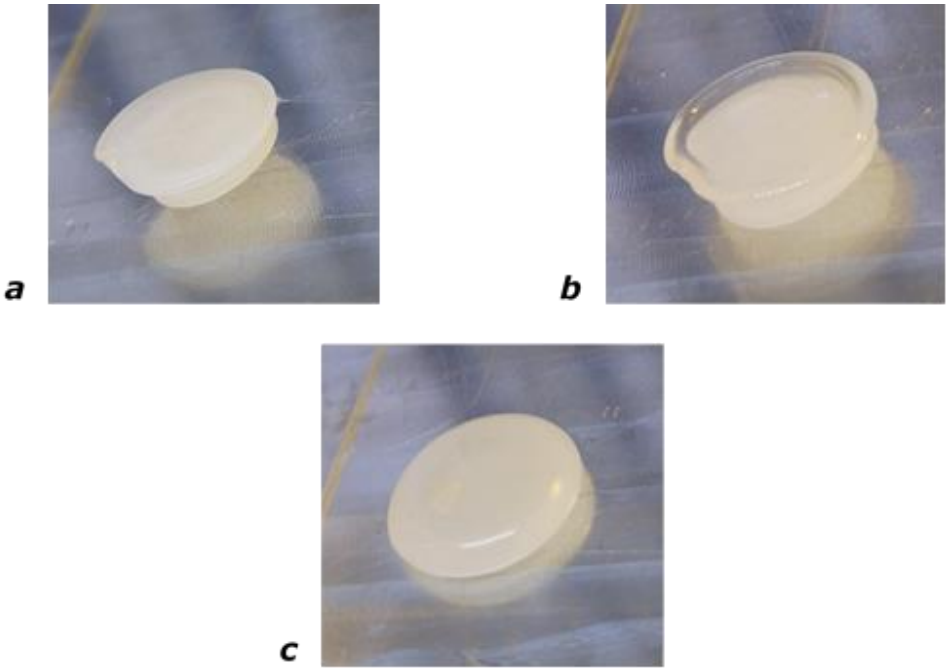

Figure S.5: *HMW PCL-LDC 5% implants printed at 110 °C with an extrusion width of 60%, pressure of 400 kPa and bed temperature of* ***(a):*** *24 °C,* ***(b):*** *30 °C and* ***(c):*** *40 °C. The bottom disc is a reflection of the printed disc on the printing platform.*

Proper selection of the print temperature could result in the fabrication of HMW PCL-LDC 5% implants with the predesigned dimensions, 10 mm length x 10 mm height x 2 mm width, since the materials extrudability could be enhanced, as previously seen. Therefore, a higher than 70 °C temperature was selected, 110 °C, since it seemed to be a promising temperature according to the printing studies of the HMW PCL-LDC 30% implants; their surface was becoming smoother after this temperature. The same parameters, as in the lower temperature studies, were applied, extrusion width of 60%, print speed of 1 mm/s and pressure of 400 kPa. The printed implant's adhesion to the building platform was investigated at various bed temperatures, room temperature or 24 °C, 30 °C and 40 °C.

Poor adhesion on the printing stage was observed at the lowest applied bed temperatures, similarly to the discs printed at a lower temperature, 70 °C. This was happening due to the fast solidification of the first layer before the printing of the rest layers. The nozzle was, thus, moving the disc which in the end did not

have the predesigned dimensions and shape and it was not homogeneously fabricated. The layers were not exactly built on top of each other, as shown in ***Figure S.5.a*** and ***Figure S.5.b***.

At the highest bed temperature, 40 °C, the implant was sufficiently stabilised on the platform as the extruded material was completely solidified after the completion of the printing process. The first layer was remaining in a semi-molten stage providing adequate adhesion of the disc to the platform for the deposition of the rest layers (***Figure S.5.c***).

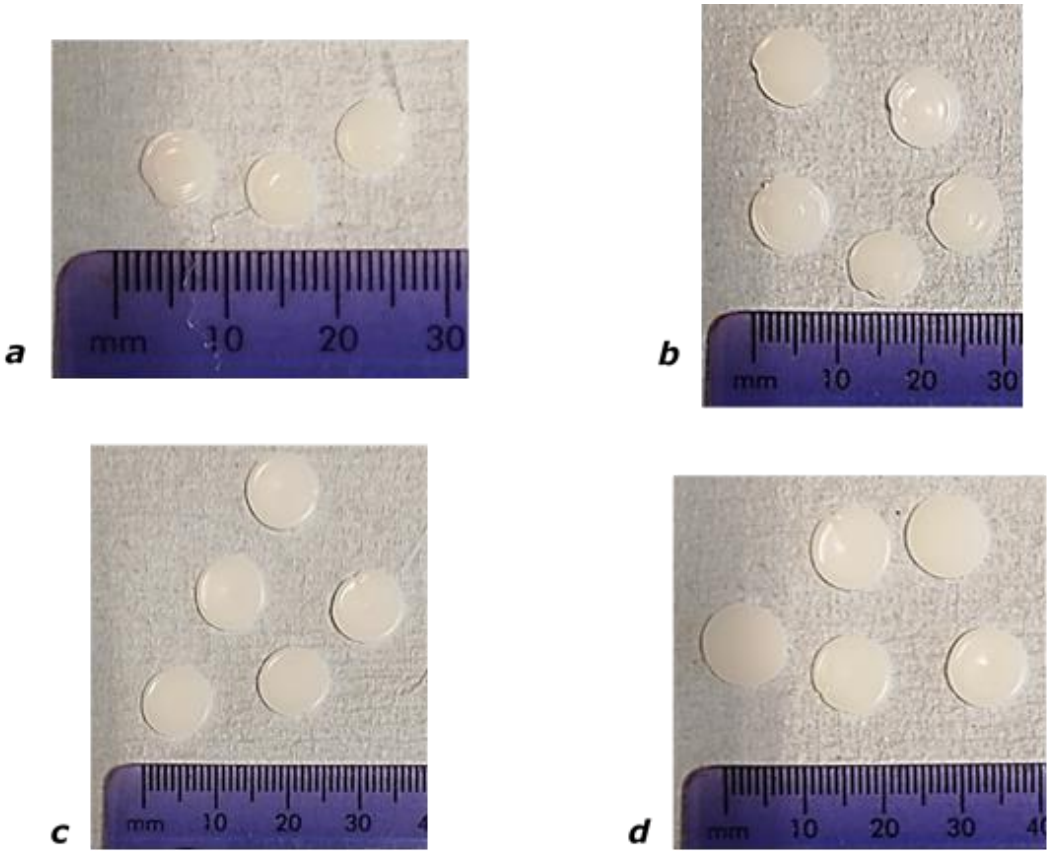

Figure S.6: *HMW PCL-LDC 5% implants printed at 110 °C, with an extrusion width of 60%, bed temperature of 40 °C and pressure of* ***(a):*** *125 kPa,* ***(b):*** *200 kPa,* ***(c):*** *300 kPa and* ***(d):*** *400 kPa.*

The manufacture of HMW PCL-LDC 5% implants at lower than 400 kPa pressures, 125, 200, 300 kPa, was also explored since a pressure of 125 kPa has been used for the production of the implants with 30% w/w lidocaine loading at 110 °C and an extrusion width setting of 60%.

Even though the implants appeared to have evenly been printed, they did not meet the desired dimensions, 10 mm length. As depicted in ***Figure S.6***, when the pressure decreased the disc size decreased, as well. This could be explained by the fact that less material was extruded when lower pressure was applied. More specifically, the dimensions of the disc printed with a pressure of 125 kPa, which was the parameter used for the printing of the HMW PCL-LDC 30% implants, were almost half the anticipated ones (***Figure S.9***). The different concentrations of the used materials, hence, led to increased viscosity of the mixture.

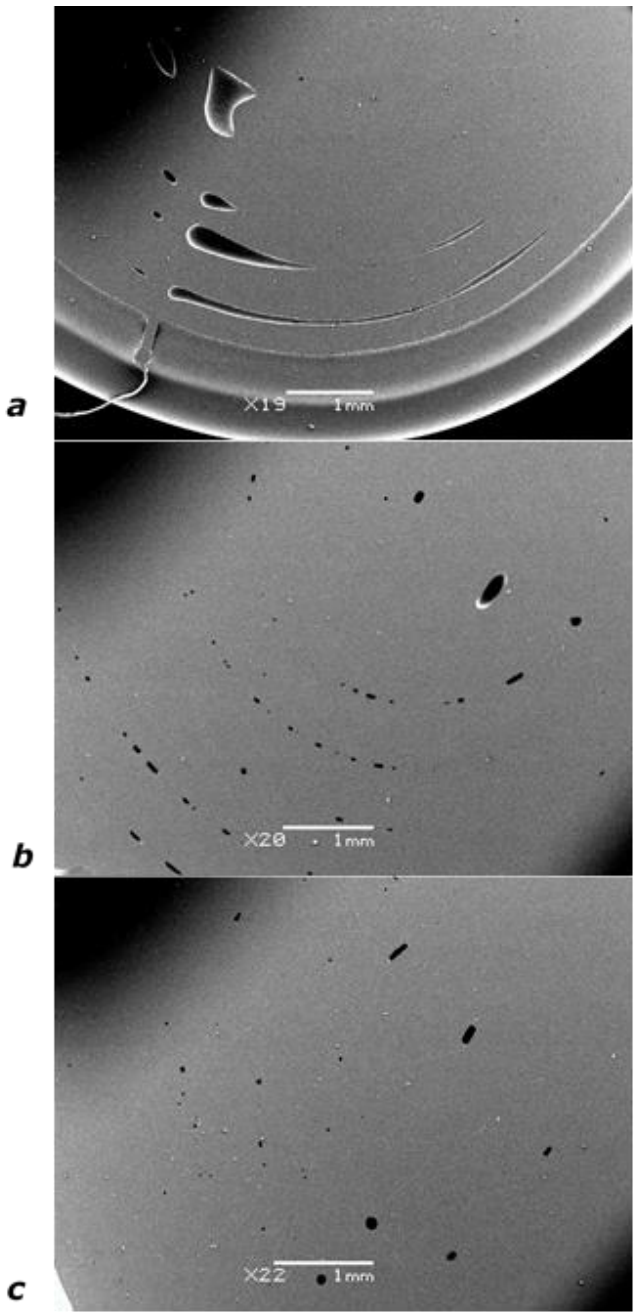

Figure S.7: *SEM images of the bottom side of HMW PCL-LDC 5% implants printed at 110 °C with an extrusion width of 60%, bed temperature 40 °C and pressure of* ***(a):*** *200 kPa,* ***(b):*** *300 kPa and* ***(c)*** *400 kPa. The magnification and the scale bar are labelled on each SEM image separately.*

The printing resolution of the 5% lidocaine loaded polycaprolactone implants was further assessed through SEM characterizations. The formulation manufactured

with the lowest pressure, 125 kPa, was not included in further analyses due to its printed size inaccuracy.

According to the SEM images in ***Figure S.7,*** some holes appeared on the surface of the implants, even when high pressure was applied during the printing process. An interesting attribute of these apertures was the fact that they seemed to be in parallel concentric cycles, which was the selected infill pattern. It was, thus, assumed that they were detected in the connection of the printed lines, since that was the area with less material extruded.

The pressure used each time affected the size and the number of cavities. The lower the pressure, as can be seen in ***Figure S.7.a***, the larger the gaps between the printed lines. In the same SEM image, fewer round apertures appeared but it was evident that the printed lines were not very well attached. When the pressure increased to 300 kPa, more round-shaped holes than gaps appeared on the implants surface and their average size was 81.5 ± 33.5 μm, based on the measurements in Image J (***Figure S.7.b***). Significantly fewer cavities were present on the surface of the HMW PCL-LDC 5% implants printed with a pressure of 400 kPa as demonstrated in ***Figure S.7.c***, which showed the impact of this parameter on the printing resolution. It was also indicated that more material was extruded when higher pressure was used. The average size of the detected holes was smaller than in the previous formulations, 41.9 ± 14.5 μm.

Nevertheless, a drug dosage form needs to be compact and without any apertures on its surface to be considered suitable for sustained drug release, otherwise, the release of the loaded drug and the degradation of the polymeric matrix will be enhanced.

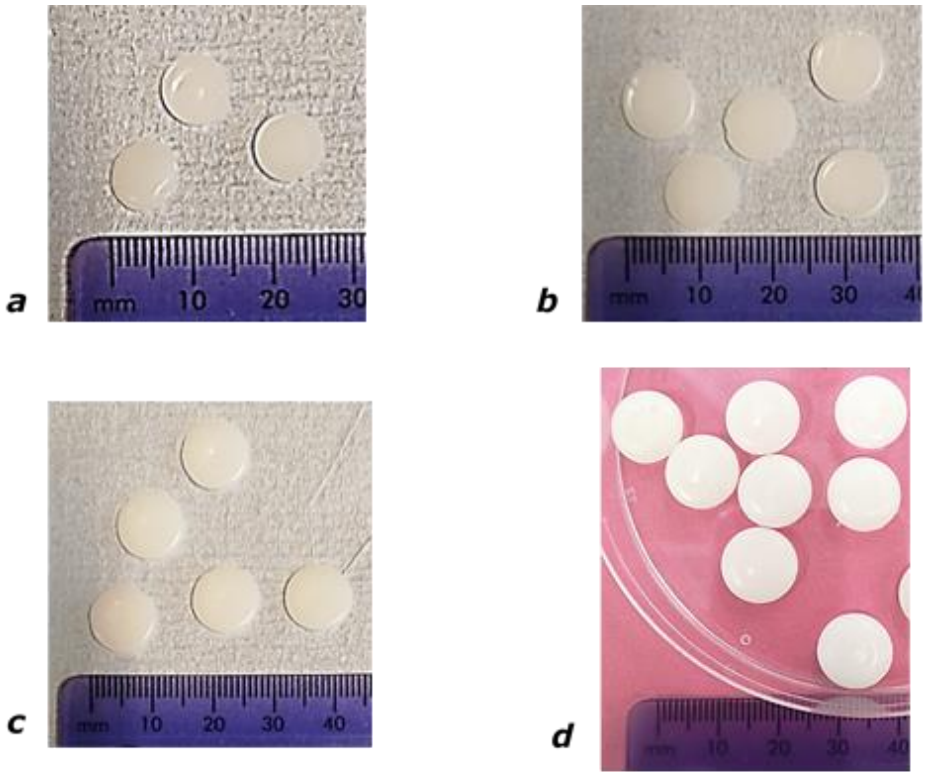

Figure S.8: *HMW PCL-LDC 5% implants printed at 110 °C, with an extrusion width of 50%, bed temperature of 40 °C and pressure of* ***(a):*** *125 kPa,* ***(b):*** *200 kPa,* ***(c):*** *300 kPa and* ***(d):*** *400 kPa.*

A similar problem, with gaps and cavities between the printed lines, has been appeared, as well, during the manufacture of the polycaprolactone implants loaded with 30% w/w lidocaine. The solution was the adjustment of the extrusion width setting to a lower value, which was also applied for the production of this formulation. The desired size could be better met by changing this parameter.

HMW PCL-LDC 5% implants were, then, printed with an extrusion width setting of 50%, while the other printing settings did not change; print temperature of 1 mm/s and bed temperature of 40 °C. Similarly to the previous printing study, four different pressures were applied, 125, 200, 300 and 400 kPa, and then, the size and the printing resolution of the produced discs were assessed.

As displayed in ***Figure S.8***, disc-shaped implants have been produced in all the explored pressures. Their size, though, differed depending on the varied

parameter; as more pressure was applied, more material was extruded from the nozzle, resulting in the manufacture of discs closer to the predesigned dimensions, 10 mm.

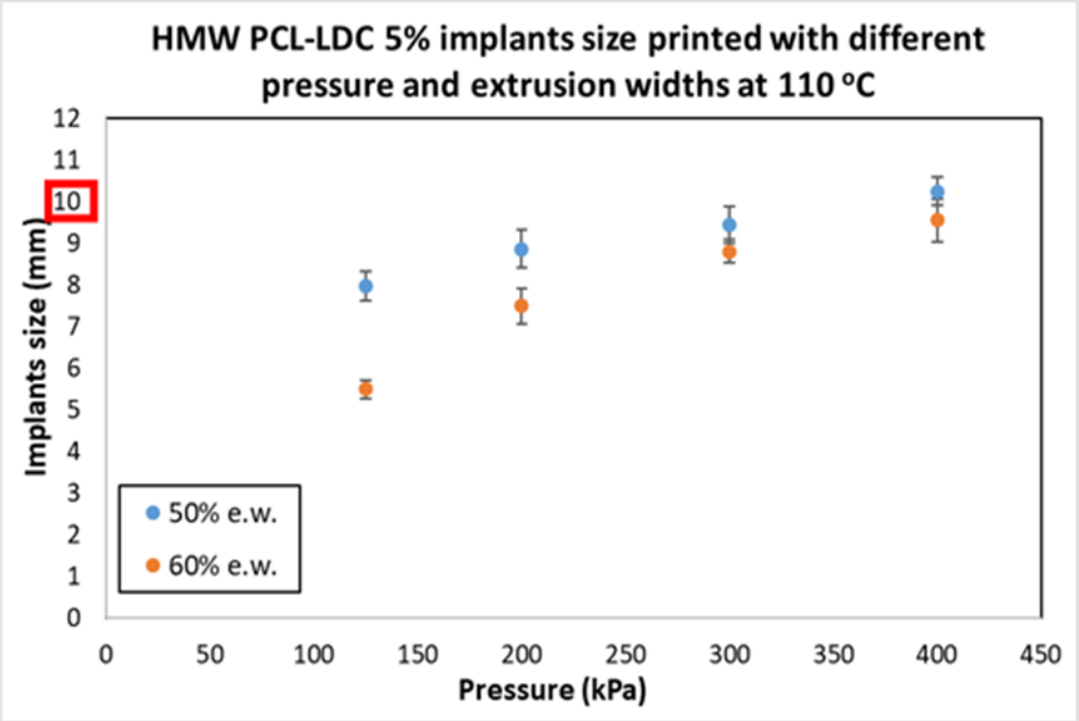

Figure S.9: *Size of the HMW PCL-LDC 5% implants printed with different pressures, a print speed of 1 mm/s, an extrusion width (e.w.) setting of 60% and 50%, bed temperature of 40 °C and temperature of 110 °C, as measured in Image J. Red boxed figure represents the theoretical dimensions of the printed disc-shaped implant as in the CAD file.*

The size of the 5% w/w lidocaine loaded polycaprolactone implants printed with an extrusion width setting of 50% was, in general, closer to 10 mm, compared to the formulations printed with the higher extrusion width, as depicted in ***Figure S.9***. More specifically, the discs printed with the highest pressure and lower extrusion width met the size requirements (***Figure S.8.d***). It was, therefore, indicated that the thinner the printed lines, the better the size accuracy of the produced object.

In contrast, the smallest discs were fabricated with the lowest applied pressure (***Figure S.8.a***). Pressure was, hence, proven to be another parameter which could regulate the size of the printed formulation.

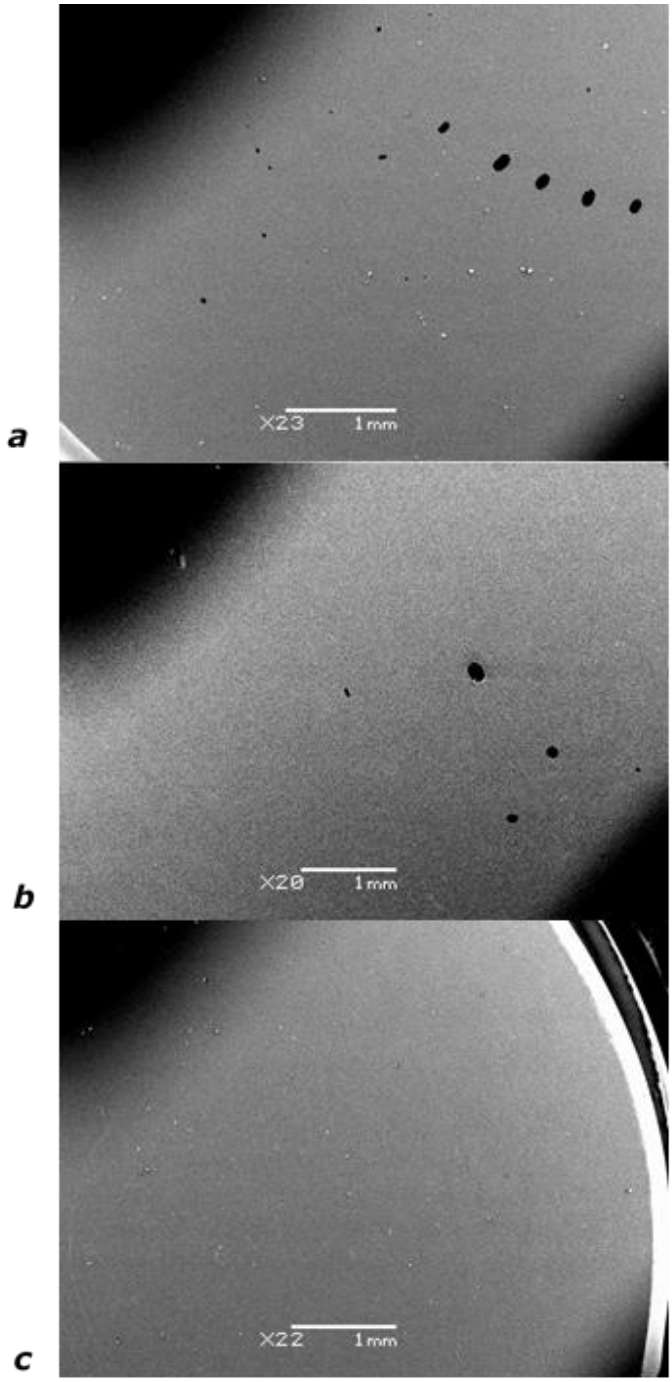

Figure S.10: *SEM images of the bottom side of HMW PCL-LDC 5% implants printed at 110 °C with an extrusion width of 50%, bed temperature of 40 °C and pressure of* ***(a):*** *200 kPa,* ***(b):*** *300 kPa and* ***(c)*** *400 kPa. The magnification and the scale bar are labelled on each SEM image separately.*

The surface of the HMW PCL-LDC 5% implants was, then, analysed in the SEM to examine if the lower extrusion width resulted in the manufacture of a more compact drug dosage form without the presence of any apertures. The implant printed with the lowest pressure, 125 kPa, was not characterized due to the low printing accuracy, as demonstrated in the size check (***Figure S.9***).

As displayed in the SEM images of the HMW PCL-LDC 5% implants printed with different pressures, 200, 300 and 400 kPa, the lower extrusion width, 50%, considerably improved the printing resolution (***Figure S.10***). Even though some holes were still present on the surface of the discs printed with pressures of 200 and 300 kPa, they were not as many as on the discs surface printed with a higher extrusion width and they were not following a concentric pattern (***Figure S.10.a, Figure S.10.b***). That indicated the better connection between the printed lines and the relatively adequate material extrusion. The average size of the detected holes decreased as the pressure increased; 121.3 ± 34.3 μm holes size when 200 kPa pressure was applied and 92.1 ± 33.3 μm holes size when 300 kPa pressure was applied. Nevertheless, according to the SEM image of the 5% w/w lidocaine loaded polycaprolactone implant, ***Figure S.10.c***, the lower extrusion width and the highest tested pressure resulted in the manufacture of a disc with a quite smooth surface without any gaps or cavities which could affect the release of the drug. This was in line with the previously discussed observations from the assessment of the disc size.

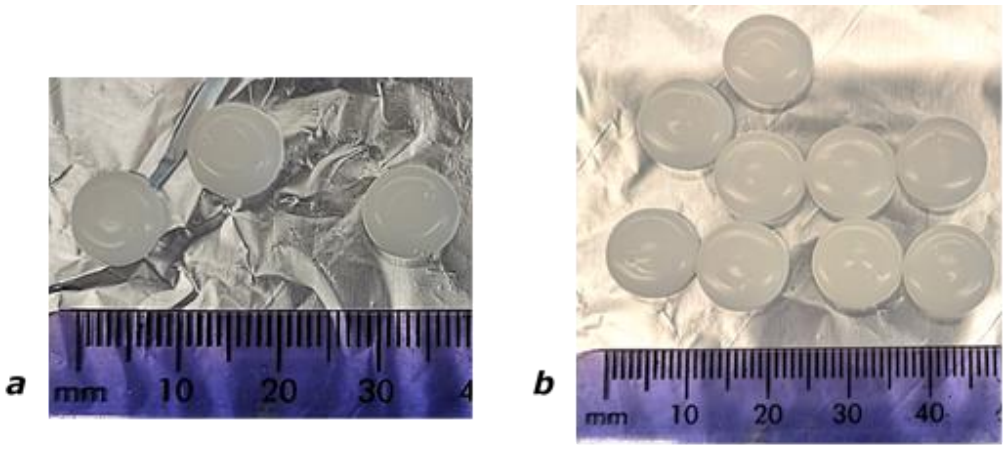

Figure S.11: *HMW PCL implants printed at 110 °C with pressure of 400 kPa, bed temperature of 40 °C and an extrusion width of* ***(a):*** *50% and* ***(b):*** *40%.*

The size of the printed polymeric discs was smaller than the predesigned one, 9.5 ± 1.2 mm (***Figure S.11.a***). This could be explained by the increased viscosity of the printing material, leading to its slower extrusion compared to the polymer-drug mixture used before. To address this issue the extrusion width was the parameter chosen to be altered since it has previously proven to be effective in the control of the size of the printed object.

Pure polycaprolactone implants were, then, printed with a lower extrusion width, 40%. As demonstrated in ***Figure S.11.b*** and after their size measurement in Image J, higher printing accuracy has been achieved compared to the discs printed with 50% extrusion width; the discs size was 10.2 ± 0.3 mm. It was, hence, indicated that this printing parameter was more appropriate for the manufacture of this formulation.

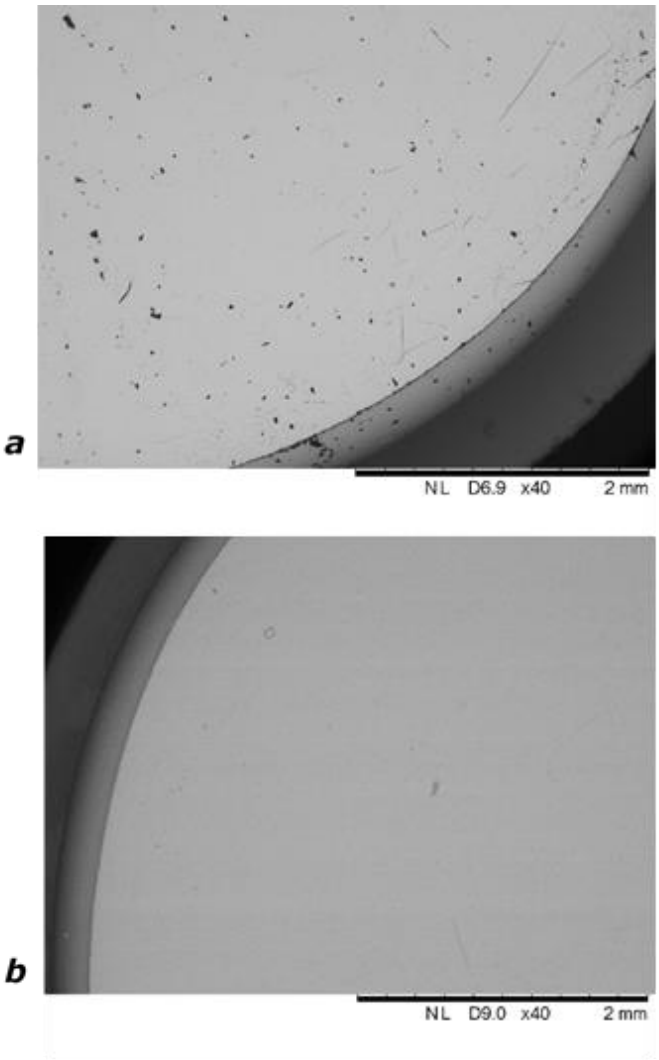

Figure S.12: *SEM images of the bottom side of HMW PCL implants printed at 110 °C with a pressure of 400 kPa, bed temperature of 40 °C and an extrusion width of* ***(a):*** *50% and* ***(b):*** *40%. The magnification is x40 and the scale bars are 2 mm and they are labelled on each SEM image separately.*

According to the SEM images in ***Figure S.12,*** contrary to the drug loaded disc there were many surface holes visible in the pure polymeric sample, indicating that the presence of drug at 5% had an impact on material properties (eg. viscosity) of the blend versus the polymer alone and hence, printing integrity (de Melo and Marijnissen-Hofste, 2012). When the printing parameters of the HMW PCL-LDC 5% implants were applied, there were many holes apparent in the pure polymeric sample (***Figure S.12.a***). Their average size was 31.6 ± 7.1 μm. The

lower used extrusion width setting of 40% reduced the appearance of surface holes and hence, improved the printing quality of the pure PCL discs (***Figure S.12.b***).

SEM observations were in line with the size measurements, both suggesting the lower applied extrusion width was the most appropriate one for the production of polycaprolactone discs with similar characteristics as the drug loaded formulations.

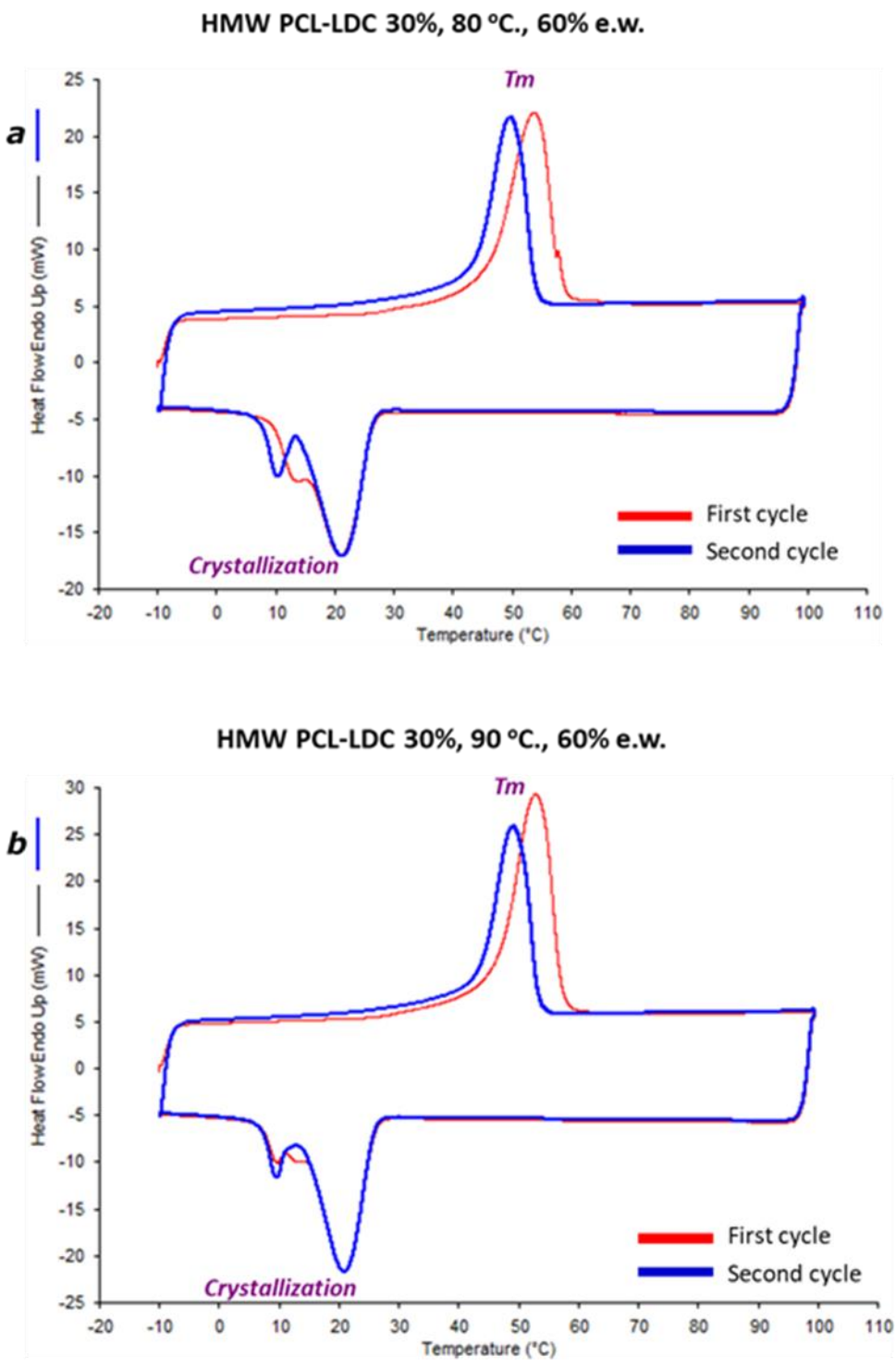

Figure S.13: *DSC thermograms of HMW PCL-LDC 30% implants printed with an extrusion width (e.w.) setting of 60% at* ***(a):*** *80 °C and* ***(b):*** *90 °C. The red line represents the first heating-cooling cycle and the blue line the second cycle.*

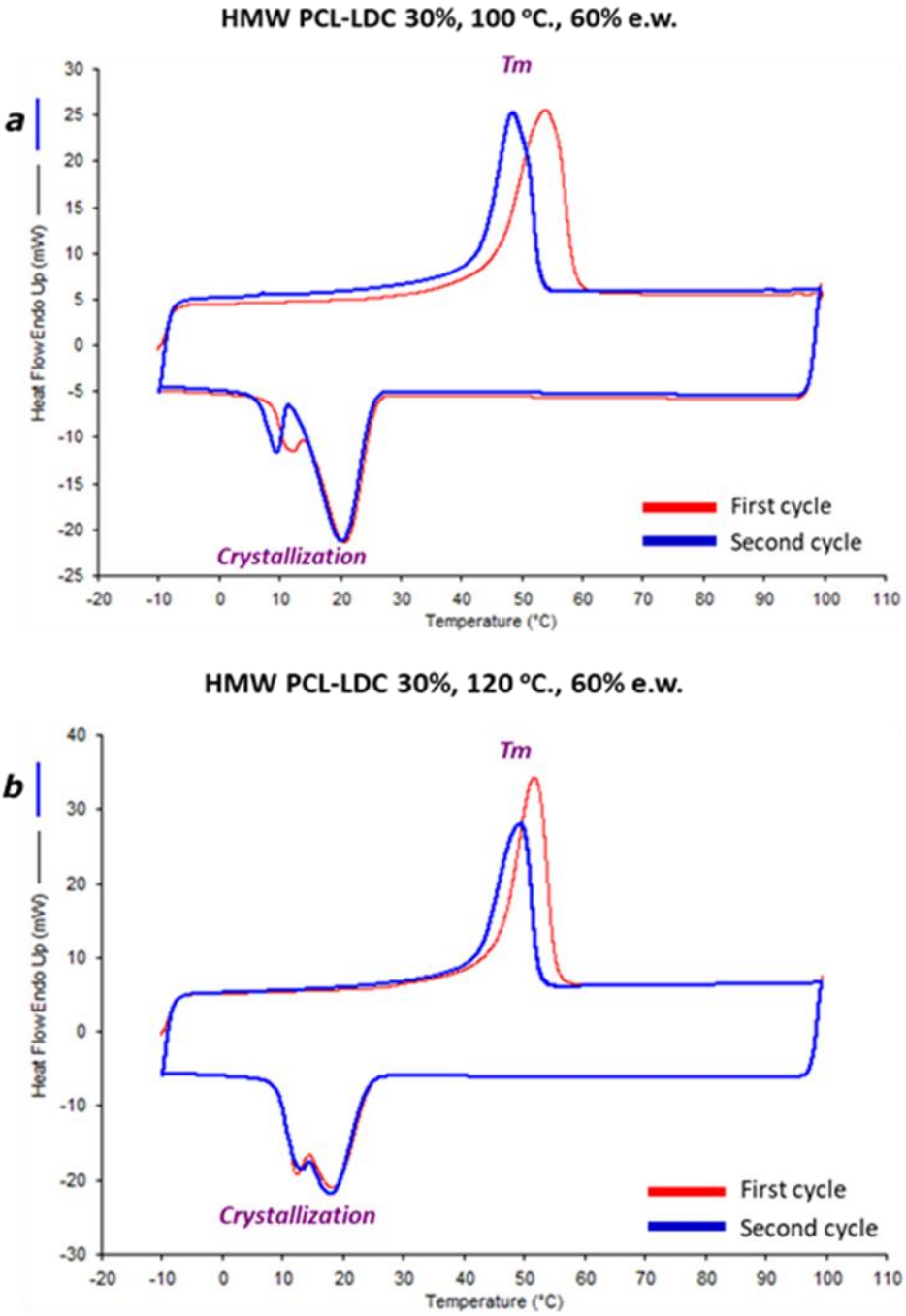

Figure S.14: *DSC thermograms of HMW PCL-LDC 30% implants printed with an extrusion width (e.w.) setting of 60% at* ***(a):*** *100 °C and* ***(b):*** *120 °C. The red line represents the first heating-cooling cycle and the blue line the second cycle.*

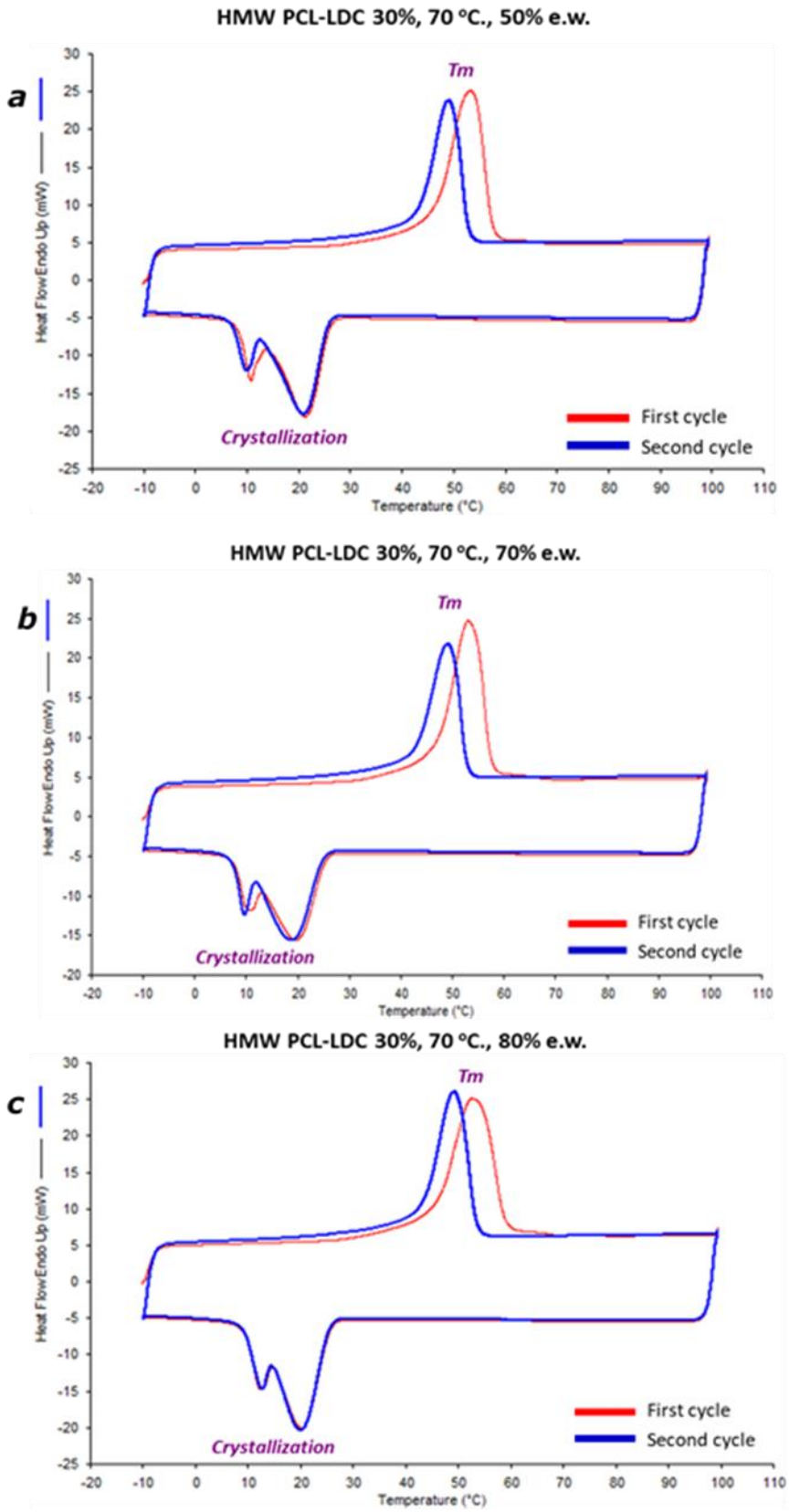

Figure S.15: *DSC thermograms of HMW PCL-LDC 30% implants printed at 70 °C with an extrusion width (e.w.) setting of* ***(a):*** *50%,* ***(b):*** *70% and* ***(c):*** *80%. The red line represents the first heating-cooling cycle and the blue line the second cycle.*

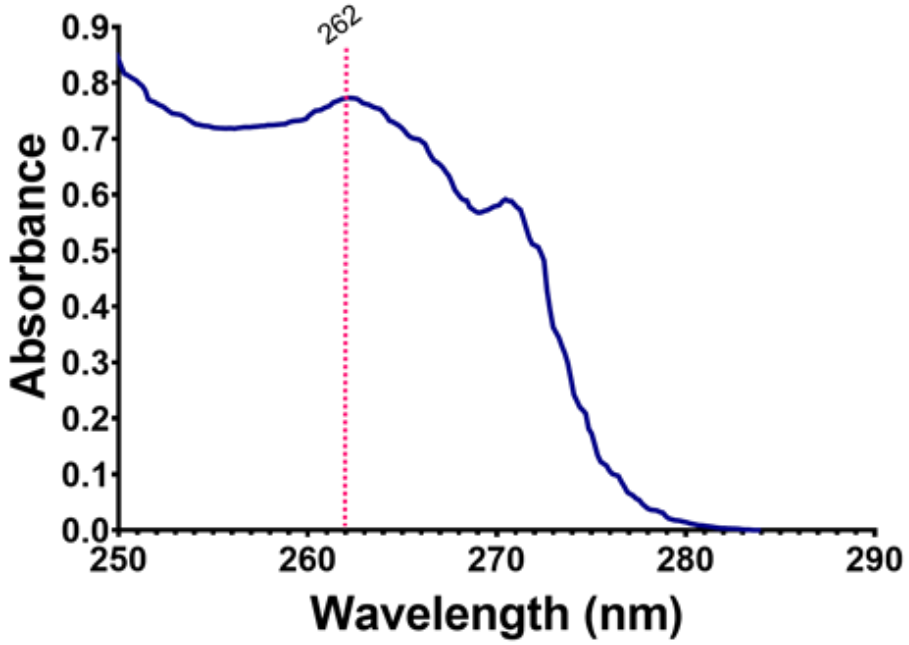

Figure S.16: *UV-Vis spectrum of lidocaine in the wavelength range of 250 – 290 nm. The pink dot-line highlights the characteristic peak of lidocaine at 262 nm in the UV-Vis spectrum.*

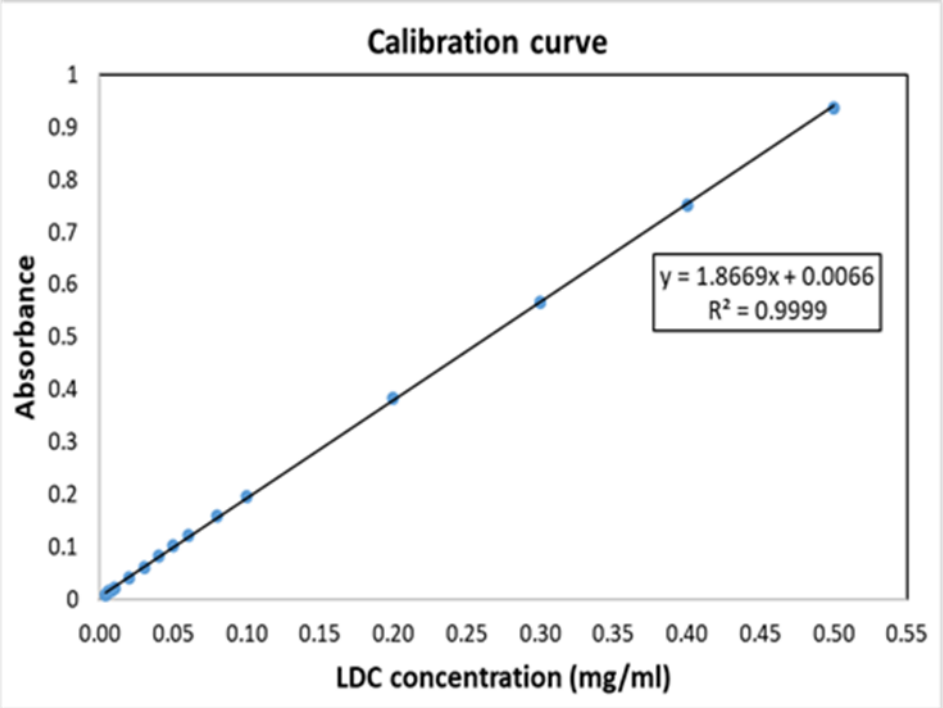

Figure S.17: *Calibration curve for the calculation of the concentration of the released lidocaine.*

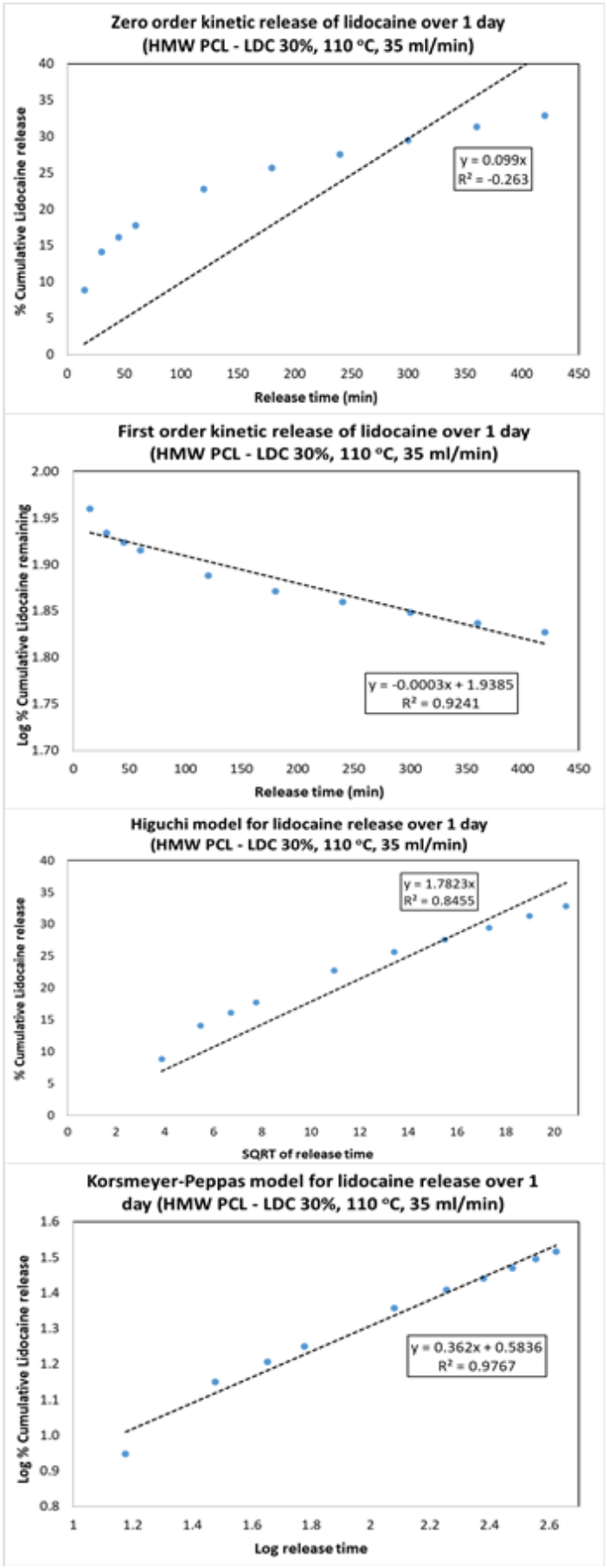

Figure S.18: (a): *Zero-order,* ***(b):*** *First-order,* ***(c):*** *Higuchi and* ***(d):*** *Korsmeyer-Peppas model kinetic release for lidocaine from HMW PCL-LDC 30% implants printed at 110 °C during day 1 of dissolution with a flow rate of 35 ml/min.*

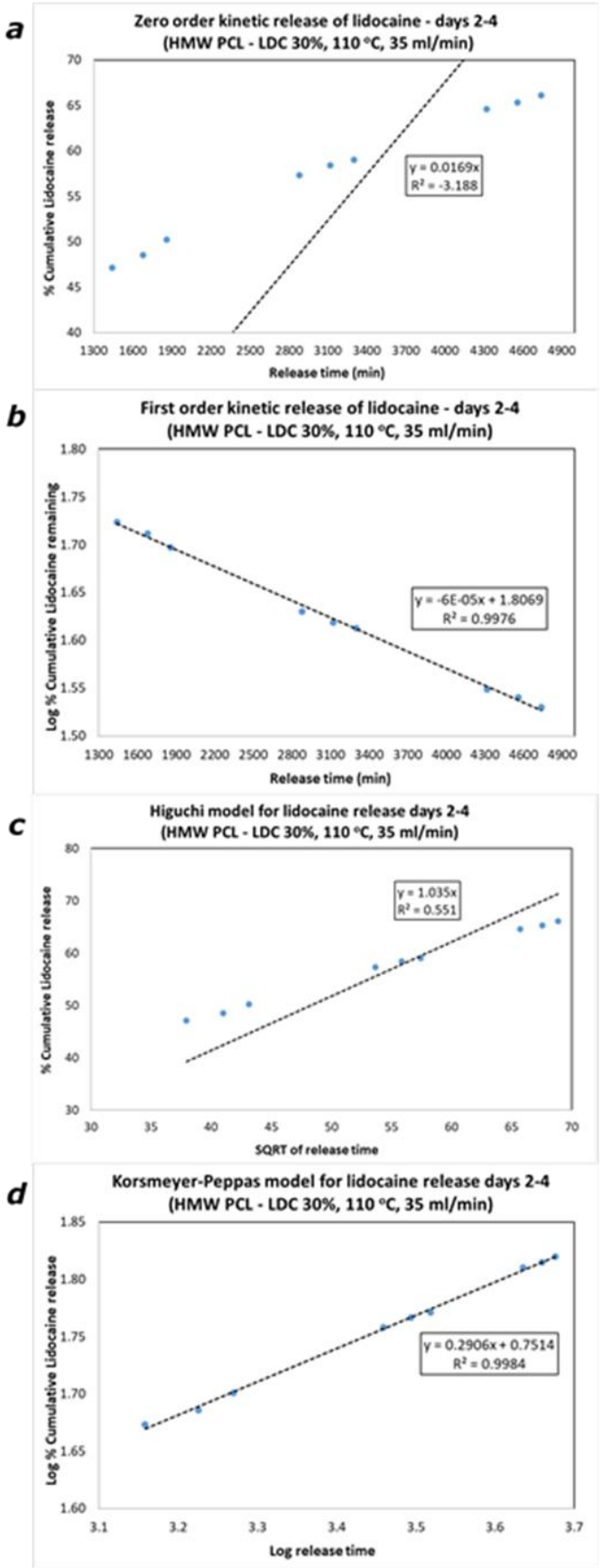

Figure S.19: (a): *Zero-order,* ***(b):*** *First-order,* ***(c):*** *Higuchi and* ***(d):*** *Korsmeyer-Peppas model kinetic release for lidocaine from HMW PCL-LDC 30% implants printed at 110 °C during days 2-4 of dissolution with a flow rate of 35 ml/min.*

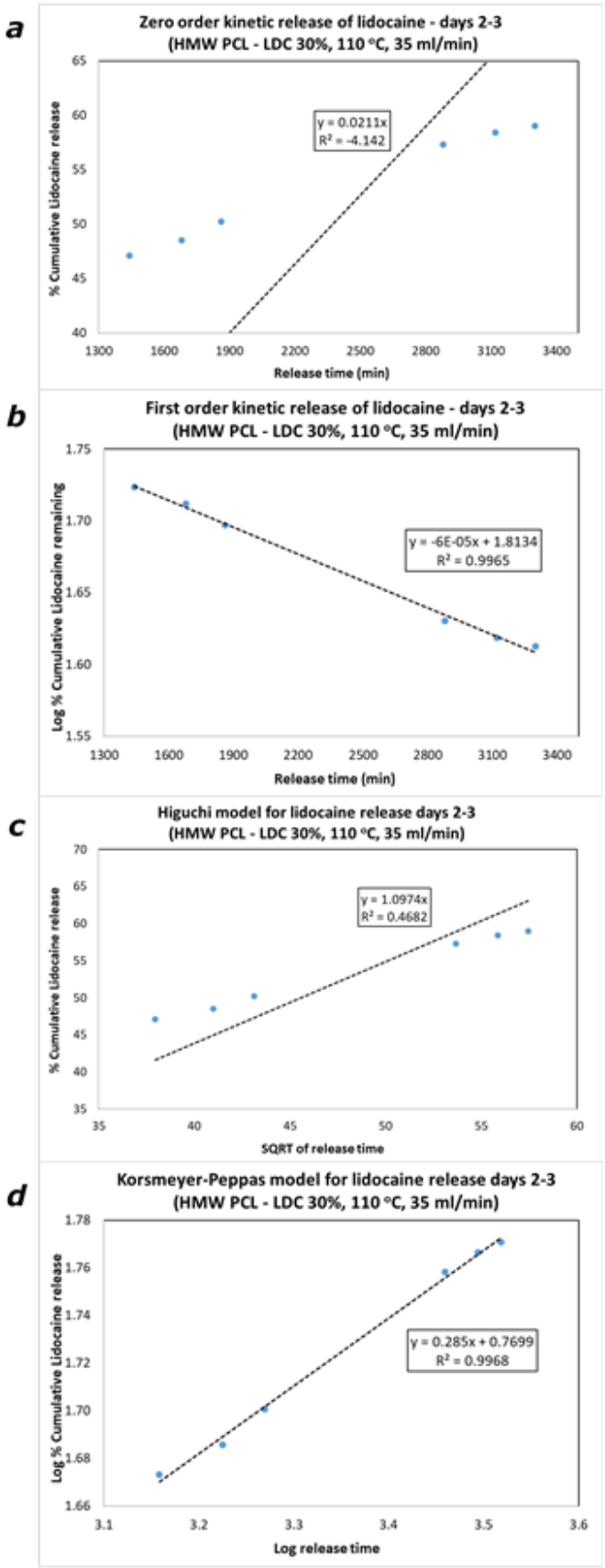

Figure S.20: (a): *Zero-order,* ***(b):*** *First-order,* ***(c):*** *Higuchi and* ***(d):*** *Korsmeyer-Peppas model kinetic release for lidocaine from HMW PCL-LDC 30% implants printed at 110 °C during days 2-3 of dissolution with a flow rate of 35 ml/min.*

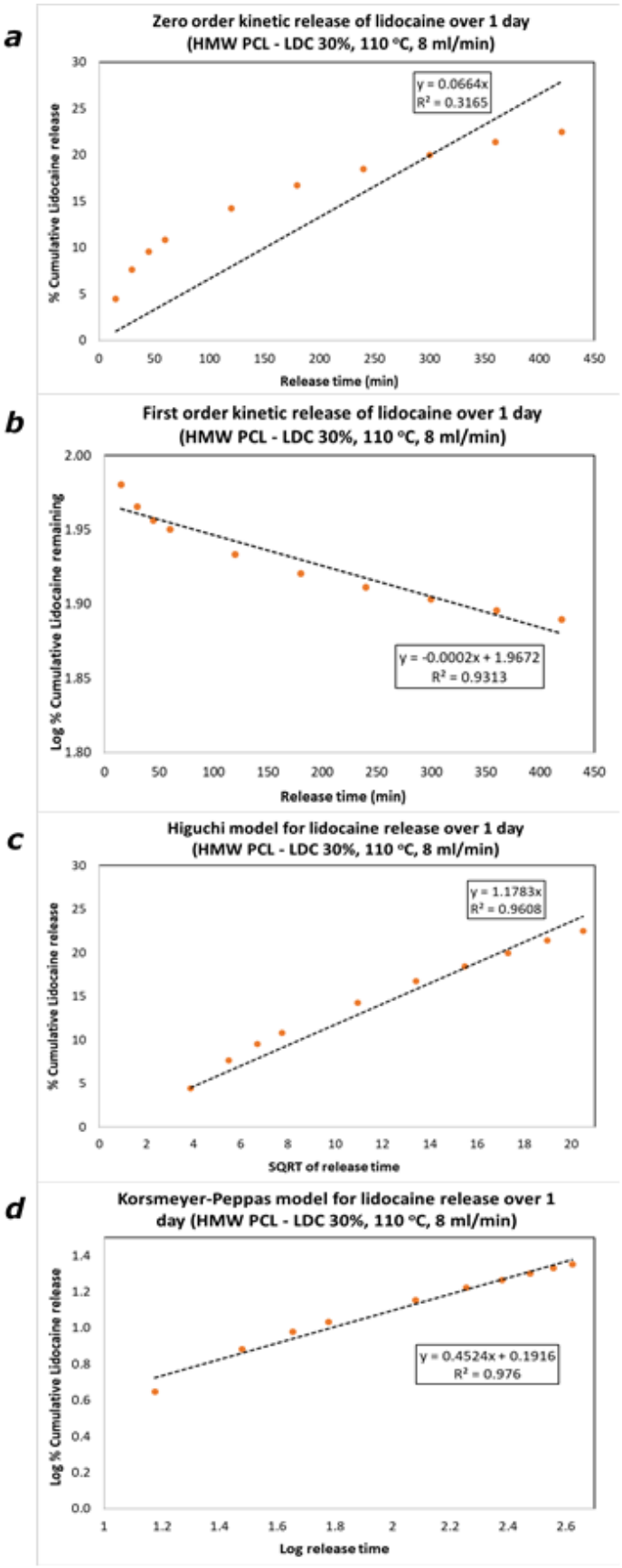

Figure S.21: (a): *Zero-order,* ***(b):*** *First-order,* ***(c):*** *Higuchi and* ***(d):*** *Korsmeyer-Peppas model kinetic release for lidocaine from HMW PCL-LDC 30% implants printed at 110 °C during day 1 of dissolution with a flow rate of 8 ml/min.*

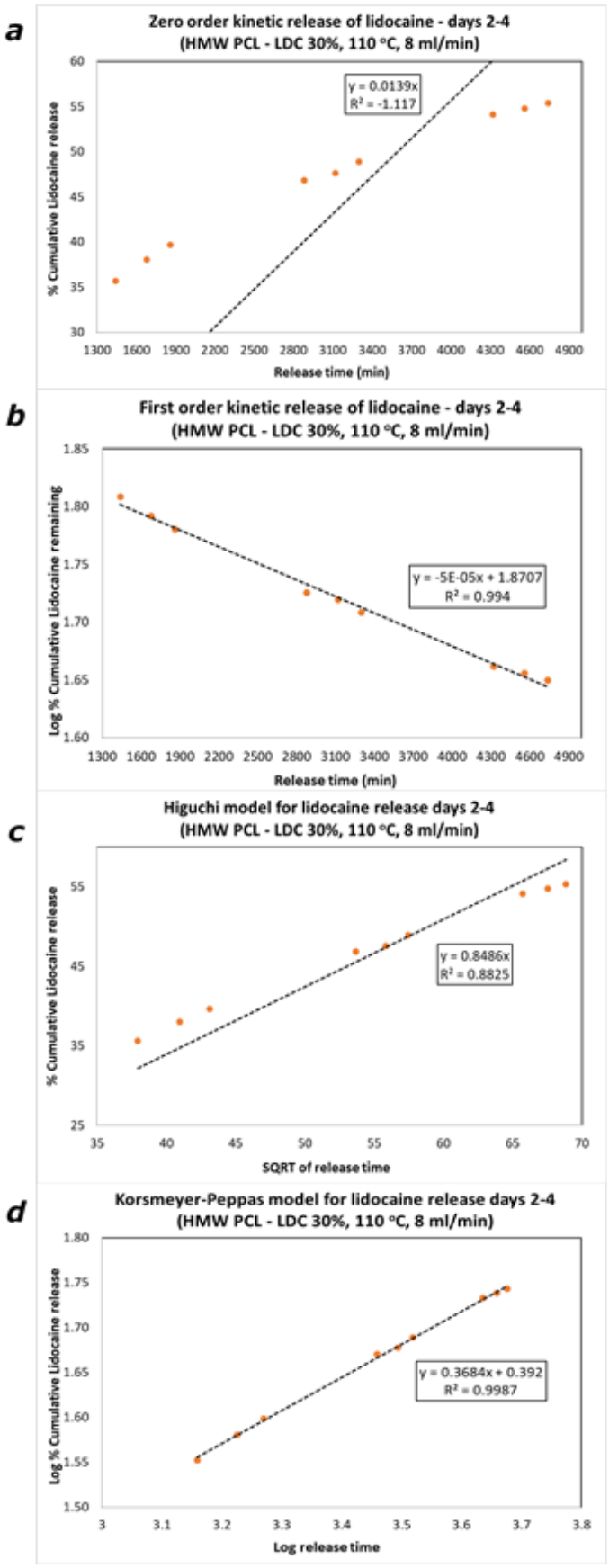

Figure S.22: (a): *Zero-order,* ***(b):*** *First-order,* ***(c):*** *Higuchi and* ***(d):*** *Korsmeyer-Peppas model kinetic release for lidocaine from HMW PCL-LDC 30% implants printed at 110 °C during days 2-4 of dissolution with a flow rate of 8 ml/min.*

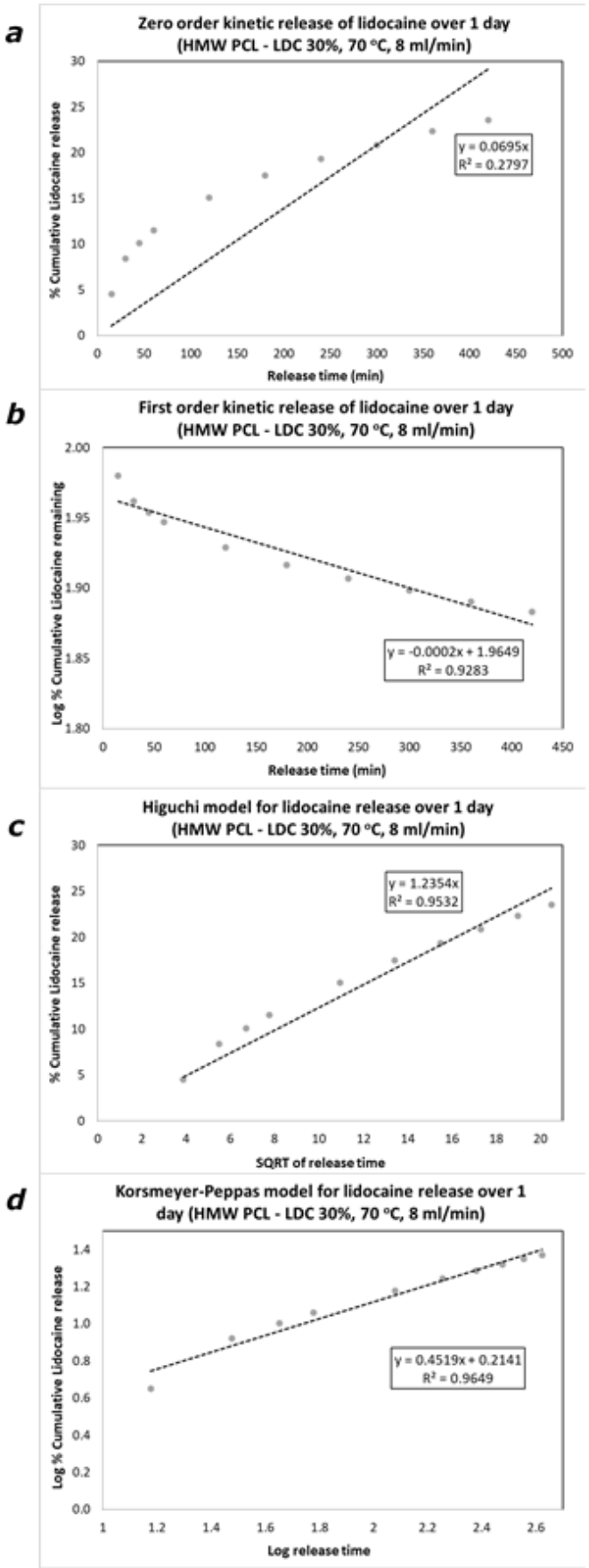

Figure S.23: (a): *Zero-order,* ***(b):*** *First-order,* ***(c):*** *Higuchi and* ***(d):*** *Korsmeyer-Peppas model kinetic release for lidocaine from HMW PCL-LDC 30% implants printed at 70 °C during day 1 of dissolution with a flow rate of 8 ml/min.*

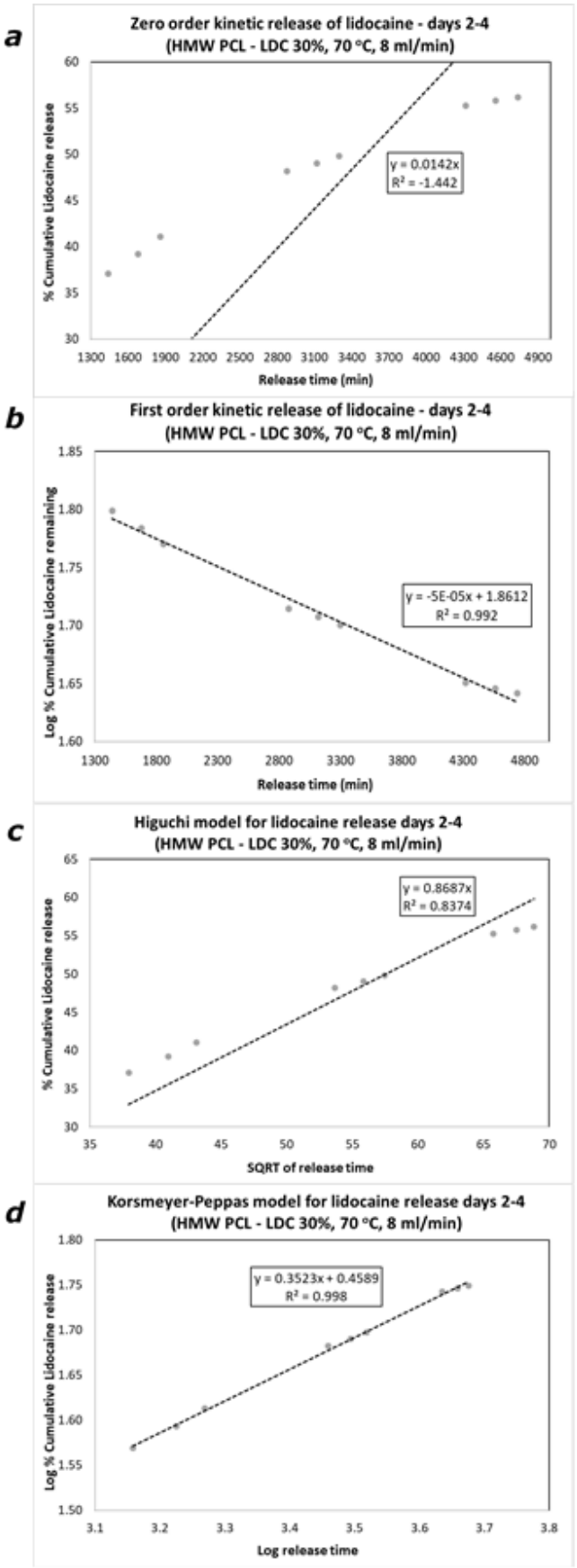

Figure S.24: (a): *Zero-order,* ***(b):*** *First-order,* ***(c):*** *Higuchi and* ***(d):*** *Korsmeyer-Peppas model kinetic release for lidocaine from HMW PCL-LDC 30% implants printed at 70 °C during days 2-4 of dissolution with a flow rate of 8 ml/min.*

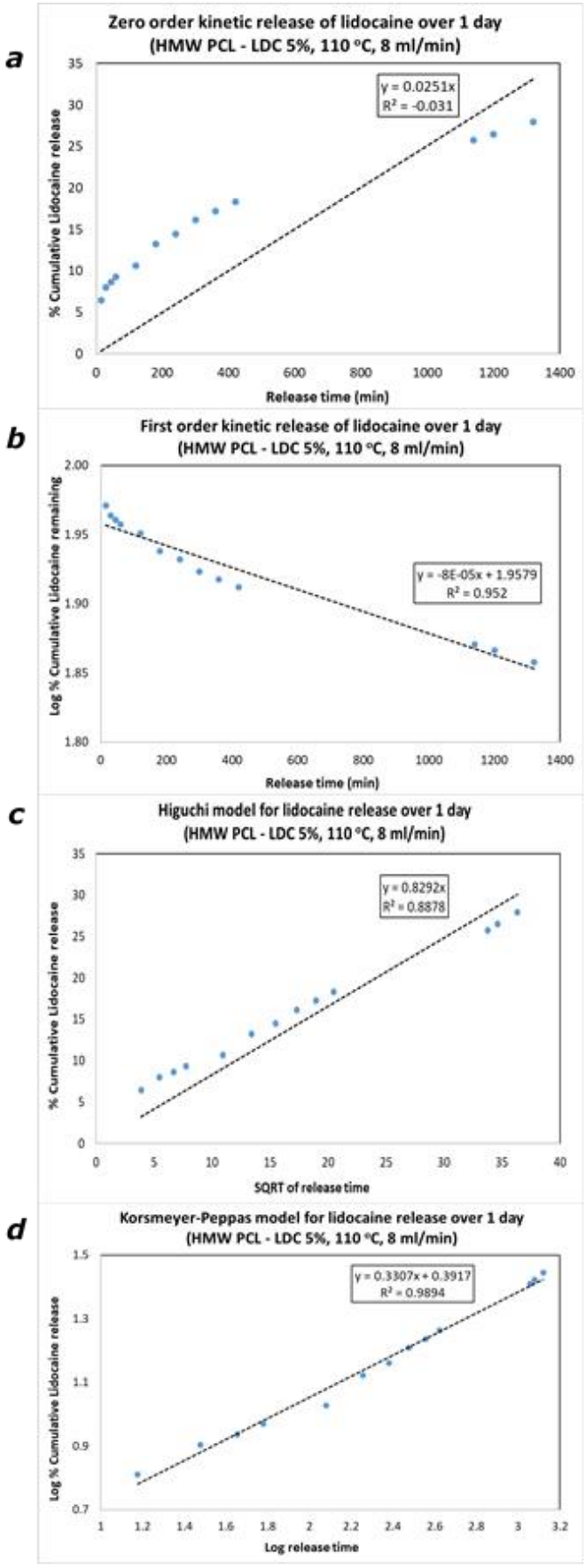

Figure S.25: (a): *Zero-order,* ***(b):*** *First-order,* ***(c):*** *Higuchi and* ***(d):*** *Korsmeyer-Peppas model kinetic release for lidocaine from HMW PCL-LDC 5% implants printed at 110 °C during day 1 of dissolution with a flow rate of 8 ml/min.*

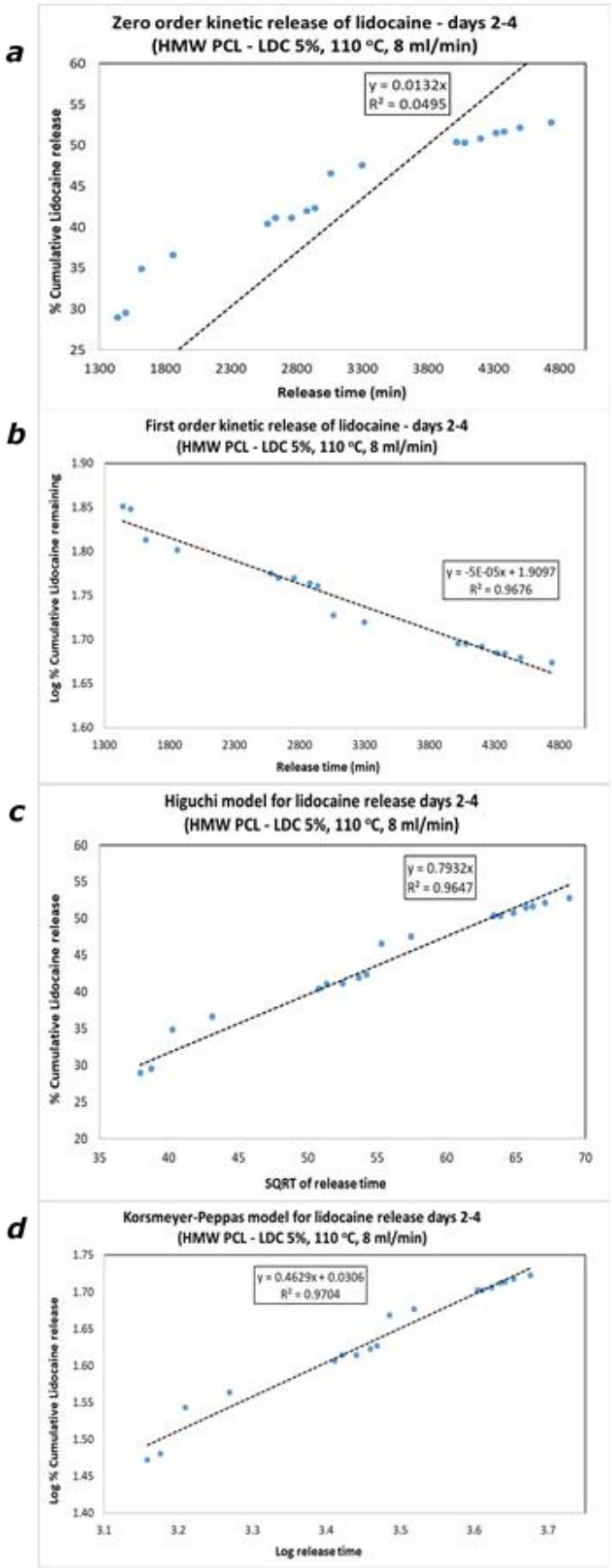

Figure S.26: (a): *Zero-order,* ***(b):*** *First-order,* ***(c):*** *Higuchi and* ***(d):*** *Korsmeyer-Peppas model kinetic release for lidocaine from HMW PCL-LDC 5% implants printed at 110 °C during days 2-4 of dissolution with a flow rate of 8 ml/min.*

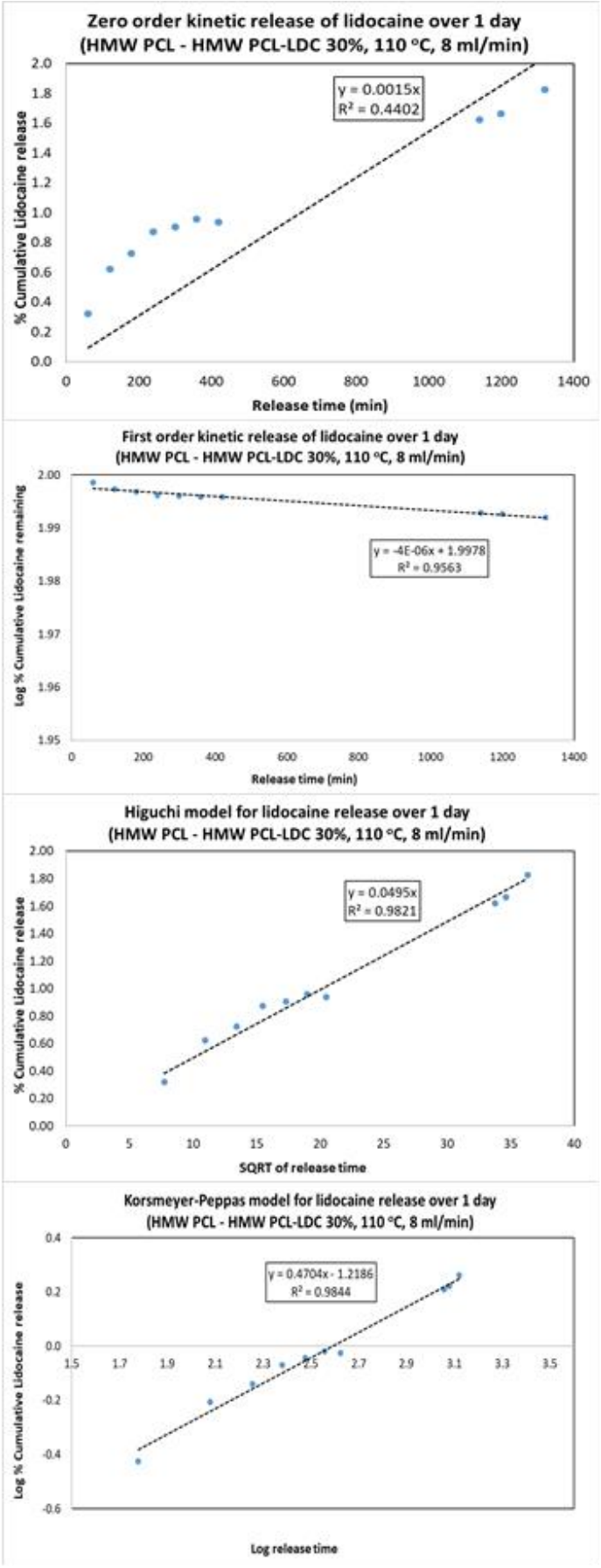

Figure S.27: (a): *Zero-order,* ***(b):*** *First-order,* ***(c):*** *Higuchi and* ***(d):*** *Korsmeyer-Peppas model kinetic release for lidocaine from HMW PCL - HMW PCL-LDC 30% implants printed at 110 °C during day 1 of dissolution with a flow rate of 8 ml/min.*

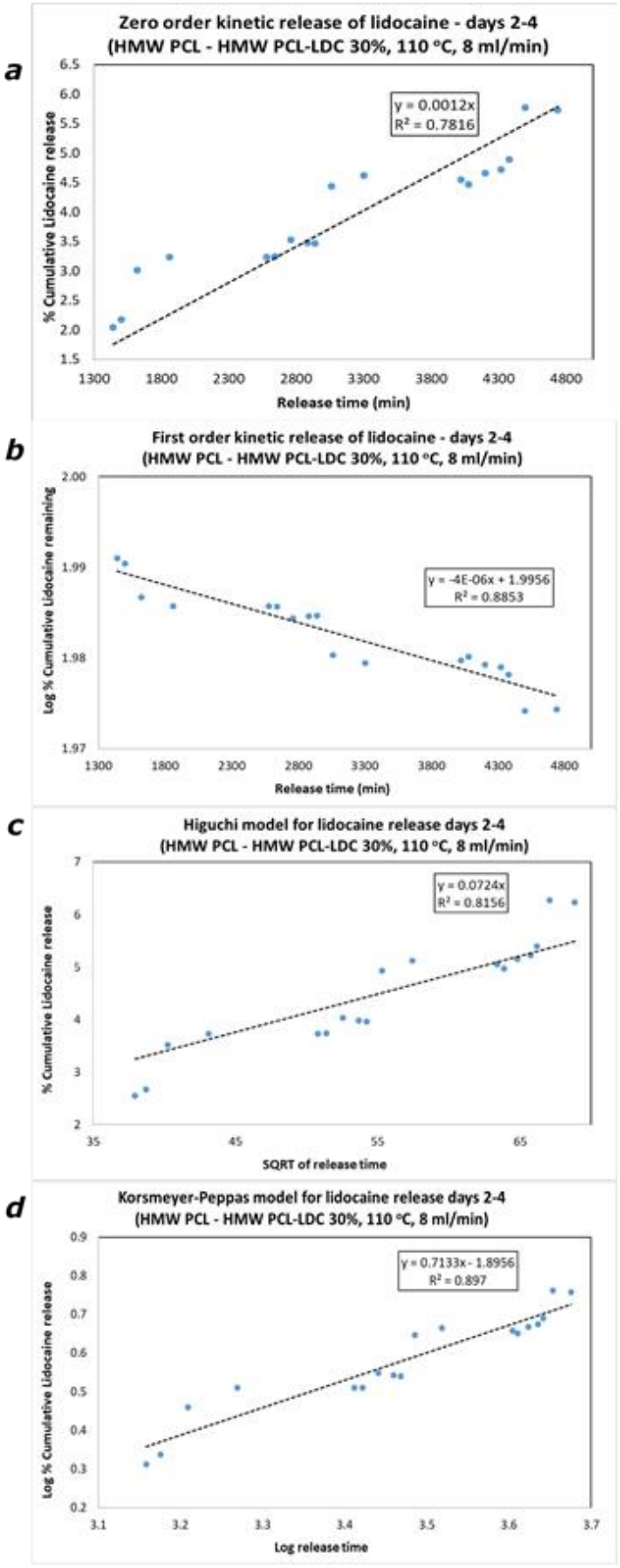

Figure S.28: (a): *Zero-order,* ***(b):*** *First-order,* ***(c):*** *Higuchi and* ***(d):*** *Korsmeyer-Peppas model kinetic release for lidocaine from HMW PCL - HMW PCL-LDC 30% implants printed at 110 °C during days 2-4 of dissolution with a flow rate of 8 ml/min.*

APPENDIX 2

A part of this thesis has been published with the relevant publication presented in the next pages (Liaskoni, Wildman and Roberts, 2021).

International Journal of Pharmaceutics 597 (2021) 120330

Contents lists available at ScienceDirect

International Journal of Pharmaceutics

journal homepage: www.elsevier.com/locate/ijpharm

3D printed polymeric drug-eluting implants

Athina Liaskoni [a], Ricky D. Wildman [b], Clive J. Roberts [a,*]

[a] Advanced Materials and Healthcare Technologies, School of Pharmacy, University of Nottingham, University Park, Nottingham NG7 2RD, UK
[b] Centre for Additive Manufacturing, Faculty of Engineering, University of Nottingham, Nottingham NG7 2RD, UK

ARTICLE INFO

Keywords:
Implant
Sustained release
Polycaprolactone
Personalised medicine
Drug delivery
3D printing

ABSTRACT

An extrusion-based 3D printer has been used for the manufacturing of sustained drug release poly(ε-caprolactone) (PCL) implants. Such implants can address issues of reduced patient compliance due to the necessary frequent administration of conventional drug delivery systems, such as tablets, capsules and solutions. The selected model drug for this study was lidocaine. Polycaprolactone core-shell implants, as well as polymeric implants with no barrier shell were printed with different drug loading, without the addition of solvents or further excipients. Scanning Electron Microscopy (SEM) analysis revealed the structural integrity of the printed formulations, while Differential Scanning Calorimetry (DSC), X-Ray Diffraction (XRD) and Attenuated Total Reflectance Fourier Transform Infrared spectroscopy (ATR-FTIR) were used to detect potential chemical interactions or modifications. Raman spectroscopy was also used to study material distribution in the prints. The drug release rate of the differently printed formulations was evaluated using a USP4 flow-through cell apparatus. All printed implants demonstrated sustained lidocaine release and the effectiveness of the PCL barrier in this regard. The Korsmeyer-Peppas model was suggested as the best fit to drug release profiles for all the produced implants. This work demonstrates that hot-melt extrusion-based 3D printing is a robust and promising technology for the production of personalisable drug-eluting implants.

1. Introduction

Personalised medicine has received interest in recent years as a means to achieve more effective patient therapies and outcomes. Within the broader framework of precision medicine usually associated with the response of the genome to the active agents, the personalisation of drug therapy both in the dosages and the proper selection of the active pharmaceutical ingredient (API) is a potentially important route to increased clinical effectiveness (Gioumouxouzis et al., 2019; Sandler and Preis, 2016). One of the most common issues arising from the administration of many currently available formulations is a relatively low patient compliance, especially in populations that have multiple and complex conditions and a consequent need to be treated with several drugs contained in different formulations (Robles-Martinez et al., 2019).

The principles of personalised medicines follow the advice of Hippocrates, "to treat the person, not the disease", since the purpose of their fabrication is to suit each patient's needs, characteristics and preferences (Alomari et al., 2015). The production of a custom-shaped drug delivery system loaded with one or more APIs could significantly improve patients' clinical outcomes, as the frequency of drugs administration would be reduced and consequently adherence enhanced (Zema et al., 2017). However, such novel individualised drug dosage forms cannot be easily fabricated using standard pharmaceutical processing methods.

It is well recognised that three-dimensional (3D) printing, also termed as Additive Manufacturing (AM) can potentially address this manufacturing issue. 3D printing has gained traction in numerous applications in various fields, including healthcare (Skowyra et al., 2015; Economidou et al., 2018). 3D Printing began in the early 1980s when Charles Hull invented the first 3D printer, then termed "stereolithography" (Hull, 1986). 3D Printing is a computer controlled additive manufacturing technique that is used for the production of solid objects in a layer-wise way through a series of cross-sectional slices according to a computer-aided design file (Moulton and Wallace, 2014).

The application of 3D printing in the pharmaceutical field makes feasible the design and fabrication of drug carriers with freedom in internal and external geometry and precise spatial drug distribution (Goyanes et al., 2015b; Khatri et al., 2018) and was importantly recognized by the FDA in 2015 of the first 3D printed drug, Spritam®, produced by Aprecia Pharmaceuticals (West and Bradbury, 2019).

* Corresponding author.
E-mail address: clive.roberts@nottingham.ac.uk (C.J. Roberts).

https://doi.org/10.1016/j.ijpharm.2021.120330
Received 4 December 2020; Received in revised form 25 January 2021; Accepted 27 January 2021
Available online 2 February 2021

Nowadays, several different Additive Manufacturing methods are commercially available with each having different operating principles and using various types of materials for the production of the predesigned parts. The most widely used methods are material jetting (MJ), binder jetting (BJ), selective laser sintering (SLS), fused deposition modelling (FDM), VAT photopolymerisation including stereolithography (SLA) and semi-solid extrusion (SSE) printing (Khaled et al., 2014; Kyobula et al., 2017; Fina et al., 2018; Infanger et al., 2019; Goyanes et al., 2015a). Many different materials can be used for 3D printing, such as plastics, metals, ceramics, polymers, hydrogels, powders, liquids, or even animal and human cells (Genina et al., 2016; Liaw and Guvendiren, 2017; Jasiuk et al., 2018). Several studies have been conducted showing the successful fabrication of drug delivery devices, orodispersible tablets and films, solid oral dosage forms and microneedles for transdermal drug delivery using various 3D printing technologies (Pissinato Pere et al., 2018; Goyanes et al., 2014; Holländer et al., 2018; Khaled et al., 2018b; Edinger et al., 2018).

Extrusion-based 3D printing methods have some similarity to conventional extrusion pharmaceutical processing technologies, and allow precise dosing with complex drug release profiles (Lamichhane et al., 2019; Khaled et al., 2015a). In this technique, a viscous semi-liquid material is extruded from a syringe on the building platform, where it solidifies typically via a drying process for the production of the desired geometry layer by layer (Tappa and Jammalamadaka, 2018). Numerous 3D printing studies have illustrated the potential of this method for the fabrication of drug dosage forms with different geometries and tuneable drug release profiles (Khaled et al., 2018a; Aita et al., 2019; Li et al., 2018).

Different types of materials can be used for extrusion, such as molten polymers, pastes, colloidal suspensions, silicones and gels (Khaled et al., 2015b; Palo et al., 2017; Ligon et al., 2017). A materials extrusion is affected by its chemical, physical and mechanical properties, often being mixed with solvents prior to their loading to the printing syringe for the desired viscosity and rheological properties to be obtained. It is necessary for the material mixtures to be free of large particulates for the nozzle to not be blocked during the 3D printing process (Sadia et al., 2018). A proper combination of the printing parameters, such as material flow rate, print temperature and print speed, also contribute to the control of materials deposition. The fact that relatively low temperatures are generally needed during the extrusion makes feasible the usage of a wide range of thermally labile active ingredients (Norman et al., 2017).

In the current study, an extrusion-based 3D printer has been used for the fabrication of an implant dosage form designed to release the active agent (usually intended to be close to the desired site of action) at a therapeutically desired rate for extended periods (da Silva et al., 2010). These can be injected or surgically inserted into the human body. These systems are generally well accepted by patients, as they only feel a small bump under the skin (Bourges et al., 2006).

Research on the manufacturing of implants with different materials, drugs, shapes and drug release profiles using various 3D printing techniques has recently been performed (Gbureck et al., 2007; Water et al., 2015; Yang et al., 2018) but not using extrusion-based methods.

The aim of the present work was the manufacture of prolonged release drug-eluting polymeric implants at the lowest temperature possible without the addition of any solvent or other materials using an extrusion-based 3D printer. For this purpose, polycaprolactone (PCL) encased in a PCL barrier shell and lidocaine loaded PCL implants with no shell have been fabricated to investigate the impact of the slow PCL degradation on the release of the drug, lidocaine. Physical and chemical characterizations have been conducted to assess the printing resolution, detect any chemical modifications or interactions occurred during the 3D printing process, as well as the chemical distribution to better understand the drug release mechanism.

2. Materials and methods

2.1. Materials

PCL with a molecular weight of 50 kDa was purchased from Polysciences Europe GmbH, (Hirschberg, Germany). Lidocaine (LDC) 97.5%, Sodium Phosphate Dibasic Anhydrous (Na_2HPO_4) ≥99%, Potassium Phosphate Monobasic (KH_2PO_4), ACS Reagent, ≥99% and Sodium Chloride (NaCl) 99.5% were purchased from Fisher Scientific UK Ltd (Loughborough, UK).

PCL was the chosen material for the fabrication of sustained release implants as it is considered non-toxic and is FDA approved. Its potential for long term degradation also contributed to its selection, as it can be used for the release of an active substance for up to several months or even years (Luong-van et al., 2006). It can be processed without difficulty due to the low melting temperature, 50–65 °C. It is compatible with many different drugs and that makes feasible the uniform distribution of the active agent in a matrix (Woodruff and Hutmacher, 2010).

The selection of the model drug that was loaded in the polymeric implants has been made in part based on its decomposition temperature, which was needed to be lower than the melting point of PCL. Lidocaine was the chosen drug as its decomposition temperature (196 °C) is higher than the melting point of the studied polymer. Its melting point (68–70.4 °C) is, however, relatively close to PCL's melting point, and therefore a similar temperature is needed for the melting and extrusion of the blended compounds (Umeda et al., 2009).

2.2. Methods

2.2.1. Extrusion-based 3D printing

Disc-shaped PCL implants loaded with 30% w/w lidocaine (PCL-LDC 30%) or 5% w/w lidocaine (PCL-LDC 5%) or drug free implants were printed using an extrusion-based 3D printer (Inkredible +, Cellink, Gothenburg, Sweden). Optimization of the printing parameters was carried out to ensure well-formed implants to be fabricated. Finally, implants with a PCL barrier-shell were manufactured based on the established settings. Characterization on the compounds before and after their mixing and extrusion was conducted to explore potential changes in their properties or any chemical interactions or modifications occurred during the 3D printing process. The process flow of manufacture and characterisation is summarised in Fig. 1.

PCL barrier-shell PCL-LDC 30% (PCL – PCL-LDC 30%) implants were printed layer by layer starting with the PCL base and outer wall shell, followed by the printing of the drug loaded polymeric formulation core (PCL-LDC 30%) and then finally a PCL cap to enclose the core (Fig. 2).

2.2.2. In vitro drug release studies

Dissolution studies were performed using a closed system USP4 flow-through cell apparatus (SOTAX CE7 smart USP 4, Foston, UK) since the test lasted for more than 24 h and any media evaporation would have had an impact on the results. Lidocaine concentration was measured in an Agilent Cary 50 Bio UV–Visible Spectrophotometer (Stockport, UK).

3. Results and discussion

3.1. Selection of printing parameters

The aim of this study was the manufacturing of polycaprolactone core-shell implants with prolonged drug release. The formulations needed are required to print evenly and continuously, without the presence of any holes in the printed structure. It was, hence, needed to establish the right combination of printing parameters for each section of the print before proceeding to the fabrication of the core-shell formulation.

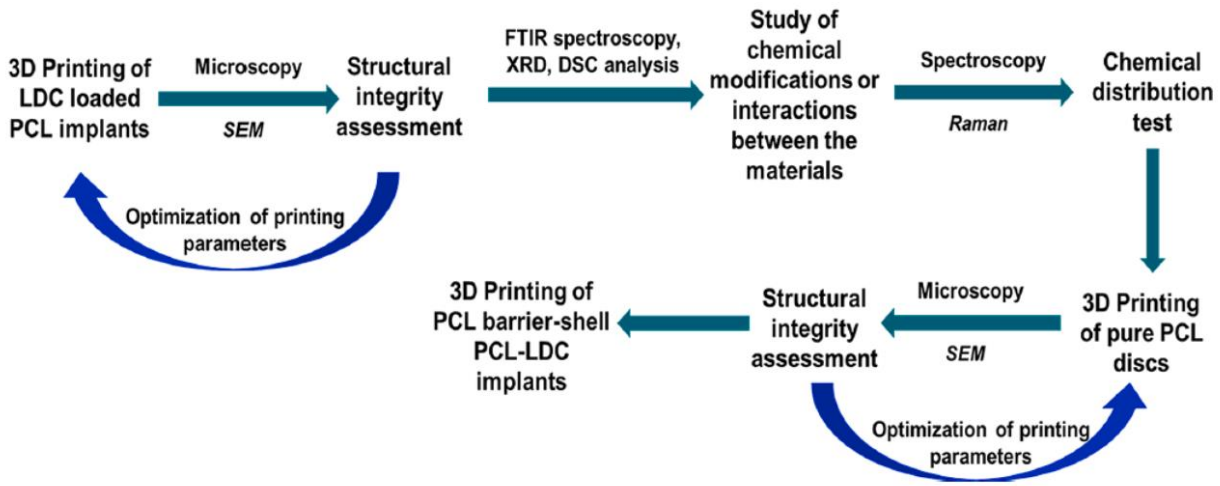

Fig. 1. Schematic diagram of the optimization procedure for the establishment of the 3D printing parameters for the manufacturing of the PCL barrier-shell PCL-LDC implants and their characterization procedures.

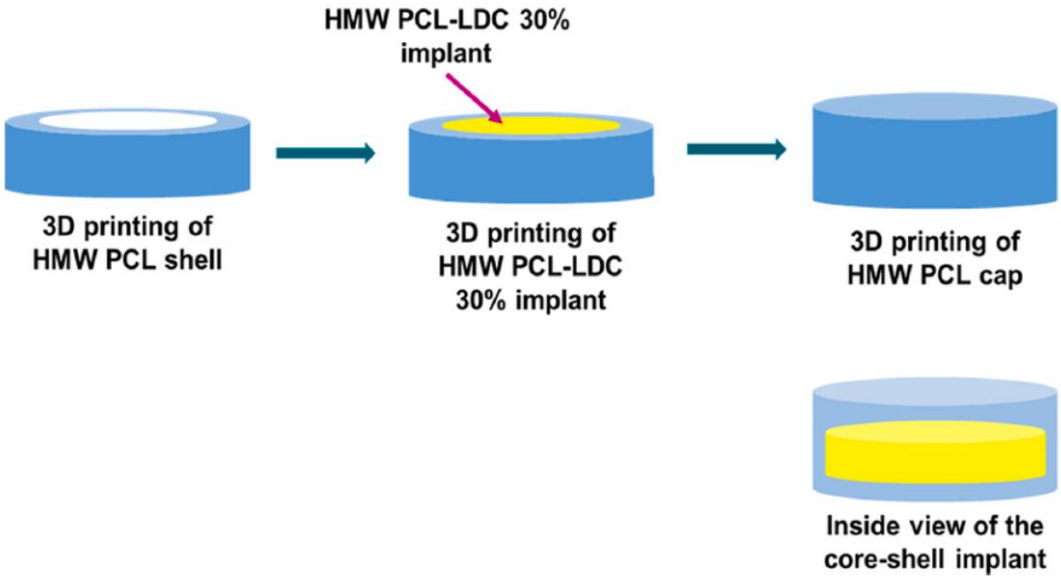

Fig. 2. Schematic diagram of 3D printing of Polycaprolactone barrier-shell PCL-LDC 30% implants in several stages. The white circle represents the gap inside the PCL shell and the yellow circle the PCL-LDC 30% implant.

3.1.1. 30% w/w lidocaine loaded polycaprolactone implants

3D printing of PCL based implants loaded with 30% w/w lidocaine was initially conducted, as this is the drug containing compartment in the PCL core-shell drug delivery system (Fig. 2).

As demonstrated in Fig. 3, the implant surfaces differ based on the selected extrusion width setting. The implant printed with an extrusion width setting of 100% (Fig. 3a), showed gaps on its surface between the printed lines. The gap size between the printed lines decreased towards zero as the extrusion width decreased (see Fig. S.2). No gap was visible on the surface of the implants printed with extrusion width settings off 50% and 60% (Fig. 3b).

The distance between the centres of the printed lines at the various applied extrusion widths was found to be almost 1.5 times higher than that defined in the printer settings based on pure geometric considerations (Fig. 4). This can be attributed to the materials swelling after their extrusion from the nozzle and before deposition and hardening. This phenomenon has been observed previously during polymer processing and is termed die or extrudate swelling or the Barus effect (Koopmans, 1999).

PCL-LDC 30% implants were, then, manufactured at different temperatures, while the printing pressure was adjusted for optimal printing at each temperature for batches of ten 2 mm discs to be produced. The higher the temperature used, the lower the pressure that was needed since more material was extruded from the nozzle due to reduced viscosity. The implants printing resolution was further explored using SEM imaging.

Even though there were no gaps present on the implant surfaces, their surfaces appeared highly featured at higher resolution (Fig. 5). This was more obvious when lower print temperatures were used, closer to the melting point of the materials (see Fig. S.3).

As demonstrated in the SEM image of the PCL-LDC 30% implant printed at 70 °C in Fig. 5a, its surface was relatively rough with some small particles on it. These particles could be attributed to either the polymer or the drug since temperatures used in printing were very close to their melting point. Therefore, 70 °C might have not been enough for the complete melting of the materials within the time of exposure in the printer. As the print temperature increased, the observed particles size decreased, and the surface of the implants became visually smoother (Fig. 6).

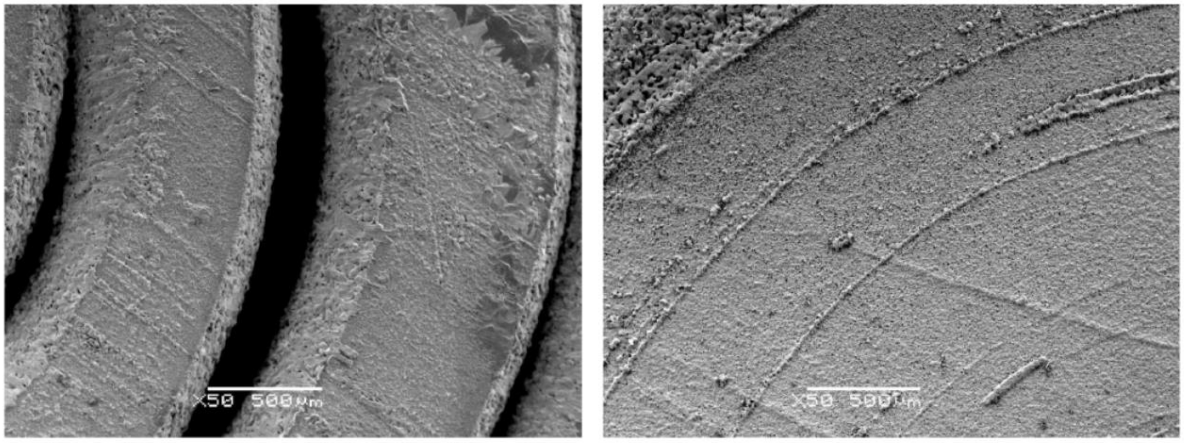

Fig. 3. SEM images of the bottom side of PCL-LDC 30% implants printed at 70 °C with an extrusion width setting of (a): 100% and (b): 60%. The magnification is ×50, the scale bar 500 μm and they are labelled on each SEM image separately.

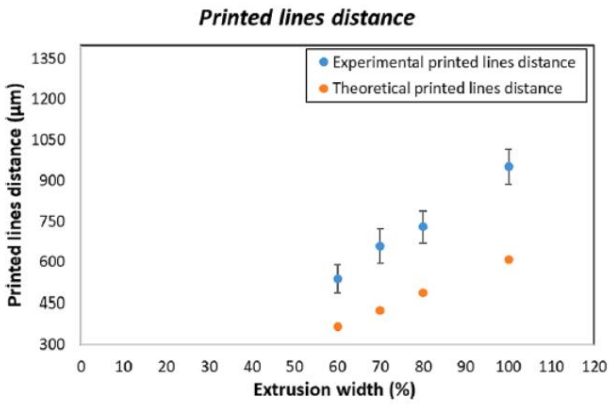

Fig. 4. Distance of the centres of the printed lines on the PCL-LDC 30% implants surface printed with different extrusion widths, 60–100%, and a print speed of 1 mm/s at 70 °C, as measured in the Image J.

3.1.2. 5% w/w lidocaine loaded polycaprolactone implants

Polymeric implants with a lower drug loading of 5% w/w, were also fabricated after optimisation of their printing parameters in a similar fashion as for the 30% loaded samples. SEM analysis of the manufactured implants revealed that the most optimal printing resolution was achieved with the lowest studied extrusion width and the highest pressure (Fig. 7b). All the other combinations of the two investigated parameters resulted in the creation of gaps on the surface of the produced discs (see Fig. S.4).

3.1.3. Pure polycaprolactone control prints

PCL discs without any drug were printed with the same settings that resulted in the most homogeneously produced PCL-LDC 5% implants. However, contrary to the drug loaded disc there were many surface holes visible in the pure polymer sample, indicating that the presence of drug at 5% had an impact on material properties (eg. viscosity) of the blend versus the polymer alone and hence, printing integrity (see Fig. S.5). The setting of the extrusion width was again altered to a lower value than that used for the fabrication of the PCL-LDC 5% implants to reduce the appearance of surface holes and hence improve the printing quality of the pure PCL discs.

3.2. Characterizations of PCL and LDC before and after 3D printing

3.2.1. DSC

The mixing and the different settings applied during the 3D printing process did not affect the thermal properties of the polymer (see Fig. S.6). No peaks for the melting point of lidocaine were detected in any of the drug loaded printed formulations, indicating a largely amorphous state of the drug within the polymer after printing and likely

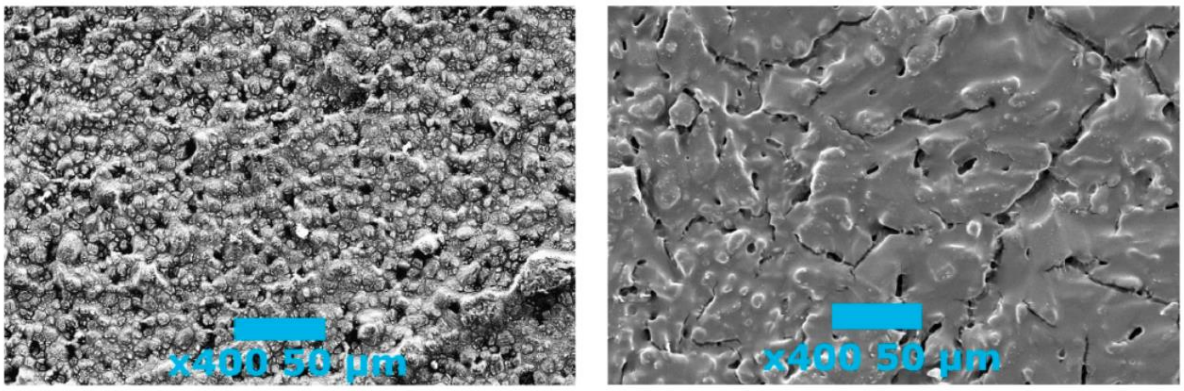

Fig. 5. SEM images of the top side of PCL-LDC 30% implants printed with an extrusion width setting of 60% at (a): 70 °C and (b): 110 °C. The magnification is ×400, the scale bar 50 μm and they are labelled on each SEM image separately.

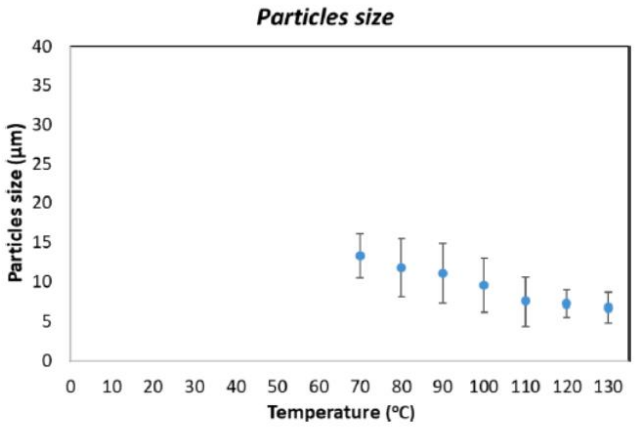

Fig. 6. Size of the particles on the surface of the PCL-LDC 30% implants printed with different temperatures, a print speed of 1 mm/s and an extrusion with setting of 60%, as measured in the Image J.

formation of a solid dispersion (Rychter et al., 2018). However, two peaks for the crystallization temperature of the PCL-LDC 30% implant appeared in the thermogram, which indicated the impact of the drug in the polymer properties. Note no T_m for the drug was observed in the second heating cycle showing that the drug had not significantly recrystallised in this first cycle. A similar thermogram, as for the crystallization temperature, was not obtained when the PCL-LDC 5% implant was characterized in the DSC. Again, there was no evidence of drug crystallisation, consistent with the higher loading also showing this phenomenon.

3.2.2. XRD

Peaks in the XRD diffractograms of the polymer and the drug verified their crystalline state before printing (Fig. 8) (Shkarina et al., 2018; Ribeiro et al., 2016). After the physical mixing of the powders and the manufacturing of PCL-LDC 30% implants with different settings, the same peaks for both materials were detected in their diffractograms, which indicated that no change in the physical form of the compounds has occurred (Fig. 8a, b).

No drug related peaks were observed for the printed PCL with 5% drug, only those associated with PCL (Fig. 8c). This is likely related to the relative lack of sensitivity of DSC compared to XRD data, where for the 30% loaded samples drug crystallisation was evident (Newman et al., 2015; Venkatesh et al., 2001). Whilst both are bulk techniques, XRD is known to be more sensitive to the presence of crystallinity than DSC, at least on their standard forms as used here, with broadly detection limits for XRD as low as 1% w/w, whereas for DSC 5% w/w is more typical (Sheokand et al., 2016). We propose that for the 30% drug loaded system, that whilst the drug is largely in an amorphous or discorded state, sufficient crystallinity remains to be detected by XRD but not DSC. Whereas, clearly for the 5% loaded sample the amount of crystallinity, if any, falls below the detection limit of both techniques.

3.2.3. FTIR

Mainly characteristic peaks of the loaded drug were detected in the FTIR spectra of the PCL implants loaded with 30% w/w lidocaine. The print temperature did not have any detectable impact on the chemical structural signature of the compounds (Fig. 9a) (Xue et al., 2014; Anacleto et al., 2018). However, fewer peaks appeared in the spectra of the fabricated implants compared to the spectrum of the physical powder mixture where more characteristic peaks for PCL were detected. A possible explanation could be the fact that only one specific area was analyzed in the FTIR for each sample and therefore, the obtained spectrum for the physical mix will have had potentially a higher amount of pure PCL present compared to the printed intimately mixed sample and hence more highly resolved peaks related to PCL in the physical mix data (Lebon et al., 2016).

The spectra of the PCL-LDC 5% powder physical mixture and printed implant, were identical indicating that at this level of loading no significant interactions could be detected (Fig. 9b). It should be noted that only the characteristic bands of the polymer were detected in these spectra since the drug loading is below the sensitivity of the technique (Lebon et al., 2016; Helmy et al., 2003).

3.2.4. Raman

The Raman spectra of the surface particles as observed in Fig. 5 and the matrix of the implant printed at 70 °C were identical and exhibited peaks related to the loaded drug (Fig. 10a) (Monteiro et al., 2016). Further analysis of the surface of the implants printed at higher temperatures, where the surface particles were smaller than those for implants printed at 70 °C showed that the spectra for the surface particles and the matrix of the implants produced at higher temperatures were identical with those of the implants fabricated with the lowest temperature (Fig. 10b). This indicated that both PCL and lidocaine were present in the matrix and the surface particles.

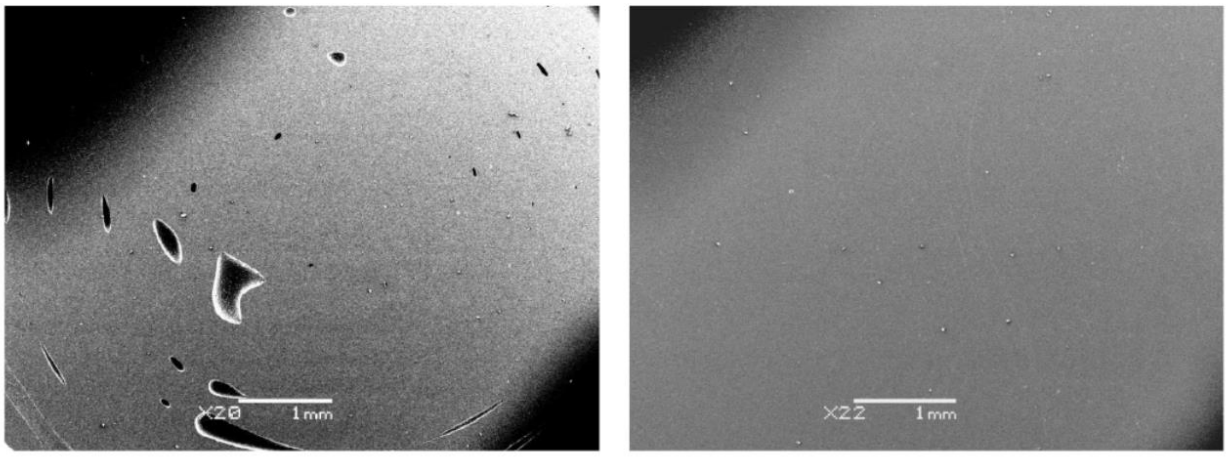

(a) (b)

Fig. 7. SEM images of the bottom side of PCL-LDC 5% implants printed at 110 °C with (a): an extrusion width setting of 60% pressure of 200 kPa and (b): an extrusion width setting of 50% pressure of 400 kPa. The magnification and the scale bar are labelled on each SEM image separately.

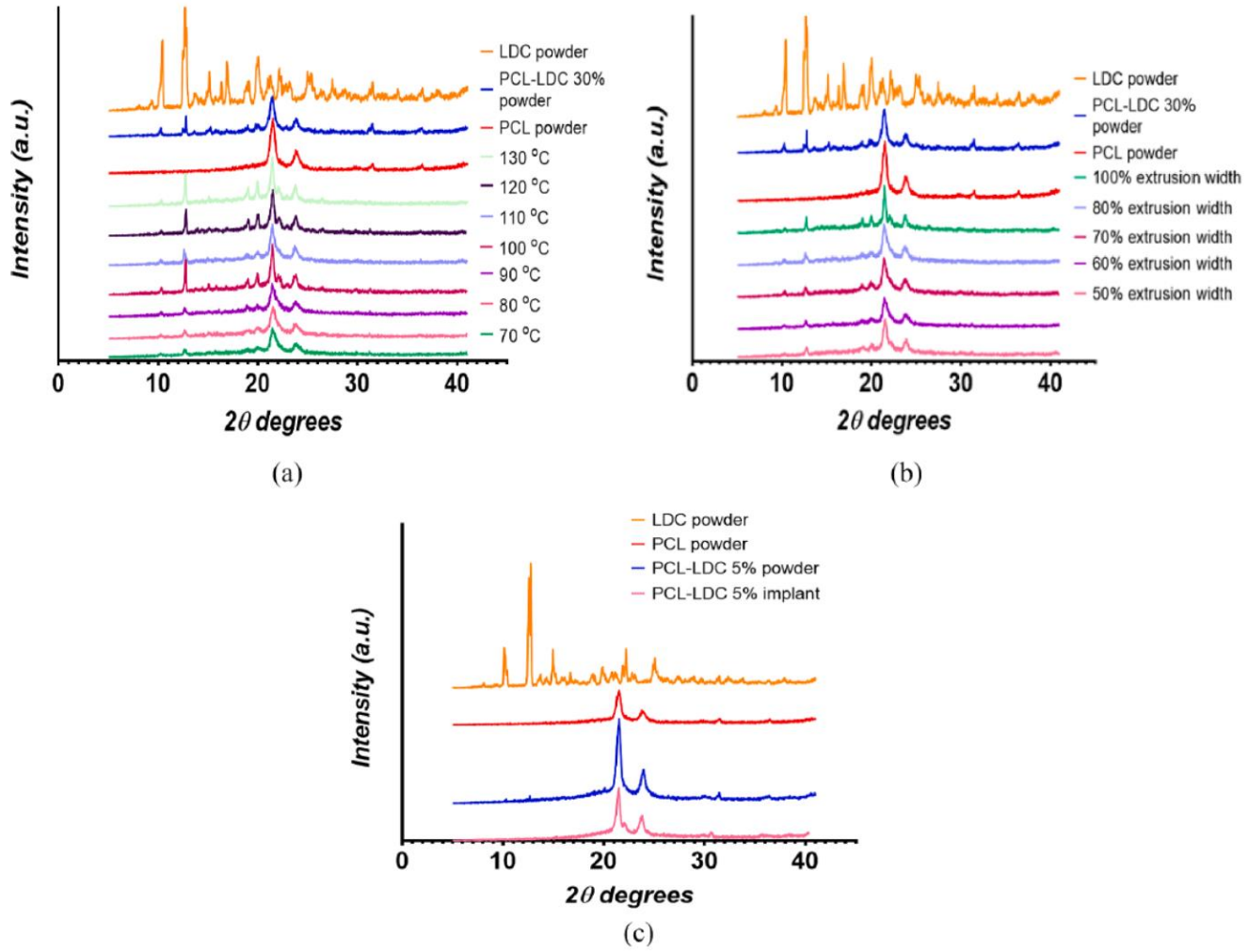

Fig. 8. XRD Diffractograms of (a): PCL-LDC 30% powder and implants printed in different temperature with an extrusion width setting of 60%, (b): PCL-LDC 30% powder and implants printed at 70 °C with different extrusion widths and (c): PCL-LDC 5% powder and implant printed at 110 °C with an extrusion width setting of 50%.

3.3. 3D printing of polycaprolactone barrier-shell PCL-LDC 30% implants

The final manufactured formulation design brings together the previously optimised elements to achieve the core-shell design goal (Fig. 2). SEM analysis was particularly important in this case since the PCL – PCL-LDC 30% implants were printed in sequential stages and the effective layer alignment and integration was needed to be investigated.

As demonstrated in the SEM images of the side view of the produced implant (Fig. 11), the printed layers were well integrated with no gaps detected, and hence, the shell as required to control drug release appears fit for purpose in terms of physical integrity.

A misalignment between the printed layers can be observed in Fig. 11a and is related to the use of a single head printer, whereby printer cartridge exchanges had to take place between sequential prints. The future use of multi-head printers with better sample stage reproducibility would relatively trivially address this issue, as it is not a fundamental issue with 3D printing rather the limitations of the printer type used here.

The individual layer height was designed to be nominally 1 mm; however, SEM images (Fig. 11a) indicated that the phenomenon of die swelling occurred during the printing of the implant layers, leading to these being approximately 1.4 times larger than expected, similar to as noted earlier.

3.4. In vitro drug release studies

Dissolution data from PCL encased and non-encased implants printed at various temperatures and with different drug loadings, in general, demonstrated sustained drug release (Fig. 12).

Polycaprolactone core-shell implants presented a particularly prolonged release, suggesting that the studied polymer provided an effective barrier to the formulation for the release of the drug. It was, thus, demonstrated the potential to achieve sustained release for a very long time based on the slow degradation of the studied polymer (Fig. 12). This was also in a good agreement with the published data of another study; combinations of different molecular weight PCL were used for the coating of 3D printed PVA-PLA implants. PCL coated formulations demonstrated sustained drug release compared to the uncoated ones, while the molecular weight of the PCL used for the coating contributed to a more extended release of the active agent (Stewart et al., 2020a).

In the PCL implants without a barrier-shell, no burst release was detected, indicating that whilst lidocaine was detected on their surface, it, nevertheless, remained sufficiently physically associated with the PCL to slow down the release. More specifically, when PCL-LDC 30% implants printed at two different temperatures, 70 and 110 °C, were tested, their lidocaine release profiles were similar (Fig. 12) and hence, they were not affected by the nature of surface particles (Fig. 5). This was consistent with the Raman analysis, where it was illustrated that the

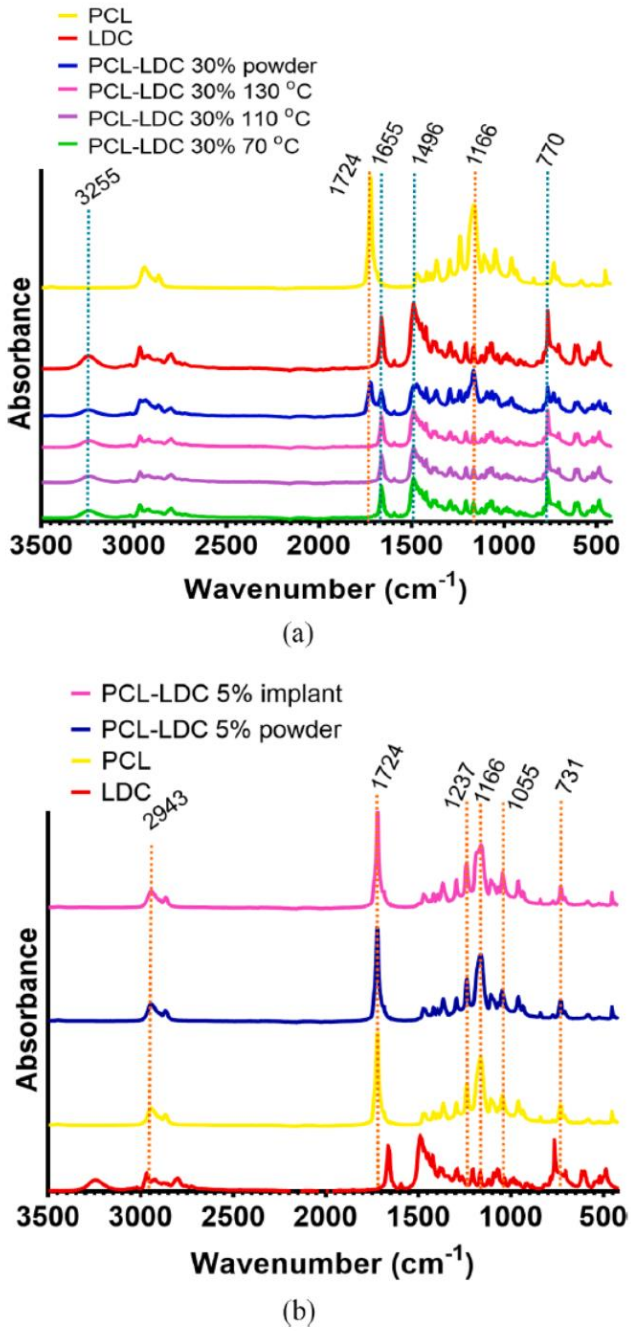

Fig. 9. FTIR spectra of (a): PCL-LDC 30% powder and implants printed in different temperature with an extrusion width setting of 60% and (b): PCL-LDC 5% powder and implant printed at 110 °C with an extrusion width setting of 50%. LDC peaks are highlighted with the blue dot-line and PCL peaks with the orange dot-line.

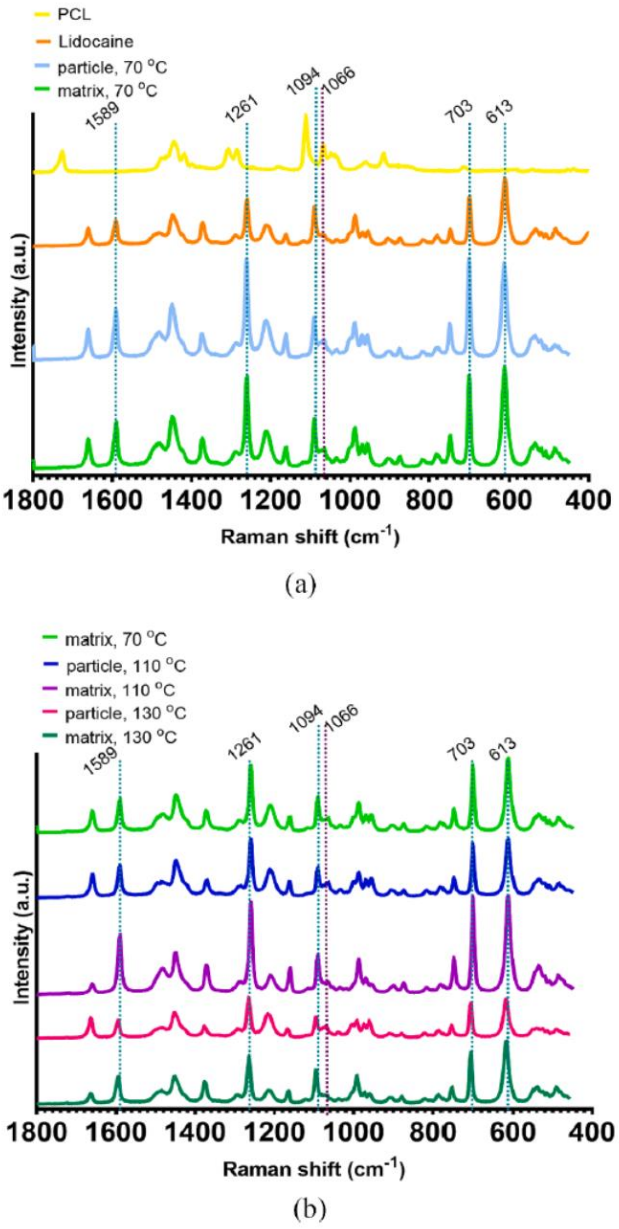

Fig. 10. Raman spectra of surface particles and matrix of (a): PCL-LDC 30% implants printed at 70 °C and (b): PCL-LDC 30% implants printed at 70, 110 and 130 °C. LDC peaks are highlighted with the blue dot-line and PCL peaks with the purple dot-line.

polymer and the drug were homogeneously distributed at the micron-scale at least, on the surface of the printed implants (Fig. 10).

As displayed in Fig. 12, when PCL implants with a lower drug loading of 5%, were tested, lidocaine was released in a similar way to the 30% LDC loaded samples, which means that no burst release had occurred, and prolonged drug release has been achieved in both cases.

According to Fig. 12 and Table S.1, the drug release rate was faster during the first day of the dissolution study in all of the differently fabricated formulations and then, it was slowing down after the second day. However, this effect was less intense in the PCL encased implants compared with the non-encased ones which indicated that the polymeric shell was degrading over time and allowing the release of the loaded drug for a particularly prolonged period.

The amount of the released lidocaine was depending on the drug loading of the tested implant and not on the previously applied printing settings; the first day of the dissolution test 32.19 ± 2.66 mg of lidocaine were released from the PCL-LDC 30% implant printed at 110 °C, 33.12 ± 0.17 mg from the PCL-LDC 30% implant printed at 70 °C, 5.68 ± 1.11 mg from the PCL-LDC 5% implant and 1.71 ± 0.53 mg from the PCL barrier-shell PCL-LDC 30% implant (Table S.1). The drug released from the 30% w/w lidocaine loaded polymeric implants was almost double the amount of the drug absorbed from the commercially available lidocaine adhesive patches, Lidoderm® and ZTLido® and below the recommended maximum total dose, 300 mg (Gudin et al., 2020; Gudin and Nalamachu, 2020). Nevertheless, the same trend was not observed in the other formulations, neither the next days of the in vitro drug release studies. This could possibly be addressed if a higher drug loading

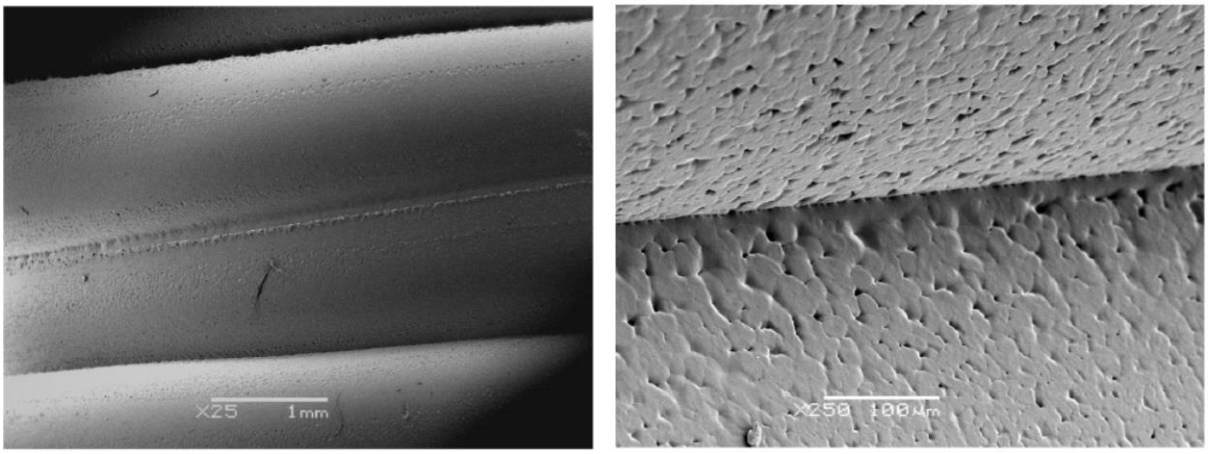

Fig. 11. SEM images of the outside layers of the 3D printed PCL barrier-shell PCL-LDC 30% implants with a magnification (a): ×25 and (b): ×250. The magnification and the scale bar are labelled on each SEM image separately.

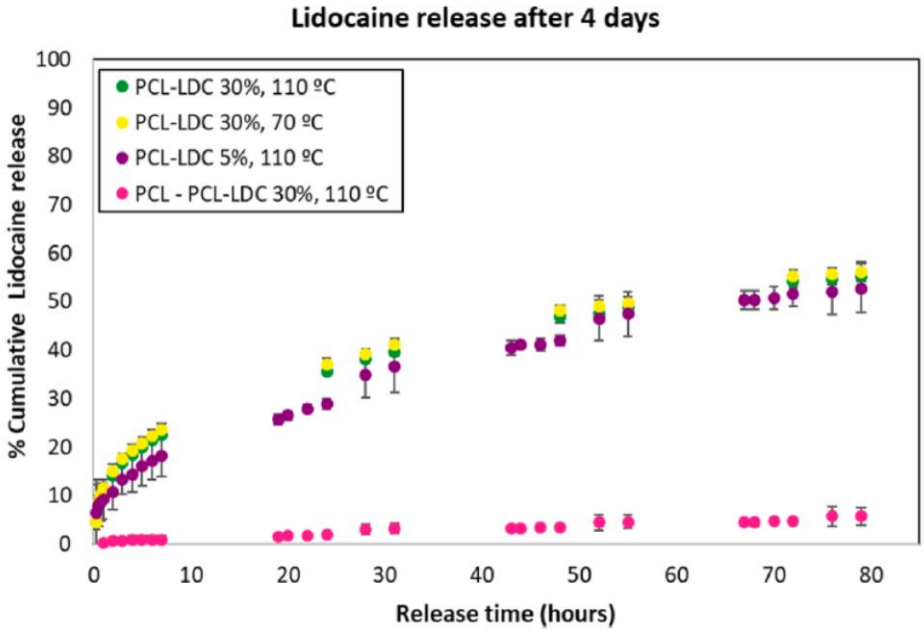

Fig. 12. Dissolution profiles of differently printed polycaprolactone non-encased and encased implants with various lidocaine loadings after 4 days.

was applied, as has already studied in other lidocaine loaded polymeric systems (Kau et al., 2014; Shao et al., 2018).

The first stages of erosion of the PCL matrix were demonstrated in the SEM images of the pure PCL discs showing surface holes (see Fig. S.8) (Díaz et al., 2014; Stewart et al., 2020b). SEM images of the lidocaine loaded polycaprolactone implants after 4 days of dissolution (Fig. 13), also showed some irregular shaped holes in the range of 25–45 µm on the surface of the implants, consistent with the release of the drug and the beginning of PCL degradation (Ferreira et al., 2017; Perale et al., 2010). PCL degradation has likely led to the smoother surface observed after drug release. These observations are consistent with drug release from the inner parts of the discs through these open channels as water penetrates into the degrading PCL matrix.

In the case of the PCL barrier-shell PCL-LDC 30% implants, the outer surface consisted of pure PCL and only a few small pores with an average size of 20 µm presented after 4 days of dissolution (see Fig. S.9). Furthermore, some gaps were detected between the printed layers, as can be seen in Fig. 14. Collectively these would have contributed to the release of the drug from the internal compartments of the manufactured implants at a rate consistent with long-term extended release.

3.5. Drug release kinetics

The drug release mechanism of the 3D printed implants was further investigated by plotting the dissolution data in different mathematical models, Zero-order, First-order, Higuchi model and Korsmeyer-Peppas model (Higuchi, 1961; Ritger and Peppas, 1987; Gouda et al., 2017).

The Korsmeyer-Peppas model was found to be the best fit for all the printed formulations (see Table S.2). More specifically, for the implants printed without a PCL shell, the release exponent value was $n < 0.45$, indicating that the drug release mechanism was diffusion related (Ritger and Peppas, 1987). PCL hydrolysis and the relaxation of the polymeric chains could also have an impact on the release of lidocaine as the aqueous medium was at 37 °C, higher than the glass transition temperature of the polymer (−60 °C) (Rychter et al., 2018). Nevertheless, this process is likely very slow and hence, the predominant mechanism

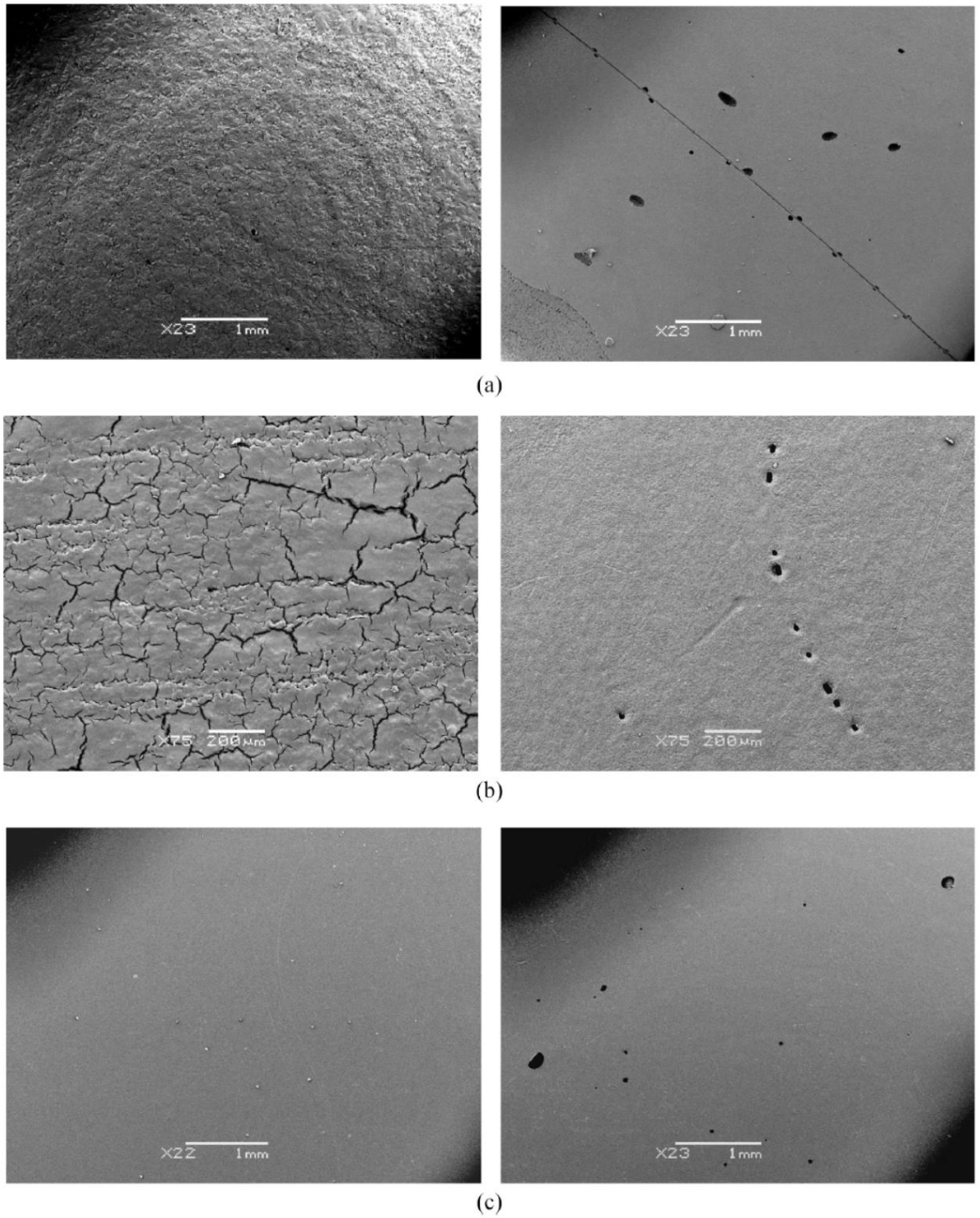

Fig. 13. SEM images before (left image) and after (right image) dissolution of the bottom side of (a): PCL-LDC 30% implants printed at 110 °C, (b): PCL-LDC 30% implants printed at 70 °C and (c): PCL-LDC 5% implants printed at 110 °C. The magnification and the scale bar are labelled on each SEM image separately.

for PCL-LDC dosage forms is proposed to be via Fickian diffusion, as is consistent with the Korsmeyer-Peppas model.

In the case of the PCL-LDC 30% implants with a PCL shell, the Korsmeyer-Peppas model also provided the highest R^2, compared to the other three kinetics models (see Table S.2). However, the obtained value of the release exponent was higher than in the non-shell formulations, $0.45 < n < 1$. It is suggested that so called 'anomalous' transport was responsible for the release of lidocaine from these implants whereby two mechanisms occurred simultaneously: diffusion and relaxation of polymeric chains (Ritger and Peppas, 1987). The latter caused by hydrolytic chain scission due to the temperature applied during the four-days in vitro drug release test. This resulted in PCL degradation and the creation of pores in the matrix. The dissolution medium could, then, gain access to the drug loaded core via these to be released through diffusion

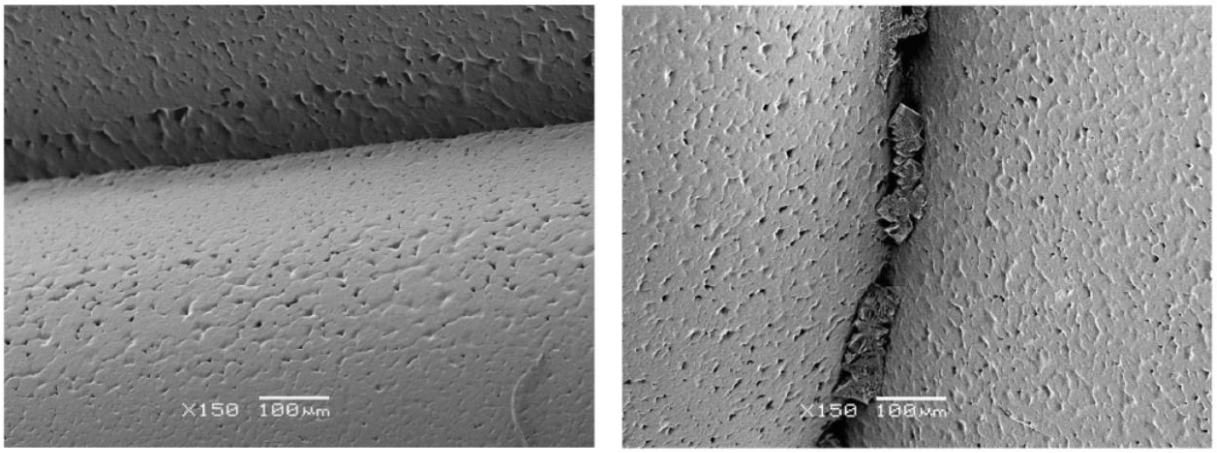

Fig. 14. SEM images (a); before (left image) and (b): after (right image) dissolution of the outside layers of PCL barrier-shell PCL-LDC 30% implants printed at 110 °C. The magnification is ×150, the scale bar 100 µm and they are labelled on each SEM image separately.

(Monteiro et al., 2016).

4. Conclusions

In summary, we have demonstrated the manufacture of a polycaprolactone core-shell formulation using a solvent-free method at a relatively low printing temperature with an extrusion-based 3D printer. Even though the studied polymer was very viscous, the proper combination of printing settings resulted in the fabrication of dosage forms without the need for additional additives. Sustained drug release has been achieved with all of the produced formulations even though different printing settings and drug loading were used. Polycaprolactone was proven to be a particularly useful polymer for the control of drug release rate due to its slow degradation. Implants encased within a PCL shell displayed low drug release (6%) compared to the non- encapsulated formulations (50–60%), verifying the effective role of the polymeric barrier. Drug release is proposed to be controlled by combined transportation mechanisms, diffusion and polymeric chain relaxation, as indicated by the Korsmeyer-Peppas model. The first stages of the PCL erosion in the polymeric matrix were observed by SEM. DSC, XRD, FTIR and Raman data exhibited that the thermal and physical properties of the polymer and the drug were unaffected by the 3D printing process and no detectable chemical interactions or modifications occurred between the used materials before and after their mixing and printing. This work clearly demonstrates that polycaprolactone has a significant potential for the production of prolonged release drug dosage forms by 3D printing. It has also been shown that drug loading can be varied in a bespoke fashion for each implant, showing that personalisable implants can be manufactured by 3D printing.

CRediT authorship contribution statement

Athina Liaskoni: Conceptualization, Methodology, Validation, Formal analysis, Data curation, Investigation, Writing - original draft, Visualization. **Ricky D. Wildman:** Conceptualization, Writing - review & editing, Supervision. **Clive J. Roberts:** Conceptualization, Writing - review & editing, Supervision.

Declaration of Competing Interest

The authors declare that they have no known competing financial interests or personal relationships that could have appeared to influence the work reported in this paper.

Acknowledgements

This work was funded by the University of Nottingham. We are grateful to Dr Graham A. Rance of the Nanoscale and Microscale Research Centre (nmRC, University of Nottingham) for assistance with Raman Spectroscopy analysis. Access to the SEM instrument was kindly provided by the nmRC (University of Nottingham).

Appendix A. Supplementary material

Supplementary data to this article can be found online at https://doi.org/10.1016/j.ijpharm.2021.120330.

References

Aita, I.E., Breitkreutz, J., Quodbach, J., 2019. On-demand manufacturing of immediate release levetiracetam tablets using pressure-assisted microsyringe printing. Eur. J. Pharm. Biopharm. 134, 29–36. https://doi.org/10.1016/j.ejpb.2018.11.008.

Alomari, M., Mohamed, F.H., Basit, A.W., Gaisford, S., 2015. Personalised dosing: Printing a dose of one's own medicine. Int. J. Pharm. 494, 568–577. https://doi.org/10.1016/j.ijpharm.2014.12.006.

Anacleto, S., Matos, M., Borges, C., Leijoto, H., Oliveira, D., Reis, A., Costa, E., Figueiredo, D., Augusto, M., Oliveira, L.D., Juliana, B., Borges, P., Antonio, M., Oliveira, D., Souza, W.D., 2018. Evaluation of physicochemical properties as supporting information on quality control of raw materials and veterinary pharmaceutical formulations. J. Pharm. Anal. 8, 168–175. https://doi.org/10.1016/j.jpha.2018.01.001.

Bourges, J.L., Bloquel, C., Thomas, A., Froussart, F., Bochot, A., Azan, F., Gurny, R., BenEzra, D., Behar-Cohen, F., 2006. Intraocular implants for extended drug delivery: Therapeutic applications. Adv. Drug Deliv. Rev. 58, 1182–1202. https://doi.org/10.1016/j.addr.2006.07.026.

da Silva, G.R., Fialho, S.L., Siqueira, R.C., Jorge, R., da Silva Cunha Júnior, A., 2010. Implants as drug delivery devices for the treatment of eye diseases. Brazilian J. Pharm. Sci. 46, 585–595. https://doi.org/10.1590/S1984-82502010000300024.

Díaz, E., Sandonis, I., Valle, M.B., 2014. In Vitro Degradation of Poly (caprolactone)/nHA Composites. J. Nanomater. 15, 1–8. https://doi.org/10.1155/2014/802435 Research.

Economidou, S.N., Lamprou, D.A., Douroumis, D., 2018. 3D printing applications for transdermal drug delivery. Int. J. Pharm. 544, 415–424. https://doi.org/10.1016/j.ijpharm.2018.01.031.

Edinger, M., Bar-Shalom, D., Sandler, N., Rantanen, J., Genina, N., 2018. QR encoded smart oral dosage forms by inkjet printing. Int. J. Pharm. 536, 138–145. https://doi.org/10.1016/j.ijpharm.2017.11.052.

Ferreira, J., Gloria, A., Cometa, S., Coelho, J.F.J., Domingos, M., 2017. Effect of in vitro enzymatic degradation on 3D printed poly(ε-caprolactone) scaffolds: morphological, chemical and mechanical properties. J. Appl. Biomater. Funct. Mater. 15, 185–195. https://doi.org/10.5301/jabfm.5000363.

Fina, F., Madla, C.M., Goyanes, A., Zhang, J., Gaisford, S., Basit, A.W., 2018. Fabricating 3D printed orally disintegrating printlets using selective laser sintering. Int. J. Pharm. 541, 101–107. https://doi.org/10.1016/j.ijpharm.2018.02.015.

Gbureck, U., Hölzel, T., Doillon, C.J., Müller, F.A., Barralet, J.E., 2007. Direct printing of bioceramic implants with spatially localized angiogenic factors. Adv. Mater. 19, 795–800. https://doi.org/10.1002/adma.200601370.

Genina, N., Holländer, J., Jukarainen, H., Mäkilä, E., Salonen, J., Sandler, N., 2016. Ethylene vinyl acetate (EVA) as a new drug carrier for 3D printed medical drug delivery devices. Eur. J. Pharm. Sci. 90, 53–63. https://doi.org/10.1016/j.ejps.2015.11.005.

Gioumouxouzis, C.I., Karavasili, C., Fatouros, D.G., 2019. Recent advances in pharmaceutical dosage forms and devices using additive manufacturing technologies. Drug Discov. Today 24, 636–643. https://doi.org/10.1016/j.drudis.2018.11.019.

Gouda, R., Baishya, H., Qing, Z., 2017. J. Develop. Drugs Appl. Math. Models Drug Release Kinet. Carbidopa Levodopa ER Tablets 6, 1–8. https://doi.org/10.4172/2329-6631.1000171.

Goyanes, A., Buanz, A.B.M., Basit, A.W., Gaisford, S., 2014. Fused-filament 3D printing (3DP) for fabrication of tablets. Int. J. Pharm. 476, 88–92. https://doi.org/10.1016/j.ijpharm.2014.09.044.

Goyanes, A., Buanz, A.B.M., Hatton, G.B., Gaisford, S., Basit, A.W., 2015a. 3D printing of modified-release aminosalicylate (4-ASA and 5-ASA) tablets. Eur. J. Pharm. Biopharm. 89, 157–162. https://doi.org/10.1016/j.ejpb.2014.12.003.

Goyanes, A., Robles, P., Buanz, A., Basit, A.W., Gaisford, S., 2015b. Effect of geometry on drug release from 3D printed tablets. Int. J. Pharm. 494, 657–663. https://doi.org/10.1016/j.ijpharm.2015.04.069.

Gudin, J., Argoff, C., Fudin, J., 2020. A Randomized, Open-Label, Bioequivalence Study of Lidocaine Topical System 1. 8 % and Lidocaine Patch 5 % in Healthy Subjects. J. Pain Res. 13, 1485–1496. https://doi.org/10.2147/JPR.S237934.

Gudin, J., Nalamachu, S., 2020. Utility of lidocaine as a topical analgesic and improvements in patch delivery systems. Postgrad. Med. 132, 28–36. https://doi.org/10.1080/00325481.2019.1702296.

Helmy, R., Zhou, G.X., Chen, Y.W., Crocker, L., Wang, T., Wenslow, R.M., Vailaya, A., 2003. Characterization and Quantitation of Aprepitant Drug Substance Polymorphs by Attenuated Total Reflectance Fourier Transform Infrared Spectroscopy FT-IR) for the identification and quantitation of two. Anal. Chem. 75, 605–611. https://doi.org/10.1021/ac020538i.

Higuchi, T., 1961. Rate of Release of Medicaments from Ointment Bases Containing Drugs in Suspension. J. Pharm. Sci. 50, 874–875. https://doi.org/10.1002/jps.2600501018.

Holländer, J., Hakala, R., Suominen, J., Moritz, N., Yliruusi, J., 2018. 3D printed UV light cured polydimethylsiloxane devices for drug delivery. Int. J. Pharm. 544, 433–442. https://doi.org/10.1016/j.ijpharm.2017.11.016.

Hull, C.W., 1986. United States Patent (19). United States Pat. 4575330 1–4.

Infanger, S., Haemmerli, A., Iliev, S., Baier, A., Stoyanov, E., Quodbach, J., 2019. Powder bed 3D-printing of highly loaded drug delivery devices with hydroxypropyl cellulose as solid binder. Int. J. Pharm. 555, 198–206. https://doi.org/10.1016/j.ijpharm.2018.11.048.

Jasiuk, I., Abueidda, D.W., Kozuch, C., Pang, S., Su, F.Y., McKittrick, J., 2018. An Overview on Additive Manufacturing of Polymers. JOM 70, 275–283. https://doi.org/10.1007/s11837-017-2730-y.

Kau, Y., Liao, C., Chen, Y., Liu, S., 2014. Sustained Release of Lidocaine from Solvent-Free Biodegradable Poly[(d, l)-Lactide-co-Glycolide] (PLGA). In Vitro and In Vivo Study. Materials (Basel). 7, 6660–6676. https://doi.org/10.3390/ma7096660.

Khaled, S.A., Alexander, M.R., Irvine, D.J., Wildman, R.D., Wallace, M.J., Sharpe, S., Yoo, J., Roberts, C.J., 2018a. Extrusion 3D Printing of Paracetamol Tablets from a Single Formulation with Tunable Release Profiles Through Control of Tablet Geometry. AAPS PharmSciTech 19, 3403–3413. https://doi.org/10.1208/s12249-018-1107-z.

Khaled, S.A., Alexander, M.R., Wildman, R.D., Wallace, M.J., Sharpe, S., Yoo, J., Roberts, C.J., 2018b. 3D extrusion printing of high drug loading immediate release paracetamol tablets. Int. J. Pharm. 538, 223–230. https://doi.org/10.1016/j.ijpharm.2018.01.024.

Khaled, S.A., Burley, J.C., Alexander, M.R., Roberts, C.J., 2014. Desktop 3D printing of controlled release pharmaceutical bilayer tablets. Int. J. Pharm. 461, 105–111. https://doi.org/10.1016/j.ijpharm.2013.11.021.

Khaled, S.A., Burley, J.C., Alexander, M.R., Yang, J., Roberts, C.J., 2015a. 3D printing of five-in-one dose combination polypill with defined immediate and sustained release profiles. J. Control. Release 217, 308–314. https://doi.org/10.1016/j.jconrel.2015.09.028.

Khaled, S.A., Burley, J.C., Alexander, M.R., Yang, J., Roberts, C.J., 2015b. 3D printing of tablets containing multiple drugs with defined release profiles. Int. J. Pharm. 494, 643–650. https://doi.org/10.1016/j.ijpharm.2015.07.067.

Khatri, P., Shah, M.K., Vora, N., 2018. Formulation strategies for solid oral dosage form using 3D printing technology: A mini-review. J. Drug Deliv. Sci. Technol. 46, 148–155. https://doi.org/10.1016/j.jddst.2018.05.009.

Koopmans, R.J., 1999. Die swell or extrudate swell. In: Karger-Kocsis, J. (Ed.), Polymer Science and Technology Series, vol. 2. Springer, Dordrecht, pp. 158–162. https://doi.org/10.1007/978-94-011-4421-6_22.

Kyobula, M., Adedeji, A., Alexander, M.R., Saleh, E., Wildman, R., Ashcroft, I., Gellert, P. R., Roberts, C.J., 2017. 3D inkjet printing of tablets exploiting bespoke complex geometries for controlled and tuneable drug release. J. Control. Release 261, 207–215. https://doi.org/10.1016/j.jconrel.2017.06.025.

Lamichhane, S., Bashyal, S., Keum, T., Noh, G., Seo, J.E., Bastola, R., Choi, J., Sohn, D.H., Lee, S., 2019. Complex formulations, simple techniques : Can 3D printing technology be the Midas touch in pharmaceutical industry ? Asian. J. Pharm. Sci. 14, 465–479. https://doi.org/10.1016/j.ajps.2018.11.008.

Lebon, M., Reiche, I., Gallet, X., Bellot-Gurlet, L., Zazzo, A., 2016. Rapid quantification of bone collagen content by ATR-FTIR spectroscopy. Radiocarbon 58, 131–146. https://doi.org/10.1017/RDC.2015.11.

Li, Q., Guan, X., Cui, M., Zhu, Z., Chen, K., Wen, H., Jia, D., Hou, J., Xu, W., Yang, X., Pan, W., 2018. Preparation and investigation of novel gastro-floating tablets with 3D extrusion-based printing. Int. J. Pharm. 535, 325–332. https://doi.org/10.1016/j.ijpharm.2017.10.037.

Liaw, C., Guvendiren, M., 2017. Current and emerging applications of 3D printing in medicine. Biofabrication 9, 1–18. https://doi.org/10.1088/1758-5090/aa7279.

Ligon, S.C., Liska, R., Stampfl, J., Gurr, M., Mulhaupt, R., 2017. Polymers for 3D Printing and Customized Additive Manufacturing. Chem. Rev. 117, 10210–10290. https://doi.org/10.1021/acs.chemrev.7b00074.

Luong-van, E., Grøndahl, L., Ngiap, K., Leong, K.W., Nurcombe, V., Cool, S.M., 2006. Controlled release of heparin from poly (e -caprolactone) electrospun fibers. Biomaterials 27, 2042–2050. https://doi.org/10.1016/j.biomaterials.2005.10.028.

Monteiro, M.S.S.B., Lunz, J., Sebastião, P.J., Inês, M., Tavares, B., 2016. Evaluation of Nevirapine Release Kinetics from Polycaprolactone Hybrids 680–701. https://doi.org/10.4236/msa.2016.711055.

Moulton, S.E., Wallace, G.G., 2014. 3-dimensional (3D) fabricated polymer based drug delivery systems. J. Control. Release 193, 27–34. https://doi.org/10.1016/j.jconrel.2014.07.005.

Newman, J.A., Schmitt, P.D., Toth, S.J., Deng, F., Zhang, S., Simpson, G.J., 2015. Parts per Million Powder X - ray Diffraction. Anal. Chem. 87, 10950–10955. https://doi.org/10.1021/acs.analchem.5b02758.

Norman, J., Madurawe, R.D., Moore, C.M.V., Khan, M.A., Khairuzzaman, A., 2017. A new chapter in pharmaceutical manufacturing: 3D-printed drug products. Adv. Drug Deliv. Rev. 108, 39–50. https://doi.org/10.1016/j.addr.2016.03.001.

Palo, M., Holländer, J., Suominen, J., Yliruusi, J., Sandler, N., 2017. 3D printed drug delivery devices: perspectives and technical challenges. Expert Rev. Med. Devices 14, 685–696. https://doi.org/10.1080/17434440.2017.1363647.

Perale, G., Casalini, T., Barri, V., Muller, M., Maccagnan, S., Masi, M., 2010. Lidocaine Release from Polycaprolactone Threads. J. Appl. Polym. Sci. Sci. 117, 3610–3614. https://doi.org/10.1002/app.

Pissinato Pere, C.P., Economidou, S.N., Lall, G., Ziraud, C., Boateng, J.S., Alexander, B. D., Lamprou, D.A., Douroumis, D., 2018. 3D printed microneedles for insulin skin delivery. Int. J. Pharm. 544, 425–432. https://doi.org/10.1016/j.ijpharm.2018.03.031.

Ribeiro, L.N.M., Franz-montan, M., Breitkreitz, M.C., Alcântara, A.C.S., Castro, S.R., Guilherme, V.A., Barbosa, R.M., Paula, E. De, 2016. Nanostructured lipid carriers as robust systems for topical lidocaine-prilocaine release in dentistry. Eur. J. Pharm. Sci. 93, 192–202. https://doi.org/10.1016/j.ejps.2016.08.030.

Ritger, P.L., Peppas, N.A., 1987. A simple equation for description of solute release I. Fickian and non-Fickian release from non-swellable devices in the form of slabs, spheres, cylinders or discs. J. Control. Release 5, 23–36. https://doi.org/10.1016/0168-3659(87)90034-4.

Robles-Martinez, P., Xu, X., Trenfield, S.J., Awad, A., Goyanes, A., Telford, R., Basit, A. W., Gaisford, S., 2019. 3D Printing of a Multi-Layered Polypill Containing Six Drugs Using a Novel Stereolithographic Method. Pharmaceutics 274, 1–16. https://doi.org/10.3390/pharmaceutics11060274.

Rychter, M., Baranowska-korczyc, A., Jarek, M., Maciejewska, B.M., Coy, E.L., Lulek, J., 2018. Cilostazol-Loaded Poly (ε -Caprolactone) Electrospun Drug Delivery System for Cardiovascular Applications. Pharm. Res. 35 https://doi.org/10.1007/s11095-017-2314-0.

Sadia, M., Alhnan, M.A., Ahmed, W., Jackson, M.J., 2018. 3D Printing of Pharmaceuticals. In: Jackson, M.J., Ahmed, W. (Eds.), Micro and Nanomanufacturing. Springer International Publishing AG 2018, pp. 467–498. https://doi.org/10.1007/978-3-319-67132-1.

Sandler, N., Preis, M., 2016. Printed Drug-Delivery Systems for Improved Patient Treatment. Trends Pharmacol. Sci. 37, 1070–1080. https://doi.org/10.1016/j.tips.2016.10.002.

Shao, J., Ma, J., Lin, L., Wang, B., Jansen, J.A., Walboomers, X.F., Zuo, Y., Yang, F., 2018. Three-Dimensional Printing of Drug-Loaded Scaffolds for Antibacterial and Analgesic Applications. Tiussue Eng. Part C 25, 1–10. https://doi.org/10.1089/ten.TEC.2018.0293.

Sheokand, S., Modi, S.R., Bansal, A.K., 2016. Quantification of low levels of amorphous content in crystalline celecoxib using dynamic vapor sorption (DVS). Eur. J. Pharm. Biopharm. 102, 77–86. https://doi.org/10.1016/j.ejpb.2016.03.006.

Shkarina, S., Shkarin, R., Weinhardt, V., Melnik, E., Vacun, G., Kluger, P., Loza, K., Epple, M., Ivlev, S.I., Baumbach, T., Surmeneva, M.A., Surmenev, R.A., 2018. 3D biodegradable scaffolds of polycaprolactone with silicate-containing hydroxyapatite microparticles for bone tissue engineering: High-resolution tomography and in vitro study. Sci. Rep. 8, 1–13. https://doi.org/10.1038/s41598-018-27097-7.

Skowyra, J., Pietrzak, K., Alhnan, M.A., 2015. Fabrication of extended-release patient-tailored prednisolone tablets via fused deposition modelling (FDM) 3D printing. Eur. J. Pharm. Sci. 68, 11–17. https://doi.org/10.1016/j.ejps.2014.11.009.

Stewart, S.A., Dom, J., Mcilorum, V.J., Gonzalez, Z., Utomo, E., Mancuso, E., Lamprou, D.A., Donnelly, R.F., Larran, E., 2020a. Poly (caprolactone) -Based Coatings on 3D-Printed Biodegradable Implants : A Novel Strategy to Prolong Delivery of Hydrophilic Drugs. Mol. Pharm. 17, 3487–3500. https://doi.org/10.1021/acs.molpharmaceut.0c00515.

Stewart, S.A., Dom, J., Mcilorum, V.J., Mancuso, E., Lamprou, D.A., Donnelly, R.F., Larrañeta, E., 2020b. Development of a Biodegradable Subcutaneous Implant for Prolonged Drug Delivery Using 3D Printing. Pharmaceutics 12, 1–16. https://doi.org/10.3390/pharmaceutics12020105.

Tappa, K., Jammalamadaka, U., 2018. Novel Biomaterials Used in Medical 3D Printing Techniques. J. Funct. Biomater. 17, 1–16. https://doi.org/10.3390/jfb9010017.

Umeda, Y., Fukami, T., Furuishi, T., Suzuki, T., Tanjoh, K., Tomono, K., 2009. Characterization of multicomponent crystal formed between indomethacin and lidocaine. Drug Dev. Ind. Pharm. 35, 843–851. https://doi.org/10.1080/03639040802660489.

Venkatesh, G.M., Barnett, M.E., Owusu-fordjour, C., Galop, M., 2001. Detection of Low Levels of the Amorphous Phase in Crystalline Pharmaceutical Materials by Current Spectrometry 1. Pharm. Res. 18, 98–103. https://doi.org/10.1023/a:1011087012826.

Water, J.J., Bohr, A., Boetker, J., Aho, J., Sandler, N., Nielsen, H.M., Rantanen, J., 2015. Three-dimensional printing of drug-eluting implants: Preparation of an antimicrobial polylactide feedstock material. J. Pharm. Sci. 104, 1099–1107. https://doi.org/10.1002/jps.24305.

West, T.G., Bradbury, T.J., 2019. 3D Printing : A Case of ZipDose Technology – World 's First Pharmaceutical Product 3D Printing Platform to Obtain FDA Approval for a Pharmaceutical Product, in: Maniruzzaman, M. (Ed.), 3D and 4D Printing in Biomedical Applications: Process Engineering and Additive Manufacturing. Wiley-VCHVerlag GmbH& Co. KGaA. 53, pp. 53–79.

Woodruff, M.A., Hutmacher, D.W., 2010. The return of a forgotten polymer - Polycaprolactone in the 21st century. Prog. Polym. Sci. 35, 1217–1256. https://doi.org/10.1016/j.progpolymsci.2010.04.002.

Xue, J., He, M., Liu, H., Niu, Y., Crawford, A., Coates, P.D., Chen, D., Shi, R., Zhang, L., 2014. Drug loaded homogeneous electrospun PCL/gelatin hybrid nano fi ber structures for anti-infective tissue regeneration membranes. Biomaterials 35, 9395–9405. https://doi.org/10.1016/j.biomaterials.2014.07.060.

Yang, N., Chen, H., Han, H., Shen, Y., Gu, S., He, Y., 2018. 3D printing and coating to fabricate a hollow bullet-shaped implant with porous surface for controlled cytoxan release. Int. J. Pharm. 552, 91–98. https://doi.org/10.1016/j.ijpharm.2018.09.042.

Zema, L., Melocchi, A., Maroni, A., Gazzaniga, A., 2017. Three-Dimensional Printing of Medicinal Products and the Challenge of Personalized Therapy. J. Pharm. Sci. 106, 1697–1705. https://doi.org/10.1016/j.xphs.2017.03.021.